

## Durham E-Theses

---

### *Deformation and fluid-rock interaction along then reactivated Outer Hebrides fault zone, Scotland*

Imber, Jonathan

#### How to cite:

---

Imber, Jonathan (1998) *Deformation and fluid-rock interaction along then reactivated Outer Hebrides fault zone, Scotland*, Durham theses, Durham University. Available at Durham E-Theses Online: <http://etheses.dur.ac.uk/2022/>

#### Use policy

---

The full-text may be used and/or reproduced, and given to third parties in any format or medium, without prior permission or charge, for personal research or study, educational, or not-for-profit purposes provided that:

- a full bibliographic reference is made to the original source
- a [link](#) is made to the metadata record in Durham E-Theses
- the full-text is not changed in any way

The full-text must not be sold in any format or medium without the formal permission of the copyright holders.

Please consult the [full Durham E-Theses policy](#) for further details.

The copyright of this thesis rests  
with the author. No quotation  
from it should be published  
without the written consent of the  
author and information derived  
from it should be acknowledged.

**DEFORMATION AND FLUID-ROCK  
INTERACTION ALONG THE REACTIVATED  
OUTER HEBRIDES FAULT ZONE, SCOTLAND.**

*by*

**Jonathan Imber**

**A thesis submitted in partial fulfilment of the requirements of the University of  
Durham for the degree of Doctor of Philosophy**

**Department of Geological Sciences  
University of Durham**

**1998**



**22 FEB 1999**

# DECLARATION

No part of this thesis has been previously submitted for a degree at this, or any other university. The work described in this thesis is entirely that of the author, except where reference is made to previously published work.



Jonathan Imber

Department of Geological Sciences,  
University of Durham

July 1998

© Jonathan Imber

**The copyright of this thesis rests with the author. No quotation or data from it should be published without the author's prior written consent and any information derived from it should be acknowledged.**

## ABSTRACT

The Outer Hebrides Fault Zone (OHFZ) is a major, moderately E- to ESE-dipping long-lived reactivated fault zone which is developed in, and cross-cuts, crystalline amphibolite to granulite grade Lewisian basement gneisses, NW Scotland. A complex assemblage of different fault rocks and structures is presently exposed along the OHFZ, which reflects deformation at a range of crustal depths and metamorphic (temperature, pressure, fluid activity) conditions. Detailed field and microstructural observations have demonstrated that segments of the fault zone which display evidence of repeated reactivation over long periods of geological time (movements range from late Laxfordian / Grenvillian to Oligocene in age) are characterised by intense, localised greenschist facies retrogression and the development of sericite- and chlorite-bearing phyllonitic shear zones. In contrast, phyllonite is absent from segments of the fault zone which have *not* suffered extensive reactivation. These observations are consistent with phyllonitisation at mid-crustal depths having caused profound long-term mechanical weakening of the OHFZ.

Two phases of retrogression and phyllonitisation have been recognised along the OHFZ:

- Upper greenschist facies, Late Laxfordian / Grenvillian phyllonitisation, which occurred at between 15 and 17km depth (Lewis and Harris only), and
- Lower greenschist facies, Caledonian phyllonitisation, which occurred at between 8 and 9km depth (Lewis, Harris and the Uists).

Microstructural and geochemical studies of selected phyllonites from reactivated segments of the OHFZ demonstrate that greenschist facies retrogression and phyllonitisation were promoted by the influx of warm (c.250 to 450°C), hydrous iron- and magnesium-bearing, oxidising fluids into the fault zone. Fluid flow during upper greenschist facies phyllonitisation was focused into pre-existing bands of highly strained quartzo-feldspathic mylonite, whilst fluid flow during lower greenschist facies phyllonitisation was focused predominantly into pre-existing brittle fractures and cataclastic crush zones. Thus, the distribution and intensity of fluid flow, and hence the distribution and intensity of retrogression and phyllonitisation were ultimately governed by the nature of pre-existing permeability pathways through the fault zone.

It is therefore concluded that the long-term *rheological* evolution of reactivated basement fault zones is inexorably linked to the mid-crustal *permeability* evolution of such structures.

## ACKNOWLEDGEMENTS

I wish to thank the following people for their input into this thesis:

- My supervisors, Bob Holdsworth and Jeremy Henderson are thanked for their guidance over the past four years. Bob's constant enthusiasm, countered by Jeremy's quiet sarcasm, have been a stimulating combination during my time in Durham. Eric Condliffe and Geoff Lloyd, my 'unofficial' supervisors in Leeds, are also thanked for their patience and guidance whilst I used their SEM.
- I am grateful to other members of staff in Durham for their help on numerous occasions. In particular, I wish to thank Andrew Peckett, Dave Hirst, Graham Pearson, Chris Ottley and Ron Hardy for their valiant attempts to introduce me to the world of microscopy and geochemistry. The geochemical studies in the thesis have also benefited from numerous discussions with, and practical help from, Alfonso Brod, Ercan Aldanmaz and Yvonne Brown.
- Cheers to Tim, Nick and Pondy for coming to the Park District of Lewis as my field assistants, and for introducing me to the joys of crab shooting.
- Thanks to the other postgrads for being making my time in Durham so thoroughly enjoyable. In particular, I would like to mention my ex-housemates and guardians of the 'departmental filth', Wayne Bailey, Alun Price and Jo Garland, and other members of the classes of '93, '94 and '95: Adam Styles, Gail Radcliffe, Simon Grant, Ziad Ahmadi, Simon Molyneux, Toby Harrold, Ian Turner, Andy Cook and Lorraine Beacom.
- My sincere thanks must also go to Simon Grant, Christina Byrne, Toby Harrold, Gail Radcliffe, Christine Orme and Martyn Stewart for their help with cutting, gluing, colouring, drawing and generally running about on my behalf over the past week. I would not be writing this now were it not for their help.
- Finally, I wish to thank Mum, Dad, Rebecca and Tamsin for their love and support over the years. It is to them I dedicate this thesis.

*Dedicated to Mum, Dad, Rebecca  
and Tamsin*

# Deformation and fluid-rock interaction along the reactivated Outer Hebrides Fault Zone, Scotland

1. INTRODUCTION.....	1
1.1 INTRODUCTION AND AIMS .....	1
1.2 STRUCTURE OF THE CONTINENTAL LITHOSPHERE .....	2
1.2.1 BUOYANCY OF THE CONTINENTAL CRUST .....	2
1.2.2 VERTICAL STRENGTH DISTRIBUTION .....	3
1.3 DEFORMATION MECHANISMS AND CRUSTAL DEFORMATION .....	5
1.3.1 FRICTIONAL DEFORMATION MECHANISMS.....	5
1.3.1.1 Fracture mechanisms.....	6
1.3.1.2 Frictional grain boundary sliding .....	7
1.3.1.3 Cataclasis .....	7
1.3.1.4 Frictional melting.....	8
1.3.2 VISCOUS DEFORMATION MECHANISMS .....	8
1.3.2.1 Diffusive mass transfer.....	8
1.3.2.2 Crystal plasticity.....	10
1.3.3 THE FRICTIONAL TO VISCOUS CREEP TRANSITION.....	12
1.3.3.1 Definition and terminology .....	13
1.3.3.2 Rheological properties of the frictional to viscous transition .....	13
1.3.3.3 Fault rocks and recognition of the frictional to viscous creep transition.....	15
1.4 RETROGRADE METAMORPHISM AND METAMORPHIC FLUID TRANSPORT IN FAULTS AND SHEAR ZONES .....	17
1.4.1 RETROGRADE METAMORPHISM IN FAULTS AND SHEAR ZONES.....	17
1.4.1.1 Chemical potential of H <sub>2</sub> O, CO <sub>2</sub> and O <sub>2</sub> .....	17
1.4.1.2 Effect of element mobility on retrograde mineral assemblages.....	18
1.4.1.3 Timing of retrogression relative to deformation.....	20
1.4.1.4 Metamorphic facies classification scheme .....	20
1.4.2 METAMORPHIC FLUID TRANSPORT WITHIN FAULTS AND SHEAR ZONES.....	20
1.4.2.1 Fluid transport in upper crustal fault zones .....	21
1.4.2.2 Fluid transport in mid- to lower crustal fault zones.....	24
1.5 FAULT ZONE WEAKENING MECHANISMS.....	26
1.5.1 SYN-TECTONIC WEAKENING MECHANISMS .....	26
1.5.1.1 High pore fluid pressure.....	26
1.5.1.2 Fluid-assisted diffusive mass transfer.....	27
1.5.1.3 Hydrolytic weakening .....	27
1.5.1.4 Generation of transient, fine grained reaction products.....	27
1.5.1.5 Transformational plasticity and volume change.....	28
1.5.2 LONG-TERM WEAKENING MECHANISMS.....	28
1.5.2.1 Reaction softening.....	28
1.5.2.2 Fabric softening.....	29
1.5.2.3 Grain size reduction .....	30
1.5.3 SUMMARY .....	30
1.6 FAULT ZONE REACTIVATION: DEFINITION AND TERMINOLOGY.....	31
1.6.1 DEFINITION AND RECOGNITION .....	31
1.6.2 STRUCTURAL TERMINOLOGY FOR REACTIVATED FAULT ZONES.....	32
1.6.2.1 The Torridon shear belt: ductile reactivation of pre- existing ductile fabrics .....	34
1.6.2.2 The Gairloch shear zone: brittle reactivation of pre- existing ductile fabrics .....	34

1.6.2.3 The Church Stretton Fault Zone: brittle reactivation of pre-existing brittle faults.....	35
1.6.2.4 New structural terminology for reactivated fault zones.....	35
1.7 DATA COLLECTION.....	37
1.7.1 FIELDWORK METHODS.....	37
1.7.2 MICROSTRUCTURAL METHODS.....	38
1.7.3 GEOCHEMICAL METHODS.....	38
1.8 THESIS OUTLINE.....	38
2. THE OUTER HEBRIDES FAULT ZONE: INTRODUCTION.....	40
2.1 INTRODUCTION.....	40
2.2 THE LEWISIAN COMPLEX IN THE OUTER HEBRIDES.....	41
2.2.1 REGIONAL CONTEXT.....	41
2.2.2 LITHOLOGIES.....	43
2.2.2.1 Quartzo-feldspathic banded gneisses.....	44
2.2.2.2 Supracrustal sequence.....	44
2.2.2.3 Major intrusives.....	44
2.2.2.4 Minor intrusives.....	45
2.2.3 THE SCOURIAN EVENT.....	46
2.2.4 THE LAXFORDIAN EVENT.....	49
2.2.5 SUMMARY.....	49
2.3 THE OUTER HEBRIDES FAULT ZONE: INTRODUCTION AND PREVIOUS WORK.....	50
2.3.1 INTRODUCTION.....	50
2.3.2 THE AGE OF THE OHFZ.....	50
2.2.3.1 Field relationships.....	51
2.2.3.2 Isotopic ages.....	51
2.3.3 FAULT ROCKS.....	52
2.3.3.1 Fault rock distribution.....	52
2.3.3.2 Distribution of low grade alteration.....	53
2.3.3.3 Late-stage faults and lineaments.....	53
2.3.4 PREVIOUS WORK: ONSHORE STUDIES.....	54
2.3.4.1 Sibson (1977a & b).....	54
2.3.4.2 White & Glasser (1987) and Walker (1990).....	56
2.3.4.3 Butler (1995) and Butler <i>et al.</i> (1995).....	57
2.3.5 PREVIOUS WORK: OFFSHORE STUDIES.....	60
2.3.5.1 Shallow structure: Stein (1988).....	60
2.3.5.2 Deep structure: Smythe <i>et al.</i> (1982), Peddy (1984) and Smythe (1987).....	61
2.4 THE STORNOWAY FORMATION.....	63
2.5 SUMMARY.....	64
3. THE OUTER HEBRIDES FAULT ZONE: OVERVIEW.....	66
3.1 INTRODUCTION.....	66
3.2 THE NORTHERN ZONE: LEWIS & SCALPAY.....	67
3.2.1 LEWISIAN PROTOLITHS OF SOUTHEAST LEWIS AND SCALPAY.....	67
3.2.2 PERVASIVE MYLONITES.....	68
3.2.2.1 Loch Sgibacleit to Loch Erisort.....	69
3.2.2.2 Scalpay.....	73
3.2.2.3 Kebock Head.....	76
3.2.2.4 Southeast Lewis.....	79
3.2.2.5 Summary and discussion.....	80
3.2.3 THE PHYLLONITE BELTS.....	84
3.2.3.1 Eishken.....	85
3.2.3.3 Kebock Head.....	89

3.2.3.3 Loch Bhrollum .....	91
3.2.3.4 Scalpay .....	95
3.2.3.5 Summary and discussion .....	98
3.2.4 NORMAL FAULTS .....	101
3.2.4.1 Gob Hais .....	101
3.2.4.2 Arnish .....	103
3.2.4.3 Dun Mor .....	104
3.2.4.4 Summary and discussion .....	105
3.2.5 SUMMARY: KINEMATIC EVOLUTION AND FLUID-ROCK INTERACTIONS ALONG THE NORTHERN ZONE OF THE OHFZ .....	106
3.3 SOUTH HARRIS .....	107
3.3.1 RUBHA VALLERIP .....	107
3.3.1.1 Protoliths .....	107
3.3.1.2 Brittle deformation .....	107
3.3.1.3 The Rubha Vallerip phyllonite belt .....	107
3.3.1.4 Microstructure .....	109
3.3.1.5 Summary and discussion .....	109
3.4 THE SOUTHERN ZONE: NORTH UIST AND ADJACENT ISLANDS .....	110
3.4.1 THE 'FORELAND' .....	111
3.4.1.1 Protoliths .....	111
3.4.1.2 Localised deformation in the 'foreland' .....	112
3.4.2 PSEUDOTACHYLYTE-ULTRACATACLASITE CRUSH ZONES AND CRUSH MELANGE .....	113
3.4.2.1 Pseudotachylyte-ultracataclasite crush zones .....	113
3.4.2.2 Crush melange .....	114
3.4.2.3 Microstructure .....	114
3.4.2.4 Summary and discussion .....	114
3.4.3 THE PHYLLOITIC FABRICS .....	116
3.4.3.1 Discrete phyllonites .....	116
3.4.3.2 Pervasive protophyllonites .....	117
3.4.3.3 The North Uist phyllonite belts .....	119
3.4.3.4 Microstructures .....	121
3.4.3.5 Summary and discussion .....	122
3.4.4 SUMMARY: KINEMATIC EVOLUTION AND FLUID-ROCK INTERACTIONS ALONG THE OHFZ IN NORTH UIST .....	125
3.5 THE SOUTHERN ZONE: SOUTH UIST AND ADJACENT ISLANDS .....	126
3.5.1 PROTOLITHS .....	127
3.5.1.1 Banded gneiss .....	127
3.5.1.2 Corodale Gneiss .....	127
3.5.2 LOCALISED DEFORMATION IN THE 'FORELAND' AND THE PSEUDOTACHYLYTE-ULTRACATACLASITE CRUSH ZONES .....	128
3.5.2.1 Localised deformation in the 'foreland' .....	128
3.5.2.2 Pseudotachylyte-ultracataclasite crush zones .....	129
3.5.2.3 Microstructure .....	129
3.5.2.4 Summary and discussion .....	129
3.5.3 THE USINISH PHYLLOITIC .....	130
3.5.3.1 Field relationships .....	130
3.5.3.2 Microstructures .....	131
3.5.3.3 Summary and discussion .....	132
3.5.4 THE MASHED GNEISS .....	133
3.5.5 SUMMARY: KINEMATIC EVOLUTION AND FLUID-ROCK INTERACTIONS ALONG THE OHFZ IN SOUTH UIST .....	134
3.6 THE SOUTHERN ZONE: ERISKAY AND THE BARRA ISLES .....	134
3.6.1 ERISKAY .....	134
3.6.2 THE BARRA ISLES .....	136
3.6.2.1 Barra, Vatersay and Sandray .....	136
3.6.2.2 Fuiay, Hellisay and Gighay .....	137

3.6.3 SUMMARY: KINEMATIC EVOLUTION AND FLUID-ROCK INTERACTIONS ALONG THE OHFZ ( <i>s.l.</i> ) ON ERISKAY AND THE BARRA ISLES .....	139
3.7 SUMMARY AND CONCLUSIONS .....	140
3.7.1 THE KINEMATIC EVOLUTION OF THE OHFZ .....	140
3.7.2 FLUID-ROCK INTERACTION ALONG THE OHFZ .....	142
3.7.3 CONCLUSIONS .....	145
4. LOCH SGIBACLEIT .....	143
4.1 INTRODUCTION .....	143
4.1.1 INTRODUCTION AND AIMS .....	143
4.1.2 STUDY AREA AND CHAPTER LAYOUT .....	143
4.2 PRIMARY FABRIC: LOWER AMPHIBOLITE FACIES MYLONITE .....	145
4.2.1 FIELD RELATIONSHIPS .....	145
4.2.1.1 Macrostructure .....	145
4.2.1.2 Lithology and mesostructure .....	145
4.2.2 MICROSTRUCTURE .....	149
4.2.2.1 Felsic mylonite and protomylonite .....	149
4.2.2.2 Felsic ultramylonite .....	151
4.2.2.3 Mafic protomylonite .....	152
4.2.2.4 Discrete ultramylonite .....	153
4.2.2.5 Pseudotachylyte .....	156
4.2.3 SUMMARY AND DISCUSSION .....	156
4.2.3.1 Metamorphic conditions during thrusting .....	157
4.2.3.2 Operative deformation mechanisms during mylonitisation .....	158
4.2.3.3 Origin and significance of the ultramylonitic fabrics .....	160
4.2.3.4 Age and significance of the 'early' pseudotachylyte veins .....	162
4.3 DERIVED FABRICS: FOLIATION-PARALLEL FAULT ZONES & CRUSH ZONES .....	162
4.3.1 FIELD RELATIONSHIPS .....	162
4.3.1.1 Macrostructure .....	163
4.3.1.2 Mesostructure .....	163
4.3.2 MICROSTRUCTURE .....	165
4.3.2.1 Pseudotachylyte fault veins, breccias and quasi-conglomerates .....	165
4.3.2.2 Pseudotachylyte-ultramylonite crush zones .....	165
4.3.3 SUMMARY AND DISCUSSION .....	166
4.3.3.1 Mechanisms of localisation and pseudotachylyte generation .....	166
4.3.3.2 Timing, kinematics and significance of brittle deformation .....	168
4.4 CROSS-CUTTING STRUCTURES .....	170
4.4.1 FIELD RELATIONSHIPS .....	170
4.4.2 MICROSTRUCTURE .....	170
4.4.3 DISCUSSION .....	171
4.5 SUMMARY .....	172
5. SCALPAY .....	179
5.1 INTRODUCTION .....	179
5.1.1 INTRODUCTION AND AIMS .....	179
5.1.2 STUDY AREA AND CHAPTER LAYOUT .....	180
5.2 PRIMARY FABRIC: UPPER GREENSCHIST FACIES MYLONITE .....	181
5.2.1 FIELD RELATIONSHIPS .....	181
5.2.1.1 Macrostructure .....	181
5.2.1.2 Lithology and mesostructure .....	182
5.2.2 MICROSTRUCTURE .....	187
5.2.2.1 Quartzo-feldspathic mylonite .....	187

5.2.2.2 Upper greenschist facies phyllonite.....	191
5.2.2.3 Protomylonitic pegmatite .....	194
5.2.2.4 Protomylonitic amphibolite.....	194
5.2.3 SUMMARY AND DISCUSSION .....	195
5.2.3.1 Retrogression and metamorphism within the mylonite belt.....	195
5.2.3.2 Operative deformation mechanisms during mylonitisation .....	196
5.3 CROSS-CUTTING STRUCTURES: THRUST-RELATED BRITTLE FAULTS & CATACLASITE SEAMS .....	201
5.4 REWORKED FABRICS: SINISTRAL STRIKE-SLIP RELATED PHYLLONITE & MYLONITE .....	201
5.4.1 FIELD RELATIONSHIPS .....	201
5.4.1.1 Macrostructure .....	201
5.4.1.2 Lithology and mesostructure .....	202
5.4.2 MICROSTRUCTURE .....	207
5.4.2.1 Felsic phyllonite ('grey-green' phyllonite).....	207
5.4.2.2 Mafic phyllonite ('dark-green' phyllonite).....	208
5.4.2.3 Strike-slip related quartzo-feldspathic mylonite.....	209
5.4.3 SUMMARY AND DISCUSSION .....	210
5.4.3.1 Retrogression and metamorphism during sinistral strike- slip.....	210
5.4.3.2 Operative deformation mechanisms during sinistral strike- slip.....	211
5.4.3.3 Timing and significance of static recrystallisation .....	213
5.4.4 SYNTHESIS .....	213
5.4.4.1 Summary .....	213
5.4.4.2 Timing and controls on shear zone localisation .....	214
5.4.4.3 A model of lower greenschist facies phyllonitisation on Scalpay .....	215
5.5 REWORKED & DERIVED FABRICS: DEXTRAL STRIKE-SLIP RELATED PHYLLONITE & DETACHMENT FAULTS.....	217
5.5.1 REWORKED FABRICS.....	217
5.5.1.1 Field relationships .....	217
5.5.1.2 Microstructure .....	219
5.5.1.3 Summary and discussion .....	220
5.5.2 DETACHMENT FAULTS .....	221
5.5.3 SYNTHESIS .....	222
5.5.3.1 Summary .....	222
5.5.3.2 Controls on the distribution of dextral strike-slip related deformation .....	223
5.5.3.3 Age and significance of detachment faults.....	223
5.6 SUMMARY .....	224
 6. NORTH UIST .....	 225
6.1 INTRODUCTION .....	225
6.1.1 INTRODUCTION AND AIMS .....	225
6.1.2 STUDY AREA AND CHAPTER LAYOUT .....	227
6.2 PRIMARY FABRIC: THE CRUSH MELANGE.....	228
6.2.1 FIELD RELATIONSHIPS.....	229
6.2.1.1 The fault zone base .....	229
6.2.1.2 The crush melange .....	229
6.2.2 MICROSTRUCTURES .....	231
6.2.2.1 Deformation microstructures.....	231
6.2.2.2 Microstructures associated with low grade alteration .....	234
6.2.3 SUMMARY AND DISCUSSION .....	236
6.2.3.1 Development of the crush melange .....	237
6.2.3.2 The distribution of low grade alteration .....	237
6.3 DERIVED FABRICS: TRANSPRESSION AND STRIKE-SLIP RELATED PHYLLONITES.....	238

6.3.1 DISCRETE PHYLLONITES.....	238
6.3.1.1 Field relationships.....	239
6.3.1.2 Microstructure.....	242
6.3.1.3 Summary and discussion.....	244
6.3.2 PERVASIVE PROTOPHYLLONITES.....	246
6.3.2.1 Field relationships.....	246
6.3.2.2 Microstructure.....	248
6.3.2.3 Summary and discussion.....	252
6.3.3 PHYLLONITE BELTS.....	256
6.3.3.1 Field relationships: macrostructure.....	258
6.3.3.2 Field relationships: lithology and mesostructure.....	258
6.3.3.3 Microstructure.....	261
6.3.3.4 Summary and discussion.....	266
6.3.4 SYNTHESIS.....	270
6.3.4.1 Summary.....	270
6.3.4.2 The spatial and temporal distribution of the phyllonitic fabrics.....	271
6.3.4.3 A model of phyllonitisation on North Uist.....	273
6.4 REWORKED FABRICS & DETACHMENT FAULTS.....	277
6.4.1 THE DISTRIBUTION OF REWORKED FABRICS IN NORTH UIST.....	277
6.4.2 TRANSTENSION-RELATED FABRICS.....	279
6.4.2.1 Field relationships.....	279
6.4.2.2 Microstructure.....	282
6.4.2.3 Summary and discussion.....	284
6.4.3 EXTENSION-RELATED FABRICS.....	286
6.4.3.1 Field relationships.....	286
6.4.3.2 Microstructure.....	292
6.4.3.3 Summary and discussion.....	299
6.4.4 DETACHMENT FAULTS.....	303
6.4.4.1 Field relationships.....	303
6.4.4.2 Origin and relative age of the detachment faults.....	305
6.4.5 SYNTHESIS.....	306
6.5 SUMMARY.....	307
7. USINISH PHYLLONITE.....	309
7.1 INTRODUCTION.....	309
7.1.1 INTRODUCTION AND AIMS.....	309
7.1.2 STUDY AREA AND CHAPTER LAYOUT.....	310
7.2 REGIONAL STRUCTURE OF THE USINISH PHYLLONITE.....	310
7.2.1 RUBHA ROSSEL.....	310
7.2.1.1 Macrostructure.....	311
7.2.1.2 Mesostructure.....	312
7.2.1.3 Detachment faults.....	316
7.2.2 RUBHA HELLISDALE TO ABHAINN LIADALE.....	316
7.2.3 RUBHA BOLUM.....	317
7.2.3.1 Macrostructure.....	317
7.2.3.2 Mesostructure.....	318
7.2.3.3 Detachment faults.....	321
7.2.4 STULEY.....	321
7.2.4.1 Macrostructure.....	321
7.2.4.2 Mesostructure.....	321
7.2.5 SUMMARY AND DISCUSSION.....	323
7.2.5.1 Kinematic evolution and regional structure of the Usinish Phyllonite.....	323
7.2.5.2 Distribution and origin of the phyllonitic fabrics.....	325
7.2.5.3 Summary.....	326

7.3 PRIMARY FABRIC: FRACTURED CORODALE GNEISS AND MASHED GNEISS.....	327
7.3.1 FRACTURED CORODALE GNEISS.....	327
7.3.1.1 Field relationships.....	327
7.3.1.2 Microstructure.....	328
7.3.2 MASHED GNEISS.....	330
7.3.2.1 Field relationships.....	330
7.3.2.2 Microstructure.....	330
7.3.3 SUMMARY AND DISCUSSION.....	332
7.3.3.1 Deformation mechanisms.....	332
7.3.3.2 Distribution of low grade alteration.....	332
7.4 DERIVED FABRICS: STRIKE-SLIP AND 'NEW' TRANSTENSION- AND EXTENSION-RELATED PHYLLONITES.....	333
7.4.1 CORODALE GNEISS-DERIVED PHYLLONITE.....	333
7.4.1.1 Protophyllonite.....	333
7.4.1.2 Phyllonite and ultraphyllonite.....	335
7.4.1.3 Summary and discussion.....	338
7.4.2 MASHED GNEISS-DERIVED PHYLLONITE.....	340
7.4.2.1 Protophyllonite.....	340
7.4.2.2 Phyllonite and ultraphyllonite.....	341
7.4.2.3 Summary and discussion.....	342
7.4.3 SYNTHESIS.....	343
7.4.3.1 Summary.....	343
7.4.3.2 A model of phyllonitisation in South Uist.....	344
7.5 REWORKED FABRICS & DETACHMENT FAULTS: TRANSTENSION- AND EXTENSION-RELATED PHYLLONITE.....	345
7.5.1 REWORKED FABRICS.....	345
7.5.1.1 Field relationships.....	345
7.5.1.2 Microstructure.....	346
7.5.1.3 Summary and discussion.....	347
7.5.2 DETACHMENT FAULTS.....	349
7.5.2.1 Field relationships.....	349
7.5.2.2 Microstructure.....	349
7.5.2.3 Summary and discussion.....	350
7.5.3 SYNTHESIS.....	351
7.5.3.1 Summary.....	351
7.5.3.2 A model of reactivation in South Uist.....	351
7.6 SUMMARY.....	353
8. GEOCHEMICAL EVOLUTION OF THE LOWER GREENSCHIST FACIES PHYLLONITES, NORTH UIST.....	355
8.1 INTRODUCTION.....	355
8.1.1 INTRODUCTION AND AIMS.....	355
8.1.2 STUDY AREA AND ANALYTICAL METHODS.....	356
8.2 SAMPLES.....	356
8.2.1 SAMPLE DESCRIPTIONS.....	358
8.2.1.1 Protoliths.....	358
8.2.1.2 Primary fabrics.....	358
8.2.1.3 Pervasive protophyllonites.....	359
8.2.1.4 Strike-slip related phyllonites and ultraphyllonites.....	359
8.2.1.5 Extension-related phyllonites and ultraphyllonites.....	360
8.2.2 FAULT ROCK DERIVATION.....	360
8.3 MAJOR ELEMENTS.....	362
8.3.1 MAJOR ELEMENT COMPOSITION.....	362
8.3.2 PROTOLITH-NORMALISED MAJOR ELEMENT COMPOSITION.....	363
8.4 RARE EARTH ELEMENTS.....	365

8.4.1	PROTOLITHS .....	366
8.4.2	CRUSH MELANGE .....	367
8.4.3	PERVASIVE PROTOPHYLLONITES AND STRIKE-SLIP RELATED PHYLLONITES.....	368
8.4.4	EXTENSIONALLY REWORKED PHYLLONITES .....	370
8.4.5	SUMMARY & DISCUSSION OF THE REE DATA .....	371
8.4.5.1	Summary .....	371
8.4.5.2	Fault rock microstructure and REE composition .....	372
8.4.5.3	Geochemical nature of the fluid phase .....	373
8.5	MULTI-ELEMENT SPIDERDIAGRAMS .....	375
8.5.1	PROTOLITHS .....	375
8.5.2	CRUSH MELANGE .....	376
8.5.3	PERVASIVE PROTOPHYLLONITES AND STRIKE-SLIP RELATED PHYLLONITES.....	378
8.5.4	EXTENSIONALLY REWORKED PHYLLONITES .....	379
8.5.5	SUMMARY & DISCUSSION.....	380
8.5.5.1	Immobile trace element data .....	381
8.5.5.2	Mobile trace element data .....	382
8.6	ELEMENT RATIO DIAGRAMS .....	383
8.6.1	U/Nb versus Rb/Nb DIAGRAM .....	383
8.6.2	U/Nb versus Sr/Nb DIAGRAM .....	384
8.6.3	U/Nb versus Ba/Nb DIAGRAM .....	385
8.6.4	U/Nb versus Cs/Nb DIAGRAM.....	386
8.6.5	SUMMARY AND DISCUSSION.....	387
8.6.5.1	Intensity of alteration .....	388
8.6.5.2	Volume changes .....	389
8.7	SUMMARY .....	389
9.	SUMMARY, DISCUSSION AND CONCLUSIONS.....	391
9.1	INTRODUCTION .....	391
9.2	TECTONIC AND METAMORPHIC EVOLUTION OF THE OHFZ.....	391
9.2.1	LEWISIAN PROTOLITHS .....	391
9.2.2	PERVASIVE MYLONITE.....	392
9.2.2.1	Timing of mylonitisation.....	392
9.2.2.2	Kinematic evolution of the pervasive mylonite belt .....	393
9.2.2.3	Textural evolution of the pervasive mylonite belt.....	393
9.2.2.4	Metamorphic conditions and crustal depths .....	395
9.2.3	CATACLASITE AND PSEUDOTACHYLYTE.....	397
9.2.3.1	Timing of brittle deformation.....	397
9.2.3.2	Fault zone kinematics during pseudotachylyte generation .....	398
9.2.3.3	Textural evolution during brittle deformation .....	399
9.2.3.4	Metamorphic conditions and crustal depths .....	400
9.2.4	LOWER GREENSCHIST FACIES FABRICS .....	401
9.2.4.1	Timing of lower greenschist facies deformation .....	401
9.2.4.2	Kinematic evolution of the lower greenschist facies fabrics .....	402
9.2.4.3	Textural evolution of the lower greenschist facies fabrics .....	403
9.2.4.4	Metamorphic conditions and crustal depths .....	405
9.2.5	LATE BRITTLE DEFORMATION: LATE DETACHMENT FAULTS AND STEEPLY DIPPING NORMAL FAULTS .....	407
9.2.5.1	Regional distribution and kinematics .....	407
9.2.5.2	Fault kinematics .....	409
9.2.5.3	Timing and kinematic model for late brittle deformation.....	411
9.2.5.4	Metamorphic conditions and crustal depths .....	413
9.2.6	TECTONIC AND METAMORPHIC MODELS OF THE OHFZ: FABRIC EVOLUTION PATHWAYS .....	414
9.2.6.1	Loch Sgibacleit pathway .....	414
9.2.6.2	Scalpay pathway.....	418

9.2.6.3 North Uist pathway .....	423
9.2.6.4 South Uist pathway .....	428
9.2.6.5 Summary and discussion .....	433
9.3 MINERAL REACTIONS, FAULT ROCK GEOCHEMISTRY AND NATURE OF THE FLUID PHASE.....	434
9.3.1 FAULT ROCK MINERALOGY AND METAMORPHIC REACTIONS .....	435
9.3.1.1 Syn-tectonic mineral assemblages.....	435
9.3.1.2 Metamorphic reactions.....	437
9.3.1.3 Summary and discussion .....	438
9.3.2 FAULT ROCK GEOCHEMISTRY.....	440
9.3.2.1 Major elements.....	440
9.3.2.2 Trace elements .....	440
9.3.2.3 Summary .....	442
9.3.3 FLUID SOURCES .....	443
9.4 MECHANISMS OF FLUID FLOW .....	443
9.4.1 UPPER GREENSCHIST FACIES MYLONITES AND PHYLLONITES.....	444
9.4.1.1 Microstructure: evidence for fluid-rock interaction .....	444
9.4.1.2 Fluid transport properties .....	444
9.4.2 CRUSH MELANGE AND PSEUDOTACHYLYTE- ULTRACATACLASITE CRUSH ZONES .....	446
9.4.2.1 Microstructure: evidence for fluid-rock interaction .....	446
9.4.2.2 Fluid transport properties .....	447
9.4.3 LOWER GREENSCHIST FACIES PHYLLONITE .....	449
9.4.3.1 Microstructure: evidence for fluid-rock interaction .....	449
9.4.3.2 Fluid transport properties of protophyllonitic gneiss .....	451
9.4.3.3 Fluid transport properties of phyllonite and ultraphyllonite .....	452
9.4.3.4 Metamorphic effects of high pore fluid pressure during reworking .....	457
9.4.4 SUMMARY .....	458
9.5 REACTIVATION, LOCALISATION AND WEAKENING ALONG THE OHFZ .....	459
9.5.1 REACTIVATION AND LOCALISATION: LOCH SGIBACLEIT.....	459
9.5.1.1 Localisation vs. weakening: clarification .....	459
9.5.1.2 Stress-strain behaviour during reactivation at Loch Sgibacleit.....	461
9.5.1.3 Controls on fault zone reactivation at Loch Sgibacleit.....	462
9.5.2 REACTIVATION AND WEAKENING: PHYLLONITE BELTS .....	462
9.5.2.1 Syn-tectonic weakening mechanisms .....	463
9.5.2.2 Long-term weakening mechanisms .....	467
9.5.2.3 Controls on fault zone reactivation along the OHFZ.....	470
9.5.3 SUMMARY .....	472
9.6 WEAKENING AND RHEOLOGICAL EVOLUTION OF THE OHFZ.....	473
9.6.1 EFFECT OF PHYLLONITISATION ON CRUSTAL STRENGTH .....	473
9.6.1.1 Methods and assumptions .....	473
9.6.1.2 Results and limitations .....	476
9.6.2 RHEOLOGICAL EVOLUTION OF THE OHFZ .....	478
9.6.2.1 Loch Sgibacleit pathway .....	478
9.6.2.2 Scalpay pathway.....	479
9.6.2.3 North and South Uist pathways.....	480
9.6.2.4 Fault zone rheology during the Mesozoic and Cenozoic.....	481
9.6.3 SUMMARY .....	482
9.7 SYNTHESIS .....	483
9.7.1 MECHANICAL SIGNIFICANCE OF BASEMENT FAULT REACTIVATION.....	483
9.7.2 CONTROLS ON PHYLLONITISATION ALONG BASEMENT FAULTS .....	484
9.7.2.1 Permeability pathways .....	485

9.7.2.2 Role of retrograde metamorphic reactions during phyllonitisation.....	486
9.8 CONCLUSIONS.....	493
REFERENCES CITED IN THE TEXT.....	494
APPENDIX A: STRUCTURAL LOGS.....	516
APPENDIX B: GEOCHEMICAL DATA.....	527

# 1. INTRODUCTION

## 1.1 INTRODUCTION AND AIMS

It is widely recognised that major faults and shear zones developed in the continental crust preserve evidence for repeated reactivation, often over long periods of geological time (e.g. Hills 1946; Watterson 1975; White *et al.* 1986; White & Muir 1989; Holdsworth *et al.* 1997). Reactivation is thought to be a consequence of the *persistent mechanical weakness* of continental fault zones (Watterson 1975).

Geophysical observations of neotectonic structures have provided additional insights into the mechanical behaviour of continental faults and shear zones. The lack of a pronounced heat flow anomaly around the San Andreas Fault Zone, California, suggests that the fault sustains much lower shear stresses than are predicted by experimental friction laws, which implies that the fault zone is weak in an *absolute* sense (Lachenbruch & Sass 1980). Furthermore, in-situ stress measurements have demonstrated that the maximum principal horizontal stress ( $S_h \max$ ) is oriented at up to  $90^\circ$  to the trace of the fault zone. This observation suggests that faults within the San Andreas system move under very low shear stresses, and is consistent with the fault zone being weak *relative* to the surrounding country rocks (Zoback *et al.* 1987). The observed weakness of the San Andreas Fault Zone has been attributed either to the presence of unusually low-friction, hydrated clay gouges (Wang 1984), or to the development of highly overpressured segments, localised along major fault strands (Byerlee 1990; Rice 1992). However, there is little direct geological evidence to support these hypotheses (Scholz 1990; Wintsch *et al.* 1995), and the proposed weakening mechanisms cannot account for the long-lived nature many major continental fault zones.

It has been postulated that the weakening mechanisms operative along long-lived, reactivated faults and shear zones must affect a major part of the continental lithosphere, and cannot be restricted to the relatively thin, brittle upper crust (Watterson 1975). The corollary of this argument is that field studies of neotectonic and upper crustal fault zones are unlikely to yield much information on the operative weakening mechanisms. In order to understand the controls on fault reactivation, it is therefore necessary to investigate exhumed, *basement* faults and shear zones, which expose deeper parts of the continental crust. White *et al.* (1986) have pointed out that reactivated basement faults typically display evidence of significant textural and mineralogical alteration, and have suggested that these processes may be fundamental to determining whether or not a fault reactivates. The principal aim of this thesis,

therefore, is to investigate the weakening mechanisms which were operative along a well exposed, reactivated basement fault zone - the Outer Hebrides Fault Zone, Scotland (Sibson 1977a & b; White & Glasser 1987; Walker 1990; Butler 1995; Butler *et al.* 1995).

The rest of this chapter briefly introduces some of the terminology, concepts and methods employed during the remainder of this study.

## **1.2 STRUCTURE OF THE CONTINENTAL LITHOSPHERE**

In order to assess the significance of basement fault zones and fault zone reactivation, it is important to have an understanding of the overall structure and mechanical behaviour of the continental lithosphere. The following section therefore summarises the main lithological and rheological features of the continental lithosphere, and briefly discusses their implications for basement fault reactivation.

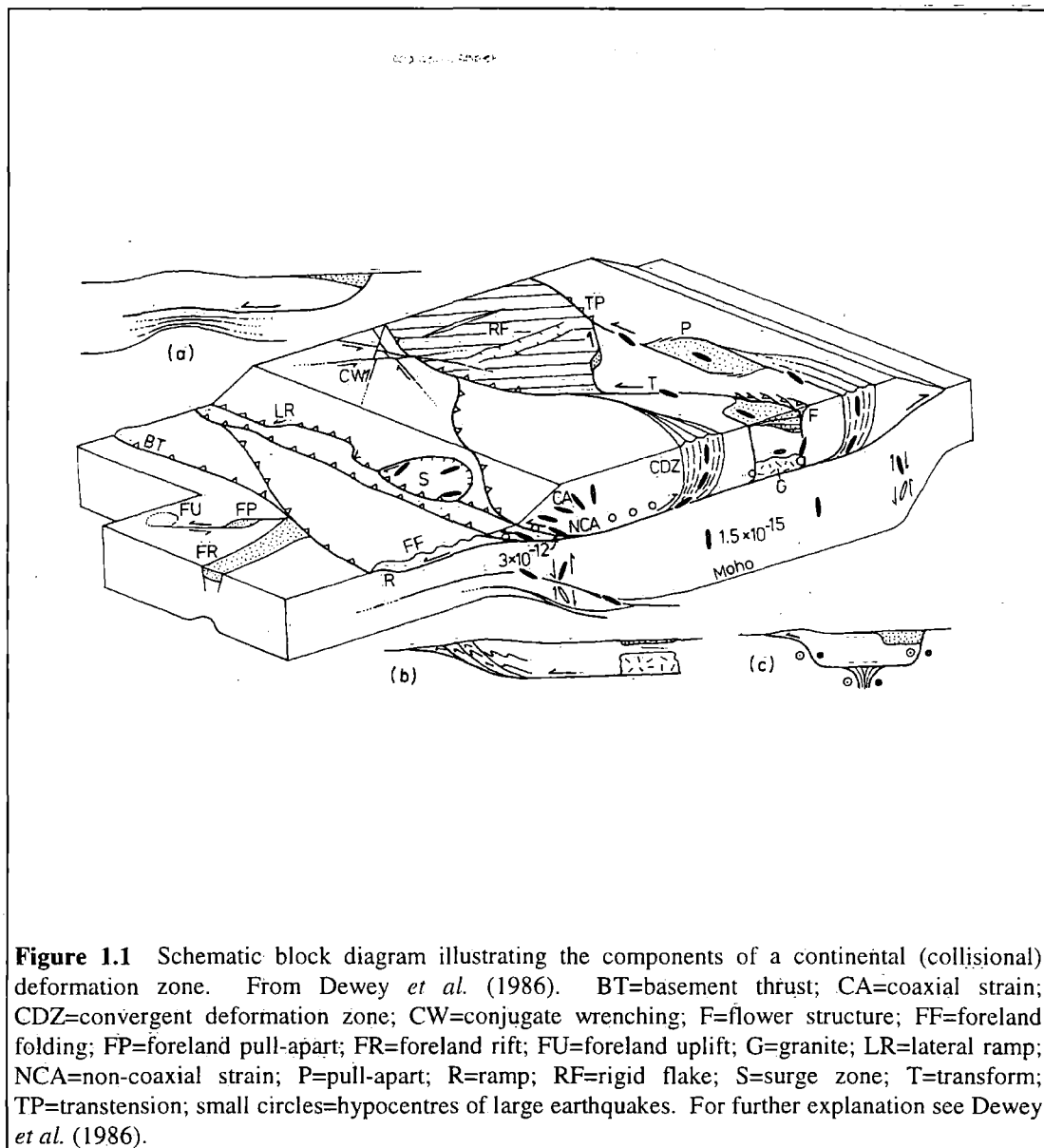
The continental lithosphere is typically between 100km and 150km thick. The uppermost 30km to 40km is composed of predominantly quartzo-feldspathic crust, which overlies the thick, olivine-dominated lithospheric upper mantle. This lithological stratification has important consequences for the mechanical behaviour of the continental lithosphere (Chen & Molnar 1983; Molnar 1988; Molnar 1992).

### **1.2.1 BUOYANCY OF THE CONTINENTAL CRUST**

Quartz and feldspar are significantly less dense than olivine. The resulting buoyancy of the thick, quartzo-feldspathic continental crust effectively prevents continental lithosphere from being subducted into the olivine-rich upper mantle. As a result, continental lithosphere is old (both in absolute terms and relative to oceanic lithosphere), and contains many ancient mechanical anisotropies, such as faults and shear zones. These faults and shear zones break the continental crust into a series of 'blocks' and 'flakes' (Oxburgh 1972; Holdsworth *et al.* 1997), which are able to deform independently of one another. Consequently, crustal deformation patterns are extremely complex, and are characterised by:

- *Strain localisation* along faults and shear zones, with very little deformation within the intervening blocks.
- *Partitioning* of the regional displacement vector into components of dip-slip and / or strike-slip along discrete faults and shear zones, and rotation of fault-bounded blocks and flakes.

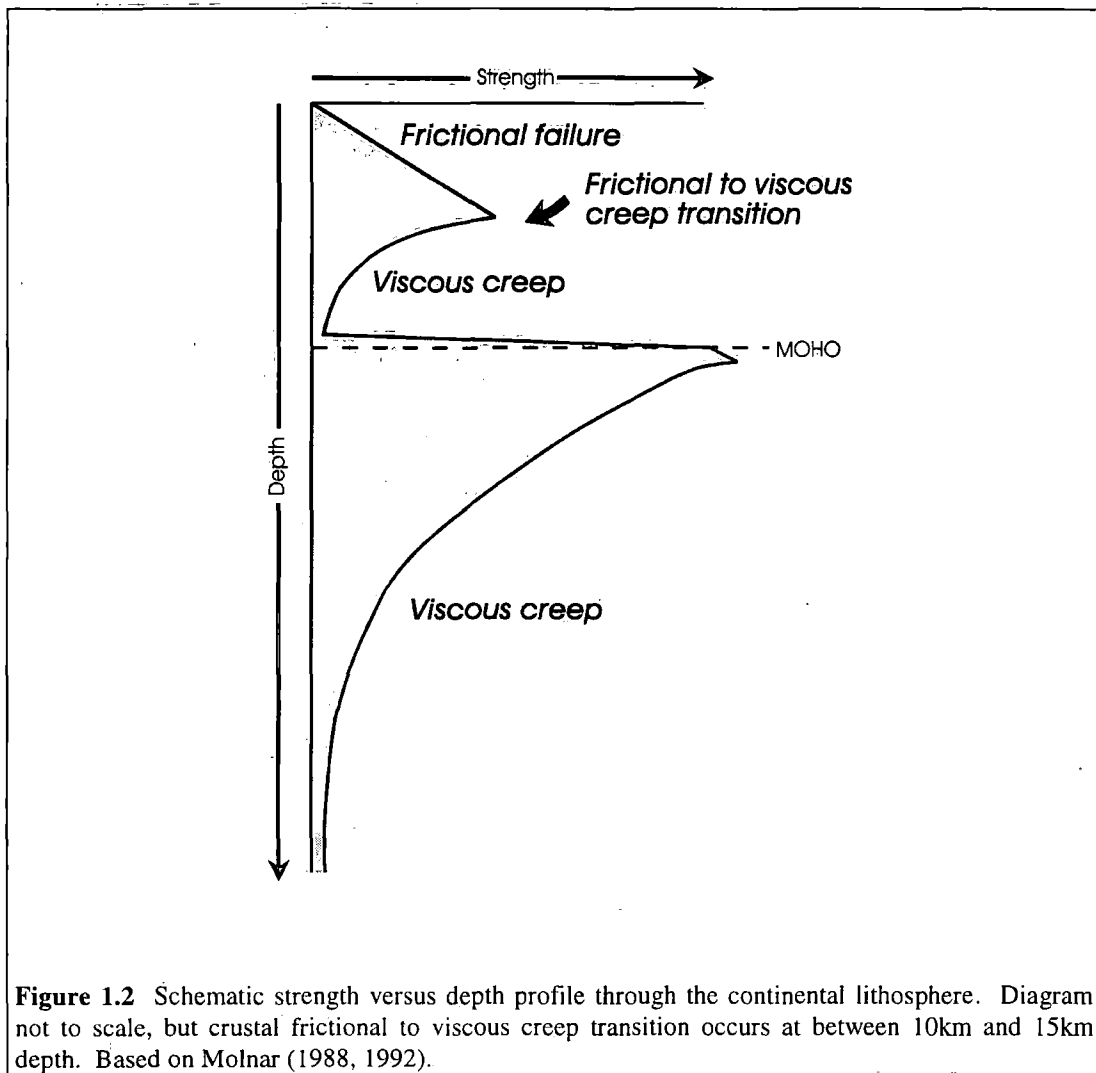
(Dewey *et al.* 1986) (Fig. 1.1)



In order to accommodate such complex strain patterns, reactivation of favourably oriented, pre-existing faults and shear zones is likely to be almost inevitable. In spite of this, not all faults and shear zones display evidence of reactivation (White *et al.* 1986). An important secondary aim of this thesis is therefore to determine why some fault zone segments suffer reactivation, whilst others do not.

## 1.2.2 VERTICAL STRENGTH DISTRIBUTION

The compositional layering imparts a complex vertical strength distribution to the continental lithosphere (Fig. 1.2). Laboratory deformation experiments (e.g. Goetze & Evans 1979), observations of natural seismicity (e.g. Chen & Molnar 1983) and field studies of naturally deformed fault rocks (e.g. Sibson 1982, 1983) suggest that



the uppermost c.10km of the continental crust deforms in a predominantly brittle (frictional) manner. Both the temperature and frictional strength of the crust increase with depth. However, above a critical temperature, it is generally accepted that thermally activated, viscous creep mechanisms become operative and as a consequence, the lower crust deforms in an essentially aseismic, ductile manner (Sibson 1982, 1983). Below the level of the 'frictional to viscous creep transition' (Schmid & Handy 1991) (see section 1.3.3), crustal strength decreases dramatically with increasing temperature (Fig. 1.2).

The base of the continental crust (i.e. the Moho) is marked by an abrupt change from quartz- and feldspar-dominated lithologies to olivine-dominated lithologies. At any given temperature, olivine is significantly stronger than either quartz or feldspar (Evans & Goetze 1979). The upper mantle is therefore strong relative to the lower crust, and is generally accepted to be the strongest region within the continental lithosphere as a whole (Molnar 1988). Below the level of the Moho, the strength of the upper mantle decreases dramatically with increasing temperature (Fig. 1.2).

The 'sawtooth' strength profile of the continental lithosphere has important consequences for understanding the nature and significance of reactivated basement fault zones. The main load-bearing region of the *lithosphere as a whole* occurs in the upper mantle, immediately below the Moho, whilst the main load-bearing region of the *crust* occurs around the frictional to viscous creep transition (Fig. 1.2). Many reactivated basement fault zones preserve fault rocks which appear to have developed around the level of the crustal frictional to viscous creep transition (e.g. White & White 1983; White *et al.* 1986). Deformation processes which are operative around the frictional to viscous creep transition (i.e. the main load-bearing region of the crust) are likely to affect the strength of the crust, but are unlikely to affect the strength of the lithospheric mantle. These observations suggest that basement fault reactivation fundamentally influences deformation *within the crust*. However, these processes may not necessarily have had any direct bearing on the larger-scale, lithospheric deformation patterns (Dewey 1988). The tectonic significance of basement fault reactivation is discussed further in Chapter 9.

### 1.3 DEFORMATION MECHANISMS AND CRUSTAL DEFORMATION

In order to identify the operative fault zone weakening processes, it is of utmost importance to determine the operative deformation mechanisms both prior to, and during reactivation (White *et al.* 1986). The following section, therefore, outlines the principal operative deformation mechanisms that are known to occur within the continental crust, and briefly describes their characteristic (optical) microstructures. Deformation mechanisms fall into two fundamentally different categories.

- Pressure-sensitive *frictional* mechanisms, and
  - Pressure-insensitive, thermally activated *viscous creep* mechanisms.
- (Schmid & Handy 1991)

#### 1.3.1 FRICTIONAL DEFORMATION MECHANISMS

Frictional deformation is pressure sensitive. The frictional strength of rocks increases proportional to the effective normal stress (section 1.5.1.1). Frictional deformation mechanisms are dominant in the uppermost c.10km of the continental crust (Sibson 1982, 1983), and encompass processes such as *fracture, frictional grain boundary sliding, cataclasis* and *frictional melting* (Sibson 1977a; Knipe 1989).

### 1.3.1.1 Fracture mechanisms

Fracture mechanisms involve the nucleation and propagation of, and displacement along, new surfaces (i.e. cracks) during deformation. The exact mechanisms of fracture nucleation and propagation are not of direct relevance to the present work (but see section 1.3.2.2), and the reader is referred to Lloyd & Knipe 1992 (and references therein) for a more detailed review. However, it is important to distinguish between fractures in dry rocks, and fractures which occur in saturated, wet rocks. Both the fracture geometry and mode of fracturing are strongly influenced by the relative magnitudes of (a) the differential stresses, (b) the pore fluid pressure and (c) the tensile strength of the host rock (Phillips 1972; Etheridge 1983; Sibson 1996). In particular, *tensile* fracturing is only possible in highly overpressured, saturated crust at low differential stresses (Table 1.1; Fig. 1.3).

Differential stress ( $\sigma_1 - \sigma_3$ )	Pore fluid pressure (pfp)	$\theta$	Fracture mode
$>8T$	Dry rock <i>or</i> $\sigma_3 > \text{pfp}$	$60^\circ$	Shear fracture in dry rock <i>or</i> shear hydraulic fracture in wet rock
$8T$	$\sigma_3 = \text{pfp}$	$60^\circ$	Shear hydraulic fracture
Between $8T$ and $4T$	$\sigma_3 < \text{pfp}$	between $60^\circ$ and $40^\circ$	Hybrid hydraulic fracture
$\leq 4T$	$\sigma_3 < \text{pfp}$ , where $(\sigma_3 - \text{pfp}) = -T$	$90^\circ$	Tensile hydraulic fracture

**Table 1.1** Table summarising the relationships between differential stress ( $\sigma_1 - \sigma_3$ ), pore fluid pressure, fracture orientation and fracture mode.  $T$  is the tensile strength of the rock;  $\theta$  is the angle between the fracture plane and the minimum principal stress ( $\sigma_3$ );  $\sigma_1$  is the maximum principal stress. Based on Phillips (1972), Etheridge (1983), Sibson (1996) and R. E. Holdsworth (*pers. comm.* 1998). See Figure 1.3.

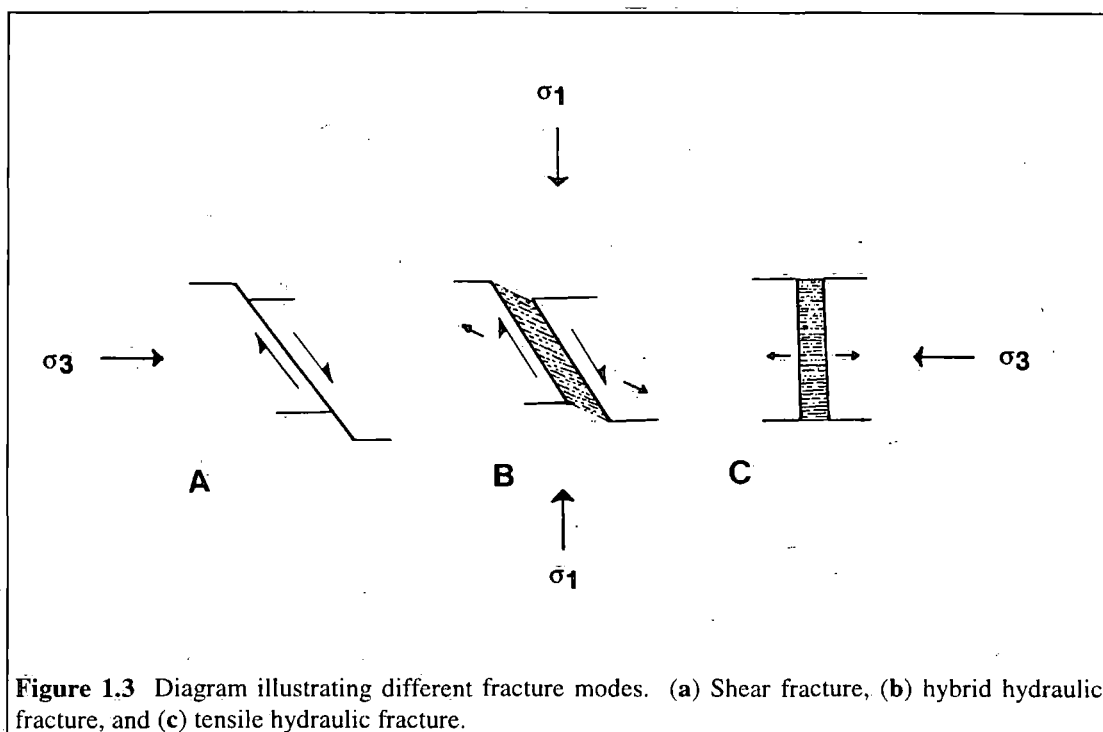


**Figure 1.3** Diagram illustrating different fracture modes. (a) Shear fracture, (b) hybrid hydraulic fracture, and (c) tensile hydraulic fracture.

### 1.3.1.2 Frictional grain boundary sliding

Frictional grain boundary sliding involves individual grains sliding past one another. Sliding occurs when the cohesion and frictional forces between the grains are overcome. In general, the grains do not suffer significant intragranular deformation. Frictional grain boundary sliding is likely to be of particular importance during deformation of partially lithified, fluid-rich sediments (e.g. Maltman 1994), and therefore will not be considered further in this thesis.

### 1.3.1.3 Cataclasis

Cataclasis involves grain-scale fracturing, frictional sliding along fracture surfaces, frictional grain boundary sliding and grain rotation. Cataclasis is favoured by moderate confining pressures and relatively high pore fluid pressures, and is thus likely to be an important deformation mechanism within the uppermost 5km to 10km of the crust (Sibson 1982, 1983; Knipe 1989). Cataclasis involves significant dilatancy (i.e. volume change), which has important implications for the fluid-transport properties of cataclastically deformed rocks (see discussions in Chapter 6, 8 and 9). Rocks deformed by cataclasis are characterised by randomly oriented, angular to rounded clasts which 'float' in a fine grained matrix. There is usually a complete gradation in grain size between the clasts and the matrix (Passchier & Trouw 1996).

#### 1.3.1.4 Frictional melting

Frictional sliding converts elastic strain energy and kinetic energy into heat energy. Thus, at high (seismic) strain rates, frictional sliding may result in localised melting of the wall rocks along fault planes (Sibson 1975). Friction-generated melts freeze rapidly to produce pseudotachylyte. Pseudotachylyte is characterised by randomly oriented, angular to well rounded clasts which float in an glassy, isotropic matrix. Clast size is extremely variable, and if the pseudotachylyte is devitrified, it is extremely difficult to distinguish from cataclasite (see discussion in Chapter 6). In general, frictional melting is promoted by dry, fluid-absent conditions (Sibson 1975, 1977a), although more recent studies suggest that some friction-melts may also be generated in fluid-rich environments (Magloughlin 1992).

It has been postulated that localised melting and pseudotachylyte generation are possible during *viscous* deformation (i.e. melting is not *controlled* by frictional sliding). The consequences of pseudotachylyte generation in the viscous regime are briefly considered in Chapter 5, but the reader is referred to Hobbs *et al.* (1986) and White (1996) for more detailed discussions.

### 1.3.2 VISCOUS DEFORMATION MECHANISMS

Viscous creep is pressure insensitive, and is characterised by linear, exponential or power-law relationships between stress and strain rate (Schmid 1982). Viscous deformation encompasses mechanisms such as *diffusive mass transfer* and *crystal plasticity* (Knipe 1989).

#### 1.3.2.1 Diffusive mass transfer

Diffusive mass transfer (DMT) involves the transport of material away from regions of high intergranular normal stress to regions of relatively low intergranular normal stress (Rutter 1983; Knipe 1989) (Fig. 1.4). Material may either be transported through the crystal lattice (Nabarro-Herring creep) or along grain boundaries. Solid-state diffusion along grain boundaries is known as Coble creep. If a fluid phase is involved in the transport of material, the process is referred to as fluid-assisted diffusive mass transfer. Diffusive mass transfer is driven by 'chemical potential gradients' within the deforming rock mass. These chemical gradients may be induced by stress variations (Wheeler 1987), fluid pressure gradients (McCaig & Knipe 1990), variations in the composition of the fluid phase and / or by variations in the internal strain energy of grains (Wintsch 1985). DMT processes are promoted by high temperatures (which lead to increased rates of solid-state diffusion during Nabarro-Herring and Coble creep), fine grain sizes (which lead to increased grain boundary

surface areas and decreased diffusion path lengths in comparison with relatively coarse grained rocks) and / or by the presence of a chemically active fluid phase (dissolved chemicals are easily transported within a fluid). The following discussion focuses on *fluid-assisted DMT* processes (McCaig 1987; McCaig & Knipe 1990), which are likely to be particularly important during fault or shear zone-related metamorphism (e.g. Beach 1980, 1982).

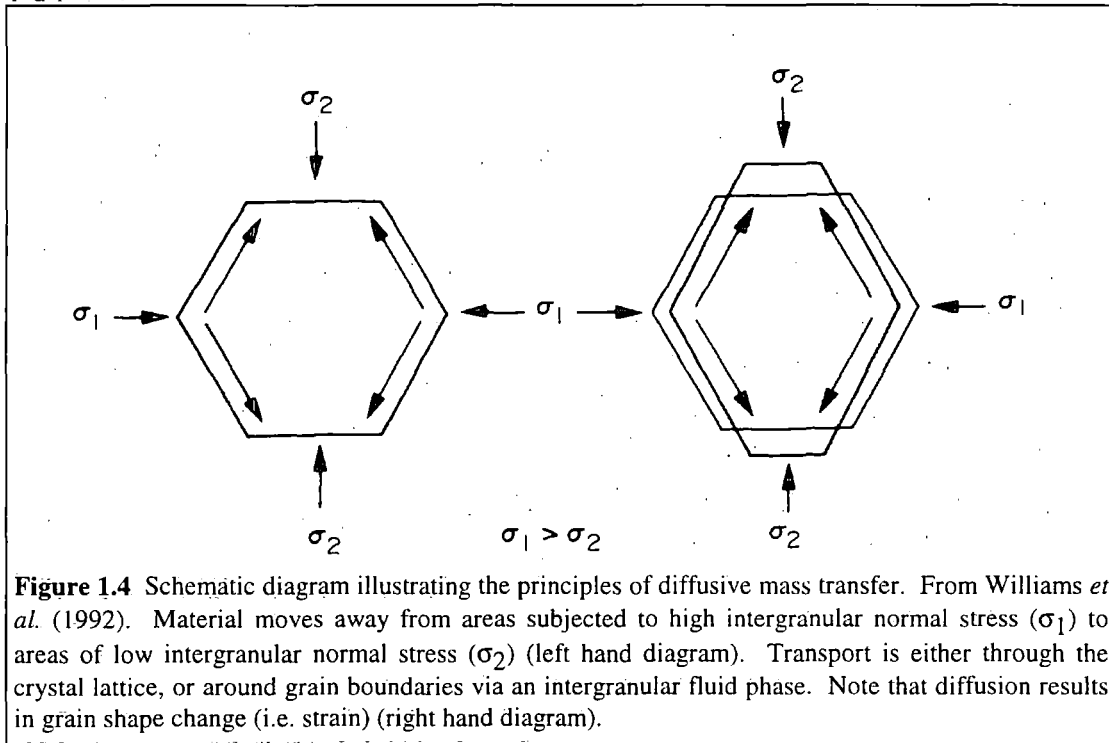


**Figure 1.4** Schematic diagram illustrating the principles of diffusive mass transfer. From Williams *et al.* (1992). Material moves away from areas subjected to high intergranular normal stress ( $\sigma_1$ ) to areas of low intergranular normal stress ( $\sigma_2$ ) (left hand diagram). Transport is either through the crystal lattice, or around grain boundaries via an intergranular fluid phase. Note that diffusion results in grain shape change (i.e. strain) (right hand diagram).

Fluid-assisted diffusive mass transfer can be considered a three-stage process (Knipe 1989). *Source mechanisms* control how material enters the diffusion pathway. Pressure solution processes, which involve chemical dissolution of material (Houseknecht 1988), are probably the most important group of source mechanisms during fluid-assisted DMT. Characteristic microstructures include stylolites (particularly in carbonate-rich rocks), truncated grains, dissolution seams (Hippertt 1994a) and crenulation cleavages (Knipe 1989). *Diffusion mechanisms* control how material is transported from the source region to the sink region. During fluid-assisted DMT, material is transported either in thin fluid films along grain boundaries (Rutter 1983), or in a bulk fluid which may be flowing through the rock (McCaig & Knipe 1987). Characteristic microstructures include voids and fluid inclusions preserved along grain boundaries (Hippertt 1994b), the localised growth of retrograde minerals (McCaig 1987) and mineralised fractures (i.e. veins) (Walther 1990). Mechanisms of fluid transport during fluid-assisted DMT are described in more detail in section 1.4. *Sink processes* control how material is deposited in sites of crystal growth. If the minerals deposited in the sinks differ in composition from the minerals removed from

the source regions, the process is referred to as 'incongruent pressure solution'. Incongruent pressure solution is an important metamorphic process (Beach 1979). In general, sinks are sites of localised dilatation and typically comprise mineralised intra-, inter- and transgranular fractures (i.e. veins), and strain shadows along the margins of rigid porphyroclasts. Note that veins provide evidence for both diffusion pathways and sink processes. Large (i.e. thin section- to outcrop-scale) transgranular veins may have transported large volumes of fluid over relatively long distances, whilst small (i.e. grain-scale), isolated intragranular veins are more likely to have been of localised importance as diffusion pathways (e.g. Walther 1990).

### **1.3.2.2 Crystal plasticity**

Crystal plasticity involves strain accommodation by intracrystalline deformation. Intracrystalline deformation is controlled by mechanical twinning and, more generally, by the movement of planar defects (dislocations) through the crystal lattice (Fig. 1.5) (Knappe 1989). In general, crystal plasticity is enhanced by trace amounts of fluids within the deforming rock mass. This 'hydrolytic weakening' effect (Tullis & Yund 1980) is discussed further in section 1.5.

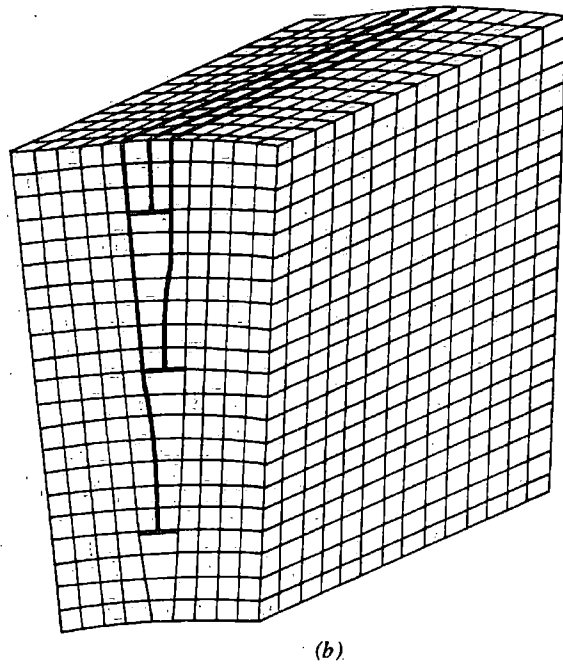
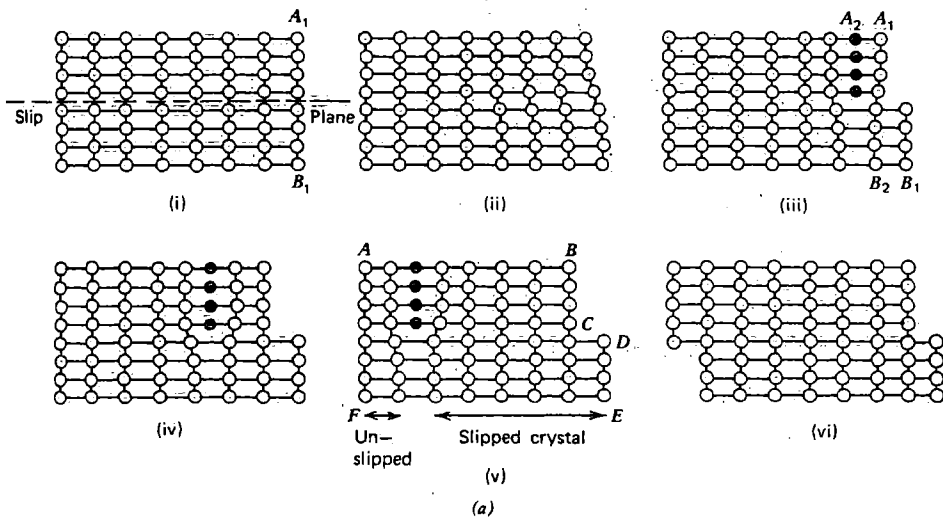


**Figure 1.5** Schematic diagram illustrating (a) dislocation glide (intracrystalline slip), and (b) angular offset of the crystal lattice across a tilt wall. If the offset is less than  $c.10^\circ$ , the tilt wall is a subgrain boundary, if the offset is greater than  $c.10^\circ$ , the tilt wall is a grain boundary. From Hobbs *et al.* (1976) and Williams *et al.* (1994).

At relatively low temperatures ( $< 0.5$  melting temperature), crystal plastic deformation is dominated by *dislocation glide* (low temperature plasticity) (Knipe 1989). However, at such temperatures, the dislocations are likely become tangled, and hence their mobility is restricted. Consequently, it becomes increasingly difficult for the dislocations to move through the crystal lattice and work hardening ensues. Low temperature plasticity and work hardening are commonly observed to be the precursors to brittle fracture and frictional sliding (Lloyd & Knipe 1992). Patchy

undulose extinction and the development of crystallographic fabrics are characteristic of dislocation glide.

At higher homologous temperatures (temperature > 0.5 melting temperature) and / or slower strain rates, the mobility of dislocations increases significantly and work hardening is counteracted by *recovery processes* (Knipe 1989). During recovery, the dislocations become re-organised into ordered configurations which lower the overall strain energy of the crystal. Recovery processes produce microstructures such as sweeping (i.e. smooth) undulose extinction, deformation bands and subgrains (Passchier & Trouw 1996). Subgrains develop as dislocations become arranged into planar boundaries, which produce small, angular offsets in the crystal lattice (Fig. 1.5b). In addition to recovery, *dynamic recrystallisation* processes contribute towards a reduction in the dislocation density / strain energy of the crystal during deformation. Recrystallisation involves the development of new, relatively strain-free grains at the expense of the older, highly strained, work-hardened grains. Two distinct dynamic recrystallisation mechanisms have been recognised (Drury and Urai 1990). *Subgrain rotation recrystallisation* is controlled by the addition of dislocations to subgrain boundaries. As more dislocations are added to the subgrain walls, the angular offset of the crystal lattice becomes progressively larger. At offsets of greater than c.10°, the subgrain is transformed into a newly recrystallised grain. Subgrain rotation recrystallisation produces distinctive 'core-and-mantle' microstructures (e.g. White 1976). These microstructures are characterised by relatively coarse, undulose porphyroclasts, which are surrounded by aggregates of fine subgrains and dynamically recrystallised grains. There is a progressive increase in the proportion of dynamically recrystallised grains away from the centre of the porphyroclast (Passchier & Trouw 1996). *Grain boundary migration recrystallisation* occurs where neighbouring crystals have significantly different dislocation densities. The grain boundaries 'sweep through' the highly deformed grains (i.e. those with high dislocation densities), leaving behind newly recrystallised grains with very low dislocation densities (Drury & Urai 1990). Grain boundary migration recrystallisation produces aggregates of interlobate grains, which are characterised by highly irregular (i.e. lobate) grain boundaries.

### **1.3.3 THE FRICTIONAL TO VISCOUS CREEP TRANSITION**

Fault rocks preserved along reactivated basement faults and shear zones typically display evidence for the operation of both frictional and viscous deformation mechanisms. These observations suggest that reactivation occurred around the level of the so-called 'frictional to viscous creep transition' (White & White 1983; White *et*

*al.* 1986) (section 1.2.2). It is therefore of utmost importance (a) to define exactly what is meant by the frictional to viscous creep transition, (b) to outline its principal rheological characteristics and (c) to recognise the frictional to viscous creep transition in naturally deformed faults and shear zones.

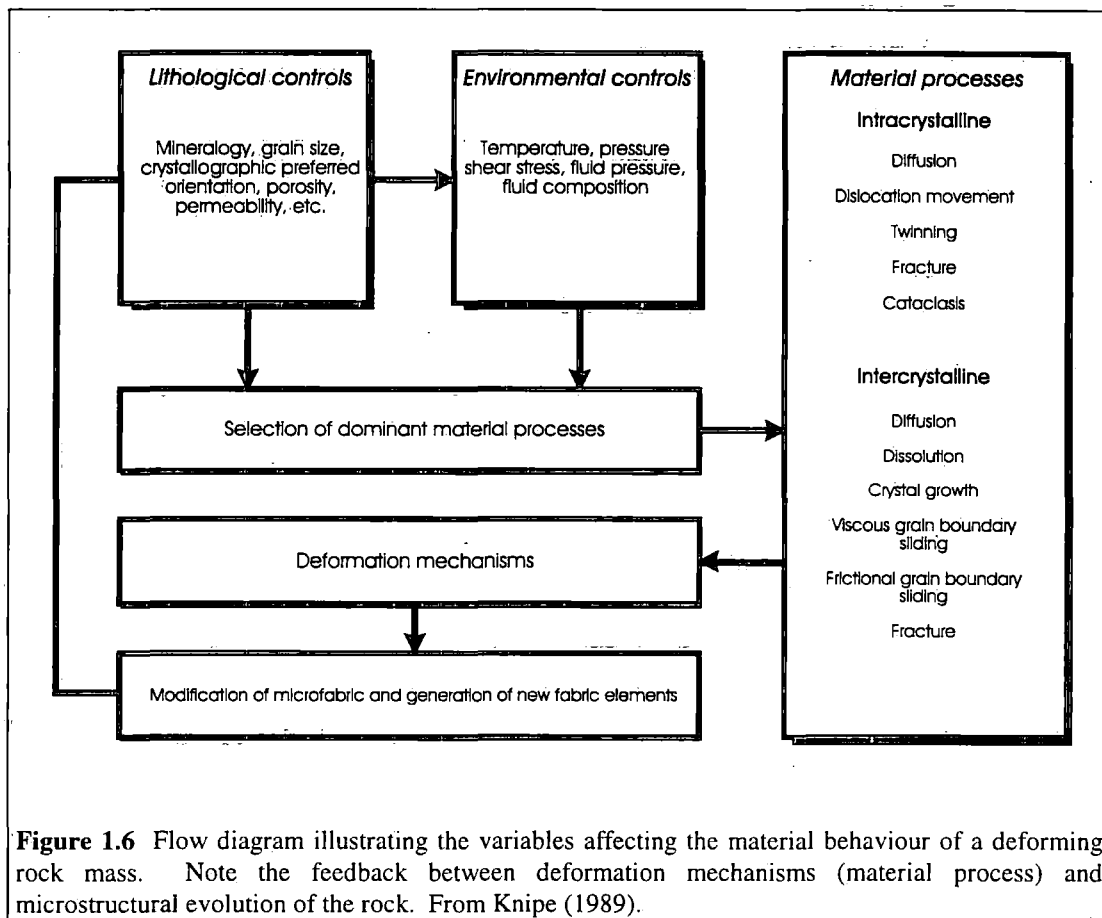
### **1.3.3.1 Definition and terminology**

The frictional to viscous transition separates the brittle, seismogenic upper crust, which deforms predominantly by fracturing, frictional sliding and cataclasis, from the essentially aseismic lower crust, which deforms predominantly by viscous creep mechanisms (Schmid & Handy 1991). This change in dominant operative deformation mechanism reflects the progressively increasing temperatures and pressures at depth within the continental crust. At relatively low temperatures and pressures (i.e. in the upper crust), the rocks are able to deform by pressure-sensitive, frictional mechanisms. However, at greater depths the increased pressure inhibits frictional sliding, whilst the increased temperature promotes the onset of thermally-activated viscous creep mechanisms.

Previous authors have used the term 'brittle-ductile transition' to describe this region of the crust (e.g. Miller *et al.* 1983). However, Rutter (1986) has pointed out that 'brittle' is a mechanistic term, which describes the processes by which a rock deforms, whilst 'ductility' is a phenomenological concept, which describes the capacity of a rock to deform in a uniform manner, by whatever mechanism. It follows that the term 'brittle-ductile' cannot adequately describe the deformation processes occurring in the region between the brittle upper crust and the viscously deforming lower crust. The use of 'brittle-ductile transition' has therefore been avoided during the present study.

### **1.3.3.2 Rheological properties of the frictional to viscous creep transition**

The mechanical behaviour of the frictional to viscous creep transition is likely to be extremely complex (Schmid & Handy 1991). This complexity arises because different minerals have different activation energies with respect to a particular viscous deformation mechanisms (Handy 1989). At any given temperature, minerals with low activation energies ('weak' minerals) will readily deform by viscous creep, whilst minerals with relatively high activation energies ('strong' minerals) will behave in a rigid manner. At low strains, the frictional to viscous creep transition will therefore occur over a broad depth range within the polymineralic (e.g. quartzofeldspathic) continental crust (Schmid & Handy 1991).



During progressive deformation, the position of the frictional to viscous creep transition is unlikely to remain static owing to complex interactions between the evolving fault rock microstructures, mineralogy and dominant operative deformation mechanisms (Knipe 1989) (Fig. 1.6). In rocks which contain or develop greater than 20% by volume 'weak' minerals, there is likely to be a strain-dependant switch from predominantly frictional to predominantly viscous deformation as the fault rock evolves from a 'load bearing framework' to an 'interconnected weak layer' microstructure and rheology (Handy 1990) (Fig. 1.12) (see section 1.5 for more detailed explanation). The corollary of this argument is the frictional to viscous creep transition will occur over a relatively *narrow* depth range in rocks which have accumulated high strains (Schmid & Handy 1991). In contrast, coarse grained rocks which contain less than 20% by volume 'weak' minerals are likely to deform by cataclasis and frictional sliding. However, cataclasis results in extreme, localised grain size reduction. If fine grained cataclasite constitutes greater than or equal to 20% of the rock volume, an interconnected weak layer microstructure may develop and localised grain size reduction may be sufficient to trigger the onset of grain size sensitive, diffusive mass transfer mechanisms (section 1.3.2.1) (e.g. Stewart *et al.* 1997). The corollary of this argument is that the frictional to viscous creep transition may *change* depth (in general, become shallower) with increasing strain. Syn-tectonic

metamorphism and the growth of new mineral phases will also alter the mechanical properties of the frictional to viscous creep transition (Handy 1989; Imber *et al.* 1997). The mineralogical and mechanical effects of metamorphism will be introduced in sections 1.4 and 1.5.

### **1.3.3.3 Fault rocks and recognition of the frictional to viscous creep transition**

The frictional to viscous creep transition is defined by changes in the operative deformation mechanisms. Each deformation mechanism is associated with a number of characteristic microstructures (section 1.2). Microstructural analysis of naturally deformed fault rocks will therefore provide an indication of whether the rock was deformed in the frictional regime, in the viscous regime, or in the frictional to viscous creep transition (Schmid & Handy 1991). Unfortunately, it is often impossible to identify the operative deformation mechanisms in the field. As a result, a purely *descriptive* fault rock classification scheme has been adopted (Sibson 1977a). It is important to emphasise that the fault rock names (e.g. 'cataclasite' and 'mylonite') are based solely on the textures observed in the field and therefore do *not* have any mechanistic connotations (Fig. 1.7).

	<i>Random fabric</i>	<i>Foliated</i>
<b>Incohesive</b>	<i>Fault breccia</i> Visible fragments > 30% rock mass	?
	<i>Fault gouge</i> Visible fragments < 30% rock mass	?
<b>Cohesive</b>	<i>Pseudotachylite</i>	?
	<i>Crush Breccia</i> <i>Fine crush breccia</i> <i>Crush microbreccia</i>	fragments > 0.5cm 0.1cm < fragments < 0.5cm fragments < 0.1cm
	<i>Protocataclasite</i> 10% to 50% matrix	<i>Protomylonite/protophyllonite</i> 10% to 50% matrix
	<i>Cataclasite</i> 50% to 90% matrix	<i>Mylonite/phyllonite</i> 50% to 90% matrix
	<i>Ultracataclasite</i> 90% to 100% matrix	<i>Ultramylonite/ultraphyllonite</i> 90% to 100% matrix
	?	<i>Blastomylonite</i>

Phyllonite is phyllosilicate-rich mylonite.  
 Blastomylonite is coarse grained mylonite which  
 has experienced significant static recrystallisation  
 (see Chapter 5).

**Figure 1.7** Descriptive fault rock classification scheme, based on textures observed in the field.  
 From Sibson (1977a).

## **1.4 RETROGRADE METAMORPHISM AND METAMORPHIC FLUID TRANSPORT IN FAULTS AND SHEAR ZONES**

Basement faults and shear zones are commonly observed to have suffered intense, localised retrograde (e.g. Beach 1980), or prograde (e.g. Holdsworth 1994) metamorphism. Furthermore, it has been suggested that fault-related metamorphism is a characteristic feature of reactivated fault zones (White *et al.* 1986) (section 1.1). In most high-grade basement rocks, the fault-related metamorphism is retrogressive as it occurs at mid- to upper crustal depths in the presence of fluids. Therefore, the following sections outline (a) the main controls on retrogressive metamorphism in faults and shear zones and (b) mechanisms of fluid transport during (retrogressive) metamorphism in faults and shear zones.

### **1.4.1 RETROGRADE METAMORPHISM IN FAULTS AND SHEAR ZONES**

Retrogressive metamorphism occurs when rocks which formed under conditions of high temperature and / or high pressure, are reworked in regions of relatively low temperature and / or low pressure. In general, retrogressive metamorphism involves the breakdown of high grade, *anhydrous* minerals (e.g. pyroxenes) to produce an assemblage of low grade, *hydrous* minerals (e.g. phyllosilicates). Retrograde metamorphic reactions can therefore be favoured by the presence of a fluid phase (Miyashiro 1994). Other important processes during retrogression include (a) cation exchange reactions, which cause pairs of minerals to change their compositions according to the prevailing pressure and temperature conditions (see Yardley 1989 and references therein), and (b) the breakdown of Ca-rich plagioclase (in high grade rocks) to albite (in low grade rocks) (Miyashiro 1994).

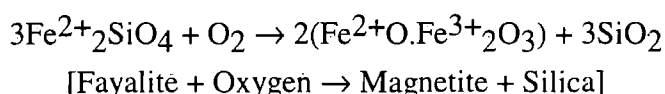
#### **1.4.1.1 Chemical potential of H<sub>2</sub>O, CO<sub>2</sub> and O<sub>2</sub>**

In general, metamorphic fluids are rich in H<sub>2</sub>O and / or CO<sub>2</sub>, with smaller amounts of CH<sub>4</sub>, N<sub>2</sub> and H<sub>2</sub> (Yardley 1989). The nature and extent of the retrograde mineral reactions will therefore depend on the chemical potential of both H<sub>2</sub>O and CO<sub>2</sub>. If H<sub>2</sub>O is present in relatively low abundance (i.e. if H<sub>2</sub>O has a relatively low chemical potential), the retrograde reactions are unlikely to go to completion. Such partially retrogressed rocks typically comprise an assemblage of metastable, 'high grade' minerals, co-existing with newly formed, hydrous, 'low grade' minerals. If H<sub>2</sub>O is readily available (i.e. if H<sub>2</sub>O has a relatively high chemical potential), the kinetics of fluid-solid metamorphism are such that the retrograde reactions are likely to be rapid (relative to solid-solid reactions) (Yardley 1989), and may go to completion. In

completely retrogressed rocks, the original high grade minerals will be completely replaced by an assemblage of hydrous, low grade minerals.

The chemical potential of CO<sub>2</sub> has a dramatic effect on retrograde mineral assemblages. In calcium-rich rocks such as metabasites, Ca-bearing silicates (e.g. actinolite, epidote and sphene) will only develop if the chemical potential of H<sub>2</sub>O is significantly *higher* than the chemical potential of CO<sub>2</sub>. Conversely, if the chemical potential of CO<sub>2</sub> is significantly higher than that of H<sub>2</sub>O, Ca-bearing silicates will break down to produce carbonates such as calcite, dolomite and ankerite (Graham *et al.* 1983; Miyashiro 1994). Thus, for the same temperature and pressure conditions, entirely different mineral assemblages may be observed depending on the nature of the fluid phase.

During retrograde metamorphism, H<sub>2</sub>O-rich fluids are likely to influence the chemical potential of O<sub>2</sub>. Fluid-rock interactions will therefore affect the oxidation state of elements such as iron, europium and uranium. The stabilities of iron-bearing silicate (e.g. hornblende, biotite and hornblende) and opaque (e.g. magnetite) minerals are particularly sensitive to the oxidation conditions during metamorphisms (Beach 1980; Yardley 1989). Under oxidising conditions, ferrous (Fe<sup>2+</sup>) minerals may break down to ferric (Fe<sup>3+</sup>) minerals, e.g.



(Gill 1989)

#### 1.4.1.2 Effect of element mobility on retrograde mineral assemblages

Retrogressive metamorphism within basement faults and shear zones is typically very intense (Oliver 1996 and references therein). This observation suggests that during retrogression, both the abundance and chemical potential of H<sub>2</sub>O are likely to have been extremely high. It has been pointed out that at high fluid-rock ratios, elements which are normally considered to be 'immobile' (i.e. those elements which are not generally redistributed during metamorphism), may display increasingly mobile behaviour (e.g. O'Hara 1990; Condie & Sinha 1996). Such 'open system' behaviour may lead to significant losses or gains in chemical components during hydrothermal metamorphism. It has been argued that the number of mineral species developed within hydrothermally altered rocks is directly related to element immobility. This relationship is expressed by Korzhinsky's phase rule:

$$P_s = C_i$$

(Korzhinsky 1959)

where  $P_S$  is the number of solid phases (i.e. mineral species) and  $C_i$  is the number of immobile components. It follows that rocks which have experienced intense retrogression and have behaved in an 'open' manner will be characterised by very restricted mineral assemblages. Furthermore, the chemical composition of *individual* minerals is likely to have been strongly influenced by the chemical composition of the fluid phase. Thus, the composition of individual minerals may *not* simply reflect the ambient pressure and temperature conditions during retrogression, as is commonly assumed (Yardley 1989).

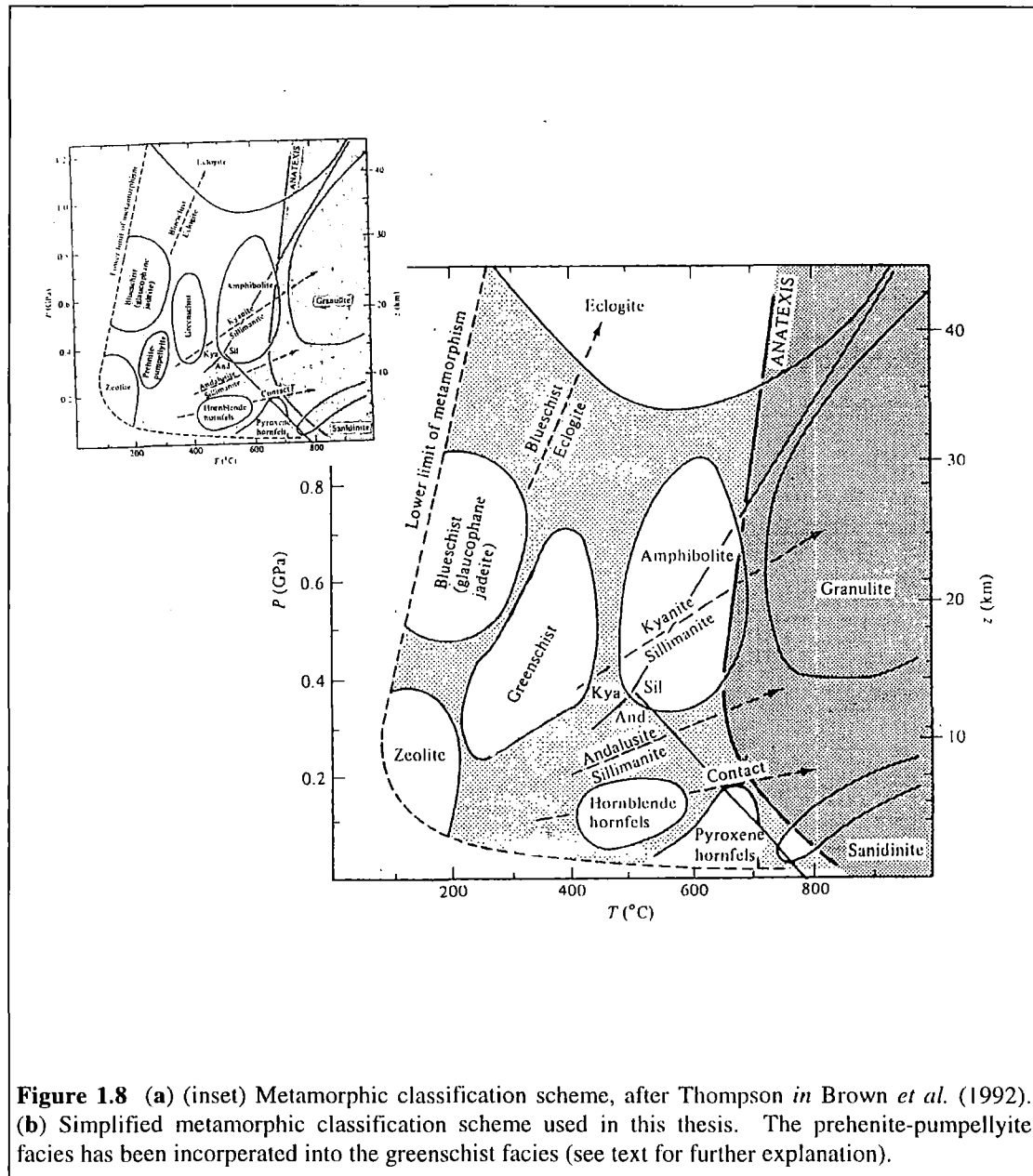


**Figure 1.8** (a) (inset) Metamorphic classification scheme, after Thompson in Brown *et al.* (1992). (b) Simplified metamorphic classification scheme used in this thesis. The prehnite-pumpellyite facies has been incorporated into the greenschist facies (see text for further explanation).

### **1.4.1.3 Timing of retrogression relative to deformation**

The timing of retrogression relative to deformation can be determined from detailed microstructural and microchemical observations (McCaig & Knipe 1990). If undeformed retrograde minerals are preserved outside the fault / shear zones, whilst deformed retrograde minerals are preserved within the fault / shear zone, it is likely that retrogression either pre-dates, or was synchronous with deformation. The most reliable evidence for syn-tectonic retrogression is the presence of strain shadows and fibrous overgrowths, which are oriented parallel to either the macroscopic foliation or mineral lineation. Such microstructures are consistent with the operation of incongruent pressure solution mechanisms (i.e. fluid-assisted diffusive mass transfer) (Beach 1979) (see section 1.3.2.1). If retrogression within the fault / shear zone entirely post-dates deformation, the retrograde minerals will be strain-free.

### **1.4.1.4 Metamorphic facies classification scheme**

Once the stable, syn-tectonic mineral assemblage has been identified, it is possible to assign each fault rock to a particular metamorphic facies. The metamorphic classification scheme used throughout this thesis is similar to that presented by Thompson (in Brown *et al.* 1992) (Fig. 1.8a). However, owing to (a) the relatively restricted chemistry of high grade quartzo-feldspathic basement complexes (in comparison with the chemical variations observed in low grade metasedimentary and metavolcanic assemblages), and to (b) enhanced element mobility during retrogressive (hydrothermal) metamorphism (section 1.4.1.2), it is likely that metamorphic mineral assemblages preserved in fault rocks derived from such complexes will also be relatively restricted. In particular, minerals characteristic of the prehnite-pumpellyite facies tend to develop only in metavolcanics or metagreywackes (Miyashiro 1994). The classification scheme used in this thesis has therefore been modified, so that the *prehnite-pumpellyite facies is included within the greenschist facies* (Fig. 1.8b).

## **1.4.2 METAMORPHIC FLUID TRANSPORT WITHIN FAULTS AND SHEAR ZONES**

Retrogressive metamorphism clearly requires an adequate supply of H<sub>2</sub>O-rich fluids. Numerous mechanisms have been proposed to explain metamorphic fluid ingress and transport in actively deforming faults and shear zones. These mechanisms are briefly reviewed in the following sections.

### 1.4.2.1 Fluid transport in upper crustal fault zones

Three principal mechanisms have been proposed to explain fluid flow through brittle, upper crustal fault zones.

#### *Fluid transport through fracture networks*

Metamorphic fluid flow in the brittle, upper crust is widely believed to be driven by convection (Taylor 1971; Fleck & Criss 1985). Convection cells develop in response to the density contrast between relatively cold, down-welling fluids and relatively hot, up-welling fluids. The viability of convection as a driving mechanism for fluid flow depends (a) on a steep thermal gradient and (b) on an interconnected porosity network (Oliver 1996). Detailed oxygen and strontium isotope studies of Hercynian metasediments led Bickle and Chapman (1990) to conclude that convection-driven flow of meteoric waters in the upper crust took place within a network of interconnected, brittle fractures.

#### *Seismic pumping*

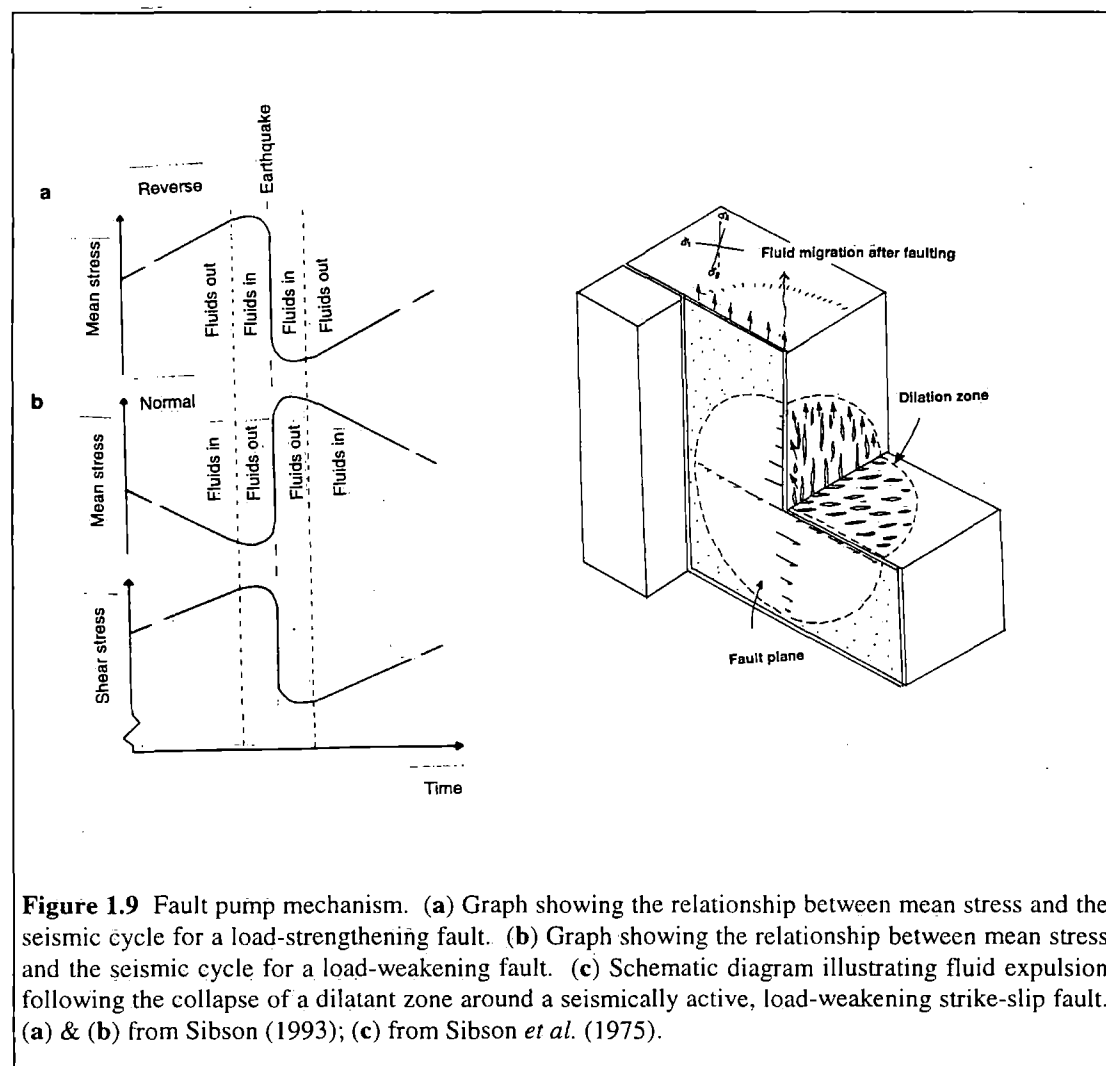


**Figure 1.9** Fault pump mechanism. (a) Graph showing the relationship between mean stress and the seismic cycle for a load-strengthening fault. (b) Graph showing the relationship between mean stress and the seismic cycle for a load-weakening fault. (c) Schematic diagram illustrating fluid expulsion following the collapse of a dilatant zone around a seismically active, load-weakening strike-slip fault. (a) & (b) from Sibson (1993); (c) from Sibson *et al.* (1975).

It has been postulated that transient fluid flow within the upper crust is driven by seismic faulting (Sibson *et al.* 1975). Faulting is characterised by relatively long periods of inactivity, punctuated by seismic events which are associated with rapid changes in both the mean stress and shear stress. A *decrease* in mean stress will tend to increase dilatancy, and will therefore draw fluids towards the fault plane. In contrast, an *increase* in mean stress will suppress dilatancy, and will therefore drive fluids away from the fault plane (Sibson 1993). The behaviour of mean stress during the seismic cycle is controlled by the kinematics of the fault zone. Compressional and transpressional faults are characterised by *load-strengthening* behaviour, whilst extensional and transtensional faults are characterised by *load-weakening* behaviour. Strike-slip faults can display either load-strengthening or load-weakening behaviour. During the interseismic period, the mean stresses around load-strengthening faults will gradually increase, thus driving fluids away from the fault zone. At failure (i.e. during the coseismic period), the mean stresses rapidly decrease, drawing fluids into the fault zone (Fig. 1.9a). In contrast, the mean stresses around load-weakening faults will gradually decrease during the interseismic period, thus fluids are drawn into the fault zone. At failure, the mean stresses rapidly increase, expelling fluids from the fault zone (Fig. 1.9b) (Sibson 1993).

The behaviour of a typical load-weakening, strike-slip fault is illustrated in Figure 1.9c. During the interseismic period, shear stresses increase, whilst the mean stresses decrease. Tensile fractures are induced in the region around the locked fault. The tensile fractures increase the dilatancy are thought to draw fluids into the region around the fault. At failure, the mean stresses rise and the network of tensile fractures collapses. The collapse of the dilatant zone is believed to rapidly expel fluids along the rupture plane, towards the surface (Sibson *et al.* 1975) (Fig. 1.9c).

### ***Fault valve behaviour***

In the fault valve model, faulting is driven by cyclic changes in fluid pressure during the seismic cycle (Sibson 1990). Fault valve behaviour is promoted by constant fluid input to the system, and by the presence of a regional permeability barrier, which help to maintain high pore fluid pressures within the fault zone. Each 'cycle' of faulting and fluid flow consists of five distinct phases (Fig. 1.10):

- Fluid input causes fluid pressures to rise along the sealed fault zone.
- The fluid pressure locally exceeds lithostatic pressure and is partially relieved by *tensile* fracturing within the fault zone.
- *Shear* hydraulic fracture occurs along the main fault zone.

- Rapid fluid discharge occurs along the shear fractures within the main fault zone.
- The fluid pressure drops, promoting mineralisation along the fracture surfaces.
- The fault zone re-seals and the cycle begins again.

Fault valve behaviour can be recognised in the field by the mutual cross-cutting relationships between multiple generations of tensile veins and shear hydraulic fractures (fault veins) within major fault zones. The fault veins, which are oriented parallel to the fault zone, are likely to be of significant lateral extent (up to the kilometre-scale). The tensile veins are between one and two orders of magnitude smaller (Sibson 1990).

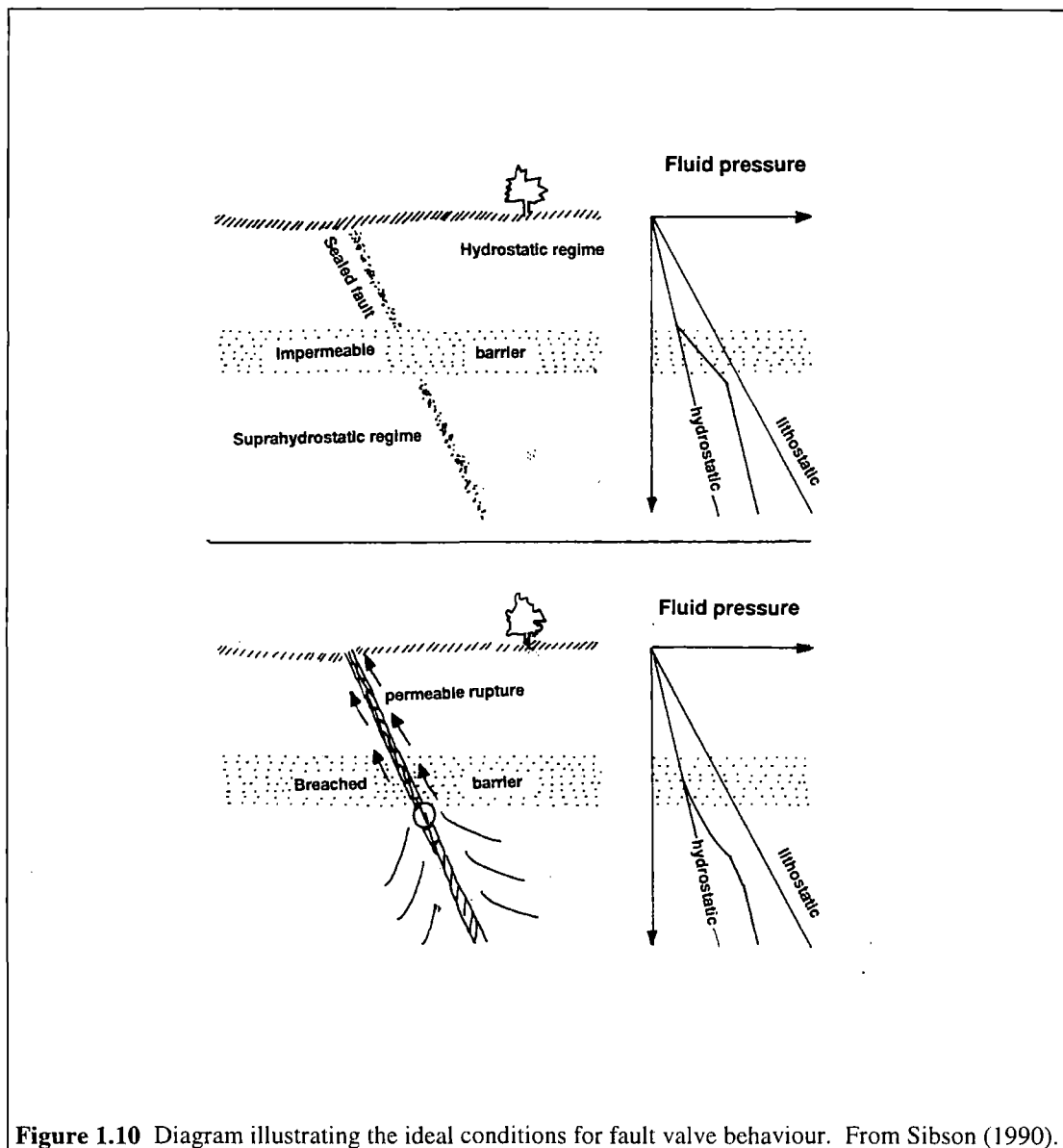


**Figure 1.10** Diagram illustrating the ideal conditions for fault valve behaviour. From Sibson (1990).

### 1.4.2.2 Fluid transport in mid- to lower crustal fault zones

Fluid flow within the mid- to lower crust is likely to be focused into actively deforming faults and shear zones. Such channelised fluid flow is promoted by strong rheological and permeability contrasts between the wall rocks and the fault rocks, and is likely to be particularly important at high magnitudes of finite strain (Oliver 1996). Three distinct groups of fluid transport mechanisms have been proposed to explain fluid transport in the mid- to lower crust.

#### *Hydraulic fracturing and dilatancy pumping*

Dilatancy pumping is thought to be the most important mechanism of fluid transport in the mid crust (Etheridge *et al.* 1983). Dilatancy pumping is driven by changes in fluid pressure, which cause hydraulic fracturing. Fluid pressures must therefore be high (fluid pressure  $\cong \sigma_3$ ) in order for dilatancy pumping to be an effective fluid-transport mechanism. In contrast to the fault valve model proposed by Sibson (1990) (section 1.4.2.1), dilatancy pumping is not necessarily linked to the seismic cycle. During macroscopically ductile deformation, cyclic variations in the pore fluid pressure may result in hydraulic fracturing. Movement along irregular fracture surfaces is likely to create voids (i.e. dilatancy), and the resulting change in hydraulic head will promote fluid movement. Fluid flow depends on the fractures being interconnected, either by other fractures or by pre-existing permeability pathways, such as bedding or foliation planes ('fracture-meshes' of Sibson 1996). The direction of fluid flow is likely to be controlled by the orientation of the permeability pathways (Sibson 1996).

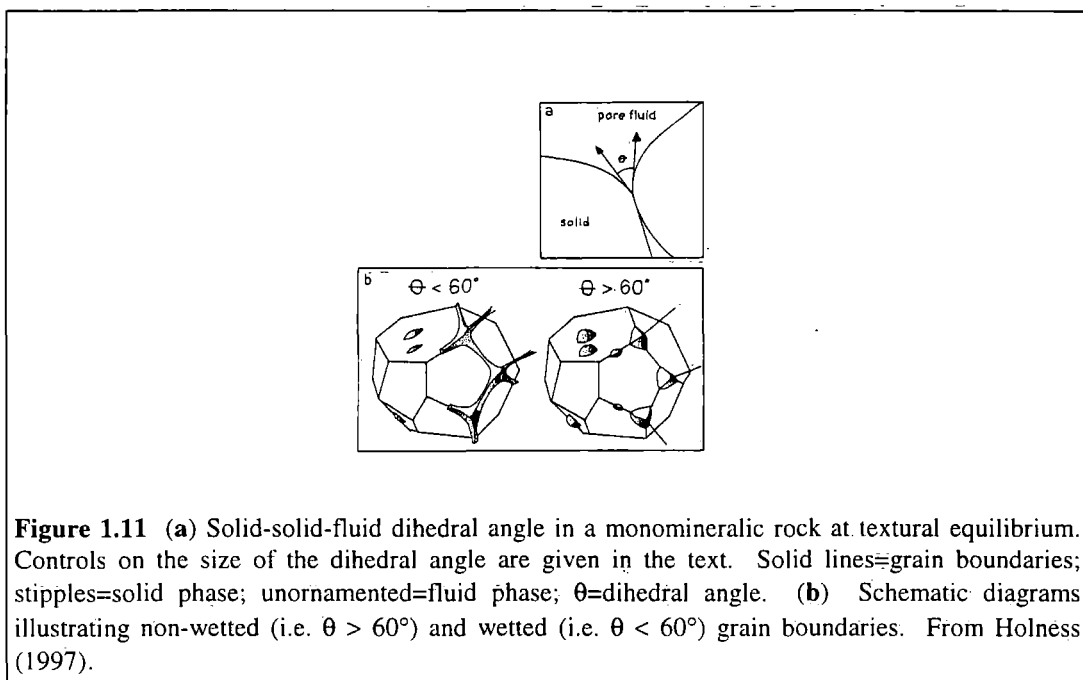


**Figure 1.11** (a) Solid-solid-fluid dihedral angle in a monomineralic rock at textural equilibrium. Controls on the size of the dihedral angle are given in the text. Solid lines=grain boundaries; stipples=solid phase; unornamented=fluid phase;  $\theta$ =dihedral angle. (b) Schematic diagrams illustrating non-wetted (i.e.  $\theta > 60^\circ$ ) and wetted (i.e.  $\theta < 60^\circ$ ) grain boundaries. From Holness (1997).

Hydraulic fracturing is characterised by the presence of small-scale (i.e. thin section-scale) vein networks and intragranular fractures. It has been postulated that hydraulic fractures are important diffusion pathways during fluid-assisted diffusive mass transfer (Cox & Etheridge 1989) (section 1.3.2.1).

### ***Fluid infiltration along grain boundaries***

Fluid infiltration along grain boundary networks is likely to be an important mechanism of fluid transport in the mid- to lower crust (McCaig & Knipe 1990), especially in rocks which are *not* highly overpressured (cf. dilatancy pumping). Experimental studies suggest that in monomineralic rocks which have achieved textural equilibrium (i.e. the grain boundaries display minimum-energy configurations), the permeability of the grain boundary network is controlled by the fluid-solid-solid dihedral angle (Holness & Graham 1991) (Fig. 1.11). If the dihedral angle is greater than  $60^\circ$ , the fluid phase will exist in isolated pores along the grain boundary network, and pervasive infiltration will not be possible. However, if the dihedral angle is less than or equal to  $60^\circ$ , the pores are interconnected and pervasive infiltration along the grain boundary network is possible (e.g. Farver & Yund 1992) (Fig. 1.11). The size of the dihedral angle depends on a number of factors, including pressure, temperature and composition of the solid and fluid phases (Holness 1993).

Deformed rocks rarely display equilibrium microstructures. This observation suggests that the porosity and permeability characteristics of the grain boundary networks in high deformed rocks are unlikely to have been controlled by the fluid-solid-solid *equilibrium* dihedral angles. Rutter (1983) has postulated that fluids are transported as thin films along grain boundaries during fluid-assisted diffusive mass transfer. Laboratory determinations of the present-day porosity characteristics of naturally deformed, macroscopically ductile mylonites suggest that fluid flow occurred through an interconnected network of micron-scale tubules (Géraud *et al.* 1995). The long axes of the tubes are typically oriented parallel to the macroscopic mineral lineation, which is consistent with the permeability having been highly directional.

### ***Microporous minerals***

Microstructural observations suggest that both plagioclase and K-feldspar display microporous textures (David *et al.* 1995). Such textures are characterised by a 'cloudy' appearance in plane polarised light. Oxygen isotope studies are consistent with fluids having infiltrated some microporous K-feldspar grains i.e. the feldspar grains appear to be *micropermeable* (David *et al.* 1995). Micropermeable feldspar grains may be important fluid pathways in metamorphic rocks which are *not* highly

overpressured (i.e. in rocks in which dilatancy pumping is unlikely to have been operative).

## 1.5 FAULT ZONE WEAKENING MECHANISMS

There is a fundamental difference between *transient, syn-tectonic weakening mechanisms*, and *long-term weakening mechanisms* (Holdsworth *et al.* 1997). Transient weakening mechanisms are operative only during active deformation, whilst long-term mechanisms are both syn-tectonic and semi-permanent, causing weakening over long periods of geological time. The following sections outline those weakening mechanisms which are likely to have been operative in retrogressed, basement fault zones. For more comprehensive reviews of weakening mechanisms operative in other regions of the crust, the reader is referred to Rubie (1990), Butler (1995) and Wintsch *et al.* (1995).

### 1.5.1 SYN-TECTONIC WEAKENING MECHANISMS

#### 1.5.1.1 High pore fluid pressure

High pore fluid pressures clearly promote fracturing and brittle failure within the crust (see sections 1.3.1.1 & 1.4.2.1). The shear stress required to initiate brittle failure is given by:

$$\tau_f = S + \mu(\sigma_n - p)$$

(Terzaghi 1936)

where  $\tau_f$  = critical shear stress required for frictional failure,  $S$  = material constant (cohesion),  $\mu$  = coefficient of friction ( $\cong 0.7$  for rocks [e.g. Byerlee 1978]),  $\sigma_n$  = normal stress,  $p$  = pore fluid pressure. This relationship suggests that an *increase* in the pore fluid pressure ( $p$ ), results in a *decrease* in the effective normal stress ( $\sigma_n - p$ ). A decrease in the effective normal stress will cause a corresponding decrease in the shear stress required for frictional failure ( $\tau_f$ ). It follows that at high pore fluid pressures, the shear stresses required for frictional failure may be relatively low. Highly overpressured faults are therefore weak. High pore fluid pressures have been invoked to explain the weakness of the San Andreas Fault (Rice 1992). However, such mechanisms are unlikely to be important in the long-term, owing to the difficulties in maintaining high pore fluid pressures over long periods of geological time (Wintsch *et al.* 1995).

During macroscopically ductile deformation, transient high pore fluid pressures can cause localised embrittlement. Embrittlement may result in grain-scale hydraulic

fractures (e.g. Cox & Etheridge 1989) (section 1.4.2.2), and / or in frictional sliding along transgranular fractures and outcrop-scale faults (e.g. Murphy 1984).

#### **1.5.1.2 Fluid-assisted diffusive mass transfer**

Localised grain size reduction and / or influx of fluids into a fault zone may promote the onset of grain size sensitive, fluid-assisted diffusive mass transfer mechanisms (see sections 1.3.2.1 & 1.3.3.2). For a given pressure, temperature and stress regime, grain size sensitive deformation mechanisms are able to sustain significantly higher strain rates than crystal plastic deformation mechanisms (see Handy 1989 and references therein). Put another way, rocks deforming by diffusion-dominated creep are able to flow under much lower stresses than rocks deforming at the same strain rate by crystal plastic mechanisms. Fine grained, fluid-rich fault zones are therefore expected to be weak.

#### **1.5.1.3 Hydrolytic weakening**

Experimental deformation of quartzo-feldspathic rocks suggests that the addition of trace amounts of water can significantly enhance the activity of crystal plastic deformation mechanisms (Tullis & Yund 1980; Kronenberg & Tullis 1994). The temperature at which the onset of crystal plasticity occurs in experimentally deformed 'wet' rocks is dependant on pressure, strain and strain rate. In rocks which are not highly overpressured, hydrolytic weakening may result in a significant strength reduction and shallowing of the frictional to viscous creep transition. However, it is not clear how significant the effects of hydrolytic weakening will be in highly overpressured, fluid-saturated crust, in which the rocks are likely to deform by predominantly by fluid-assisted DMT and hydraulic fracture processes.

#### **1.5.1.4 Generation of transient, fine grained reaction products**

The formation of new minerals during metamorphism occurs in two distinct stages. *Nucleation* involves the production of fine grained mineral nuclei, whilst *growth* occurs as material is deposited on the stable nuclei (Fyfe *et al.* 1978). Experimental data suggest that significant stress drops are associated with shear zone localisation during the development of fine grained reaction products (i.e. nucleation) (Brodie & Rutter 1987). This weakening effect has been attributed to the onset of diffusion-dominated, grain size sensitive deformation mechanisms within the shear zones (Rubie 1990 and references therein). However, provided the rocks remain at sufficiently high temperatures, and the supply of reactants is not exhausted, the nuclei are likely to become coarser as growth occurs. The rocks are therefore likely to undergo subsequent strain *hardening* as diffusion dominated deformation mechanisms

are suppressed by grain growth. Any weakening effects are, therefore, likely to be short-lived.

#### **1.5.1.5 Transformational plasticity and volume change**

Transformational plasticity is thought to occur during metamorphic reactions which involve significant volume change. Volume change may induce internal stresses within the new minerals, which help overcome the yield strength of the material (White & Knipe 1978). Thus, relatively small external (i.e. applied) stresses are required for the material to deform. However, unless there is repeated cycling across a phase boundary, transformational plasticity is unlikely to cause significant long-term weakening (Rubie 1990). A more significant consequence of volume change during metamorphism is likely to be the development of fractures within the surrounding minerals (e.g. O'Hanley & Offler 1992).

### **1.5.2 LONG-TERM WEAKENING MECHANISMS**

#### **1.5.2.1 Reaction softening**

Reaction softening is a process whereby relatively strong minerals are replaced by *intrinsically weak* minerals during syn-tectonic metamorphism (White & Knipe 1978; Rubie 1990; Wintsch *et al.* 1995). Experimentally deformed single muscovite crystals are able to accommodate strain by dislocation glide under a wide range of pressure and temperature conditions. Muscovite (and biotite) are thus characterised by low activation energies with respect to dislocation glide, and are likely to be intrinsically weak at a wide range of crustal depths (Mares & Kronenberg 1993). Furthermore, well foliated, micaceous rocks appear to be significantly weaker than massive, quartzo-feldspathic rocks deformed experimentally under similar pressure, temperature and strain rate conditions (Shea & Kronenberg 1993). It follows that syn-tectonic chemical breakdown of feldspar to aggregates of white mica (e.g. Beach 1980) constitutes an important reaction softening process (Wintsch *et al.* 1995). Other reaction softening processes, which are probably important at higher levels in the crust, involve the precipitation of clay minerals or zeolites (Byerlee 1978). Reaction softening is likely to be an important long-term weakening mechanism. However, changes in the ambient temperature and pressure conditions and / or fluid composition may favour subsequent re-precipitation of relatively strong minerals. Such processes may result in *reaction hardening* of the fault zone (see discussion in Wintsch *et al.* 1995).

### 1.5.2.2 Fabric softening

Fabric softening encompasses both foliation weakening (Jordan 1987), and the development of crystallographic fabrics (White *et al.* 1986).

#### *Foliation weakening*

Most unmodified basement rocks are characterised by granoblastic textures, in which interlocking networks of relatively strong minerals (e.g. feldspar and hornblende) isolate pockets of relatively weak minerals, such as quartz and biotite. The rheology of most unmodified basement rocks is therefore controlled by the rheological behaviour of the relatively strong, interlocking mineral phases. Granoblastic textures which are dominated by aggregates of strong minerals have been termed *load bearing framework microstructures* (LBF) (Handy 1990) (Fig. 1.12). At the onset of deformation, relatively strong minerals remain rigid and deform predominantly by fracturing. In contrast, relatively weak minerals, such as quartz, are able to deform in a plastic (macroscopically ductile) manner. With progressively increasing strain, the plastically deforming minerals become stretched. Eventually, the deformed weak phase becomes interconnected, and wraps around isolated, rigid porphyroclasts. The rheology of the deformed aggregate will thenceforth be controlled by the rheology of the contiguous weak phase. Such *interconnected weak layer microstructures* (IWL) (Handy 1990) (Fig. 1.14) will develop provided the weak phase constitutes 20% or more by volume of the undeformed protolith (Schmid & Handy 1991). The switch from a LBF-dominated rheology to an IWL-dominated rheology will clearly weaken the fault rocks relative to undeformed protoliths of the same composition. This

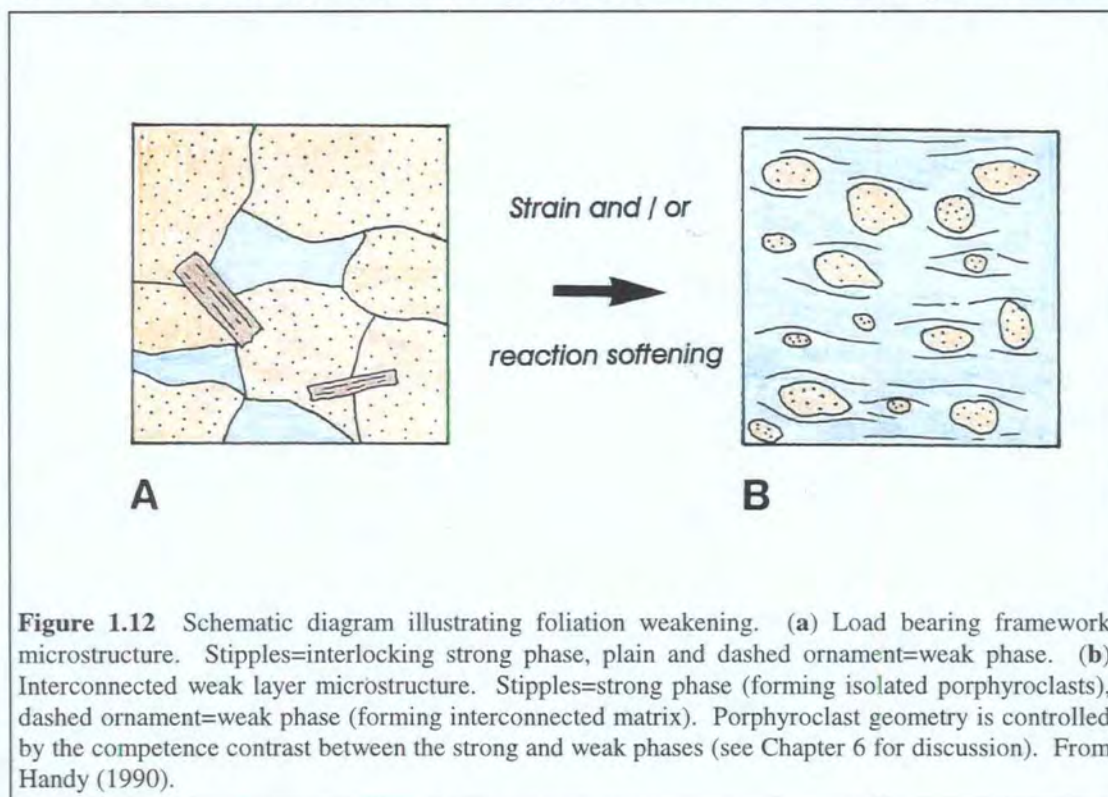


**Figure 1.12** Schematic diagram illustrating foliation weakening. (a) Load bearing framework microstructure. Stipples=interlocking strong phase, plain and dashed ornament=weak phase. (b) Interconnected weak layer microstructure. Stipples=strong phase (forming isolated porphyroclasts), dashed ornament=weak phase (forming interconnected matrix). Porphyroclast geometry is controlled by the competence contrast between the strong and weak phases (see Chapter 6 for discussion). From Handy (1990).

process is referred to as *foliation weakening* (Jordan 1987; Handy 1992). Foliation weakening is enhanced by syn-tectonic metamorphic reactions which produce aggregates of highly aligned, contiguous phyllosilicate minerals (Handy 1990).

#### ***Development of crystallographic fabrics***

During crystal plastic flow, the crystallographic axes of deformed minerals become aligned according to (a) which intracrystalline slip systems were operative (which, in turn, are controlled by the fault rock mineralogy, and pressure, temperature and strain-rate conditions), and (b) according to the kinematics and direction of movement (Law 1990). If the movement direction during reactivation corresponds closely to the movement direction during a previous deformation event, the slip systems within the previously deformed grains may be ideally oriented for 'easy' intracrystalline deformation. However, if the movement directions during successive deformation events do *not* coincide, a strong crystallographic fabric is unlikely to weaken the fault zone, and may even result in hardening (White *et al.* 1986).

#### **1.5.2.3 Grain size reduction**

Watterson (1975) postulated that grain size reduction is a fundamental control on the persistent mechanical weakness of basement faults and shear zones. Grain size reduction, either by cataclasis or dynamic recrystallisation, is likely to promote the onset of grain size sensitive, diffusion-dominated deformation mechanisms (sections 1.3.2.1 & 1.3.3.2). Furthermore, grain size reduction increases the total grain boundary surface area, which renders fine-grained rocks more susceptible to metamorphism than coarse-grained rocks of a similar composition (Brodie & Rutter 1985). Both grain size sensitive deformation and syn-tectonic metamorphism are thought to contribute significantly to fault zone weakening (see sections 1.5.1.2, 1.5.1.4 & 1.5.2.1). However, the importance of grain size reduction as a *long-term* weakening mechanism depends on the fault zone remaining at sufficiently low temperatures to prevent grain growth during static recrystallisation (Passchier & Trouw 1996) (see Chapter 6 for further discussion on the mechanisms of static recrystallisation).

#### **1.5.3 SUMMARY**

A number of different syn-tectonic and long-term weakening mechanisms have been proposed in the literature. However, the most widely invoked operative weakening mechanisms in reactivated basement fault zones involve hydrous fluids. High syn-tectonic pore fluid pressures can significantly reduce frictional strength, promoting hydraulic fracturing and embrittlement. Syn-tectonic retrogression (i.e. hydration) is

likely to enhance reaction softening and foliation weakening, and may also be an important mechanism during diffusive mass transfer. The role of fluids is clearly central to understanding fault zone weakening and reactivation. An underlying theme of this thesis is therefore to document the mechanical and chemical effects of fluid-rock interaction during retrogression and subsequent reactivation along the Outer Hebrides Fault Zone (OHFZ).

## **1.6 FAULT ZONE REACTIVATION: DEFINITION AND TERMINOLOGY**

### **1.6.1 DEFINITION AND RECOGNITION**

In ancient settings, reactivation is defined as '*the accommodation of geologically separable displacement events along pre-existing structures*'. In general, the periods of inactivity between successive events must be greater than c.1Ma (the limit of resolution for most geological data) (Holdsworth *et al.* 1997). In basement faults and shear zones, reactivation can be recognised by one or more of the following structural and geochronological criteria (Butler 1995; Holdsworth *et al.* 1997):

- Overprinting relationships between different fault rocks may suggest that a fault zone has experienced a polyphase kinematic history, which is consistent with reactivation (Fig. 1.13b).
- Changes in fault rock distribution and the style of deformation through time are consistent with a fault zone having experienced a polyphase history, and having been reactivated under different pressure and temperature conditions (Fig. 1.13b).
- Direct isotopic dating of deformation products may indicate that different fault rocks formed during separate deformation events (Fig. 1.13c).
- Dating of intrusions (or sedimentary units) which cross-cut, and / or are cross-cut by, faults may provide evidence for repeated activity along a fault zone (Fig. 1.13a & c).
- Stratigraphic evidence, such as basin inversion geometries and repeated footwall uplift unconformities (Fig. 1.13a).
- Neotectonic criteria, such as present-day seismic activity along the line of ancient fault zones (Fig. 1.13d).

## 1.6.2 STRUCTURAL TERMINOLOGY FOR REACTIVATED FAULT ZONES

Holdsworth *et al.* (1997) have recognised two distinct types of reactivated fault. Reactivated structures which display the *same* sense of relative displacement during successive deformation events are said to have experienced *kinematic reactivation*. In contrast, faults which display *different* senses of relative displacement during successive events are said to have experienced *geometric reactivation* (Fig. 1.14).

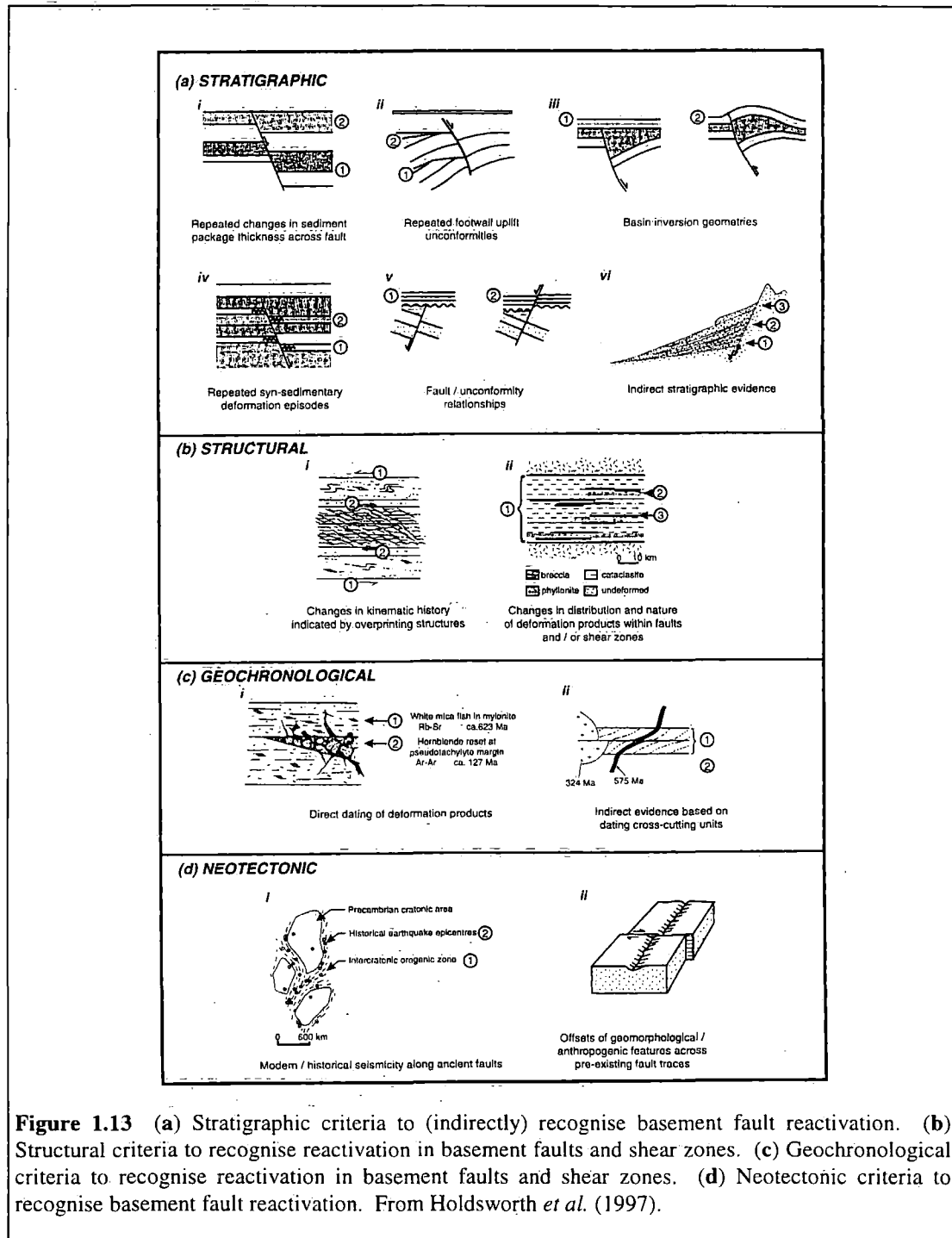


**Figure 1.13** (a) Stratigraphic criteria to (indirectly) recognise basement fault reactivation. (b) Structural criteria to recognise reactivation in basement faults and shear zones. (c) Geochronological criteria to recognise reactivation in basement faults and shear zones. (d) Neotectonic criteria to recognise basement fault reactivation. From Holdsworth *et al.* (1997).

To date, however, there have been few systematic attempts to describe the *spatial and temporal relationships* between successive generations of fault rocks in reactivated fault zones (but see Grocott 1977). Changes in the distribution and style of deformation are likely to record important changes in the ambient metamorphic conditions and dominant operative deformation and localisation mechanisms through time. Such changes are likely to have profound implications for the operative fault zone weakening mechanisms, and are therefore fundamental in understanding the controls on fault zone reactivation. The importance of defining the precise relationships between successive generations of fault rocks in reactivated fault zones is highlighted by the following examples.

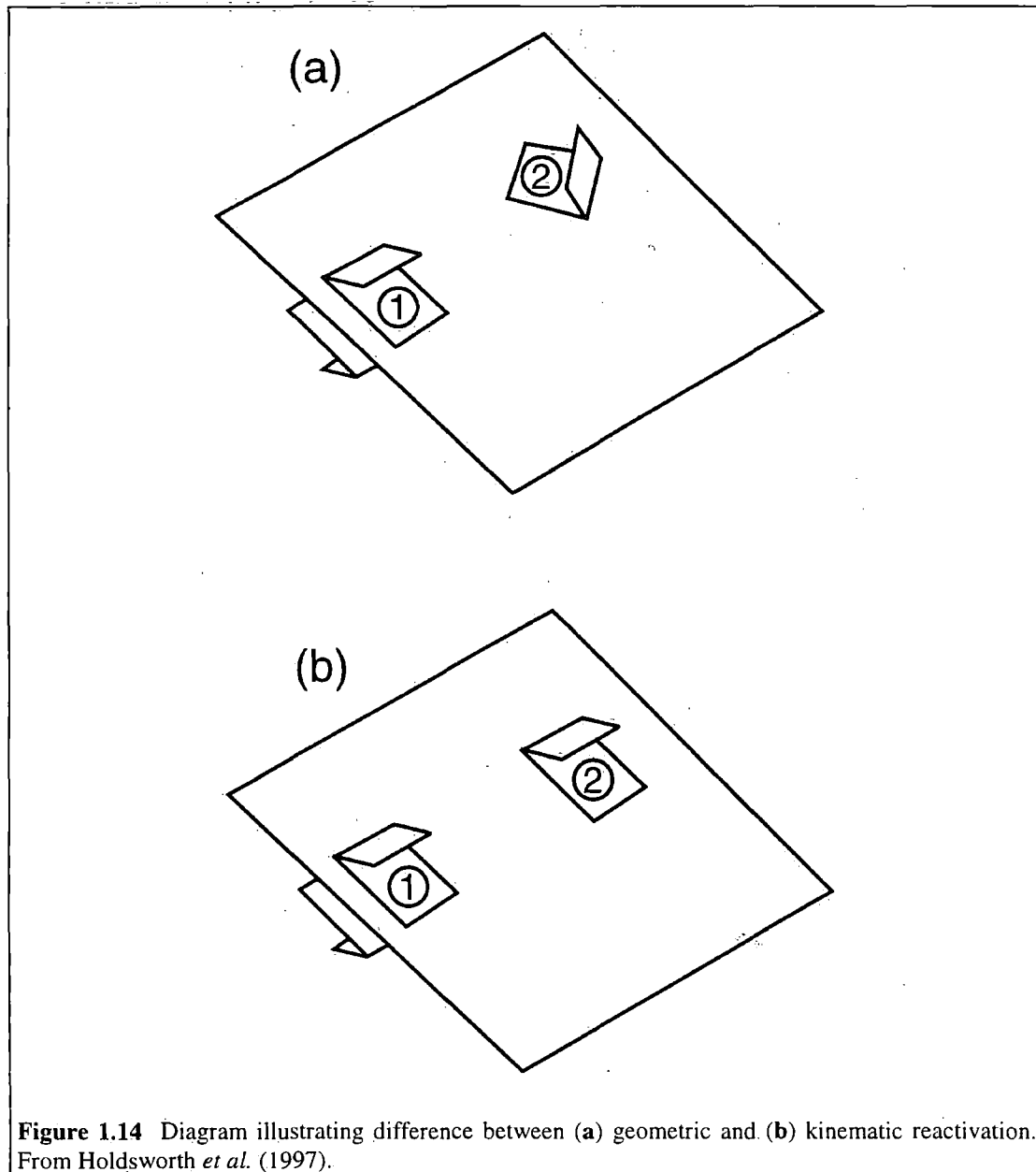


**Figure 1.14** Diagram illustrating difference between (a) geometric and (b) kinematic reactivation. From Holdsworth *et al.* (1997).

### **1.6.2.1 The Torridon shear belt: ductile reactivation of pre-existing ductile fabrics**

The Torridon shear belt is a major NW-SE trending structure developed within Precambrian Lewisian gneisses, northwest Scotland. Two main deformation events, separated by the intrusion of a mafic dyke swarm, have been recognised within the Torridon shear belt (Wheeler *et al.* 1987). The earliest ('Inverian' - see Chapter 2) deformation event was characterised by the development of a strong, macroscopically ductile mylonitic fabric. Inverian deformation within the shear zone was post-dated by the intrusion of the mafic Scourie dyke suite (c.2.39Ga [Chapman 1979]). Subsequent macroscopically ductile Laxfordian deformation (c.1.7Ga [Park 1973]) appears to have been coaxial with the earlier Inverian deformation event, and was particularly intense within and along the margins of the Scourie dykes (Wheeler *et al.* 1987). These observations suggest that the macroscopically ductile Inverian shear zone fabrics were locally reactivated during macroscopically ductile, Laxfordian deformation. Laxfordian deformation within the Torridon shear belt is an example of kinematic reactivation.

### **1.6.2.2 The Gairloch shear zone: brittle reactivation of pre-existing ductile fabrics**

The Gairloch shear zone is a steeply dipping, NW-SE trending structure developed within Precambrian Lewisian gneisses of northwest Scotland. The Gairloch shear zone belongs to the same set of structures as the NW-SE trending Torridon shear belt discussed in the previous section (Coward & Park 1987). At least three different phases of deformation have been recognised within the Gairloch shear zone (Shihe & Park 1993; Beacom *et al.* 1997). The earlier phase of deformation (c.1.7Ga [Shihe & Park 1993]) was characterised by the development of a broad, amphibolite facies shear zone. Subsequent greenschist facies retrogression (c.1.5Ga [Shihe & Park 1993]) was associated with localised shearing within steeply dipping, NW-SE trending shear zones. The macroscopically ductile, greenschist facies fabrics are commonly observed to be deformed by relatively narrow, foliation-parallel 'crush belts' (i.e. zones of intense cataclastic deformation). Shear criteria are consistent with the greenschist facies shear zones and the crush belts both having developed during dextral strike-slip (Shihe & Park 1993; Beacom *et al.* 1997). The shear zones and crush belts are cross-cut by predominantly N-S trending, brittle faults. These observations suggest that the macroscopically ductile, greenschist facies fabrics were kinematically reactivated (*sensu* Holdsworth *et al.* 1997) during the development of the crush belts. However, the N-S trending faults do *not* reactivate earlier fabrics.

### 1.6.2.3 The Church Stretton Fault Zone: brittle reactivation of pre-existing brittle faults

The Church Stretton Fault Zone (CSFZ) is a steeply dipping, NE-SW trending structure, developed within late Precambrian to early Palaeozoic (Silurian) sediments in the Welsh Borders (Woodcock 1988). At Dolyhir Quarry, the CSFZ comprises two sets of steeply dipping, anastomosing NNE-SSW and NW-SE trending faults. Faults which deform the late Precambrian sediments, but which do *not* cross-cut the Precambrian - Silurian unconformity are commonly observed to be associated with down-dip plunging slickenlines. In contrast, faults which cross-cut the unconformity are associated predominantly sub-horizontal slickenlines. It has been postulated that brittle, pre-Silurian dip-slip faults were reactivated as brittle, post-Silurian transcurrent faults (Woodcock 1992). Post-Silurian brittle deformation along the CSFZ is therefore an example of geometric reactivation.

### 1.6.2.4 New structural terminology for reactivated fault zones

These field studies clearly demonstrate that fault zone reactivation occurs at all levels in the crust. However, the style and distribution of deformation during reactivation are different in each example. Fault zone reactivation at mid-crustal depths, around the level of the frictional to viscous transition (e.g. the Torridon and Gairloch shear zones) is likely to have important implications for the strength of the crust as a whole (section 1.3.3). In contrast, fault zone reactivation at upper-crustal depths (e.g. the Church Stretton Fault Zone) is unlikely to affect total crustal strength. These observations underline the importance of rigorously describing the exact relationships between successive generations of fault rocks and structures in reactivated fault zones. The following terminology has been adopted throughout this thesis:

- ***Protoliths*** are rocks which pre-date localised deformation along a fault or shear zone. The Lewisian gneiss of Gairloch and Torridon, and the Precambrian and Silurian sediments of the Welsh Borders are examples of protoliths (sections 1.6.2.1, 1.6.2.2 & 1.6.2.3).
- ***Primary fabrics / structures*** are the oldest fault rocks or structures recognised along a fault or shear zone. The mineralogy, microstructure and / or fluid transport properties of the primary fabrics may be to some extent influenced by the protoliths. The Inverian fabrics within the Torridon shear belt, the amphibolite facies mylonites within the Gairloch shear zone and the pre-Silurian dip-slip faults along the Church Stretton Fault Zone are examples of primary fabrics and structures (sections 1.6.2.1, 1.6.2.2 & 1.6.2.3).
- ***Derived fabrics / structures*** are fault rocks or structures whose geometry is clearly inherited from that of the primary fabrics, but which do *not* simply

rework the pre-existing fault rocks and structures. The mineralogy, microstructures and / or fluid transport properties of the inherited fabrics may differ significantly from those of the older fault zone fabrics. Derived fabrics are thought to develop when the prevailing metamorphic conditions during reactivation differ significantly from the prevailing conditions during the previous deformation event. The crush belts within the Gairloch shear zone are examples of derived fabrics (section 1.6.2.2).

- **Reworked fabrics / structures** are fault rocks or structures which are *directly* deformed during a subsequent deformation episode. Reworking does not necessarily involve significant changes to the mineralogy, microstructure and / or fluid transport properties of the pre-existing fault rocks or structures. Reworked fabrics are thought to develop when the prevailing metamorphic conditions during reactivation were similar to the prevailing conditions during the previous deformation event. The Laxfordian shear zones which localised along the margins of Scourie dykes within the Torridon shear belt, and the post-Silurian strike-slip faults within the Church Stretton Fault Zone are examples of reworked fabrics and structures (sections 1.6.2.1 & 1.6.2.3).
- **Cross-cutting fabrics / structures** are fault rocks or structures which overprint pre-existing fault zone fabrics, but whose geometry, mineralogy, microstructure and / or fluid-transport properties are clearly *not* influenced by the pre-existing architecture of the fault zone. Cross-cutting fabrics are thought to develop either if (a) the orientation of the regional stress field does not favour reactivation of pre-existing structures (e.g. Sibson 1975), and / or (b) if there is a marked *decrease* in the ambient pressure and temperature conditions between successive deformation events. The N-S trending faults which cross-cut the Gairloch shear zone are examples of cross-cutting structures (section 1.6.2.2).

The terminology presented in this section can be applied to reactivated faults and shear zones in general, and is complementary to the terminology advocated by Holdsworth *et al.* (1997).

## 1.7 DATA COLLECTION

The following section briefly outlines the main field and microstructural techniques employed during this study.

### 1.7.1 FIELDWORK METHODS

The OHFZ has been comprehensively mapped by previous authors (Coward 1969; Sibson 1977b; Walker 1990; Fettes *et al.* 1992; Butler 1995). High quality maps (generally at 1:10000 scale) of the different fault rocks are provided by Sibson (1977b) and Butler (1995). These maps have been extensively referred to throughout the present study.

Geologically significant, well exposed field localities were selected with reference to Sibson (1977b) and Butler (1995). In order to document the complex relationships between the different fault rocks and structures, a technique of *structural logging* has been devised (Appendix A). A structural log is a graphical representation of the fault rocks encountered along a chosen one-dimensional traverse through the fault zone. Each structural log comprises (a) a *geometric log*, which provides information on the orientation of the foliation, mineral lineation, fault planes etc. along the line of the traverse, (b) a *kinematic log*, which provides information on the fault zone kinematics along the line of the traverse, and (c) a *lithological log*, which illustrates the mineralogical and textural characteristics of the fault rocks along the line of the traverse. The field sheets (although not the clean copy versions) include additional information, such as the location of samples and photographs. The scale of the structural logs can be varied according to the nature of the study. The logs in this thesis are presented at scales of 1:5, 1:10, 1:50 or 1:100. In regions of predominantly brittle fault rocks, the traverses were designed to be oriented parallel to the inferred bulk transport direction, and were conducted in surfaces normal to the regional fault planes. In regions of macroscopically ductile fault rocks, the traverses were conducted parallel to the transport direction, in surfaces parallel to the inferred XZ plane of the finite strain ellipsoid (i.e. parallel to the mineral stretching lineation and perpendicular to the regional foliation). However, the location of each traverse was to some extent limited by the available exposure.

Additional reconnaissance mapping, at a scale of 1:10000, was carried out in regions for which detailed structural maps were unavailable (notably the Loch Bhrollum and Kebock Head regions of southeast Lewis, the Lees region of eastern North Uist and the Rubha Hellisdale region of eastern South Uist) (Chapter 3).

## 1.7.2 MICROSTRUCTURAL METHODS

The samples collected during each structural traverse were studied using standard petrographic thin sections. Selected textures were analysed using the backscattered detector attached to a CamScan scanning electron microscope in the Electron Microscopy Unit at the University of Leeds. Semi-quantitative analyses of selected minerals were obtained using the energy dispersive X-ray detector attached to the SEM.

## 1.7.3 GEOCHEMICAL METHODS

Details of the geochemical techniques employed during this study are presented in Chapter 8 and Appendix B.

## 1.8 THESIS OUTLINE

Following this introduction, the thesis comprises:

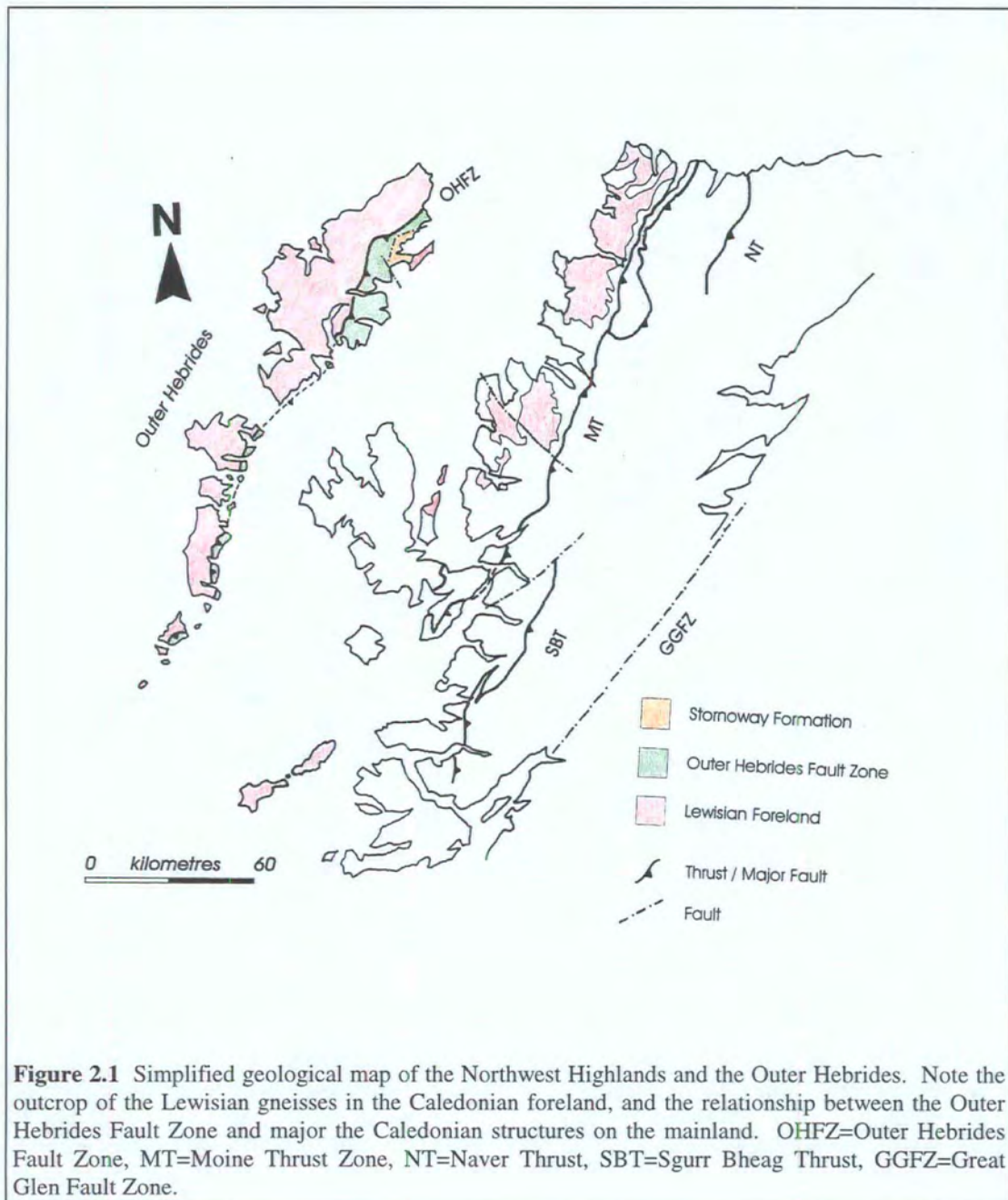
- *Chapter 2* - an introduction to the regional geology of the Outer Hebrides, including a summary of previous work on the Outer Hebrides Fault Zone.
- *Chapter 3* - an overview of kinematic, metamorphic and textural evolution of the entire Outer Hebrides Fault Zone, based on the present author's observations, supplemented by previous work where necessary. The aim of Chapter 3 is to provide a context in which to understand the detailed field and microstructural studies presented in Chapters 4, 5, 6 and 7.
- *Chapters 4 to 7* - these chapters present detailed field and microstructural observations from key localities along the OHFZ (Loch Sgibacleit, southeast Lewis; Scalpay, south Harris; eastern North Uist; eastern South Uist). Each chapter describes the local textural and metamorphic evolution of the fault zone. Particular emphasis is placed on (a) the spatial and temporal relationships between different generations of fault rocks, and on (b) interpreting the fault rock textures in terms of the operative deformation mechanisms and (where appropriate) in terms of fluid-rock interaction.
- *Chapter 8* - this chapter presents the results of a geochemical study of selected fault rocks from eastern North Uist. The geochemical data are interpreted in terms of the metamorphic processes, operative deformation mechanisms and fluid-rock interaction during fault zone reactivation.

- *Chapter 9* - this chapter synthesis the observations and interpretations made in previous sections, to provide a model of fault zone weakening and reactivation for the Outer Hebrides Fault Zone. The significance of fault zone weakening and fluid-rock interaction during reactivation will be discussed.

## 2. THE OUTER HEBRIDES FAULT ZONE: INTRODUCTION

### 2.1 INTRODUCTION

The Outer Hebrides (Lewis, Harris, North Uist, Benbecula, South Uist, Barra and numerous smaller islands and skerries) lie off the northwest coast of Scotland and extend for over 200km, from the Butt of Lewis in the north to Barra Head in the south. The geology of the Outer Hebrides can be divided into three fundamental units (Fig. 2.1), which form the basis for the subdivision of this chapter:



- (1) The *Lewisian Complex*, which comprises amphibolite to granulite facies basement gneisses (e.g. Fettes *et al.* 1992; section 2.2 of the present work).
- (2) The *Outer Hebrides Fault Zone* (OHFZ), which comprises a variety of different fault rocks, all of which were derived from the Lewisian gneisses (e.g. Sibson 1977b; section 2.3 and following chapters of the present work).
- (3) The *Stornoway Formation*, which comprises a thick succession of undeformed and unmetamorphosed ?Permo-Triassic conglomerates and sandstones (Steel & Wilson 1975; section 2.4 of the present work).

The aims of this chapter are twofold. (1) To introduce the regional geology of the Outer Hebrides, as a context in which to discuss the structural and metamorphic evolution of the Outer Hebrides Fault Zone (sections 2.2 & 2.4), and (2) to introduce and summarise previous work on the Outer Hebrides Fault Zone (section 2.3).

## 2.2 THE LEWISIAN COMPLEX IN THE OUTER HEBRIDES

The fault rocks which comprise the Outer Hebrides Fault Zone were, without exception, derived from Lewisian protoliths. An appreciation of the Lewisian geology is therefore essential in order to understand the nature and style of deformation observed along the OHFZ. The following sections summarise the metamorphic and structural evolution of the Lewisian gneisses in the Outer Hebrides.

### 2.2.1 REGIONAL CONTEXT

The Outer Hebrides predominantly comprise an assemblage of high-grade Archaean to Early Proterozoic gneisses, which are collectively referred to as the 'Lewisian Complex' (e.g. Dearnley 1962). The Lewisian Complex, which is exposed in the Outer Hebrides and on the Scottish mainland (Fig. 2.1), belongs to a group of Precambrian basement terrains which outcrop extensively around the North Atlantic region. Palaeogeographic reconstructions of the North Atlantic region suggest that the Scottish Lewisian Complex is closely related to the Nagssugtoqidian gneisses of East Greenland, which together formed part of a major Early Proterozoic mobile belt (the 'Inverian - Nagssugtoqidian mobile belt'; Le Pichon *et al.* 1977; Myers 1987; Coward & Park 1987; Fig. 2.2).

Sutton & Watson (1951) recognised two principal tectonothermal events in the Lewisian Complex of the Scottish mainland. The oldest ('Scourian') event pre-dates

the intrusion of a suite of tholeiitic dykes (the 'Scourie Dykes'), whilst the younger ('Laxfordian') event largely post-dates the intrusion of the Scourie Dykes.

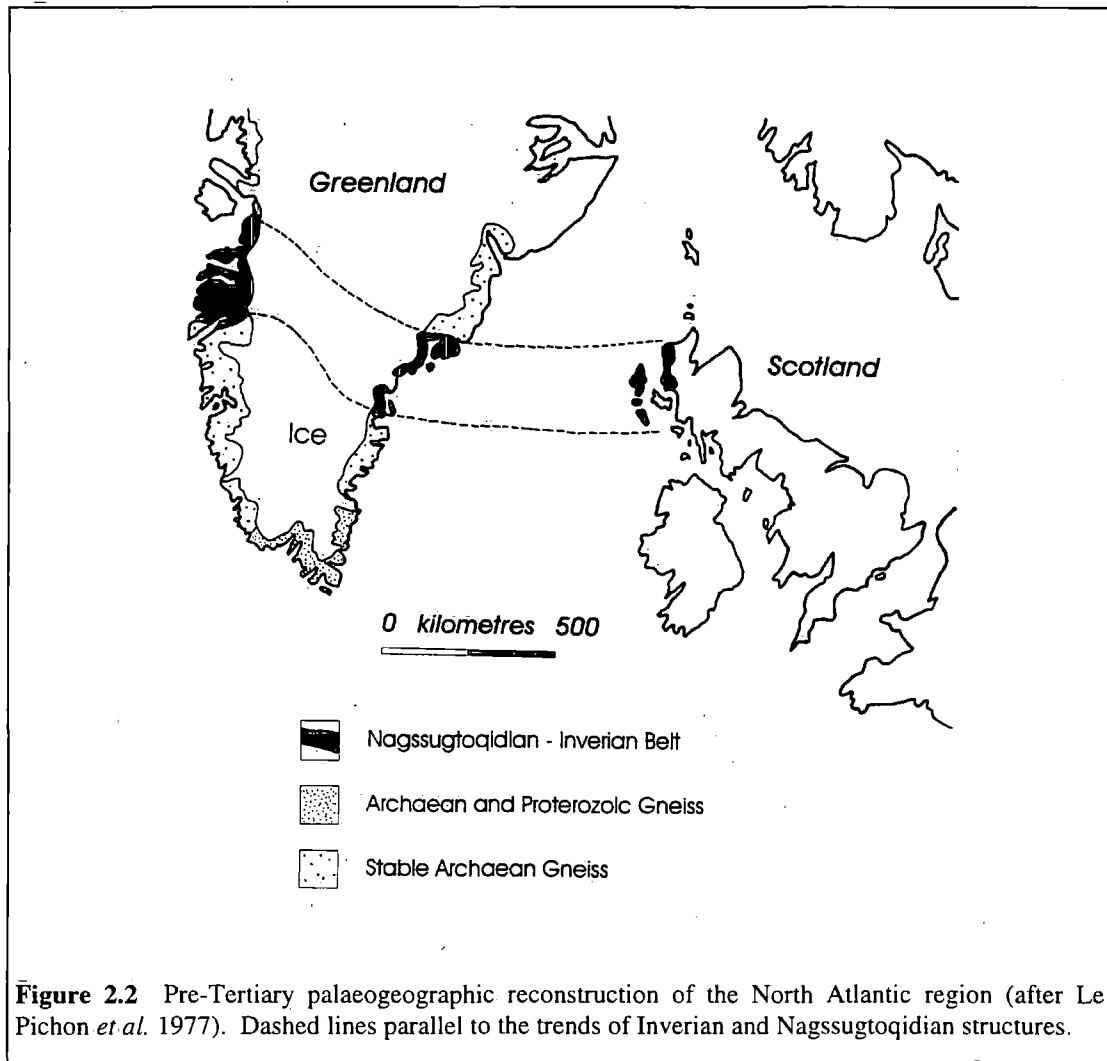


**Figure 2.2** Pre-Tertiary palaeogeographic reconstruction of the North Atlantic region (after Le Pichon *et al.* 1977). Dashed lines parallel to the trends of Inverian and Nagssugtoqidian structures.

A similar sequence of events has been identified in the Lewisian of the Outer Hebrides (Dearnley 1962). The 'Scourian' event (2900Ma to 2400Ma) pre-dates the intrusion of a suite of basic dykes (the 'Younger Basics' of Fettes *et al.* 1992), whilst the 'Laxfordian' event (2400Ma to 1400Ma) largely post-dates the intrusion of the Younger Basics. Geochronological and geochemical studies (e.g. Lambert *et al.* 1970; Fettes *et al.* 1992) suggest that the Younger Basics belong to the same suite of minor intrusions as the Scourie Dykes. The 'Scourian' and 'Laxfordian' events recognised in the Outer Hebrides are thus broadly equivalent to the Scourian and Laxfordian events as originally defined on the Scottish mainland (Sutton & Watson 1951).

## 2.2.2 LITHOLOGIES

The gneisses of the Outer Hebrides fall into four broad lithological groups, which are described below. The relative ages and structural relationships of the different gneisses are defined in sections 2.2.3 and 2.2.4.

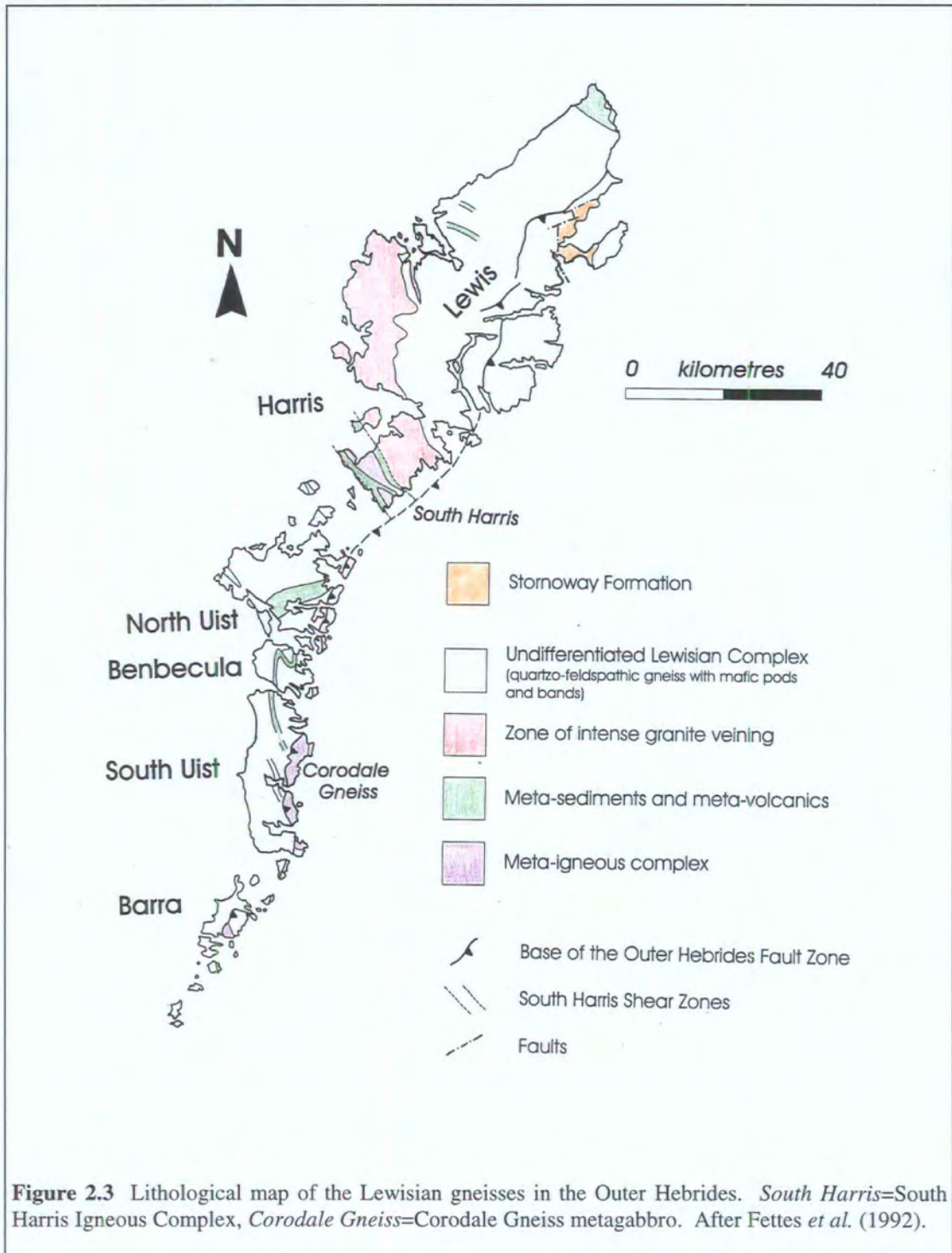


**Figure 2.3** Lithological map of the Lewisian gneisses in the Outer Hebrides. *South Harris*=South Harris Igneous Complex, *Corodale Gneiss*=Corodale Gneiss metagabbro. After Fettes *et al.* (1992).

### 2.2.2.1 Quartzo-feldspathic banded gneisses

The most commonly observed lithology in the Outer Hebrides is quartzo-feldspathic banded gneiss (the 'grey gneiss' of Dearnley 1962 & Walker 1990). The banded gneisses are medium to coarse grained, crystalline rocks comprising feldspar (moderately calcic plagioclase and lesser amounts of K-feldspar), quartz, hornblende, biotite  $\pm$  pyroxene. The feldspars typically form equigranular, polygonal aggregates which surround isolated pockets of flattened quartz grains, laths of biotite and subhedral to euhedral hornblende grains. The mafic minerals define pronounced, though laterally discontinuous compositional bands (bands are centimetres to tens of centimetres thick). The flattened quartz grains and biotite laths are typically oriented parallel to the banding and define a crude 'gneissose foliation' (Fettes *et al.* 1992). The quartzo-feldspathic banded gneisses are locally associated with distinct mafic pods, (the 'Older Basics' of Fettes *et al.* 1992), which may be up to several hundreds of metres in diameter. The Older Basics comprise medium to coarse grained, equigranular aggregates of plagioclase and hornblende  $\pm$  pyroxene, with subordinate bands of quartzo-feldspathic material. The quartzo-feldspathic banded gneisses and the Older Basics are depicted as 'Undifferentiated Lewisian Complex' in Figure 2.3 and together form the most important group of protoliths to the fault rocks of the Outer Hebrides Fault Zone (Chapters 3 to 7).

### 2.2.2.2 Supracrustal sequence

Distinct bands of quartzite, marble and garnet  $\pm$  kyanite  $\pm$  sillimanite-bearing schist occur throughout the Outer Hebrides. These 'exotic' lithologies are thought to be metasedimentary or metavolcanic in origin and may represent the remnants of an Archaean supracrustal sequence (Coward *et al.* 1969; Fettes *et al.* 1992; section 2.2.3 of the present work). The largest bands of metasedimentary / metavolcanic rocks are preserved in the Uists and within the South Harris Shear Zones (Fig. 2.3). Very few of the fault rocks from the Outer Hebrides Fault Zone appear to be derived from either metasedimentary or metavolcanic protoliths.

### 2.2.2.3 Major intrusives

Two major meta-igneous complexes outcrop in the Outer Hebrides. The South Harris Igneous Complex is closely associated with the South Harris supracrustal sequence (Fig. 2.3) and comprises four distinct bodies of metagabbro, meta-anorthosite, metanorite and metadiorite (Jehu & Craig 1927). The phyllonitic mylonites exposed at Rubha Vallerip (NG 060 830; Chapter 3) were derived from the meta-anorthosite, but overall, very few of the fault rocks associated with the Outer Hebrides Fault Zone were derived from the meta-igneous rocks of South Harris.

The other major meta-igneous body (the Corodale Gneiss), is a pyroxene-rich metagabbro which is exposed in the hangingwall of the Outer Hebrides Fault Zone in South Uist (Coward 1969; Coward 1972; Fig. 2.3). The Corodale Gneiss is locally highly crushed and fractured. This brittle deformation has been attributed to top-to-the-W (i.e. thrust sense) movements along the Outer Hebrides Fault Zone (Coward 1972; Sibson 1977b; Butler 1995). A belt of phyllosilicate-rich mylonite is exposed in eastern South Uist and is thought to have been derived predominantly from the Corodale Gneiss (Fig. 2.5; see section 2.3.2 & Chapter 7).

#### **2.2.2.4 Minor intrusives**

Several suites of minor intrusives have been recognised in the Outer Hebrides. The earliest is a group of widespread, though not abundantly developed, fine grained metadiorite dykes and pegmatite veins (Fettes & Mendum 1987). The dykes and veins (typically  $\leq 30\text{cm}$  thick) are collectively referred to as the 'Late Scourian Suite' (Fettes *et al.* 1992) and are well exposed in regions of low Laxfordian strain (see Plate 2.1 of Butler 1995).

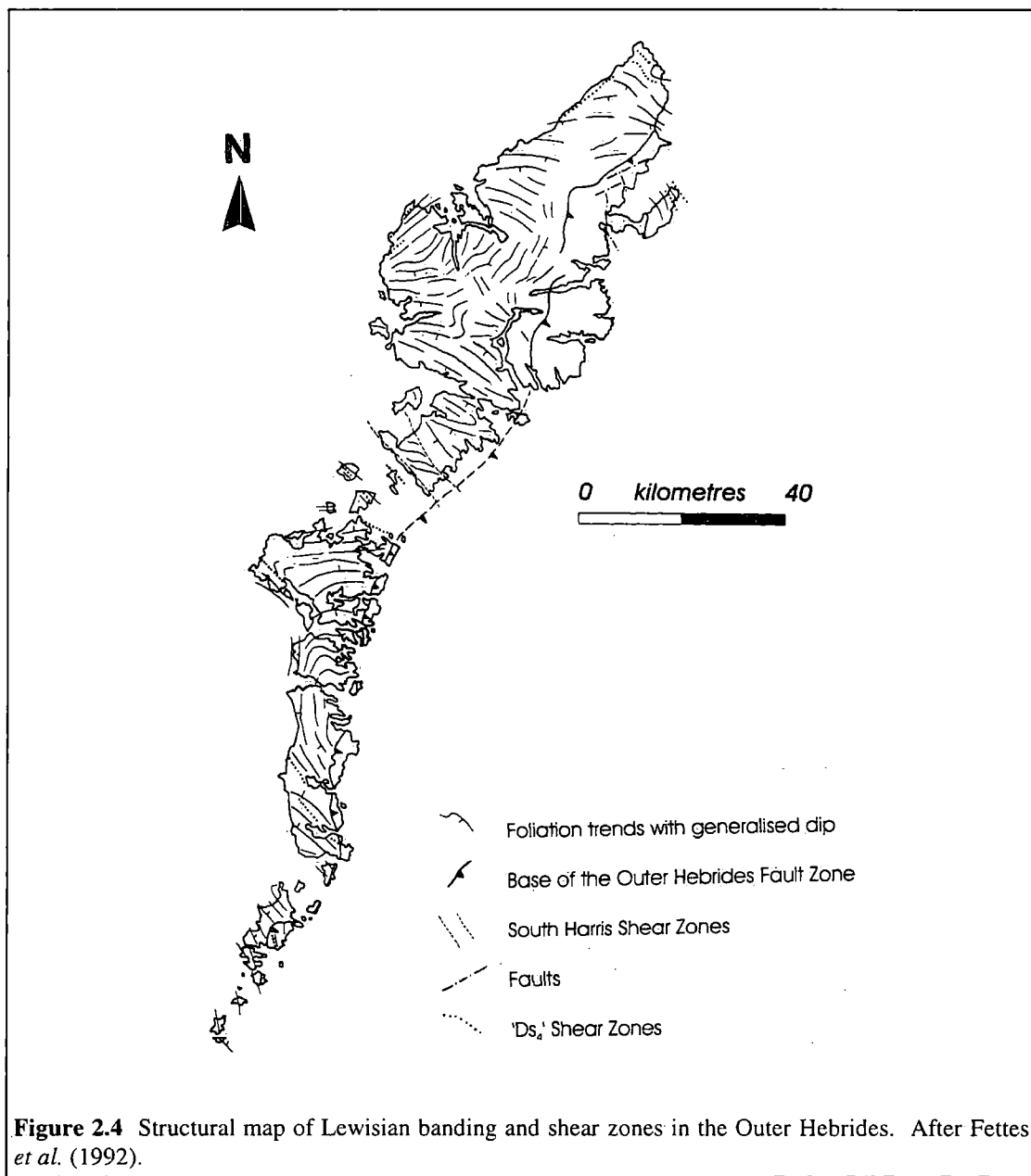
The E-W to NW-SE trending Younger Basic dykes are widespread and abundant throughout the Outer Hebrides. The dykes are locally up to 3m thick and comprise a suite of metadolerites with subordinate dunite, peridotite, norite and picrite sheets (Fettes & Mendum 1987). The metadolerites comprise equigranular, polygonal to subhedral aggregates of plagioclase and hornblende which surround isolated garnet, quartz and / or pyroxene grains. Some of the fault rocks associated with the Outer Hebrides Fault Zone were undoubtedly derived from either Younger Basic or Late Scourian Suite dykes (Chapter 3). However, the volume of fault rocks derived from these minor intrusions is not thought to be great.

Late Laxfordian pegmatite dykes and veins are widespread throughout the Outer Hebrides and are locally abundant in the Uig Hills-Harris granite-migmatite complex of western Lewis and Harris (Myers 1971; Fettes *et al.* 1992; Fig. 2.3). The pegmatites and granite veins are typically highly discordant to the gneissose banding and comprise a coarse grained assemblage of K-feldspar, plagioclase, quartz, biotite, muscovite  $\pm$  chlorite after biotite. In Lewis and Harris, a significant proportion of the fault rocks associated with the Outer Hebrides Fault Zone were derived from Laxfordian pegmatites (Fettes *et al.* 1992; section 2.2.4, Chapters 3, 4 & 5).

### 2.2.3 THE SCOURIAN EVENT

The Scourian event in the Outer Hebrides is thought to have spanned the period from c.2900Ma to 2400Ma (Fettes & Mendum 1987). Radiometric age dating and the use of igneous intrusions (the Late Scourian Suite and Younger Basics) as time markers has allowed Fettes *et al.* (1992) to recognise four distinct phases of Scourian metamorphism and / or deformation.

The supracrustal sequence of metasediments and metavolcanics is believed to have been deposited or extruded c.2900Ma and subsequently subjected to a phase of 'early' Scourian deformation and metamorphism ( $Ds_1$ ' of Fettes *et al.* 1992). An important episode of igneous activity followed, in which large volumes of tonalite and granodiorite magmas were injected into the deformed supracrustal sequence. Recent whole-rock Sm-Nd and Pb-Pb isotopic age dates (Whitehouse 1993) suggest that the igneous protoliths to the Corodale Gneiss may have originated during this period of Scourian igneous activity. The upper amphibolite to granulite facies 'main' Scourian event ( $Ds_2$ ' or 'gneissification event' of Fettes *et al.* 1992), was characterised by intense, penetrative deformation and is thought to have been responsible transforming the tonalites and granodiorites into the banded quartzo-feldspathic gneisses which dominate the geology of the Outer Hebrides at the present day.



Fettes *et al.* (1992) have identified two further phases of Scourian deformation following the 'gneissification event'. 'Ds<sub>3</sub>' partly pre-dates the intrusion of the Late Scourian Suite and is characterised by regional-scale asymmetric folds with NNE-SSW trending long limbs. 'Ds<sub>4</sub>' post-dates the Late Scourian Suite and was associated with the development of the NW-SE (locally NE-SW) trending shear zones (Fig. 2.4). 'Ds<sub>4</sub>' may be equivalent to the Inverian event identified on the Scottish mainland and appears to have been broadly contemporaneous with the intrusion of the Younger Basic dykes. Sm-Nd age dating suggests that the South Harris Igneous Complex may have originated during the latest Scourian or earliest Laxfordian (c.2200Ma, Cliff *et al.* 1983), although its exact relationship to the banded gneiss country rocks remains unclear.

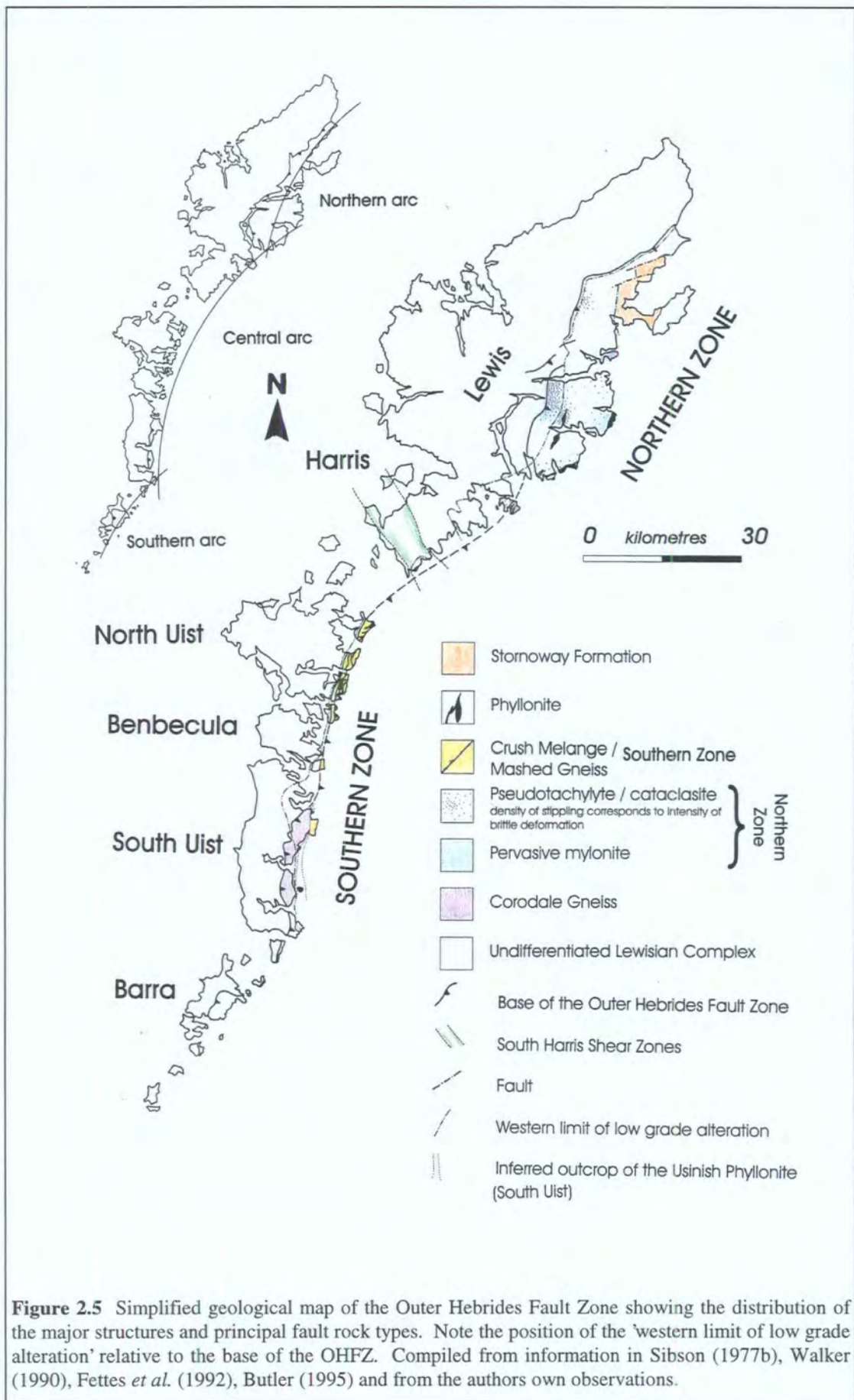


**Figure 2.5** Simplified geological map of the Outer Hebrides Fault Zone showing the distribution of the major structures and principal fault rock types. Note the position of the 'western limit of low grade alteration' relative to the base of the OHFZ. Compiled from information in Sibson (1977b), Walker (1990), Fettes *et al.* (1992), Butler (1995) and from the authors own observations.

## 2.2.4 THE LAXFORDIAN EVENT

The earliest Laxfordian event recognised in the Outer Hebrides ('D<sub>1</sub>' of Fettes *et al.* 1992) may have been synchronous with late Scourian ('D<sub>s4</sub>') shearing (Fettes *et al.* 1992). Structures associated with the 'main' amphibolite facies Laxfordian tectonothermal event ('D<sub>2</sub>' and 'D<sub>3</sub>' of Fettes *et al.* 1992) are widespread and accentuate the strong NW-SE trending structural grain observed throughout the islands (Fig. 2.4). Gently plunging, flat-lying open to isoclinal folds originated during the 'D<sub>2</sub>' event, whilst 'D<sub>3</sub>' is characterised by highly asymmetric, upright, regional-scale folds with NW-SE trending axial planes (Fig. 2.4). The vertical limbs of the latter folds are typically attenuated and sheared.

The amphibolite facies 'D<sub>2</sub>' and 'D<sub>3</sub>' events were followed by the widespread intrusion of granite and pegmatite veins and the development of the Uig Hills-Harris granite-migmatite complex (Myers 1971; Fig. 2.3). Fettes *et al.* (1992) noted that the granite sheets preserved in the Uig Hills (west Lewis) are locally overprinted by an amphibolite to upper greenschist facies mylonitic fabric ± pseudotachylyte veins. The geometry of the mylonitic fabric is consistent with top-to-the-WSW directed thrusting (Fettes & Mendum 1987). It has been suggested that these thrust-related mylonitic fabrics are late Laxfordian in age and were the precursors to localised deformation along the Outer Hebrides Fault Zone in Lewis ('D<sub>5</sub>' and 'D<sub>6</sub>' of Fettes *et al.* 1992). The nature and age of the mylonitic fabrics and the role of pegmatites in localising deformation along the Outer Hebrides Fault Zone in Lewis are discussed further in Chapters 3, 4 and 5.

## 2.2.5 SUMMARY

It is apparent from the preceding descriptions that the Lewisian Complex of the Outer Hebrides has suffered a protracted history deformation, metamorphism and igneous intrusion. The highest metamorphic grades were associated with penetrative deformation during the main Scourian 'gneissification' event. Subsequent Scourian and Laxfordian events were characterised by progressively decreasing metamorphic grades and increasingly localised deformation. These observations are consistent with the progressive exhumation of the Lewisian Complex in the Outer Hebrides from the Proterozoic onwards (cf. Grocott 1977).

The gneissose fabric elements (e.g. banding, fold axial planes and shear zones) define a strong NW-SE structural grain throughout the Outer Hebrides (Fig. 2.4). This structural grain appears to have been a long-lived feature which originated during the Scourian, but was subsequently reinforced and imprinted during the main Laxfordian

tectonothermal event ('D<sub>12</sub>' and 'D<sub>13</sub>') (Fettes & Mendum 1987). However, the trace of the Outer Hebrides Fault Zone clearly cross-cuts the gneissose fabric on a regional scale, the discordance being particularly strong on Harris and in the Uists (Fig. 2.4). It is therefore unlikely that the gneissose fabric was the primary control on the localisation of strain along the OHFZ either on Harris or in the Uists. The influence of the pre-existing basement fabrics on the distribution of deformation along the OHFZ is discussed further in Chapter 3.

## **2.3 THE OUTER HEBRIDES FAULT ZONE: INTRODUCTION AND PREVIOUS WORK**

### **2.3.1 INTRODUCTION**

The Outer Hebrides Fault Zone (OHFZ) is one of the largest tectonic lineaments in the British Isles. It outcrops for approximately 190km along the eastern seaboard of the Outer Hebrides and lies some 85km to the west of the better known Moine Thrust Zone (Fig. 2.1). In contrast to the Moine Thrust Zone, the OHFZ cross-cuts relatively homogeneous Lewisian basement gneisses (section 2.2) and therefore does not displace any laterally continuous stratigraphic marker horizons. The Outer Hebrides Fault Zone dips moderately towards the SE or ESE and the onshore trace of the OHFZ defines three concave-to-the-east arcs (Sibson 1977b) (Fig. 2.5 inset).

A number of Mesozoic sedimentary basins are developed in the hangingwall of the Outer Hebrides Fault Zone (Fig. 2.7) and are discussed further in sections 2.3.4 and 2.3.5.

### **2.3.2 THE AGE OF THE OHFZ**

It is extremely difficult to precisely constrain the age of deformation along the Outer Hebrides Fault Zone. Firstly, unlike the Moine Thrust Zone, the OHFZ does not cross-cut a stratigraphically datable sedimentary succession. Secondly, the different fault rock assemblages exposed along the OHFZ (section 2.3.3.1) are unlikely to have developed during a single deformation event (section 2.3.3.4). Finally, most of the fault rocks preserved in the Outer Hebrides have experienced significant syn- and / or post-tectonic retrogressive metamorphism and hydration (section 2.3.3.2). Retrogression could significantly affect the isotopic systems used for dating the deformation events.

### 2.2.3.1 Field relationships

The fault rocks and structures exposed along the OHFZ deform both the Younger Basic dykes and the Laxfordian pegmatite sheets (section 2.2.2.4) (Sibson 1977b; Butler 1995; Chapter 5 of the present work, but cf. Lailey *et al.* 1989). The oldest possible deformation event along the OHFZ must therefore post-date, or have been synchronous with, the last stages of the Laxfordian tectonothermal event (section 2.2.4).

On South Uist and Barra, the OHFZ is cross-cut by a number of WNW-ESE trending quartz-diorite and camptonite dykes (Fettes *et al.* 1992). Rb-Sr ages obtained from biotite grains contained within the dykes are consistent with intrusion between 304Ma and 280Ma (i.e. during the Permo-Carboniferous). Fettes *et al.* (1992) have therefore concluded that the latest deformation event along the OHFZ on South Uist and Barra must have been pre-Permo-Carboniferous in age.

In northeast Lewis, some of the pebbles contained within undeformed Permo-Triassic conglomerates (Fig. 2.5, section 2.4) appear to have been derived from pseudotachylyte- and cataclasite-bearing gneisses (Steel & Wilson 1975; Butler 1995). The sediment source region is thought to have been local (Steel & Wilson 1975), which is consistent with the pseudotachylyte- and cataclasite-bearing clasts having been derived from the nearby OHFZ (Fig. 2.5, section 2.3.3.1). Sibson (in Steel & Wilson 1975 & 1977b) has therefore suggested that cataclasis and pseudotachylyte generation along the OHFZ in northeast Lewis must pre-date the deposition of the Permo-Triassic conglomerates.

### 2.2.3.2 Isotopic ages

Isotopic ages have been obtained from a number of different fault rocks from along the OHFZ (D. C. Rex in Sibson 1977b; Kelley 1994).

Whole rock K-Ar ages obtained from samples of pseudotachylyte, cataclasite and phyllonite are presented in Sibson (1977b). The pseudotachylytes returned ages of  $442 \pm 17$  to  $2056 \pm 80$ Ma, the cataclasites yielded ages of  $1000 \pm 40$  to  $1926 \pm 76$ Ma whilst ages in the range  $394 \pm 16$  to  $947 \pm 40$ Ma were obtained from samples of lower greenschist facies phyllonite. Despite the wide range, the K-Ar ages cluster around 397Ma. Sibson (1977b) therefore concluded that the main phase of deformation along the OHFZ occurred c. 400Ma, and was broadly synchronous with Caledonian thrusting along the Moine Thrust Zone (Fig. 2.1).

More recently, laser probe  $^{40}\text{Ar}$ - $^{39}\text{Ar}$  dating of a pseudotachylyte vein from the region immediately to the west of the OHFZ has yielded a mean age of  $430 \pm 6$ Ma (Kelley *et al.* 1994). Kelley *et al.* (1994) have therefore suggested that pseudotachylyte generation in the Outer Hebrides was broadly coeval with deformation along the Moine Thrust Zone (e.g. Kelley 1988).

### 2.3.3 FAULT ROCKS

#### 2.3.3.1 Fault rock distribution

A complex array of structures and associated fault rocks, including cataclasites, pseudotachylytes, mylonites and phyllonites (Sibson 1977a & b) are exposed along the length of the Outer Hebrides Fault Zone (Fig. 2.5). Previous workers have noted systematic, regional-scale variations in the style of deformation, both parallel and perpendicular to the strike of the Outer Hebrides Fault Zone. Sibson (1977b) suggested that from north to south, there is a *progressive* along-strike decrease in the proportion of macroscopically ductile fault rocks (i.e. mylonites and phyllonites) to brittle fault rocks (i.e. cataclasites, pseudotachylytes etc.). He also observed that brittle fault rocks are most commonly preserved immediately above the base of the fault zone (i.e. in the west), whilst macroscopically ductile fault rocks (in particular phyllonites) typically outcrop in the east of the fault zone (Sibson 1977b). More recent authors (Butler 1995; Butler *et al.* 1995) have suggested that parallel to the strike of the OHFZ, there is an *abrupt* change in the nature of the fault rocks across the South Harris Shear Zones. Based on my own observations (Chapter 3) and a review of the existing literature (Sibson 1977a & b; Lailey *et al.* 1989; Walker 1990; Fettes *et al.* 1992; Butler 1995; Butler *et al.* 1995), the present author concurs with Butler (1995) and Butler *et al.* (1995) and suggests that there is a fundamental difference in the fault rock assemblages preserved to the north and south of the South Harris Shear Zones.

The *Northern Zone* of the OHFZ comprises the islands of Lewis and Scalpay and lies to the north of the South Harris Shear Zones (Fig. 2.5). The *Southern Zone* of the OHFZ comprises the Uists and Barra Isles and lies to the south of the South Harris Shear Zones (Fig. 2.5).

The Northern Zone is relatively poorly exposed and inaccessible but is characterised by a thick sequence of quartzo-feldspathic mylonites (the 'pervasive mylonites') and a number of relatively large, though laterally discontinuous, belts of green micaceous phyllonite (Figs. 2.5). Brittle fault rocks (pseudotachylytes and cataclasites) and fractures are widely, albeit heterogeneously developed in the Northern Zone (Fig 2.5). The relationship between the mylonites and pseudotachylytes is complex and is described at length in Chapters 3, 4 and 5.

The Southern Zone is characterised by an absence of pervasive mylonite. The style of deformation is extremely variable along the strike of the Southern Zone (Fig. 2.5). In the North Uist region, the OHFZ comprises a thick sequence of cataclasites and pseudotachylytes (the 'crush melange' of Sibson 1977b), which are overprinted by a crude protophyllonitic fabric (the 'early cataclastic foliation' of Sibson 1977b). The

most highly strained regions comprise a network of anastomosing phyllonitic shear zones (Fig. 2.5). The relationships between the crush melange and the phyllonitic fabrics are described in Chapter 6. In South Uist, the style of deformation is strongly influenced by the presence of the meta-igneous Corodale Gneiss (Fig. 2.5; section 2.2.2). The base of the OHFZ in this area marks the lower boundary of the Corodale Gneiss, which is defined by relatively planar eastward-dipping faults and laterally discontinuous 'pseudotachylite-ultracataclasite crush zones' (Coward 1972; Butler 1995 and Chapter 3 of the present work). A single belt of micaceous green phyllonite (the 'Usinish Phyllonite' of Butler 1995; Chapter 7 of the present work) outcrops immediately to the east of the Corodale Gneiss (Fig. 2.5). Note that the crush melange and braided phyllonite belts observed further north are *not* present on South Uist. On Barra, the OHFZ comprises several laterally discontinuous pseudotachylite-bearing crush zones which are cross-cut by a number of brittle faults (Sibson 1977b). Phyllonite does not outcrop on Barra itself, although MacInnes & Alsop (1997) have reported belts of micaceous green phyllonite on the islands of Hellisay, Gighay and Fuiay in the Sound of Barra (Fig. 3.42; Chapter 3).

#### **2.3.3.2 Distribution of low grade alteration**

Most of the rocks which outcrop within the Outer Hebrides Fault Zone have experienced significant post-Laxfordian metamorphic retrogression i.e. the mineral assemblages preserved within the OHFZ generally reflect lower temperature and pressure conditions than the mineral assemblages preserved within the protolith Lewisian gneisses to the west of the fault zone. Fettes *et al.* (1992) have defined a moderately to steeply E-dipping surface (the 'western limit of low grade alteration' in Fig. 2.5) which separates 'pristine' gneisses in the west from retrogressed gneisses in the east. In northeast Lewis and on North Uist, the limit of low grade alteration closely follows the base of the OHFZ. However, in the Park district of southeast Lewis, the retrogressed rocks lie some 4km to the east of the fault zone base. On Harris and in northern South Uist, a zone of retrogressed gneiss is developed up to 5km to the *west* of the base of the OHFZ (Fig. 2.5). In central South Uist, the limit of low grade alteration lies to the east of the fault zone base and is closely associated with the outcrop of the Usinish Phyllonite (Fig. 2.5). The fault rocks and gneisses preserved on Barra have not experienced significant post-Laxfordian alteration (Fettes *et al.* 1992, cf. MacInnes & Alsop 1997).

#### **2.3.3.3 Late-stage faults and lineaments**

The Outer Hebrides Fault Zone is cross-cut by numerous sub-vertical, E-W and NW-SE trending brittle fractures and lineaments (Sibson 1977b). The largest (km-scale) fractures are rarely exposed, but are associated with prominent topographic features

such as linear gullies and sea lochs. Smaller (m-scale) fractures are commonly exposed along coastal sections and are locally associated with sub-horizontal slickenlines and / or carbonate-rich breccias. Although the fractures clearly post-date the latest movements along the OHFZ, the fractures and lineaments rarely displace either the trace of the OHFZ or the western limit of low grade alteration.

There has been much debate amongst previous workers regarding (a) the fault zone kinematics and relative ages of the different fault rocks, and (b) the significance and timing of low grade alteration along the OHFZ. This had led different authors to reach widely differing conclusions concerning the deformation environment of the fault zone. The results of the most important onshore and offshore studies are summarised below (sections 2.3.4 & 2.3.5).

## 2.3.4 PREVIOUS WORK: ONSHORE STUDIES

### 2.3.4.1 Sibson (1977a & b)

Detailed field studies led Sibson (1977b) to conclude that the Outer Hebrides Fault Zone developed in response to westward-directed Caledonian compression. The kinematic and textural evolution of the OHFZ after Sibson (1977b) is summarised below.

- *Inception phase (D<sub>0</sub>)*: A variety of different structures formed in response to westward-directed compression. In North Uist, brittle deformation associated with the development of the crush melange (section 2.3.3) was accompanied by macroscopically ductile shearing and the development of a crude protomylonitic fabric (the 'early cataclastic foliation' of Sibson 1977b) further east. In southeast Lewis, deformation was localised along a broad, eastward dipping ductile shear zone (= pervasive mylonite; section 2.3.3).
- *Main thrust phase (D<sub>1</sub>)*: Continued top-to-the-W thrusting in North Uist was associated with ductile shearing along belts of highly strained, greenschist facies mylonite (= phyllonite; section 2.3.3). In southeast Lewis, mylonitisation was accompanied by transient frictional melting, to produce a complex assemblage of mutually overprinting mylonites and pseudotachylytes (Sibson 1980).
- *Lag sliding phase (D<sub>2</sub>)*: A phase of normal (top-to-the-E) movements followed the cessation of active thrusting along the OHFZ. The extensional displacements were accommodated by 'down-dip' shearing along pre-existing belts of mylonite and phyllonite.

*Phase of late faulting (D<sub>3</sub>):* Late faults are commonly observed at the margins of crush zones and phyllonite belts and are thought to have developed in response to continued 'lag sliding' down the dip of the OHFZ.

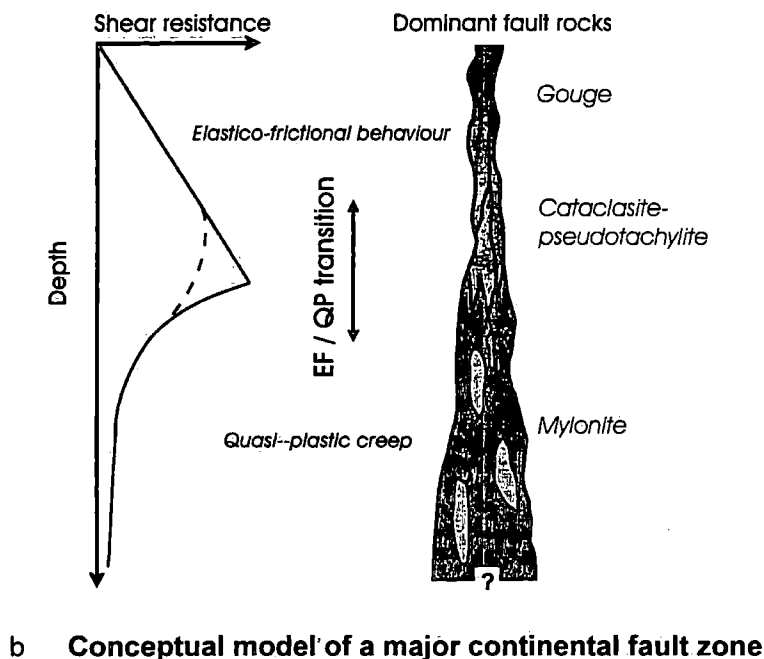
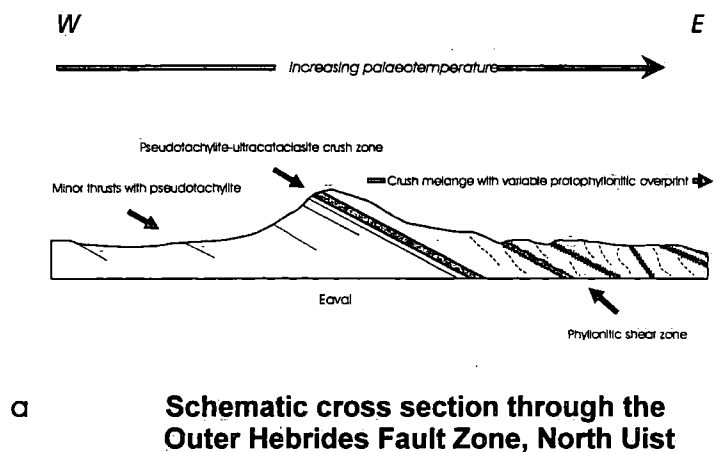


**Figure 2.6** (a) Schematic cross-section across the Outer Hebrides Fault Zone on North Uist after Sibson (1977a & b). Note the distribution of the different fault rocks. (b) Conceptual model of a major continental fault zone, modified from Sibson (1977a, 1982, 1983). The crush melange / pseudotachylite was thought to have been generated in the 'elastico-frictional regime', whilst the phyllonitic shear zones were developed entirely within the 'quasi-plastic regime'.

It was thought that the cataclasites, pseudotachylytes, mylonites and phyllonites all formed in response to top-to-the-W thrusting and must therefore be of broadly the same age (Sibson 1977b). On North Uist, it was also observed (a) that the crush melange consistently outcrops adjacent to the base of the OHFZ and has *not* suffered intense post-Laxfordian metamorphism; and (b) that the phyllonite belts consistently outcrop to the east of the crush melange and are associated with intense, post-Laxfordian greenschist facies metamorphism and hydrothermal alteration.

Sibson (1977a & b) suggested that the pattern of brittle deformation in the west and ductile, greenschist facies deformation in the east reflects a progressive increase in palaeotemperature from west to east across the present-day strike of OHFZ (Fig. 2.6a). The apparent eastward increase in palaeotemperature could be explained if the outcrop of the OHFZ on North Uist represents an exhumed depth profile through the continental crust. It was argued that brittle faulting, cataclasis and pseudotachylyte generation took place at relatively low temperatures and pressures within the upper-crustal 'elastico-frictional regime' (Fig. 2.6b). In contrast, the continuous 'quasi-plastic' deformation observed in the phyllonite belts must have occurred at relatively high temperatures and pressures i.e. at greater depths within the crust (Fig. 2.6b) (Sibson 1977a & b).

The pseudotachylyte-mylonite assemblage observed in southeast Lewis was thought to have developed at depths equivalent to the elastico-frictional / quasi-plastic transition zone (Sibson 1977b but cf. Sibson 1980 and White 1996) (Fig. 2.6b).

#### **2.3.4.2 White & Glasser (1987) and Walker (1990)**

Walker (1990) proposed that the Outer Hebrides Fault Zone experienced a two phase kinematic history, with at least two phases of fault rock generation. The kinematic and textural evolution of the OHFZ after Walker (1990) is summarised below.

- *Phase of Caledonian thrusting* A broad zone of quartzo-feldspathic 'r-type' (White 1982) mylonites (= pervasive mylonite) developed during top-to-the-W thrusting and is presently exposed in southeast Lewis. In the Uists, thrusting was associated with brittle deformation and the widespread development of 'microbreccia' (= crush melange). The r-type mylonites were deformed at relatively deep crustal levels ( $\geq 12$ km depth), whilst brecciation took place at no greater than 7 kilometres depth.
- *Phase of ?Tertiary extension* Top-to-the-E extension was associated with the development of 'c-type' (White 1982) mylonite bands (= phyllonite).

Mylonitisation was accompanied by intense syn-tectonic greenschist facies metamorphism and hydrothermal activity.

The conclusions of White & Glasser (1987) differ significantly from those of Sibson (1977a & b). The former authors argued that the *c*-type mylonites (phyllonites) are significantly *younger* than either the microbreccias (crush melange) or the *r*-type mylonites (pervasive mylonites). The present day outcrop of the OHFZ cannot therefore represent an exhumed crustal depth profile through the continental crust (White & Glasser 1987).

On the basis of microstructural and geochemical analyses, it was argued that extensional deformation was accompanied by an influx of chemically active, hydrous fluids into the fault zone (Walker 1990). Microstructural observations suggested that the fluids initially entered the fault zone along fractures within the microbreccia. The fluids were responsible for the breakdown of plagioclase and K-feldspar to aggregates of fine grained sericite, epidote and clay minerals along fracture planes (White & Glasser 1987; Walker 1990). It was suggested that grain size reduction further facilitated fluid influx into the fault zone (White & Glasser 1987), whilst the growth of intrinsically weak sheet silicates would have promoted localised deformation in the most highly retrogressed regions (Walker 1990). This combination of retrogression and strain localisation resulted in the development of *c*-type mylonite bands.

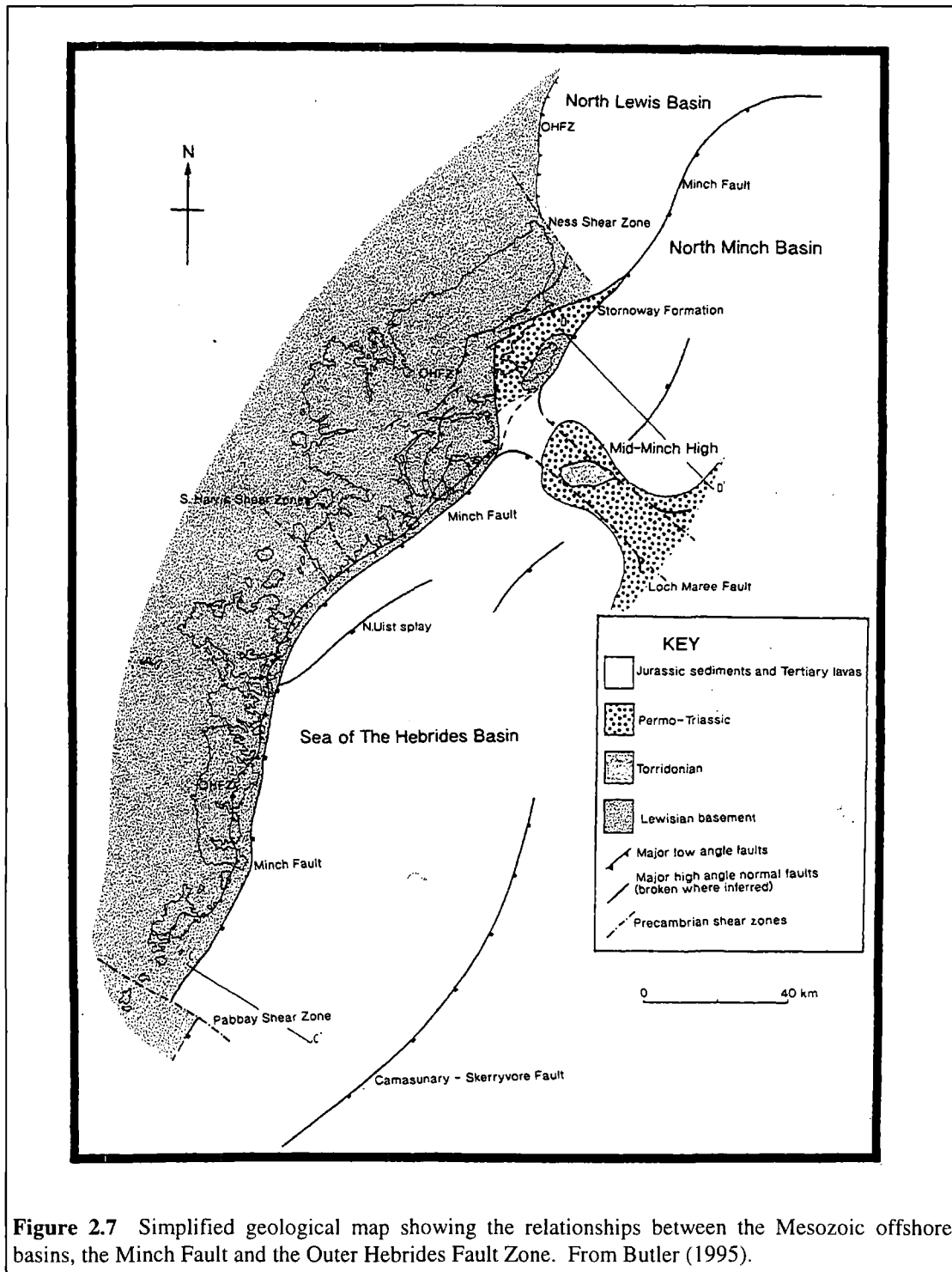
Walker (1990) has presented whole-rock major and trace element analyses of the Lewisian protoliths (banded gneiss and Corodale gneiss) and a variety of different fault rocks (including samples of microbreccia and *c*-type mylonite). The results of geochemical mass balance calculations suggest (a) that the microbreccias have experienced a slight gain in SiO<sub>2</sub> relative to the banded gneiss protoliths and (b) that the *c*-type mylonites have experienced a significant loss in SiO<sub>2</sub> and a concomitant gain in MgO and Fe<sub>2</sub>O<sub>3</sub> relative to the banded gneiss protoliths. In order to bring about the observed chemical and mineralogical changes, Walker (1990) concluded that the fluids must have been enriched in magnesium and iron and that they entered the fault zone at temperatures of between 250°C and 350°C. It was postulated that the fluids were derived from basic magmas associated with Tertiary rifting and crustal extension in the North Atlantic region.

#### **2.3.4.3 Butler (1995) and Butler *et al.* (1995)**

On the basis of extensive field mapping, Butler (1995) proposed that the Outer Hebrides Fault Zone was active from the late Laxfordian to the Mesozoic. Following the earliest phase of deformation along the OHFZ, Butler (1995) has inferred significant displacements across the South Harris Shear Zones (SHSZ) (Fig. 2.5). The

kinematic and textural evolution of the OHFZ and SHSZ after Butler (1995) is summarised below.

- *Late Laxfordian - Grenvillian thrusting along the OHFZ* A thick belt of upper greenschist facies mylonite (= pervasive mylonite) developed during top-to-the-NW thrusting. The mylonites are presently exposed to the north of the SHSZ (i.e. only in the Northern Zone; section 2.3.3), although Butler (1995) has inferred that they may have originally extended southward.
- *Grenvillian displacements along the SHSZ* Oblique-dextral movements across the steeply dipping South Harris Shear Zones offset the rocks to the south of the SHSZ towards the NW, relative to the rocks to the north of the SHSZ. As a result, the inferred southward continuation of the upper greenschist facies mylonite belt is not exposed onshore in the Outer Hebrides.
- *Caledonian thrusting along the OHFZ* Widespread cataclasis, pseudotachylyte generation and brittle faulting was associated with top-to-the-NW thrusting along the length of the OHFZ.
- *Caledonian strike-slip along the OHFZ* The onset of top-to-the-NE sinistral strike-slip was associated with the influx of hydrous fluids into the fault zone. The fluids were responsible for widespread syn-tectonic retrogression and the development of the lower greenschist facies phyllonitic shear zones.
- *Late Caledonian extension along the OHFZ* Top-to-the-ESE (locally top-to-the-SSW) extensional strains were focused almost exclusively into the pre-existing phyllonitic shear zones.
- *Mesozoic steep normal faulting* Steeply dipping normal faults accommodated top-to-the-E or top-to-the-NE extension. The faults which are exposed onshore may have been associated with the development of the offshore North Minch and Sea of the Hebrides Basins to the east (Fig. 2.7).



On the basis of field and microstructural observations, it has been suggested that fluid influx and phyllonitisation along the OHFZ were synchronous with and ultimately controlled by a change in the kinematic regime, from top-to-the-NW thrusting to top-to-the-NE sinistral strike-slip (Butler *et al.* 1995, cf. White & Glasser 1987). Butler (1995) and Butler *et al.* (1995) have therefore argued that the phyllonite belts *originated* during sinistral strike-slip and were subsequently *reactivated* during top-to-

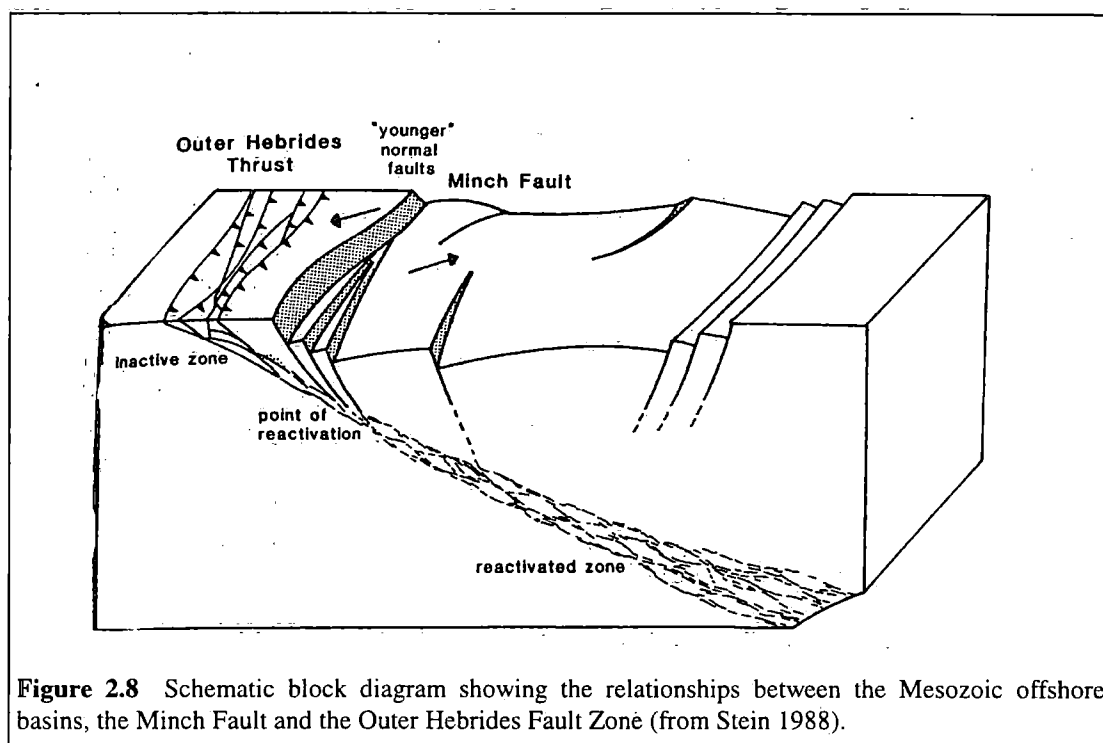


**Figure 2.8** Schematic block diagram showing the relationships between the Mesozoic offshore basins, the Minch Fault and the Outer Hebrides Fault Zone (from Stein 1988).

the-ESE extension. The observation that subsequent extensional strain was focused almost entirely into the pre-existing phyllonite belts led Butler *et al.* (1995) to conclude that the phyllonite belts constitute reaction softened zones which are weak, relative to both the Lewisian gneisses and to the earlier cataclastic fault rocks. It was suggested that the presence of rheologically weak phyllonite belts along the Outer Hebrides Fault Zone strongly influenced the architecture of the offshore Sea of the Hebrides and North Minch Basins (Butler *et al.* 1995, cf. Stein 1988).

### 2.3.5 PREVIOUS WORK: OFFSHORE STUDIES

#### 2.3.5.1 Shallow structure: Stein (1988)

The structural development of the Mesozoic offshore North Minch, North Lewis and Sea of the Hebrides basins has been studied using shallow seismic reflection data ( $\leq 6$ s two-way travel time) (Stein 1988) (Fig. 2.7). The seismic profiles suggest that the offshore basins are half-graben structures developed in the hangingwall of the Outer Hebrides Fault Zone. The basins are infilled by packages of gently westward dipping ?late Palaeozoic to Mesozoic sediments.

The Sea of the Hebrides basin and the northern North Minch basin are bounded to the west by the steeply E-dipping Minch Fault. The western boundary of the southern North Minch basin is defined by a number of steeply dipping normal faults which splay off from the main Minch Fault near the mouth of Stornoway Bay (Fig. 2.7). These normal faults are locally exposed onshore (section 2.5) and define the western margin of the Permo-Triassic Stornoway Formation (section 2.4). The North Lewis

basin lies en-echelon to the North Minch Basin and is bounded to the west by the OHFZ and to the east by the Minch Fault (Fig. 2.7). This en-echelon basin geometry is thought to reflect a major strike-swing in the OHFZ to the north of the Butt of Lewis (Fig. 2.7).

The inferred trace of the Minch Fault clearly follows the onshore outcrop of the Outer Hebrides Fault Zone. At depth ( $\cong$  5s two-way travel time), the Minch Fault appears to root down into the OHFZ (Fig. 2.8). Stein (1988) has suggested that extensional displacements on the Minch Fault were transferred at depth onto the OHFZ. The shallow seismic reflection data are therefore consistent with *partial* reactivation of the OHFZ as an extensional detachment, probably during the late Palaeozoic and Mesozoic.

#### **2.3.5.2 Deep structure: Smythe *et al.* (1982), Peddy (1984) and Smythe (1987)**

The deep structure of the Caledonian foreland has been studied using deep seismic reflection data ( $\leq$  15s two-way travel time) (e.g. Smythe *et al.* 1982). The Outer Hebrides Fault Zone is visible on the MOIST and WINCH surveys (Smythe 1987; see Fig. 2.9) as a strong, moderately eastward dipping reflector which can be traced almost to the base of the continental crust. In the uppermost 15km of the sections, the sediments of the North Lewis and North Minch basins produce strong, W-dipping reflectors in the hangingwall of the OHFZ. In contrast, the Lewisian basement in the footwall of the OHFZ is remarkably unreflective (Smythe *et al.* 1982). On migrated, depth converted profiles, the OHFZ appears to flatten out parallel to the Moho (at approximately 25km depth) and does not, apparently, continue into the upper mantle. Peddy (1984) suggested that the sediments preserved in the overlying North Lewis and North Minch basins have significantly lower seismic velocities than the Lewisian basement. As a result, the apparent depths of the OHFZ and Moho reflectors beneath the hangingwall basins calculated by Smythe *et al.* (1982) may be incorrect. Seismic modelling, which takes into account variations in seismic velocity, suggests that the OHFZ cuts the base of the crust and produces an apparent 3km normal displacement of the Moho reflector (Peddy 1984).

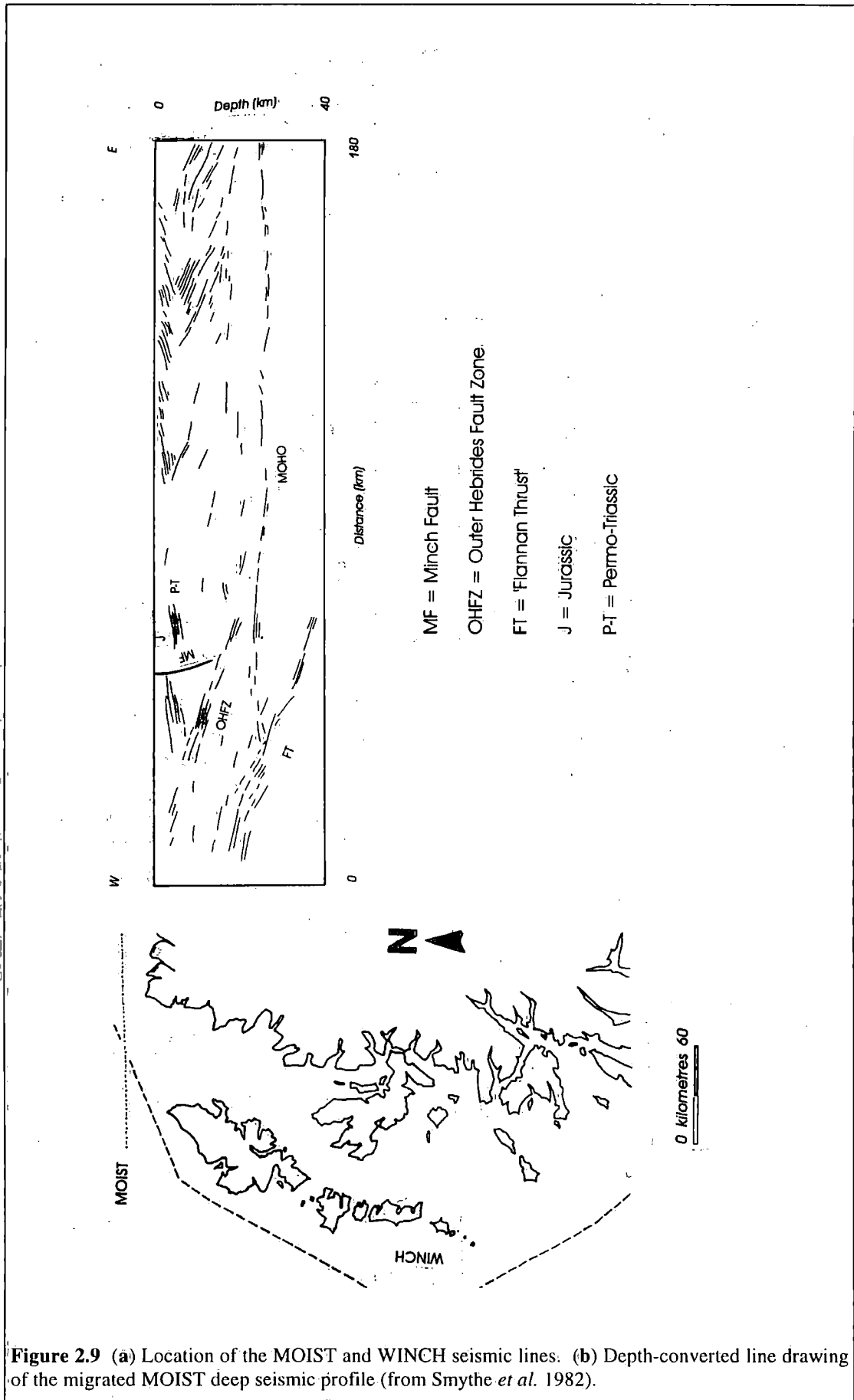


**Figure 2.9** (a) Location of the MOIST and WINCH seismic lines. (b) Depth-converted line drawing of the migrated MOIST deep seismic profile (from Smythe *et al.* 1982).

## 2.4 THE STORNOWAY FORMATION

The Stornoway Formation comprises a succession ( $\leq 4000\text{m}$  thick) of undeformed, unmetamorphosed conglomerates, red sandstones and conglstones (Steel & Wilson 1975). The Formation is exposed to the north and east of Stornoway and at Arnish Point (NB 430 306) to the south (Figs. 2.5). Analysis of the clasts contained within the conglomerates suggests that the Stornoway Formation sediments were derived from both 'pristine' Lewisian gneisses and from fault rocks (pseudotachylytes and phyllonites) associated with the Outer Hebrides Fault Zone (Sibson in Steel & Wilson 1975; Sibson 1977b; Butler 1995).

Sedimentological studies (Steel & Wilson 1975) have identified three principal 'depositional units' within the Stornoway Formation. Each unit comprises a number of westward-dipping, coarsening-upwards  $\pm$  fining-upwards sedimentary sequences. Deposition appears to have been markedly diachronous and the units young to the west. Steel & Wilson (1975) have suggested that the coarsening-upwards sequences are the result of continued uplift of the sediment source region in the footwalls of a number of E-dipping syn-tectonic normal faults (Fig. 2.10). The diachronous nature of the sediments can be explained by the progressive westward migration of these basin-bounding faults through time. The faults which define the present-day western margin of the Stornoway Formation (Figs. 2.5 & 2.7) are thus believed to be the youngest of a series of E-dipping normal faults. The location of the earlier faults beneath the Eye Peninsula has been inferred from the distribution of the different sedimentary sequences (Steel & Wilson 1975) (Fig. 2.10).

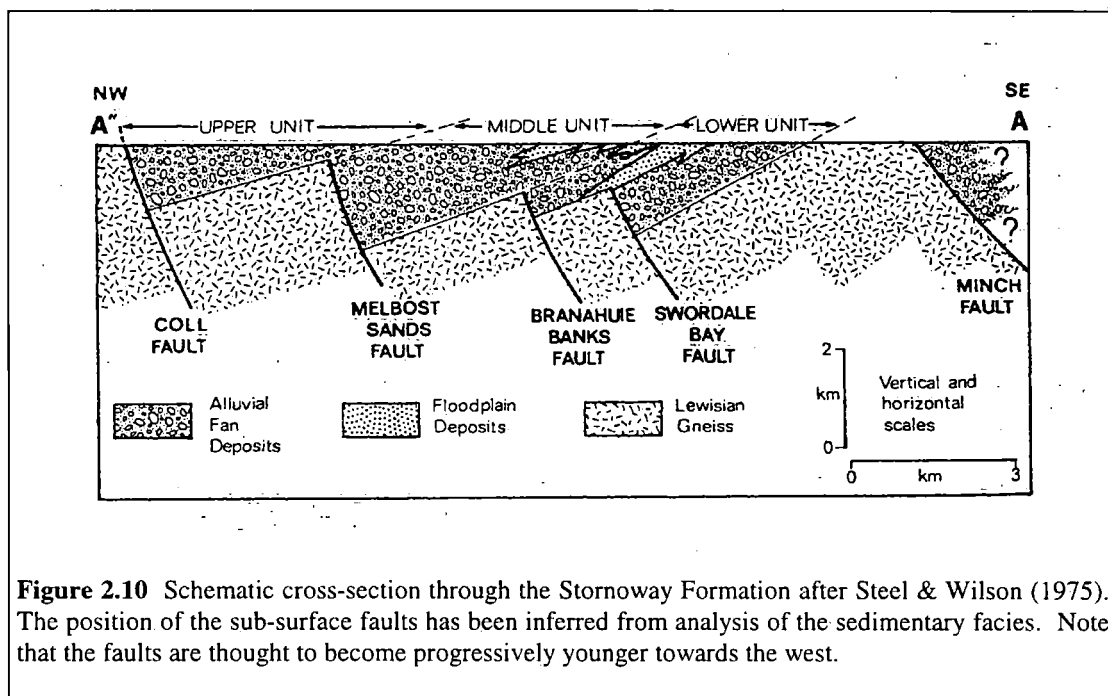


**Figure 2.10** Schematic cross-section through the Stornoway Formation after Steel & Wilson (1975). The position of the sub-surface faults has been inferred from analysis of the sedimentary facies. Note that the faults are thought to become progressively younger towards the west.

The present-day basin bounding faults appear to be associated with a number of steeply dipping normal faults which are developed within the adjacent Lewisian gneisses. The geometry and style of deformation associated with these normal faults is described below (Chapter 3).

## 2.5 SUMMARY

It is clear that a wide variety of different fault rocks are preserved along the length of the Outer Hebrides Fault Zone. In particular, it has been recognised that:

- The different fault rocks may have developed at different depths within the continental crust.
- The belt of pervasive mylonites exposed in southeast Lewis developed in response to top-to-the-NW thrusting and was deformed at relatively deep levels within the crust.
- The development of the phyllonite belts was controlled by syn-tectonic greenschist facies metamorphism and fluid influx into the fault zone. Fluids entered the fault zone through pre-existing fractures in the crush melange.
- The Outer Hebrides Fault Zone appears to have had a profound influence on the geometry and location of the Mesozoic North Minch, North Lewis and Sea of the Hebrides basins.
- The latest movements on the Outer Hebrides Fault Zone were probably synchronous with normal faulting and the deposition of the Permo-Triassic Stornoway Formation.

However, a number of important questions remain to be answered:

- (1) To determine the relative age and kinematic regime under which the different fault rocks were developed, and to relate this to the spatial distribution and timing of fluid influx into the fault zone.
- (2) To determine the range of operative deformation mechanisms associated with each group of fault rocks and how these mechanisms may have evolved with increasing strain.
- (3) To determine the precise mechanisms of fluid infiltration into the fault zone and how these mechanisms may have evolved with increasing strain.

- . (4) To understand the interactions between fluid influx, the operative deformation mechanisms and the rheological evolution of the fault zone.
- . (5) To synthesise these results in order to determine the underlying controls on the pattern of the reactivation observed along the Outer Hebrides Fault Zone.

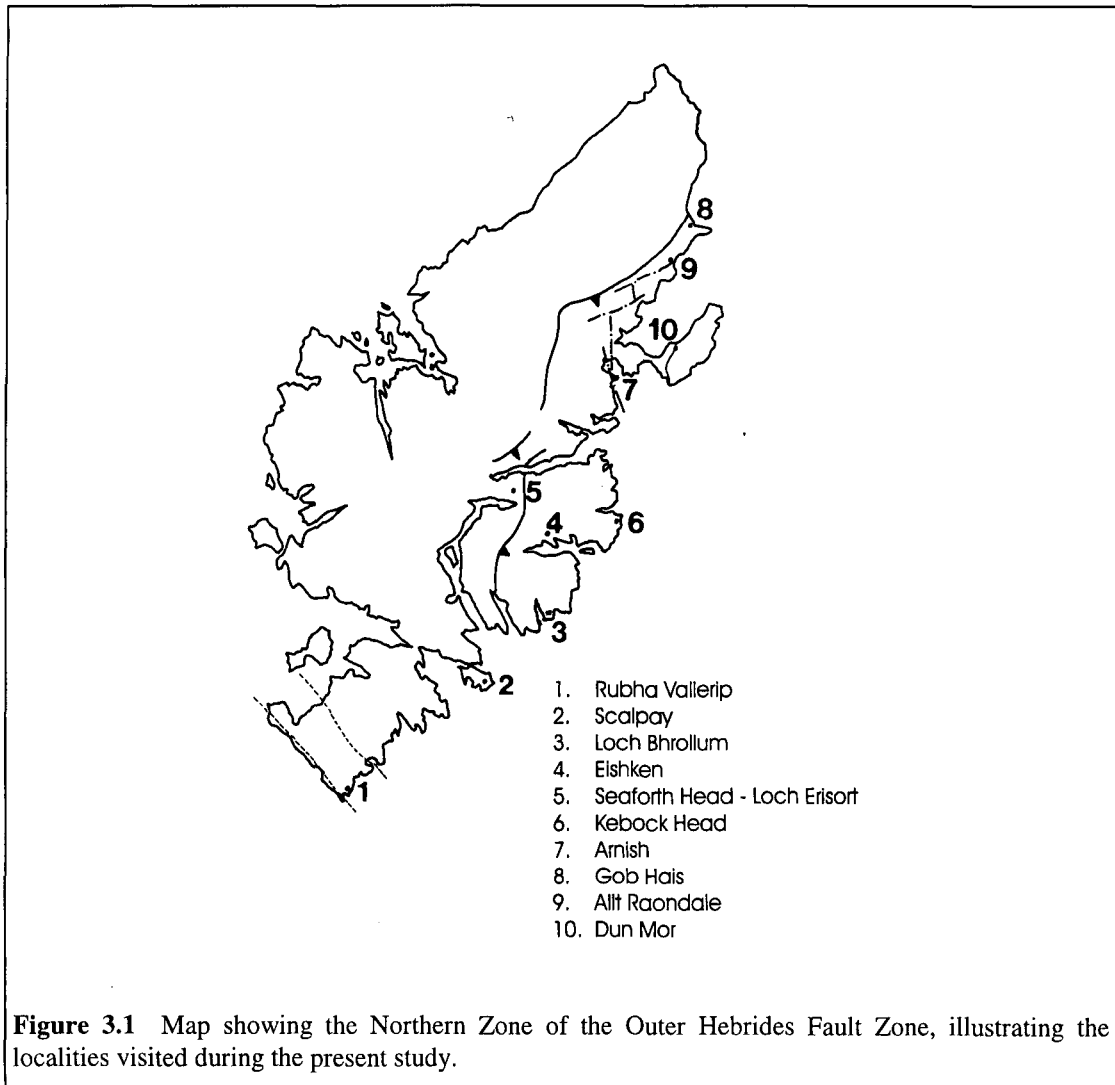
The aim of the latter part of this thesis is to begin to answer some of these questions.

### 3. THE OUTER HEBRIDES FAULT ZONE: OVERVIEW

#### 3.1 INTRODUCTION

The aim of this chapter is to provide a comprehensive description of the kinematic, textural and metamorphic evolution of the Outer Hebrides Fault Zone. The fault rock descriptions are based primarily upon field and generalised microstructural observations made during the present study, which are supplemented by the observations of previous authors where necessary. The chapter is organised on an island-by-island basis, the fabrics preserved in each geographical area being described in chronological order. Unfortunately, a degree of repetition is inevitable.

The final section (section 3.7) summarises the spatial and temporal relationships between the different fault rocks, and identifies the possible mechanisms which could account for the apparently long-lived nature of the Outer Hebrides Fault Zone. These mechanisms will then be discussed in greater detail in the subsequent chapters of this thesis (Chapter 4 to 8).

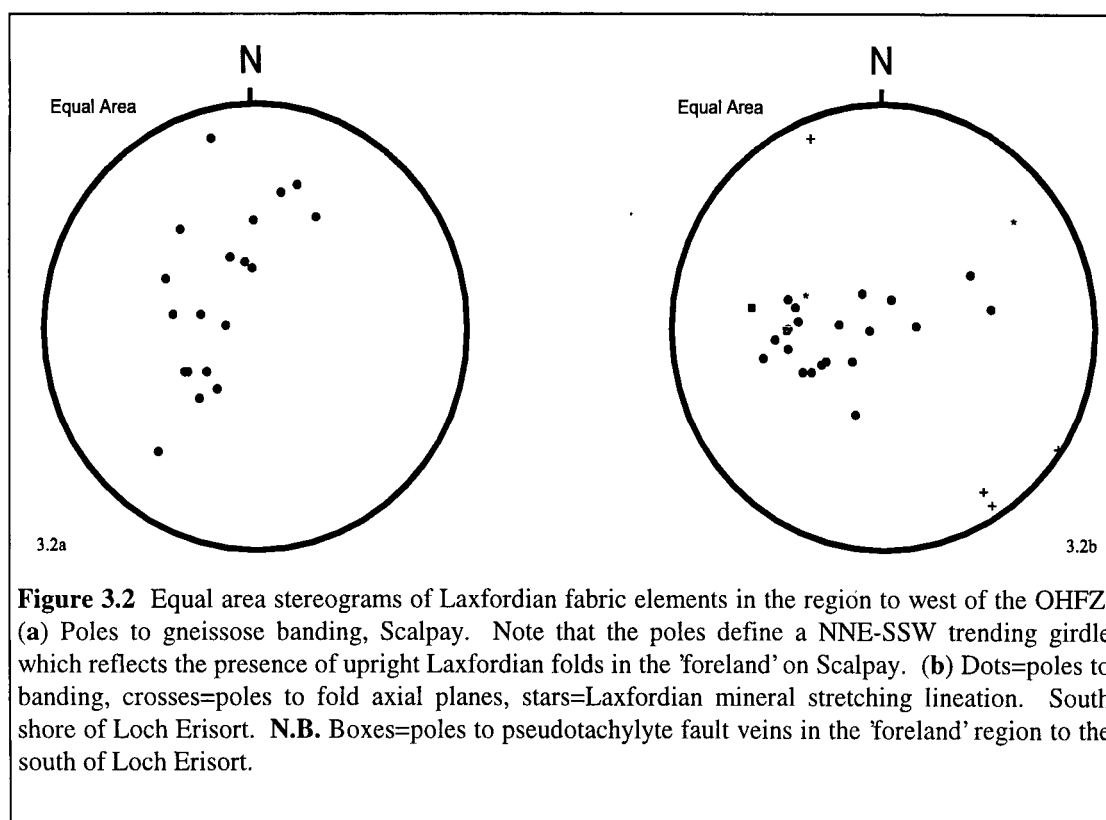


### 3.2 THE NORTHERN ZONE: LEWIS & SCALPAY

The following section comprises descriptions of (1) the Lewisian protoliths (section 3.2.1), (2) the pervasive mylonite belt preserved in southeast Lewis and Scalpay (section 3.2.2), (3) the phyllonite belts preserved in southeast Lewis and Scalpay (section 3.2.3) and (4) the steep normal faults preserved in northeast Lewis (section 3.2.4). There are significant geographical variations along the OHFZ throughout Lewis and Scalpay. Sections 3.2.2 to 3.2.4 are therefore divided into separate geographical localities.

#### 3.2.1 LEWISIAN PROTOLITHS OF SOUTHEAST LEWIS AND SCALPAY

The Lewisian rocks preserved within and immediately to the west of the Outer Hebrides Fault Zone in Lewis and on Scalpay comprise quartzo-feldspathic banded gneisses, amphibolite pods ( $\leq 200\text{m}$  thick) (the Older Basics; section 2.2.2.1), amphibolite sheets ( $\leq 2\text{m}$  thick) (the Younger Basics; section 2.2.2.4) and Laxfordian pegmatites (section 2.2.2.4). Older Basic pods are widely observed throughout southeast Lewis (e.g. around Loch Sgibacleit, Loch Bhrollum and at Kebock Head; Fig. 3.1), but are relatively rare on Scalpay (Fig. 3.1). In contrast, extensive Laxfordian pegmatite sheets ( $\leq 5\text{m}$  thick) are well developed on Scalpay, but are less commonly observed in southeast Lewis.



The predominantly E-dipping gneissose banding is locally deformed by shallowly plunging cm- to m-scale folds. The folds, which are thought to be of Laxfordian age ('D13' of Fettes *et al.* 1992; section 2.2.4 of the present work), are associated with vertical to moderately E-dipping axial planes (Figs. 3.2a & b).

The gneisses preserved in the 'foreland' region in Lewis have not experienced significant post-Laxfordian (post 'D13' of Fettes *et al.* 1992) retrogression. In contrast, the gneisses preserved in the footwall of the OHFZ on Scalpay have suffered significant post-Laxfordian retrogression and hydration under greenschist facies conditions (Fig. 2.5).

### 3.2.2 PERVASIVE MYLONITES

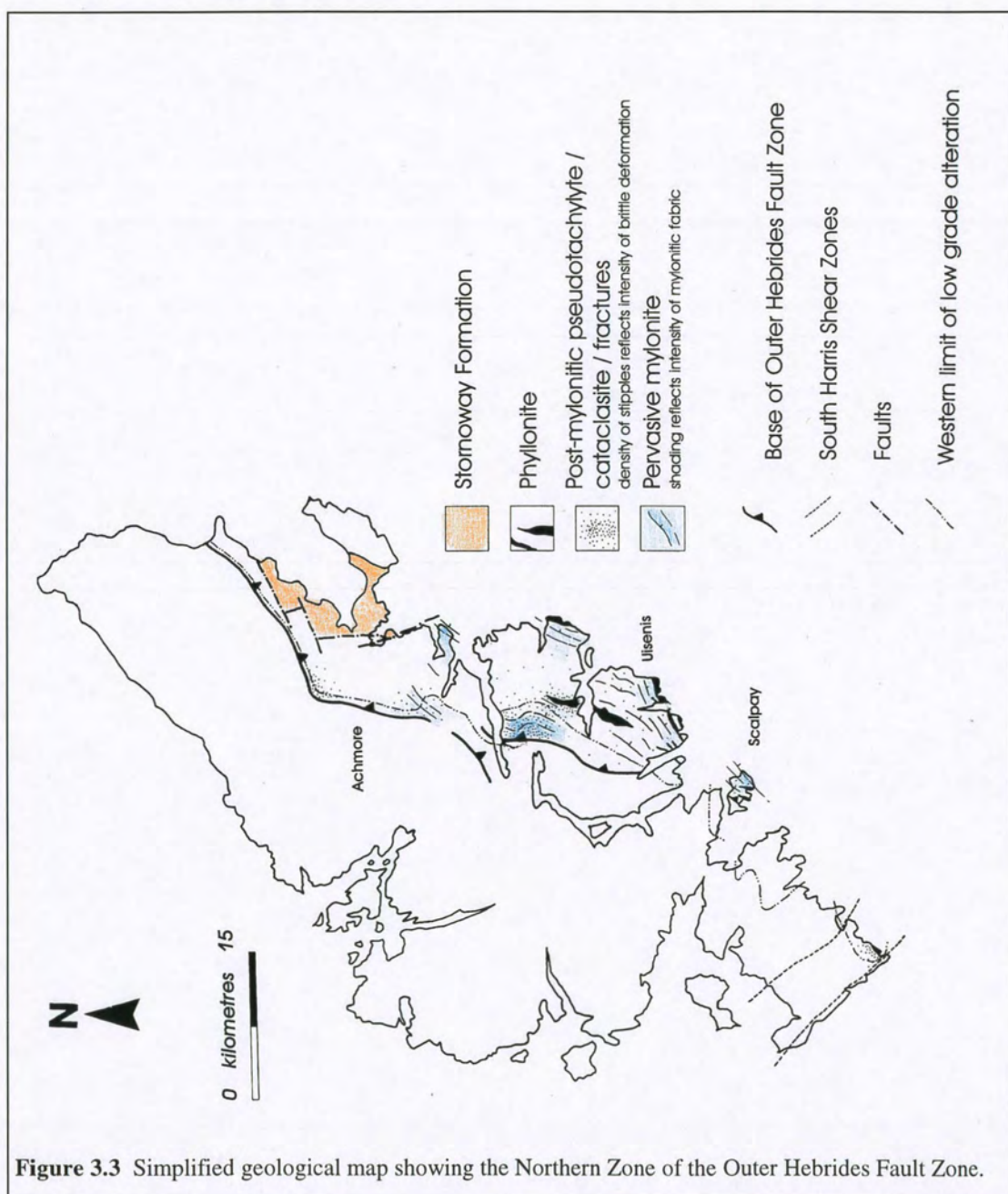


**Figure 3.3** Simplified geological map showing the Northern Zone of the Outer Hebrides Fault Zone.

A belt of eastward dipping quartzo-feldspathic mylonites (the 'pervasive mylonites'; section 2.3.3.1) outcrops extensively in southeast and central Lewis and on Scalpay (Fig. 3.3). Exposure is poor, but the belt is known to extend from Scalpay in the south, at least as far as Achmore (NB 310 300) in the north (Sibson 1977b; Fettes *et al.* 1992; Butler 1995) (Figs. 3.1 & 3.3). The pervasive mylonites are locally overprinted by belts of lower greenschist facies phyllonite (Figs. 3.1 & 3.3). The relationship between the pervasive mylonites and phyllonite belts is discussed further in section 3.2.3.

Fettes *et al.* (1992) have compiled a form-line map illustrating the general trend of the mylonitic foliation in Lewis and on Scalpay (Fig. 3.3). Although there are significant localised variations, the trace of the foliation defines two regional-scale strike-swings. The northern strike-swing takes place between Achmore, where the foliation trends ENE-WSW or NE-SW, and Loch Erisort, where the foliation strikes predominantly N-S or NNE-WSW (Fig. 3.3). Poor exposure and the effects of later brittle deformation (Fettes *et al.* 1992; section 2.3.3.3 of the present work) preclude any analysis of the geometry of the northern strike-swing. The southern strike-swing appears to be very abrupt and occurs between Uisenis (NB 337 068) and Loch Bhrollum (NB 322 031) (Figs. 3.1 & 3.3). The foliation strikes predominantly NNE-WSW to the north of Uisenis, but strikes NE-SW along the southeast coast of Lewis and on Scalpay.

During the present survey, N-S trending segments of the pervasive mylonite belt have been studied in detail around Loch Sgibacleit and Loch Erisort (NB 295 164 - NB 305 197), and in the region to the west of Kebock Head (NB 406 140 - 520 138). A NE-SW trending segment of the pervasive mylonite belt has been studied on Scalpay (NG 225 950 - NG 247 946) (Fig. 3.1).

### **3.2.2.1 Loch Sgibacleit to Loch Erisort**

A N-S trending segment of the pervasive mylonite belt outcrops in the region between Loch Sgibacleit (NB 295 164) and Loch Erisort (NB 294 202) (Figs. 3.3 & 3.4). Relatively unmodified Lewisian gneisses in the region immediately to the west of the pervasive mylonite belt are well exposed in road cuttings to the south of Loch Erisort (NB 273 195 to NB 305 196). The mylonites themselves are well exposed on the hills to the north and south of Loch Sgibacleit (Mullach Breac Malasgair, NB 301 166 & Creag na h-Uamha, NB 306 153) (Fig. 3.4).

**Localised deformation in the 'foreland'**

Evidence for localised deformation (e.g. bands of protomylonite, brittle faults and pseudotachylite veins, breccias and quasi-conglomerates) in the 'foreland' is widespread, but is never very intense. Overall, fault rocks probably account for less than 5% of the total rocks exposed in the 'foreland'.

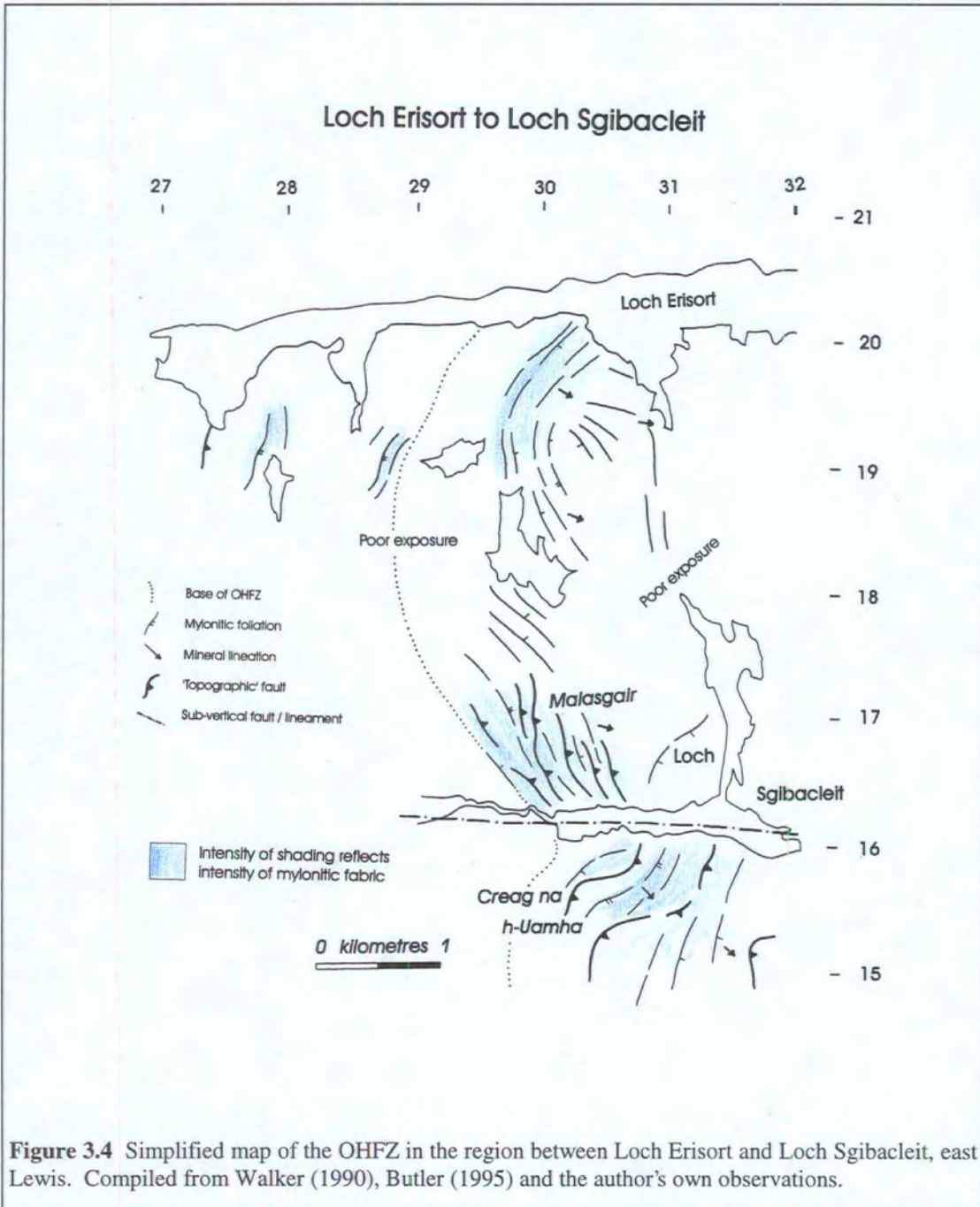


**Figure 3.4** Simplified map of the OHFZ in the region between Loch Erisort and Loch Sgibacleit, east Lewis. Compiled from Walker (1990), Butler (1995) and the author's own observations.

The E-dipping bands of protomylonite are typically associated with WNW-ESE trending mineral lineations. Well developed  $\sigma$ -type feldspar porphyroclasts observed in surfaces parallel to the mineral lineation and perpendicular to the foliation are

consistent with top-to-the-W directed shear during mylonitisation. The predominantly eastward dipping brittle faults produce apparent compressional thrust-sense (i.e. top-to-the-W) displacements of the gneissose banding. In contrast, the geometries of pseudotachylyte injection veins (Sibson 1975) are consistent with pseudotachylyte generation during localised compression *or* extension (i.e. top-to-the-E).

***The pervasive mylonite belt around Loch Sgibacleit***

Around Loch Sgibacleit, the pervasive mylonite belt comprises a predominantly E- or SE-dipping assemblage of protomylonites, mylonites, ultramylonites and concordant pseudotachylyte veins (Figs. 3.5 & 3.6). The mylonitic fabrics and 'early' concordant pseudotachylyte veins are themselves deformed by 'late' concordant and discordant pseudotachylyte-bearing fault zones, brittle folds and by a network of brittle fractures and joints.

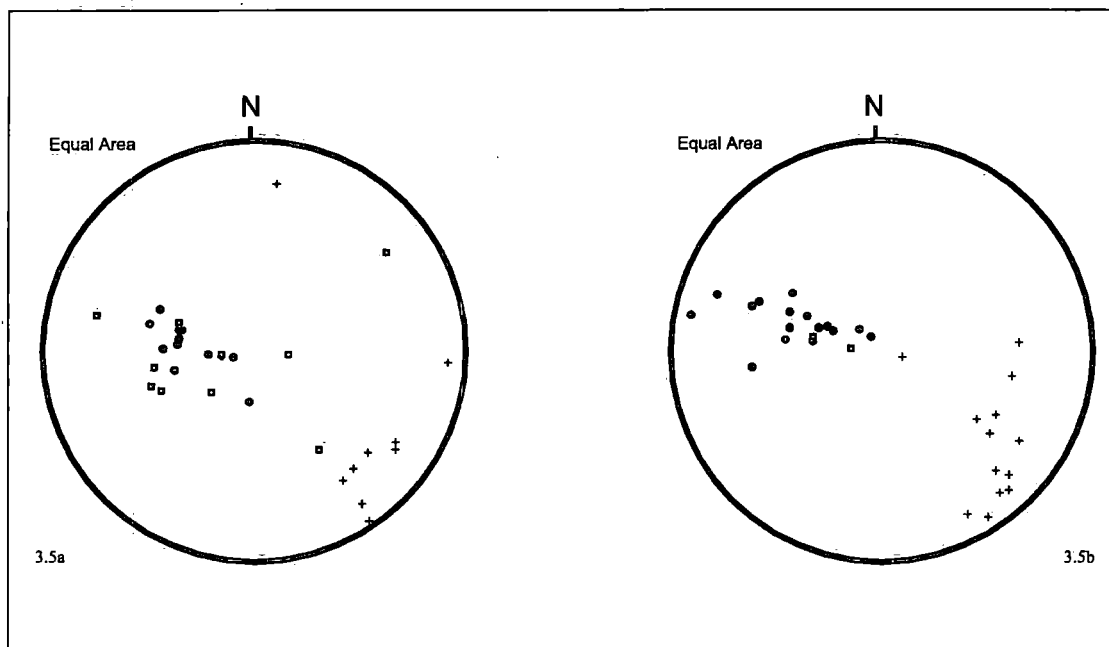


**Figure 3.5** Equal area stereograms of mylonitic fabric elements within the lower amphibolite facies pervasive mylonite belt, Loch Sgibacleit region. (a) Dots=poles to mylonitic foliation, crosses=mineral lineations, boxes=poles to pseudotachylyte fault veins. North shore of Loch Sgibacleit. (b) Dots=poles to mylonitic foliation, crosses=mineral lineations, boxes=poles to pseudotachylyte fault veins. South shore of Loch Sgibacleit.

The mylonitic fabrics are associated with a strong, SE- to ESE-plunging mineral lineation (Figs. 3.5a & b). Kinematic indicators ( $\sigma$ - and  $\delta$ -type feldspar porphyroclasts and asymmetric shear bands) viewed in surfaces parallel to the mineral lineation and perpendicular to the foliation are consistent with top-to-the-NW or -WNW shearing during mylonitisation.

The geometries of the concordant and discordant pseudotachylyte-bearing fault zones which overprint the mylonitic foliation are consistent with either localised compression or localised extension during pseudotachylyte generation. Similarly, the brittle faults, which themselves post-date pseudotachylyte generation, appear to have accommodated either extensional (top-to-the-ESE) or compressional (top-to-the-WNW) displacements.

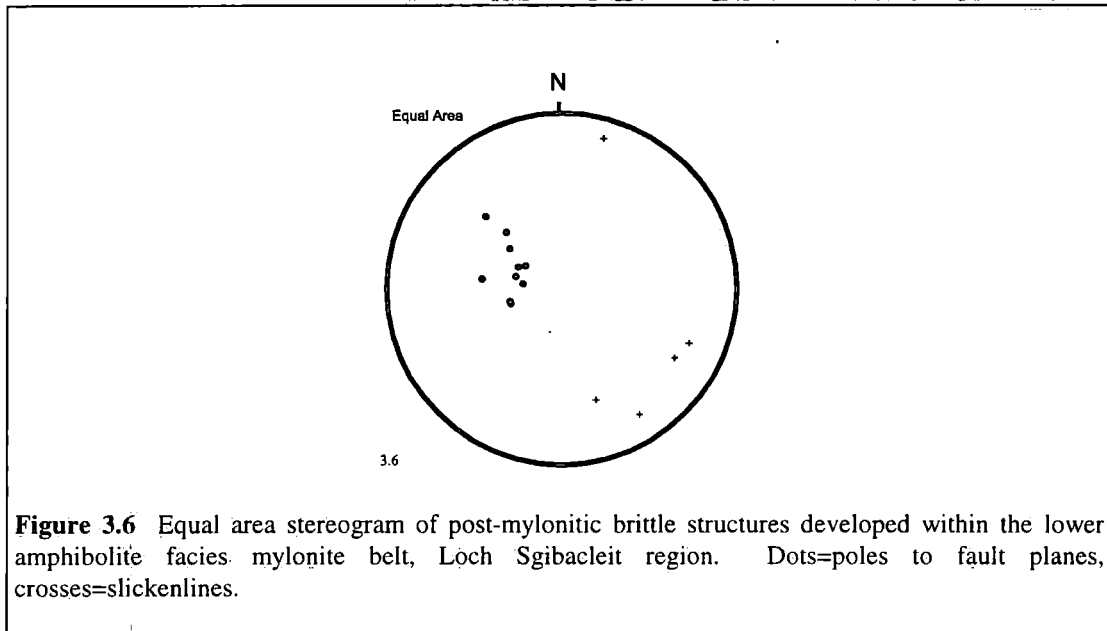


**Figure 3.6** Equal area stereogram of post-mylonitic brittle structures developed within the lower amphibolite facies mylonite belt, Loch Sgibacleit region. Dots=poles to fault planes, crosses=slickenlines.

### ***Microstructure***

***Mylonites.*** The mylonites are characterised by feldspar (oligoclase  $\pm$  K-feldspar), garnet or hornblende porphyroclasts which 'float' in an ultrafine grained polyminerally matrix. The matrix comprises polycrystalline quartz and feldspar ribbons and / or bands of viscously deformed pseudotachylyte (Sibson 1980; White 1996; Chapter 4 of the present work).

The porphyroclasts are typically well rounded and are cross-cut by intragranular fractures. The fractures are infilled by aggregates of recrystallised feldspar, hornblende and / or viscously deformed pseudotachylyte. Feldspar, hornblende and garnet appear to have been stable during mylonitisation and there is little evidence to suggest that the fault rocks have experienced significant syn- or post-tectonic retrogression.

### ***Summary and discussion***

The mylonite belt exposed in the Loch Sgibacleit region developed under a regime regional top-to-the-NW thrusting. The apparently stable mineral assemblage of garnet, hornblende and moderately calcic plagioclase is consistent with either (a) deformation in an amphibolite facies environment, or with (b) a meta-stable mineral

assemblage which survived deformation at temperatures and pressures either above or below amphibolite facies conditions. However, the observed deformation microstructures (extensive recrystallisation of quartz and partial recrystallisation and / or fracturing of feldspar and hornblende grains) suggest that thrusting took place at temperatures and pressures consistent with lower amphibolite facies conditions (White 1996 and Chapter 4 of the present work). Microstructural evidence (Sibson 1980; White 1996; Chapter 4 of the present work) suggests that the 'early' concordant pseudotachylyte veins may have developed *synchronously* with macroscopically ductile top-to-the-NW thrusting and mylonitisation.

Brittle faulting and generation of both concordant and discordant pseudotachylyte-bearing structures took place following the cessation of mylonitisation. Pseudotachylyte generation and brittle faulting occurred during *localised* compression or extension. It is therefore not possible to unequivocally determine the *regional* kinematic regime from the structures and fault rocks preserved within the pervasive mylonite belt. On theoretical grounds (Sibson 1977a, 1983), Butler (1995) has argued that pseudotachylyte generation is more likely to take place in a load strengthening (i.e. compressional) environment than in a load weakening (i.e. extensional) environment (Sibson 1993). Given the lack of convincing evidence to the contrary, the present author concurs with Butler (1995) and suggests that brittle faulting and the generation of discordant pseudotachylyte-bearing structures around Loch Sgibacleit took place under a regime of regional compression (i.e. top-to-the-W thrusting) along the OHFZ.

### 3.2.2.2 Scalpay

The island of Scalpay lies at the mouth of East Loch Tarbert (Fig. 3.1). A NE-SW trending segment of the pervasive mylonite belt has been studied along the well exposed southeast coast of the island, between Lag na Laire (NG 235 941) and Geo an Ear (NG 247 949). The unmodified gneisses of the 'foreland' are exposed along coastal sections in northwest Scalpay (Fig. 3.7).

#### *Localised deformation in the 'foreland'*

Evidence for localised deformation in the 'foreland' is widespread, but is never very intense. Overall, fault rocks probably account for much less than 5% of the total rocks exposed in the 'foreland'.

Rare SE-dipping brittle faults and / or cataclasite seams cross-cut the gneissose banding and locally displace individual bands (offsets  $\leq 10\text{cm}$ ) in an apparent reverse sense (i.e. top-to-the-NW). Isolated exposures of mylonitised pegmatite have been observed in the 'foreland' (C. A. Butler *pers. comm.* 1997). The mylonitic foliation is

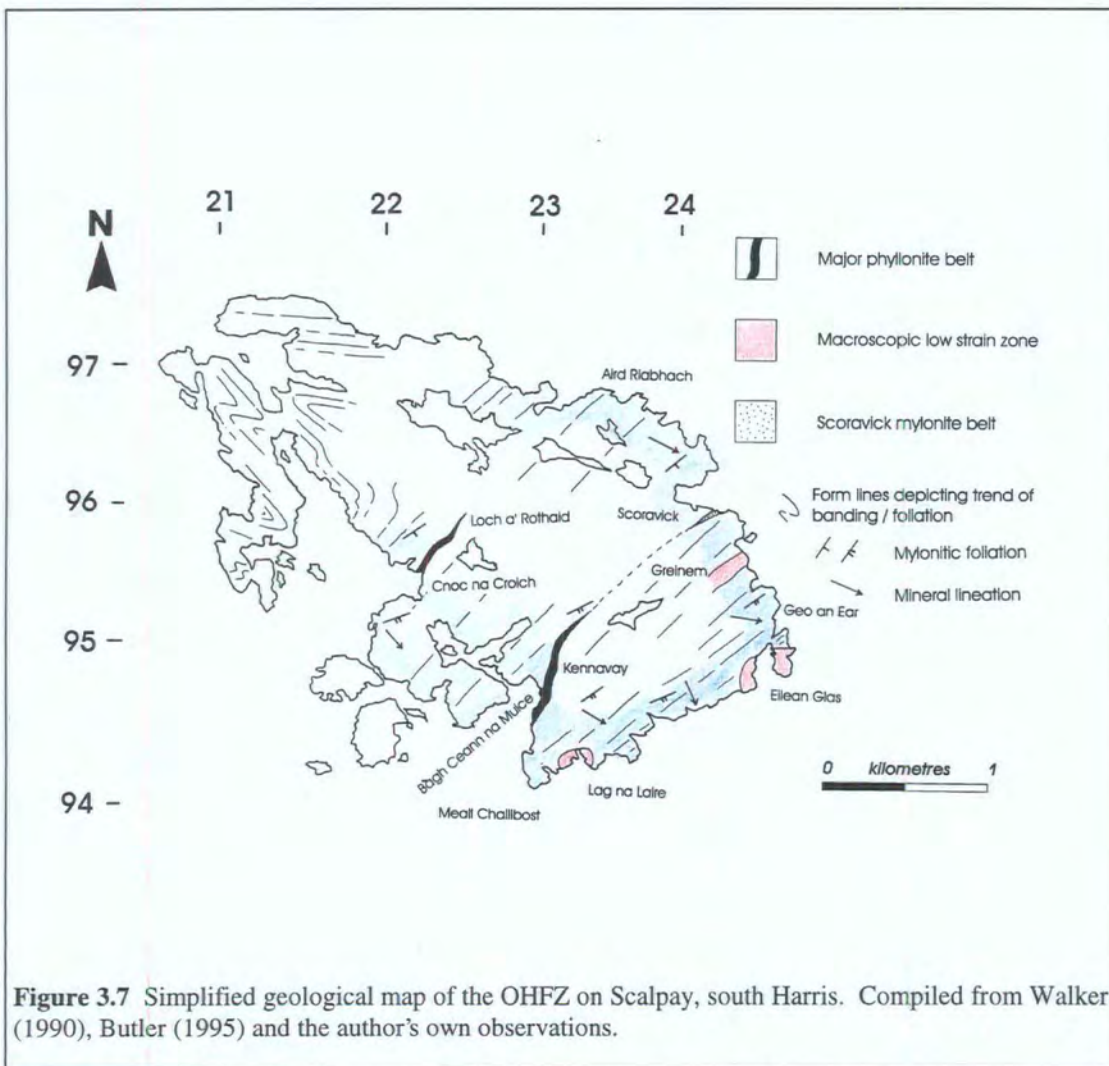


**Figure 3.7** Simplified geological map of the OHFZ on Scalpay, south Harris. Compiled from Walker (1990), Butler (1995) and the author's own observations.

associated with a NW-SE trending mineral lineation. Kinematic indicators ( $\delta$ -type feldspar porphyroclasts) viewed in surfaces parallel to the mineral lineation and perpendicular to the foliation are consistent with top-to-the-NW directed shear (i.e. localised thrusting).

### ***The pervasive mylonite belt on Scalpay***

The pervasive mylonite belt comprises interbanded quartzo-feldspathic and phyllosilicate-rich mylonites. Overall, phyllosilicate-rich mylonites probably account for less than 50% of the total mylonitic fault rocks exposed on Scalpay. The mylonitic foliation consistently dips towards the southeast and is associated with a strong SE-plunging mineral lineation (Fig. 3.8). Kinematic indicators ( $\sigma$ -type feldspar porphyroclasts) viewed in surfaces parallel to the mineral lineation and perpendicular to the foliation are consistent with top-to-the-NW directed shear (i.e. regional thrusting). Within the phyllosilicate-rich bands, the mylonitic fabric is locally deformed by ESE-plunging crenulations or SW-verging cm-scale folds. The geometry of the folds is consistent with localised top-to-the-SW shear within the phyllosilicate-

rich bands following the cessation of top-to-the-NW thrusting (discussed in section 3.2.3.4).

Neither fresh, nor viscously deformed pseudotachylyte veins have been observed within the pervasive mylonite belt on Scalpay.

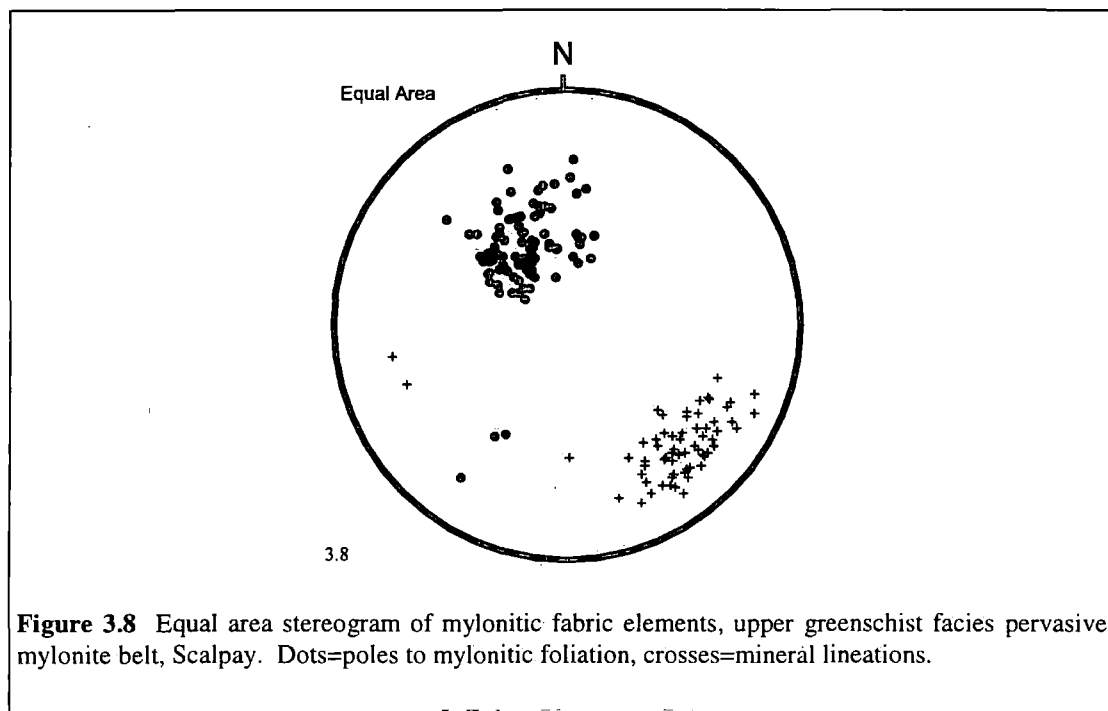


**Figure 3.8** Equal area stereogram of mylonitic fabric elements, upper greenschist facies pervasive mylonite belt, Scalpay. Dots=poles to mylonitic foliation, crosses=mineral lineations.

### ***Microstructure***

***Mylonites*** The microstructure of the quartzo-feldspathic mylonites is characterised by polycrystalline quartz ribbons which are interbanded with flattened, partially sericitised and / or partially recrystallised feldspar grains. The feldspar grains are locally cross-cut by intragranular fractures, which are infilled by aggregates of ultrafine grained recrystallised feldspar. Hornblende porphyroclasts are locally preserved and are typically cross-cut by intra- and transgranular fractures, which are infilled by aggregates of fibrous actinolite and / or quartz. Actinolite strain shadows are locally developed along the margins of hornblende grains. The actinolite / quartz fibres within the fractures and strain shadows are oriented parallel to the NW-SE trending mineral lineation.

The microstructure of the phyllosilicate-rich mylonites is characterised by interconnected sericite strands (Chapter 1) and polycrystalline quartz ribbons, which anastomose around partially sericitised and / or partially recrystallised feldspar grains. The sericite strands locally contain 'cores' of relatively unaltered relict feldspar.

The mylonitised pegmatite preserved in the 'foreland' region on Scalpay contains viscously deformed pseudotachylyte veins and is microstructurally very similar to the lower amphibolite facies mylonites from Loch Sgibaeleit (section 3.2.2.1).

### ***Summary and discussion***

The NE-SW trending segment of the pervasive mylonite belt exposed on Scalpay comprises an assemblage of quartzo-feldspathic and phyllosilicate-rich mylonites, which developed during regional top-to-the-NW thrusting. Phyllosilicate-rich mylonite bands were subsequently reactivated during top-to-the-SW directed shear.

The strain shadows and fibrous fracture infills observed within the quartzo-feldspathic mylonites are consistent with the operation of fluid-assisted diffusive mass transfer (DMT) mechanisms during thrusting (Chapter 1). Fluid-assisted DMT can only take place in the presence of a syn-tectonic fluid phase, which suggests that there was a significant influx of fluids into the pervasive mylonite belt during top-to-the-NW thrusting. Furthermore, feldspar sericitisation reactions cannot occur in the absence of a chemically active fluid phase (Chapter 1). The observation that feldspar was breaking down to produce aggregates of highly aligned sericite needles is also consistent with syn-tectonic fluid influx into the fault zone during thrusting.

Syn-tectonic actinolite growth, extensive recrystallisation of quartz and partial recrystallisation and / or fracturing of the feldspar grains are consistent with deformation and retrogression at pressures and temperatures equivalent to upper greenschist facies conditions (Chapter 1).

The age of the brittle faults observed in the 'foreland' relative to the age of mylonitisation is unclear from the field relationships and is discussed below, in the light of evidence from Kebock Head (section 3.2.1.3).

#### **3.2.2.3 Kebock Head**

Kebock Head (Fig. 3.1) is situated on the east coast of Lewis, some 10km orthogonal to the regional strike of the mylonitic fabric from Loch Sgibacleit (Fig. 3.3). A N-S trending segment of the pervasive mylonite belt is moderately well exposed along the north coast of the Kebock Head peninsular, between Creag an Easa Duibh (NB 410 140) and Kebock Head itself (NB 427 139). Sporadic exposures of pervasive mylonite have been observed along the south coast of the peninsular, between Lemreway (NB 383 115) and Mòl Stiogh' a' Chragain (NB 413 112) (Fig. 3.9).

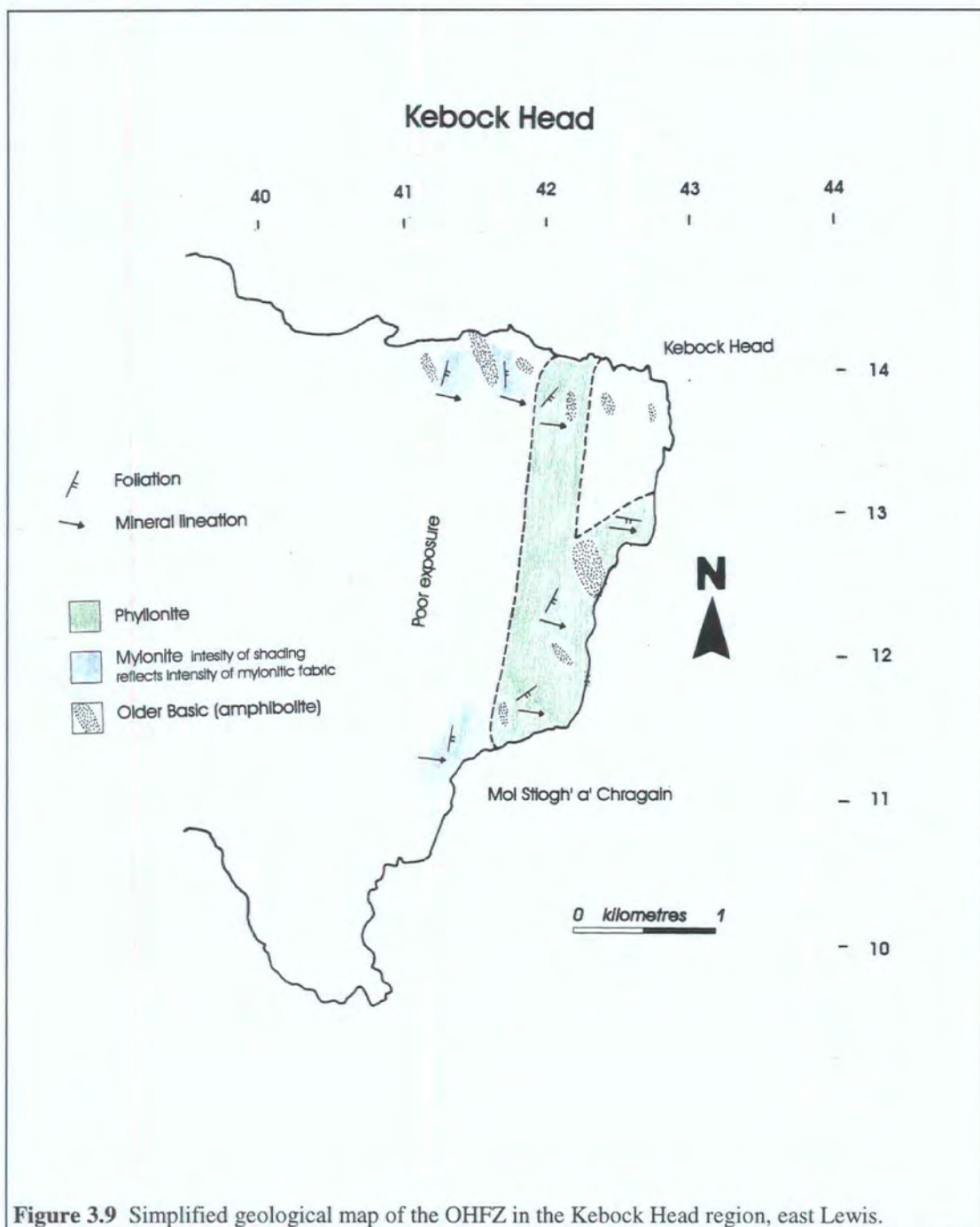


**Figure 3.9** Simplified geological map of the OHFZ in the Kebock Head region, east Lewis.

### ***The pervasive mylonite belt around Kebock Head***

The pervasive mylonite belt comprises quartzo-feldspathic protomylonites and mylonites. The predominantly E- to ESE-dipping mylonitic foliation locally wraps around relatively undeformed pods of massive amphibolite (Older Basics; section 2.2.2.1). The mylonitic fabric is associated with a shallowly E- to ESE-plunging mineral lineation (Fig. 3.10). Kinematic indicators ( $\sigma$ -type feldspar porphyroclasts) viewed in surfaces parallel to the mineral lineation and perpendicular to the foliation are consistent with top-to-the-W or -WNW directed shearing (i.e. regional thrusting)

during mylonitisation. Pseudotachylyte has not been observed in the Kebock Head region.

The mylonitic fabric is locally cross-cut by cataclasite seams ( $\leq 2\text{cm}$  thick) and brittle fractures. The cataclasites and brittle fractures are typically oriented sub-parallel to the mylonitic foliation / gneissose banding. However, individual bands are occasionally observed to be displaced (offsets  $\leq 5\text{cm}$ ) in an apparent reverse (i.e. top-to-the-W) sense.

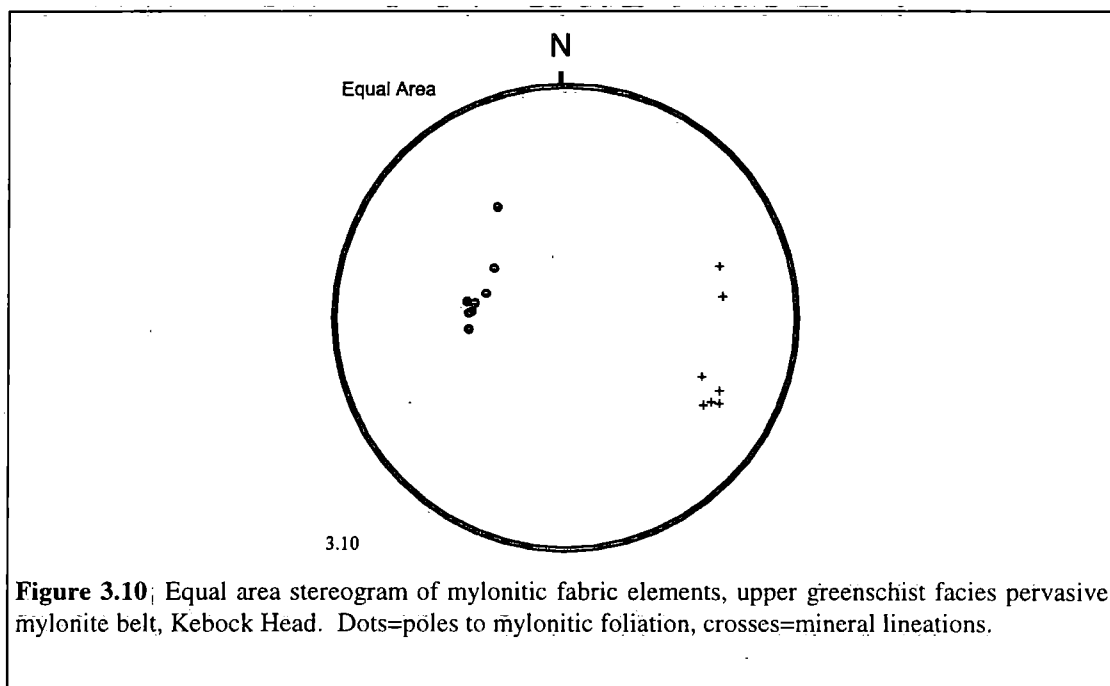


**Figure 3.10** Equal area stereogram of mylonitic fabric elements, upper greenschist facies pervasive mylonite belt, Kebock Head. Dots=poles to mylonitic foliation, crosses=mineral lineations.

### *Microstructure*

The mylonites from Kebock Head possess similar microstructures to the quartzofeldspathic mylonites from Scalpay (section 3.2.1.2).

### *Summary and discussion*

The N-S trending segment of the pervasive mylonite belt exposed at Kebock Head developed during regional top-to-the-W or -WNW thrusting along the Outer Hebrides Fault Zone. The microstructural similarities between the Kebock Head mylonites and the Scalpay mylonites (section 3.2.1.2) suggest that, at Kebock Head, top-to-the-W thrusting probably took place under upper greenschist facies conditions and was accompanied by significant syn-tectonic fluid influx into the fault zone.

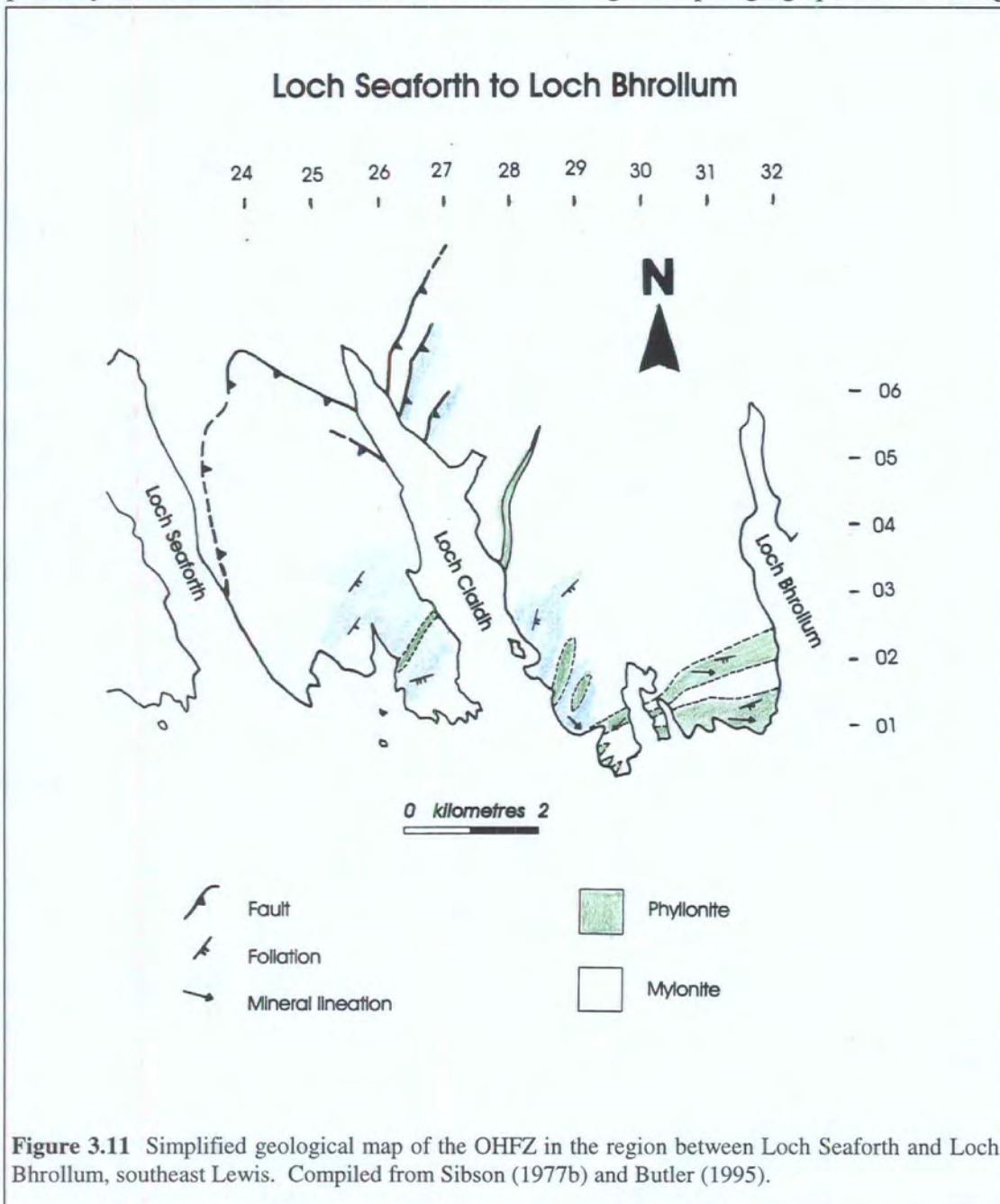
Top-to-the-W brittle deformation clearly post-dates mylonitisation at Kebock Head. The style and intensity of brittle deformation at Kebock Head is comparable with that observed on Scalpay (section 3.2.1.2). Given the lack of direct field evidence, it is tentatively suggested that the brittle faults and cataclasite seams preserved on Scalpay

are of broadly similar age as the brittle faults and cataclasite seams preserved at Kebock Head.

### 3.2.2.4 Southeast Lewis

The field relationships in southeast Lewis are of critical importance as the region lies astride the southern strike-swing of the pervasive mylonite belt. Unfortunately, the present author did not make the opportunity to spend enough time in the region to carry out a detailed study of the mylonites.

The results of a reconnaissance survey in the Loch Claidh region (NB 253 067 - NB 293 004) are presented by Sibson (1977b) (Fig. 3.11). A pervasive ESE-dipping protomylonitic foliation is associated with a strong ESE-plunging quartz stretching



lineation. Concordant bands of ultramylonite ( $\leq 5\text{cm}$  thick) and laterally discontinuous pseudotachylyte lenses ( $\leq 7\text{m}$  thick) are locally preserved. It has been suggested that both the mylonitic fabrics and pseudotachylyte-bearing structures developed in response to thrusting along the Outer Hebrides Fault Zone (Sibson 1977b).

Butler (1995) has reported exposures of steeply SE-dipping mylonites in the region to the west of Loch Bhallamus (NB 286 009) (Fig. 3.11). The mylonites are associated with a SE-plunging mineral lineation and are thought to have developed in response to top-to-the-NW thrusting along the Outer Hebrides Fault Zone (Butler 1995).

### **3.2.2.5 Summary and discussion**

From the preceding descriptions, it is clear that: (1) the N-S trending segments of the pervasive mylonite belt have accommodated top-to-the-NW or -WNW shear; (2) the NE-SW trending segments of the pervasive mylonite belt have accommodated top-to-the-NW shear; (3) regional thrusting around Loch Sgibacleit is inferred to have occurred under 'dry' lower amphibolite facies conditions; (4) regional thrusting and mylonitisation at Kebock Head and on Scalpay are inferred to have taken place under fluid-rich upper greenschist facies conditions; (5) cataclasis, generation of discordant pseudotachylyte-bearing fault zones and brittle faulting post-date lower amphibolite and upper greenschist facies mylonitisation. The intensity of brittle deformation is greatest in regions of lower amphibolite facies mylonite. The foliation trends, mineral lineation azimuths and the distribution of syn-tectonic retrogression throughout the pervasive mylonite belt are summarised in Figure 3.12.

Two important questions which need to be addressed are:

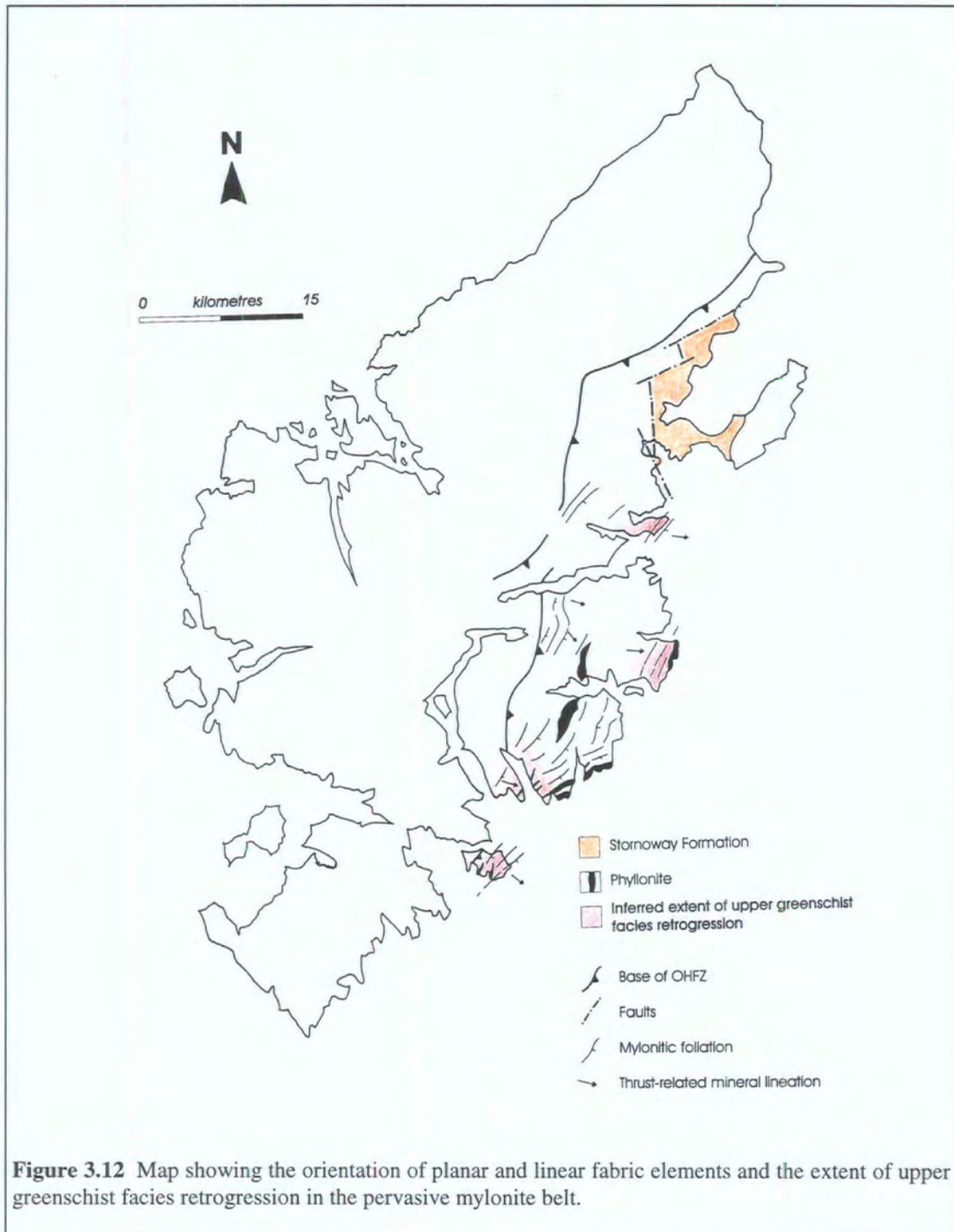
- What are the relative ages of hydrous upper greenschist facies deformation and anhydrous lower amphibolite facies deformation?
- What is the overall geometry of the pervasive mylonite belt and what are the possible causes of the strike-swing?

In discussing these problems, it is important to bear in mind the limited nature of the dataset, caused by the inaccessibility of the area and by the comparative lack of exposure in southeast Lewis.

### *The relative age of upper greenschist facies retrogression*

There are three possible alternatives regarding the relative ages of the upper greenschist and lower amphibolite facies mylonites.

- Scenario 1 - upper greenschist facies retrogression and mylonitisation significantly pre-dates lower amphibolite facies mylonitisation and pseudotachylyte generation.
- Scenario 2 - upper greenschist facies retrogression and mylonitisation



significantly post-dates lower amphibolite facies mylonitisation and pseudotachylyte generation.

- Scenario 3 - upper greenschist facies retrogression and mylonitisation was broadly synchronous with lower amphibolite facies mylonitisation and pseudotachylyte generation.

Assuming that the upper greenschist facies mylonites are significantly *older* than the lower amphibolite facies mylonites and pseudotachylytes (Scenario 1), there is an implied *increase* in metamorphic grade between the two deformation events. However, the mineral assemblage preserved in the Loch Sgibacleit mylonite appears to be completely stable under lower amphibolite facies conditions and there is no textural evidence (e.g. the growth of new garnet porphyroblasts) to suggest that the mylonite was derived from a pre-existing upper greenschist facies assemblage. Moreover, it is difficult to envisage a mechanism whereby significant areas of greenschist facies mylonite completely survived prograde metamorphism, whilst the mylonite at Loch Sgibacleit appears to be in complete equilibrium with lower amphibolite facies conditions (Fig. 3.12). It is therefore *unlikely that greenschist facies retrogression pre-dates amphibolite facies mylonitisation*.

Assuming that the upper greenschist facies mylonites are significantly *younger* than the lower amphibolite facies mylonites and pseudotachylytes (Scenario 2), it is not unreasonable to expect that the earlier 'high temperature' fault rocks would have been reworked during greenschist facies deformation and retrogression. Thus, reworked pseudotachylyte veins and / or relict lower amphibolite facies mineral assemblages should be commonly observed within regions of upper greenschist facies retrogression and mylonitisation. However, neither fresh nor reworked pseudotachylyte veins are preserved within the upper greenschist facies mylonites exposed at Kebock Head or on Scalpay. Furthermore, relict amphibolite facies mineral assemblages (e.g. garnet + quartz + moderately calcic plagioclase) have not been observed in areas of upper greenschist facies retrogression. These observations suggest that *the upper greenschist facies mylonites cannot have been derived from reworked lower amphibolite facies fabrics*. Given the poor exposure and the distance between individual localities (Fig. 3.1), it is impossible to provide an unambiguous explanation of these field relationships. The two most likely interpretations are that (1) retrogression was restricted to areas of previously unmodified gneiss (i.e. low strain 'windows' within the belt of lower amphibolite facies mylonite), or (2) that the greenschist facies mylonites are of broadly the same age as the amphibolite facies fabrics. Field studies and theoretical considerations suggest that the permeability of deformed, anisotropic fault rocks (e.g. mylonites) is likely much greater than the

permeability of unmodified crystalline basement gneisses (e.g. Oliver 1996; Ord & Oliver 1997). It is therefore unlikely that retrogression was simply focused into low strain 'windows' within a pre-existing belt of amphibolite facies mylonite.

The intriguing possibility which remains is that *the lower amphibolite facies pseudotachylytes and mylonites are of broadly the same age as the upper greenschist facies mylonites* (Scenario 3). The spatially restricted pattern of retrogression (Fig. 3.12) is consistent with fluid influx into an actively deforming shear zone (Oliver 1996). Furthermore, the apparent lack of pseudotachylyte generation during upper greenschist facies deformation can be explained on theoretical grounds by the presence of a fluid phase and / or by locally high pore fluid pressures during mylonitisation (Sibson 1975; White 1996; Chapter 8 of the present work). The mylonitised pegmatite preserved in the 'foreland' region on Scalpay (section 3.2.1.2) is associated with viscously deformed pseudotachylyte veins and is microstructurally very similar to the lower amphibolite facies mylonites from Loch Sgibacleit (section 3.2.1.1). The implication is that deformation on Scalpay *initially* took place under dry, lower amphibolite facies conditions, but that retrogression and fluid influx occurred soon after the onset of localised deformation and prevented widespread pseudotachylyte generation.

### ***Geometry of the pervasive mylonite belt***

The inference that the upper greenschist and lower amphibolite facies fabrics are of the same age strongly suggests that the strike-swing of the pervasive mylonite belt observed in southeast Lewis is a primary feature, and was not caused by a re-orientation of the mylonitic fabric during a later deformation event. Butler (1995) has suggested that the mylonite belt bifurcates in the region to the north of Loch Erisort and forms two distinct 'arms', which are thought to outcrop in an area of no exposure around Stornoway (Fig. 3.13a). However, observations made by the present author have not substantiated Butler's (1995) interpretation, and it is suggested that the mylonites exposed throughout eastern Lewis and Scalpay in fact form part of a single broad mylonite belt. To a first order approximation, the N-S trending segment of the mylonite belt may represent a frontal ramp, whilst the NE-SW trending segment exposed in southeast Lewis and on Scalpay may represent an oblique ramp (or vice-versa) of a mid-crustal thrust system (Fig. 3.13b). It is possible that the distribution of syn-tectonic upper greenschist facies retrogression along the fault zone was in some way influenced by the regional geometry of the pervasive mylonite belt. Unfortunately, a lack of exposure in southeast Lewis precludes any detailed analysis of these hypotheses.

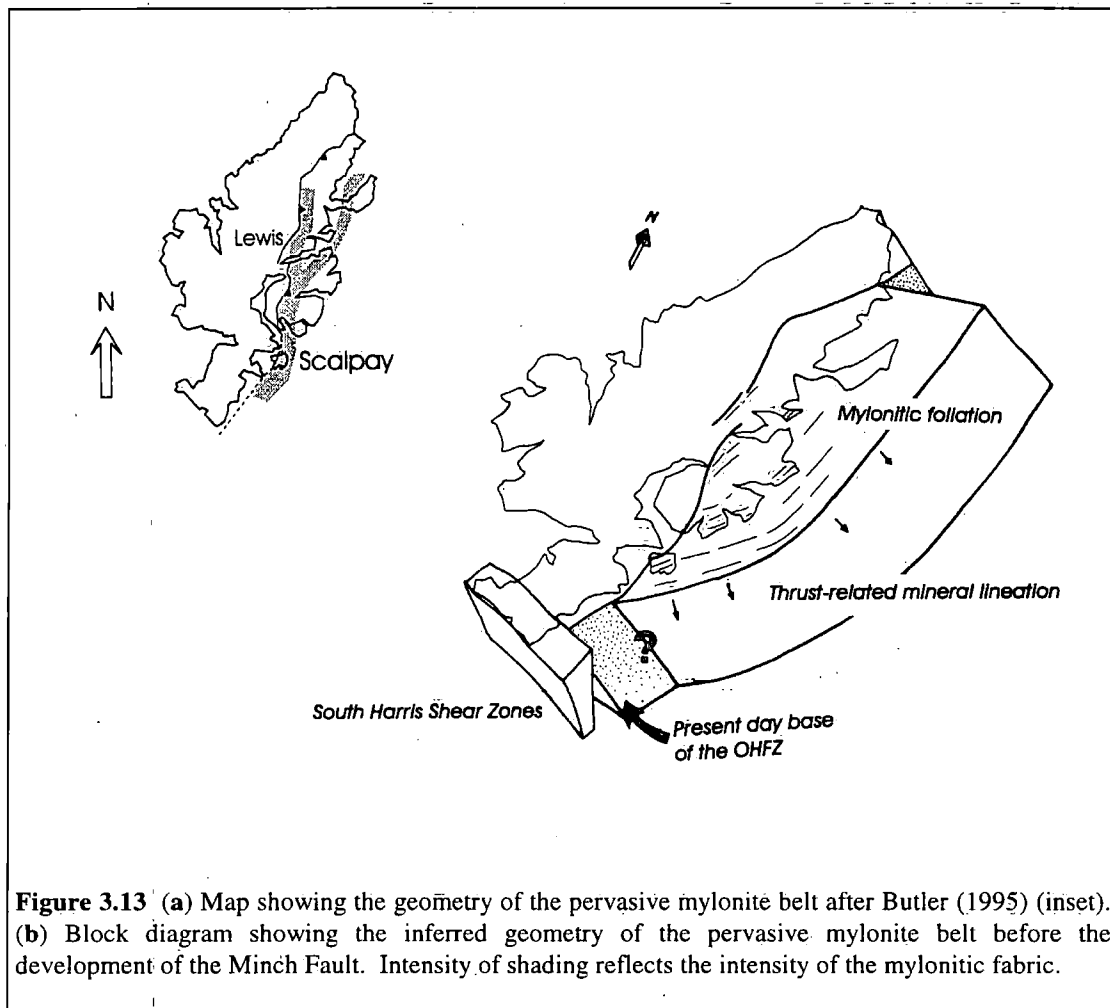


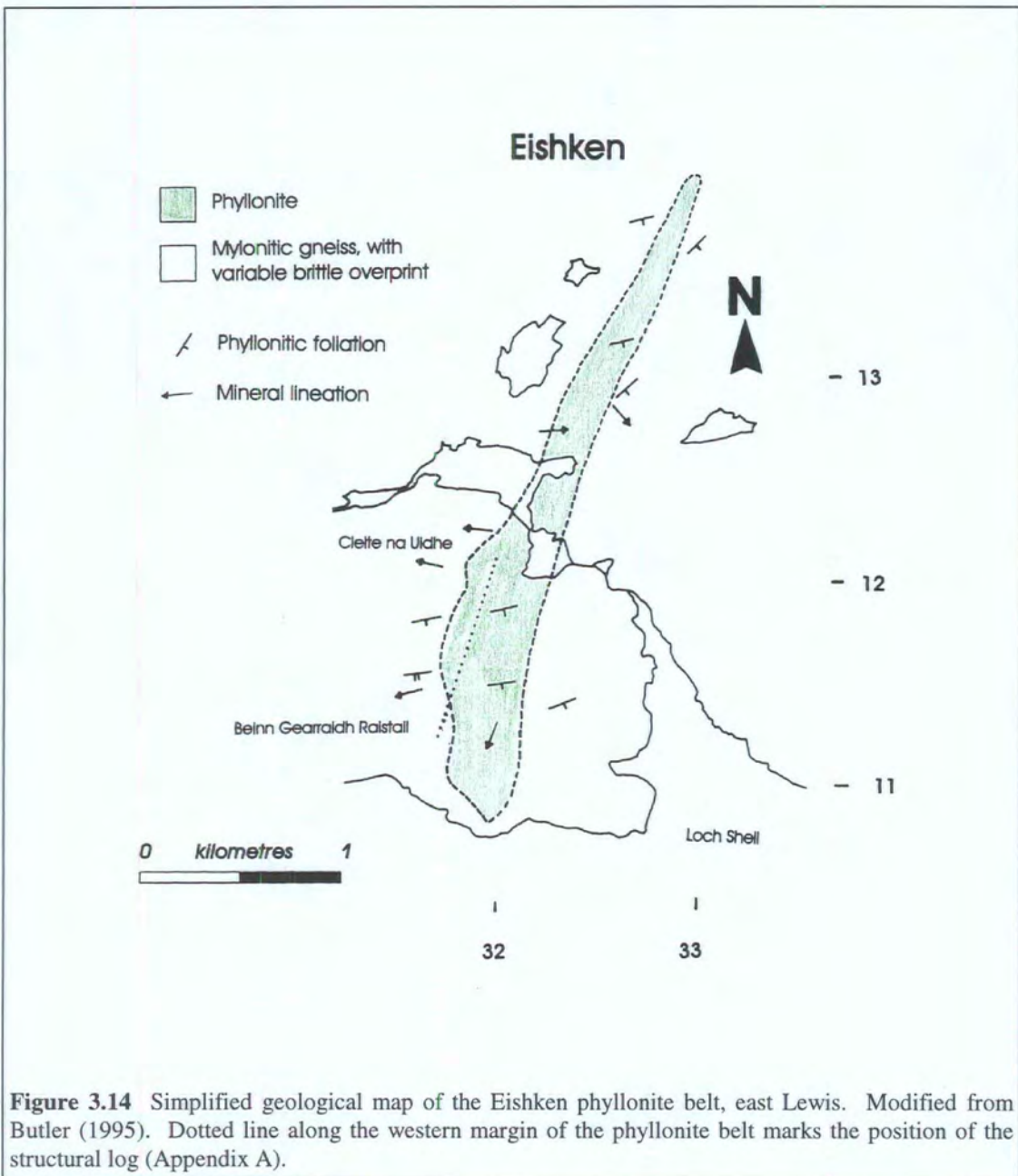
**Figure 3.13** (a) Map showing the geometry of the pervasive mylonite belt after Butler (1995) (inset). (b) Block diagram showing the inferred geometry of the pervasive mylonite belt before the development of the Minch Fault. Intensity of shading reflects the intensity of the mylonitic fabric.

### 3.2.3 THE PHYLLONITE BELTS

A number of S- and E-dipping belts of phyllonite outcrop in central Scalpay (NG 223 955 & NG 230 944), along the southeast coast of Lewis (NB 283 013 - NB 357 034), on Corlabhadh hill (NB 302 058 - NB 323 100), to the north of Eishken (NB 319 109 - NB 330 140) and at Kebock Head (NB 427 139 - NB 415 114) (Figs. 3.1 & 3.3).

In the following sections, it will become apparent that the phyllonitic fabrics post-date the thrust-related pervasive mylonites, brittle fractures, cataclases and pseudotachylytes (section 3.2.2). However, on a regional scale the phyllonite belts clearly trend sub-parallel to the earlier mylonitic foliation. The phyllonite belts thus follow distinct NE-SW or N-S trends (see also Butler 1995) (Fig. 3.3).

During the present study, N-S trending phyllonite belts have been investigated in the Eishken and Kebock Head areas, whilst NE-SW trending phyllonite belts have been studied in southeast Lewis (Loch Bhrollum; NB 320 032 - NB 357 034) and on Scalpay (Fig. 3.1).



### 3.2.3.1 Eishken

The N-S to NNE-WSW trending phyllonite belt outcrops between Loch Shell (NB 319 109) and Lochan na Uidhean Beaga (NB 330 140) (Butler 1995) (Fig. 3.14). A detailed structural log has been constructed along the well exposed western margin of the phyllonite belt (Beinn Gearraidh Raistail, NB 317 116 to Cleite na Uidhe, NB 320 122) (Appendix A), whilst reconnaissance studies have been conducted in the region to the north and west of the phyllonite belt (e.g. Cleit na Ceardaich; NB 318 154) (Fig. 3.14).

### ***Protoliths***

The geology of the region immediately to the west of the phyllonite belt is dominated by pervasive mylonite, pegmatite and banded gneiss. The gneisses and mylonites are cross-cut by veins of pale green cataclasite and / or devitrified pseudotachylyte, which are themselves cross-cut by a network of closely spaced brittle fractures. The intensity of brittle fracturing at Eishken appears to be much greater than that observed in the Loch Sgibacleit area (section 3.2.2.1).

### ***Discrete phyllonites***

The western margin of the phyllonite belt is characterised by a number of narrow ( $\leq 10\text{cm}$  thick), laterally discontinuous bands of phyllonite and protophyllonite ('discrete phyllonites'). The margins of the discrete phyllonite bands are extremely abrupt (cf. the 'discontinuous shear zones' of Tourigny & Tremblay 1997) and are typically oriented parallel to either the pre-existing mylonitic foliation or to the fractures (Fig. 3.15).

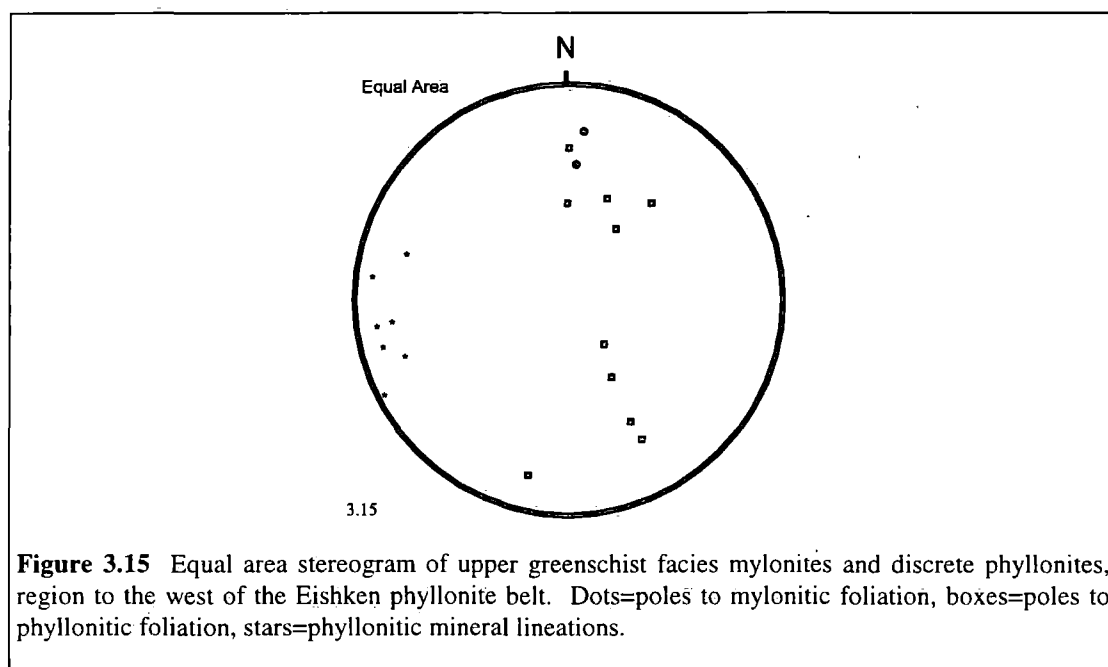


**Figure 3.15** Equal area stereogram of upper greenschist facies mylonites and discrete phyllonites, region to the west of the Eishken phyllonite belt. Dots=poles to mylonitic foliation, boxes=poles to phyllonitic foliation, stars=phyllonitic mineral lineations.

The phyllonitic / protophyllonitic foliation dips moderately towards the NNW or towards the SSW and is associated with a WSW- or WNW-plunging mineral lineation (Fig. 3.15). Kinematic indicators are rare, but  $\sigma$ -type feldspar and hornblende porphyroclasts viewed in surfaces parallel to the mineral lineation and perpendicular to the foliation are consistent with top-to-the-E shear.

The discrete phyllonites and the fractured country rock are cross-cut by a set of steeply dipping, N-S trending quartz veins (the 'post-fold' veins - see below).

### *The Eishken phyllonite belt*

The phyllonite belt comprises an assemblage of fine grained phyllonites and ultraphyllonites. The foliation dips predominantly towards the south and is associated with a sub-horizontal ENE-WSW to ESE-WNW trending mineral lineation (Fig. 3.16a).

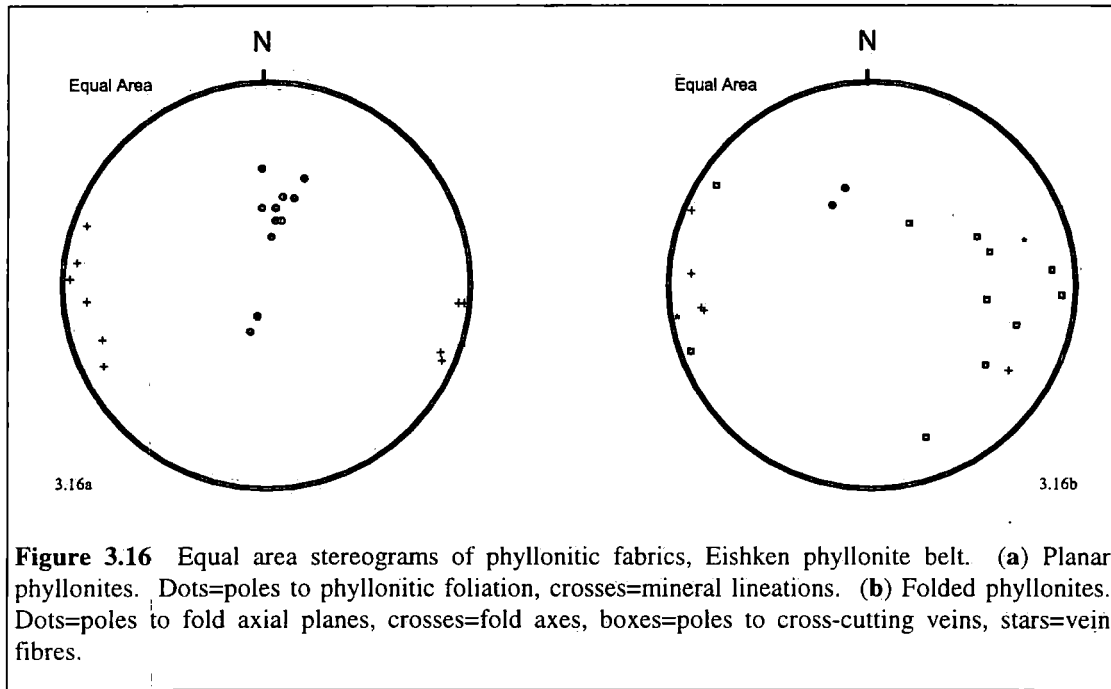


**Figure 3.16** Equal area stereograms of phyllonitic fabrics, Eishken phyllonite belt. (a) Planar phyllonites. Dots=poles to phyllonitic foliation, crosses=mineral lineations. (b) Folded phyllonites. Dots=poles to fold axial planes, crosses=fold axes, boxes=poles to cross-cutting veins, stars=vein fibres.

The phyllonitic foliation is commonly observed to be deformed by cascades of gently WNW- or ESE-plunging open warps and chevron folds (wavelengths  $\leq 10\text{cm}$ ) (Fig. 3.16b). The folds typically verge towards the south, although anomalously N-verging folds are locally preserved in an area of northward dipping ultraphyllonite (Cleite na Uidhe, NB 320 122) (Fig. 3.14). A set of 'early' (i.e. pre-folding) foliation-parallel to discordant quartz-epidote-chlorite veins are widely developed within the phyllonite belt. The folds are themselves cross-cut by a set of undeformed axial planar quartz veins and by a set of sub-vertical N-S trending quartz veins (Fig. 3.16). The orientation of the fibrous infill associated with the latter set of 'post-fold' veins is consistent with ENE-WSW extension.

### *Microstructure*

*Protoliths* The microstructures of the banded gneiss and pervasive mylonite are described in section 3.2.2.1.

*Phyllonites (including the 'discrete phyllonites')* The phyllonitic fault rocks are characterised by domains of ultrafine grained, viscously deformed pseudotachylyte, which are interbanded with domains of relatively coarse grained quartzo-feldspathic aggregates. The boundaries between the two domains are extremely abrupt. It is

thought that the quartzo-feldspathic domains were derived from the wallrocks to the original pseudotachylyte veins (cf. Chapter 4). Asymmetric shear bands are locally developed within domains of viscously deformed pseudotachylyte and are consistent with top-to-the-ENE or -ESE directed shear.

The microstructure of the quartzo-feldspathic domains is dominated by relatively coarse ( $\leq 2$ mm diameter) quartz grains and aggregates of partially sericitised feldspar. The quartz grains display intense patchy undulose extinction and are locally cross-cut by arrays of intragranular fractures. The fractures are infilled by fine grained aggregates of fine grained (?dynamically recrystallised) quartz, although overall, evidence for widespread recrystallisation is not commonly observed. Hornblende grains are locally preserved within the quartzo-feldspathic domains. The hornblende is partially replaced by aggregates of chlorite and epidote.

The viscously deformed pseudotachylyte veins contain numerous opaque grains, polycrystalline quartz ribbons and sericite strands. The opaque grains are typically fringed by fibrous quartz-chlorite strain shadows and are locally boudinaged parallel to the macroscopic mineral lineation.

### ***Summary and discussion***

The geometries of the discrete phyllonite bands preserved to the west of the Eishken belt are consistent with top-to-the-E directed shear. The laterally discontinuous nature of the discrete phyllonites suggests that individual bands have not accommodated large finite strains. These observations suggest that phyllonitisation in the region to the west of the present day Eishken phyllonite belt was synchronous with top-to-the-E shear (Chapter 1).

The geometries of the planar phyllonites and ultraphyllonites preserved *within* the Eishken phyllonite belt are also consistent with top-to-the-E shear. Although low strain fabrics are not preserved within the phyllonite belt, it does not seem unreasonable to suggest that phyllonitisation in region presently occupied by the Eishken belt was synchronous with top-to-the-E shear (Chapter 1).

The phyllonites and ultraphyllonites preserved within the Eishken belt were subsequently reworked and deformed by a series of southward (and locally northward) verging folds. The observed fold geometries are consistent with a regime of predominantly top-to-the-S extension, directed down the regional dip of the foliation (Fig. 3.17).

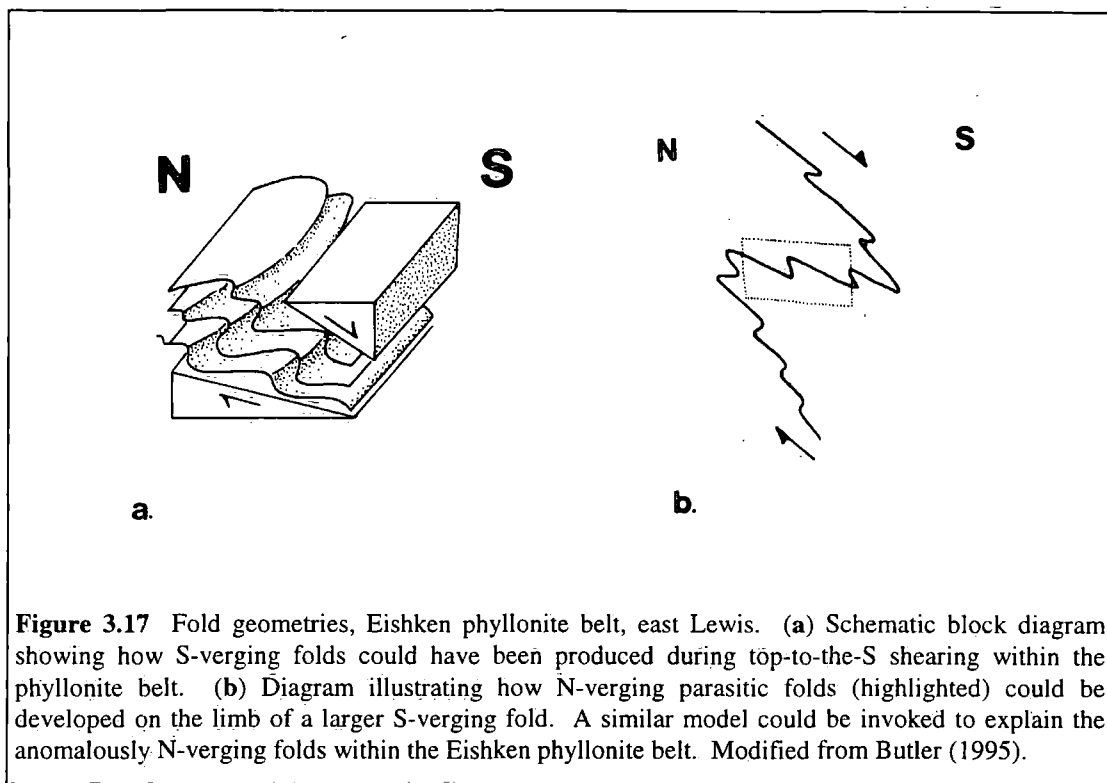


**Figure 3.17** Fold geometries, Eishken phyllonite belt, east Lewis. (a) Schematic block diagram showing how S-verging folds could have been produced during top-to-the-S shearing within the phyllonite belt. (b) Diagram illustrating how N-verging parasitic folds (highlighted) could be developed on the limb of a larger S-verging fold. A similar model could be invoked to explain the anomalously N-verging folds within the Eishken phyllonite belt. Modified from Butler (1995).

The geometries of the chlorite strain shadows preserved within domains of viscously deformed pseudotachylite are consistent with the operation of fluid-assisted diffusive mass transfer (DMT) mechanisms during top-to-the-E shearing (Chapter 1). Fluid-assisted DMT can only take place in the presence of a syn-tectonic fluid phase, which suggests that there was a significant influx of fluids into the fault zone during top-to-the-E shearing. Furthermore, feldspar sericitisation reactions cannot occur in the absence of a chemically active fluid phase (Chapter 1). The observation that feldspar was breaking down to produce aggregates of highly aligned sericite needles is also consistent with significant fluid influx during E-directed shear.

The syn-tectonic breakdown of feldspar and hornblende to produce aggregates of sericite and chlorite, together with the observed quartz deformation microstructures suggest that phyllonitisation took place at temperatures and pressures consistent with lower greenschist facies conditions (Chapter 1).

### 3.2.3.3 Kebock Head

A NNE-SSW trending phyllonite belt outcrops along the east coast of the Kebock Head peninsular, between Geodha Ruadh (NB 415 114) and Kebock Head (NB 427 137) (Fig. 3.9). The phyllonite belt is fairly well exposed in scattered crags along the cliff tops, although further inland the rocks are badly weathered.

### *Protoliths*

The geology of the region to the west of the phyllonite belt is dominated by unmodified banded gneisses, thick amphibolite pods and upper greenschist facies pervasive mylonites (section 3.2.2.3).

### *Discrete phyllonites*

The region immediately to the west of the phyllonite belt is characterised by laterally discontinuous bands ( $\leq 10\text{cm}$  thick) of discrete phyllonite and protophyllonite. The phyllonitic foliation dips moderately towards the east and is associated with a gently E-plunging mineral lineation (Fig. 3.18a). Kinematic indicators are rare, but the sigmoidal strike-swing of the protophyllonitic foliation, viewed in surfaces parallel to the mineral lineation and perpendicular to the foliation, is consistent with top-to-the-E shear. Bands of discrete phyllonite are locally deformed by cascades of small, S-verging folds (wavelength  $\leq 5\text{cm}$ ).

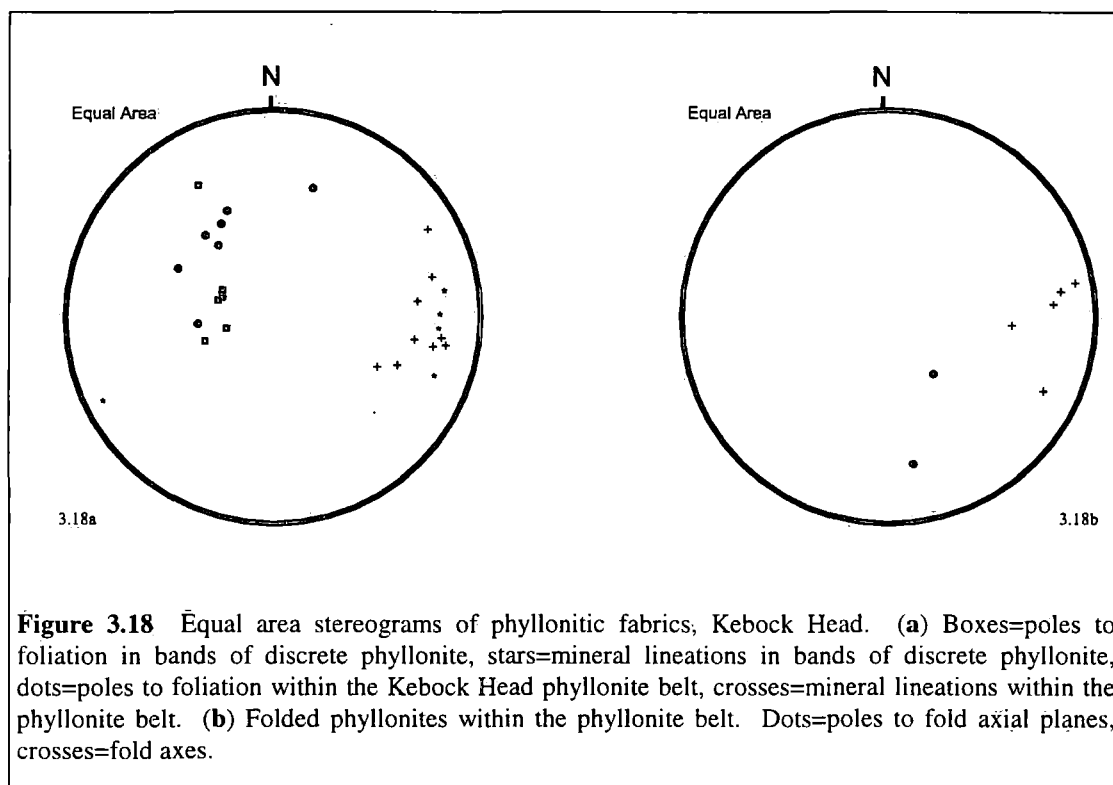


**Figure 3.18** Equal area stereograms of phyllonitic fabrics, Kebock Head. (a) Boxes=poles to foliation in bands of discrete phyllonite, stars=mineral lineations in bands of discrete phyllonite, dots=poles to foliation within the Kebock Head phyllonite belt, crosses=mineral lineations within the phyllonite belt. (b) Folded phyllonites within the phyllonite belt. Dots=poles to fold axial planes, crosses=fold axes.

### *The Kebock Head phyllonite belt*

The Kebock Head phyllonite belt comprises an assemblage of phyllonite, protophyllonite and ultraphyllonite. The foliation dips moderately towards the E or SE and is associated with a NE- to ESE-plunging mineral lineation (Fig. 3.18a). Rare  $\sigma$ -type feldspar porphyroclasts viewed in surfaces parallel to the mineral lineation and perpendicular to the foliation are consistent with top-to-the-E shear across the

phyllonite belt. Pods of unfoliated amphibolite ( $\leq 100\text{m}$  diameter) are preserved throughout the phyllonite belt and are locally 'wrapped' by the phyllonitic foliation. The phyllonitic fabric is commonly observed to be deformed by cascades of gently eastward plunging open warps, chevron folds or crenulations (Fig. 3.18b). The folds typically verge towards the south.

### ***Microstructure***

The microstructures of the Kebock Head, Loch Bhrollum and Scalpay phyllonites appear to be very similar and thus described together in section 3.2.3.4.

### ***Summary and discussion***

The geometries of the discrete phyllonite bands preserved around Kebock Head are consistent with top-to-the-E directed shear. The laterally discontinuous nature of many of the discrete protophyllonites suggests that individual bands have not accommodated large finite strains. These observations are consistent with phyllonitisation during top-to-the-E directed shear (Chapter 1).

The phyllonitic and ultraphyllonitic fabrics were subsequently reactivated and deformed by a series of S- and SW-verging minor folds. The overall geometry of the folds is consistent with oblique (top-to-the-S) dextral transtension across the Kebock Head phyllonite belt.

The metamorphic and hydrogeologic environment during phyllonitisation at Kebock Head is discussed in section 3.2.3.4.

### **3.2.3.3 Loch Bhrollum**

The ENE-WSW trending Loch Bhrollum phyllonite belt outcrops along the southeast coast of Lewis, between Rubha na Faing (NB 324 023) and Geodha na Beairt (NB 357 035). The phyllonite belt is exposed in scattered crags along the coast, but further inland, the rocks are badly weathered. A subsidiary phyllonite belt is exposed along the coast at Aird Dubh (NB 322 030) (Figs. 3.1 & 3.19).

### ***Protoliths***

The geology of the region to the north of the Loch Bhrollum phyllonite belt is dominated by unmodified banded gneisses, pods of massive amphibolite (Older Basics; section 2.2.2.1) and by a poorly developed SE-dipping belt of upper greenschist facies pervasive mylonite (section 3.2.2.4) (e.g. Tòb Bhrollum; NB 322 033) (Fig. 3.19).

### Discrete phyllonites

Bands of discrete phyllonite and protophyllonite ( $\leq 5\text{cm}$  thick) are preserved around Tòb Bhrollum (NB 322 033). In contrast to the discrete phyllonitic fabrics observed in the Eishken and Kebock Head regions, the phyllonite bands which are exposed to the east of Loch Bhrollum are laterally continuous ( $\leq 5\text{m}$  long) and typically form interconnected networks. The SE- to NW-dipping phyllonitic foliation is oriented sub-parallel to the gneissose banding / mylonitic foliation of the host rock, and is associated with a sub-horizontal E-W to ENE-WSW trending mineral lineation (Fig. 3.20a). Asymmetric shear band fabrics viewed in surfaces parallel to the mineral lineation and perpendicular to the foliation are consistent with top-to-the-E directed shear.

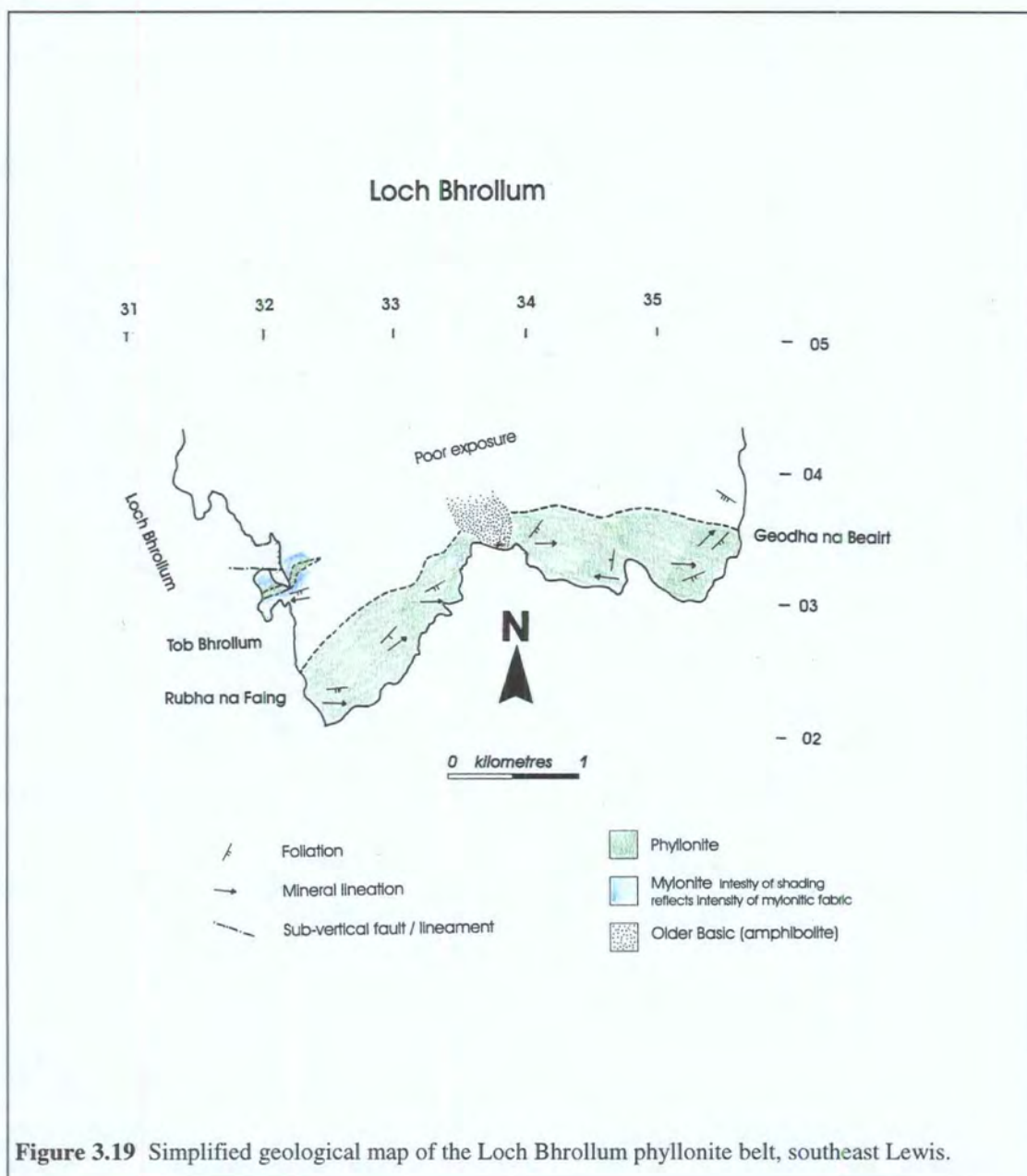


**Figure 3.19** Simplified geological map of the Loch Bhrollum phyllonite belt, southeast Lewis.

### *The Loch Bhrollum phyllonite belt*

The Loch Bhrollum belt comprises an assemblage of protophyllonite, phyllonite and ultraphyllonite. The foliation dips predominantly towards the SSE and is associated with a sub-horizontal NW-SE to NE-SW trending mineral lineation (Fig. 3.20b). Asymmetric shear bands and  $\sigma$ -type hornblende and feldspar porphyroclasts viewed in surfaces parallel to the mineral lineation and perpendicular to the foliation are consistent with top-to-the-E directed shear. A massive mafic to ultramafic body ( $\leq 200\text{m}$  thick) outcrops within the Loch Bhrollum phyllonite belt and is exposed at Camas Thomascro (NB 336 033). Although the mafic and ultramafic material appears to be completely undeformed and unaltered, felsic segregations contained within the hornblende-rich host display a crude protomylonitic foliation.

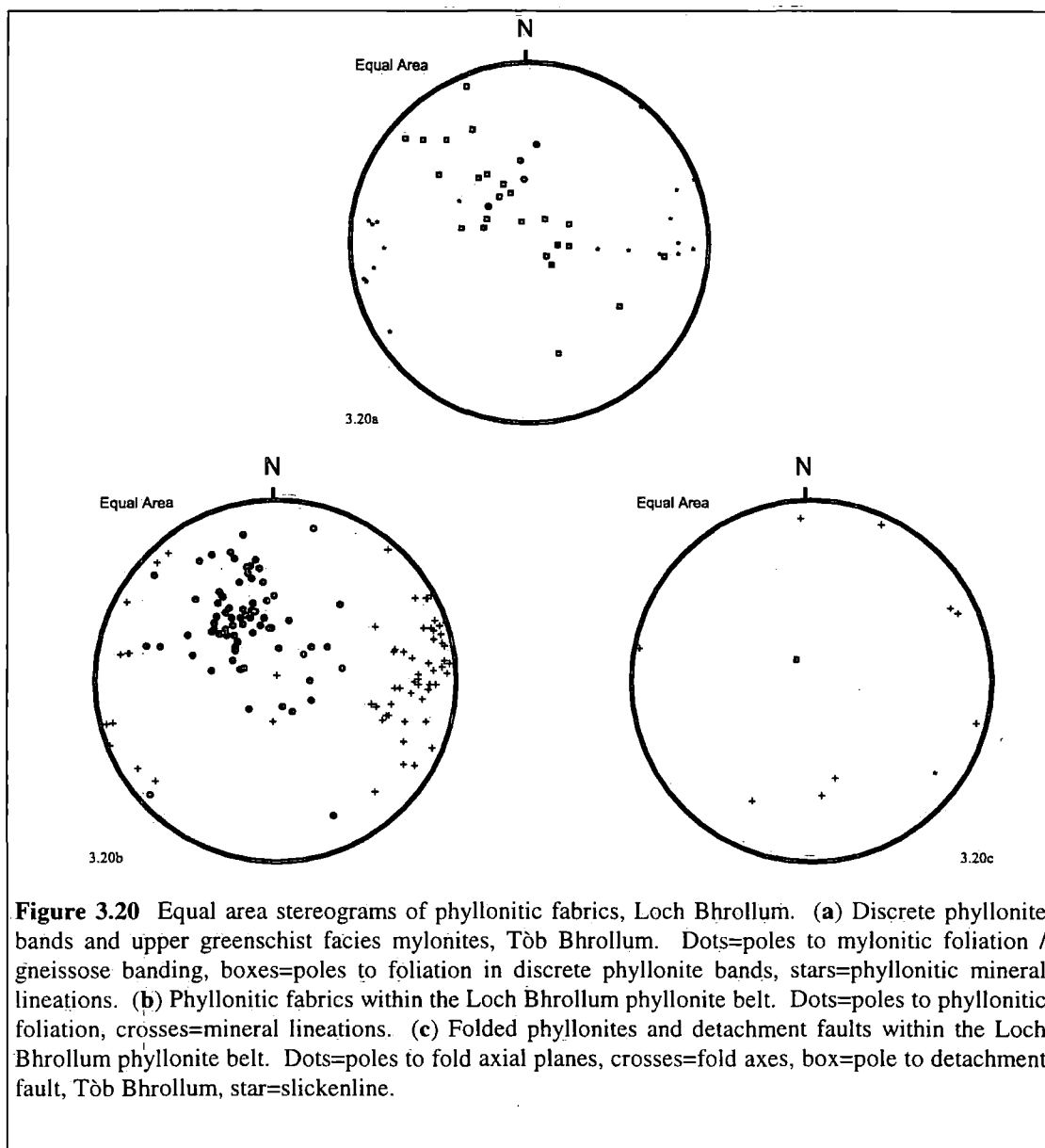


**Figure 3.20** Equal area stereograms of phyllonitic fabrics, Loch Bhrollum. (a) Discrete phyllonite bands and upper greenschist facies mylonites, Tòb Bhrollum. Dots=poles to mylonitic foliation / gneissose banding, boxes=poles to foliation in discrete phyllonite bands, stars=phyllonitic mineral lineations. (b) Phyllonitic fabrics within the Loch Bhrollum phyllonite belt. Dots=poles to phyllonitic foliation, crosses=mineral lineations. (c) Folded phyllonites and detachment faults within the Loch Bhrollum phyllonite belt. Dots=poles to fold axial planes, crosses=fold axes, box=pole to detachment fault, Tòb Bhrollum, star=slickenline.

Cascades of highly curvilinear, gently plunging recumbant folds are commonly observed to deform the phyllonitic fabrics within the Loch Bhrollum belt (Fig. 3.20c). The folds consistently verge towards the S or SSE and aggregates of coarse grained quartz or quartz-carbonate are commonly preserved within the fold hinge regions. The quartz and quartz-carbonate aggregates (hereafter referred to as 'saddle reefs') are clearly wrapped by the phyllonitic foliation and locally, are themselves folded. Shallowly SE- and SSW-dipping brittle faults ('detachments') are *locally* developed and are clearly visible in N-S trending vertical cliff sections (e.g. Geodha Mol Laoigh; NB 358 031). The detachment faults are oriented sub-parallel to the phyllonitic foliation and are typically either developed within, or at the margins of the phyllonite belt. Two sub-parallel detachment faults are exposed at Tòb Bhrollum (NB 320 032) (Fig. 3.19). The detachments are lined by angular clasts of brecciated phyllonite which 'float' in a fine grained clay-rich gouge. SE-plunging slickenlines have locally been observed, although it has not been possible to determine the sense of displacement along any of the detachment surfaces. Butler (1995) has mapped the westward extension of the Loch Bhrollum phyllonite belt, (in the Loch Bhallamus region; NB 284 014 to NB 311 027), and has reported the absence of detachment faults.

### ***Microstructure***

The microstructures of the Kebock Head, Loch Bhrollum and Scalpay phyllonites appear to be very similar and thus described together in section 3.2.3.4.

### ***Summary and discussion***

The geometries of the interconnected phyllonite and protophyllonite bands exposed at Tòb Bhrollum are consistent with top-to-the-E directed shear. The interconnected nature of the protophyllonite bands suggests that they may have accommodated a greater magnitude of strain than the laterally discontinuous discrete phyllonites exposed at Eishken and Kebock Head (sections 3.2.3.1 & 3.3.3.2). However, there is no evidence to suggest that the protophyllonitic fabrics exposed at Tòb Bhrollum have been reworked or reactivated. These observations therefore suggest that phyllonitisation was synchronous with top-to-the-E directed shear (Chapter 1). The geometries of the planar phyllonitic and ultraphyllonitic fabrics preserved within the Loch Bhrollum phyllonite belt are consistent with top-to-the-E shear. Although low strain fabrics have not been observed within the phyllonite belt, it is likely that phyllonitisation in the region presently occupied by the Loch Bhrollum phyllonite belt was also synchronous with top-to-the-E shear.

The phyllonitic and ultraphyllonitic fabrics were subsequently reactivated and deformed by a series of S- and SSE-verging minor folds. The overall geometry of the folds is consistent with top-to-the-S extension, down the dip of the pre-existing phyllonitic foliation.

The metamorphic environment during phyllonitisation at Kebock Head is discussed in section 3.2.3.4.

#### **3.2.3.4 Scalpay**

Several NE-SW and NNE-SSW trending phyllonite belts, which overprint the thrust-related pervasive mylonites (section 3.2.2.2), have been observed in central and southeast Scalpay. The two principal phyllonite belts outcrop between Cnoc na Croich (NG 223 955) and Loch a' Rothaid (NG 227 958) and between Bàgh Ceann na Muice (NG 230 944) and Kennavay (NG 234 952) (Fig. 3.7). Exposure is good along coastal sections and in the Cnoc na Croich quarry, but the rocks are badly weathered further inland.

#### ***Protoliths***

The geology of southeast Scalpay is dominated by upper greenschist facies pervasive mylonite (section 3.2.2.2), with subordinate amounts of unmodified banded gneiss (sections 2.2.2.1 & 3.2.1).

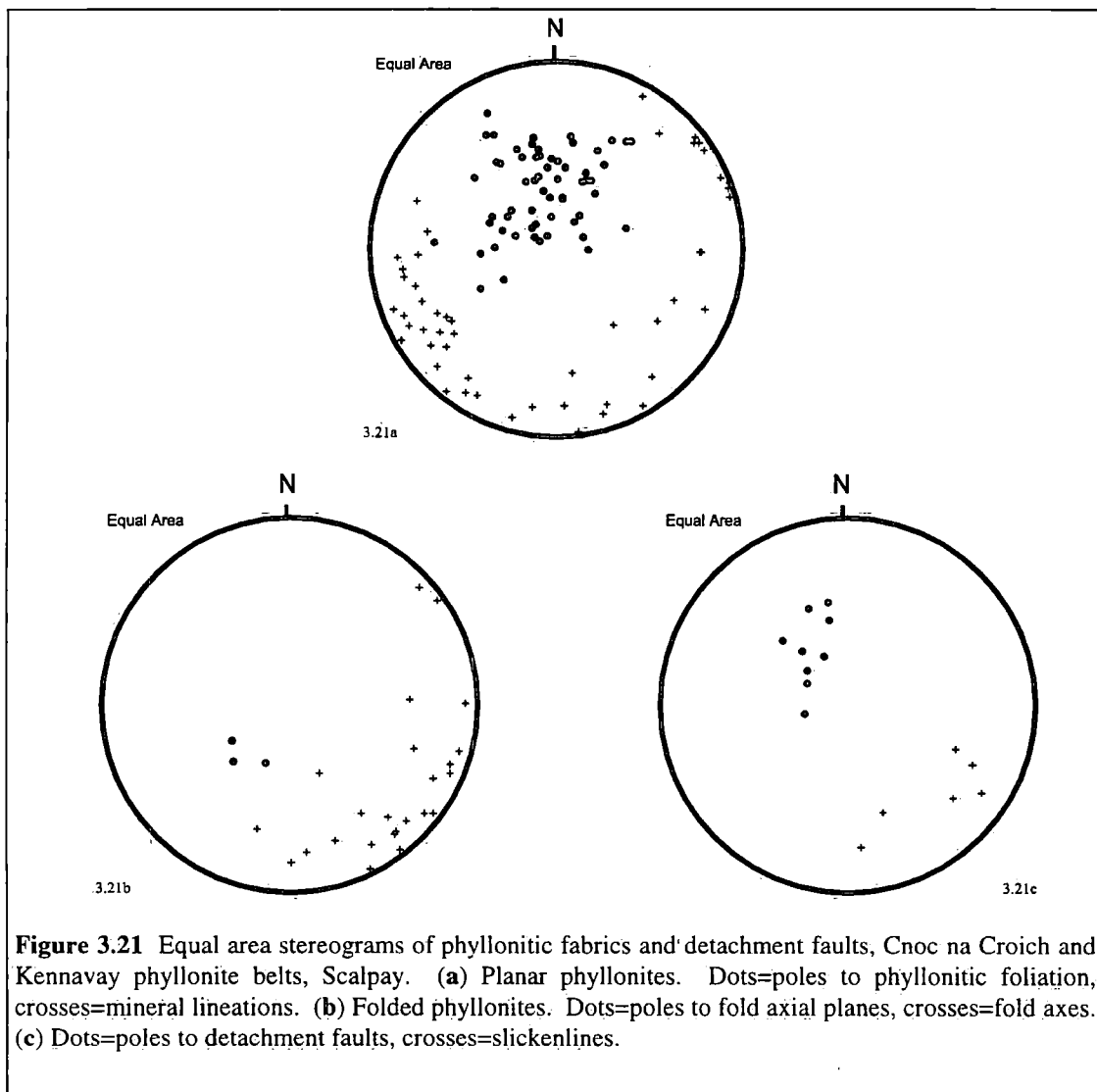
The 'phyllonites' described in the present section are distinguished from the earlier 'phyllosilicate-rich mylonites' (section 3.2.2.2) by an absence of actinolite and by the complete retrogression of minor amphibolite bodies (e.g. Younger Basic dykes; section 2.2.2.4) to aggregates of chlorite and partially sericitised feldspar.

#### ***The Cnoc na Croich and Kennavay phyllonite belts***

The Cnoc na Croich and Kennavay phyllonite belts comprise an assemblage of protophyllonite / protomylonite, phyllonite and ultraphyllonite. The foliation dips moderately towards the SSW or SSE and is associated with a predominantly sub-horizontal, strike-parallel NE-SW trending mineral lineation (Fig. 3.21a). Asymmetric shear bands viewed in surfaces parallel to the mineral lineation and perpendicular to the foliation are consistent with top-to-the-NE directed shear (i.e. sinistral strike-slip; see also Butler *et al.* 1995). NNW- and SE-plunging mineral lineations are locally preserved within protophyllonitic / protomylonitic lithologies which are exposed at the base of the Kennavay phyllonite belt (NG 230 944) (Fig. 3.21a).  $\sigma$ -type feldspar porphyroclasts viewed in surfaces parallel to the down-dip plunging mineral lineation and perpendicular to the foliation are consistent with top-to-the-NW or -NNW directed shear (i.e. thrusting / transpression) (Chapter 5).

The phyllonitic fabrics in both the Cnoc an Croich and Kennavay belts are commonly observed to be deformed by cascades of highly curvilinear SW-verging folds (wavelengths  $\leq 20\text{cm}$ ) (Fig. 3.21b). Aggregates of coarse grained quartz-carbonate-albite-chlorite ('saddle reefs') are commonly preserved in fold hinge regions. The coarse grained aggregates are clearly wrapped by the phyllonitic foliation and locally, are themselves deformed by folding.

SE-dipping detachment faults are developed at the margins of the Cnoc na Croich and Kennavay phyllonite belts. The detachment faults are oriented sub-parallel to the phyllonitic foliation and are associated with shallowly SE- and SSE-plunging slickenlines (Fig. 3.21c). The geometry of the minor fault planes associated with individual detachment surfaces are consistent with top-to-the-SE or -SSE displacements.



### ***Microstructure***

*Protoliths* The microstructures of the upper greenschist facies pervasive mylonite are described in section 3.2.2.2.

*Phyllonites* The phyllonitic fabrics from the Scalpay, Kebock Head and Loch Bhrollum belts are characterised by partially sericitised feldspar porphyroclasts which 'float' in a matrix of interconnected sericite or chlorite strands, polycrystalline quartz ribbons and aggregates of ultrafine grained recrystallised feldspar.

Small, partially chloritised hornblende grains ( $\leq 0.1\text{mm}$  diameter) are locally preserved and are commonly observed to be boudinaged parallel to the macroscopic mineral lineation. The boudin necks and strain shadows associated with these deformed hornblende grains are typically infilled by chlorite laths which are aligned parallel to the macroscopic mineral lineation. Asymmetric shear bands preserved in planar phyllonites are commonly observed to be infilled by aggregates of chlorite and twinned calcite grains, whilst the 'saddle reefs' associated with the folded phyllonites comprise aggregates of chlorite, twinned calcite and partially recrystallised quartz and feldspar grains.

### ***Summary and discussion***

The geometries of the fabrics preserved at the base of the Kennavay phyllonite belt are consistent with a progressive change in kinematic regime, from localised top-to-the-NW thrusting to localised top-to-the-NE (sinistral) strike-slip deformation on Scalpay. Sinistral strike-slip related fabrics are commonly observed in both the Cnoc na Croich and Kennavay belts. These observations suggest that the *onset* of phyllonitisation may have been synchronous with the change in kinematic regime from thrusting to strike-slip, and that either (a) the thrust-related phyllonites were extensively reworked during strike-slip, or that (b) the *main* phase of phyllonitisation was synchronous with sinistral strike-slip.

The phyllonitic fabrics were subsequently reactivated and deformed by a series of SW-verging folds. The geometry of the folds is consistent with top-to-the-SW directed dextral strike-slip within the Cnoc na Croich and Kennavay phyllonite belts. Top-to-the-SE normal displacements were localised along the shallowly dipping detachment faults following the cessation of shearing within the phyllonite belts.

Microstructural observations of the Scalpay, Kebock Head and Loch Bhrollum phyllonites suggest that similar deformation mechanisms and metamorphic conditions prevailed during phyllonitisation at all three localities. Boudinaged hornblende grains are locally 'fringed' by fibrous chlorite strain shadows, which suggests that sites of localised dilatation acted as DMT sinks during top-to-the-E or -NE directed shearing. The presence of deformed quartz-calcite-chlorite-albite aggregates within asymmetric

shear band and in fold hinges is consistent with the operation of fluid-assisted DMT during top-to-the-S or -SW shearing and reworking of the phyllonitic fabrics. Fluid-assisted DMT mechanisms are operative in the presence of a syn-tectonic fluid phase, which suggests that there was a significant influx of fluids into the fault zone during phyllonitisation and possibly also extensional reworking (see Chapter 9).

The syn-tectonic breakdown of feldspar and hornblende to produce aggregates of sericite and chlorite, together with the observed quartz deformation microstructures suggest that phyllonitisation took place at temperatures and pressures consistent with lower greenschist facies conditions (Chapter 1).

### **3.2.3.5 Summary and discussion**

The phyllonite belts preserved in the Northern Zone of the Outer Hebrides Fault Zone have experienced a polyphase kinematic and textural evolution. At each of the localities studied, phyllonitisation was associated with localised lower greenschist facies retrogression and syn-tectonic fluid influx into the fault zone. The Eishken, Kebock Head and Loch Bhrollum phyllonite belts originated during top-to-the-E directed shear and were subsequently reactivated during top-to-the-S directed extension. In contrast, the onset of phyllonitisation on Scalpay was synchronous with the transition from top-to-the-NW thrusting to top-to-the-NE sinistral strike-slip. The phyllonitic fabrics on Scalpay were subsequently reworked during top-to-the-SW directed dextral strike-slip.

A phase of top-to-the-SE normal faulting has been recognised on Scalpay, but appears to be largely absent further north.

Two important questions which need to be addressed are:

- Were phyllonitisation and reactivation on Scalpay broadly synchronous with phyllonitisation and reactivation at Eishken, Kebock Head and Loch Bhrollum?
- Can the kinematic histories recognised within individual phyllonite belts be integrated to provide a kinematic model for the entire Northern Zone?

#### ***The relative timing of phyllonitisation and reactivation***

At Eishken, phyllonitisation clearly post-dates lower amphibolite facies mylonitisation, pseudotachylyte generation and brittle fracturing (section 3.2.3.1). At Kebock Head, Loch Bhrollum and on Scalpay, phyllonitisation clearly post-dates upper greenschist facies thrust-related mylonitisation and subsequent cataclasis and brittle fracturing (sections 3.2.2.2, 3.2.2.3 & 3.2.2.4).

The earliest phase of phyllonitisation recognised at Eishken, Kebock Head and Loch Bhrollum was associated with macroscopically ductile top-to-the-E directed shearing

under fluid-rich, lower greenschist facies conditions. These observations suggest that phyllonitisation throughout southeast Lewis took place under similar kinematic and environmental regimes.

Although the onset of phyllonitisation on Scalpay was associated with top-to-the-NW or -NNW thrusting / transpression, the *principal* phase of phyllonitisation probably took place under a regime of top-to-the-NE sinistral strike-slip (see also Butler *et al.* 1995). The style of deformation and the inferred grade of metamorphism associated with strike-slip displacements on Scalpay are indistinguishable from the style of deformation and the inferred grade of metamorphism associated with top-to-the-E directed shear at Eishken, Kebock Head and Loch Bhrollum. In the absence of any evidence to the contrary, it is suggested that phyllonitisation and sinistral strike-slip on Scalpay were broadly synchronous with phyllonitisation and top-to-the-E shear at Eishken, Kebock Head and Loch Bhrollum.

The phyllonitic fabrics at each locality were subsequently reworked and folded during top-to-the-S (at Eishken, Kebock Head and Loch Bhrollum), or top-to-the-SW (on Scalpay) directed shear. The mineral assemblages and the style of deformation observed in packages of reworked phyllonites are very similar at each locality. It is therefore inferred that reworking of the Scalpay, Eishken, Kebock Head and Loch Bhrollum phyllonite belts took place under similar metamorphic regimes. In the absence of any evidence to the contrary, it is therefore suggested that top-to-the-SW shearing on Scalpay was broadly synchronous with top-to-the-S shearing at Eishken, Kebock Head and Loch Bhrollum. As both the ENE-WSW trending Loch Bhrollum phyllonite belt and the N-S trending Eishken and Kebock Head phyllonite belts preserve evidence which is consistent with top-to-the-S directed shear, it is suggested that the *regional* displacement vector was towards the south. In the following section, it will be shown that the unique kinematic history associated with the phyllonite belts exposed on Scalpay can be explained by the overall geometry of the Northern Zone phyllonite belts (see also Butler 1995 & Butler *et al.* 1995).

#### ***A kinematic model for the Northern Zone phyllonite belts***

The geometry of the phyllonite belts preserved in the Northern Zone of the Outer Hebrides Fault Zone has clearly been influenced by the geometry of the pre-existing pervasive mylonite belt (Fig. 3.3; section 3.2.1.5). The controls on this geological inheritance are discussed below (section 3.7; see also Butler 1995). However, it is adequate to note here that as a result, some of the Northern Zone phyllonite belts were not 'ideally' oriented to accommodate regional top-to-the-S displacements. In particular, the NNE-SSW to NE-SW trending Cnoc na Croich and Kennavay phyllonite belts (section 3.2.3.4) are oriented oblique to the regional S-directed

displacement vector (Fig. 3.22). There are two possible kinematic models which explain how regional top-to-the-S displacements were accommodated in Scalpay:

- (1) Oblique, top-to-the-S shear (i.e. dextral transtension) within the phyllonite belts on Scalpay.
- (2) Kinematic partitioning of the overall top-to-the-S displacement into a relatively large component of dextral strike-slip and a relatively small component of top-to-the-SE dip-slip on Scalpay (Fig. 3.22).

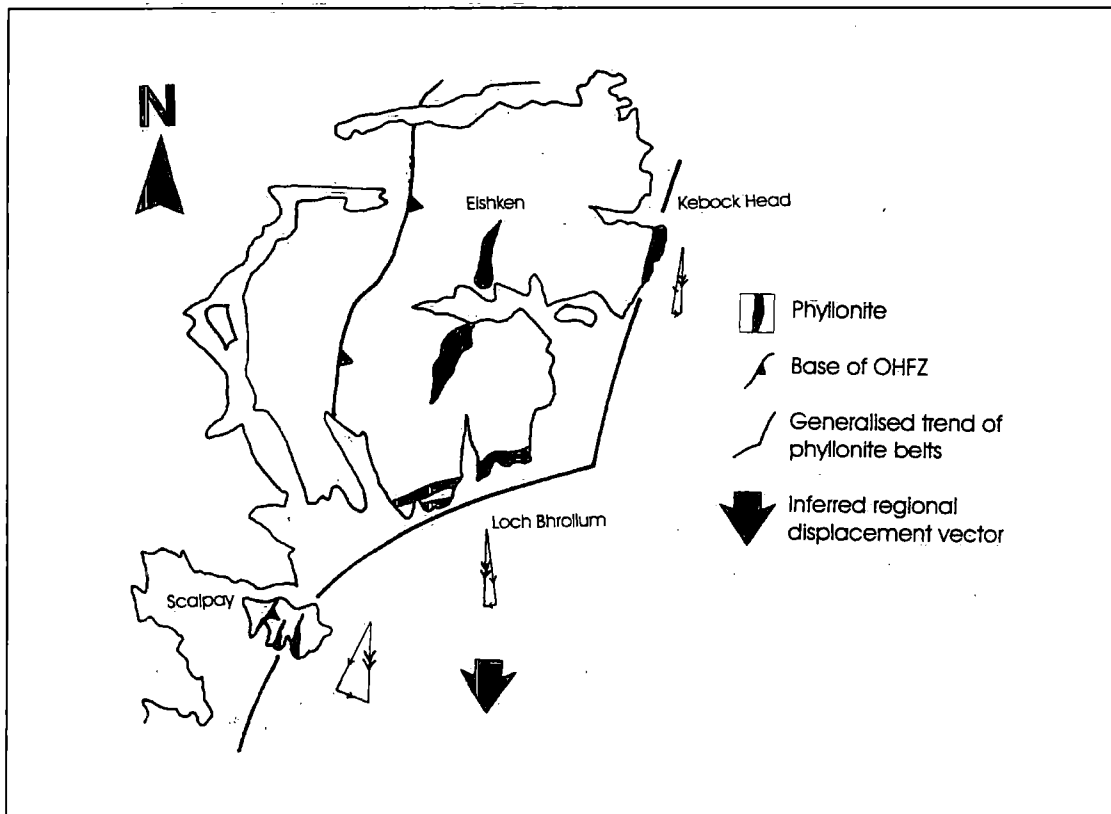


**Figure 3.22** Simplified map showing the possible kinematic regime during top-to-the-S extension in the Northern Zone of the OHFZ. The deformation can be accommodated by dip-slip down the phyllonitic foliation in the Eishken, Kebock Head and Loch Bhrollum phyllonite belts. The phyllonite belts exposed on Scalpay occupy a 'hinge' region of the OHFZ and the foliation is therefore oriented oblique to the regional extension vector. On Scalpay, the deformation can therefore be accommodated by dextral strike-slip within the phyllonite belts and by top-to-the-SE dip-slip along SE-dipping detachment faults. An arbitrary magnitude has been assigned to the regional S-directed extension vector, but the extension vector is assumed to be of the same magnitude throughout southeast Lewis and on Scalpay.

The geometries of the folded phyllonites preserved within the Cnoc na Croich and Kennavay belts on Scalpay are consistent with top-to-the-SW dextral strike-slip (section 3.2.3.4). It is therefore unlikely that significant oblique-slip displacements were localised within the phyllonite belts on Scalpay. However, in order to invoke kinematic partitioning of the regional top-to-the-S movement vector, it is necessary to account for the top-to-the-SE dip-slip component (Fig. 3.22).

SE-dipping detachment faults are developed along the margins of the Cnoc na Croich and Kennavay phyllonite belts (section 3.2.3.4). The detachment faults are associated with SE-plunging slickenlines and are inferred to have accommodated predominantly normal (i.e. top-to-the-SE) displacements. Whilst the latest movements along the detachments clearly post-date the latest movements along the phyllonite belts, it is feasible that the detachment faults were *initiated* during top-to-the-SW reworking of the phyllonitic fabrics. It is therefore suggested that kinematic partitioning on Scalpay was achieved by a small component of top-to-the-SE dip-slip along a system of detachment faults and by significant dextral strike-slip displacements across the Cnoc na Croich and Kennavay phyllonite belts. Whilst the field relationships preserved on Scalpay do not provide unequivocal evidence for kinematic partitioning of the regional top-to-the-S displacement vector, the partitioning model is consistent with the virtual absence of detachment faults in southeast Lewis (Fig. 3.22).

### 3.2.4 NORMAL FAULTS

A set of steeply dipping faults are widely developed throughout the Northern Zone of the Outer Hebrides Fault Zone (Butler 1995). These faults post-date the pervasive mylonites, phyllonites and detachment faults and are thought to have been associated with the development of the Mesozoic North Minch and Sea of the Hebrides basins (Butler 1995; Chapter 2 of the present work). The distribution and regional significance of 'late' faulting has been discussed in some detail by previous authors (e.g. Steel & Wilson 1975; Butler 1995). The aim of the present work is to describe the geometry and style of faulting and in particular, to assess the possible role fluids may have played during deformation. A number of well exposed localities in northeast Lewis are described in the following sections (Fig. 3.1).

#### 3.2.4.1 Gob Hais

A network of brittle faults, which cross-cut otherwise unmodified Lewisian gneisses, and are particularly well exposed in a N-S trending cliff section to the south of Gob Hais (NB 537 494) (Figs. 3.1 & 3.23).

Three different sets of faults have been identified at Gob Hais. A set of shallowly to moderately SE-dipping faults is clearly offset by a set of steeply SW-dipping faults and by a set of steeply NE-dipping faults (Figs. 3.23 & 3.26). The relative ages of the NE- and SW-dipping faults are unclear from the field relationships, but Butler (1995) has suggested that both sets of structures are of broadly the same age.

The shallowly to moderately SE-dipping fault planes are typically lined by thin ( $\leq 10$ cm thick) layers of clay-rich gouge  $\pm$  clasts of brecciated gneiss. Slickenlines have not been observed, but offsets of gneissose banding and amphibolite pods are



consistent with both apparent compressional and apparent extensional displacements across these shallowly to moderately SE-dipping faults.

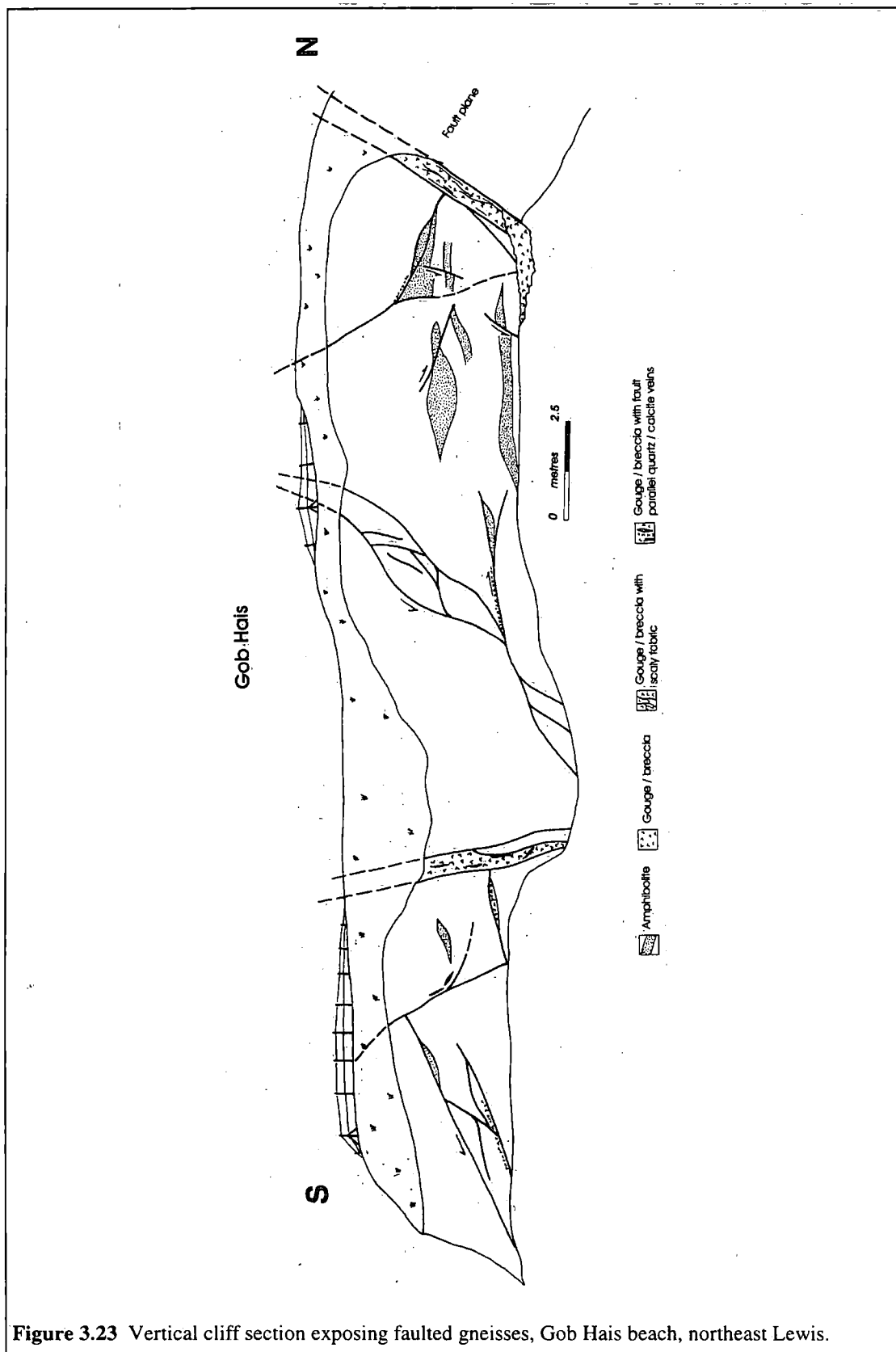
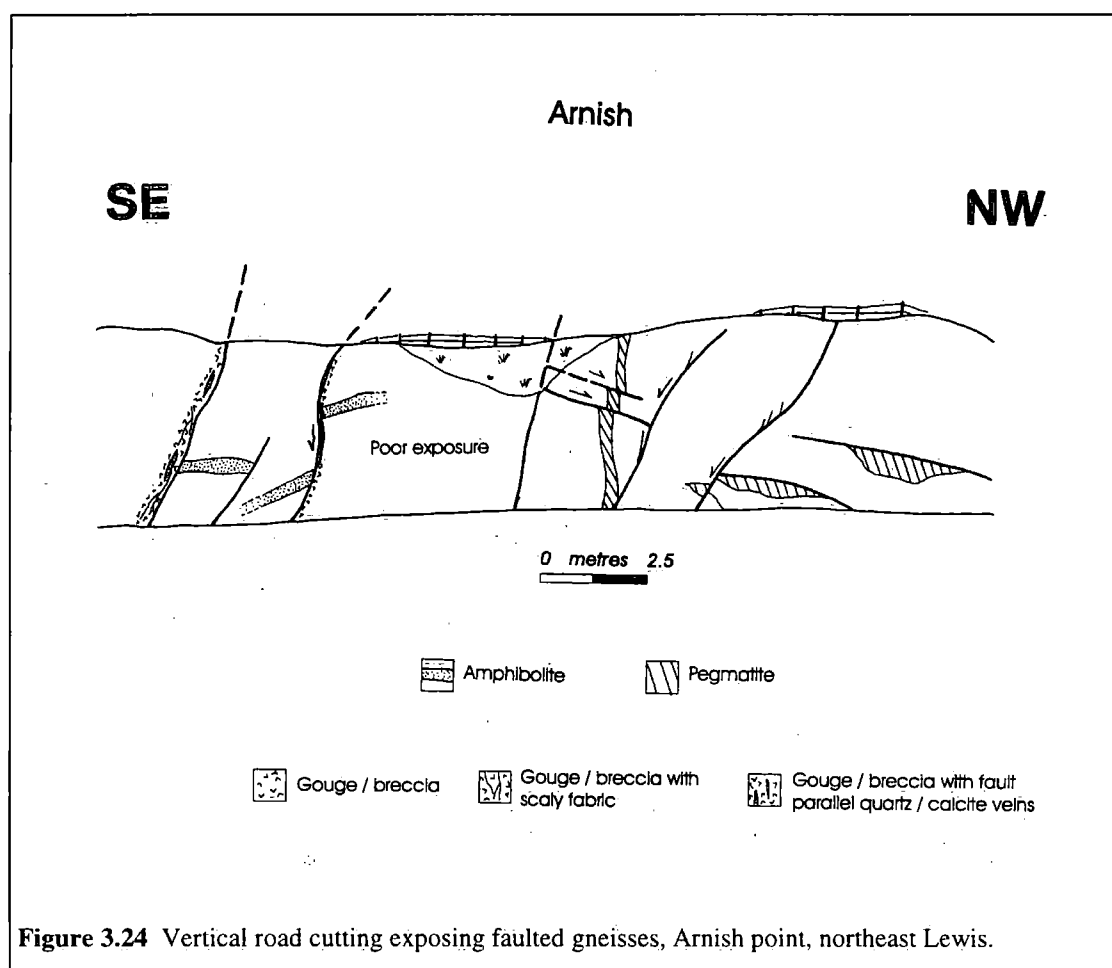


Figure 3.23 Vertical cliff section exposing faulted gneisses, Gob Hais beach, northeast Lewis.

The steeply SW- and NE-dipping faults are commonly observed to be lined by scaly, clay-rich gouges ( $\leq 5\text{cm}$  thick) and / or bands of brecciated gneiss. Quartz-carbonate veins ( $\leq 0.5\text{cm}$  thick) are locally developed *within* gouge / breccia zones and are oriented sub-parallel to the host fault plane (Fig. 3.23). Down dip-plunging slickenlines are locally preserved on both SW- and NE-dipping fault planes. The geometries of subsidiary fracture arrays are consistent with predominantly extensional displacements along the steeply SW- and NE-dipping faults.

### 3.2.4.2 Arnish

Brittle faults, which cross-cut otherwise unmodified Lewisian gneisses, are well exposed in a NW-SE trending road cutting to the west of Arnish Point (NB 425 303) (Figs. 3.1 & 3.24).



Two different sets of faults have been recognised at Arnish. A set of shallowly NW-dipping faults are clearly cross-cut by a set of steeply E- and SE-dipping faults (Figs. 3.24 & 3.26). The shallowly NW-dipping structures are typically discrete fractures which are not associated with gouge / breccia layers. Slickenlines have not been

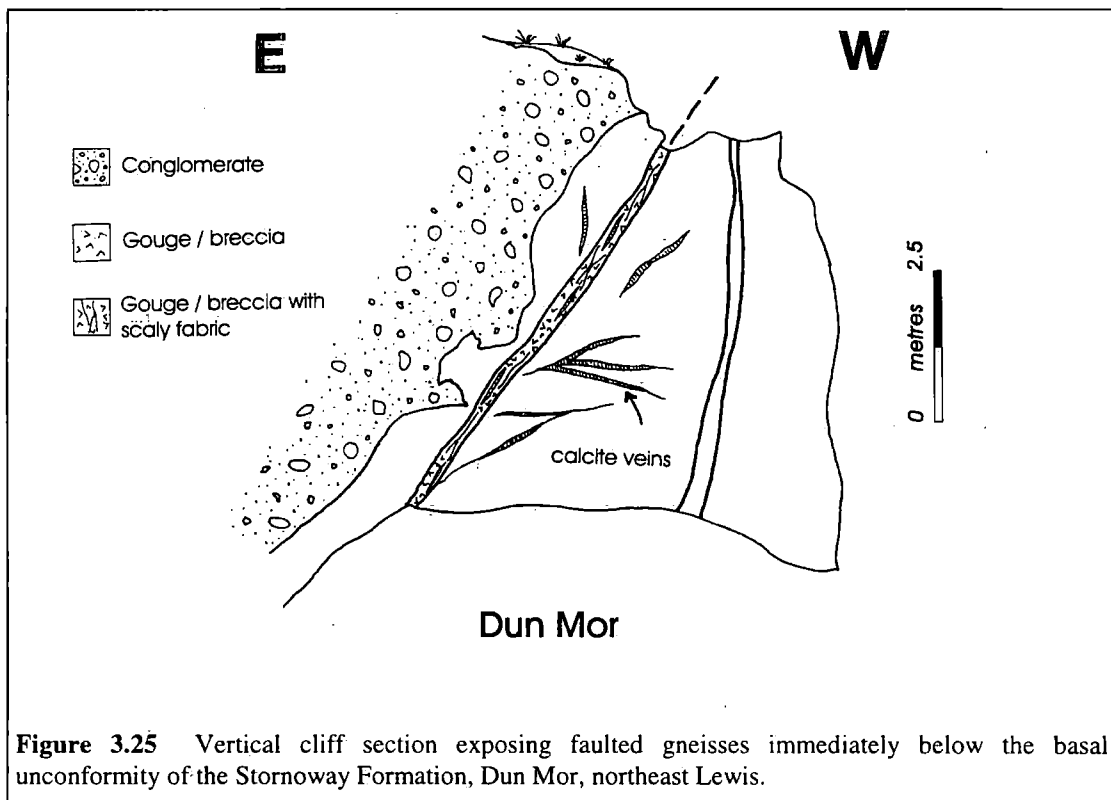
observed, but the geometries of offset pegmatite veins are consistent with apparent extensional displacements across the shallowly NW-dipping faults.

The steeply dipping faults are locally associated with zones of severely crushed gneiss ( $\leq 30\text{cm}$  thick on either side of the fault plane). Scaly gouges ( $\leq 20\text{cm}$  thick), which contain fault-parallel calcite veins, have been observed along some of the steeply dipping fault surfaces (Fig. 3.24). Both E- and SE-dipping faults are associated with predominantly down-dip plunging slickenlines. The geometries of displaced amphibolite bodies and the geometries of subsidiary fracture arrays are consistent with extensional displacements across the steeply E- and SE-dipping fault planes.

### 3.2.4.3 Dun Mor

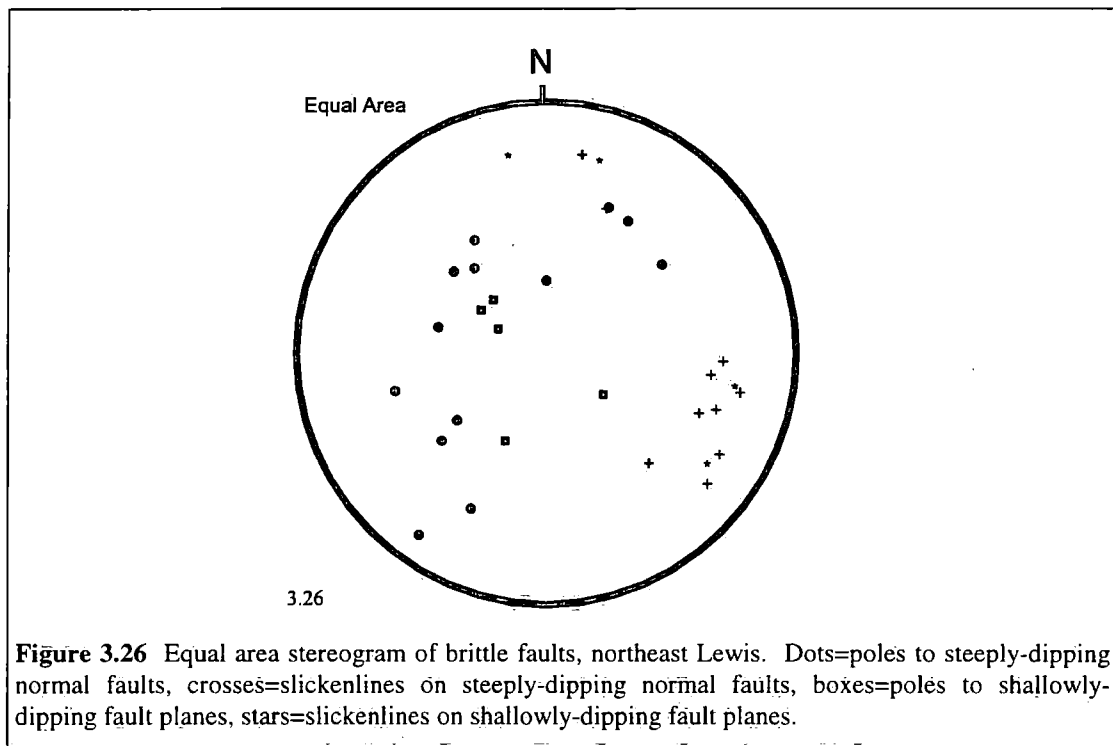
The basal unconformity of the Permo-Triassic Stornoway Formation (Steel & Wilson; Chapter 2 of the present work) is exposed at Dun Mor (NB 515 340) on the Eye Peninsular (Figs. 3.3 & 3.25). The unconformity itself is *not* faulted, but a steeply E-dipping fault cross-cuts gneisses immediately below the surface of the unconformity (Fig. 3.25).

The fault is lined by up to 30cm of scaly red gouge which contains a number of undulating, fault-parallel calcite veins. Slickenlines have not been observed. The gneisses (and locally the conglomerates) are cross-cut by an irregular network of calcite veins (Fig. 3.25).



#### 3.2.4.4 Summary and discussion

A set of 'early', shallowly dipping normal and reverse faults is cross-cut up to two sets of steeply dipping normal faults (Fig. 3.26). The shallowly dipping faults are associated with an extremely brittle style of deformation and there is little evidence to suggest that fluids played an important role during deformation. In contrast, the steeply dipping normal faults are typically associated with scaly clay-rich gouges  $\pm$  fault-parallel quartz or calcite veins. The development of fault-parallel veins is consistent with localised, transient high pore fluid pressures during faulting. The fluids appear to have been saturated with respect to calcite and silica.



### 3.2.5 SUMMARY: KINEMATIC EVOLUTION AND FLUID-ROCK INTERACTIONS ALONG THE NORTHERN ZONE OF THE OHFZ

The kinematic, textural and metamorphic evolution of the Northern Zone of the Outer Hebrides Fault Zone is summarised in Table 3.1.

<b>Kinematic regime</b>	<b>Fault rocks / structures</b>	<b>Metamorphism / fluids</b>
<b>1. Regional top-to-NW thrusting</b> (Oldest)	Mylonites and pseudotachylytes developed in the region between Loch Erisort and Loch Sgibacleit. Mylonites developed at Kebock Head and on Scalpay.	'Dry' lower amphibolite facies conditions prevailed in the region between Loch Sgibacleit and Loch Erisort. Localised syn-tectonic fluid influx and upper greenschist facies retrogression at Kebock Head and on Scalpay.
<b>2. ?Regional top-to-W or -NW thrusting</b>	Cataclasites, brittle faults and localised pseudotachylytes. Brittle deformation most intense in regions of lower amphibolite mylonite, but virtually absent in regions of upper greenschist facies mylonite.	Fluid absent?
<b>3. Regional top-to-E shear (top-to-NE on Scalpay)</b>	Phyllonite belts.	Localised syn-tectonic fluid influx and lower greenschist facies retrogression associated with phyllonitisation.
<b>4. Regional top-to-S shear</b>	Reworking of phyllonitic fabrics. Possibly associated with localised brittle faulting on Scalpay.	Fluids present, probably associated with continued lower greenschist facies retrogression.
<b>5. Top-to-E normal faulting</b> (Youngest)	Mainly steep normal faults with gouges and breccias.	Upper crustal conditions. Transient high pore fluid pressures during faulting.

**Table 3.1.** Summary of the kinematic, textural and metamorphic evolution of the Northern Zone of the OHFZ.

### 3.3 SOUTH HARRIS

The only onshore outcrops of the OHFZ in South Harris are preserved on the small east coast promontories of Rubha Vallerip (NG 059 830) and Rubha Quidnish (NG 098 864). At both these localities, the OHFZ is characterised by a zone ( $\leq 200\text{m}$  thick) of intense brittle deformation, which is overprinted by NNE-SSW trending belts of phyllonite (Fettes *et al.* 1992). Note that pervasive mylonite has not been observed on the mainland of South Harris. Unfortunately, the author did not visit Rubha Quidnish, so the following section is limited to a description of the rocks exposed at Rubha Vallerip.

#### 3.3.1 RUBHA VALLERIP

Rubha Vallerip occupies a unique position in that it lies along strike of the South Harris Shear Zones (Figs. 3.1 & 3.3) and strictly speaking, does not belong to either the Northern or Southern Zones of the OHFZ. The kinematic and textural evolution of the OHFZ at Rubha Vallerip is therefore of crucial importance in understanding the geological relationship between the Northern and Southern Zones.

##### 3.3.1.1 Protoliths

The fault rocks are entirely derived from the granulite facies meta-anorthosite body which outcrops immediately to the west of Rubha Vallerip (Fettes *et al.* 1992; section 2.2.2.3 of the present work).

##### 3.3.1.2 Brittle deformation

The effects of brittle deformation are widespread, but heterogeneously distributed. Blocks ( $\leq 10\text{m}$  wide) of relatively undeformed meta-anorthosite 'float' in a matrix of crushed meta-anorthosite, pale green cataclasite and seams of devitrified pseudotachylyte. The size of the meta-anorthosite blocks and the proportion of blocks to matrix both decrease towards the east coast. The cataclasite and / or devitrified pseudotachylyte seams appear to be randomly oriented and cross-cutting relationships suggest that there have been several phases of cataclasis and / or pseudotachylyte generation. The cataclasite and pseudotachylyte seams are themselves cross-cut by a network of closely spaced brittle fractures.

##### 3.3.1.3 The Rubha Vallerip phyllonite belt

A NNE-SSW trending phyllonite belt outcrops along the east coast of Rubha Vallerip. The phyllonite belt is at least 10m thick, although its upper margin is not exposed onshore. The phyllonite belt comprises an assemblage of protophyllonites, phyllonites

and ultraphyllonites which 'wrap' clasts ( $\leq 2\text{m}$  thick) of highly altered, cataclastically deformed meta-anorthosite.

The moderately ESE-dipping protophyllonitic foliation is associated with either a NW-SE or an E-W trending mineral lineation (Fig. 3.27a). Kinematic indicators have not been observed in protophyllonites which are associated with a NW-SE trending mineral lineation. However, asymmetric shear bands viewed in surfaces parallel to the E-W trending mineral lineation are consistent with top-to-the-E directed shear (i.e. extension).

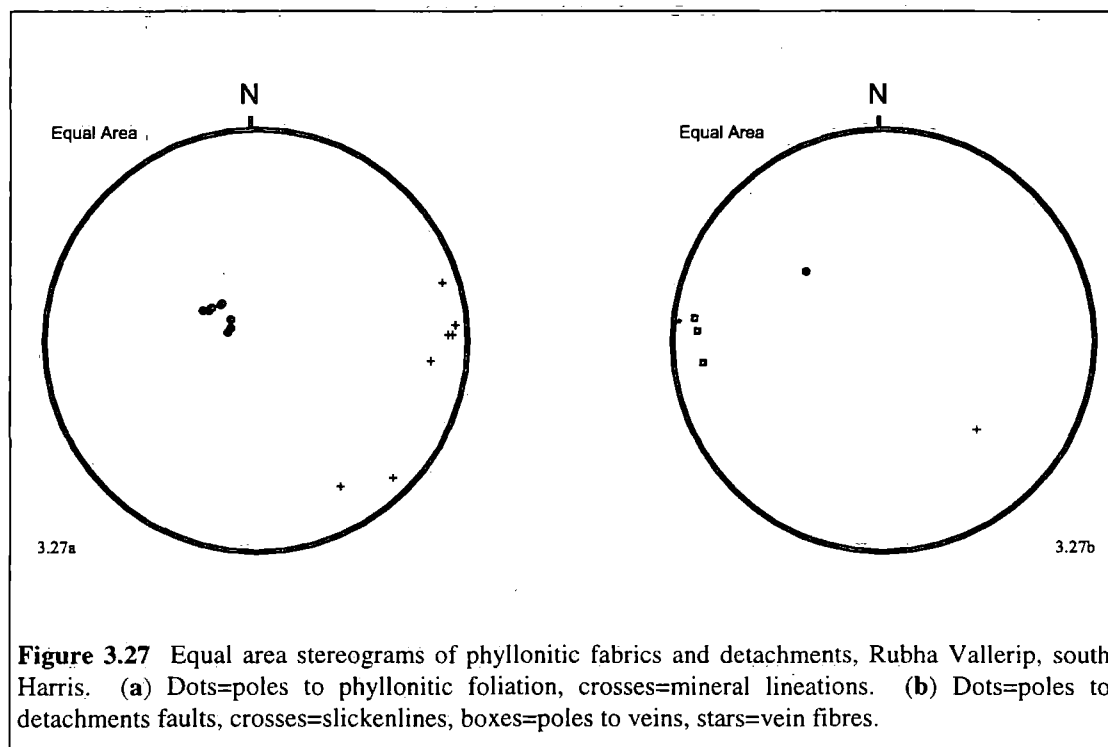


**Figure 3.27** Equal area stereograms of phyllonitic fabrics and detachments, Rubha Vallerip, south Harris. (a) Dots=poles to phyllonitic foliation, crosses=mineral lineations. (b) Dots=poles to detachments faults, crosses=slickenlines, boxes=poles to veins, stars=vein fibres.

The protophyllonitic fabrics clearly overprint the pre-existing 'cataclasite' seams, although the precise geometry of the deformed 'cataclasite' seams is very variable. Relict 'cataclasite' seams which are overprinted by protophyllonitic fabrics associated with a NW-SE trending mineral lineation are clearly discordant to the protophyllonitic foliation. In contrast, relict 'cataclasite' seams preserved in extension-related protophyllonites are oriented sub-parallel to the protophyllonitic foliation.

Moderately ESE-dipping phyllonites and ultraphyllonites are locally well developed. The phyllonitic / ultraphyllonitic foliation is associated with an E-W trending mineral lineation and asymmetric shear bands and poorly developed  $\sigma$ -type feldspar porphyroclasts viewed in surfaces parallel to the mineral lineation and perpendicular to the foliation are consistent with top-to-the-E shearing (i.e. extension). The phyllonitic / ultraphyllonitic fabrics are cross-cut by an array of undeformed, N-S

trending quartz veins. The orientation of the quartz fibres is consistent with E-W extension (Fig. 3.27b).

The phyllonite belt is cross-cut by a number of poorly exposed SE-dipping detachment faults. The detachment faults are developed at the margins of crushed meta-anorthosite blocks and are associated with SE-plunging slickenlines. The sense of displacement across the detachment faults is not known.

#### **3.3.1.4 Microstructure**

*Crushed meta-anorthosite* The blocks of crushed meta-anorthosite comprise an assemblage of partially sericitised feldspar (?plagioclase), hornblende, chlorite, quartz and epidote, which is cross-cut by a network of brittle fractures. The hornblende grains are partially replaced by aggregates of chlorite and epidote, whilst the fractures are host to aggregates of fine grained, undeformed epidote.

*Protophyllonite* The protophyllonites comprise locally interconnected sericite strands which enclose mm-scale augen of crushed meta-anorthosite.

*Phyllonite and ultraphyllonite* The microstructures of the phyllonites and ultraphyllonites are characterised by viscously deformed cataclasite and pseudotachylyte veins which contain sericite strands and porphyroclasts of quartz and partially sericitised feldspar (cf. section 3.2.2.1). The quartz grains display strong patchy undulose extinction. Aggregates of fibrous chlorite are locally developed in strain shadows around the margins of the quartz porphyroclasts..

#### **3.3.1.5 Summary and discussion**

It is clear from the preceding descriptions that a phase of cataclasis, pseudotachylyte generation and brittle faulting was post-dated by an episode of phyllonitisation and macroscopically ductile deformation. The phyllonites are apparently post-dated by a number of sub-parallel brittle detachment faults.

The age and overall kinematic regime under which cataclasis, pseudotachylyte generation and brittle faulting took place are rather unclear from the limited exposure available at Rubha Vallerip. However, the overall style of deformation observed at Rubha Vallerip is reminiscent of the North Uist crush melange which is thought to have developed during a phase of regional top-to-the-W thrusting (Sibson 1977b; Butler 1995; section 3.4 of the present work). It is therefore tentatively suggested that cataclasis, pseudotachylyte generation and brittle faulting at Rubha Vallerip were associated with top-to-the-W thrusting.

The protophyllonitic foliation developed near the margins of the phyllonite belt is associated with both NW-SE and E-W trending mineral lineations. It is unclear from field and microstructural observations whether or not these fabrics are of the same age, and whether or not they developed under the same kinematic regime.

The geometry of the relict 'cataclasite' seams preserved in the protophyllonites is a qualitative indicator of the magnitude of finite strain (Chapter 1). The discordance between the protophyllonitic foliation and the 'cataclasite' seams suggests that the protophyllonites associated with a NW-SE trending mineral lineation have experienced a relatively low magnitude of finite strain. This observation is consistent with an episode of phyllonitisation during NW-SE directed shearing at Rubha Vallerip (Chapter 1). In contrast, the presence of concordant 'cataclasite' seams suggests that the extension-related phyllonites have experienced a relatively high magnitude of finite strain. It is thus possible that the protophyllonitic fabrics which are associated with a NW-SE trending mineral lineation are relict fabrics (i.e. low strain 'windows'), which escaped reworking during subsequent top-to-the-E extension. However, observations of the phyllonitic fabrics preserved in South Uist suggest that relatively unstrained fabrics are *not* necessarily younger than relatively high strain fabrics (section 3.5; Chapter 7). In the absence of isotopic age dates, the relative ages of the different phyllonitic fabrics at Rubha Vallerip therefore remain uncertain.

The mineral assemblage which is preserved in the blocks of crushed meta-anorthosite suggests that the rocks have experienced partial retrogression and hydration under lower greenschist facies conditions. The presence of undeformed epidote aggregates along fracture planes is consistent with retrogression subsequent to the cessation of brittle deformation.

The microstructures associated with the phyllonitic fault rocks are very similar to those observed in the Eishken phyllonite belt (section 3.2.2.1). It is thus inferred that phyllonitisation was associated with syn-tectonic fluid influx into the fault zone at temperatures and pressures consistent with lower greenschist facies conditions. Partial retrogression of the meta-anorthosite was probably synchronous with phyllonitisation.

#### **3.4 THE SOUTHERN ZONE: NORTH UIST AND ADJACENT ISLANDS**

The following section comprises descriptions of (1) the local Lewisian geology and possible OHFZ-related localised deformation in the 'foreland' (section 3.4.1), (2) the crush melange and pseudotachylite-ultracataclasite crush zones (section 3.4.2) and (3) the phyllonitic fabrics (section 3.4.3), (Fig. 3.28). In contrast to the Northern Zone (section 3.2), the geology of the OHFZ in the North Uist region is fairly consistent (Figs. 2.5 & 3.28). As a result, the following sections are not sub-divided into individual localities, although attention will be drawn to any significant geographical variations. The localities visited during the present study are illustrated in Figure 3.29.

### 3.4.1 THE 'FORELAND'

#### 3.4.1.1 Protoliths

The 'foreland' is dominated by medium to coarse grained quartzo-feldspathic banded gneisses, which are associated with pods and lenses of coarse grained amphibolite ('Older Basics'; section 2.2.2.1). The gneissose banding predominantly dips moderately towards the north (Figs. 2.4 & 3.30a) and is widely observed to be deformed by flat lying metre-scale isoclinal folds. The folds are well exposed at Bàgh a' Bhiorain (NF 9075 6277) and Loch Eport (NF 895 630) and are thought to be of Laxfordian ('Dl<sub>2</sub>') age (Fettes *et al.* 1992; Chapter 2 of the present work). Note that the trace of the OHFZ clearly cross-cuts the regional Laxfordian structures preserved in the 'foreland' (Fig. 2.4). There is little evidence of widespread low grade alteration of the gneisses to the west of the OHFZ on North Uist (Fig. 3.28).

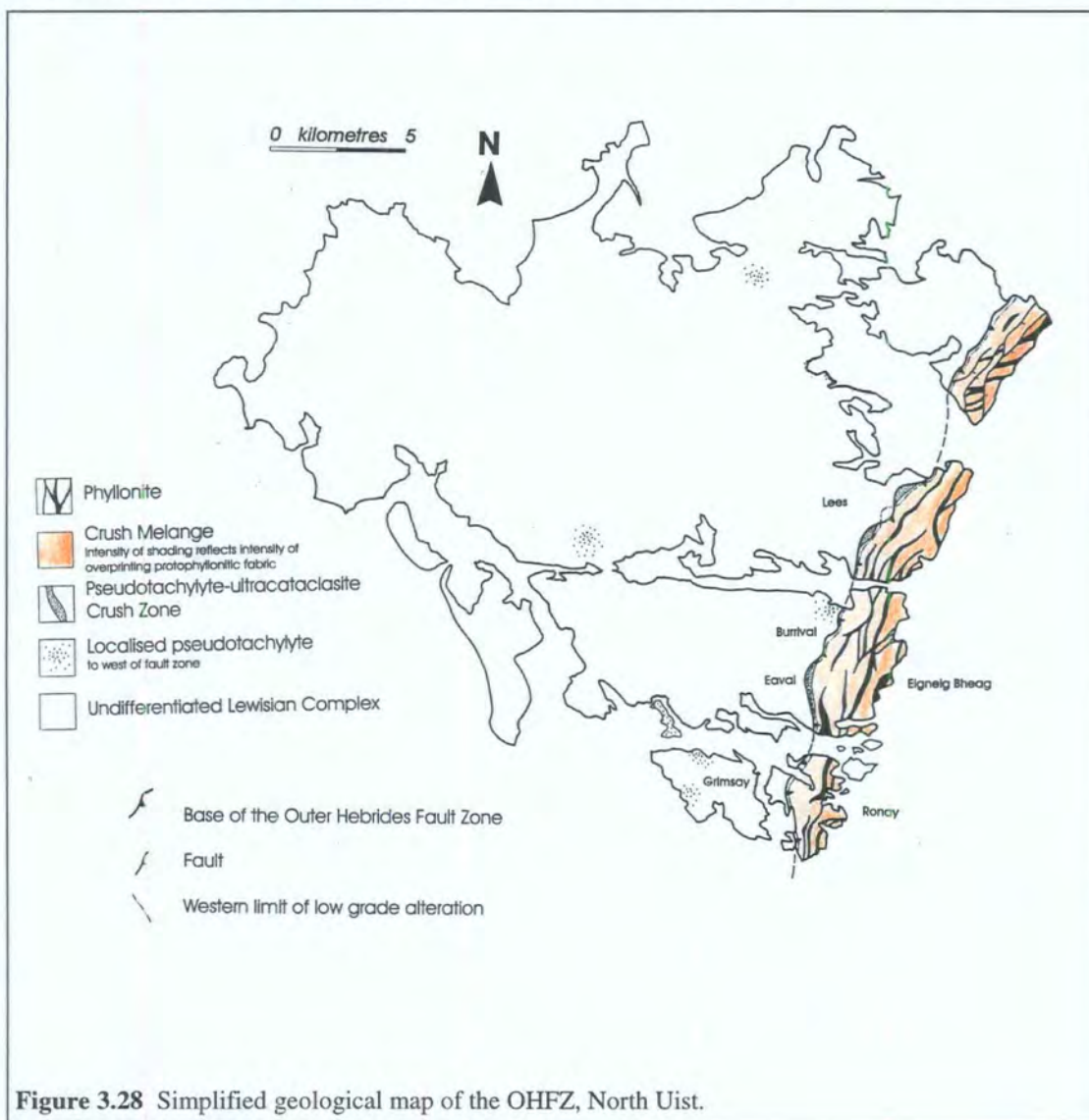


Figure 3.28 Simplified geological map of the OHFZ, North Uist.

### 3.4.1.2 Localised deformation in the 'foreland'

Evidence for localised deformation in the 'foreland' is widespread, but is rarely very intense (e.g. Fig. 3.28). The principal fault rocks / structures observed in the 'foreland' are (1) pseudotachylyte-bearing veins, breccias and quasi-conglomerates and (2) pseudotachylyte-barren brittle faults (Sibson 1977b; Butler 1995).

Moderately E- and / or W-dipping pseudotachylyte veins and brittle faults are well exposed on the small islands of Grimsay (e.g. NF 855 576) and Gairbh-eilean (NF 847 588) (Fig. 3.28). Apparent offsets of the gneissose banding are typically consistent with reverse (i.e. top-to-the-E or top-to-the-W) displacements during pseudotachylyte generation and brittle faulting (Butler 1995). The observed displacements rarely exceed more than a few tens of centimetres. Excellent examples of top-to-the-W reverse faults are exposed immediately to the west of the OHFZ on the southern shore of Loch Eport (NF 9054 6233).

The pseudotachylyte preserved at localities some distance to the west of the OHFZ (e.g. Grimsay, Gairbh-eilean and Clachan na Luib, NF 816 644; Fig. 3.32) is black in colour and appears to be fresh and glassy. In contrast, the pseudotachylyte preserved immediately below the base of the OHFZ (e.g. Bàgh a' Bhiorain; NF 9075 6277 - NF 9080 6275), is pale green in colour and appears to be completely devitrified. The devitrified pseudotachylyte veins are spatially associated with, and are locally cross-cut by a network of thin epidote veins ( $\leq 2$ cm thick) (Fig. 3.30b).

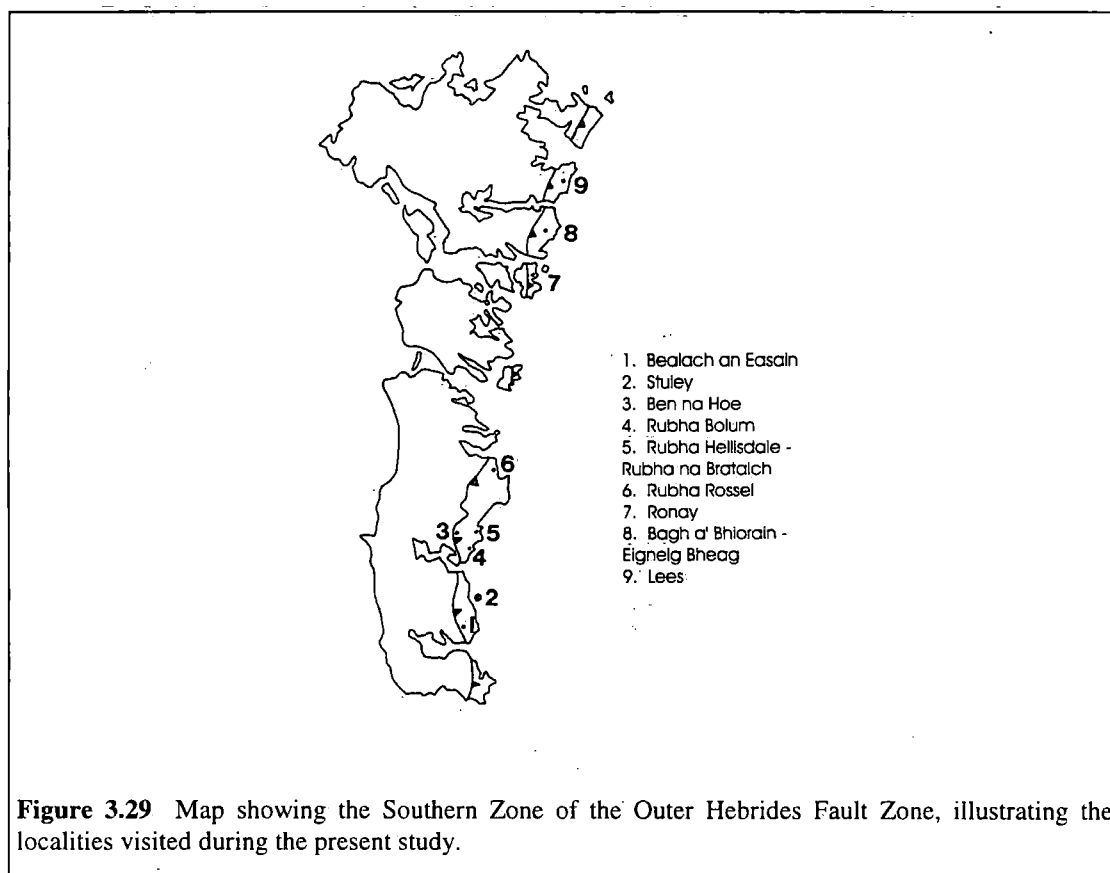


**Figure 3.29** Map showing the Southern Zone of the Outer Hebrides Fault Zone, illustrating the localities visited during the present study.

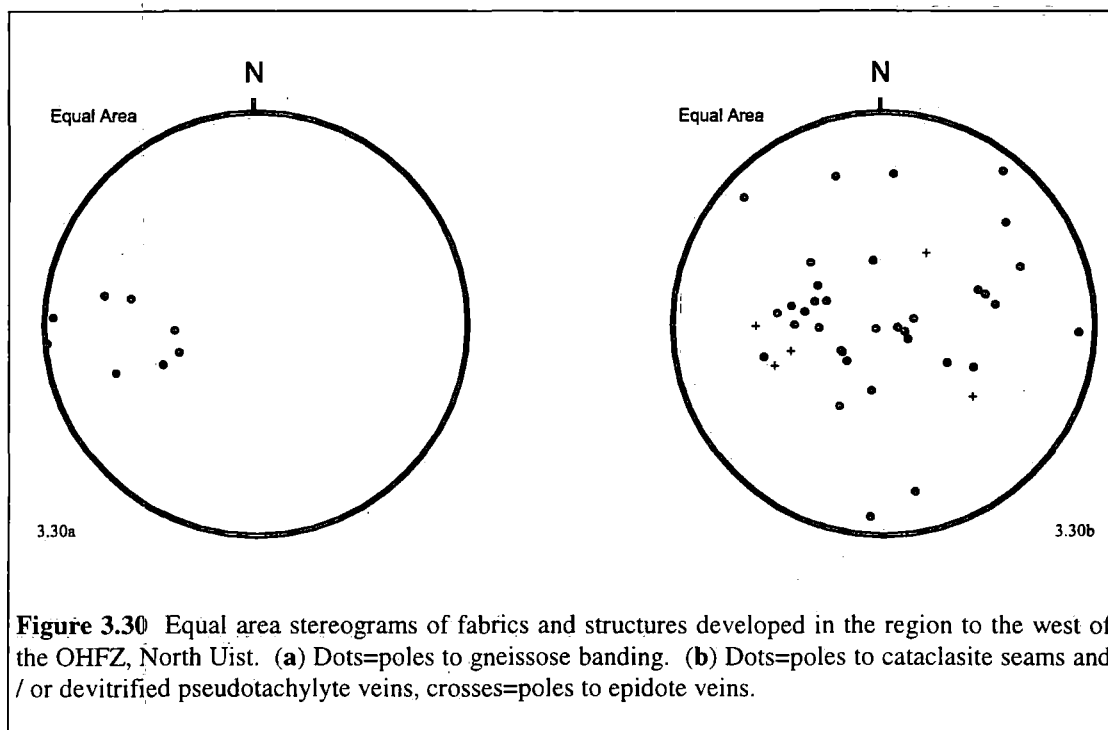


**Figure 3.30** Equal area stereograms of fabrics and structures developed in the region to the west of the OHFZ, North Uist. (a) Dots=poles to gneissose banding. (b) Dots=poles to cataclasite seams and / or devitrified pseudotachylyte veins, crosses=poles to epidote veins.

### 3.4.2 PSEUDOTACHYLYTE-ULTRACATACLASITE CRUSH ZONES AND CRUSH MELANGE

On North Uist, the OHFZ is characterised by a broad ( $\geq 1000\text{m}$  thick), E-dipping zone of intense brittle deformation. These 'cataclastic' fault rocks fall into two groups; (1) pseudotachylyte-ultracataclasite crush zones and (2) crush melange (Sibson 1977b) (Fig. 3.28).

#### 3.4.2.1 Pseudotachylyte-ultracataclasite crush zones

The pseudotachylyte-ultracataclasite crush zones are laterally discontinuous, fault-bounded lenses ( $\leq 30\text{m}$  thick) of pseudotachylyte, ultracataclasite and cataclasite which outcrop along the base of the OHFZ (Fig. 3.28). Crush zones are exposed immediately below the summits of North Lee (NF 932 667), South Lee (NF 919 650) and Eaval (NF 899 605) (Fig. 3.29) (Sibson 1977b). In regions where crush zones are absent (e.g. Burrival, NF 909 622), the topography is more subdued.

The crush zones are characterised by a few randomly oriented blocks of gneiss (typically  $\leq 1\text{m}$  diameter) which 'float' in a matrix of dark green, aphanitic ultracataclasite, cataclasite and devitrified pseudotachylyte (matrix  $\leq 70\%$  by volume). The entire assemblage is cross-cut by a network of apparently randomly oriented, closely spaced brittle fractures and joints. As a result, it is virtually impossible to make sense of the structures developed within the crush zones. However, Butler (1995) noted that the geometries of pseudotachylyte-bearing faults developed in

regions adjacent to the crush zones are typically consistent with top-to-the-W compression.

### 3.4.2.2 Crush melange

The crush melange is widely developed throughout eastern North Uist and outcrops to the east of the pseudotachylyte-ultracataclasite crush zones (Fig. 3.28).

The crush melange is characterised by blocks of relatively undeformed gneiss (typically  $\leq 5\text{m}$  diameter; locally  $\leq 100\text{m}$  diameter) which 'float' in a matrix of crushed gneiss, cataclasite and / or devitrified pseudotachylyte. The geometries of pseudotachylyte-bearing faults are consistent with either localised compression or localised extension. The overall proportion of pseudotachylyte / cataclasite is lower in the crush melange than in the pseudotachylyte-ultracataclasite crush zones.

The crush melange is cross-cut by a network of moderately E- and W-dipping cm- to m-scale brittle faults which predominantly display apparent reverse displacements (Butler 1995). A set of undeformed N-S trending quartz veins is locally developed within parts of the crush melange. The orientation of the fibrous vein infills are consistent with E-W extension during vein opening (White & Glasser 1987).

### 3.4.2.3 Microstructure

*Cataclasite / devitrified pseudotachylyte* The cataclasite / devitrified pseudotachylyte veins comprise an ultrafine grained mixture of quartz, feldspar (?albite), sericite and epidote which contains clasts of partially sericitised feldspar and fractured quartz. The margins of both the clasts and the 'cataclasite' seams appear to be overgrown by fine grained aggregates of undeformed epidote.

*Relict gneiss* The blocks of relatively undeformed gneiss comprise an assemblage of partially sericitised feldspar (predominantly albitic plagioclase  $\pm$  K-feldspar), hornblende, chlorite (after biotite), quartz and epidote. Individual quartz and feldspar grains are deformed by intragranular fractures and most quartz grains display intense patchy undulose extinction. In contrast, hornblende grains comparatively undeformed and unaltered. Transgranular fractures are widely developed and are infilled by fine grained aggregates of undeformed epidote.

### 3.4.2.4 Summary and discussion

It is clear from the preceding descriptions that there has been at least one phase of intense brittle deformation in the North Uist region, which involved cataclasis, pseudotachylyte generation and brittle faulting.

However, several important questions remain, the answers to which are not immediately obvious from the observed field relationships:

- (1) What are the relative ages of the pseudotachylyte-ultracataclasite crush zones and the crush melange?
- (2) What was the overall kinematic regime under which brittle deformation took place?
- (3) What was the prevailing metamorphic environment during deformation?

### ***Relative age of the crush zones and crush melange***

The pseudotachylyte-ultracataclasite crush zones are typically fault bounded. It is therefore not possible to directly determine the relative ages of the crush zones and the crush melange. However, the deformation microstructures observed in the crush melange and in the crush zones are very similar. Furthermore, although the *proportion* of individual constituents is different, the same *variety* of fault rocks have been observed in the crush zones and in the crush melange. It is therefore suggested that the crush zones and the crush melange developed under similar deformation regimes and in a similar metamorphic environment (see below). If this inference is correct, it is possible that both fault rock assemblages are of broadly the same age. Previous authors have suggested that the pseudotachylyte-ultracataclasite crush zones represent regions of comparatively high finite strain which developed against a 'background' of less intense deformation within the crush melange (e.g. Sibson 1977b; White & Glasser 1987).

### ***Kinematic regime of the crush zones and the crush melange***

The fine grained, jointed nature of the crush zones precludes any direct study of the kinematic environment during crush zone generation. Comparison with better exposed structures preserved in the crush melange suggests that pseudotachylyte generation and brittle faulting took place during either localised compression or localised extension. Previous authors have inferred an *overall* compressional (i.e. regional top-to-the-W shear) environment from the preponderance of E-dipping reverse faults preserved in the 'foreland' immediately to the west of the OHFZ (section 3.4.1) (Sibson 1977b; Butler 1995). However, White & Glasser (1987) cite the N-S trending extensional quartz veins within the crush melange as evidence for bulk extension (i.e. regional top-to-the-E shear) during brittle deformation. It will be shown in the following section (section 3.4.3) that these veins relate to a later phase of deformation, which post-dates the generation of the crush melange. In the absence of more compelling evidence to the contrary, the present author concurs with Sibson (1977b) and Butler (1995) and tentatively suggests that cataclasis, pseudotachylyte generation and brittle deformation were synchronous with overall top-to-the-W shear.

### ***The metamorphic conditions during deformation and relative timing of retrogression and devitrification***

The mineral assemblages preserved in blocks of crushed gneiss suggest that the crush melange and the pseudotachylyte-ultracataclasite crush zones have experienced partial retrogression and hydration under lower greenschist facies conditions (Chapter 1). However, there is little microstructural evidence consistent with the operation of either fluid assisted DMT or fluid assisted fracture mechanisms during deformation. This observation suggests either that fluids were absent and / or that fluid pressures were low during brittle deformation.

The abundance of cataclasites and pseudotachylytes suggests that deformation took place predominantly within the frictional regime (Chapter 1). Quartz grains preserved within blocks of relict gneiss are typically fractured and display very strong patchy undulose extinction, and there is little evidence for widespread recrystallisation of quartz. These observations are consistent with deformation in a 'dry' environment at, or below lower greenschist facies conditions, probably at relatively high strain rates (Chapter 1). Walker (1990) has suggested that the fault rocks and structures observed within crush melange are consistent with deformation at depths of approximately 5km within the crust.

The presence of undeformed epidote  $\pm$  chlorite aggregates along fracture planes, cataclasite seams and devitrified pseudotachylyte veins is consistent with retrogression following the cessation of brittle deformation. Retrogression (and devitrification) are therefore thought to post-date the development of both the pseudotachylyte-ultracataclasite crush zones and the crush melange.

The deformation environment and the significance of low grade alteration are discussed in more detail in Chapter 6.

### **3.4.3 THE PHYLLONITIC FABRICS**

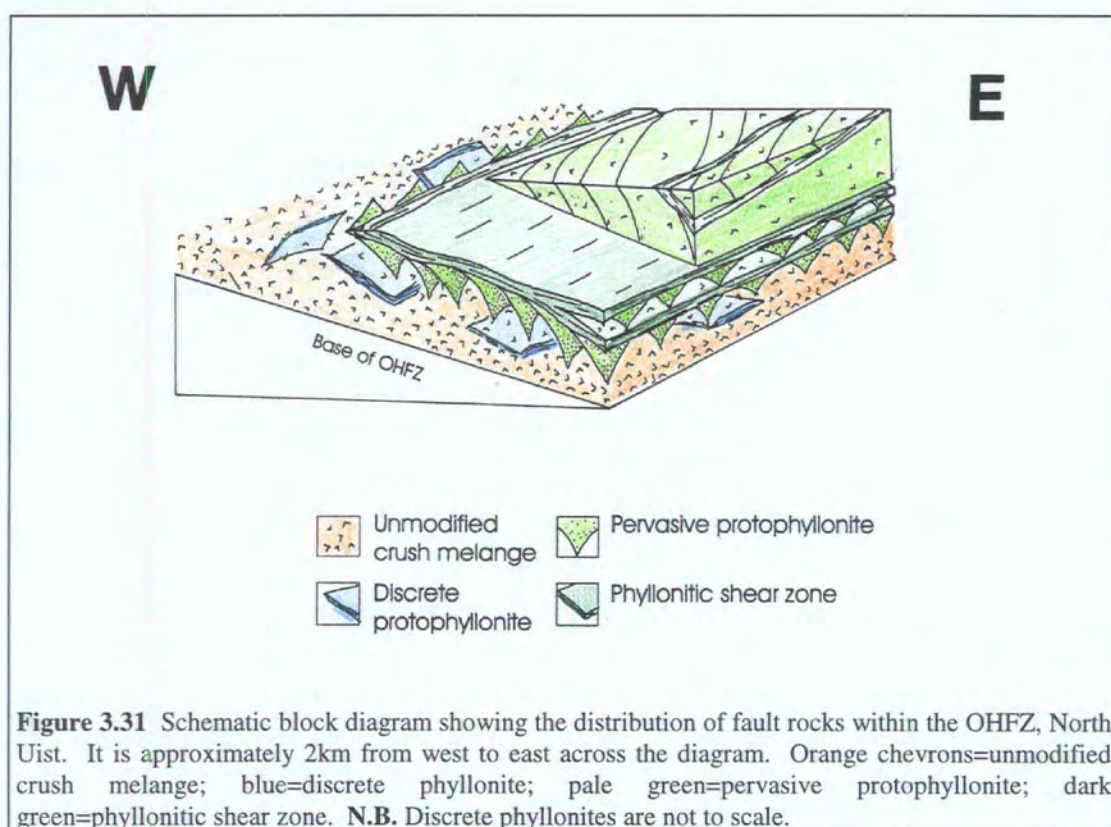
The crush melange is overprinted by a macroscopically ductile phyllonitic fabric (Fig. 3.28). The intensity of the phyllonitic overprint is extremely heterogeneous. Bands of discrete phyllonite are developed in the lowermost 500m of the crush melange, and a pervasive protophyllonitic fabric is developed in the uppermost 500m of the exposed crush melange. In the most highly strained regions, the ductile fabric is very intense and defines an anastomosing network of metre- to kilometre-scale phyllonitic shear zones (Figs. 3.28 & 3.31).

#### **3.4.3.1 Discrete phyllonites**

Narrow ( $\leq 20$ cm wide), laterally discontinuous bands of discrete phyllonite are locally exposed between Burrival and Loch a' Ghlinne-dorcha (between NF 913 625 to NF

913 618 and NF 917 625 to NF 918 617) (Figs. 3.28 & 3.29). Discrete phyllonites have *not* been observed either in the region to the east of the Lees or on Ronay, although it should be emphasised that the exposure is relatively poor in these latter two areas.

The discrete phyllonites are characterised by a sub-horizontal to moderately E-, W- or SE-dipping foliation, which is associated with an E-W, WNW-ESE or NE-SW trending mineral lineation (Fig. 3.32). Kinematic indicators (e.g.  $\sigma$ -type quartz porphyroclasts) viewed in surfaces parallel to the mineral lineation and perpendicular to the foliation are consistent with localised top-to-the-W, -WNW or -NE directed shear (i.e. regional compression, sinistral transpression or sinistral strike-slip respectively).



### 3.4.3.2 Pervasive protophyllonites

A pervasive protophyllonitic fabric overprints the crush melange in the region to the east of the Lees (between NF 938 671 to NF 953 674 and NF 913 637 to NF 930 637), in the region between Loch a' Ghlinne-dorcha and Eigneig Bheag (between NF 915 630 to NF 930 630 and NF 913 590 to NF 920 590) and to the east of Beinn a' Charnain (NF 890 564) on Ronay (Figs. 3.28 & 3.29). In the region to the east of the Lees, the foliation dips moderately towards the south, whilst to the east of Loch a' Ghlinne-dorcha it dips moderately to steeply towards the southeast or northwest. Butler (1995) has reported a moderately SE-dipping protophyllonitic foliation on

Ronay. At each of these localities, the protophyllonitic foliation is associated with a sub-horizontal NE-SW trending mineral lineation (Figs. 3.33a & b). Asymmetric shear bands and  $\sigma$ -type quartz and feldspar porphyroclasts viewed in surfaces parallel to the mineral lineation and perpendicular to the foliation are consistent with top-to-the-NE shear (i.e. regional sinistral strike-slip).

The protophyllonitic fabrics are cross-cut by a set of undeformed N-S trending quartz veins. The orientation of the fibrous vein infills is consistent with E-W directed extension. These veins are identical to the N-S trending veins which cross-cut the crush melange.

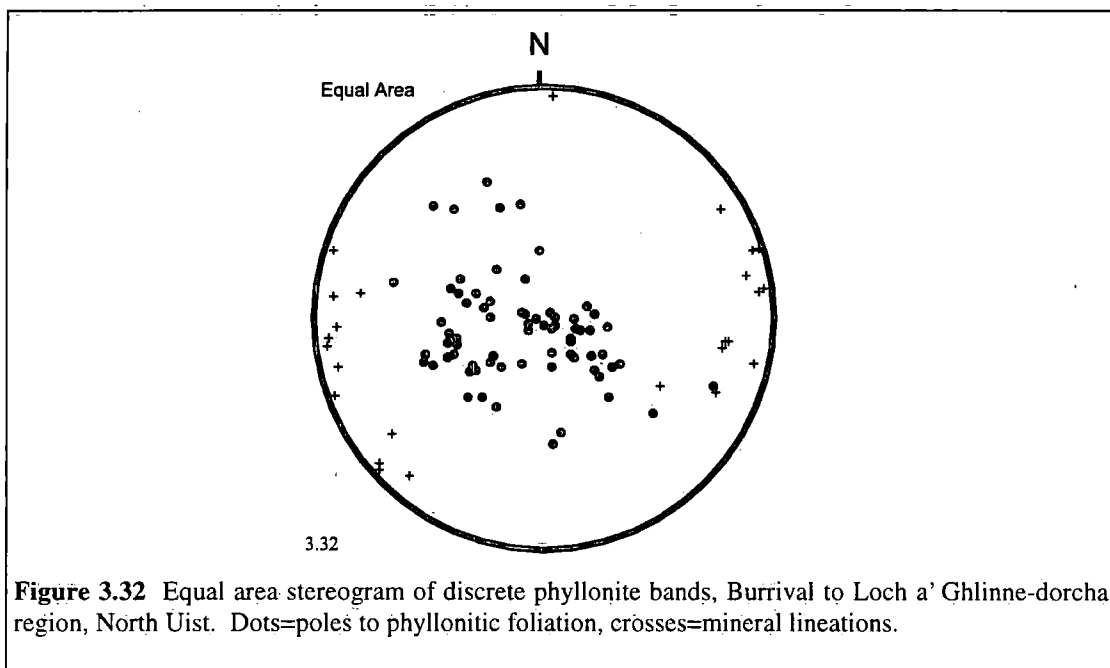


**Figure 3.32** Equal area stereogram of discrete phyllonite bands, Burrival to Loch a' Ghlinne-dorcha region, North Uist. Dots=poles to phyllonitic foliation, crosses=mineral lineations.

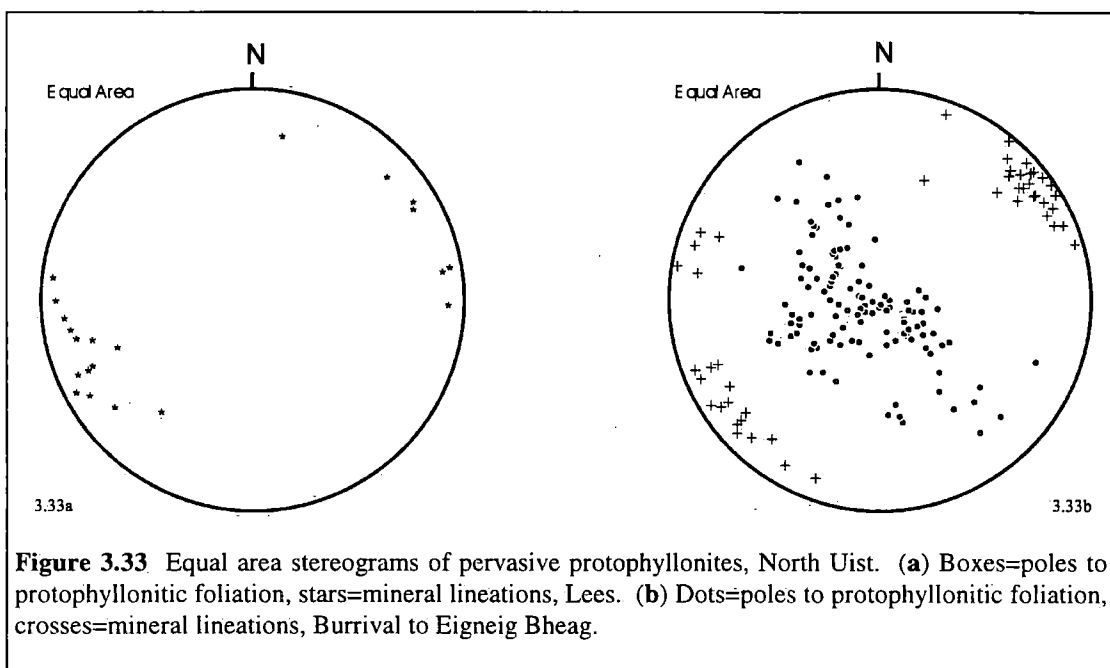


**Figure 3.33** Equal area stereograms of pervasive protophyllonites, North Uist. (a) Boxes=poles to protophyllonitic foliation, stars=mineral lineations, Lees. (b) Dots=poles to protophyllonitic foliation, crosses=mineral lineations, Burrival to Eigneig Bheag.

### 3.4.3.3 The North Uist phyllonite belts

A number of NNE-SSW and NE-SW trending phyllonite belts outcrop within the OHFZ on North Uist. The phyllonite belts are typically interconnected and define an anastomosing network which encloses elongate augen ( $\leq 2\text{km}$  long) of protophyllonitic crush melange (Figs. 3.28 & 3.31).

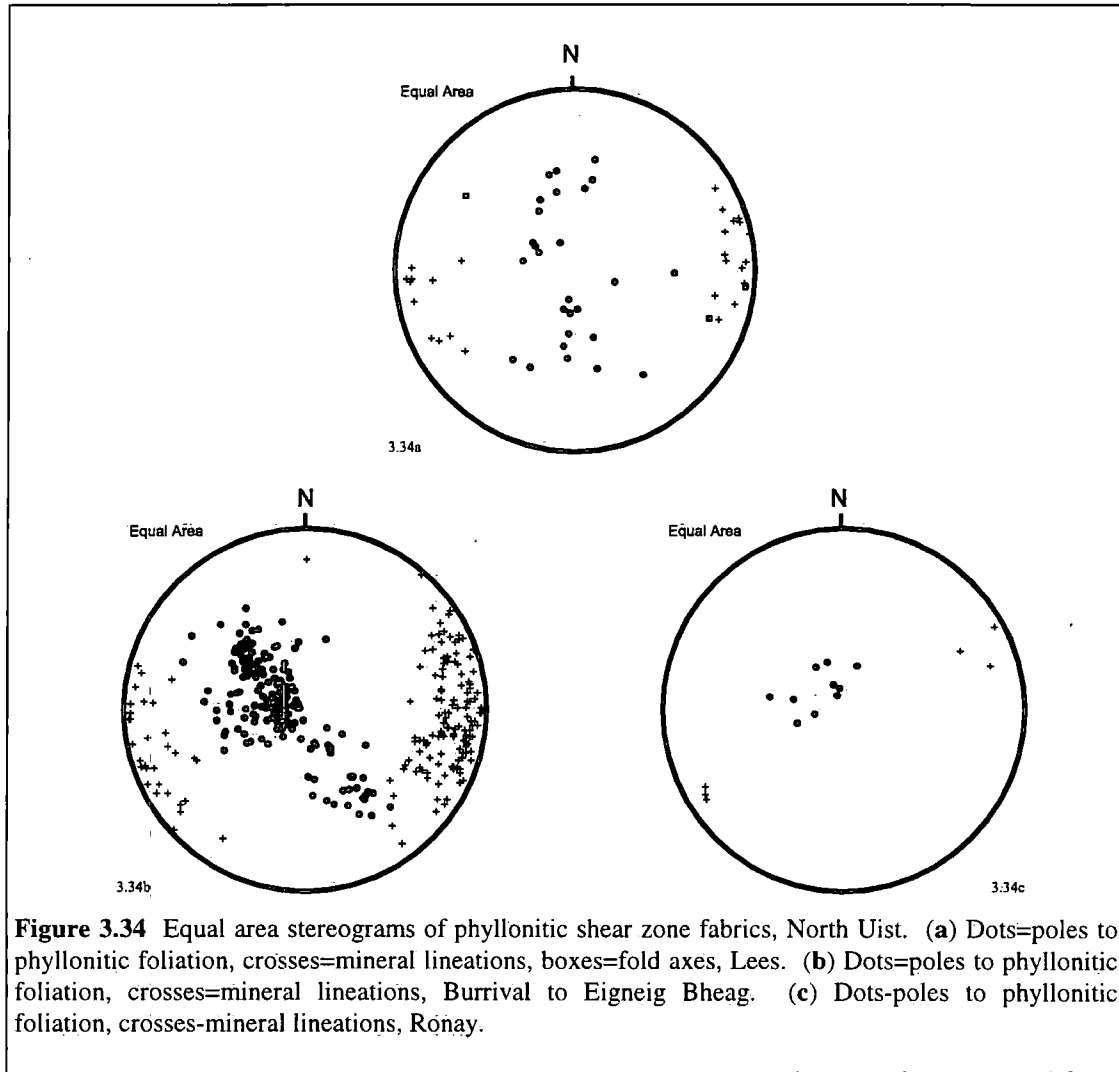
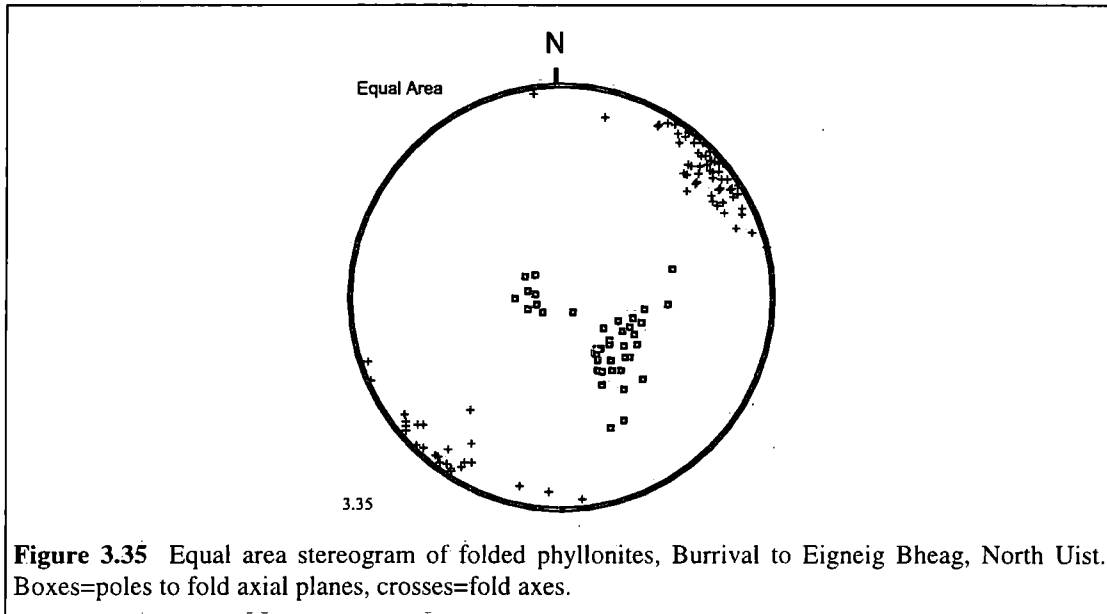


**Figure 3.34** Equal area stereograms of phyllonitic shear zone fabrics, North Uist. (a) Dots=poles to phyllonitic foliation, crosses=mineral lineations, boxes=fold axes, Lees. (b) Dots=poles to phyllonitic foliation, crosses=mineral lineations, Burrival to Eigneig Bheag. (c) Dots=poles to phyllonitic foliation, crosses=mineral lineations, Ronay.

In the region to the east of the Lees (Fig. 3.29), the phyllonitic / ultraphyllonitic shear zone foliation dips moderately towards the south or towards the north and is associated with a NE-SW to E-W trending mineral lineation (Fig. 3.34a). In the region between Loch a' Ghlinne-dorcha and Eigneig Bheag, the foliation dips moderately towards the southeast or towards the northwest and is associated with a NE-SW to SE-NW trending mineral lineation (Fig. 3.34b). On Ronay, the gently SE-dipping foliation is associated with a sub-horizontal NE-SW trending mineral lineation and is cross-cut by a number of N-S quartz and quartz-chlorite veins. The orientation of the fibrous vein infills is consistent with E-W extension (Fig. 3.36a).

$\sigma$ -type quartz and feldspar porphyroclasts viewed in surfaces parallel to the NE-SW trending mineral lineation are consistent with top-to-the-NE shear (i.e. sinistral strike-slip). In contrast, asymmetric shear bands viewed in surfaces parallel to the ENE-WSW and SE-NW trending mineral lineations are consistent with top-to-the-ENE or top-to-the-SE shear (i.e. eastward-directed transtension or extension).

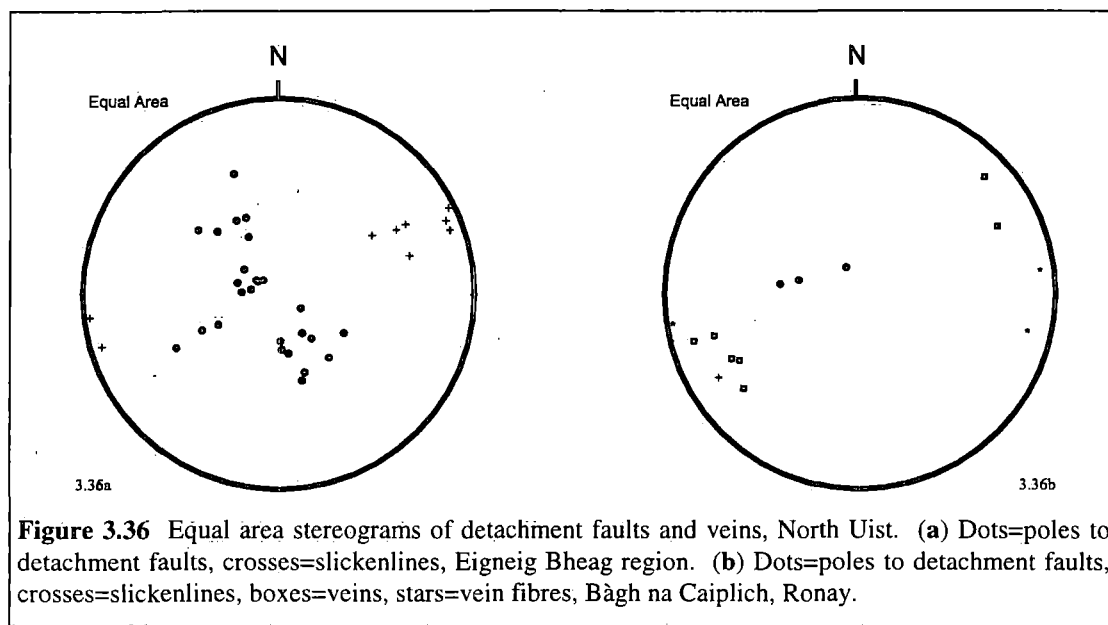


The phyllonitic fabrics are commonly observed to be deformed by cascades of gently plunging, curvilinear SE-verging warps and chevron folds (Figs. 3.34a & 3.35). The folds are typically associated with a 'new' axial planar crenulation cleavage. The axial planar foliation, which is locally the dominant fabric, carries E-W or NW-SE trending mineral lineations and is itself locally deformed by SE-verging folds and crenulations. These observations suggest that the crenulation fabric and the SE-verging folds are of broadly the same age and that both developed during top-to-the-ENE or -SE directed shear. Syn-tectonic quartz-carbonate-chlorite veins and 'saddle reefs' (section 3.2.3.4) are commonly observed within units of folded phyllonite. The veins and 'saddle reefs' are themselves deformed by folding. Folded phyllonites have not been observed on Ronay.

The phyllonite belts are typically cross-cut by arrays of sub-parallel SE-dipping detachment faults. Bands of incohesive breccia ( $\leq 10$ cm thick) and / or NE-SW trending slickenlines are commonly observed to be developed along detachment surfaces (Figs. 3.36a & b). The geometries of the fracture patterns which are associated with the principal detachment planes are consistent with top-to-the-NE displacements (i.e. localised sinistral strike-slip).

### 3.4.3.4 Microstructures

*Pervasive protophyllonites* The pervasive protophyllonites comprise an assemblage of quartz, partially sericitised feldspar (mostly albite) and hornblende grains which are 'wrapped' by laterally discontinuous strands of chlorite and sericite. The microstructures of the quartz and feldspar grains preserved in the pervasive protophyllonites are similar to the microstructures of the quartz and feldspar grains observed within the crush melange (section 3.4.2).



The hornblende grains are locally cross-cut by intragranular fractures which are infilled by aggregates of actinolite fibres and chlorite aggregates. Actinolite and / or chlorite strain shadows are commonly observed to be associated with the hornblende grains.

*Discrete phyllonites and phyllonitic / ultraphyllonitic shear zone fabrics* The microstructures preserved in the discrete phyllonite bands are similar to the microstructures associated with the phyllonitic / ultraphyllonitic shear zone fabrics. Polycrystalline quartz ribbons, opaque grains, sericite strands and partially sericitised feldspar porphyroclasts 'float' in an ultrafine grained mixture of albite, chlorite, epidote and quartz. Chlorite stains shadows are locally associated with the opaque grains.

Folded phyllonites are typically cross-cut by an axial planar crenulation cleavage, which is locally observed to be the dominant fabric. Actinolite has not been observed in extensionally reworked phyllonites.

### 3.4.3.5 Summary and discussion

It is clear from the preceding descriptions that the thrust-related fault rocks of the crush melange were overprinted by a macroscopically ductile phyllonitic fabric. The pervasive protophyllonites and the phyllonitic shear zones developed during top-to-the-NE sinistral strike-slip. The strike-slip related shear zone fabrics were subsequently reworked during eastward-directed transtension / extension (see also Butler 1995 and Butler *et al.* 1995). A new, extension-related (crenulation) fabric is locally developed within some shear zones. Top-to-the-NE displacements along a network of brittle detachment faults appear to post-date macroscopically ductile deformation within the phyllonite belts.

The development of actinolite / chlorite strain shadows and fracture infills within the pervasive protophyllonites suggests that fluid assisted DMT mechanisms were operative during strike-slip related phyllonitisation. The continued operation of fluid assisted DMT mechanisms during shear zone reactivation is inferred from the development of syn-tectonic veins within packages of reworked phyllonite. These observations are consistent with the presence of a chemically active fluid phase during both strike-slip and subsequent extensional reactivation (Chapter 1). The syn-tectonic breakdown of hornblende to aggregates of actinolite and chlorite, and the breakdown of feldspar to aggregates of sericite and albite suggest that phyllonitisation took place at temperatures and pressures consistent with lower greenschist facies conditions (Chapter 1).

Two important questions remain, the answers to which are not immediately obvious from the observed field and microstructural relationships:

- (1) What is the relative age of the discrete phyllonite bands and what role did they play during deformation along the OHFZ in North Uist?
- (2) Was the change in kinematic regime from strike-slip to extension the manifestation of a single progressive deformation event?

#### ***The role of the discrete phyllonite bands and the kinematic regime at the onset of phyllonitisation***

The geometries of the discrete phyllonite bands are consistent with either top-to-the-W thrusting, top-to-the-NW transpression or sinistral strike-slip. The microstructures preserved in the discrete phyllonite bands are similar to the microstructures observed in strike-slip related phyllonites. The prevailing metamorphic environment during the each of these fabric-forming events is therefore thought to have been similar. It is suggested that the discrete phyllonite bands which are associated with strike-parallel (i.e. NE-SW trending) mineral lineations are broadly the same age as the strike-slip

related pervasive protophyllonites. However, the ages of the thrust- and transpression-related discrete phyllonites is less clear.

The operation of fluid assisted DMT mechanisms during phyllonitisation strongly suggests that deformation was controlled by a chemically active fluid phase (see above). The trace element geochemistry of the phyllonitic fault rocks must therefore have been influenced by the composition, temperature and pore pressure of the syn-tectonic fluid phase (e.g. Condie & Sinha 1996). The protolith-normalised rare earth element (REE) patterns (Chapter 8) obtained from samples of thrust / transpression-related discrete phyllonite and strike-slip related phyllonite are relatively similar (Fig. 3.37; see Chapter 8 for a more detailed discussion of the fault rock geochemistry). This observation suggests that the fluids which were responsible for *strike-slip* related phyllonitisation had similar geochemical characteristics compared to the fluids which were responsible for *thrust / transpression*-related phyllonitisation. It is therefore postulated that both the thrust / transpression- and strike-slip related phyllonites developed during a single 'phase' of fluid-rock interaction (Chapter 8). If these inferences are correct, *the thrust / transpression-related discrete phyllonite bands may be of a similar age to the strike-slip related phyllonites*. The restricted outcrop pattern and the laterally discontinuous nature of the thrust / transpression-related discrete phyllonite bands suggests that the discrete phyllonites have accommodated relatively low magnitudes of finite strain in comparison with the strike-slip related phyllonitic shear zones. There are two possible kinematic models which could account for the observed fabric distribution:

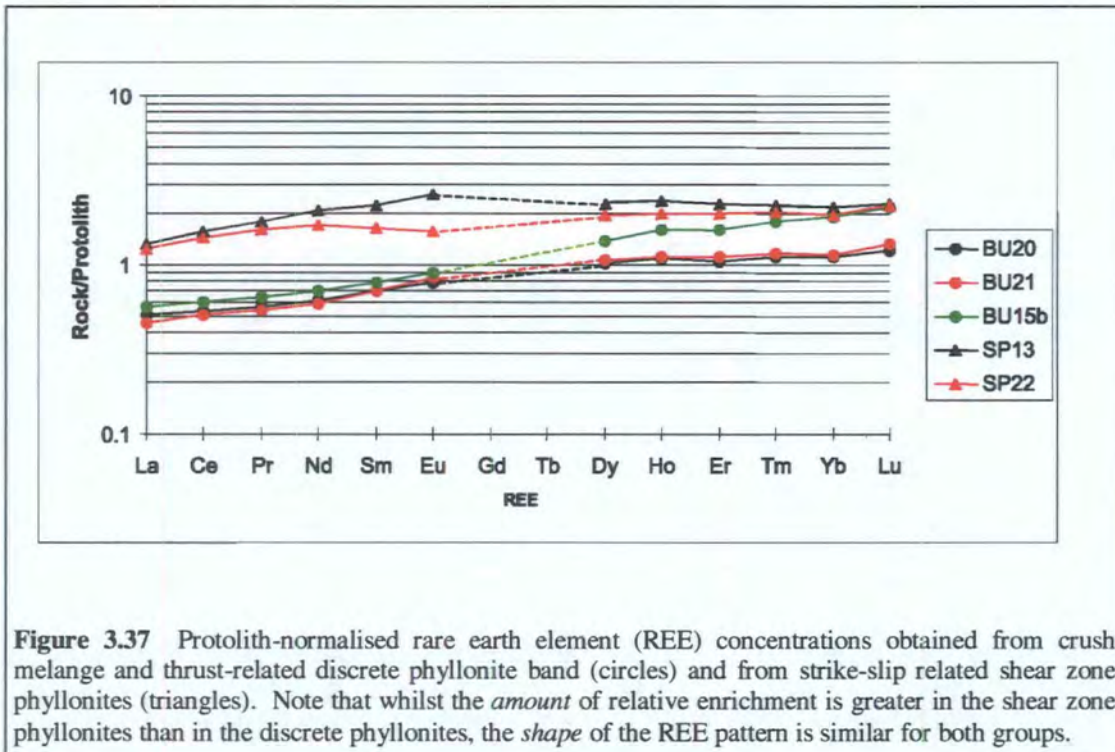


**Figure 3.37** Protolith-normalised rare earth element (REE) concentrations obtained from crush melange and thrust-related discrete phyllonite band (circles) and from strike-slip related shear zone phyllonites (triangles). Note that whilst the *amount* of relative enrichment is greater in the shear zone phyllonites than in the discrete phyllonites, the *shape* of the REE pattern is similar for both groups.

- **Model 1** The onset of phyllonitisation may have been associated with a progressive change in kinematic regime, from top-to-the-W thrusting to sinistral transpression to regional sinistral strike-slip.
- **Model 2** A regime of regional sinistral transpression may have been partitioned into components of pure sinistral strike-slip (within the pervasive protophyllonites and the phyllonitic shear zones) and pure top-to-the-W dip-slip (within the discrete phyllonite bands).

If there was a progressive change in kinematic regime, from thrusting to sinistral strike-slip (Model 1), the limited outcrop of thrust-sense discrete phyllonites and the apparent absence of thrust-related fabrics either within the pervasive protophyllonites or within the phyllonitic shear zones suggests (a) that phyllonitisation was probably associated with the final stages of thrusting, and that (b) thrust-related fabrics were generally restricted to the region to the west of Loch a' Ghlinne-dorcha. However, if regional oblique compression was partitioned into separate components of pure strike-slip and pure-dip slip (Model 2), the limited outcrop of thrust-sense discrete phyllonites suggests (a) that the regional movement vector was oriented at low angles to the overall trend of the fault zone (cf. Holdsworth & Strachan 1991 and the 'wrench-dominated transpression' model of Teyssier *et al.* 1995) and (b) that regional transpression probably quickly gave way to a regime of regional sinistral strike-slip. In the absence of accurate and precise isotopic age dates, it is virtually impossible to identify which of these kinematic models may have been applicable to the OHFZ on North Uist. Whichever model is correct, it can be confidently argued that the main phase of phyllonitisation in North Uist appears to have been associated with regional top-to-the-NE sinistral strike-slip (Chapter 6).

#### ***The transition from strike-slip to extension***

The shear zone fabrics are associated with NE-SW to NW-SE trending mineral lineations. The mineral lineation azimuths do not show a bimodal distribution, but are evenly spread through c.50° (e.g. Fig. 3.34b).

NE-SW to ENE-WSW trending mineral lineations are typically observed in packages of planar phyllonite which display little evidence of folding and / or extensive reworking. In contrast, E-W to NW-SE trending mineral lineations are typically associated with 'new' axial planar crenulation fabrics which cross-cut packages of highly deformed and folded phyllonite. It is therefore suggested that the *least* strained fabrics preserve evidence of top-to-the-NE or -ENE directed shear (i.e. regional strike-slip or transtension), whilst more *highly* strained packages of phyllonite and

ultraphyllonite tend to preserve evidence of top-to-the-ESE or -SE directed shear (i.e. regional extension). These observations suggest that the progressive clockwise rotation of the mineral lineation from a NE-SW to a NW-SE trend was accompanied by a progressive increase in the apparent degree of reworking of the phyllonitic fabrics. The distribution of reworked fabrics is consistent with a progressive change in the kinematic regime, from regional top-to-the-NE sinistral strike-slip to regional top-to-the-SE extension (see also Butler 1995 and Butler *et al.* 1995).

### 3.4.4 SUMMARY: KINEMATIC EVOLUTION AND FLUID-ROCK INTERACTIONS ALONG THE OHFZ IN NORTH UIST

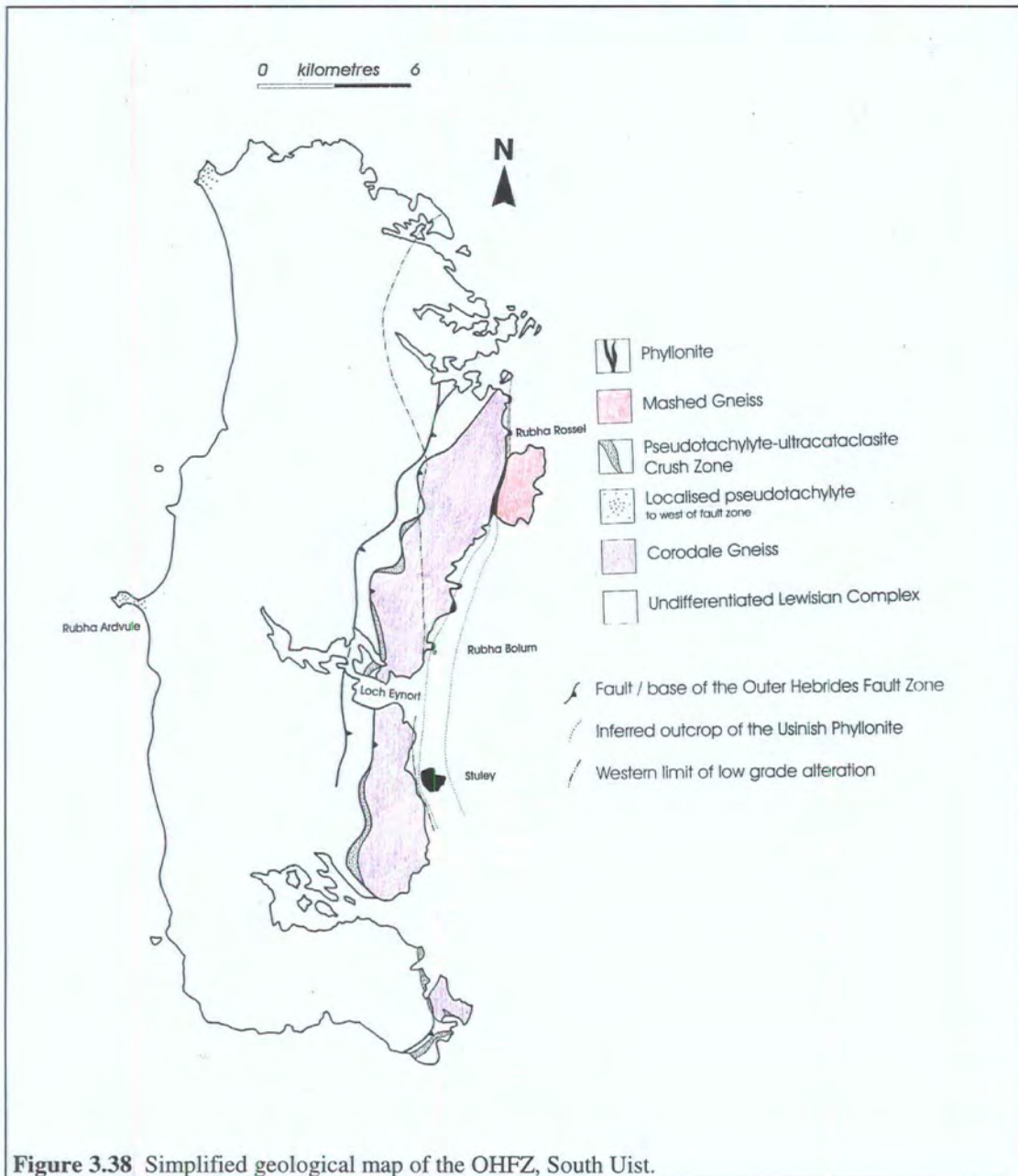
The kinematic, textural and metamorphic evolution of the OHFZ on North Uist and Ronay is summarised in Table 3.2.

<b>Kinematic regime</b>	<b>Fault rocks / structures</b>	<b>Metamorphism / fluids</b>
<b>1. ?Regional top-to-W thrusting</b> (Oldest)	Cataclasites, pseudotachylytes and brittle faults in the crush melange and pseudotachylyte-ultracataclasite crush zones.	Temperatures at or below lower greenschist facies conditions. Fluids absent or not significant during deformation.
<b>2. Regional sinistral transpression</b>	Discrete phyllonites, pervasive protophyllonites and phyllonitic shear zones.	Lower greenschist facies conditions, in the presence of a syn-tectonic fluid phase.
<b>3. Regional top-to-NE sinistral strike-slip</b>	Phyllonitic shear zones $\pm$ pervasive protophyllonites.	Lower greenschist facies conditions, in the presence of a syn-tectonic fluid phase.
<b>4. Regional sinistral transtension</b>	Reworking of phyllonitic shear zone fabrics. Not observed on Ronay.	Lower greenschist facies conditions, in the presence of a syn-tectonic fluid phase.
<b>5. Regional top-to-SE extension</b>	Reworking of phyllonitic shear zone fabrics. Development of folds and 'new' foliation. Not observed on Ronay.	Lower greenschist facies conditions, in the presence of a syn-tectonic fluid phase.
<b>6. Top-to-NE faulting</b> (Youngest)	Brittle detachment faults, typically developed along shear zone margins.	Fluids absent, sub-greenschist facies (upper crustal) conditions.

**Table 3.2.** Summary of the kinematic, textural and metamorphic evolution of the OHFZ on North Uist and Ronay.

### 3.5 THE SOUTHERN ZONE: SOUTH UIST AND ADJACENT ISLANDS

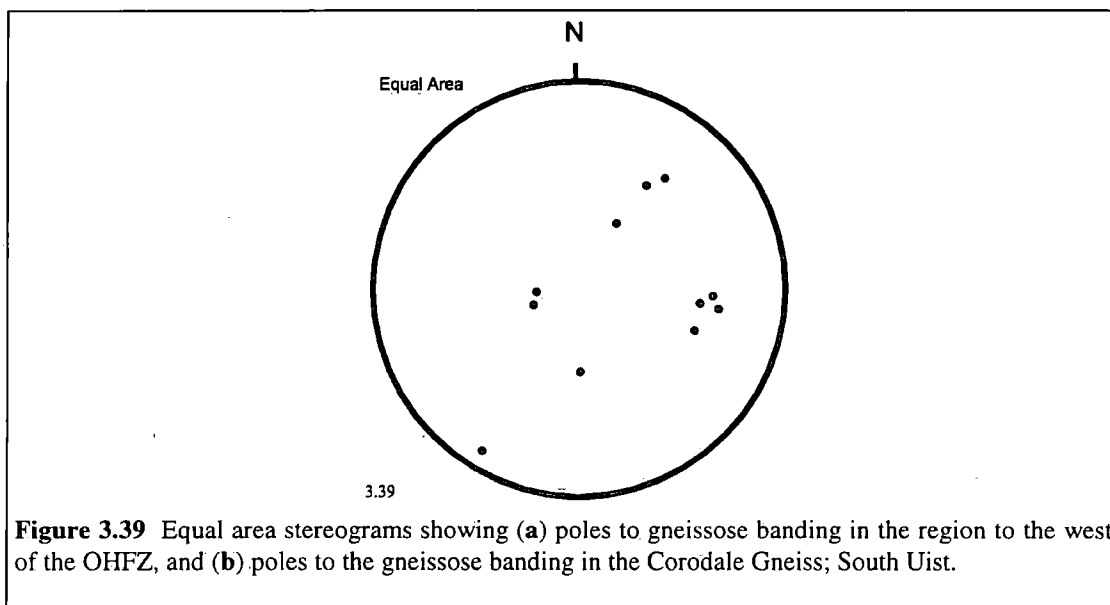
The following section comprises descriptions of (1) the Lewisian protoliths (section 3.5.1), (2) localised deformation in the 'foreland' and the pseudotachylyte-ultracataclasite crush zones (section 3.5.2), (3) the Usinish Phyllonite (section 3.5.3) and (4) the Mashed Gneiss (section 3.5.4), (Fig. 3.38). The following sections are not sub-divided into descriptions of individual localities (Fig. 3.29), although attention will be drawn to any significant geographical variations in the geology.



### 3.5.1 PROTOLITHS

#### 3.5.1.1 Banded gneiss

The geology of the region to the west of the OHFZ (the 'foreland') is dominated by amphibolite facies quartzo-feldspathic banded gneisses (section 2.2.2.1), concordant to discordant Younger Basic sheets and discordant pegmatite veins (section 2.2.2.4). The gneissose banding is deformed by regional-scale NW-SE trending Laxfordian folds ('D1<sub>3</sub>' of Fettes *et al.* 1992) (Figs. 2.4 & 3.39a; section 2.2.4). Note that the trace of the OHFZ clearly cross-cuts the regional Laxfordian structures preserved in the 'foreland' (Fig. 2.4).



#### 3.5.1.2 Corodale Gneiss

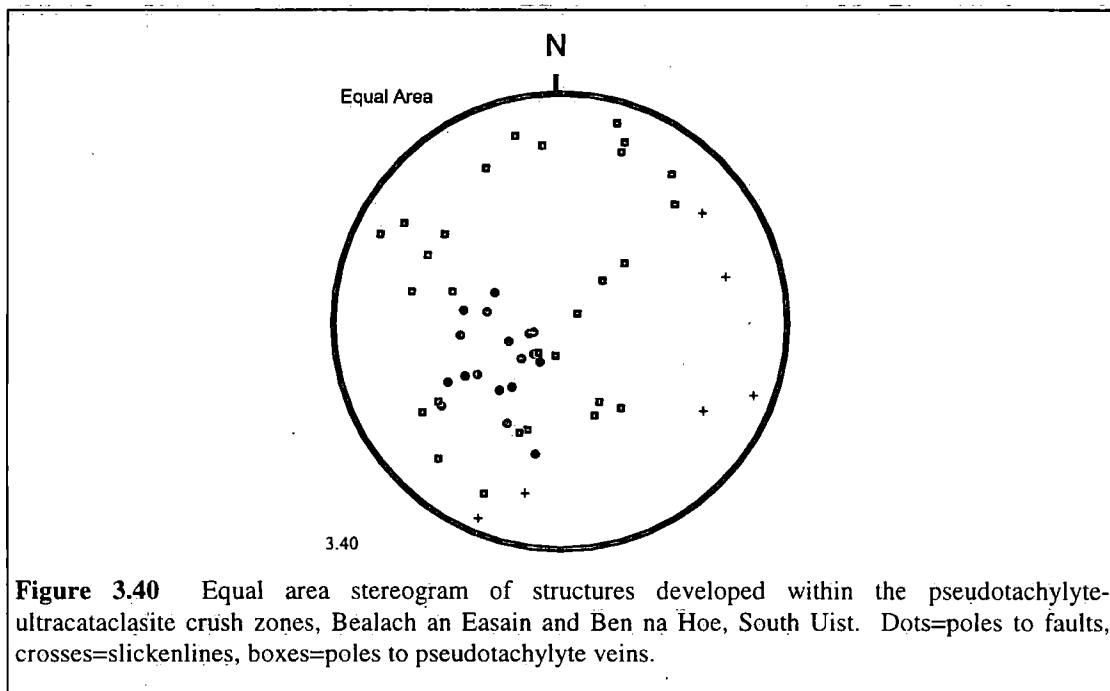
The geology of the region to the east of the OHFZ is dominated by the granulite facies meta-igneous Corodale Gneiss (section 2.2.2.3). The NE-SW to NNE-SSW trending banding developed within the Corodale Gneiss (Fig. 3.39b) is locally cross-cut by brittle faults, cataclasite seams and devitrified pseudotachylyte veins (e.g. NF 856 366; Fig. 3.29). Localised brittle deformation within the Corodale Gneiss has been attributed by previous authors to a phase of top-to-the-W thrusting along the OHFZ (Coward 1972; Sibson 1977b). The structural base of the Corodale Gneiss is defined by an E-dipping zone of intense brittle deformation (Fig. 3.38 & section 3.5.2), whilst its upper margin is defined by an E-dipping phyllonitic shear zone (the 'Usinish Phyllonite') (Fig. 3.38 & section 3.5.3).

### 3.5.2 LOCALISED DEFORMATION IN THE 'FORELAND' AND THE PSEUDOTACHYLYTE-ULTRACATACLASITE CRUSH ZONES

#### 3.5.2.1 Localised deformation in the 'foreland'

Evidence for localised brittle deformation in the 'foreland' is widespread, but is never very intense. The principal fault rocks / structures observed in the 'foreland' are (1) pseudotachylyte-bearing veins, breccias and quasi-conglomerates and (2) pseudotachylyte-barren brittle faults (Sibson 1977b; Butler 1995).

Although previous authors (Coward 1972; Sibson 1977b) have reported pseudotachylyte breccias at localities up to 9km to the west of the OHFZ (e.g. Ardivachar Point, NF 742 464; Rubha Ardvule NF 710 300) (Fig. 3.38), the effects of localised brittle deformation are more commonly observed in the region immediately below the base of the fault zone (e.g. Loch Eynort - Ben na Hoe, NF 808 285; Loch Boisdale - Bealach an Easain, NF 803 207). The brittle faults and pseudotachylyte veins preserved in the footwall of the OHFZ typically dip towards the east, although there are significant local variations in their orientation (Fig. 3.40). The geometries of subsidiary fractures and injection veins are consistent with either apparent compressional or apparent extensional displacements during faulting / pseudotachylyte generation in the 'foreland'. Butler (1995) has noted a preponderance of compressional (i.e. top-to-the-W) structures in the 'foreland'.



### **3.5.2.2 Pseudotachylyte-ultracataclasite crush zones**

For much of its length, the base of the OHFZ in South Uist is defined by a number of E-dipping fault-bounded pseudotachylyte-ultracataclasite crush zones (Fig. 3.38). The crush zones are locally up to 30m thick and form prominent upstanding topographic features.

The crush zones are characterised by a few randomly oriented blocks of gneiss and pegmatite (typically  $\leq 2\text{m}$  diameter) which 'float' in a matrix of dark green, aphanitic ultracataclasite, cataclasite and devitrified pseudotachylyte (matrix  $\leq 90\%$  by volume). The entire assemblage is cross-cut by a network of closely spaced joints and a number of cm- to m-scale E-and NE-dipping brittle faults. The faults are associated with NE-SW to ESE-WNW trending slickenlines (Fig. 3.40) and are locally lined by a thin layer of incohesive gouge or breccia ( $\leq 2\text{cm}$  thick). The geometries of minor fractures are consistent with either normal or, less commonly, reverse displacements during brittle faulting.

### **3.5.2.3 Microstructure**

Microstructural observations of the gneissose blocks preserved within the fine grained pseudotachylyte-ultracataclasite matrix suggest that the fault rocks which constitute the crush zones have been derived from both quartz-rich banded gneisses of the 'foreland' and from the quartz-poor Corodale Gneiss.

The deformation microstructures associated with the South Uist crush zones are very similar to those observed in the pseudotachylyte-ultracataclasite crush zones of North Uist (see section 3.4.2.3 for a more detailed description). Feldspar and hornblende clasts are partially altered to aggregates of sericite and chlorite, and the pseudotachylyte matrix is locally cross-cut by a network of undeformed mm-scale quartz-calcite-epidote-chlorite veins. However, the overall degree of alteration appears to be less than that associated with the North Uist crush zones.

### **3.5.2.4 Summary and discussion**

It is clear from the preceding descriptions that there has been at least one phase of intense brittle deformation in the South Uist region, which involved cataclasis, pseudotachylyte generation and brittle faulting. Crush zone generation was post-dated by predominantly normal (i.e. top-to-the-E or -NE) movements along brittle fault planes.

The microstructural similarities between the North and South Uist crush zones suggest that similar deformation regimes prevailed during cataclasis and pseudotachylyte generation throughout the Uists (i.e. temperatures and pressures at or below lower greenschist facies conditions, in a predominantly dry, relatively high strain rate environment; section 3.4.2.4). The observation that undeformed quartz-calcite-

epidote-chlorite veins locally cross-cut pseudotachylyte seams, suggests that retrogression and devitrification in South Uist post-dates pseudotachylyte generation. However, the timing of retrogression and devitrification relative to normal faulting is unclear from the observed field and microstructural relationships.

The prevailing kinematic regime during crush zone generation is not immediately obvious from the structures preserved within the crush zones themselves. However, previous authors have inferred an *overall* compressional (i.e. regional top-to-the-W shear) environment from the preponderance of E-dipping reverse faults preserved in the 'foreland' immediately to the west of the OHFZ (section 3.4.1) (Sibson 1977b; Butler 1995). In the absence of convincing evidence to the contrary, the present author tentatively agrees with the suggestion that the crush zones developed during regional thrusting along the OHFZ in South Uist.

### 3.5.3 THE USINISH PHYLLONITE

The phyllonitic fault rocks of South Uist, here collectively referred to as the 'Usinish Phyllonite' (*sensu* Butler 1995), are exposed in a series of east coast promontories and islands (Ornish, NF 858 376; Rubha Rossel, NF 858 365; Rubha Hellisdale, NF 840 307; Rubha Bolum, NF 828 284 and Stuley island, NF 830 235) (Figs. 3.29 & 3.38). Most workers have inferred a continuous N-S to NNE-SSW trending phyllonite belt which widens progressively towards the south (e.g. Coward 1969; Sibson 1977b; Walker 1990; Butler 1995). The phyllonite belt dips moderately to the east, separating intensely fractured feldspar-rich Corodale Gneiss (section 3.5.1) in the footwall from the quartzo-feldspathic Mashed Gneiss (section 3.5.4) in the hangingwall (Fig. 3.38).

#### 3.5.3.1 Field relationships

The internal structure of the Usinish Phyllonite is complex and comprises a number of detachment-bounded packages of protophyllonite, phyllonite and ultraphyllonite. The phyllonitic foliation dips moderately towards the south or north and is associated with a NE-SW (locally NNE-SSW) to E-W trending mineral lineation (Fig. 3.41a and Chapter 7).  $\delta$ -type quartz and feldspar porphyroclasts viewed in surfaces parallel to the NE-SW trending mineral lineation are consistent with top-to-the-NE (locally top-to-the-NNE) shear (i.e. regional sinistral strike-slip / transtensional displacements), whilst asymmetric shear bands viewed in surfaces parallel to the E-W trending mineral lineation are consistent with top-to-the-E shear (i.e. regional extension). Note that both strike-slip and extension-related mineral lineations have been observed within packages of relatively undeformed *protophyllonite* (e.g. at Rubha Bolum, NF 828 284; Figs. 3.29 & 3.41a). This contrasts with the North Uist phyllonite belts

where extension-related mineral lineations are observed only in the most highly strained packages of phyllonite (section 3.4.3.5). The strike-slip / transtension-related fabrics are locally deformed by cascades of E-verging folds (e.g. south of Rubha Hellisdale, NF 8370 3036) (Fig. 3.29). The folds are typically associated with a well developed axial planar foliation, which carries an E-W trending mineral lineation. Folded phyllonitic fabrics are less commonly observed within the Usinish Phyllonite than within the North Uist phyllonite belts.

The macroscopically ductile phyllonitic fabrics are cross-cut by a number of brittle detachment faults. The detachment faults are typically oriented sub-parallel to the phyllonitic foliation and are associated with NNE- to ESE-plunging slickenlines. (Fig. 3.41b). The geometries of subsidiary fractures are consistent with predominantly top-to-the-NNE, -ENE or -ESE (i.e. sinistral transtensional or extensional) displacements along the detachment surfaces.

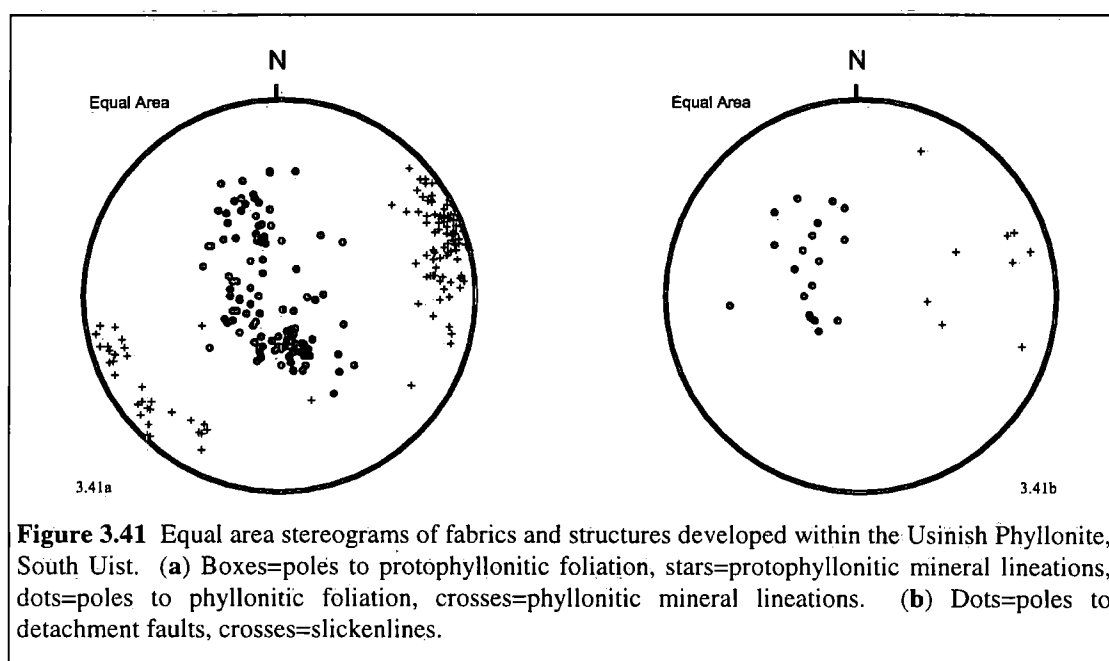


**Figure 3.41** Equal area stereograms of fabrics and structures developed within the Usinish Phyllonite, South Uist. (a) Boxes=poles to protophyllonitic foliation, stars=protophyllonitic mineral lineations, dots=poles to phyllonitic foliation, crosses=phyllonitic mineral lineations. (b) Dots=poles to detachment faults, crosses=slickenlines.

### 3.5.3.2 Microstructures

Microstructural observations suggest that the fault rocks which comprise the Usinish Phyllonite were derived from either the quartz-poor Corodale Gneiss (section 3.5.1) or from the quartz-rich Mashed Gneiss (section 3.5.4).

*Protophyllonites* The strike-slip / transtension and extension-related protophyllonites comprise an assemblage of feldspar, hornblende  $\pm$  quartz porphyroclasts, which 'float' in a matrix of altered cataclasite / pseudotachylite and partially altered, flattened feldspar grains which are cross-cut by laterally discontinuous sericite strands. The seams of altered 'cataclasite' comprise mixtures of fine grained epidote, chlorite and

albite, and the margins of the seams are typically overgrown by aggregates of relatively undeformed epidote.

Quartz displays strong patchy undulose extinction and locally shows evidence of extensive recrystallisation. Both quartz and feldspar porphyroclasts are cross-cut by arrays of intragranular fractures and are occasionally observed to be associated with chlorite strain shadows.

*Phyllonites and ultraphyllonites* The phyllonites and ultraphyllonites are characterised by fractured feldspar porphyroclasts which 'float' in a fine grained matrix of interconnected sericite strands and bands of recrystallised quartz and feldspar. The intragranular fractures within feldspar porphyroclasts are typically infilled by aggregates of recrystallised feldspar and / or fibrous chlorite. Small scale ( $\leq 1$ mm long) asymmetric shear bands, which are lined by deformed chlorite aggregates, are locally developed in extension-related phyllonites and ultraphyllonites.

### 3.5.3.3 Summary and discussion

The strike-slip / transtension- and extension-related phyllonitic fabrics of the Usinish Phyllonite overprint, and therefore post-date, the cataclasite seams and pseudotachylite veins observed within the Corodale Gneiss. The phyllonitic fabrics are themselves cross-cut by sinistral-oblique and extension-related detachment faults. The presence of strike-slip / transtension- and extension-related *protophyllonites* suggests that there have been at least two phases of phyllonitisation along the ÖHFZ in South Uist (Chapter 1). The earliest phyllonitisation event appears to have been synchronous with top-to-the-NE (locally top-to-the-NNE) directed shear, whilst the later event was associated with eastward directed extension. The field relationships therefore suggest that regional extension was accommodated either by reworking of the pre-existing strike-slip / transtension-related fabrics *or* by the generation of new fabrics within previously un-phyllonitised areas (e.g. Rubha Bolum, section 3.5.3.1 & Chapter 7). However, the relatively poor exposure and the fault-bounded nature of the different packages of phyllonite precludes detailed analysis of the transition from regional strike-slip / transtension to regional extension. Similarly, it has not been possible to unequivocally identify a phase of sinistral transpression in the South Uist region (cf. Table 3.2). The kinematic evolution of the Usinish Phyllonite is discussed in more detail in Chapter 7.

The development of chlorite strain shadows and chlorite-rich shear bands suggests that sites of localised dilatation within both strike-slip / transtension- and extension-related phyllonites acted as DMT sinks during deformation. The operation of fluid assisted DMT mechanisms is consistent with the presence of a chemically active fluid phase during deformation within the Usinish Phyllonite (Chapter 1). The observed

quartz and feldspar deformation microstructures (section 3.5.3.2) and the apparent syn-tectonic breakdown of feldspar and hornblende to aggregates of sericite and epidote and chlorite respectively suggest that deformation and retrogression took place under lower greenschist facies conditions (Chapter 1).

It is not clear from the observed field relationships whether the faults which cross-cut the pseudotachylite-ultracataclasite crush zones (section 3.5.3.2) developed synchronously with the detachment faults which cross-cut the Usinish Phyllonite. However, given the kinematic and structural similarities, it is suggested that both sets of faults developed at broadly the same time, within a regime of sinistral transtension or regional eastward-directed extension (see also Butler 1995).

### **3.5.4 THE MASHED GNEISS**

The quartzo-feldspathic Mashed Gneiss outcrops in the hangingwall of the Usinish Phyllonite (see Chapter 7) (Fig. 3.38). Detailed field studies of the Mashed Gneiss have not been conducted during the present study, although preliminary observations suggest that it closely resembles the crush melange of North Uist (section 3.4.2.2) (see also Sibson 1977b; Butler 1995). The Mashed Gneiss is intensely fractured and is structurally isotropic, although a crude strike-slip / transtension-related protophyllonitic fabric locally overprints the Mashed Gneiss in the immediate hangingwall of the Usinish Phyllonite (e.g. Rubha Rossel, NF 858 365).

Geochemical studies (Walker 1990) suggest that the Mashed Gneiss has experienced extreme alteration and retrogression under fluid-rich lower greenschist facies conditions. Field and microstructural observations of Mashed Gneiss 'inliers' within the Usinish Phyllonite (Chapter 7) are consistent with alteration and retrogression synchronous with phyllonitisation and top-to-the-NE shear.

### 3.5.5 SUMMARY: KINEMATIC EVOLUTION AND FLUID-ROCK INTERACTIONS ALONG THE OHFZ IN SOUTH UIST

The kinematic, textural and metamorphic evolution of the OHFZ on South Uist summarised in Table 3.3.

<b>Kinematic regime</b>	<b>Fault rocks / structures</b>	<b>Metamorphism / fluids</b>
<b>1. ?Regional top-to-W thrusting</b> (Oldest)	Cataclasites and pseudotachylytes in the pseudotachylyte-ultracataclasite crush zones.	Temperatures at or below lower greenschist facies conditions. Fluids not important during deformation.
<b>2. Regional top-to-NE (locally top-to-NNE) strike-slip / transtension</b>	Protophyllonites, phyllonites and ultraphyllonites within Usinish Phyllonite.	Fluid-rich lower greenschist facies environment.
<b>3. Regional top-to-E extension</b>	Reworking of pre-existing phyllonitic fabrics <i>and</i> phase of further phyllonitisation along Usinish Phyllonite.	Fluid-rich lower greenschist facies environment.
<b>4. Top-to-NNE, -ENE or -ESE faulting</b> (Youngest)	Brittle normal faults within crush zones and the Usinish Phyllonite.	Fluids absent, sub-greenschist facies (upper crustal) conditions.

**Table 3.3** Table summarising the kinematic, textural and metamorphic evolution of the OHFZ in South Uist.

### 3.6 THE SOUTHERN ZONE: ERISKAY AND THE BARRA ISLES

The author briefly visited Eriskay, Vatersay and Barra during the present survey. The following sections are therefore supplemented by more detailed accounts provided in Francis (1973), Sibson (1977b), Fettes *et al.* (1992), Butler (1995) and MacInnes & Alsop (1997).

#### 3.6.1 ERISKAY

The island of Eriskay (NF 782 124 to NF 793 082) lies in the Sound of Barra, off the south coast of South Uist (Fig. 3.42). The Lewisian geology of the island is dominated by quartzo-feldspathic banded gneisses (section 2.2.2.1) (Fettes *et al.* 1992;

Butler 1995). In eastern Eriskay, the banded gneisses are cross-cut by predominantly E-dipping pseudotachylyte-bearing fault veins, breccias and quasi-conglomerates. The effects of brittle deformation are locally very intense, and in places, the fault rocks closely resemble crush melange observed in North Uist (section 3.4.2.2; Chapter 6). The geometries of pseudotachylyte injection veins and subsidiary fractures suggest that pseudotachylyte generation took place during either localised extensional or compressional faulting.

Along the east coast (between Sloc Caol, NF 808 123 and Sloc a' Mhaide, NF 806 117), the crush melange is *locally* overprinted either by E-dipping, macroscopically ductile discrete phyllonite bands or by an E- to SE-dipping pervasive protophyllonitic fabric. Both the discrete phyllonite bands and the pervasive protophyllonitic foliation are associated with a well developed, NE-SW trending, sub-horizontal quartz stretching lineation. Kinematic indicators ( $\sigma$ -type quartz and feldspar porphyroclasts and the sigmoidal geometry of the protophyllonitic foliation) viewed in surfaces parallel to the mineral lineation and perpendicular to the foliation are consistent with top-to-the-NE shear during phyllonitisation. However, it should be emphasised that well developed phyllonitic shear zones have *not* been observed on Eriskay.

Both the pseudotachylyte-bearing faults and the phyllonitic fabrics are both cross-cut by a number of moderately E-dipping normal faults (e.g. NF 802 097).

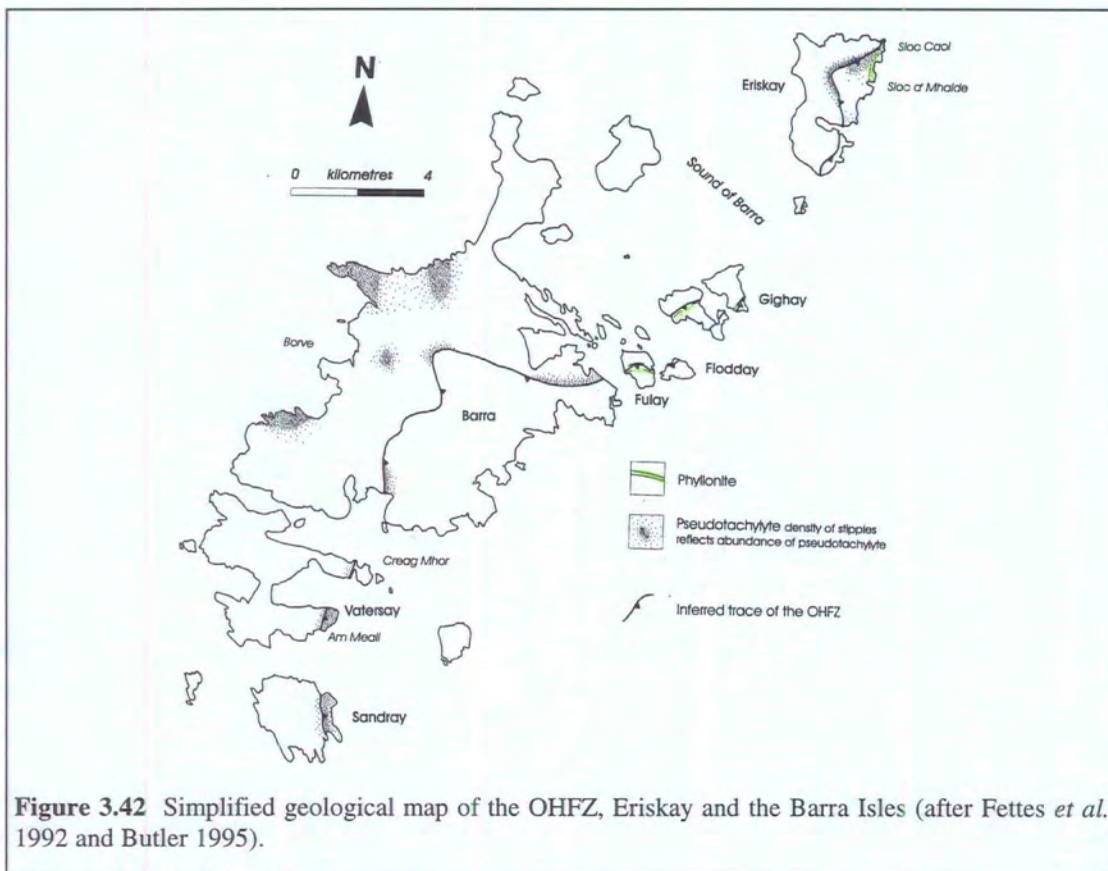


**Figure 3.42** Simplified geological map of the OHFZ, Eriskay and the Barra Isles (after Fettes *et al.* 1992 and Butler 1995).

### 3.6.2 THE BARRA ISLES

The Lewisian geology of the Barra Isles (Gighay, Hellisay, Flodday, Fuiay, Barra, Watersay and Sandray) is dominated by amphibolite facies banded gneisses (section 2.2.2.1) which generally outcrop in the *footwall* of the inferred fault zone trace, and by orthopyroxene-bearing granulite facies gneisses which generally outcrop in the *hangingwall* of the inferred fault zone trace (Fig. 3.42) (Francis 1973).

#### 3.6.2.1 Barra, Watersay and Sandray

There has been some debate concerning the exact outcrop and significance of the fault zone exposed on Barra. Some authors (Francis 1973; Fettes *et al.* 1992) have inferred a major strike-swing in the trace of the OHFZ, from a predominantly NE-SW trend in the southern reaches of the Sound of Barra, to a predominantly E-W trend in northern Barra (Fig. 3.42). In contrast, Sibson (1977b) and Butler (1995) have suggested that the fault zone exposed on Barra could in fact be a subsidiary *splay* off from the main Outer Hebrides Fault Zone (Fig. 3.43a). The implication of the latter interpretation is that the OHFZ (*s.s.*) lies offshore, some way to the east of Barra. A third possibility, favoured by Butler (1995), is that the OHFZ (*s.s.*) is exposed on Barra, but that it has been displaced relative to the trace of the OHFZ on Eriskay and South Uist by a number of NW-SE trending dextral transfer faults / shear zones in the Sound of Barra (Fig. 3.43b).

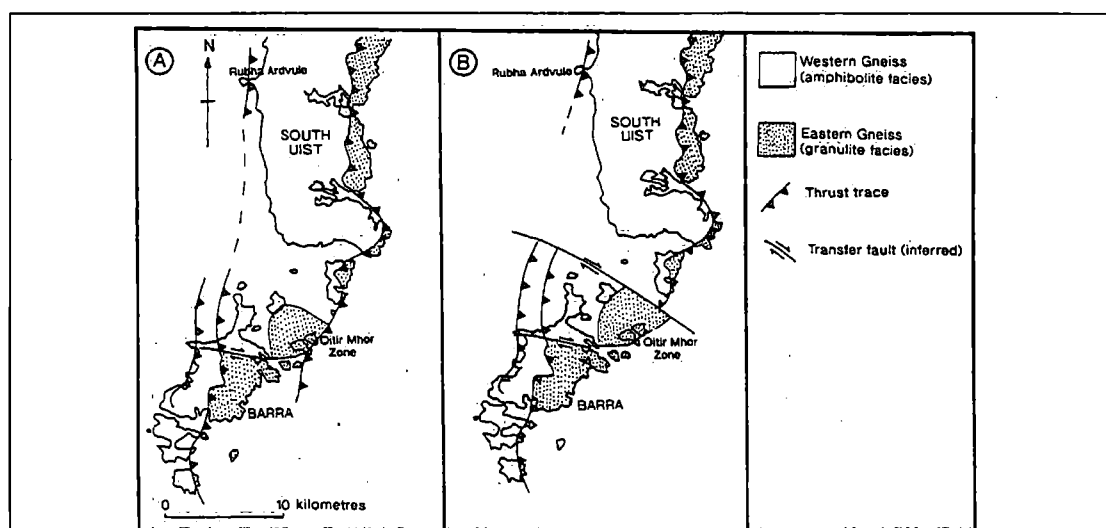


**Figure 3.43** Possible re-interpretation of the trace of the fault zone exposed on Barra, and its relationship with the structures exposed on South Uist. (a) Fault zone segment exposed on Barra is *not* the OHFZ, but is the southward continuation of a fault zone which outcrops to the west of South Uist (after Sibson 1977b and Butler 1995). (b) Fault zone segment exposed on Barra *is* the OHFZ, but the trace of the OHFZ has been displaced in an apparent dextral sense by unexposed WNW-ESE trending faults / shear zones in the Sound of Barra (after Butler 1995).

The trace of the fault zone on Barra, Vatersay and Sandray is marked, for much of its length, by a prominent E-dipping topographic break-of-slope (Fig. 3.42). E-dipping brittle faults, cataclasite seams, pseudotachylyte-bearing fault veins, and minor pseudotachylyte-ultracataclasite crush zones are commonly observed in the gneisses adjacent to these 'topographic faults' (Sibson 1977b; Butler 1995). The pseudotachylyte-bearing fault veins display apparent top-to-the-W, -NW or -E extensional and compressional displacements. Microstructural observations of the crushed gneisses suggest that the conditions of deformation and metamorphism during pseudotachylyte generation on Barra were very similar to those inferred during pseudotachylyte generation in the Uists (sections 3.4.2.4 & 3.5.2.4). However, the pseudotachylytes exposed in the Barra Isles display comparatively little evidence for significant post-tectonic retrogression (Butler 1995). Previous authors have suggested that the pseudotachylyte-bearing structures developed in a regime of *regional* top-to-the-W thrusting (Francis 1973; Sibson 1977b; Fettes *et al.* 1992; Butler 1995). However, neither the present author, nor subsequent workers (G. I. Alsop & G. Oliver *pers. comm.* 1998) could find any convincing evidence to substantiate this claim.

Minor pseudotachylyte-ultracataclasite crush zones ( $\leq 3\text{m}$  thick) outcrop in southern Vatersay (Am Meall, NL 653 944), and are cross-cut by a number of poorly exposed, E-dipping detachment faults. A moderately E-dipping detachment fault, which cross-cuts unmodified banded gneisses, is exposed in northern Vatersay (Creag Mhór, NL 663 954). The fault plane is associated with NW-SE trending slickenlines, and the geometries of subsidiary fractures are consistent with extensional displacements along the main fault plane. A zone of steeply E-dipping normal faults is developed in the hangingwall of the detachment fault. The detachment fault does *not* appear to have been offset by displacements along the steeply dipping normal faults. This observation suggests that *the detachment fault and the steeply dipping normal fault developed at the same time*, and has important implications for the relative age of the detachment faults (Chapter 9).

### 3.6.2.2 Fuiay, Hellisay and Gighay

Recent work by MacInnes & Alsop (1997) has been concerned with those segments of the OHFZ which are exposed on the islands of Fuiay, Hellisay and Gighay in the Sound of Barra (Fig. 3.42).

The granulite to upper amphibolite facies Lewisian protoliths are overprinted by a broad zone ( $\leq 1\text{km}$  wide) of macroscopically ductile blastomylonites. The foliation dips shallowly towards the ESE and is associated with a SE-plunging mineral lineation. Asymmetric quartz and feldspar augen viewed in surfaces parallel to the mineral lineation and perpendicular to the foliation are consistent with top-to-the-NW

directed shear. Similar blastomylonitic fabrics, which are exposed in western Barra (Borve Point, NF 650 021), are cross-cut by undeformed Laxfordian pegmatite veins i.e. the blastomylonites are probably of pre-Laxfordian origin. This observation is consistent with the blastomylonites exposed on Gighay, Fuiay and Hellisay being significantly older than either the pseudotachylyte- or phyllonite-bearing structures.

The mylonite belt on Gighay, Fuiay and Hellisay is overprinted by cataclasites and pseudotachylytes, which are thought to have developed in response to brittle top-to-the-NW thrusting (MacInnes & Alsop 1997). The brittle fault rocks are themselves post-dated by a network of SE- and NW-dipping phyllonitic shear zones. The phyllonitic foliation is associated with a NW-SE trending mineral lineation.  $\sigma$ -type porphyroclasts viewed in surfaces parallel to the mineral lineation and perpendicular to the foliation are consistent with top-to-the-SE displacements along the phyllonitic shear zones. MacInnes & Alsop (1997) have *not* reported NE-SW trending mineral lineations within the Sound of Barra phyllonite belts. These observations suggest that phyllonitisation in the Sound of Barra region was synchronous with top-to-the-SE extension (cf. sections 3.4.3.4 and 3.5.3.3). The phyllonitic fabrics are cross-cut, and therefore post-dated by a number of steeply SE-dipping normal faults.

An interesting corollary of MacInnes & Alsop's (1997) study is that the fault zone segments exposed on Fuiay, Hellisay and Gighay are more akin to the phyllonite-bearing fault zones exposed in the Uists than to the phyllonite-barren fault zone segments exposed on Barra, Vatersay and Sandray. This observation lends support to Sibson's (1997b) and Butler's (1995) suggestion that the trace of the OHFZ (*s.s.*) in fact lies offshore, some way to the east of Barra (Fig. 3.43a). However, the age and significance of the early, thrust-related mylonites exposed on Fuiay, Hellisay and Gighay are not known.

### 3.6.3 SUMMARY: KINEMATIC EVOLUTION AND FLUID-ROCK INTERACTIONS ALONG THE OHFZ (*s.l.*) ON ERISKAY AND THE BARRA ISLES

The kinematic, textural and metamorphic evolution of the OHFZ (*s.l.*) exposed on Eriskay and in the Barra Isles is summarised in Table 3.4.

<b>Kinematic regime</b>	<b>Fault rocks / structures</b>	<b>Metamorphism / fluids</b>
<b>1. ?Regional top-to-NW thrusting (?Laxfordian)</b> (Oldest)	Blastomylonites, only exposed in western Barra and in the Sound of Barra.	Data currently unavailable.
<b>2. ?Regional top-to-NW thrusting</b>	Cataclasites, pseudotachylytes and brittle faults.	Temperatures at or below lower greenschist facies conditions. Fluids not important during deformation.
<b>3. ?Localised top-to-the-NE sinistral strike-slip</b>	Discrete phyllonite bands and pervasive protophyllonites, only exposed in eastern Eriskay.	Data currently unavailable, but presumably involved significant fluid influx into the fault zone.
<b>4. ?Localised top-to-SE extension</b>	Phyllonitic shear zone fabrics, only exposed on the islands of Gighay, Fuiay and Hellisay in the Sound of Barra.	Data currently unavailable, but presumably involved significant fluid influx into the fault zone.
<b>5. Top-to-SE faulting</b> (Youngest)	Brittle normal faults.	?Upper crustal environment.

**Table 3.4** Table summarising the known kinematic, textural and metamorphic evolution of the OHFZ on Eriskay and in the Barra Isles, based upon the work of previous authors (see text).

## 3.7 SUMMARY AND CONCLUSIONS

### 3.7.1 THE KINEMATIC EVOLUTION OF THE OHFZ

Although the Northern and Southern Zones share broadly similar kinematic and structural histories, significant differences exist between the two zones. In the following discussion, the fault zone segments exposed in the Barra Isles are excluded, as it is unclear how these structures relate to the segment of the OHFZ exposed in South Uist (section 3.6.2.1). Overall, the observed differences between the Northern and Southern Zones of the OHFZ can be adequately explained by the kinematic model of Butler (1995) (section 2.3.3.3). The main point of Butler's (1995) argument is that following the cessation of macroscopically ductile top-to-the-NW thrusting and mylonitisation in the Outer Hebrides region, oblique dextral displacements across the South Harris Shear Zones (SHSZ) (Fig. 2.5) displaced the southern portion of the mylonite belt towards the NW, relative to the portion of the mylonite belt which is exposed in Lewis and Harris. As a result, the inferred southward continuation of the mylonite belt presently lies offshore, some way to the west of the region occupied by the present day Southern Zone of the OHFZ (Butler 1995; see section 2.3.3.3 of the present work).

Evidence for top-to-the-W brittle deformation is observed along the entire length of the present day OHFZ. Brittle deformation is thought to have taken place in a similar deformation environment along the entire length of the fault zone. However, the relative age of brittle deformation in the Northern Zone compared to brittle deformation in the Southern Zone is not immediately obvious from the field evidence, and is discussed further in Chapter 4.

An episode of phyllonitisation and lower greenschist facies retrogression, which clearly post-dates brittle thrusting, has been recognised along the entire length of the OHFZ. Phyllonitisation in the Northern Zone was synchronous with a change in the kinematic regime from local thrusting / sinistral transpression to regional top-to-the-E sinistral strike-slip. Phyllonitisation in the Uists was synchronous with a change in the kinematic regime from regional thrusting / sinistral transpression to top-to-the-NE sinistral strike-slip. Although the inferred movement vector in the Northern Zone appears to have been different to the inferred movement vector in the Uists, the style of deformation and the inferred grade of metamorphism during phyllonitisation were similar along the entire length of the OHFZ. It is therefore suggested that the main phase of phyllonitisation recognised in Lewis and on Scalpay was broadly synchronous with the main phase of phyllonitisation recognised throughout the Uists. The timing of thrust-related phyllonitisation relative to thrust-related brittle

deformation in the Northern Zone is unclear from field and microstructural observations. The thrust-related phyllonitic fabrics are never cross-cut by cataclasite / pseudotachylyte veins, but conversely, the cataclasite / pseudotachylyte veins do not appear to have been reworked during thrust-related phyllonitisation. It is therefore not unlikely that thrust-related brittle deformation was broadly synchronous with thrust-related phyllonitisation in the Northern Zone. This possibility is explored further in Chapter 5.

The phyllonitic fabrics were subsequently reworked during an episode of regional top-to-the-S extension in the Northern Zone and regional top-to-the-E or -SE extension in the Uists. Although the prevailing kinematic regime in the Northern Zone was clearly different to the prevailing kinematic regime in the Uists, the style of deformation and the inferred grade of metamorphism during reworking were similar along the entire length of the OHFZ. It is therefore suggested that the phase of extensional reworking recognised in Lewis and on Scalpay was broadly synchronous with the phase of extensional reworking recognised throughout the Uists.

The phyllonite belts and pseudotachylyte-ultracataclasite crush zones are locally cross-cut by networks of brittle detachment faults. Although the *initiation* of localised brittle deformation may have been synchronous with reworking of the phyllonitic fabrics (e.g. section 3.2.3.4; see Chapter 6 for more detailed discussion), the latest movements along the detachment faults clearly post-date deformation within the phyllonite belts. The detachment faults exposed on Scalpay preserve evidence for top-to-the-SE normal displacements, the detachment faults exposed on North Uist preserve evidence for top-to-the-NE strike-slip displacements, whilst the detachments exposed on South Uist preserve evidence for top-to-the-NNE, -ENE or -ESE displacements.

Steeply dipping normal faults, which appear to have been associated with bulk E-W extension, are well exposed in northeast Lewis and represent the latest deformation event for which onshore evidence is preserved in the Outer Hebrides. In the Southern Zone of the OHFZ, steeply-dipping normal faults are locally exposed onshore in Watersay, and appear to have developed synchronously with the moderately-dipping brittle detachment faults.

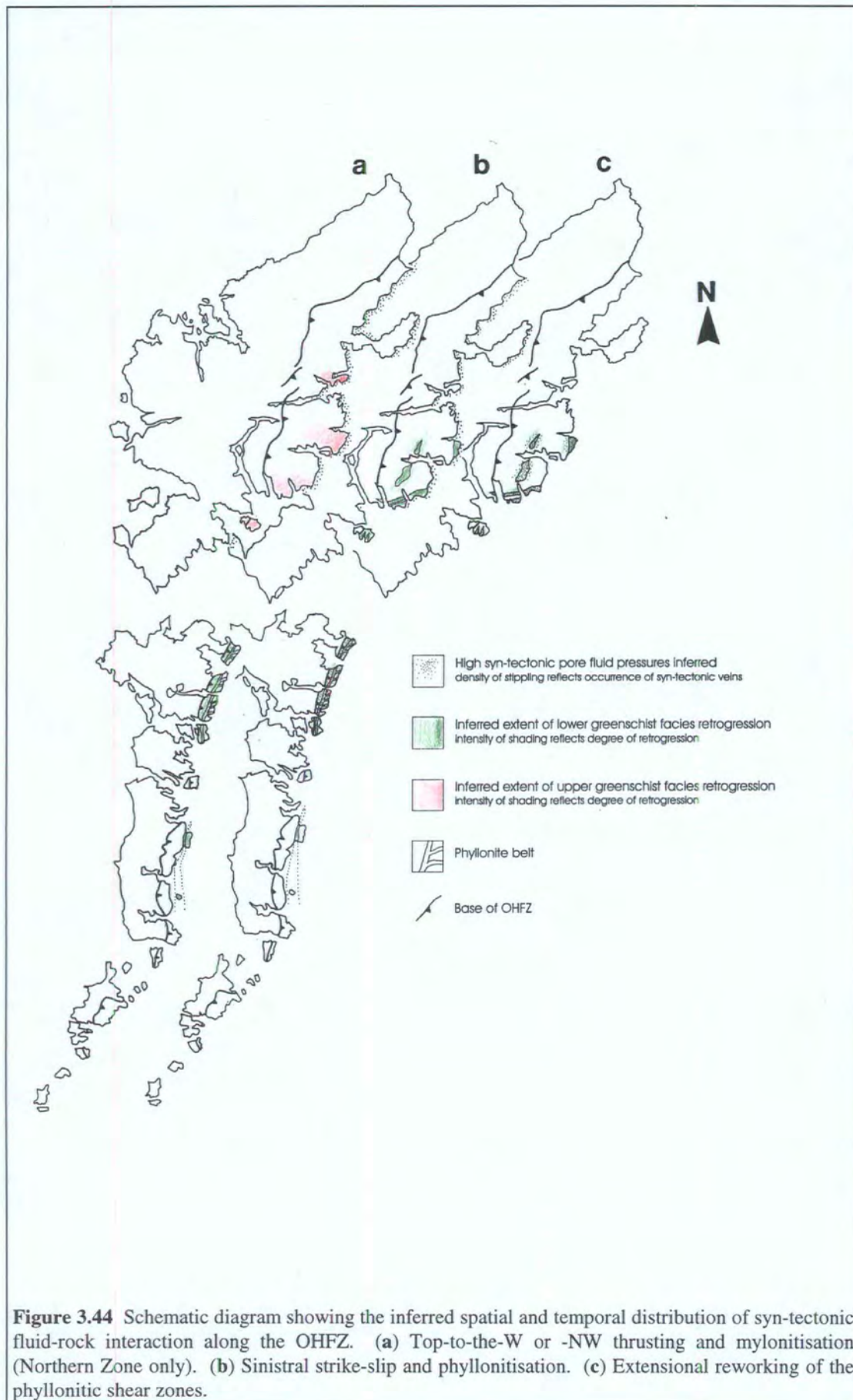
The inferred kinematic and structural evolution of the Outer Hebrides Fault Zone in Lewis, Scalpay and the Uists is summarised in Table 3.5.

<b>Northern Zone</b>	<b>Southern Zone</b> (excluding the Barra Isles)
Regional <b>top-to-W</b> or <b>-NW thrusting</b> ; upper greenschist and lower amphibolite facies mylonites $\pm$ pseudotachylyte.	No equivalent deformation recognised.
?Regional <b>top-to-W thrusting</b> ; cataclasites, pseudotachylytes and brittle faults locally overprint earlier lower amphibolite facies mylonites. The timing relative to brittle deformation in the Southern Zone is unclear.	?Regional <b>top-to-W thrusting</b> ; cataclasites, pseudotachylytes and brittle faults - development of the crush melange and / or pseudotachylyte-ultracataclasite crush zones. The timing relative to brittle deformation in the Northern Zone is unclear.
?Localised <b>sinistral transpression</b> (only observed on Scalpay); onset of phyllonitisation.	Regional <b>sinistral transpression</b> inferred throughout the Uists; onset of phyllonitisation.
Regional <b>top-to-E sinistral strike-slip / transtension</b> ; widespread phyllonitisation.	Regional <b>top-to-NE sinistral strike-slip / transtension</b> ; widespread phyllonitisation.
Regional <b>top-to-S extension</b> ; reactivation of phyllonitic fabrics and initiation of detachment faults.	Regional <b>top-to-E or -SE extension</b> ; reactivation of phyllonitic fabrics and initiation of detachment faults.
Localised <b>top-to-SE extension</b> along detachment faults.	Localised <b>top-to-NE, -ENE or -ESE strike-slip</b> or extension along detachment faults.
<b>Top-to-E extension</b> ; steeply dipping normal faults.	No equivalent deformation recognised in the Uists, although steeply E-dipping normal faults locally developed on Vatersay.

**Table 3.5** Table summarising the kinematic and structural evolution of the Northern and Southern Zones of the OHFZ. The fault zone exposed in the Barra Isles has not been included owing to its uncertain affinity with the OHFZ (*s.s.*) (section 3.6.2). Modified from Butler (1995).

### 3.7.2 FLUID-ROCK INTERACTION ALONG THE OHFZ

There have clearly been several phases of syn-tectonic retrogression and / or fluid-rock interaction along the Outer Hebrides Fault Zone. The inferred distribution of fluid-rock interaction during top-to-the-W thrusting, top-to-the-E or -NE sinistral strike-slip and top-to-the-S or -SE extension is illustrated in Figure 3.44 and is summarised in Table 3.6.



The important points to note are: (a) fluid-rock interaction resulted in localised retrogressive metamorphism and localised high pore fluid pressures; (b) retrogression appears to have been most intense within the hangingwall of the fault zone; (c) at the onset of phyllonitisation, the locus of significant fluid-rock interaction appears to have been focused either into areas of pre-existing upper greenschist facies mylonite (Northern Zone only) or into areas of intense brittle deformation (Northern and Southern Zones); (d) during extensional reactivation, the locus of significant fluid rock interaction appears to have been focused into actively deforming shear zones (Fig. 3.44).

<b>Kinematic regime</b>	<b>Locus of intense retrogression / fluid-rock interaction</b>
<b>Top-to-W or -NW thrusting</b> (Northern Zone only)	<p><i>N-S trending segments of mylonite belt:</i> retrogression largely confined to hangingwall of fault zone.</p> <p><i>NE-SW trending segments of mylonite belt:</i> retrogression observed throughout fault zone (Fig. 3.46a).</p>
<b>Sinistral transpression / strike-slip / transtension</b>	Retrogression of crush melange, Mashed Gneiss and pervasive protophyllonites. Intense retrogression in phyllonitic shear zones (Fig. 3.46b).
<b>Top-to-E, -SE or -S extension</b>	Continued retrogression within reworked phyllonitic shear zones. Evidence for locally high pore fluid pressures within the crush melange and pervasive protophyllonites (Fig. 3.46c).
<b>Top-to-E normal faulting</b>	Localised, transient high pore fluid pressures both along in, and adjacent to, actively deforming normal faults (Fig. 3.46d).

**Table 3.6** Table summarising the inferred distribution of syn-tectonic fluid-rock interactions along the Outer Hebrides Fault Zone.

### 3.7.3 CONCLUSIONS

The Outer Hebrides Fault Zone is clearly a long-lived structure, which has been the focus for long-lived *tectonic activity* and *retrogressive fluid-rock interaction* from the late Precambrian to the Mesozoic (Lailey *et al.* 1995; Butler 1995). The fault rocks and structures presently exposed along the OHFZ must therefore have been influenced (a) by the *changing kinematic and metamorphic environment* during each successive deformation event, and (b) by the *pre-existing fault zone fabrics*.

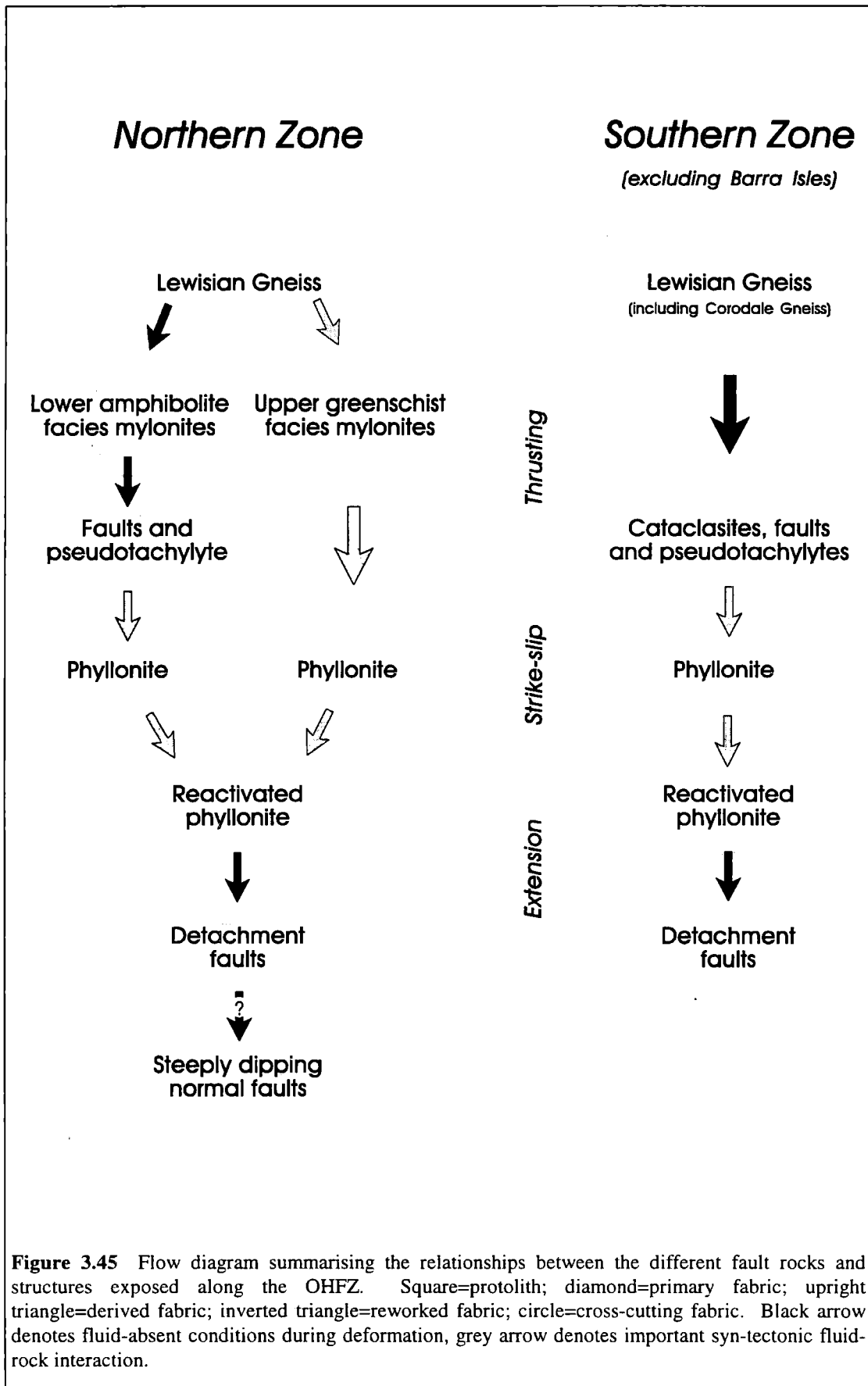
In order to assess the role played by the pre-existing fabrics during reactivation of the OHFZ, it is important to determine how the different fault rocks and structures relate to one another (see discussion in Chapter 1). Derived, reworked and cross-cutting fabrics have all been recognised along the OHFZ. The relationships between the different fabrics are illustrated in Figure 3.45 and are summarised in Table 3.7.

The geometries of the phyllonite belts in particular have clearly been influenced by the pre-existing architecture of the fault zone. In southeast Lewis and on Scalpay, the transpression / strike-slip related phyllonitic fabrics directly rework the thrust-related upper greenschist facies phyllosilicate-rich mylonites, whilst at Eishken and in the Uists, the geometry of the phyllonite belts appears to have been inherited from the thrust-related brittle fractures and pseudotachylyte-bearing fault zones (Figs. 3.3, 3.28, 3.38 & 3.45).

The phyllonite belts were subsequently reactivated during regional top-to-the-S or -SE extension. On Lewis, Scalpay and North Uist, the phyllonitic fabrics were directly reworked (Fig. 3.45), and extensional deformation was focused almost entirely into the pre-existing strike-slip related shear zones. On South Uist, extension was accommodated both by reactivation of the pre-existing strike-slip related fabrics, and by the generation of new phyllonitic fabrics. However, in regions where phyllonite is absent (e.g. Loch Sgibacleit), the effects of extension are far less intense. These observations suggest that *the phyllonitic shear zones were weak, relative both to the surrounding Lewisian gneisses and to the cataclastic / mylonitic host rocks* (Butler *et al.* 1995).

The next four chapters present detailed field and microstructural studies of the fault rocks and structures conducted at several well exposed, geologically important localities. Each chapter comprises descriptions of the primary, derived and reworked fabrics, and discusses the spatial and temporal relationships between successive generations of fault rocks. Chapter 4 is a study of the lower amphibolite facies mylonites and pseudotachylyte-bearing fault zones exposed in southeast Lewis. The aim of Chapter 4 is to determine why the lower amphibolite facies mylonites were *not* reworked during E-directed extension. Chapters 5, 6 and 7 describe the meso- and

microstructural evolution of the OHFZ on Scalpay, North Uist and South Uist respectively. Particular emphasis will be placed on describing (a) the relationships between the primary fabrics and the phyllonitic (i.e. derived and / or reworked) fabrics, and (b) the style and distribution of deformation during extensional reactivation.



<b>Fabric</b>	<b>Northern Zone</b>	<b>Southern Zone</b> (excluding the Barra Isles)
<b>Protoliths</b>	Quartzo-feldspathic banded gneisses, Older Basics, Younger Basics and Laxfordian pegmatites.	Quartzo-feldspathic banded gneisses, Older Basics, Younger Basics, Laxfordian pegmatites and the meta-igneous Corodale Gneiss.
<b>Primary fabrics</b>	Upper greenschist and lower amphibolite facies pervasive mylonites.	Crush melange and pseudotachylyte-ultracataclastic crush zones.
<b>Derived fabrics</b>	(1) Foliation-parallel brittle faults in Loch Sgibacleit region; (2) strike-slip related phyllonitic fabrics at Eishken; (3) detachment faults on Scalpay.	(1) Strike-slip and transpression-related phyllonitic fabrics in North Uist; (2) strike-slip, and locally, extension-related fabrics in the Usinish Phyllonite; (3) detachment faults in the Uists.
<b>Reworked fabrics</b>	(1) Strike-slip and / or thrust-related phyllonitic fabrics at Kebock Head, Loch Bhrollum and on Scalpay; (2) extension-related phyllonitic fabrics at Eishken, Kebock Head, Loch Bhrollum and on Scalpay.	(1) Extension-related phyllonitic fabrics in North Uist; (2) some extension-related fabrics in the Usinish Phyllonite.
<b>Cross-cutting fabrics</b>	(1) Steeply dipping normal faults in northeast Lewis and Loch Sgibacleit region; (2) E-W trending lineaments / strike-slip faults.	(1) E-W trending lineaments / strike-slip faults.

**Table 3.7** Table summarising the distribution of primary, derived, reactivated and cross-cutting fabrics along the Outer Hebrides Fault Zone.

## 4. LOCH SGIBACLEIT

### 4.1 INTRODUCTION

#### 4.1.1 INTRODUCTION AND AIMS

The predominantly N-S trending segment of the Outer Hebrides Fault Zone exposed in the region between Loch Erisort and Loch Sgibacleit has experienced a complex history of both brittle and macroscopically ductile deformation (section 3.2.2.1).

Regional top-to-the-NW thrusting was accommodated by macroscopically ductile deformation and *localised* pseudotachylyte generation within a lower amphibolite facies mylonite belt, which forms part of the pervasive mylonite belt described in section 3.2.2 (see also Sibson 1977b, 1980; White 1996). The macroscopically ductile mylonitic fabrics (i.e. the primary fabrics) are overprinted by foliation-parallel and discordant pseudotachylyte-bearing fault zones (i.e. the derived fabrics), which are themselves cross-cut by highly discordant pseudotachylyte-barren brittle faults and joints. There is little evidence to suggest that significant fluid-rock interaction occurred either during mylonitisation or during subsequent brittle deformation.

The aims of this chapter are twofold:

- (1) To describe the textural evolution of the 'dry' lower amphibolite facies mylonites, in order to provide a comparison with the reactivated, hydrated, upper greenschist facies mylonites preserved on Scalpay (Chapters 5 & 9).
- (2) To determine the relationships between the mylonites (i.e. the primary fabric) and derived and cross-cutting brittle structures.

#### 4.1.2 STUDY AREA AND CHAPTER LAYOUT

Loch Sgibacleit lies in a steep-sided, E-W trending valley which affords a section through the lower amphibolite facies mylonite belt. Exposure is excellent on the crags immediately above the loch, but is poor in areas of undulating peat-covered moorland to either side. Consequently, detailed studies of the mylonite belt and overprinting brittle structures have been conducted on the well exposed hillsides immediately to the north and south of Loch Sgibacleit (Mullach Breac Malasgair, NB 302 166 and Creag na h-Uamha, NB 307 158 respectively) (Figs. 3.4 & 4.1; LOGS - Appendix A). This chapter comprises detailed field and microstructural descriptions of the different fault rocks and structures which outcrop in the Loch Sgibacleit region. An account of

the primary fabric (i.e. the lower amphibolite facies mylonites and 'early' pseudotachylytes) (section 4.2) is followed by descriptions of the foliation-parallel pseudotachylyte-bearing fault zones (i.e. the derived fabrics) (section 4.3) and the predominantly discordant joints and brittle faults (i.e. the cross-cutting structures; section 4.4). The structural evolution of the OHFZ in the Loch Sgibacleit region is summarised in section 4.5.

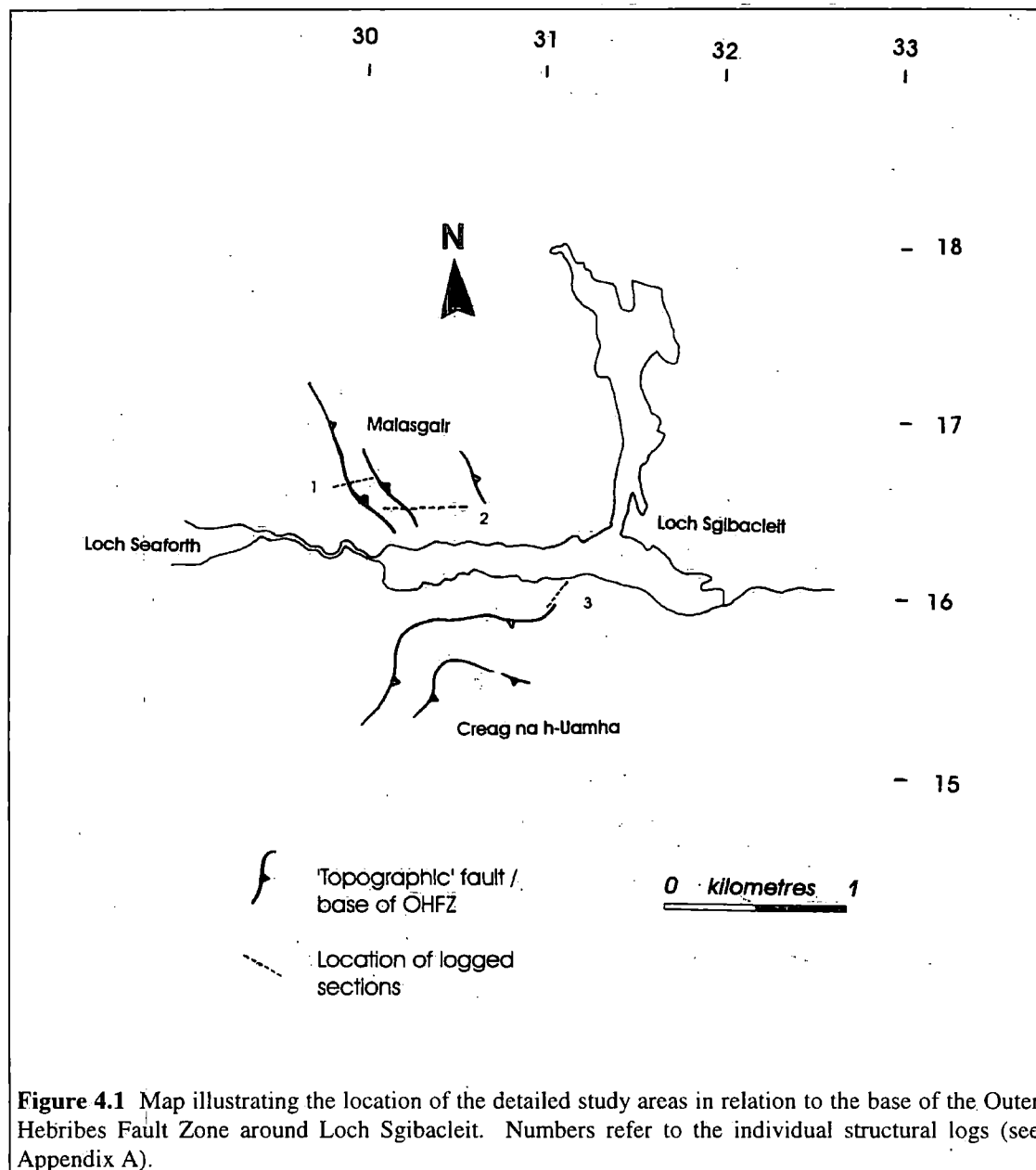


**Figure 4.1** Map illustrating the location of the detailed study areas in relation to the base of the Outer Hebrides Fault Zone around Loch Sgibacleit. Numbers refer to the individual structural logs (see Appendix A).

## 4.2 PRIMARY FABRIC: LOWER AMPHIBOLITE FACIES MYLONITE

### 4.2.1 FIELD RELATIONSHIPS

The aims of this section are (a) to describe the overall geometry of the mylonite belt (i.e. the macrostructure) and (b) to describe the lithologies and textures of the fabrics preserved within the mylonite belt (i.e. the mesostructure).

#### 4.2.1.1 Macrostructure

The SE- or E-dipping lower amphibolite facies mylonites (Fig. 3.5) overprint and deform the relatively unmodified, folded Laxfordian gneisses of the 'foreland' (section 3.2.1). The mylonite belt is at least c.600m thick, and its lower margin is defined by a series of E-dipping 'topographic' faults which outcrop along the western and southern flanks of Mullach Breac Malasgair (NB 302 166) and along the western and northern flanks of Creag na h-Uamha (NB 307 158) (see section 4.4) (Fig. 3.4). The upper margin of the mylonite belt is poorly exposed, but it appears to be gradational and is defined by a progressive eastward decrease in the intensity of the mylonitic fabric. Pervasive mylonitic fabrics are *not* commonly observed in the region immediately to the east of Loch Sgibacleit (Fig. 3.4).

#### 4.2.1.2 Lithology and mesostructure

The primary fabric comprises interbanded packages of quartzo-feldspathic mylonite, protomylonite and ultramylonite, variably deformed amphibolite pods and concordant to discordant pseudotachylyte veins.

#### *Quartzo-feldspathic mylonite and protomylonite*

Quartzo-feldspathic mylonites and protomylonites (*sensu* Sibson 1977a) account for c.70% of the exposed macroscopically ductile faults rocks, and are characterised by a platy, E- to SE-dipping foliation. The foliation, which is typically associated with a well developed SE-plunging quartz stretching lineation, is defined by re-oriented, attenuated lithological banding, undulating quartz ribbons (aspect ratios  $\leq 1:50$ ) and aligned biotite flakes (Figs. 3.5a & b). Asymmetric shear bands and  $\sigma$ - and  $\delta$ -type feldspar porphyroclasts ( $\leq 4$ mm diameter) viewed in surfaces parallel to the mineral lineation and perpendicular to the foliation are always consistent with top-to-the-NW shear (Plate 4.1).

### *Ultramylonite*

Ultramylonite accounts for between 10% and 20% of the macroscopically ductile fault rocks exposed in the Loch Sgibacleit region. Two distinct varieties of ultramylonite have been recognised. Bands of concordant *pervasive ultramylonite* ( $\leq 1\text{m}$  thick) are widely observed within packages of quartzo-feldspathic mylonite and protomylonite, and are characterised by isolated  $\sigma$ - and  $\delta$ -type feldspar porphyroclasts ( $\leq 1\text{cm}$  diameter) which 'float' in a matrix of quartz ribbons (ribbons  $\leq 1\text{mm}$  thick; aspect ratios  $\geq 50:1$ ). The pervasive ultramylonitic foliation is continuous with the regional mylonitic fabric and the margins of the pervasive ultramylonite bands are gradational (Plate 4.2).



**Plate 4.1** Typical quartzo-feldspathic mylonite, Loch Sgibacleit region (NB 302 166). Asymmetric feldspar porphyroclasts (pink) in a matrix of highly strained, undulating quartz ribbons (black). NW to left, viewed in surface parallel to the mineral lineation and perpendicular to the foliation.

*Discrete ultramylonite bands* ( $\leq 8\text{cm}$  thick; typically  $\cong 2\text{cm}$  thick) are commonly observed within packages of felsic and mafic mylonite, protomylonite and pervasive ultramylonite. The discrete ultramylonite bands comprise isolated  $\delta$ - and  $\sigma$ -type quartz and feldspar porphyroclasts ( $\ll 1\text{mm}$  diameter) which 'float' in a foliated, aphanitic matrix. The foliation is defined by ultrafine quartz ribbons ( $\ll 0.5\text{mm}$  thick; aspect ratios  $\geq 50:1$ ) and millimetre-scale colour banding. Discrete ultramylonite bands possess sharply defined margins, which are either concordant or (locally) discordant to the regional mylonitic fabric (angular discordance  $\leq 30^\circ$ ). The ultramylonitic foliation is typically oriented parallel to the margins of the host ultramylonite band, regardless of whether the band is concordant or discordant to the regional fabric. In three dimensions, ultramylonite bands are bifurcating, planar or

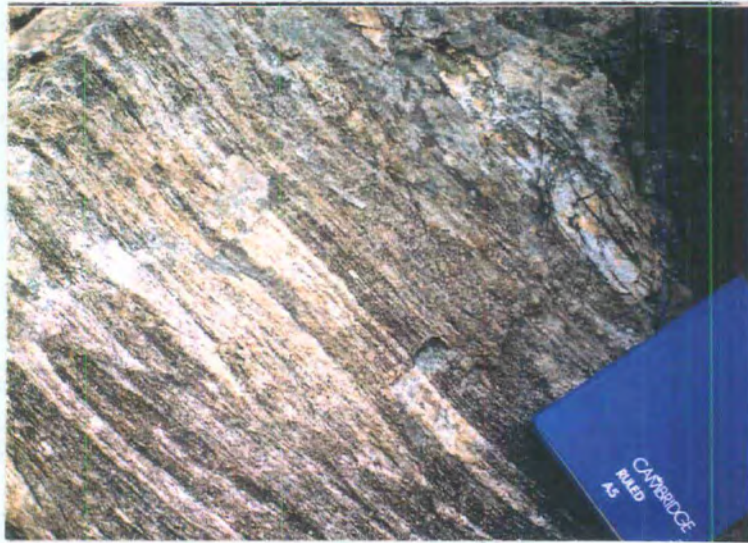


**Plate 4.2** Package of pervasive quartzo-feldspathic ultramylonite, Loch Sgibacleit region (NB 303 166). Well developed, SE-dipping foliation is defined by highly strained, planar quartz ribbons. Note that very few porphyroclasts are visible in the field. SE to right, viewed in surface parallel to the mineral lineation and perpendicular to the foliation.

wedge shaped bodies, which appear to terminate either as 'hairline' fractures and / or in a number of splays oriented at low angles to the regional mylonitic foliation (Fig. 4.2).

#### ***Protomylonitic amphibolite***

Amphibolite pods and sheets account for c.10% of the rocks exposed in the Loch Sgibacleit region. Boudinaged amphibolites ( $\leq 200\text{m}$  thick; typically  $\leq 2\text{m}$  thick) are commonly observed within the mylonite belt, and are typically oriented sub-parallel to the regional mylonitic foliation. A crude protomylonitic fabric is locally observed to overprint the boudin margins. The protomylonitic foliation is defined by undulating quartz ribbons (aspect ratios  $\leq 5:1$ ), which wrap around apparently undeformed garnet, hornblende and feldspar grains.

#### ***'Early' pseudotachylyte***

It has been suggested that localised melting and pseudotachylyte generation were synchronous with macroscopically ductile deformation (Sibson 1977b, 1980; White 1996; section 3.2.2.1 of the present work). 'Early' (i.e. syn-mylonitisation) pseudotachylyte veins (up to 10cm thick, but typically  $\leq 5\text{cm}$  thick;  $\leq 50\text{cm}$  long) are commonly observed within packages of felsic and mafic mylonite and protomylonite. The aphanitic, dark brown or black matrix is well jointed and contains numerous angular to rounded clasts of quartz and feldspar  $\pm$  hornblende ( $\leq 1\text{mm}$  diameter). The pseudotachylyte veins typically display pinch-and-swell geometries (Sibson 1975,

1977b) and are either concordant, or (locally) discordant to the regional mylonitic foliation. The pinch-and-swell veins are locally associated with branching injection veins, which are oriented at up to 45° to the regional foliation (Fig. 4.3). The origin and relative age of the 'early' pseudotachylyte veins is discussed further in section 4.2.3.

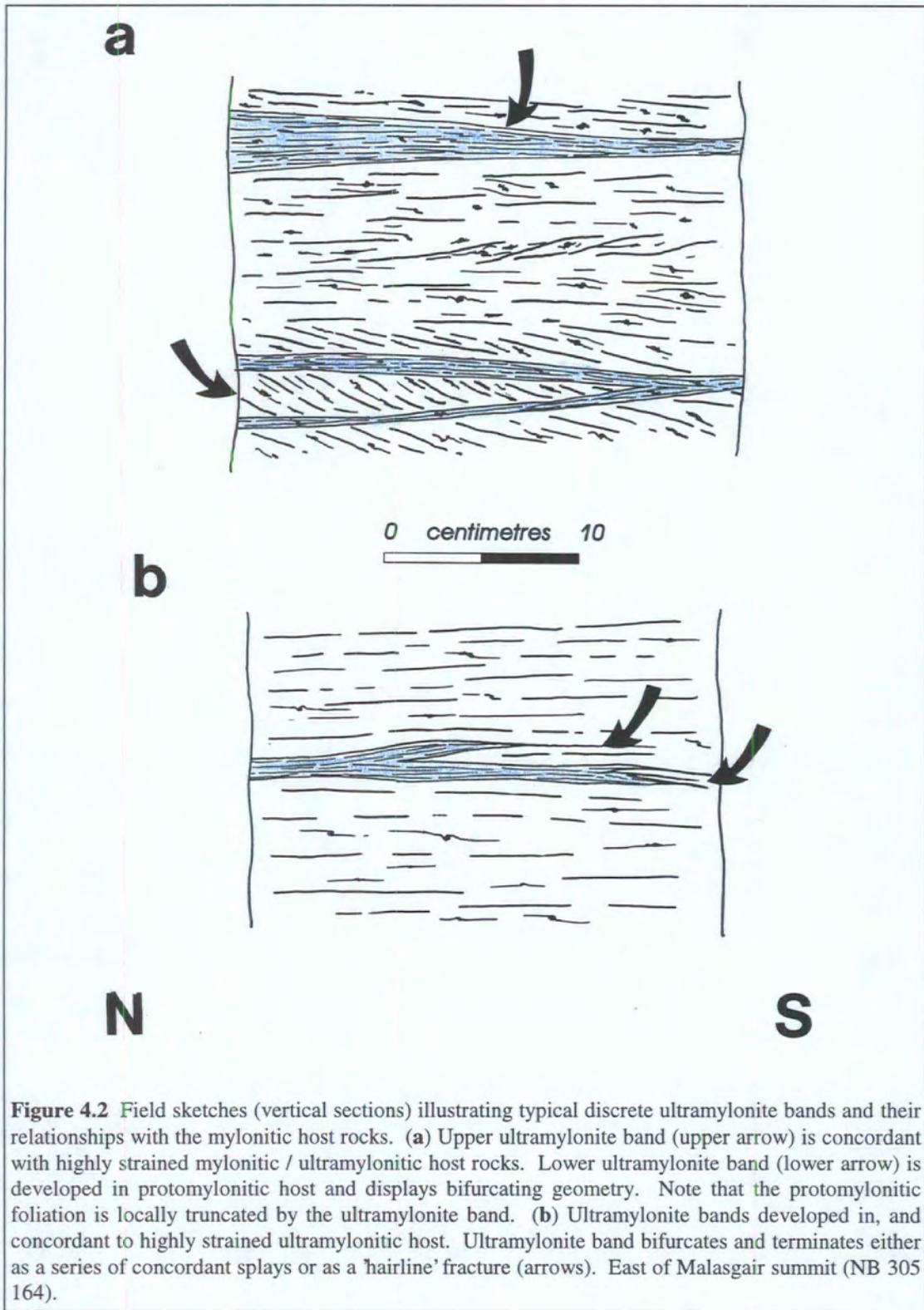
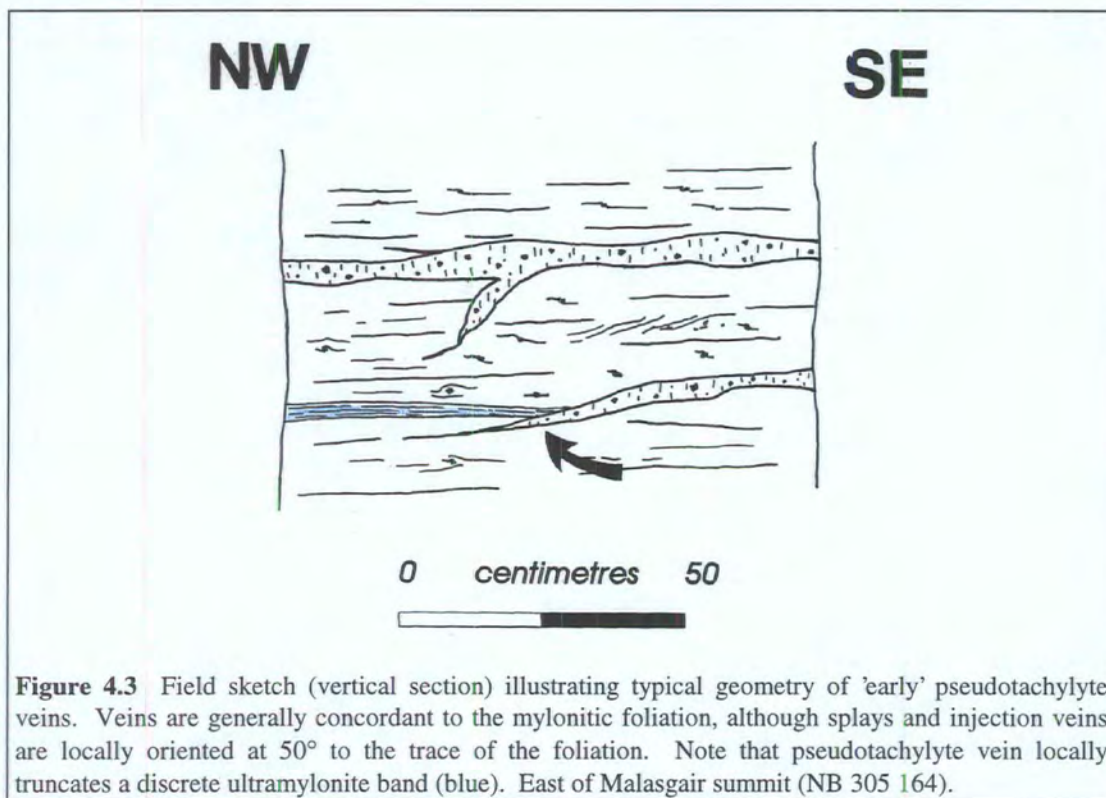


**Figure 4.2** Field sketches (vertical sections) illustrating typical discrete ultramylonite bands and their relationships with the mylonitic host rocks. (a) Upper ultramylonite band (upper arrow) is concordant with highly strained mylonitic / ultramylonitic host rocks. Lower ultramylonite band (lower arrow) is developed in protomylonitic host and displays bifurcating geometry. Note that the protomylonitic foliation is locally truncated by the ultramylonite band. (b) Ultramylonite bands developed in, and concordant to highly strained ultramylonitic host. Ultramylonite band bifurcates and terminates either as a series of concordant splays or as a 'hairline' fracture (arrows). East of Malasgair summit (NB 305 164).



## 4.2.2 MICROSTRUCTURE

The following section describes the typical fault rock microstructures observed in the Loch Sgibacleit region. The microstructures of the protolith gneisses are described briefly in Chapter 3.

### 4.2.2.1 Felsic mylonite and protomylonite

Domains of felsic mylonite and protomylonite correspond to the packages of quartzofeldspathic mylonite and protomylonite observed in the field. Domains of mylonitised felsic gneiss comprise  $\delta$ -,  $\sigma$ - and  $\phi$ -type feldspar  $\pm$  hornblende porphyroclasts, which are wrapped by a network of anastomosing, polycrystalline quartz ribbons, bands of ultrafine-grained feldspar and, locally, by bands of ultrafine-grained biotite (Plate 4.3). Insertion of a sensitive tint plate suggests that the aggregates of fine grained quartz and feldspar both display strong crystallographic preferred orientations. Asymmetric shear bands, whose geometries are consistent with top-to-the-NW shear, are typically developed in domains of felsic protomylonite (Plate 4.4).

The quartz ribbons ( $\leq 1$ mm thick) display a variety of microstructures. Ribbons with relatively low aspect ratios ( $\leq 30:1$ ) typically comprise monocrystalline 'cores', which display strong patchy to sweeping undulose extinction, and which are surrounded by

'mantles' of optical subgrains and aggregates of equigranular-interlobate quartz grains ( $\leq 0.01\text{mm}$  diameter). The lobate quartz grains display aspect ratios of up to 5:1, and their long axes are oriented at up to  $50^\circ$  to the trace of the macroscopic foliation. Ribbons with relatively high aspect ratios ( $\leq 100:1$ ) are composed entirely of elongate, equigranular-interlobate quartz grains (individual grains  $\leq 0.01\text{mm}$  diameter). The fine, elongate quartz grains locally define an oblique secondary foliation, whose geometry is consistent with top-to-the-NW shear (Lister & Snoke 1984) (Plate 4.5).

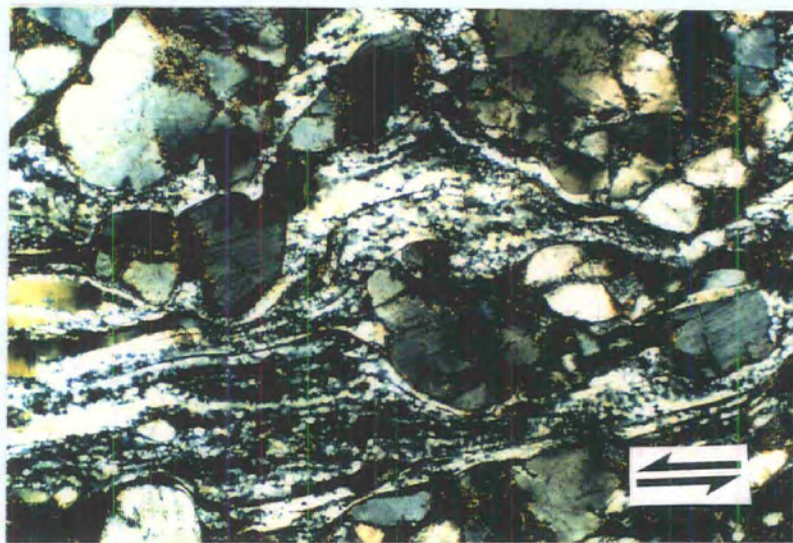


**Plate 4.3** Quartzo-feldspathic protomylonite. Relatively undeformed, asymmetric feldspar porphyroclasts are wrapped by an anastomosing network of highly strained, polycrystalline quartz ribbons. Split arrows parallel to mineral lineation, top-to-NW shear. Field of view  $3 \times 1.9\text{mm}$ , crossed polars.

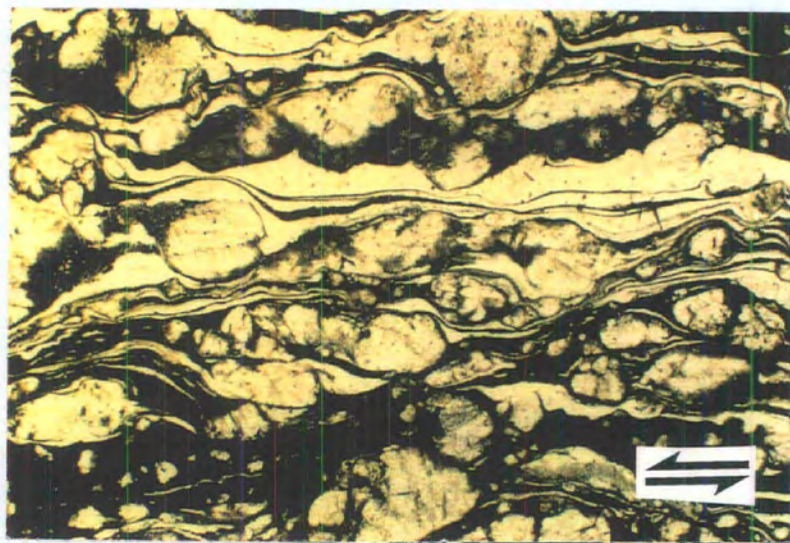


**Plate 4.4** Asymmetric extensional shear bands developed in quartzo-feldspathic mylonite. Rounded feldspar porphyroclasts wrapped by undulating quartz ribbons and bands of ultrafine grained biotite (dark material). Split arrows parallel to mineral lineation, top-to-the-NW shear. Field of view  $6 \times 3.7\text{mm}$ , plane polarised light.

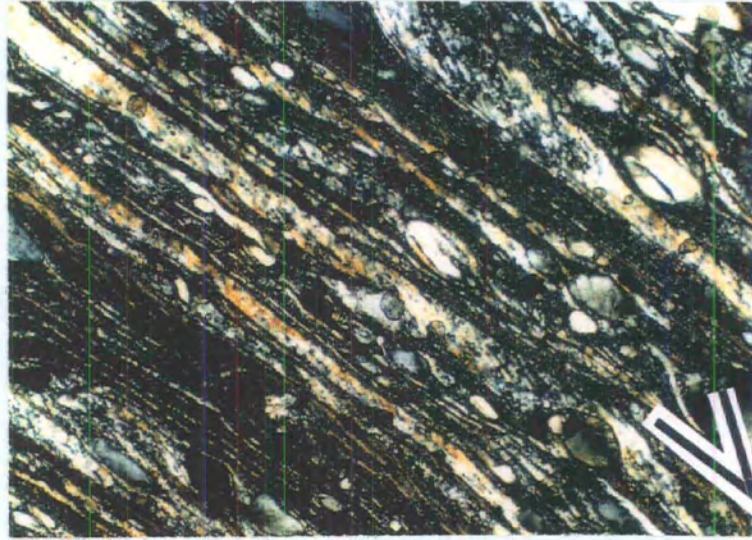


**Plate 4.5** Felsic mylonite / ultramylonite. Small, well rounded feldspar porphyroclasts 'float' in a matrix of polycrystalline quartz ribbons and ultrafine grained biotite. Recrystallised quartz grains within quartz ribbons define a well developed, oblique secondary foliation. Long bar parallel to primary foliation, short bar parallel to secondary foliation. NW to left, top-to-NW shear. Field of view 3×1.9mm, crossed polars.

Feldspar (moderately calcic plagioclase and K-feldspar) porphyroclasts ( $\leq 2$ mm diameter but typically  $\cong 0.025$ mm diameter; aspect ratios  $\leq 5:1$ ) preserved in domains of felsic mylonite are subangular to well rounded and typically display strong patchy to sweeping undulose extinction and / or gently curved twin planes. The largest feldspar porphyroclasts ( $\geq 1$ mm diameter) are locally cross-cut by arrays of intragranular extension fractures and 'bookshelf' shear fractures which extend the host grain parallel to the trace of the macroscopic foliation. The intragranular fractures are typically infilled by aggregates of ultrafine grained feldspar. Both plagioclase and K-feldspar porphyroclasts are surrounded by narrow mantles (between 0.05mm and 0.005mm thick) which comprise aggregates of ultrafine, equigranular-interlobate feldspar grains (individual grains  $\leq 0.005$ mm diameter). The mantles are typically 'drawn out' to form laterally continuous (on the thin section-scale) tails and bands which are oriented parallel to the trace of the macroscopic foliation.

#### 4.2.2.2 Felsic ultramylonite

Domains of felsic ultramylonite correspond to the pervasive quartzo-feldspathic ultramylonites observed in the field. Felsic ultramylonite comprises rounded to subrounded feldspar (moderately calcic plagioclase and K-feldspar) porphyroclasts (typically  $\leq 0.1$ mm diameter; aspect ratios  $\leq 3:1$ ), which are wrapped by

polycrystalline quartz ribbons ( $\leq 0.05\text{mm}$  wide) and bands of ultrafine grained feldspar. Asymmetric shear bands are rarely observed (Plate 4.6).

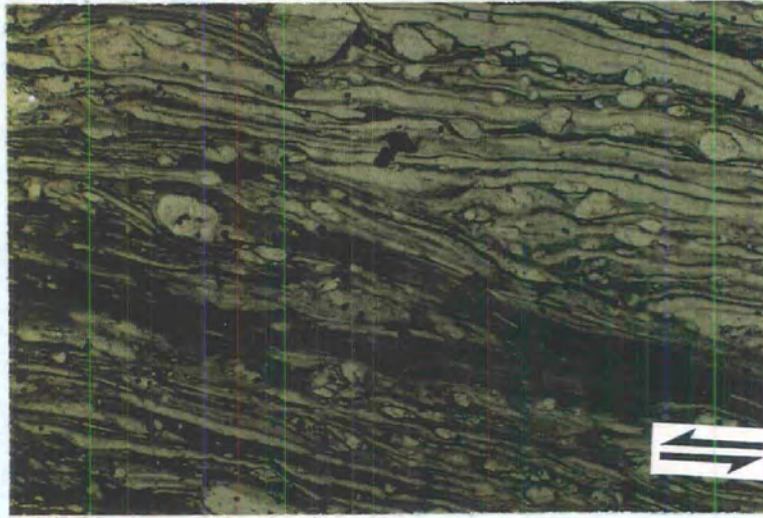


**Plate 4.6** Felsic ultramylonite. Well rounded feldspar porphyroclasts 'float' in a matrix of highly strained quartz ribbons. Note bands of highly strained, concordant and slightly discordant *discrete* ultramylonite (dark brown) contain very few porphyroclasts (see text for discussion). Split arrows parallel mineral lineation, top-to-NW shear. Field of view  $3 \times 1.9\text{mm}$ , plane polarised light.

The quartz ribbons are typically planar and comprise aggregates of fine, elongate, equigranular-interlobate quartz grains (individual grains  $\leq 0.01\text{mm}$  diameter). The long axes of the lobate quartz grains are typically oriented at between  $30^\circ$  and  $40^\circ$  to the trace of the macroscopic foliation, and thus define an oblique secondary foliation. The asymmetry of the oblique foliation is consistent with top-to-the-NW shear. Quartz core-and-mantle microstructures have *not* been observed in domains of felsic ultramylonite. The intracrystalline microstructures displayed by feldspar grains preserved in domains of felsic ultramylonite are indistinguishable from those observed in domains of felsic mylonite and protomylonite.

#### 4.2.2.3 Mafic protomylonite

Domains of mafic protomylonite correspond to the protomylonitic amphibolites observed in the field. Domains of mafic protomylonite comprise relatively undeformed garnet-feldspar-hornblende augen ( $\leq 5\text{cm}$  diameter), and feldspar and hornblende porphyroclasts, which are *locally* wrapped by anastomosing quartz ribbons and bands of ultrafine-grained feldspar (Plate 4.7). The quartz ribbons ( $\leq 0.1\text{mm}$  wide; aspect ratios  $\leq 4:1$ ) display well developed core-and-mantle microstructures, which are similar to those observed in domains of felsic protomylonite (section 4.2.2.1).



**Plate 4.7** Protomylonitic amphibolite. Relatively undeformed hornblende (green and brown) and garnet porphyroclasts 'float' in a matrix of undulating quartz ribbons. Note the aspect ratios of the quartz ribbons are significantly lower than those observed in felsic mylonites and ultramylonites (e.g. Plate 4.5). Bar parallel mineral lineation, shear sense not determined. Field of view  $3 \times 1.9$ mm, plane polarised light.

Feldspar porphyroclasts ( $\leq 0.3$ mm diameter) typically display strong, patchy undulose extinction, and are commonly observed to be cross-cut by arrays of en-echelon, intragranular shear fractures. These 'bookshelf' fractures are generally infilled by aggregates of ultrafine-grained feldspar  $\pm$  opaque grains and appear to extend the host porphyroclast parallel to the trace of the macroscopic foliation. Narrow mantles (between 0.003mm and 0.05mm thick) of ultrafine, equigranular-interlobate feldspar grains (individual grains  $\leq 0.003$ mm diameter) are locally developed along the margins of feldspar porphyroclasts, and are typically drawn out into tails and bands which are oriented parallel to the trace of the macroscopic foliation.

The angular to subangular hornblende porphyroclasts (between 0.2mm and 0.05mm diameter) are characterised by strong, patchy undulose extinction, and are locally cross-cut by narrow kink bands and / or intragranular shear fractures. Some hornblende porphyroclasts are surrounded by narrow mantles of fine-grained ( $\leq 0.008$ mm diameter) green pleochroic hornblende and finely disseminated opaque minerals. Less commonly, the margins of mantles comprise aggregates of ultrafine grained biotite.

#### **4.2.2.4 Discrete ultramylonite**

Domains of discrete ultramylonite correspond to the discrete ultramylonite bands observed in the field. Less deformed discrete ultramylonite bands comprise isolated feldspar, quartz and less commonly, hornblende porphyroclasts which 'float' in an

ultrafine-grained, brown matrix (Plate 4.8). More highly deformed ultramylonite bands comprise fine polycrystalline quartz and feldspar ribbons ( $\geq 0.01\text{mm}$  thick) which 'float' in a similar ultrafine-grained, brown matrix. The foliation is defined by delicate colour banding (bands  $\leq 0.005\text{mm}$  wide) and strung-out trails of opaque minerals (individual grains  $\leq 0.01\text{mm}$  diameter) (Plate 4.6). Backscattered scanning electron microscope images suggest that the matrix comprises aggregates of ultrafine grained, equant feldspar (predominantly plagioclase) and amphibole grains (White 1996).

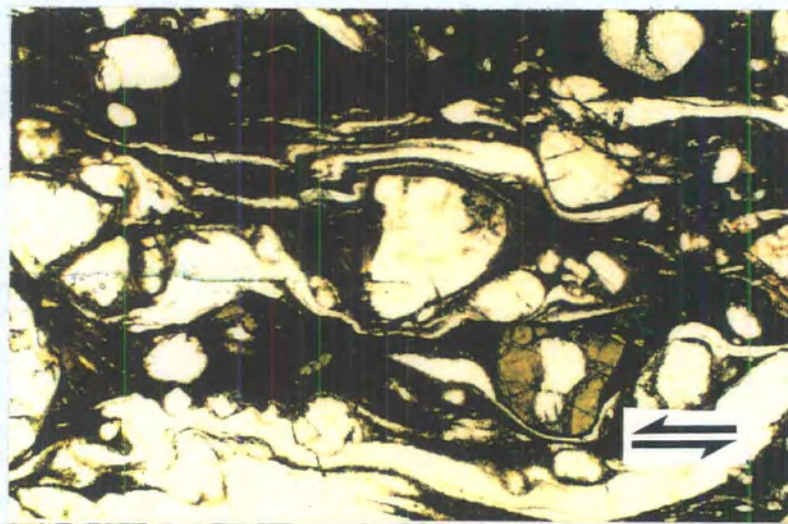


**Plate 4.8** Moderately strained discrete ultramylonite band. Rounded feldspar porphyroclasts (and rare green hornblende grains) 'float' in a matrix of elongate quartz ribbons and ultrafine grained, dark brown matrix. Dark brown matrix is thought to be viscously deformed pseudotachylyte. See text for discussion. Split arrows parallel mineral lineation, top-to-NW shear. Field of view  $3 \times 1.9\text{mm}$ , plane polarised light.

The plagioclase and K-feldspar porphyroclasts preserved within domains of discrete ultramylonite are typically equant (aspect ratios  $\leq 2:1$ ), well rounded and display a wide range of grain sizes (porphyroclasts vary from  $1.5\text{mm}$  to less than  $0.05\text{mm}$  diameter). The feldspar porphyroclasts are characterised by strong patchy undulose extinction, although core-and-mantle microstructures and intragranular fractures are not commonly observed (cf. section 4.2.2.1). The margins of relatively undeformed feldspar porphyroclasts are locally 'intruded' by a number of wedge-shaped embayments ( $\leq 0.05\text{mm}$  long). These embayments are infilled by aggregates of ultrafine grained biotite (Plate 4.9).

The gently undulating margins of the discrete ultramylonite bands are very sharply defined and are typically oriented sub-parallel to the trace of the macroscopic foliation. However, wedge shaped apophyses locally splay off from the parent band into the wallrock and are oriented at up to  $30^\circ$  to the trace of the foliation. Discordant

ultramylonite bands are typically preserved in domains of felsic or mafic protomylonite (Plate 4.10), whilst those preserved in domains of more highly deformed felsic mylonite and pervasive ultramylonite are typically concordant. As noted previously, the ultramylonitic foliation is usually concordant to the margins of the host ultramylonite band, regardless of the orientation of the regional mylonitic foliation (Plates 4.6 & 4.10). The relationships between the host rocks and the discrete ultramylonites are summarised in Figure 4.4, and are discussed in section 4.2.3.

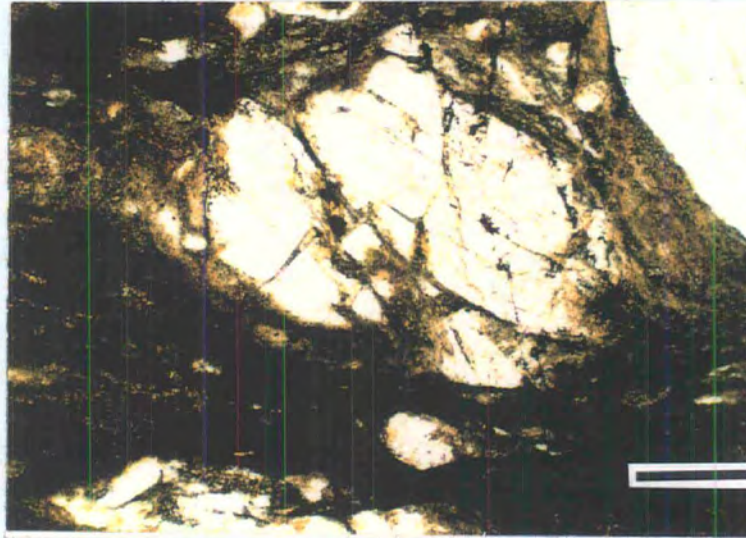


**Plate 4.9** Detail of feldspar porphyroclast preserved in moderately strained discrete ultramylonite band. Porphyroclast is highly fractured. Fractures are infilled by aggregates of ultrafine grained biotite which appear to be in optical continuity with the surrounding matrix. Bar parallel to mineral lineation, sense of shear not known. Field of view  $1.3 \times 0.77$  mm, plane polarised light.

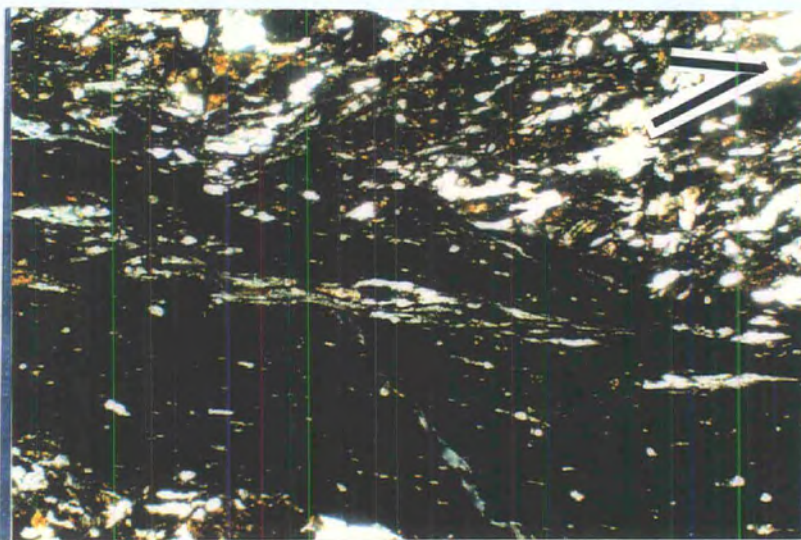


**Plate 4.10** High discordant discrete ultramylonite band (dark brown) in mafic protomylonite host. Note that the trace of the ultramylonitic foliation is parallel to the margins of the ultramylonite band, but highly discordant to the regional mylonitic foliation developed within the protomylonitic host. Long bar parallel to the regional foliation, short bar parallel to the foliation within the ultramylonite band. Field of view  $6 \times 3.7$  mm, plane polarised light.

#### 4.2.2.5 Pseudotachylyte

Concordant and discordant (Fig. 3.5) (Plate 4.11) 'early' pseudotachylyte veins are commonly observed in domains of felsic and mafic protomylonite and mylonite, but are rarely observed in domains of pervasive ultramylonite. 'Early' pseudotachylyte veins comprise angular to rounded clasts of quartz and feldspar  $\pm$  hornblende ( $\leq 2$ mm diameter, although grain size is variable), and elongate slivers of the wallrock, which 'float' in an optically isotropic, devitrified brown or black matrix. Quartz and feldspar clasts are locally intruded by tapering injection veins ( $\leq 1$ mm long), which are infilled by devitrified pseudotachylyte (Plate 4.12).

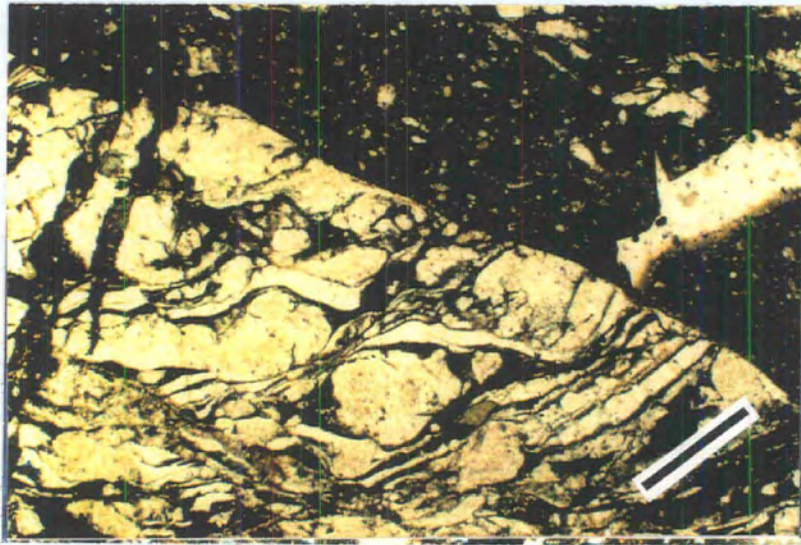


**Plate 4.11** Highly discordant 'early' pseudotachylyte band (dark brown) cross-cutting felsic protomylonite. Bar parallel to trace of protomylonitic foliation, shear sense not known. Field of view  $6 \times 3.7$ mm, plane polarised light.

The early pseudotachylyte veins possess sharply defined, undulating margins. Undulating, concordant and discordant (angular discordance  $\leq 45^\circ$ ) injection veins and apophyses are commonly observed to intrude the wallrocks.

#### 4.2.3 SUMMARY AND DISCUSSION

The macroscopically ductile primary fabric comprises interbanded packages of felsic mylonite, protomylonite and ultramylonite, protomylonitic amphibolite, discrete ultramylonite bands and narrow, concordant and discordant pseudotachylyte veins. The deformation microstructures observed in packages of mylonitised felsic and mafic gneiss are characterised by fractured feldspar porphyroclasts which 'float' in a matrix of interconnected quartz ribbons and bands of ultrafine grained feldspar. The discrete

ultramylonite bands are characterised by rounded feldspar and quartz porphyroclasts and ribbons which 'float' in an ultrafine grained matrix.

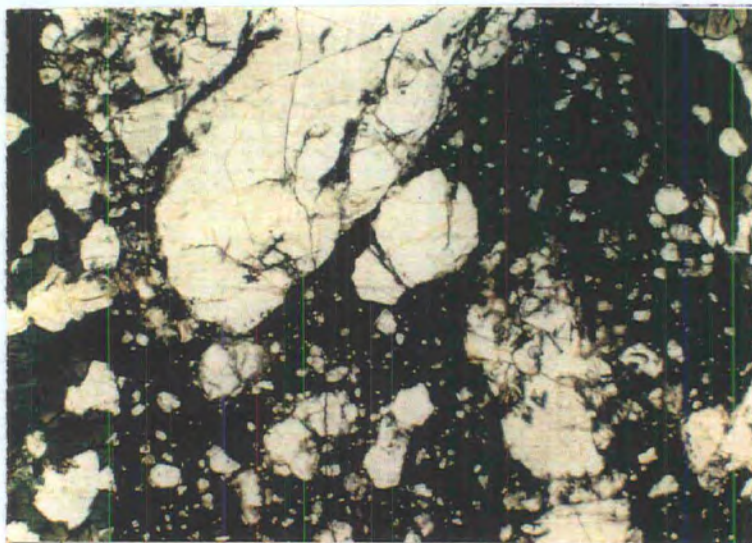


**Plate 4.12** Subangular feldspar clasts within 'early' pseudotachylyte matrix (dark brown). Note that the clasts are locally intruded by small pseudotachylyte injection veins (arrowed). Field of view  $3\times 1.9\text{mm}$ , plane polarised light.

#### 4.2.3.1 Metamorphic conditions during thrusting

Felsic mylonites display an apparently stable mineral assemblage of moderately calcic plagioclase, K-feldspar, quartz and biotite. Mafic mylonites comprise an apparently stable mineral assemblage of green hornblende, moderately calcic plagioclase and garnet. There is *no* evidence to suggest that deformation was accompanied by significant fluid-rock interaction (cf. the upper greenschist facies mylonite belt exposed on Scalpay; section 5.2). These observations suggest either that (a) in the absence of available syn-tectonic fluids, the original amphibolite facies mineral assemblage was preserved in a metastable state, or that (b) thrusting and mylonitisation took place under amphibolite facies conditions.

The quartz grains preserved in packages of felsic and mafic mylonite have experienced widespread dynamic recrystallisation, and an oblique foliation is locally developed (section 4.2.3.2). These observations are consistent with deformation having occurred at temperatures of between  $400^{\circ}\text{C}$  and  $700^{\circ}\text{C}$  (Passchier & Trouw 1996). The deformation microstructures associated with plagioclase and K-feldspar porphyroclasts (localised intragranular fracturing and widespread development of core-and-mantle microstructures) suggest that deformation took place at temperatures of between  $400^{\circ}\text{C}$  and  $500^{\circ}\text{C}$  (White 1975; Fitz Gerald & Stünitz 1993). It is therefore postulated that the macroscopically ductile primary fabrics developed in a 'dry', lower amphibolite facies metamorphic environment (see also White 1996).

#### 4.2.3.2 Operative deformation mechanisms during mylonitisation

The microstructural similarities between packages of felsic and mafic mylonite suggest that both groups of fault rock deformed in a similar manner. The inferred operative deformation mechanisms within the discrete ultramylonite bands will be discussed in a subsequent section.

##### *Felsic and mafic mylonite*

Packages of felsic and mafic mylonite comprise *isolated* feldspar and / or hornblende and / or garnet porphyroclasts which 'float' in a matrix of interconnected quartz ribbons and bands of ultrafine grained feldspar. The porphyroclasts display low aspect ratios and appear to be relatively undeformed. In contrast, the quartz ribbons and feldspar-rich bands display comparatively high aspect ratios and appear to be very highly strained. These observations suggest that the rheological behaviour of the highly strained mylonitic fault rocks was primarily controlled by the rheological behaviour of the quartz ribbons and bands of ultrafine grained feldspar (Handy 1990). Quartz ribbons with relatively low aspect ratios are commonly observed in packages of felsic and mafic protomylonite and comprise monocrystalline undulose 'cores', which are surrounded by mantles of optical subgrains and aggregates of fine grained equigranular-interlobate quartz (sections 4.2.2.1 & 4.2.2.3). Quartz ribbons with relatively high aspect ratios, which are commonly observed in packages of felsic mylonite and ultramylonite, comprise aggregates of elongate, equigranular-interlobate quartz grains (section 4.2.2.1). The long axes of the lobate quartz grains are typically oriented at up to 50° to the trace of the regional mylonitic foliation and thus define an oblique secondary foliation. These observations suggest that during mylonitisation, the quartz grains deformed primarily by intracrystalline crystal plastic mechanisms. The core-and-mantle microstructures suggest that at relatively low strains, deformation was primarily accommodated by dislocation glide and subgrain rotation recrystallisation (White 1976; Hirth & Tullis 1992). However, more highly strained quartz ribbons are characterised by an oblique foliation, which is consistent with the operation of grain boundary migration recrystallisation mechanisms (Hirth & Tullis 1992). Means (1981) has postulated that oblique foliations may develop during non-coaxial steady-state deformation. If this inference is correct, it is likely that packages of felsic mylonite and pervasive ultramylonite which contain abundant polycrystalline quartz ribbons have accommodated very high magnitudes of finite shear strain. The largest feldspar porphyroclasts ( $\geq 1$ mm diameter) are commonly observed to be cross-cut by arrays of intragranular extension and shear fractures. The shear fractures typically extend the host porphyroclasts in a direction parallel to the macroscopic

mineral lineation. Both the extension and shear fractures are healed by aggregates of ultrafine grained feldspar, and there is *no* textural evidence (e.g. fibrous vein infills) to suggest that fracture opening was associated with localised high pore fluid pressures. Smaller porphyroclasts are rarely observed to be fractured. It is therefore postulated that intragranular fracturing was an important mechanism of grain size reduction within *larger* feldspar porphyroclasts, especially at the onset of mylonitisation (Michibayashi 1996).

The majority of feldspar porphyroclasts display strong patchy undulose extinction and are surrounded by tails and mantles of ultrafine, equigranular-interlobate feldspar grains. The lobate feldspar grains display a strong crystallographic preferred orientation, and are consistently finer than the elongate, lobate quartz grains described above. Similar microstructures have been observed in experimentally deformed albite aggregates, and are thought to have developed in response to recrystallisation-accommodated dislocation creep  $\pm$  grain boundary sliding processes (Tullis & Yund 1985). Unfortunately, the fine grain size precludes detailed optical examination, and in the absence of TEM data, it is tentatively suggested that deformation within the bands of ultrafine grained feldspar was primarily accommodated by dislocation creep and / or by solid-state grain size sensitive (GSS) mechanisms. If these inferences are correct, grain size reduction, which was primarily controlled by intragranular fracture and dynamic recrystallisation mechanisms, may have resulted in a switch from *grain size insensitive* to *grain size sensitive* deformation within feldspar-rich bands during mylonitisation. It is important to emphasise that there is no evidence for the operation of *fluid-assisted* GSS creep mechanisms (cf. the hydrated upper greenschist facies mylonites from Scalpay; Chapter 5).

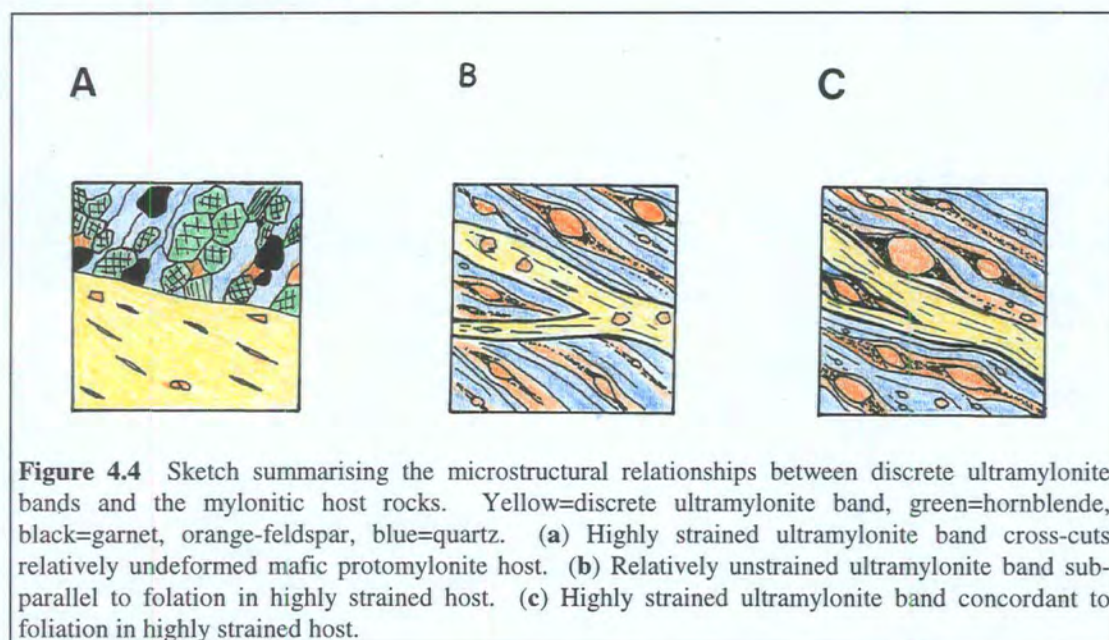
### ***Discrete ultramylonites***

Discrete ultramylonite bands comprise isolated feldspar and quartz porphyroclasts and ribbons, which 'float' in a foliated, ultrafine grained matrix. It is likely that the rheological behaviour of the ultramylonite bands was controlled by the rheological behaviour of the ultrafine grained, interconnected matrix (Handy 1990).

Highly discordant, highly deformed ultramylonite bands locally truncate the coarse, protomylonitic foliation developed in relatively undeformed host rocks. This observation suggests that at relatively low bulk finite strains, the coarse grained protomylonitic host rocks, which deformed predominantly by dislocation glide and subgrain rotation recrystallisation in quartz and intragranular fracturing in feldspar, were significantly more competent than the highly strained ultramylonite bands (cf. Fliervoet *et al.* 1997). It is unlikely that the ultrafine-grained discrete ultramylonite bands deformed by intragranular fracturing / subgrain rotation recrystallisation.

Conversely, ultramylonite bands developed in packages of highly deformed mylonite and pervasive ultramylonite are typically concordant to the regional foliation (Fig. 4.4). This observation suggests that at relatively high bulk finite strains, the competence contrast between the fine grained host rocks and the fine grained ultramylonite bands was relatively low. Similar deformation mechanisms may have been operative within the ultramylonite bands and the highly deformed mylonitic host rocks. The quartzo-feldspathic mylonites and pervasive ultramylonites appear to have deformed by dislocation creep-dominated mechanisms in quartz-rich layers, and by dislocation creep and / or grain size sensitive (GSS) processes in the ultrafine grained feldspar-rich layers. It is therefore suggested that *the ultrafine grained discrete ultramylonite bands deformed by dislocation creep and / or grain size sensitive processes, regardless of the operative deformation mechanisms within the host rocks* (cf. Fliervoet *et al.* 1997).

The discordant geometries displayed by some discrete ultramylonite bands are discussed in the following section.



#### 4.2.3.3 Origin and significance of the ultramylonitic fabrics

Two distinct mechanisms have been proposed to explain the origin of ultramylonite. The most widely accepted interpretation is that ultramylonites develop during *progressive* deformation within macroscopically ductile mylonitic shear zones (Sibson 1977a & b; White *et al.* 1980). However, it has also been suggested that some ultramylonite bands are derived from pseudotachylyte veins, which have been deformed in a macroscopically ductile manner (Sibson 1980; Passchier 1982; Hobbs *et al.* 1986). The following sections discuss the origins of the pervasive

ultramylonites and the discrete ultramylonite bands preserved within the Loch Sgibacleit mylonite belt.

### ***Pervasive ultramylonites***

Packages of pervasive ultramylonite are typically oriented parallel to the regional mylonitic foliation, and appear to 'grade into' neighbouring bands of mylonite and protomylonite. The microstructures of the mylonitic and protomylonitic host rocks clearly demonstrate that progressively increasing strain was associated (a) with a progressive *decrease* in both the number and size of the porphyroclasts, and (b) with a concomitant *increase* in the relative proportion of fine grained matrix. Grain size reduction was primarily controlled by intragranular fracturing within large feldspar porphyroclasts, and by dynamic recrystallisation of the quartz and smaller feldspar grains. These observations suggest that packages of pervasive ultramylonite are regions in which intense dynamic recrystallisation and intragranular fracturing have reduced most of the original porphyroclasts to foliated aggregates of fine grained quartz and feldspar i.e. *the pervasive ultramylonites appear to have developed during progressive mylonitisation.*

### ***Discrete ultramylonite bands***

Discrete ultramylonite bands are characterised by very abrupt margins, and highly strained ultramylonite bands are locally developed in, and cross-cut relatively undeformed protomylonitic hosts (Fig. 4.4). These observations suggest that the discrete ultramylonite bands are *unlikely* to have developed by progressive grain size reduction during mylonitisation. It is therefore postulated that the discrete ultramylonite bands nucleated along *pre-existing* zones of ultrafine-grained or glassy material within the mylonite belt.

The concordant and discordant 'early' pseudotachylyte veins (typically  $\leq 5\text{cm}$  thick) preserved within the Loch Sgibacleit mylonite belt comprise angular to rounded feldspar and quartz clasts (of very variable grainsize) which 'float' in an ultrafine grained, isotropic matrix of devitrified pseudotachylyte matrix. The quartz and feldspar clasts are locally 'intruded' by wedge shaped apophyses, which taper towards the centre of the host grain and appear to be infilled by devitrified pseudotachylyte. These microstructures are thought to preserve evidence for partial melting and / or melt injection along grain margins during pseudotachylyte generation (Sibson 1975; Maddock 1986; Magloughlin 1992).

Relatively unstrained discrete ultramylonite bands comprise rounded feldspar and quartz porphyroclasts, and quartz and feldspar ribbons, which 'float' in an ultrafine grained, foliated matrix. The porphyroclast margins are locally 'intruded' by wedge

shaped apophyses, which are infilled by fine biotite laths ( $\leq 0.01$  mm long) and / or by ultramylonitic matrix. It is postulated that these grain boundary microstructures may have originated as injection veins, which suggests that the ultramylonitic fabrics rework material that may have originated as a melt (Passchier 1982). Both relatively undeformed and strongly deformed discrete ultramylonite bands are locally discordant to the regional fabric and are commonly observed to bifurcate (Figs. 4.2 & 4.4). It is conceivable that these geometries were inherited from precursor pseudotachylyte veins. In particular, bifurcating ultramylonite bands may have been derived from splays or injection veins. The available field and microstructural evidence is therefore consistent with *the discrete ultramylonite bands having nucleated along veins of concordant and discordant pseudotachylyte* within the Loch Sgibacleit mylonite belt (see also Sibson 1980; Walker 1990; White 1996, but cf. Butler 1995).

#### **4.2.3.4 Age and significance of the 'early' pseudotachylyte veins**

The inference that the discrete ultramylonite bands nucleated along pseudotachylyte veins suggests either (a) that the 'early' pseudotachylyte veins *pre-date* mylonitisation (Walker 1990), or (b) that the veins developed *during* mylonitisation (Sibson 1980; White 1996). Field and microstructural observations demonstrate that *unmodified* early pseudotachylyte veins are preserved in both relatively undeformed protomylonitic hosts and in highly deformed mylonites. *Deformed* pseudotachylyte veins (i.e. discrete ultramylonite bands) have been observed in both relatively undeformed protomylonitic hosts and in packages of highly strained pervasive ultramylonite. These observations are clearly inconsistent with the notion that the early pseudotachylyte veins pre-date the onset of mylonitisation. It is therefore suggested that *the early pseudotachylyte veins developed synchronous with macroscopically ductile deformation and mylonitisation at Loch Sgibacleit*.

A discussion of the mechanisms of pseudotachylyte generation during mylonitisation are beyond the scope of this chapter, and the reader is referred to Sibson 1977b, Sibson 1980, White 1996.

### **4.3 DERIVED FABRICS: FOLIATION-PARALLEL FAULT ZONES & CRUSH ZONES**

#### **4.3.1 FIELD RELATIONSHIPS**

The mylonitic foliation (i.e. the primary fabric) is disrupted by predominantly foliation-parallel bands of intense brittle deformation. These bands comprise (a) pseudotachylyte-bearing brittle fault zones and (b) pseudotachylyte-ultramylonite

crush zones (Sibson 1977b). The following sections describe the overall distribution of brittle deformation (i.e. the macrostructure; section 4.3.1.1), and the hand specimen- and outcrop-scale brittle fabrics (i.e. the mesostructure; section 4.3.1.2).

#### 4.3.1.1 Macrostructure

Foliation-parallel pseudotachylyte-bearing fault zones ( $\leq 2\text{m}$  thick;  $\leq 20\text{m}$  along strike) are commonly observed to overprint packages of macroscopically ductile quartzo-feldspathic mylonite and ultramylonite. Foliation-parallel fault zones have *not* been observed either in regions of unmodified gneiss or within packages of protomylonitic amphibolite, although foliation-parallel fault zones are locally developed along the *margins* of boudinaged amphibolite sheets. The fault zones appear to be evenly distributed throughout the mylonite belt, although the effects of steeply-dipping, cross-cutting faults (section 4.4) precludes detailed analysis of the fault zone distribution and spacing.

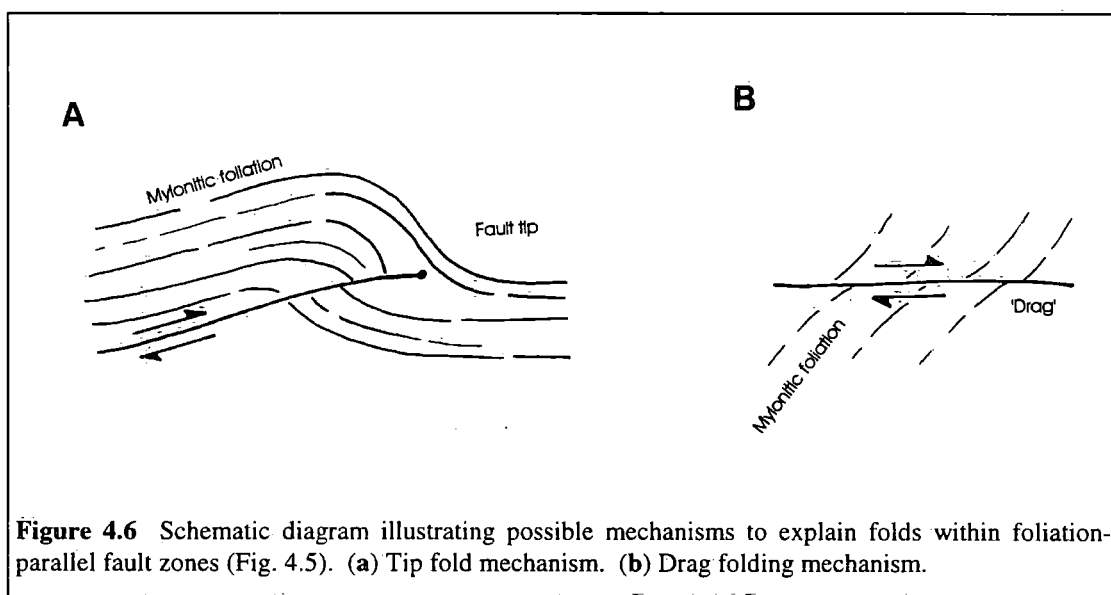
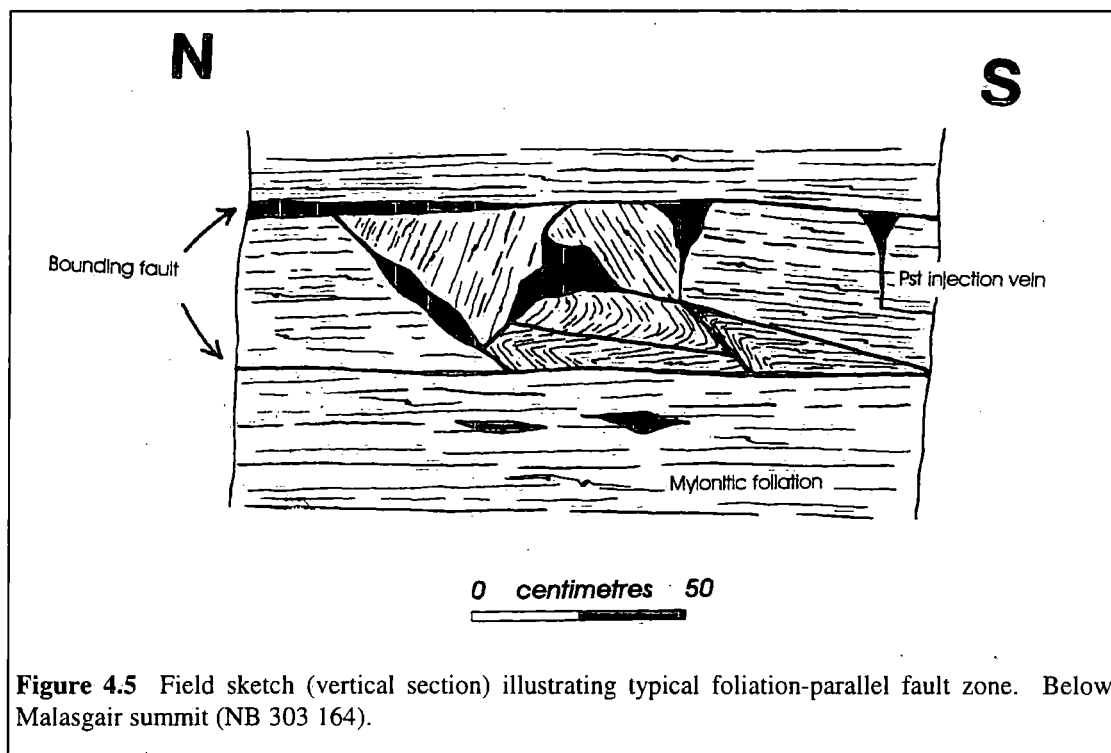
Pseudotachylyte-ultramylonite crush zones ( $\leq 5\text{m}$  thick;  $\leq 50\text{m}$  along strike) are preserved in the basal 50m of the mylonite belt, but have not been observed in regions to the east of Malasgair summit (NB 302 166). The crush zones appear to be more widely spaced than the foliation-parallel fault zones, although the effects of steeply-dipping, cross-cutting normal faults (section 4.4) precludes detailed analysis of the crush zone distribution.

Packages of relatively unmodified mylonite preserved in between foliation-parallel fault zones and pseudotachylyte-ultramylonite crush zones are *locally* disrupted by concordant and discordant pseudotachylyte-bearing extensional and compressional faults.

#### 4.3.1.2 Mesostructure

The foliation-parallel fault zones comprise tabular bands ( $\leq 5\text{m}$  thick) of intensely fractured, disrupted mylonite, which are locally enclosed, or bounded on one side, by laterally continuous ( $\leq 10\text{m}$  long), foliation-parallel faults (Figs. 3.6 & 4.5). These 'bounding' faults are typically lined by narrow pseudotachylyte veins ( $\leq 10\text{cm}$  thick), which generally pinch out along the strike of the host fault plane. The tabular zones of disrupted mylonite are characterised by abundant barren and pseudotachylyte-bearing brittle fractures ( $\leq 1\text{m}$  long, typically c.10cm long), and by centimetre-scale pseudotachylyte injection veins. The brittle fractures are oriented either at high or low angles to the strike of the regional fabric, and serve to isolate angular blocks of mylonite ( $\leq 20\text{cm}$  thick) (Fig. 4.5). The foliation within the fault-bounded blocks is typically oriented at between  $10^\circ$  and  $20^\circ$  (locally up to  $50^\circ$ ) to the regional fabric. This observation suggests that the blocks have experienced a significant amount of

rotation. In regions adjacent to the brittle fractures, the mylonitic fabric is locally deformed by sub-rounded to angular, open to tight folds. It is unclear whether these structures are drag folds, or whether they formed in order to maintain strain compatibility ahead of propagating faults (cf. Grocott 1981; but see models of Williams 1987 & Holdsworth 1989) (Fig. 4.6). In either event, the fold asymmetry is consistent either with apparent localised extensional or apparent localised compressional movements along the associated fault planes. Slickenlines are rarely exposed either on paired bounding fault surfaces or on subsidiary fracture planes.



The crush zones comprise ultrafine grained aggregates of pseudotachylyte, ultramylonite and ultracataclasite. The aphanitic fault rocks are typically cross-cut by closely spaced joints and steeply dipping normal faults (section 4.4), which precludes detailed analysis of the internal structure of these zones. The crush zone margins are typically defined by concordant or cross-cutting pseudotachylyte-barren brittle faults. However, in regions where the original field relationships are preserved (e.g. NB 307 158), the crush zones appear to grade into pseudotachylyte-bearing foliation-parallel fault zones. These observations suggest that the crush zones and the foliation-parallel fault zones may have developed at broadly the same time.

Centimetre- to metre-scale pseudotachylyte-bearing faults locally disrupt regions of relatively unmodified mylonite. The faults are typically lined by narrow, undulating pseudotachylyte veins ( $\leq 2\text{cm}$  thick), although thicker pseudotachylyte breccias and quasi-conglomerates ( $\leq 1\text{m}$  thick) (Sibson 1975) are locally developed. Slickenlines are rarely exposed, although the geometries of subsidiary fractures are consistent either with localised apparent extensional or localised apparent compressional displacements during pseudotachylyte generation.

### **4.3.2 MICROSTRUCTURE**

#### **4.3.2.1 Pseudotachylyte fault veins, breccias and quasi-conglomerates**

The pseudotachylyte fault veins, breccias and quasi-conglomerates comprise angular to rounded clasts of feldspar and quartz  $\pm$  hornblende (between 0.05mm and 20cm diameter; clast size depends on the width of the host vein), which 'float' in an ultrafine grained, pale to dark brown matrix. The matrix appears to be completely devitrified and neither microlitic or vesicular textures (Magloughlin 1992) have been observed. The margins of the pseudotachylyte veins are extremely sharply defined and planar (cf. the undulating margins of some 'early' pseudotachylyte veins), and the wall rocks are commonly observed to be intruded by highly discordant, planar injection veins.

#### **4.3.2.2 Pseudotachylyte-ultramylonite crush zones**

The pseudotachylyte-ultramylonite crush zones comprise angular blocks and 'slivers' ( $\leq 20\text{cm}$  thick) of mylonite, pervasive ultramylonite and discrete ultramylonite, which 'float' in an isotropic matrix of devitrified pseudotachylyte. The entire assemblage is cross-cut by randomly oriented brittle fractures ( $\leq 7\text{cm}$  long) (Plate 4.13). The foliation preserved within the fracture-bounded blocks is locally oriented at up to  $30^\circ$  to the mylonitic fabric. This observation suggests that the blocks have experienced significant rotation. In regions immediately adjacent to the brittle fractures, the

foliation is deformed by asymmetric, millimetre-scale folds, which are exactly analogous to the mesoscopic folds observed within foliation-parallel fault zones (section 4.3.1.2). The folds do not display a consistent sense of vergence.

Subtle colour variations suggest that the matrix is composed of many individual pseudotachylyte veins (at least five veins,  $\leq 5\text{mm}$  thick, have been observed within a single thin section). Cross-cutting relationships between the different pseudotachylyte veins are consistent with the pseudotachylyte-ultramylonite crush zones having developed during several phases of pseudotachylyte generation and / or injection.

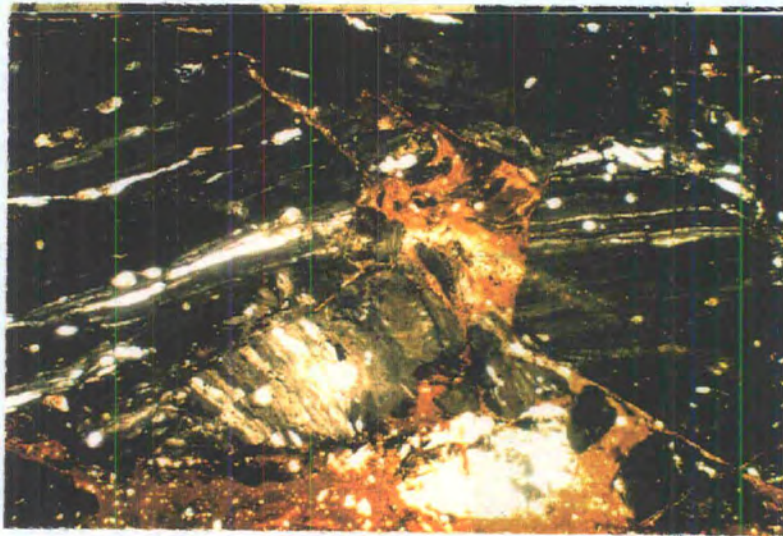


**Plate 4.13** Part of pseudotachylyte-ultramylonite crush zone. Clasts of fractured and randomly oriented ultramylonite (dark brown) are intruded by irregular pseudotachylyte veins (pale brown). Field of view  $6 \times 3.7\text{mm}$ , plane polarised light.

### 4.3.3 SUMMARY AND DISCUSSION

The mylonitic fabrics at Loch Sgibacleit are locally deformed by pseudotachylyte-bearing foliation-parallel brittle fault zones and by thick pseudotachylyte-ultramylonite crush zones. Both sets of structures appear to be of the same age, and both are localised within packages of highly strained quartzo-feldspathic mylonite. The effects of brittle deformation outside these foliation-parallel zones are relatively minor.

#### 4.3.3.1 Mechanisms of localisation and pseudotachylyte generation

The close spatial association between the foliation-parallel brittle fault zones and concentrations of pseudotachylyte is consistent with pseudotachylyte generation having occurred during localised frictional sliding and melting (Sibson 1975; Grocott

1981; Swanson 1992). Unfortunately, insufficient data have been collected to produce a detailed model of how the foliation-parallel fault zones may have evolved (cf. Grocott 1981). However, two important conclusions can be drawn from the observations presented in this section. Firstly, the foliation-parallel fault zones are *not* associated with cataclaste-bearing structures (cf. Sibson 1977b), and the pseudotachylyte veins do not display vesicular textures (although it is possible that the vesicles may have been destroyed during devitrification) (Magloughlin 1992). These observations are consistent with pseudotachylyte generation at Loch Sgibacleit having occurred *at or near the base of the seismogenic zone* i.e. at depths of between 10km and 15km (Swanson 1992).

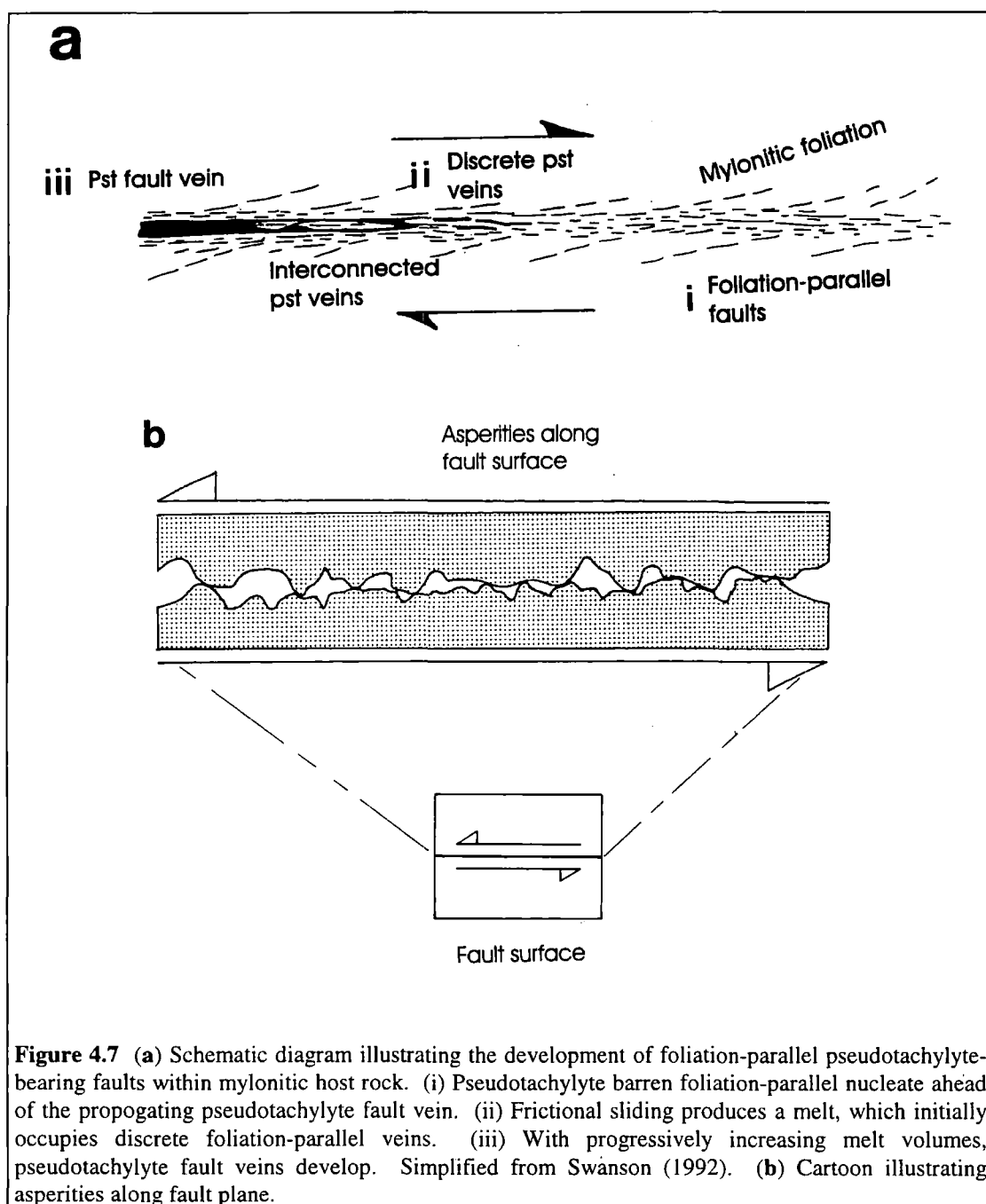


**Figure 4.7** (a) Schematic diagram illustrating the development of foliation-parallel pseudotachylyte-bearing faults within mylonitic host rock. (i) Pseudotachylyte barren foliation-parallel nucleate ahead of the propagating pseudotachylyte fault vein. (ii) Frictional sliding produces a melt, which initially occupies discrete foliation-parallel veins. (iii) With progressively increasing melt volumes, pseudotachylyte fault veins develop. Simplified from Swanson (1992). (b) Cartoon illustrating asperities along fault plane.

Secondly, it is clear that the pre-existing mylonitic foliation was an important control on the localisation of brittle deformation and melt generation. In particular, the foliation-parallel fault zones appear to have localised within packages of highly strained mylonite and ultramylonite. Swanson (1992) has postulated that near the base of the seismogenic zone, melt generation occurs by frictional sliding ('adhesive wear') along pre-existing mylonitic foliation surfaces (Fig. 4.7a). It is therefore tentatively suggested that pseudotachylyte generation principally took place along the laterally continuous, foliation-parallel faults (section 4.3.1.2). At any given depth, the static and dynamic resistance to frictional sliding will depend upon the adhesion between asperities (i.e. small irregularities) developed along the slip plane (Swanson 1992) (Fig. 4.7b). Highly strained mylonites and ultramylonites are characterised by a well developed, planar foliation (on both the meso- and micro-scales), whilst the less strained protomylonites are characterised by a poorly developed, undulating foliation (on both the meso- and micro-scales). It is therefore postulated that the regular *mylonitic* and *ultramylonitic* foliation planes provided 'easy' slip surfaces during frictional sliding compared to the irregular protomylonitic foliation surfaces. As a result, the pseudotachylyte-generating fault zones may have become preferentially localised into packages of highly strained mylonite.

Pseudotachylyte-ultramylonite crush zones are regions in which the mylonitic fabric has been completely disrupted by several phases of pseudotachylyte generation and / or injection. The apparently chaotic structure of the ultrafine grained fault rocks makes it extremely difficult to determine either the causes of crush zone localisation or the mechanisms of melt generation. However, in regions where the original field relationships are preserved, the crush zones appear 'grade into' pseudotachylyte-bearing foliation-parallel fault zones. Furthermore, the millimetre-scale fractures and folds preserved within the crush zones are exactly analogous to the centimetre- and metre scale fractures and folds observed with foliation-parallel fault zones (sections 4.3.1.2 & 4.3.2.2). It is therefore postulated that the operative localisation and melt-generation mechanisms during the development of the crush zones were similar to those operating during the development of the foliation-parallel fault zones.

#### **4.3.3.2 Timing, kinematics and significance of brittle deformation**

In the absence of isotopic age dates, the timing and significance of brittle deformation and pseudotachylyte generation at Loch Sgibacleit is a matter for speculation. However, the observed change in dominant operative deformation mechanism, from predominantly viscous creep during mylonitisation to predominantly frictional sliding during pseudotachylyte generation, can be attributed to a decrease in the ambient pressure and temperature conditions (Passchier 1982, 1984; Schmid & Handy 1991)

(see Chapter 9 for a more detailed discussion). There are two plausible 'end-member' models which could explain this decrease in the pressure and temperature conditions. Firstly, it is possible that both the primary (i.e. mylonitic) and derived (i.e. brittle) fabrics developed during a *single, progressive deformation event*. Increasing embrittlement and localisation of deformation may therefore have been the manifestation of the falling pressure and temperature conditions during progressive exhumation of the fault zone (Grocott 1977). Secondly, it is possible that the primary and derived fabrics developed during *two distinct and entirely unrelated deformation events*. This model implies that the decrease in pressure and temperature conditions occurred following the cessation of macroscopically ductile deformation, but prior to the onset of brittle deformation.

It has been postulated that the absence of cataclasite and the non-vesicular nature of the pseudotachylyte implies that melt generation took place at between 10km and 15km depth (Swanson 1992) (section 4.3.3.1). However, the thermally controlled transition from predominantly frictional to predominantly viscous deformation is also expected to occur within a similar depth range (Sibson 1982, 1983) (see Chapter 9 for a more detailed discussion). These observations suggest that the onset of brittle deformation and frictional melting at the present-day erosion level may have occurred whilst that part of the fault zone was still relatively deep, certainly within a few kilometres of the thermally controlled frictional to viscous transition. If this inference is correct, it is conceivable that *the mylonitic fabrics, the pseudotachylyte-bearing foliation-parallel fault zones and the pseudotachylyte-ultramylonite crush zones developed during a single, progressive deformation event, around the region of the thermally controlled frictional to viscous transition*.

Kinematic indicators (e.g. the geometries of pseudotachylyte injection veins and the geometries of minor faults) suggest that pseudotachylyte generation occurred during localised compressional and localised extensional faulting. The *overall* kinematic regime under which brittle deformation and pseudotachylyte generation took place is therefore unclear. However, it is postulated that both the brittle and macroscopically ductile fabrics developed during a single progressive deformation event. If this inference is correct, it is likely that both fabrics developed under the same kinematic regime. It is therefore tentatively suggested that *the pseudotachylyte-bearing foliation-parallel fault zones and the pseudotachylyte-ultramylonite crush zones developed during top-to-the-NW-thrusting*. A corollary of these arguments is that the foliation-parallel faults and pseudotachylyte veins at Loch Sgibacleit may be significantly older, and entirely unrelated to, the crush melange and pseudotachylyte-ultracataclasite crush zones observed in the Uists (Chapters 3 & 6) (cf. Sibson 1977b; Butler 1995). However, it is entirely possible that at least *some* of the

pseudotachylyte-bearing structures preserved at Loch Sgibacleit (in particular, the pseudotachylyte-bearing compressional and extensional faults preserved in regions *between* foliation-parallel fault zones) may have developed synchronous with brittle deformation in the Uists.

## 4.4 CROSS-CUTTING STRUCTURES

### 4.4.1 FIELD RELATIONSHIPS

The mylonitic fabrics, the pseudotachylyte-bearing faults and the crush zones are commonly observed to be cross-cut by pseudotachylyte-barren brittle faults. Two distinct groups of cross-cutting structures have been recognised (Butler 1995). Firstly, a kilometre-scale array of moderately E-dipping faults outcrops in the region immediately above the fault zone base (Fig. 3.4) (section 4.2.1.1). The fault planes are not exposed, but their outcrop is marked by a number of distinct topographic notches which are visible along the western and southern flanks of Mullach Breac Malasgair (NB 302 166) and along the western and northern flanks of Creag na h-Uamha (NB 307 158). These 'topographic' faults do not appear to be cross-cut by other structures, which suggests that they developed relatively late in the structural history of the OHFZ in the Loch Sgibacleit region (Sibson 1977b; Butler 1995). Owing to poor exposure, the sense-of-shear along the 'topographic' faults is not known.

Secondly, the primary and derived fabrics are widely observed to be cross-cut by steeply E-dipping, centimetre- to metre-scale brittle faults. Offsets of the mylonitic foliation and of earlier brittle faults are consistent with apparent normal displacements across the steeply dipping fault planes. The effects of normal faulting are most intense within pseudotachylyte-ultramylonite crush zones. These observations suggest that whilst the *geometry* of the steeply dipping normal faults was not controlled either by the primary or derived fabrics, the *intensity* of brittle deformation appears to have been influenced by lithological variations within the mylonite belt.

### 4.4.2 MICROSTRUCTURE

The steeply dipping normal faults are typically lined by bands ( $\leq 0.3$ mm thick) of fine grained breccia. The breccias comprise angular to rounded clasts of quartz and feldspar ( $\leq 0.2$ mm diameter, but grain size is extremely variable), which 'float' in a matrix of comminuted quartz, feldspar and hornblende grains (individual grains  $\leq 0.005$ mm diameter) and / or in an amorphous 'gouge' (Plate 4.14). Brown iron

staining is locally observed within the breccia layers and, less commonly, within the adjacent wall rocks. These observations suggest iron-rich fluids may have been channelled along the steeply dipping fault planes.

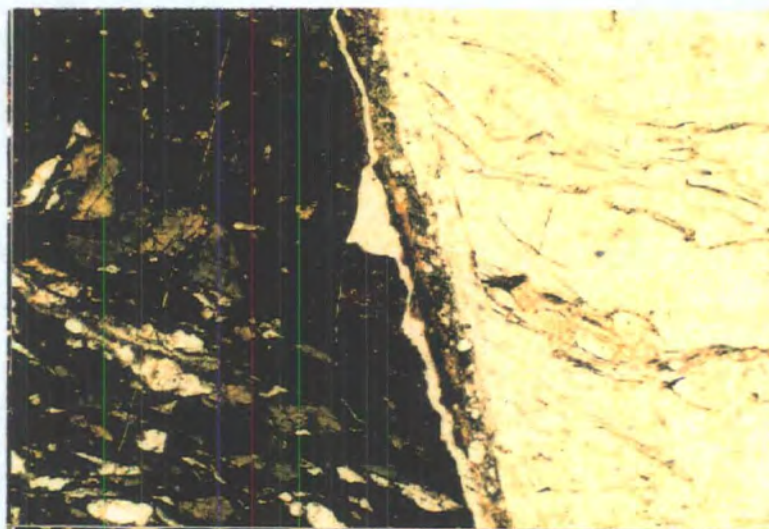


**Plate 4.14** Brittle fault juxtaposing unit of felsic mylonite (pale grey) against discrete ultramylonite band (dark brown). Fault is lined by narrow band of quartz-rich breccia (sub-vertical brown band). Field of view  $3 \times 1.9$ mm, plane polarised light.

#### 4.4.3 DISCUSSION

The style of deformation associated with the steeply dipping normal faults suggests that deformation took place at relatively high levels within the crust (probably within 5km of the surface) (Sibson 1977a & b). If this inference is correct, the normal faults are likely to be *significantly* younger than foliation-parallel fault zones and the pseudotachylyte-ultramylonite crush zones. Butler (1995) has suggested that the normal faults preserved in the Loch Sgibacleit region developed synchronously with the normal faults exposed in northeast Lewis (sections 2.4 & 3.2.4). In the absence of more compelling evidence to the contrary, the present author concurs with Butler (1995), and suggests that the normal faults around Loch Sgibacleit may have been associated with the development of the offshore Mesozoic hangingwall basins (sections 2.3.4 & 2.4).

## 4.5 SUMMARY

- Top-to-the-NW thrusting was associated with anhydrous, lower amphibolite facies macroscopically ductile deformation and mylonitisation.
- Deformation appears to have been localised into bands of mylonitised quartzofeldspathic gneiss, and was accommodated primarily by intracrystalline crystal plastic mechanisms and / or by grain size sensitive creep at high strains.
- Mylonitisation was accompanied by localised melting and pseudotachylyte generation. The 'early' pseudotachylyte veins were subjected to macroscopically ductile, viscous deformation and were transformed into ultramylonite bands.
- Progressive uplift / exhumation of the fault zone promoted a transition from predominantly viscous creep to predominantly frictional deformation.
- Frictional faulting and widespread pseudotachylyte generation were associated with the development of foliation-parallel fault zones and crush zones. The foliation parallel damage zones are localised within packages of highly strained mylonite and ultramylonite i.e. the distribution of brittle deformation was strongly influenced by the primary fabric.
- The pseudotachylyte-bearing foliation-parallel structures are cross-cut by steeply dipping Mesozoic normal faults. Normal faults are preferentially developed within pseudotachylyte-ultramylonite crush zones.

The textural evolution of the OHFZ in the Loch Sgibacleit region is summarised in Figure 9.2a, and will be discussed in Chapter 9.

## 5. SCALPAY

### 5.1 INTRODUCTION

#### 5.1.1 INTRODUCTION AND AIMS

The predominantly NE-SW trending segment of the Outer Hebrides Fault Zone exposed on the island of Scalpay has experienced a polyphase kinematic, textural and metamorphic evolution (sections 3.2.2.2 & 3.2.3.4; Table 3.1).

Regional top-to-the-NW thrusting was associated with the development of an upper greenschist facies mylonite belt, which forms part of the pervasive mylonite belt described in section 3.2.2. Predominantly SE-dipping compressional faults and cataclastic seams post-date the macroscopically ductile mylonites, although the effects of brittle deformation are not very intense on Scalpay (cf. Loch Sgibacleit; Chapter 4). Brittle deformation was followed by an episode of lower greenschist facies retrogression, hydration and phyllonitisation synchronous with a change in the kinematic regime from localised top-to-the-NW thrusting to localised top-to-the-NE sinistral strike-slip. The locus of intense lower greenschist facies retrogression and fluid-rock interaction appears to have been focused into certain pre-existing bands of upper greenschist facies mylonite. This observation suggests that the primary fabric exerted a strong control on the distribution of the lower greenschist facies phyllonitic fabrics. The phyllonite belts were subsequently reworked during localised top-to-the-SW dextral strike-slip. Intense retrogression and fluid-rock interaction appears to have been focused into the actively deforming phyllonitic shear zones. These observations suggest (a) that the phyllonitic shear zones were weak relative to both the Lewisian gneisses and to the upper greenschist facies quartzo-feldspathic mylonites and (b) that the phyllonitic shear zones acted as long-lived fluid pathways.

The aims of this chapter are threefold:

- (1) To describe the textural evolution of the hydrated, thrust-related upper greenschist facies mylonites, in order to provide a comparison with the dry, lower amphibolite facies mylonites from Loch Sgibacleit (Chapters 4 & 9).
- (2) To examine the relationships between the upper greenschist facies mylonites (i.e. the primary fabric) and the thrust- / sinistral strike-slip related phyllonitic fabrics (i.e. the reworked fabrics).
- (3) To determine the controls on the distribution of dextral strike-slip related fabrics.

### 5.1.2 STUDY AREA AND CHAPTER LAYOUT

The island of Scalpay is situated in the mouth of East Loch Tarbert. The island measures 4.5km long by 2.5km wide and is characterised by undulating, heather-clad moorland and which is dissected by numerous small lochans. Exposure is excellent along coastal sections, although the rocks are rather weathered further inland. Detailed field studies of the fault rocks have therefore been conducted at well exposed localities along the northwest, southeast and southwest coasts of Scalpay (Fig. 5.1).

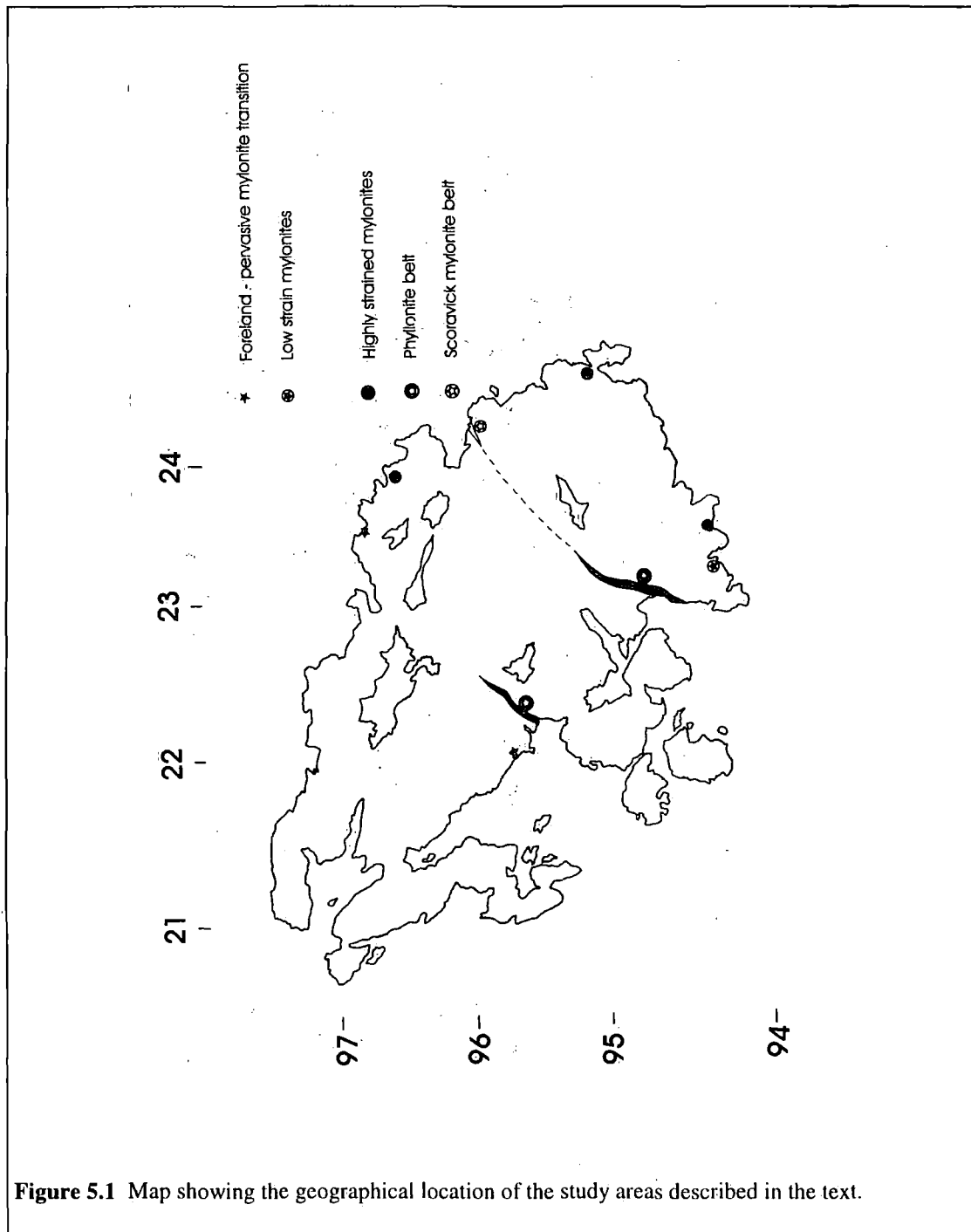


**Figure 5.1** Map showing the geographical location of the study areas described in the text.

The NW part of Scalpay (i.e. the 'foreland') comprises relatively unmodified Laxfordian gneisses, pegmatite veins and amphibolite sheets (Younger Basic dykes) (sections 2.2.2.4 & 3.2.1). In the SE part of the island, the basement assemblage is overprinted and deformed by a SE-dipping zone of pervasive, upper greenschist facies mylonite (Fig. 3.8). The mylonites are themselves locally overprinted by several sub-concordant belts of ESE- to SE-dipping lower greenschist facies phyllonite (Figs. 3.7 & 3.21a). Lower greenschist facies phyllonite has not been observed in the 'foreland'. The remainder of this chapter comprises detailed field and microstructural descriptions of the different fault rocks and structures which outcrop in southeast Scalpay. A description of the upper greenschist facies mylonites (section 5.2) is followed by a brief account of the brittle thrust-related structures (section 5.3). The thrust- and sinistral strike-slip related lower greenschist facies phyllonites will be described in section 5.4, whilst the final part of this chapter (section 5.5) examines the distribution and style of deformation associated with dextral reworking.

## **5.2 PRIMARY FABRIC: UPPER GREENSCHIST FACIES MYLONITE**

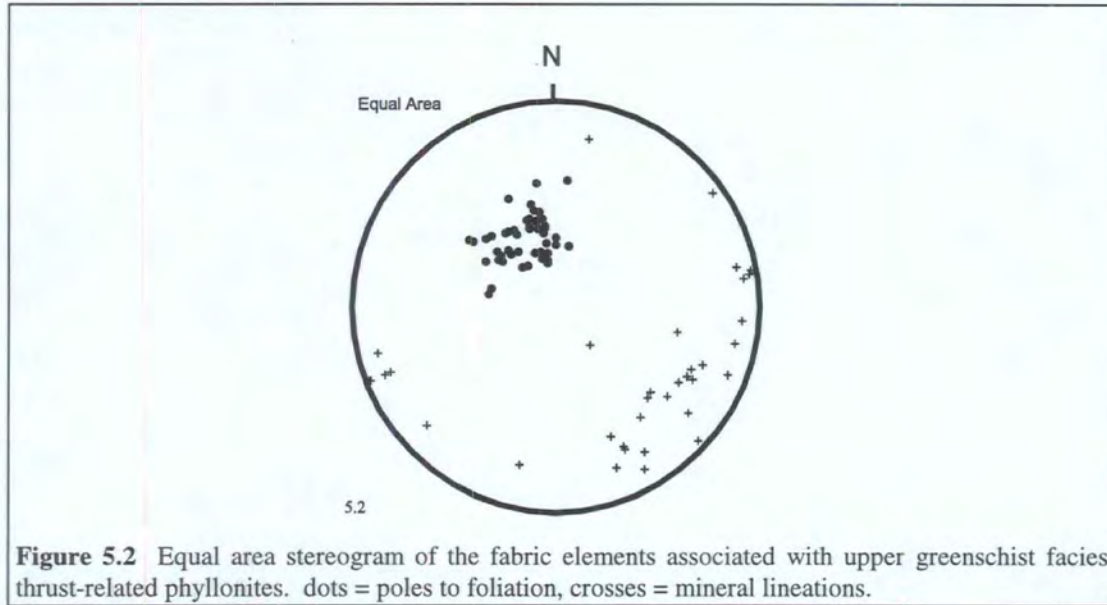
### **5.2.1 FIELD RELATIONSHIPS**

The aims of this section are (a) to describe the overall geometry of the mylonite belt (i.e. the macrostructure) and (b) to describe the hand specimen / outcrop-scale lithologies and textures of the fabrics preserved within the mylonite belt (i.e. the mesostructure).

#### **5.2.1.1 Macrostructure**

The SE-dipping upper greenschist facies mylonites overprint and deform the relatively unmodified, folded Laxfordian gneisses of the 'foreland'. The lower margin of the mylonite belt is gradational, and is characterised by a progressive change in the orientation of the lithological banding, from a predominantly NW-SE trend in the 'foreland' to a NE-SW trend within the mylonite belt (Fig. 3.7 and compare Fig. 3.2a with Fig. 3.8). The upper margin is not exposed onshore, which suggests that the mylonite belt must be at least c.1000m thick. Overall, the mylonitic fabric appears to intensify towards the southeast coast (Sibson 1977b; Lailey *et al.* 1989; Walker 1990; Butler 1995). However, augen (up to 100m in diameter) of relatively low macroscopically ductile finite strain are preserved within the pervasive mylonite belt at Lag na Laire (NG 232 942), Eilean Glas (NG 245 946) and Greinem (NG 245 955) (Fig. 3.7) (see also Butler 1995).

### 5.2.1.2 Lithology and mesostructure



The pervasive mylonite belt comprises interbanded packages of quartzo-feldspathic mylonite and protomylonite, packages of upper greenschist facies phyllonite, protophyllonite and ultraphyllonite, protomylonitic pegmatites and variably deformed amphibolite sheets. Quartzo-feldspathic mylonites are characterised by a platy, SE-dipping foliation, which is defined by re-oriented, attenuated lithological banding, quartz ribbons (aspect ratios  $\leq 1:20$ ) and flattened feldspar grains (aspect ratios  $\leq 5:1$ ) (Plate 5.1). The foliation is typically associated with a well developed, SE-plunging quartz stretching lineation (Fig. 3.8).

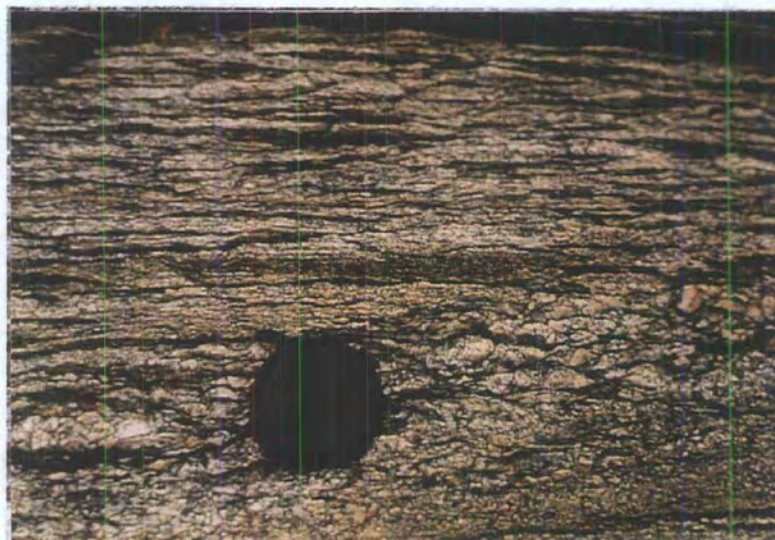


**Plate 5.1** Typical quartzo-feldspathic mylonite from Scalpay. Foliation defined by undulating quartz ribbons and reoriented, attenuated lithological banding. NW to left.

Asymmetric shear bands and  $\sigma$ - and  $\delta$ -type feldspar porphyroclasts ( $\leq 4$ mm diameter) viewed in surfaces parallel to the mineral lineation and perpendicular to the foliation are consistent with top-to-the-NW shear. Packages of grey-green upper greenschist facies phyllonite are characterised by a strong, SE-dipping foliation, which is defined by aligned phyllosilicate minerals, and by a predominantly SE-plunging mineral lineation, which is defined by aligned actinolite needles and stretched quartz grains (Fig. 5.2).  $\phi$ - and  $\sigma$ -type quartz, feldspar and hornblende porphyroclasts are locally preserved, but are absent from the most highly strained ultraphyllonites. Coarse grained, pink protomylonitic pegmatites, which vary from 2cm to 2m in thickness, are commonly observed within the mylonite belt. The protomylonitic foliation is defined by anastomosing quartz ribbons and / or aligned chlorite laths, which wrap around large  $\sigma$ -type quartz and feldspar porphyroclasts ( $\leq 2$ cm diameter). The moderately SE-dipping foliation is typically associated with a well developed, SE-plunging mineral lineation (Fig. 5.3).

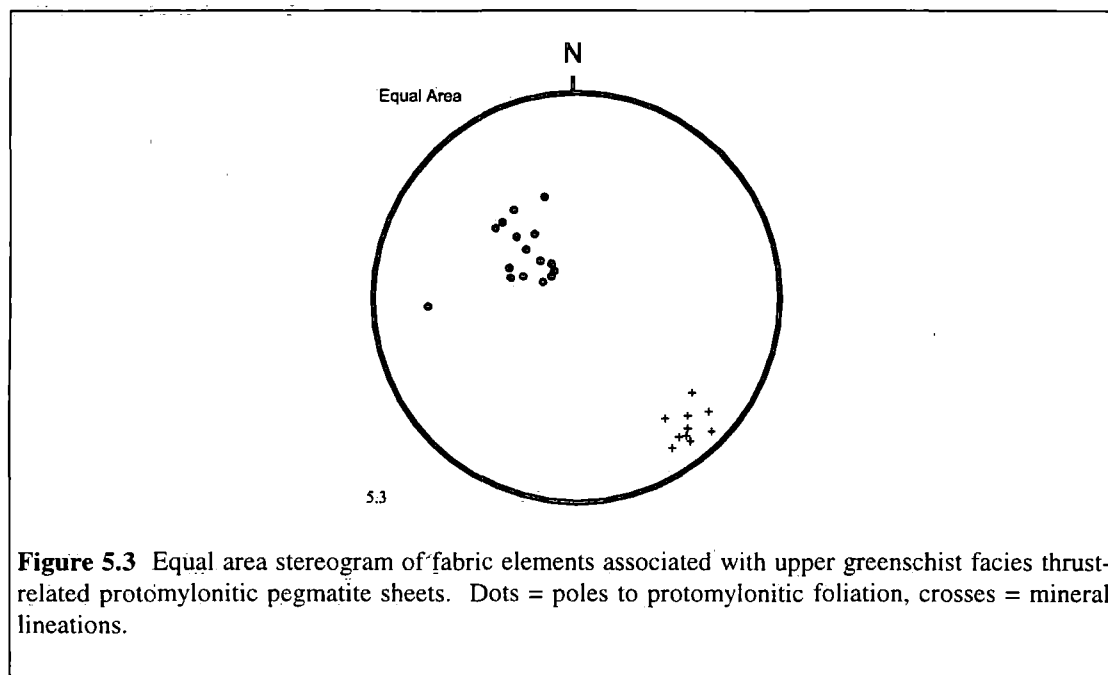


**Figure 5.3** Equal area stereogram of fabric elements associated with upper greenschist facies thrust-related protomylonitic pegmatite sheets. Dots = poles to protomylonitic foliation, crosses = mineral lineations.

Asymmetric chlorite-rich shear bands and quartz and feldspar porphyroclasts viewed in surfaces parallel to the mineral lineation and perpendicular to the foliation are consistent with top-to-the-NW thrusting. Deformed amphibolite sheets ( $\leq 1$ m thick) are commonly observed around southeastern Scalpay. The SE-dipping protomylonitic foliation is defined by flattened feldspar grains, and is locally associated with a poorly defined SE-plunging mineral lineation. The relative proportions of quartzofeldspathic mylonite, upper greenschist facies phyllonite and protomylonitic pegmatite and amphibolite vary considerably throughout the pervasive mylonite belt. These lithological variations reflect both the original lithological diversity observed within

the Laxfordian protoliths (section 3.2.1) and variations in the magnitude of macroscopically ductile finite strain within the mylonite belt. The following sections therefore describe the structures and fault rocks observed within packages of 'low' strain and 'highly' strained mylonite.

### *Low strain mylonite*

The orientation of Younger Basic dykes relative to the orientation of the mylonitic fabric is a particularly useful qualitative strain marker (Sutton & Watson 1951; Lailey *et al.* 1989; Butler 1995). In the present work, zones of 'low' strain are defined as those regions in which the Younger Basic amphibolite sheets are generally discordant to the mylonitic fabric, i.e. the magnitude of macroscopically ductile strain was insufficient to re-orient the originally discordant Younger Basics into parallelism with the mylonitic fabric. Packages of low strain mylonite are exposed (a) along the lower margin of the mylonite belt at Aird Riabhach (NG 236 966) and Cnoc na Croich (NG 222 956) and (b) in macroscopic low strain augen within the mylonite belt (section 5.2.1.1). Low strain mylonites comprise packages of protomylonitic pegmatite, quartzo-feldspathic protomylonite and mylonite and protomylonitic amphibolite sheets. Upper greenschist facies phyllonites are rarely observed in low strain zones.



**Plate 5.2** View of typical low strain mylonite, Lag na Laire (NG 232 942). Southeast to left. Mylonitic foliation dips towards the left and is clearly cross-cut by discordant Younger Basic amphibolite sheets (dark bands). See also Figure 5.4 for explanation.

Along the base of the mylonite belt (at Aird Riabhach, NG 236 966 and Cnoc na Croich, NG 222 956), protomylonitic fabrics are commonly observed to overprint S- and SE-dipping pegmatite sheets, but are *not* developed in N- or W-dipping pegmatite sheets. At Aird Riabhach, bands of protomylonite ( $\leq 0.5\text{m}$  thick)

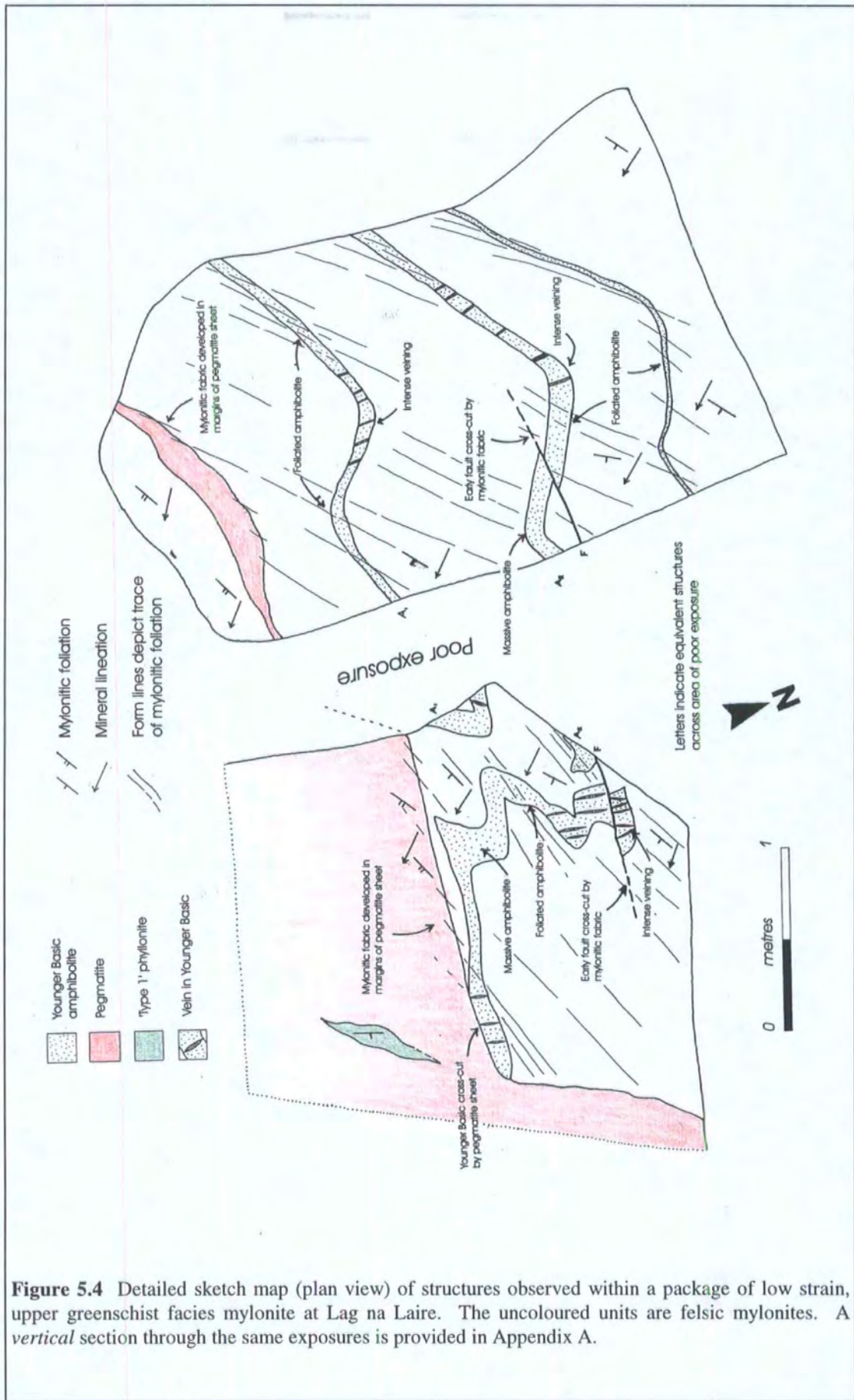


**Figure 5.4** Detailed sketch map (plan view) of structures observed within a package of low strain, upper greenschist facies mylonite at Lag na Laire. The uncoloured units are felsic mylonites. A vertical section through the same exposures is provided in Appendix A.

are locally developed in quartzo-feldspathic banded gneisses adjacent to massive amphibolite sheets. These observations suggest that at low strains, deformation was extremely heterogeneous and was localised within favourably oriented pegmatite sheets and / or along favourably oriented competence boundaries.

A *pervasive* protomylonitic fabric overprints the quartzo-feldspathic gneisses, pegmatite veins and discordant and concordant amphibolite sheets preserved within the low strain augen at Lag na Laire (NG 232 942 to NG 234 942) (Figs. 3.7 & 5.4). The discordant amphibolite sheets ( $\leq 0.5\text{m}$  thick) preserve relict ?Laxfordian folds, whose axial planes are oriented parallel to the protomylonitic foliation (Plate 5.2). Arrays of NE-SW to N-S trending, fibrous quartz-epidote veins cross-cut the thickest amphibolite sheets (Figs. 5.4 & 5.5). The orientation of the fibres is generally consistent with vein opening in a direction parallel to the SE-plunging mineral lineation. Concordant amphibolite sheets ( $\leq 0.25\text{m}$  thick) are typically boudinaged and stretched parallel to the mineral lineation. Arrays of sub-vertical, fibrous quartz-epidote veins are commonly observed in the boudin necks.

These observations suggest that vein opening was synchronous with mylonitisation during top-to-the-NW thrusting.

### ***Highly strained mylonite***

Zones of 'highly' strained mylonite are defined as those regions in which the planar fabric elements are typically oriented parallel to the mylonitic foliation. Packages of highly strained mylonite were examined at localities to the east of Lag na Laire (NG 234 942 and NG 235 941), at Geo an Ear (NG 247 949) and to the south of Aird Riabhach (NG 239 265) (Figs. 3.7 & 5.1). Highly strained mylonite comprises packages of quartzo-feldspathic mylonite and protomylonite, upper greenschist facies phyllonite, protophyllonite and ultraphyllonite, protomylonitic pegmatite and concordant, protomylonitic amphibolite sheets. Bands of upper greenschist facies phyllonite are up to 1.5m in thickness and locally contain elongate augen ( $\leq 30\text{cm}$  long) of flattened, relict pegmatite. In general, the phyllonitic fabric grades abruptly into the surrounding quartzo-feldspathic mylonite, although to the south of Aird Riabhach (NG 239 265), the base of a prominent phyllonite band is marked by a SE-dipping brittle detachment fault. The significance of this and other detachment faults will be discussed in section 5.5.

Highly strained mylonites are typically associated with a SE-plunging mineral lineation (e.g. Figs. 3.8 & 5.2). However, at Geo an Ear (NG 247 949), small (wavelength  $\cong 1\text{cm}$ ), SW-verging folds and crenulations are developed in bands of highly strained phyllonite and ultraphyllonite. These folds are thought to be related to

a subsequent phase of localised top-to-the-SW dextral strike-slip. The significance of these dextral strike-slip related fabrics will be discussed in section 5.5.

## 5.2.2 MICROSTRUCTURE

### 5.2.2.1 Quartzo-feldspathic mylonite

Quartzo-feldspathic mylonites and protomylonites comprise aggregates of polycrystalline quartz ribbons, partially sericitised, flattened feldspar grains (Plate 5.3a) and, less commonly, strands of aligned sericite grains (Plate 5.3b) and kinked biotites (biotite grains  $\leq 60\mu\text{m}$  long) (Fig.5.6). Well-formed  $\sigma$ - and  $\delta$ -type feldspar porphyroclasts are *locally* preserved.

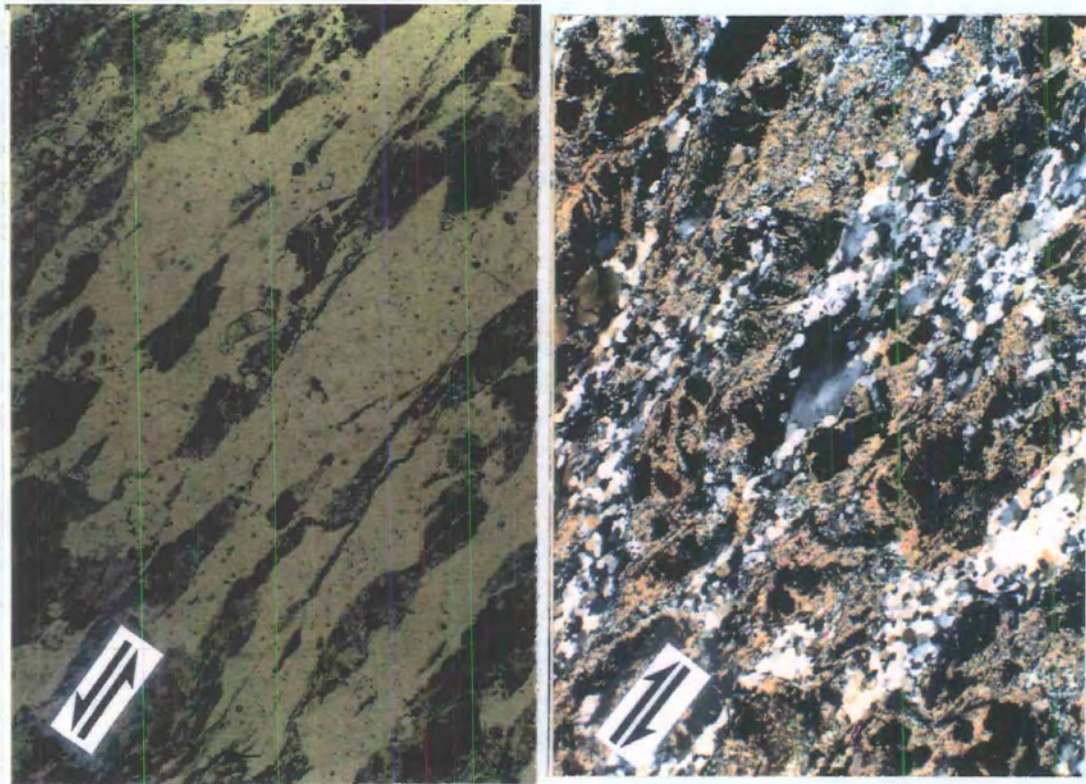


**Plate 5.3** Quartzo-feldspathic mylonite. (a) Partially sericitised feldspar porphyroclasts (dark grey) 'float' in a matrix of interconnected polycrystalline quartz ribbons. Split arrows parallel mineral lineation, top-to-NW shear. Field of view  $6\times 3.7\text{mm}$ , plane polarised light. (b) Crossed polars view of same mylonite illustrating the effects of sericitisation. Feldspar porphyroclasts (dark brown) locally altered to aggregates of sericite (pale brown speckles), particularly along grain margins. Split arrows parallel mineral lineation, top-to-NW sense of shear. Field of view  $6\times 3.7\text{mm}$ , crossed polars.

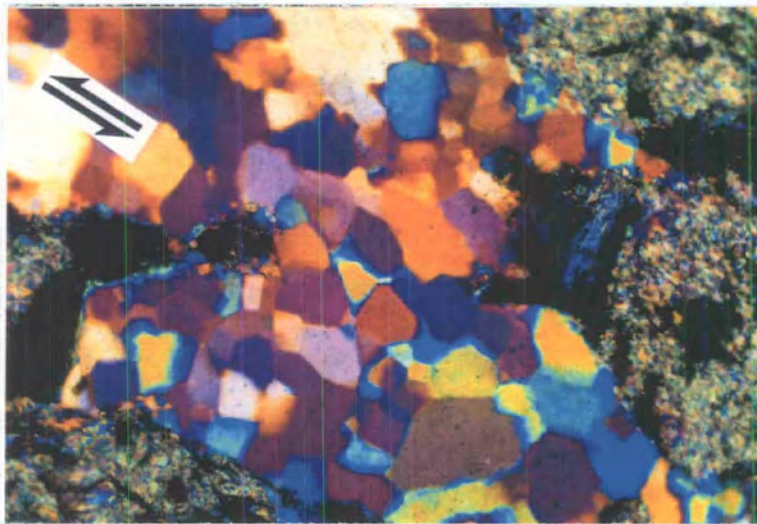
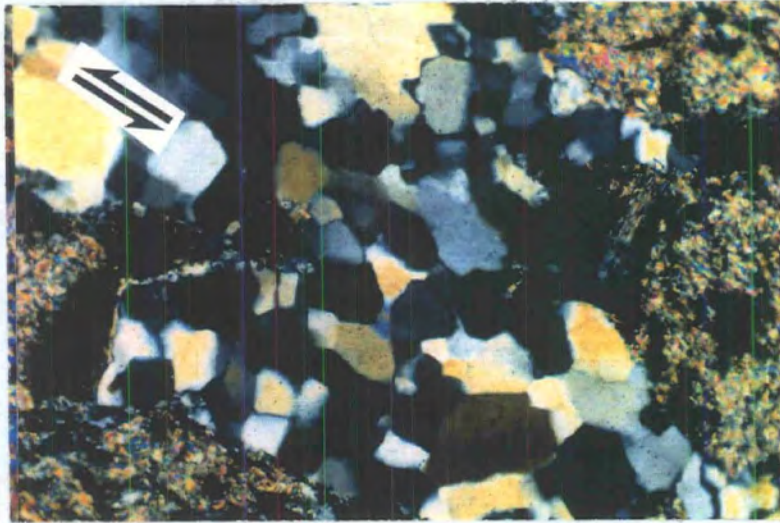


**Plate 5.4** (a) The intracrystalline microstructure of many quartz ribbons preserved in quartz-feldspathic mylonite is characterised by equant recrystallised grains which possess straight to curvilinear grain boundaries.  $120^\circ$  triple junctions between grains are occasionally observed. Split arrows parallel to mineral lineation, top-to-NW sense of shear. Field of view  $1.3 \times 0.77$  mm, crossed polars. (b) The same view as (a), but a sensitive tint plate has been inserted. The range of colours suggests that crystallographic axes of the recrystallised grains are not uniformly oriented.

The polycrystalline quartz ribbons typically comprise (a) relatively coarse, equigranular-polygonal aggregates, in which individual grains ( $\leq 0.3$  mm diameter) display straight to faintly undulose extinction and weak crystallographic preferred orientations (Plates 5.4a & b), or (b) relatively fine, equigranular-interlobate aggregates, in which individual grains ( $\leq 0.2$  mm diameter) display aspect ratios of up to 6:1. The long axes of these elongate grains are oriented at between  $0^\circ$  and  $40^\circ$  to the overall trend of the foliation. Quartz 'core-and-mantle' microstructures (White

1976) are locally preserved (Plate 5.5). Monocrystalline 'cores' (aspect ratios  $\leq 20:1$ ) are characterised by strong patchy to sweeping undulose extinction, and equant to elongate subgrains are locally very well developed ( $\leq 0.2\text{mm}$  diameter; aspect ratios between 1:1 to 5:1).

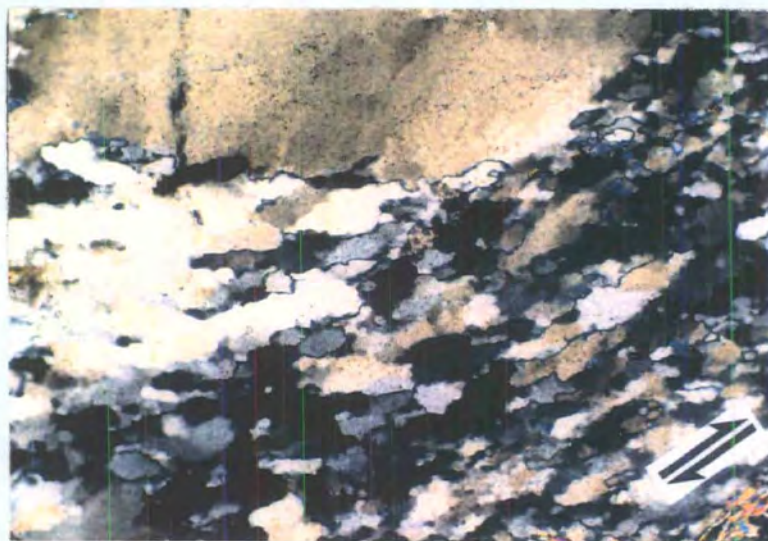


**Plate 5.5** Quartzo-feldspathic mylonite. Unrecrystallised quartz grain (top left) with poorly developed subgrains surrounded by a mantle of recrystallised quartz. Note that the recrystallised quartz grains are flattened parallel to the trace of the foliation and display irregular grain boundary geometries. Split arrows parallel to mineral lineation, top-to-NW shear. Field of view  $1.3 \times 0.77\text{mm}$ , crossed polars.

Feldspar grains preserved within quartzo-feldspathic mylonite are typically flattened parallel to the trace of the foliation and display varying degrees of sericitisation (sericite accounts for between 5% and 80% of the surface area of the host grain). Sericite typically forms stubby laths ( $\leq 0.125\text{mm}$  long; aspect ratios  $\leq 2:1$ ) or needles, and laterally discontinuous (on the grain scale) sericite strands are locally developed along the margins of flattened feldspar grains. Relatively unaltered porphyroclasts of K-feldspar and calcic plagioclase display strong patchy undulose extinction and appear to be cloudy in plane polarised light. Intragranular extension fractures, which are infilled by fine grained aggregates of albitic feldspar are commonly observed to cross-cut feldspar porphyroclasts. Seriate-interlobate aggregates of fine grained albite (individual grains  $\leq 0.05\text{mm}$  diameter; aspect ratios between 1:1 and 3:1) have also been observed along the margins of relatively unaltered porphyroclasts (Plate 5.6; Fig. 5.7). The albite grains appear to be clear in plane polarised light, although the grain boundaries are decorated by numerous fine, high relief fluid inclusions ( $\ll 0.01\text{mm}$  diameter).

Fibrous quartz and quartz-epidote veins are locally preserved within quartzo-feldspathic mylonites. Undeformed veins are oriented perpendicular to the foliation

and the vein fibres are typically aligned parallel to the macroscopic mineral lineation. Deformed veins are oriented sub-parallel to the trace of the foliation and are boudinaged. These observations suggest that vein opening was broadly synchronous with mylonitisation (Plate 5.7).

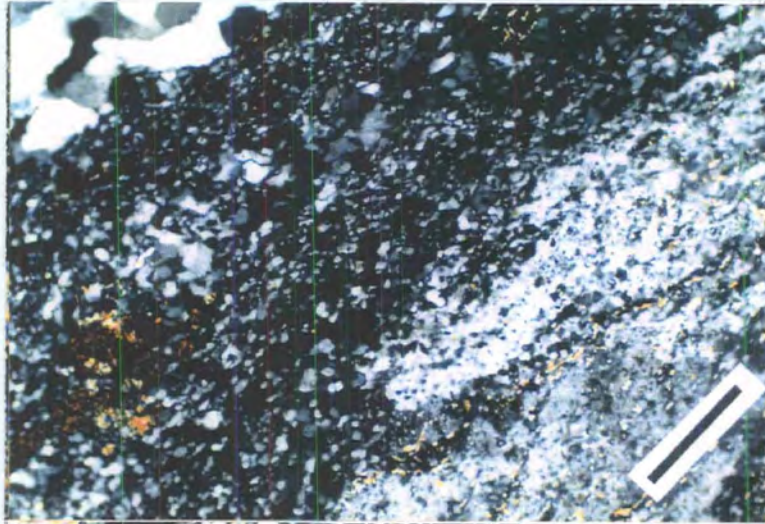


**Plate 5.6** Quartzo-feldspathic mylonite. Ultrafine grained neocrystallised albite aggregates (dark grey, low relief) surrounding relict 'cores' of partially altered, K-feldspar (bottom right), see text for explanation. Bar parallel to the trace of the foliation, shear sense not known. Field of view  $0.66 \times 0.4\text{mm}$ , crossed polars.

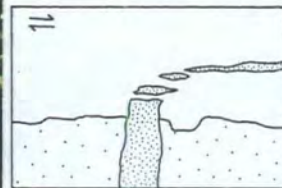


**Plate 5.7** The contact between an amphibolite sheet (dark brown) and quartzo-feldspathic mylonite (pale brown). Note the transcrystalline vein appears to be undeformed within the amphibolite sheet, but that the vein is highly sheared within the quartzo-feldspathic mylonite. Split arrows parallel to mineral lineation, top-to-NW shear. Field of view  $12 \times 7.2\text{mm}$ , crossed polars. Inset is a line drawing of the photomicrograph; amphibolite = coarse stipples, vein = fine stipples.

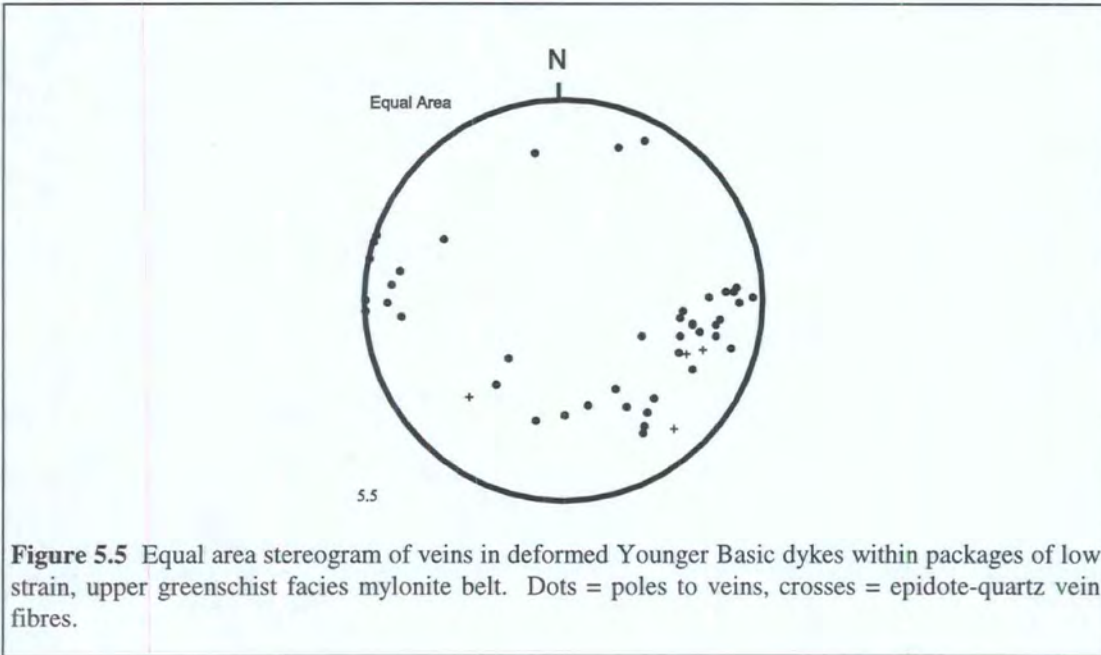


**Figure 5.5** Equal area stereogram of veins in deformed Younger Basic dykes within packages of low strain, upper greenschist facies mylonite belt. Dots = poles to veins, crosses = epidote-quartz vein fibres.

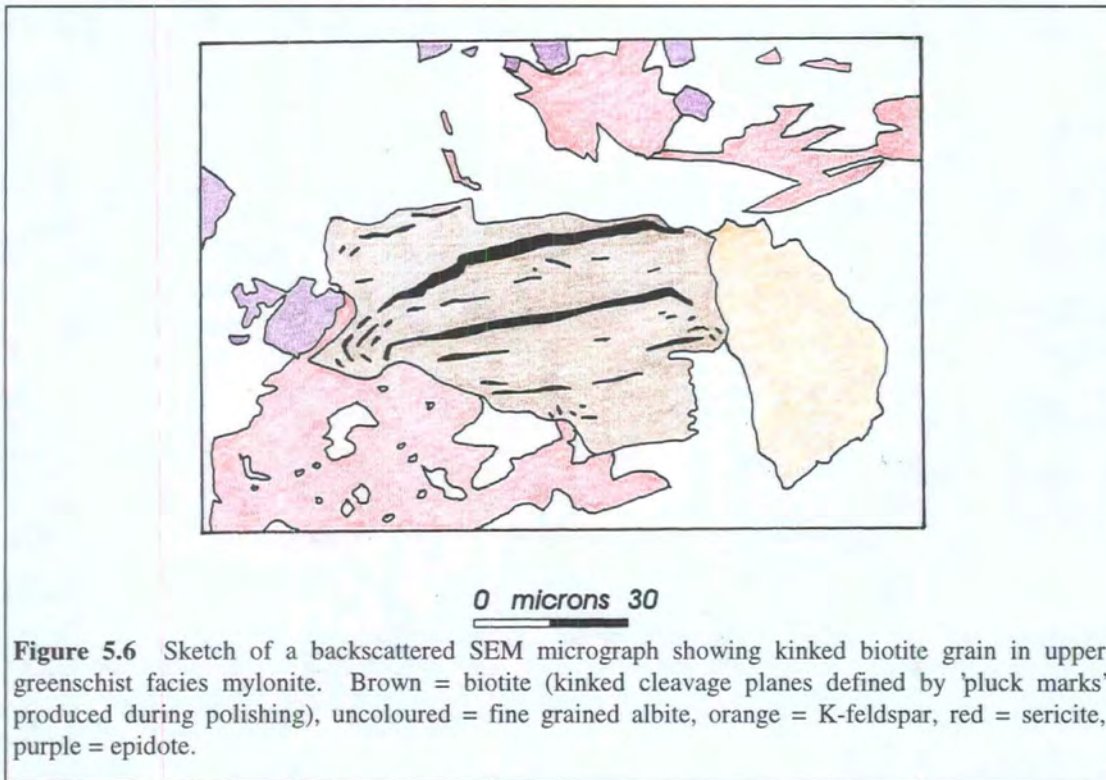
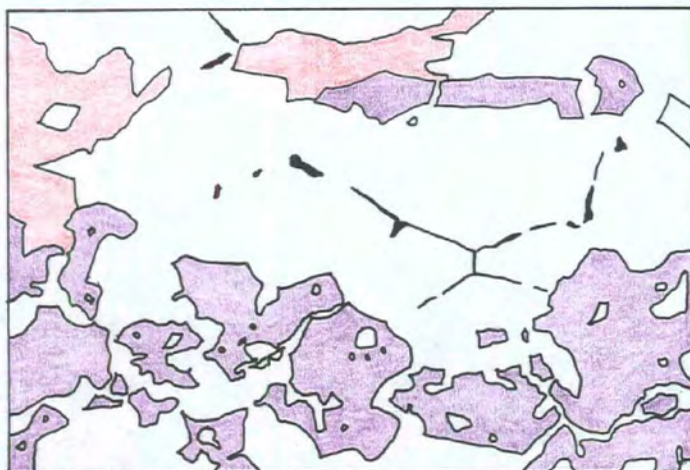


**Figure 5.6** Sketch of a backscattered SEM micrograph showing kinked biotite grain in upper greenschist facies mylonite. Brown = biotite (kinked cleavage planes defined by 'pluck marks' produced during polishing), uncoloured = fine grained albite, orange = K-feldspar, red = sericite, purple = epidote.

### 5.2.2.2 Upper greenschist facies phyllonite

Upper greenschist facies phyllonite comprises flattened, partially sericitised feldspar grains and relatively unaltered hornblende porphyroclasts, which are wrapped by interconnected, transgranular sericite strands, anastomosing quartz ribbons and trails of epidote grains (Plate 5.8). The sericite strands comprise aggregates of intensely aligned sericite needles, which are oriented parallel to the trace of the macroscopic foliation. Individual needles display patchy undulose extinction, but are rarely observed to be kinked or fractured. The microstructures of the quartz and feldspar

grains preserved within packages of upper greenschist facies phyllonite are identical to those observed within the quartzo-feldspathic mylonites.



0 microns 10

**Figure 5.7** Sketch of a backscattered SEM micrograph showing aggregates of fine grained neocrystallised albite (uncoloured) in upper greenschist facies mylonite. Albite grain boundaries (discontinuous black lines) defined by 'pluck marks' produced during polishing. Red = sericite, purple = epidote.

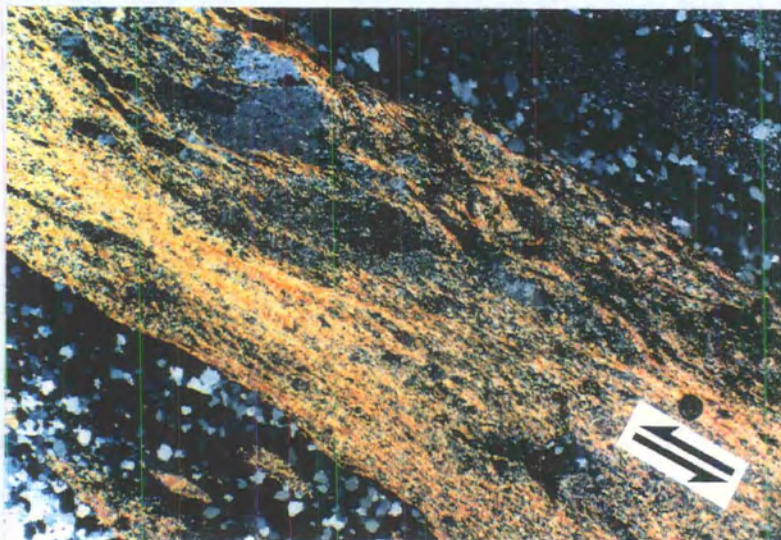


**Plate 5.8** Upper greenschist facies thrust-related phyllonite. The foliation is defined by interconnected sericite strands (high birefringence material), polycrystalline quartz ribbons (bottom left) and bands of ultrafine grained neocrystallised feldspar (top right). Split arrows parallel mineral lineation, top-to-NW shear. Field of view 6x3.7mm, crossed polars.

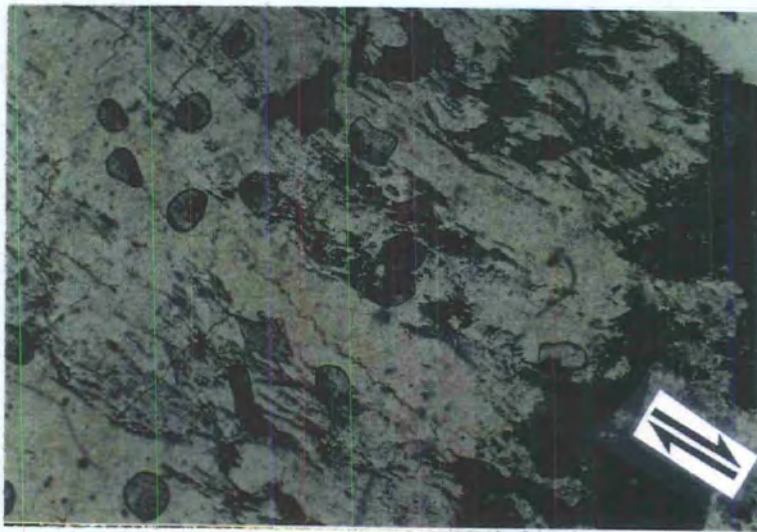


**Plate 5.9** (a) Intragranular tensile fractures cross-cutting hornblende grain (green-brown) preserved in upper greenschist facies phyllonite. Fractures are infilled with quartz (colourless, low relief) and actinolite needles (low relief, pale green) which are oriented parallel to the macroscopic mineral lineation. Note that actinolite is much more commonly observed than chlorite. Bar parallel mineral lineation, shear sense not known. Field of view 1.3×0.77mm, plane polarised light. (b) Detail of tensile intragranular fracture within hornblende. Note trails of hornblende and actinolite inclusions (trending top right to bottom left), consistent with crack-seal opening. Field of view 0.33×0.25mm, plane polarised light.

The hornblende porphyroclasts are *locally* altered to actinolite ± chlorite along cleavages planes (actinolite accounts for less than 5% of the total surface area of the host grain). Arrays of intragranular extension fractures are commonly observed to cross-cut the hornblende porphyroclasts. The fractures are oriented at high angles to the trace of the foliation and are typically infilled by aggregates of fibrous actinolite and quartz (Plate 5.9a). The fibres are aligned parallel to the macroscopic mineral lineation, and crack-seal textures (Ramsay 1980a) are locally preserved (Plate 5.9b).

Actinolite strain shadows are typically developed around the margins of hornblende porphyroclasts. These observations suggest that intragranular fracturing and the growth of actinolite were synchronous with top-to-the-NW thrusting.

### **5.2.2.3 Protomylonitic pegmatite**

Protomylonitic pegmatites comprise anastomosing, polycrystalline quartz ribbons, aligned chlorite flakes and laterally discontinuous sericite strands which wrap around coarse ( $\leq 20$ mm diameter) porphyroclasts of feldspar and quartz and augen of coarse, randomly oriented chlorite laths ( $\leq 5$ mm long). The microstructures of the quartz ribbons preserved within the protomylonitic pegmatites are identical to those observed in quartzo-feldspathic mylonites.

The K-feldspar porphyroclasts preserved within relatively deformed pegmatite sheets are typically cross-cut by arrays of variably oriented intragranular extension fractures. The fractures are infilled by aggregates of fine grained albite.

### **5.2.2.4 Protomylonitic amphibolite**

Protomylonitic amphibolites comprise aggregates of hornblende and flattened, partially sericitised feldspar grains. Quartz is rare to absent. The feldspar grains are highly sericitised (stubby sericite laths account for up to 70% of the surface area of the host grain), and are locally cross-cut by intragranular sericite strands. In contrast, the hornblende grains are relatively unaltered (actinolite  $\pm$  chlorite lamellae are locally developed along cleavage planes, but account for less than 10% of the surface area of the host grain) (Plate 5.10). Arrays of intragranular extension fractures, which are oriented at high angles to the trace of the foliation are commonly observed to cross-cut hornblende porphyroclasts. The fractures are infilled by aggregates of fibrous quartz and actinolite, which are aligned parallel to the macroscopic mineral lineation. Actinolite strain shadows are widely developed at the margins of hornblende porphyroclasts.

Transgranular, fibrous quartz-epidote  $\pm$  actinolite extension fractures are commonly observed to cross-cut protomylonitic amphibolites. The fibrous infills are oriented parallel to the macroscopic mineral lineation (Fig. 5.5) and locally contain laterally discontinuous trails of high relief fluid inclusions and fragments of the wall rock, which are oriented parallel to the vein margins. Where transgranular veins cross-cut the contacts between protomylonitic amphibolites and quartzo-feldspathic mylonites, the veins typically appear to be completely undeformed within amphibolite hosts, but are highly sheared and attenuated within the quartzo-feldspathic mylonites. These observations suggest that both the intra- and transgranular veins opened synchronous with top-to-the-NW thrusting.



**Plate 5.10** Upper greenschist facies protomylonitic amphibolite. Relatively undeformed, unaltered hornblende (green-brown) and highly altered feldspar porphyroclasts (black) are wrapped by laterally discontinuous sericite strands (speckled brown). Split arrows parallel mineral lineation, top-to-NW shear. Field of view 6×3.7mm, crossed polars.

### 5.2.3 SUMMARY AND DISCUSSION

A belt of SE-dipping mylonite, which developed during regional top-to-the-NW thrusting, outcrops in southeast Scalpay. The belt comprises packages of quartzofeldspathic mylonite and protomylonite, packages of phyllonitic mylonite, bands of protomylonitic pegmatite and deformed amphibolite sheets. Overall, the mylonitic fabric intensifies towards the southeast, although low strain augen are commonly observed throughout the mylonite belt. The most highly strained regions are characterised by bands of phyllonite, protophyllonite and ultraphyllonite. The presence of syn-tectonic quartz and quartz-epidote-actinolite veins suggests that significant fluid-rock interaction occurred during top-to-the-NW thrusting on Scalpay.

#### 5.2.3.1 Retrogression and metamorphism within the mylonite belt

The mylonite belt comprises an assemblage of quartz, feldspar (calcic plagioclase + K-feldspar porphyroclasts and fine grained albitic feldspar), hornblende, biotite, sericite, actinolite, chlorite and epidote. The relative abundance of hydrous mineral phases (in particular actinolite and sericite) in comparison with the relatively unmodified amphibolite facies gneisses of the 'foreland' (section 3.2.1) suggests that the hydrous minerals may have developed during localised retrograde metamorphism

within the mylonite belt. The textural relationships between the hornblende porphyroclasts and the actinolite fibres / chlorite lamellae are critical to determining more precisely the timing and the conditions under which retrogression occurred. Hornblende porphyroclasts are commonly observed to be fringed by well developed actinolite strain shadows. In contrast, chlorite is rarely observed and is only developed along cleavage planes within hornblende grains. The chlorite lamellae appear to be completely undeformed. The textural evidence therefore suggests that the actinolite fibres developed synchronous with top-to-the-NW thrusting, but that the chlorite lamellae probably *post-date* deformation. The absence of chlorite and the co-existence of actinolite and hornblende are consistent with deformation and retrogression having taken place under upper greenschist facies conditions (Miyashiro 1994 and Chapter 1 of the present work).

### 5.2.3.2 Operative deformation mechanisms during mylonitisation

#### *Quartzo-feldspathic mylonites*

The quartzo-feldspathic mylonites (and the protomylonitic pegmatites) are characterised by a network of interconnected quartz ribbons, which isolate flattened, partially sericitised feldspar grains. This observation suggests that the overall rheological behaviour of the quartzo-feldspathic mylonites may have been controlled by rheological behaviour of the deforming quartz ribbons (Jordan 1987; Handy 1990 & 1994). The quartz ribbons typically comprise polycrystalline aggregates of equant, equigranular-polygonal and, less commonly, elongate, equigranular-interlobate grains. Flattened, undulose monocrystalline 'cores' are locally preserved, which are surrounded by mantles of elongate, equigranular-interlobate subgrains. The equant, polygonal grains rarely display well developed undulose extinction. Stain-free polygonal grains are thought to develop in response to grain boundary area reduction (GBAR) processes, and are consistent with a phase of static recrystallisation following the cessation of active deformation (Passchier & Trouw 1996). These observations therefore suggest (a) that the mylonites experienced an episode of static recrystallisation following the cessation of macroscopically ductile thrusting, and (b) that the quartz deformation microstructures were largely destroyed by GBAR. The timing and significance of static recrystallisation is discussed further in section 5.4. However, the monocrystalline ribbons, elongate subgrains and elongate equigranular-interlobate aggregates are probably *deformation* microstructures which survived static recrystallisation. The well developed subgrains and core-and-mantle microstructures suggest that recovery and subgrain rotation recrystallisation may have been important processes during mylonitisation ('Regime 2' of Hirth & Tullis 1992). Experimental

evidence suggests that these microstructures are characteristic of quartz grains deformed at pressures, temperatures and strain rates which are either equivalent to natural mid- to upper greenschist facies conditions (Hirth & Tullis 1992; Passchier & Trouw 1996). The mylonitic foliation is locally cross-cut by syn-tectonic fibrous quartz and quartz-epidote veins. This observation suggests that brittle fracturing during macroscopically ductile deformation may have been controlled by localised, transient increases in the pore fluid pressure (Handy 1989).

### *Upper greenschist facies phyllonites*

The upper greenschist facies phyllonites are characterised by a network of interconnected polycrystalline quartz ribbons and sericite strands, which wrap around flattened, partially sericitised feldspar grains. The microstructural evidence therefore suggests that the overall rheological behaviour of the phyllonites was controlled by the rheological behaviour of the quartz ribbons and sericite strands. The microstructures of the polycrystalline quartz ribbons are identical to the microstructures of the quartz ribbons preserved in packages of quartzo-feldspathic mylonite. These observations suggest that the quartz grains experienced a phase of intracrystalline plastic deformation, which was followed by an episode of grain boundary area reduction during static recrystallisation. Strands of intensely aligned sericite needles are typically preserved adjacent to polycrystalline quartz ribbons. Significant deformation within the sericite strands must have been required in order to maintain strain compatibility with neighbouring, highly deformed quartz ribbons. Although the sericite needles display strong patchy undulose extinction, there is little evidence to suggest that *individual* sericite grains have experienced large strains. There are three possible models to explain this paradox. Firstly, static recrystallisation following the cessation of thrusting could have destroyed any intracrystalline deformation microstructures within the sericite needles. Secondly, the undulose extinction, intense alignment and euhedral form of the sericite needles suggests that sericite may have accommodated deformation by intracrystalline slip (?dislocation glide) and dynamic recrystallisation mechanisms (Mares & Kronenberg 1993; Goodwin & Wenk 1995). Finally, strain within the sericite strands may have been accommodated by *aggregate-scale* deformation mechanisms, such as viscous grain boundary sliding, which do not result in significant intracrystalline deformation (Behrmann & Mainprice 1987; Stünitz & Fitz Gerald 1993). Unfortunately, it is not possible to determine which, (if any), of these models is correct without the use of TEM.

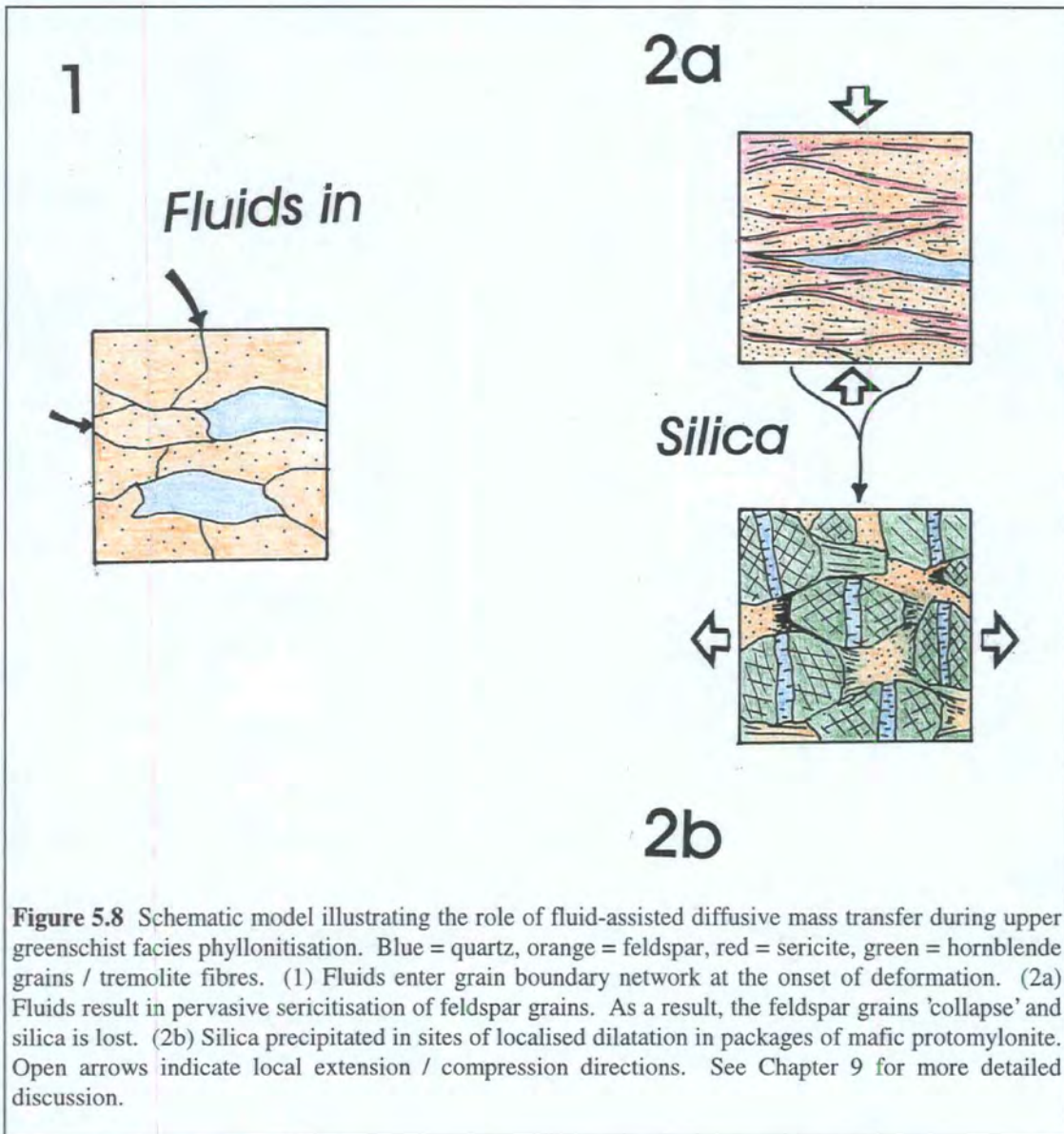


**Figure 5.8** Schematic model illustrating the role of fluid-assisted diffusive mass transfer during upper greenschist facies phyllonitisation. Blue = quartz, orange = feldspar, red = sericite, green = hornblende grains / tremolite fibres. (1) Fluids enter grain boundary network at the onset of deformation. (2a) Fluids result in pervasive sericitisation of feldspar grains. As a result, the feldspar grains 'collapse' and silica is lost. (2b) Silica precipitated in sites of localised dilatation in packages of mafic protomylonite. Open arrows indicate local extension / compression directions. See Chapter 9 for more detailed discussion.

Hornblende grains preserved within packages of protomylonitic amphibolite and packages of upper greenschist facies phyllonite are commonly observed to be fringed by fibrous actinolite strain shadows, and are cross-cut by arrays of intragranular extension fractures. The fractures are typically infilled by fibrous quartz and / or quartz-actinolite aggregates, which are oriented parallel to the macroscopic mineral lineation. There is little evidence to suggest that individual hornblende grains experienced significant intracrystalline plastic deformation. These observations suggest that sites of localised dilatation within and along the margins of the relatively competent hornblende grains acted as fluid-assisted diffusive mass transfer sinks (Knipe 1989) during top-to-the-NW thrusting. Protomylonitic amphibolites are commonly observed to be cross-cut by *undeformed* transgranular quartz and quartz-epidote veins. The vein fibres are oriented parallel to the macroscopic mineral

lineation, and the internal textures are generally consistent with crack-seal fracture growth (Ramsay 1980). These observations suggest (a) that the protomylonitic amphibolites did not experience significant macroscopically ductile strain, and (b) that brittle fracturing was probably caused by transient, localised increases in the pore fluid pressure during macroscopically ductile deformation within surrounding packages of quartzo-feldspathic and phyllosilicate-rich mylonite.

Feldspar grains preserved throughout the mylonite belt have experienced pervasive alteration to aggregates of sericite and epidote. Sericitisation reactions, which require the presence of a chemically active fluid phase, typically involve the loss of silica from the host grain (Hemley & Jones 1964; Beach 1980). The feldspar grains may therefore have behaved as effective diffusive mass transfer sources (Knipe 1989) during deformation and sericitisation. The most highly strained regions within the mylonite belt typically contain packages of upper greenschist facies phyllonite, which are characterised by intensely sericitised feldspar porphyroclasts. This observation suggests that fluid-assisted DMT processes may have been particularly important in the most highly strained packages of mylonite. A schematic model, which illustrates the possible role of fluid-assisted DMT during mylonitisation is presented in Figure 5.8. The significance of fluid-assisted DMT as a metamorphic process is discussed in more detail in Chapter 9.

Relatively *unaltered* plagioclase and K-feldspar porphyroclasts are locally preserved. Unaltered feldspar porphyroclasts display patchy undulose extinction and are commonly observed to be surrounded by irregular mantles of fine grained, seriate-interlobate albite. Experimental evidence suggests that recovery and dynamic recrystallisation should not be significant in either plagioclase or K-feldspar at temperatures of less than 400°C to 500°C (Passchier & Trouw 1996). The aggregates of fine grained albitic feldspar are therefore unlikely to have formed in response to dynamic recrystallisation or recovery processes. Two mechanisms have been proposed to explain the development of fine grained feldspar aggregates in greenschist facies tectonites (Tullis & Yund 1992; Fitz Gerald & Stünitz 1993). Firstly, it has been suggested that optical microstructures resembling those produced by dynamic recrystallisation may develop in response to grain-scale fracturing and 'micro-cataclasis' of feldspar grains (Tullis & Yund 1992). Secondly, Fitz Gerald & Stünitz (1993) have proposed that both plagioclase and K-feldspar porphyroclasts may undergo metamorphism during deformation in a *fluid-rich*, greenschist facies environment, to produce aggregates of fine grained albite, white mica, clinozoisite and quartz. This process, whereby the mineralogy and / or chemical composition of the 'daughter' grains differ significantly from the mineralogy and / or chemical composition of the parent porphyroclast has been termed 'neocrystallisation' (Fitz

Gerald & Stünitz 1993). The aggregates of fine grained feldspar are consistently more albitic in composition than the coarse grained feldspar porphyroclasts. This observation suggests that neocrystallisation mechanisms may have been responsible for the observed grain size reduction. However, it could be argued that micro-cataclasis would render the resulting fine grained plagioclase / K-feldspar more susceptible to albitisation (i.e. alteration) than the coarse grained porphyroclasts. Two further lines of microstructural evidence suggest that cataclasis was unlikely. Firstly, the aggregates of fine grained albite tend to be equigranular, whereas cataclasis is more likely to result in a random grain size distribution. Secondly, fluid inclusions are typically concentrated along albite grain boundaries, whilst the albite grains themselves appear to be clear in plane polarised light. In contrast, the feldspar porphyroclasts are characteristically 'cloudy' in plane polarised light. These observations suggest that (a) the porphyroclasts display a 'microporous' texture (i.e. pores are distributed throughout the parent grain), but that (b) pores are restricted to the margins of the albite grains (David *et al.* 1995). Drury & Urai (1990) have demonstrated that in recrystallised quartz grains, fluid inclusions may become concentrated into grain boundary networks and are *not* homogeneously distributed. It is therefore postulated that the fine grained albite aggregates developed in response to neocrystallisation of the parent plagioclase and K-feldspar porphyroclasts during mylonitisation.

In conclusion, it has been demonstrated that there were a number of different operative deformation mechanisms during top-to-the-NW thrusting and mylonitisation. The overall rheological behaviour of the mylonite belt appears to have been controlled by intracrystalline plastic deformation within quartz grains and / or by deformation along sericite strands. Intra- and transgranular brittle fractures are commonly observed, and probably represent localised, transient brittle deformation events which developed in response to syn-tectonic fluctuations in the pore fluid pressure. Fluid assisted diffusive mass transfer mechanisms are also inferred to have been important operative deformation mechanisms, particularly within packages of the most highly strained mylonite. There is clearly a close relationship between retrograde metamorphism and deformation by fluid-assisted diffusive mass transfer processes. This relationship will be discussed further in Chapter 9.

### **5.3 CROSS-CUTTING STRUCTURES: THRUST-RELATED BRITTLE FAULTS & CATACLASITE SEAMS**

Butler (1995) has described widely spaced, steeply SE-dipping brittle faults and cataclasite seams which locally cross-cut the gneissose banding in the 'foreland' and the mylonitic foliation preserved in macroscopic low strain augen. The brittle faults produce apparent, centimetre-scale thrust-sense offsets in the gneissose banding (Butler 1995). These observations suggest (a) that brittle thrusting post-dates macroscopically ductile thrusting, and (b) that neither the brittle faults nor the cataclasite seams localised along pre-existing mylonitic foliation surfaces.

### **5.4 REWORKED FABRICS: SINISTRAL STRIKE-SLIP RELATED PHYLLONITE & MYLONITE**

Evidence for sinistral strike-slip (i.e. top-to-the-NE shear) is preserved in a number of macroscopically ductile shear zones which outcrop throughout southeast Scalpay. The shear zones appear to deform and rework the thrust-related upper greenschist facies mylonites (section 3.2.3.4). The sinistral strike-slip related fabrics are described in the following section, with the aim of understanding how the primary fabric (i.e. the upper greenschist facies mylonites) may have influenced the distribution and style of deformation within the sinistral strike-slip related shear zones (i.e. the reworked fabrics).

#### **5.4.1 FIELD RELATIONSHIPS**

The aims of this section are (a) to describe the overall distribution of the sinistral strike-slip related shear zones (i.e. the macrostructure) and (b) to describe the hand specimen and outcrop-scale lithologies and textures of the fabrics preserved within the shear zones (i.e. the mesostructure).

##### **5.4.1.1 Macrostructure**

Three major SE- to SSE-dipping sinistral strike-slip related shear zones are exposed in southeast Scalpay. The shear zones are oriented sub-parallel to the pre-existing thrust-related mylonitic foliation, and are typically bounded by foliation-parallel brittle detachment faults (section 5.5). The NE-trending Cnoc na Croich belt (at least 5m thick) outcrops between Cnoc na Croich (NG 223 955) and Loch a' Rothaid (NG 227 958) and appears to pinch out laterally towards the northeast. The NNE- to NE-trending Kennavay belt (at least 5m thick) outcrops between Bàgh Ceann na Muice

(NG 230 944) and Kennavay (NG 234 952), but is lost in an area of poor exposure towards the northeast. The NE-trending Scoravick belt (at least 4m thick) outcrops along the northeast coast of Scalpay (NG 244 958) and appears to be the along-strike continuation of the Kennavay belt (Figs. 3.7 & 5.1). The Cnoc na Croich and Kennavay belts comprise packages of distinctive lower greenschist facies phyllonite, whilst the Scoravick belt is composed of quartzo-felspathic mylonite. Narrow bands of sinistral strike-slip related phyllonite ( $\leq 50\text{cm}$  thick) are preserved throughout southeast Scalpay, and are particularly well exposed in the region to the east of Lag na Laire (NG 235 941).

#### **5.4.1.2 Lithology and mesostructure**

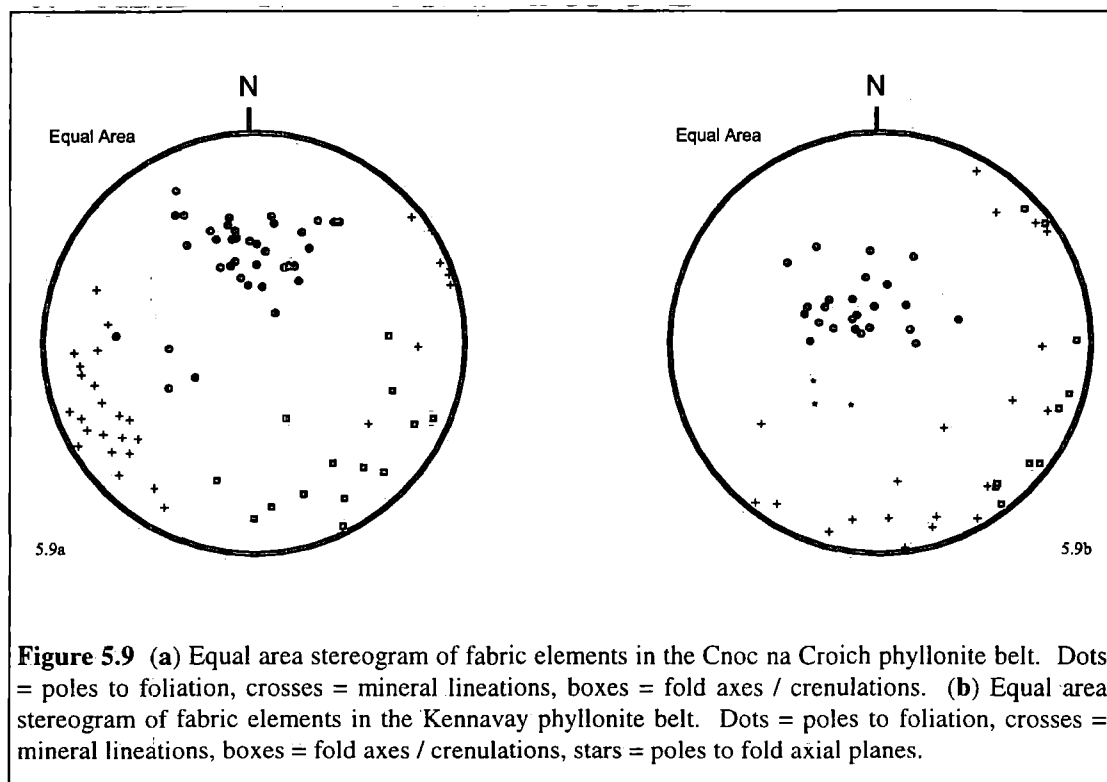
The Cnoc na Croich and Kennavay belts (and subsidiary phyllonite bands) comprise interbanded packages of grey-green and dark-green phyllonite. Microstructural observations suggest that the grey-green phyllonites were derived from felsic protoliths, whilst the dark-green phyllonites were derived from mafic protoliths (section 5.4.2). Grey-green phyllonite, protophyllonite and ultraphyllonite comprise  $\phi$  -,  $\sigma$ - and  $\delta$ -type quartz  $\pm$  feldspar porphyroclasts (locally  $\leq 10\text{cm}$  diameter; typically  $\leq 5\text{mm}$  diameter) which are wrapped by undulating quartz ribbons ( $\leq 1\text{mm}$  thick; aspect ratios  $\leq 100:1$ ) and aggregates of fine grained, intensely aligned phyllosilicate minerals. Dark green phyllonite, ultraphyllonite and protophyllonite are extremely fissile and comprise flattened  $\phi$ -type feldspar porphyroclasts which are wrapped by aggregates of fine grained, intensely aligned phyllosilicate minerals.

The Scoravick belt comprises fine grained quartzo-feldspathic mylonite, protomylonite and ultramylonite, in which  $\delta$ - and  $\sigma$ -type feldspar porphyroclasts ( $\leq 0.5\text{mm}$  diameter) are wrapped by aggregates of highly attenuated quartz ribbons ( $\ll 1\text{mm}$  thick; aspect ratios  $\leq 100:1$ ).

#### ***The Cnoc na Croich phyllonite belt***

The Cnoc na Croich phyllonite belt is particularly well exposed in a small quarry on the southwest coast of Scalpay (NG 223 955). The upper margin of the shear zone is defined by a SE-dipping brittle detachment fault (section 5.5), which separates a band of upper greenschist facies, thrust related mylonite in its hangingwall from lower greenschist facies sinistral strike-slip related phyllonite in its footwall. The base of the shear zone is not exposed. The predominantly southward dipping phyllonitic foliation is associated with a sub-horizontal, NE-SW trending mineral lineation (Fig. 5.9a). Kinematic indicators ( $\sigma$ - and  $\delta$ -type quartz and feldspar porphyroclasts and asymmetric shear bands) viewed in surfaces parallel to the mineral lineation and perpendicular to the foliation are consistent with top-to-the-NE shear (i.e. sinistral

strike-slip). The phyllonitic fabric is locally deformed by centimetre-scale folds, which are thought to have developed during a phase of subsequent dextral strike-slip (see sections 3.2.3.4 & 5.5). In general, the effects of folding are not very intense and unmodified sinistral strike-slip related fabrics account for approximately 75% of the total rocks exposed within the Cnoc na Croich belt.

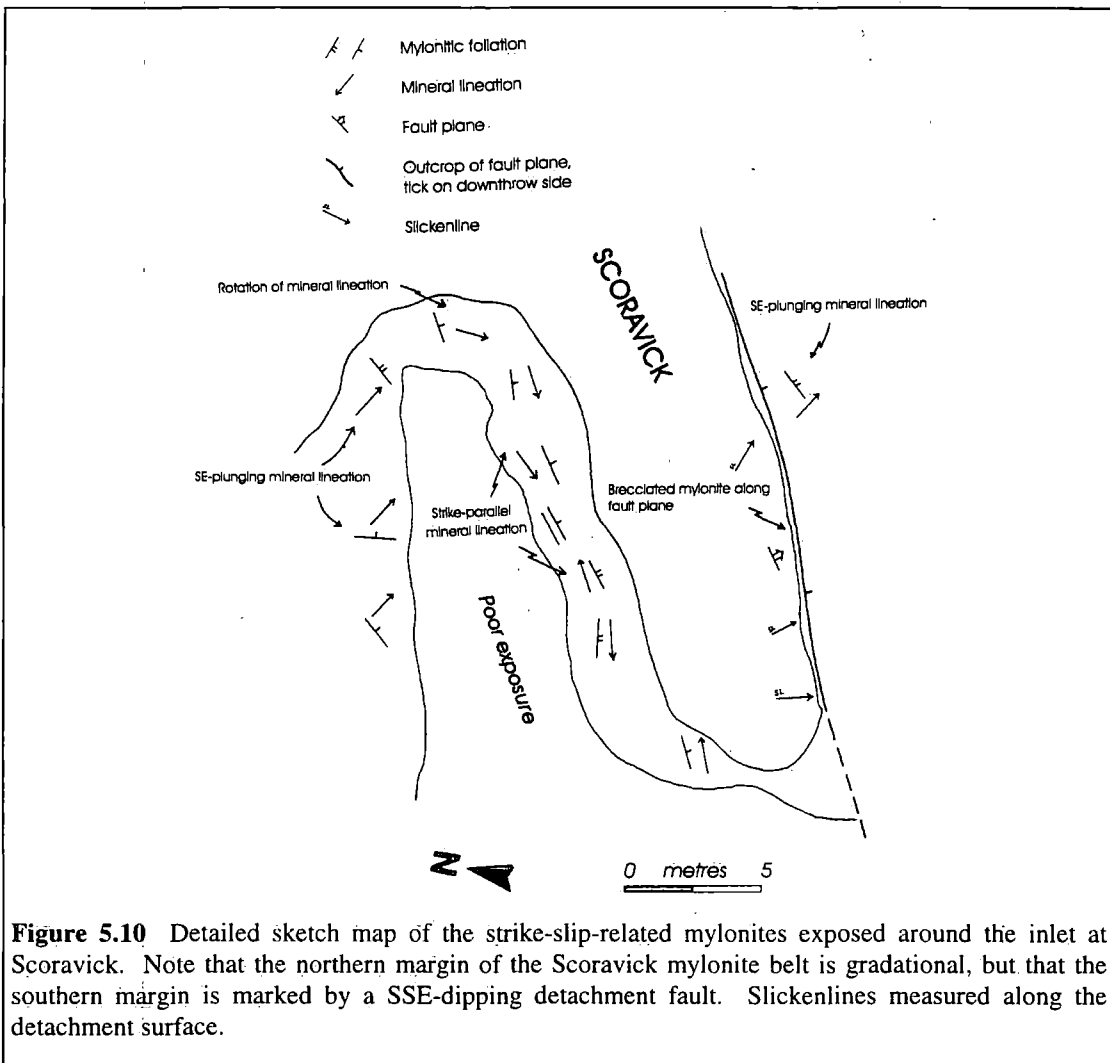


### *The Kennavay phyllonite belt*

The base of the Kennavay belt is exposed just above the high water mark along the east side of Bàgh Ceann na Muice (NG 2309 9454), whilst its upper margin is exposed in a steep cliff at NG 2316 9473. The upper margin is defined by a foliation-parallel brittle detachment fault (section 5.5), which separates a package of highly strained, upper greenschist facies thrust-related mylonite in the hangingwall from folded, dark-green lower greenschist facies phyllonite in its footwall. In contrast, the base of the phyllonite belt is locally unaffected by brittle faulting and the original shear zone fabrics are preserved. The footwall of the Kennavay belt is characterised by interbanded packages of highly strained mylonite and phyllonite (section 5.2.1.2). The predominantly S- to SE-dipping mylonitic / phyllonitic foliation is associated with a SE-, SSE- to SSW-plunging mineral lineation. The mineral lineation appears to undergo a progressive change in orientation towards the base of the Kennavay belt, from a NW-SE to a NNE-SSW trend (Fig. 5.9b).  $\sigma$ -type quartz porphyroclasts viewed in surfaces parallel to the NW-SE trending mineral lineation are consistent with top-

to-the-NW shear (i.e. thrusting), whilst  $\sigma$ -type quartz porphyroclasts and asymmetric shear bands viewed in surfaces parallel to the NNE-SSW trending mineral lineation are consistent with top-to-the-NNE shear (i.e. sinistral strike-slip). These observations suggest (a) that *the pre-existing thrust-related fabrics were reworked during lower greenschist facies phyllonitisation*, and (b) that *reworking and phyllonitisation were synchronous with a change in kinematic regime from top-to-the-NW thrusting to sinistral strike-slip*. The Kennavay belt itself is characterised by predominantly SE-dipping packages of grey-green and dark-green phyllonite, which are commonly observed to be deformed by cascades of centimetre-scale folds. The folds are thought to have developed during a subsequent phase of dextral strike-slip (sections 3.2.3.4 & 5.5).

### The Scoravick mylonite belt



A SE-dipping belt of highly strained, sinistral strike-slip related quartzo-feldspathic mylonite occupies an E-W trending inlet at Scoravick (NG 244 958) (Fig. 3.7). The upper margin of the Scoravick belt is defined by a SE-dipping brittle detachment fault

(section 5.5), which separates thrust-related mylonites in the hangingwall from strike-slip related mylonites in its footwall. In contrast, the base of the Scoravick belt is unaffected by brittle deformation and the original shear zone fabrics are preserved. The footwall of the Scoravick belt is characterised by highly strained, SE-dipping quartzo-feldspathic mylonites and protomylonites, which are associated with a SE-plunging mineral lineation. However, the mineral lineation appears to undergo a progressive change in orientation towards the base of the Scoravick belt, from a NW-SE to a NE-SW trend (Figs. 5.10 & 5.11).  $\sigma$ -type feldspar porphyroclasts viewed in surfaces parallel to the NW-SE trending mineral lineation are consistent with top-to-the-NW shear (i.e. thrusting), whilst  $\delta$ - and  $\sigma$ -type feldspar porphyroclasts viewed in surfaces parallel to the NE-SW trending mineral lineation are consistent with top-to-the-NE shear (i.e. sinistral strike-slip). These observations suggest that at Scoravick, the *pre-existing thrust-related fabrics were reworked during sinistral strike-slip, but that reworking was not associated with the development of lower greenschist facies phyllonitic fabrics.*

The strike-slip related mylonitic fabrics are locally cross-cut by *undeformed* quartz and quartz-chlorite veins (Fig. 5.11).

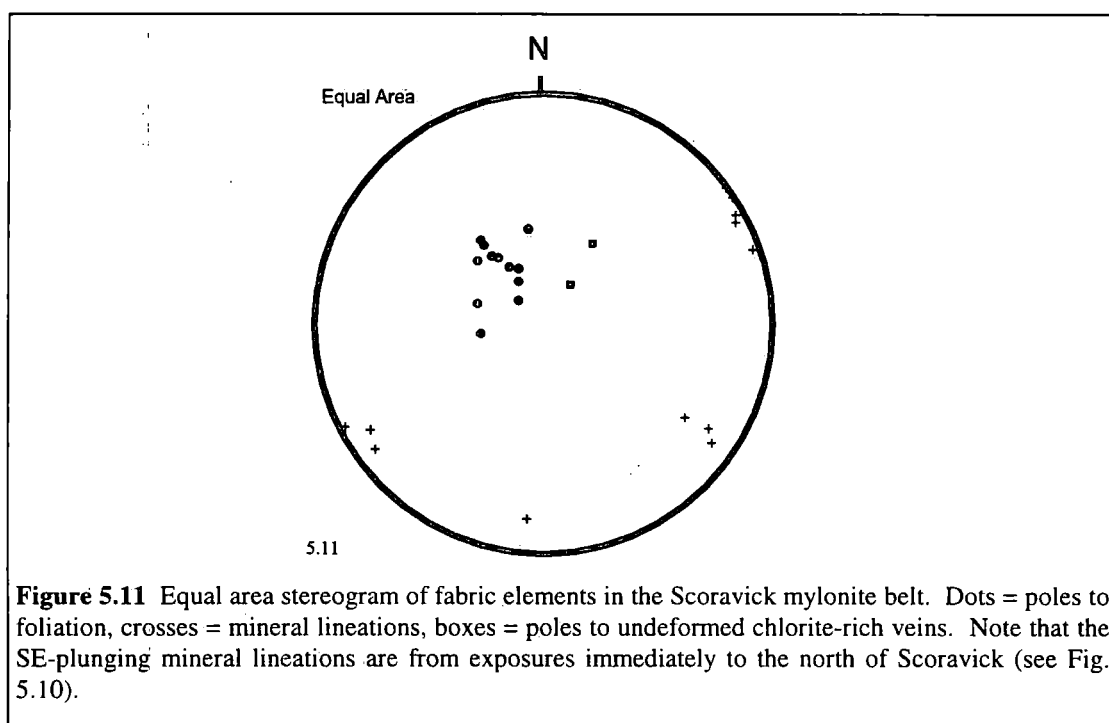


**Figure 5.11** Equal area stereogram of fabric elements in the Scoravick mylonite belt. Dots = poles to foliation, crosses = mineral lineations, boxes = poles to undeformed chlorite-rich veins. Note that the SE-plunging mineral lineations are from exposures immediately to the north of Scoravick (see Fig. 5.10).

### ***Subsidiary phyllonite bands***

A band of dark-green, lower greenschist facies phyllonite and ultraphyllonite ( $\leq 10$ cm thick) is exposed in a wave-polished surface to east of Lag na Laire (NG 235 941). The lower greenschist facies phyllonites are developed within, and are concordant to, a package of highly strained, upper greenschist facies, thrust-related quartzo-

feldspathic mylonites. The margins of the phyllonite band are very abrupt, but do *not* appear to be defined by brittle faults. The S- to SE-dipping phyllonitic foliation is associated with sub-horizontal E-W to NE-SW trending mineral lineations (Fig. 5.12).  $\sigma$ -type quartz porphyroclasts viewed in surfaces parallel to the mineral lineation and perpendicular to the foliation are consistent with top-to-the-E or -NE shear.

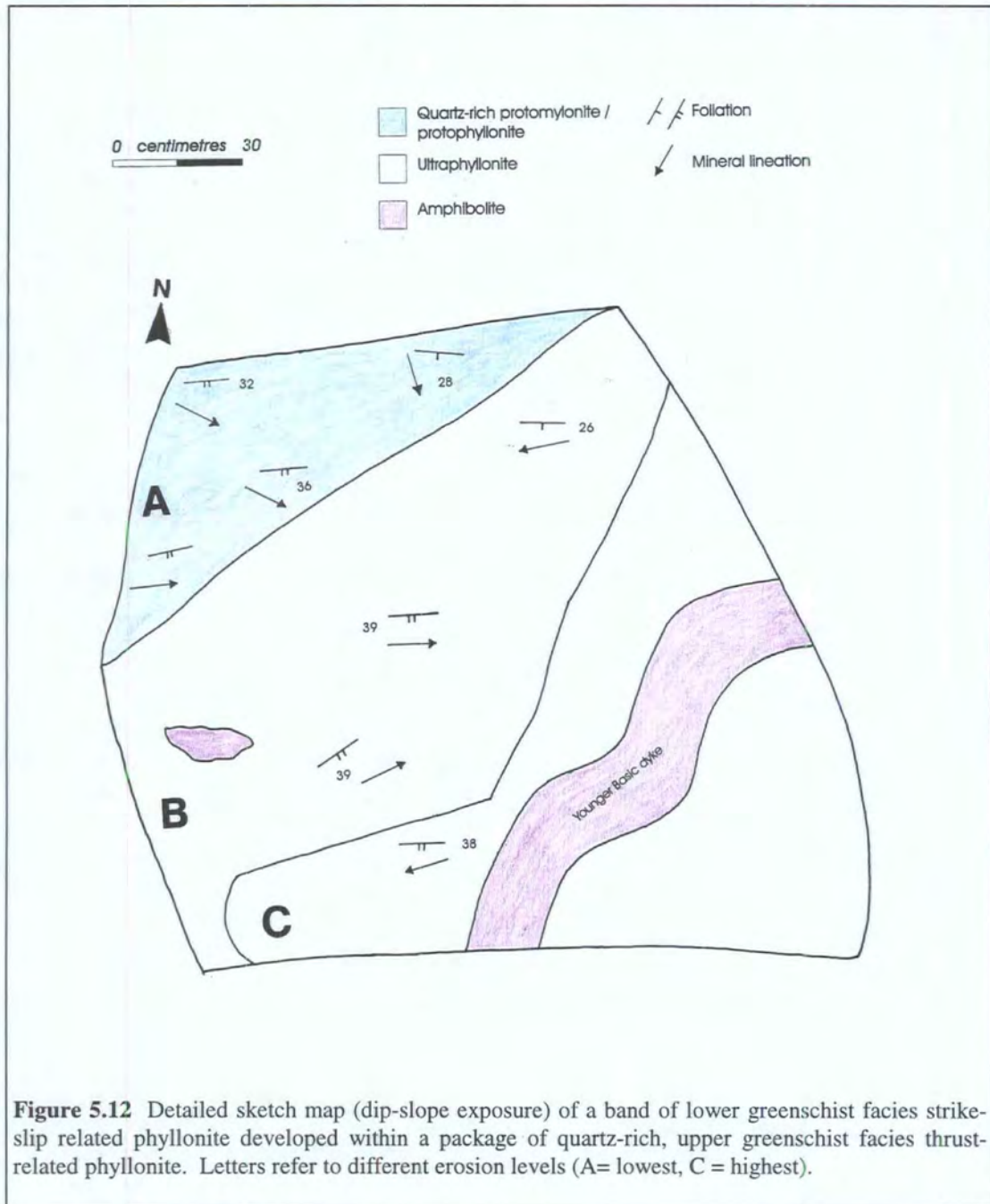


**Figure 5.12** Detailed sketch map (dip-slope exposure) of a band of lower greenschist facies strike-slip related phyllonite developed within a package of quartz-rich, upper greenschist facies thrust-related phyllonite. Letters refer to different erosion levels (A= lowest, C = highest).

## 5.4.2 MICROSTRUCTURE

### 5.4.2.1 Felsic phyllonite ('grey-green' phyllonite)

Felsic ('grey-green') phyllonite comprises quartz and feldspar porphyroclasts and isolated polycrystalline quartz ribbons, which are wrapped by a network of interconnected sericite strands  $\pm$  laterally discontinuous trails of fine grained epidote (Plate 5.11). The anastomosing sericite strands, which locally define an asymmetric shear band foliation, comprise aggregates of intensely aligned sericite needles. Individual sericite needles typically display patchy undulose extinction, but are rarely observed to be kinked or fractured. Prismatic opaque grains ( $\leq 0.1\text{mm}$  diameter), which are typically fringed by fibrous quartz strain shadows, are widely observed within sericite strands. Chlorite strain shadows are *locally* developed along the margins of quartz and feldspar porphyroclasts.

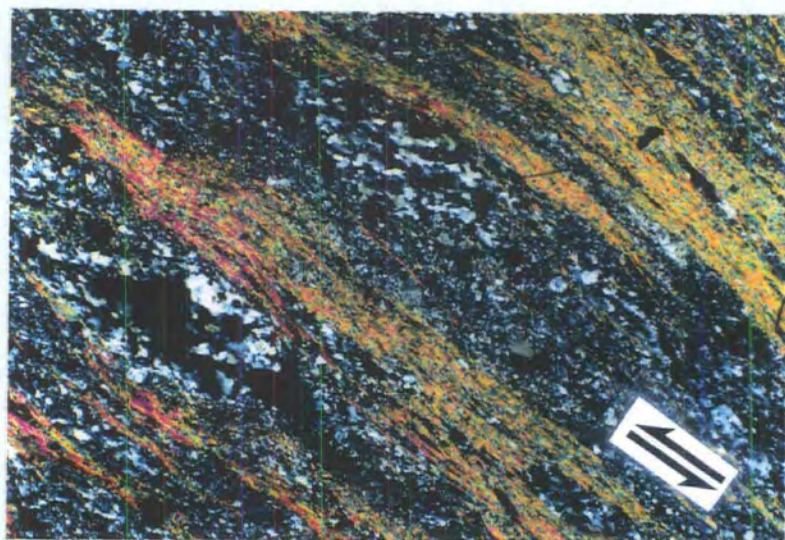


**Plate 5.11** Lower greenschist facies felsic phyllonite. The foliation is defined by highly birefringent sericite strands and bands of fine-grained recrystallised quartz and ultrafine-grained neocrystallised feldspar (low relief). Split arrows parallel mineral lineation, top-to-NE shear. Field of view  $6\times 3.7\text{mm}$ , crossed polars.

Quartz porphyroclasts are flattened parallel to the trace of the foliation ( $\leq 4\text{mm}$  long; aspect ratios  $\leq 3:1$ ) and display well developed core-and-mantle microstructures. The cores typically exhibit strong patchy to sweeping undulose extinction, although elongate, equigranular-polygonal subgrains ( $\leq 0.05\text{mm}$  long; aspect ratios  $\leq 4:1$ ) are locally developed. The porphyroclast mantles and the polycrystalline ribbons comprise aggregates of elongate, seriate-interlobate quartz grains ( $\leq 0.1\text{mm}$  long; aspect ratios  $\leq 4:1$ ). Arrays of ultrafine, high relief fluid inclusions ( $\ll 0.01\text{mm}$  diameter) are commonly observed to decorate quartz grain and subgrain boundaries.

Feldspar porphyroclasts are relatively rare (feldspar accounts for approximately 10% of the porphyroclasts preserved within domains of felsic phyllonite) and typically display partial to complete alteration to aggregates of fine grained sericite needles (needles  $\leq 0.05\text{mm}$  long; aspect ratios  $\leq 1:5$ ). Relatively unaltered feldspar grains display strong patchy undulose extinction, and are locally surrounded by irregular patches of fine grained, seriate-interlobate albite (individual grains  $< 0.01\text{mm}$  diameter).

#### 5.4.2.2 Mafic phyllonite ('dark-green' phyllonite)

Mafic phyllonite comprises a network of anastomosing chlorite strands which isolate pockets of flattened ( $\leq 1\text{mm}$  long; aspect ratios  $\leq 3:1$ ), partially sericitised feldspar grains (sericite accounts for up to 20% of the surface area of the host grain) and small ( $\leq 0.1\text{mm}$  diameter), equant hornblende inclusions (Plate 5.12).

The chlorite strands comprise aggregates of highly aligned chlorite laths. Individual chlorite grains display patchy undulose extinction, but are rarely observed to be kinked or fractured. Feldspar grains are typically cross-cut by intragranular sericite strands, which are oriented parallel to the trace of the foliation.



**Plate 5.12** Lower greenschist facies mafic phyllonite. The foliation is defined by an interconnected network of chlorite strands (green) and flattened, partially sericitised feldspar grains (pale brown). Note that virtually no hornblende remains. Split arrows parallel mineral lineation, top-to-NE shear. Field of view  $6 \times 3.7\text{mm}$ , plane polarised light.

### 5.4.2.3 Strike-slip related quartzo-feldspathic mylonite

The strike-slip related quartzo-feldspathic mylonites from Scoravick consist of unaltered K-feldspar porphyroclasts and flattened, partially sericitised feldspar grains, which are wrapped by bands of ultrafine grained polycrystalline albite  $\pm$  epidote and undulating polycrystalline quartz ribbons (Plate 5.13). The quartz ribbons (between 0.5mm and 7cm long) comprise polycrystalline aggregates of equigranular-polygonal grains (individual grains  $\leq$  0.1mm diameter; aspect ratios  $\cong$  1:1). Core-and-mantle microstructures have not been observed.



**Plate 5.13** Lower greenschist facies quartzo-feldspathic mylonite from Scoravick. The foliation is defined by bands of recrystallised quartz and feldspar (grey), laterally discontinuous sericite strands (brown). Subrounded, pristine K-feldspar grains are common observed to be cross-cut by intragranular tensile fractures (arrowed). Split arrows parallel mineral lineation, top-to-NE shear. Field of view 6x3.7mm, crossed polars.

Pristine, tartan-twinned and untwinned K-feldspar porphyroclasts (between 0.06mm and 2mm in diameter; aspect ratios between 1:1 and 4:1) display strong patchy undulose extinction and are locally cross-cut by intragranular extension fractures. The fractures are typically infilled by aggregates of fine grained albite, fibrous quartz or massive calcite grains. 'Flame perthite' (Pryer & Robin 1995) is locally developed in K-feldspar porphyroclasts. The 'flames' are between 0.03mm long and 0.25mm long and tend to 'point' away from porphyroclast margins and intragranular fractures. Bands of ultrafine grained (individual grains  $\leq$  0.007mm diameter), equigranular-interlobate albite aggregates are commonly observed to form 'tails' around the margins of pristine feldspar porphyroclasts. Altered feldspar grains (sericite accounts for up to 70% of the surface area of the host grain) are typically flattened parallel to the trace of the foliation and are cross-cut by well developed intragranular sericite strands. The distribution of pristine and sericitised feldspar grains does *not* appear to be related to

the deformation microstructures. The preponderance of pristine K-feldspar porphyroclasts therefore suggests that plagioclase may have been preferentially sericitised.

### **5.4.3 SUMMARY AND DISCUSSION**

Sinistral strike-slip  $\pm$  thrust-related fabrics are developed in a number of discrete, macroscopically ductile shear zones, which overprint and rework the earlier thrust-related upper greenschist facies mylonites. The strike-slip related shear zones typically comprise packages of felsic and mafic phyllonite, although a band of quartzo-feldspathic mylonite is locally preserved.

#### **5.4.3.1 Retrogression and metamorphism during sinistral strike-slip**

Mineralogical and microstructural observations suggest that the sinistral strike-slip related phyllonites preserved within the Cnoc na Croich and Kennavay belts and the quartzo-feldspathic mylonites preserved within the Scoravick belt may have developed under different metamorphic conditions.

The phyllonites comprise a stable assemblage of sericite, chlorite, fine grained albite, quartz, epidote and opaque minerals. The original plagioclase, K-feldspar and hornblende grains have suffered intense (locally complete) alteration to aggregates of hydrous phyllosilicate minerals  $\pm$  albite and epidote. The retrograde minerals typically display strong grain shape preferred orientation. In particular, fibrous chlorite is locally developed in strain shadows around the margins of quartz and opaque grains, whilst aggregates of sericite or chlorite form interconnected strands in which the (001) cleavage planes are oriented parallel to the trace of the macroscopic foliation. These observations suggest (a) that the sinistral strike-slip related phyllonites have experienced intense lower greenschist facies metamorphism and hydration, and (b) that retrogression was synchronous with deformation.

The sinistral strike-slip related mylonites from Scoravick comprise an assemblage of K-feldspar, partially sericitised (?) plagioclase, flame perthite, fine grained albite, quartz and calcite. Pryer & Robin (1995) have postulated that flame perthite develops during greenschist facies deformation (temperature between 250°C and 450°C), provided the partial pressure of water is low.

In the Scoravick mylonites, tails and mantles of fine grained albite are commonly observed to wrap around asymmetric K-feldspar porphyroclasts, and the (001) cleavage planes of sericite needles are typically oriented parallel to the trace of the macroscopic foliation. These observations suggest that albitisation and sericitisation, both of which are characteristic of greenschist facies metamorphism (Miyashiro

1994), were synchronous with sinistral strike-slip. Syn-tectonic transgranular vein arrays have not been observed within the Scoravick mylonites. However, K-feldspar porphyroclasts are commonly observed to be cross-cut by intragranular extension fractures. The fractures are *locally* infilled by aggregates of calcite and quartz. These observations suggest (a) that both H<sub>2</sub>O and CO<sub>2</sub> were present in *limited* amounts during mylonitisation, and (b) that the fluid pressure during deformation were generally low. Since the *total* fluid pressure depends on the *partial* pressures of all the fluid phases (Miyashiro 1994), the partial pressure of H<sub>2</sub>O during mylonitisation may have been particularly low. It is therefore postulated that both the sinistral strike-slip related phyllonites and the sinistral strike-slip related quartzo-feldspathic mylonites developed under lower greenschist facies conditions. The different deformation microstructures and mineral assemblages can be explained by differences in the availability of water during deformation. Possible controls on the availability of water during sinistral strike-slip are discussed in section 5.4.4.

#### **5.4.3.2 Operative deformation mechanisms during sinistral strike-slip**

##### ***Sinistral strike-slip related phyllonites***

Sericitised feldspar grains are commonly observed within packages of felsic and mafic phyllonite. Sericitisation reactions require a chemically active fluid phase and typically involve the loss of silica from the parent grain (Hemley & Jones 1964; Beach 1980). The chlorite strands preserved in mafic phyllonite appear to have been derived from the syn-tectonic breakdown of hornblende. Chloritisation reactions also require a chemically active fluid phase, and also involve the loss of silica from the parent grain (Beach 1980). These observations suggest that feldspar and hornblende grains may have acted as diffusive mass transfer (DMT) sources during phyllonitisation. It is postulated that the syn-tectonic growth of sericite and chlorite was controlled by fluid-assisted DMT mechanisms. If this inference is correct, fluid-assisted DMT processes ultimately controlled the development of the sericite and chlorite strands, and thus fundamentally influenced the textural and rheological evolution of the phyllonitic shear zones (see below).

Felsic phyllonite comprises isolated quartz ribbons and feldspar porphyroclasts, which are wrapped by a network of interconnected sericite strands. Mafic phyllonite comprises isolated feldspar grains, which are wrapped by a network of interconnected chlorite strands. These observations are consistent with the overall rheological behaviour of the felsic and mafic phyllonites having been controlled by deformation within the phyllosilicate-rich strands (Jordan 1987; Handy 1990, 1994). Aggregates of phyllosilicate grains locally define well developed asymmetric shear band fabrics,

which is also consistent with the sericite and chlorite strands having accommodated a significant component of shear strain (O'Brien *et al.* 1987). However, apart from displaying strong patchy undulose extinction, individual sericite and chlorite needles do not appear to have suffered significant deformation. Static recrystallisation following the cessation of sinistral strike-slip could have destroyed any deformation microstructures within the sericite or chlorite strands. However, there is no evidence to suggest that other minerals preserved within packages of strike-slip related phyllonite (e.g. quartz) underwent static recrystallisation. It is therefore postulated that the sericite and chlorite grains preserve the original deformation microstructures. In the absence of TEM studies, it is not possible to determine the operative deformation mechanisms within the fine grained phyllosilicate strands. However, it is tentatively suggested that deformation was accommodated by intracrystalline slip and recrystallisation processes (Bons 1988; Mares & Kronenberg 1993; Goodwin & Wenk 1995) (but see section 5.2.3.2 for further discussion).

### ***Scoravick mylonites***

The sinistral strike-slip related mylonites from Scoravick are characterised by isolated K-feldspar porphyroclasts and partially sericitised (?) plagioclase grains, which are wrapped by quartz ribbons and aggregates of fine grained albite. These observations suggest that the rheological behaviour of the quartzo-feldspathic mylonites may have been controlled by deformation within the quartz ribbons and albite bands. The fine grain size has hampered detailed optical study of the albite aggregates, and it has not been possible to positively identify the dominant operative deformation mechanism(s). However, Stünitz & Fitz Gerald (1993) have proposed that fine grained, greenschist facies albite-rich mylonites may accommodate deformation by viscous grain boundary sliding mechanisms.

The polycrystalline quartz ribbons comprise aggregates of equant, equigranular-polygonal grains. The polygonal grains rarely display well developed undulose extinction. Stain-free polygonal grains are thought to develop in response to grain boundary area reduction (GBAR) processes, and are consistent with a phase of static recrystallisation following the cessation of active deformation (Passchier & Trouw 1996). These observations therefore suggest (a) that the mylonites experienced an episode of static recrystallisation following the cessation of sinistral strike-slip, and (b) that the quartz deformation microstructures were destroyed by GBAR. In the absence of deformation microstructures, it is tentatively suggested that the quartz ribbons developed by intracrystalline plastic deformation mechanisms (Hirth & Tullis 1992).

### 5.4.3.3 Timing and significance of static recrystallisation

Quartz ribbons preserved in packages of thrust- *and* sinistral strike-slip related mylonite are widely inferred to have undergone a phase of static recrystallisation following the cessation of active deformation (sections 5.2.3.2 & 5.4.3.2). The latest phase of static recrystallisation must therefore post-date sinistral strike-slip, although its age relative to dextral strike-slip (section 5.5) is unclear.

Static recrystallisation is thought to be controlled by grain boundary area reduction (GBAR) processes. GBAR is promoted either by elevated temperatures or by the presence of fluids along grain boundaries following the cessation of deformation (Passchier & Trouw 1996). There is no evidence to suggest that there was a major heating event following sinistral strike-slip on Scalpay. However, there *is* evidence for the presence of fluids within areas of highly deformed mylonite (e.g. section 5.4.1.2). It is therefore suggested that static recrystallisation was caused by fluids 'trapped' within the fault rocks after deformation had ceased (see also Stewart 1997).

## 5.4.4 SYNTHESIS

### 5.4.4.1 Summary

Lower greenschist facies thrust- and sinistral strike-slip related fabrics are preserved within discrete shear zones throughout southeast Scalpay. The lower greenschist facies fabrics *locally* deform and rework the pre-existing upper greenschist facies mylonites. The margins of the lower greenschist facies shear zones are typically cross-cut by later brittle detachment faults. However, in regions where the original shear zone geometries are preserved, it appears that there was a progressive change in the kinematic regime, from top-to-the-NW thrusting to top-to-the-NE sinistral strike-slip during reworking.

In general, the reworked fabrics are completely retrogressed and comprise sericite- or chlorite-rich phyllonites and ultraphyllonites. However, a belt of *partially* retrogressed, sinistral strike-slip related lower greenschist facies quartzo-feldspathic mylonite is locally preserved on the NE coast of Scalpay (Fig. 3.7). These observations suggest that the distribution of intense fluid-rock interaction was extremely heterogeneous during reworking. The two important questions which will be addressed in the following sections are therefore:

- What were the principal controls on shear zone localisation during reworking (section 5.4.4.2)?
- What were the principal controls on the distribution of fluid-rock interaction during reworking (section 5.4.4.3)?

#### 5.4.4.2 Timing and controls on shear zone localisation

An appreciation of the *absolute* ages of the upper greenschist facies deformation and the lower greenschist reworking events is vital in order to understand the mechanisms of shear zone localisation. Unfortunately, there are no reliable isotopic age dates available for either the upper or lower greenschist facies fabrics. However, there are two plausible 'end-member' models which could explain the spatial and temporal distribution of the upper and lower greenschist facies fabrics. Firstly, it is possible that both fabrics developed during a *single, progressive deformation event*. The differences in metamorphic grade and style of deformation may have been caused by progressive exhumation of the fault zone during deformation. If this model is correct, the lower greenschist facies shear zones are probably the manifestation of increasingly localised deformation, which resulted from the falling pressure and temperature conditions during thrusting and subsequent sinistral strike-slip (cf. Grocott 1977). Secondly, it is possible that the upper and lower greenschist facies fabrics developed during *two distinct and entirely unrelated deformation events*. If this model is correct, the lower greenschist facies shear zones probably localised along pre-existing anisotropies within the upper greenschist facies mylonite belt.

The macroscopically ductile, upper greenschist facies fabrics are locally cross-cut by brittle thrust faults and cataclasite seams (Butler 1995). In contrast, brittle thrust-related structures have not been observed to cross-cut the lower greenschist facies fabrics. This observation suggests that macroscopically ductile thrusting had ceased prior to the onset of lower greenschist facies reworking. Thrust-related mylonites are only preserved in the Northern Zone of the OHFZ (i.e. in the region to the north of the South Harris Shear Zones), whilst lower greenschist facies fabrics have been observed along the entire length of the fault zone (section 2.3.3.1). The kinematics of the South Harris Shear Zones (SHSZ) and the regional distribution upper and lower greenschist fabrics are consistent with the thrust-related mylonites *pre-dating* the latest movements across the SHSZ, whilst the strike-slip related fabrics must *post-date* the latest movements across the SHSZ (Butler 1995; see also Chapters 2 & 3 of the present work). These observations suggest (a) that the lower greenschist facies fabrics are *significantly* younger than the upper greenschist facies fabrics, and (b) that these fabrics probably developed during two *separate* deformation events. If these inferences are correct, it is likely that the lower greenschist facies shear zones localised along pre-existing anisotropies within the primary fabric (i.e. within the upper greenschist facies mylonite belt).

Narrow bands of lower greenschist facies phyllonite, which have accommodated relatively low magnitudes of finite strain and have *not* been modified by the effects of

later brittle deformation, are locally developed within packages of *highly strained, upper greenschist facies phyllonite* (Fig. 5.12; section 5.4.1.2). The footwall of the Kennavay phyllonite belt, which has not been modified by the effects of later brittle deformation, is also characterised by bands of *upper greenschist facies phyllonite*. However, the lower greenschist facies Scoravick mylonite belt, which appears to be the along-strike continuation of the Kennavay belt (Butler 1995), is developed within a package of highly strained upper greenschist facies *quartzo-feldspathic mylonite*. These observations suggest (a) that bands of pre-existing, highly strained, upper greenschist facies phyllonite and mylonite were preferentially reworked at the onset of lower greenschist facies thrusting and / or during subsequent sinistral strike-slip, and (b) that bands of *lower greenschist facies phyllonite* localised along pre-existing zones of highly strained *upper greenschist facies phyllonite*.

#### **5.4.4.3 A model of lower greenschist facies phyllonitisation on Scalpay**

*Lower greenschist facies phyllonitic* fabrics are developed in discrete shear zones which deform and overprint packages of highly strained, *upper greenschist facies phyllonite*. Deformation within the lower greenschist facies phyllonite belts was ultimately controlled by fluid-assisted diffusive mass transfer processes, and the original feldspar, hornblende and biotite grains have suffered extreme retrogression to aggregates of hydrous phyllosilicates. These observations suggest (a) that lower greenschist facies phyllonitisation and deformation were characterised by intense fluid-rock interaction, and (b) that fluids were 'channellised' into the phyllonitic shear zones during reworking. In contrast, the quartzo-feldspathic mylonites preserved in the Scoravick belt have suffered relatively limited retrogression, and the deformation microstructures are consistent with relatively low fluid pressures during reworking. These observations suggest that fluids were less abundant in the Scoravick belt than in either the Cnoc na Croich or Kennavay belts. A model of lower greenschist facies phyllonitisation must therefore explain (a) the 'channellised' nature of fluid-rock interaction, and (b) the limited availability of fluids within the Scoravick belt.

Studies of naturally deformed metamorphic rocks (Oliver 1996) and numerical models of fluid flow during regional metamorphism (Ord & Oliver 1997) suggest that channellised fluid flow is likely to occur within highly strained, actively deforming regions in which the rheology of the deforming rocks contrasts significantly with the rheology of the wallrock. Weak shear zones are thus ideal conduits for channellised fluid flow.

At the onset of reworking, bands of highly strained, upper greenschist facies phyllonite appear to have been preferentially reactivated. A number of recent studies suggest that, under the same pressure and temperature conditions, phyllosilicate-rich

fault rocks are substantially weaker than quartzo-feldspathic fault rocks (e.g. Janecke & Evans 1998; Shea & Kronenberg 1993; Wintsch *et al.* 1995). These observations

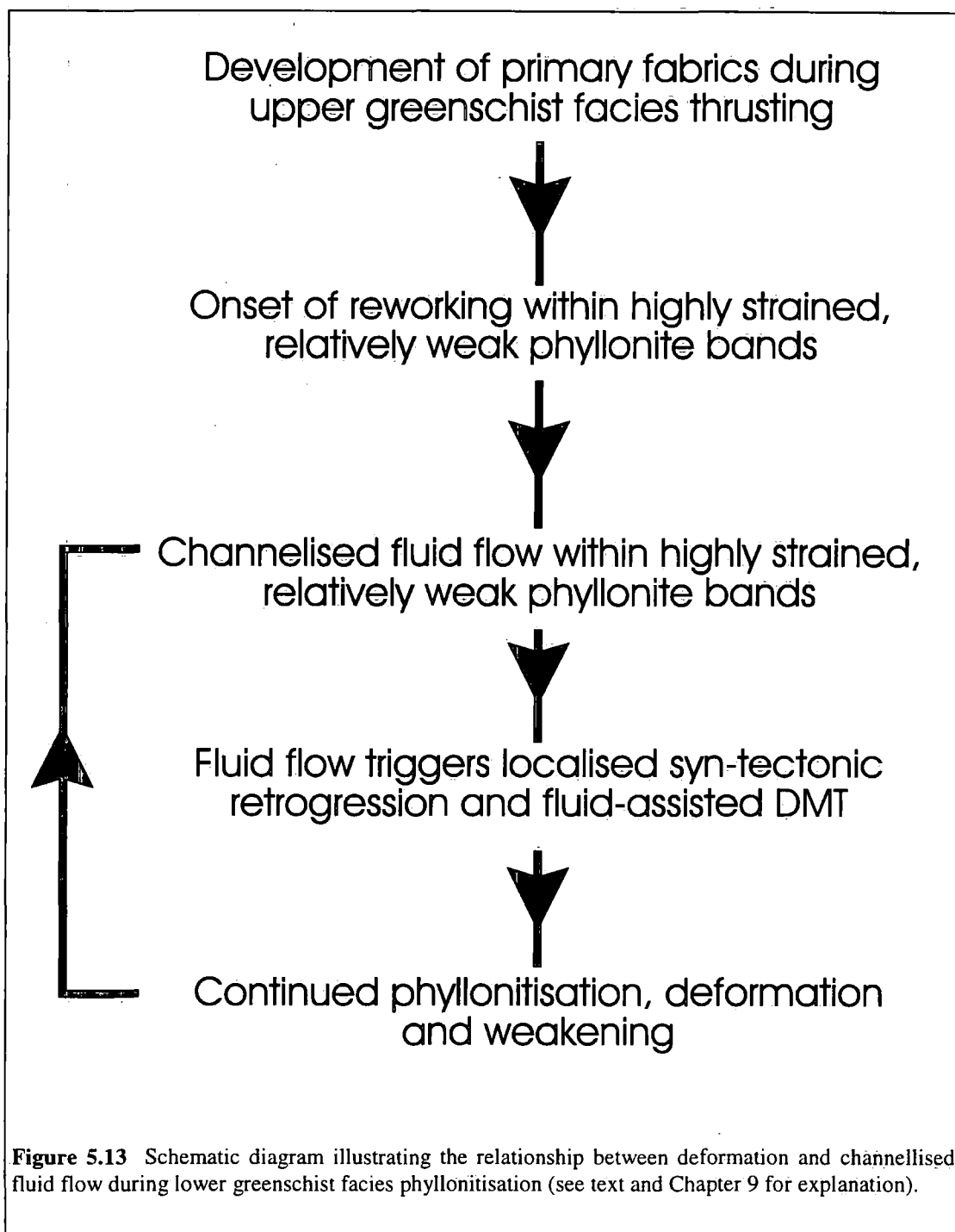


**Figure 5.13** Schematic diagram illustrating the relationship between deformation and channelled fluid flow during lower greenschist facies phyllonitisation (see text and Chapter 9 for explanation).

suggest that the rheology of the highly strained upper greenschist facies phyllonites may have been significantly weaker than that of the surrounding quartzo-feldspathic mylonites (see also section 5.5). It is therefore proposed that at the onset of reworking, the upper greenschist facies phyllonite bands were suitable fluid conduits. If this inference is correct, fluid flow (and therefore retrogression and fluid-rock

interaction) became focused within the phyllosilicate-rich bands. The operation of fluid-assisted DMT processes and the generation of further phyllosilicate minerals could have further weakened the phyllonite belts (see Chapter 6 for a discussion of the role of fluid-assisted DMT). A positive feedback between deformation, fluid-rock interaction and fluid channelling is envisaged, with the result that fluid flow became increasingly focused within the actively deforming, macroscopically ductile phyllonitic shear zones (Fig. 5.13). It is important to emphasise that the outcrop-scale brittle thrusts / cataclasite seams do *not* appear to have been significant fluid pathways during phyllonitisation (cf. the North Uist phyllonite belts; Chapter 6).

Poor inland exposure precludes a detailed study of the relationship between the Scoravick and Kennavay belts. As a result, it is difficult to speculate on the causes of the limited fluid availability within the Scoravick belt. However, the lower greenschist facies *quartzo-feldspathic* Scoravick mylonites appear to have been developed within a package of highly strained upper greenschist facies *quartzo-feldspathic* mylonite. In the absence of more compelling evidence, it is tentatively suggested that the rheological contrast between the Scoravick mylonites and the quartzo-feldspathic host rocks may not have been sufficient to result in channelled fluid flow.

## **5.5 REWORKED & DERIVED FABRICS: DEXTRAL STRIKE-SLIP RELATED PHYLLONITE & DETACHMENT FAULTS**

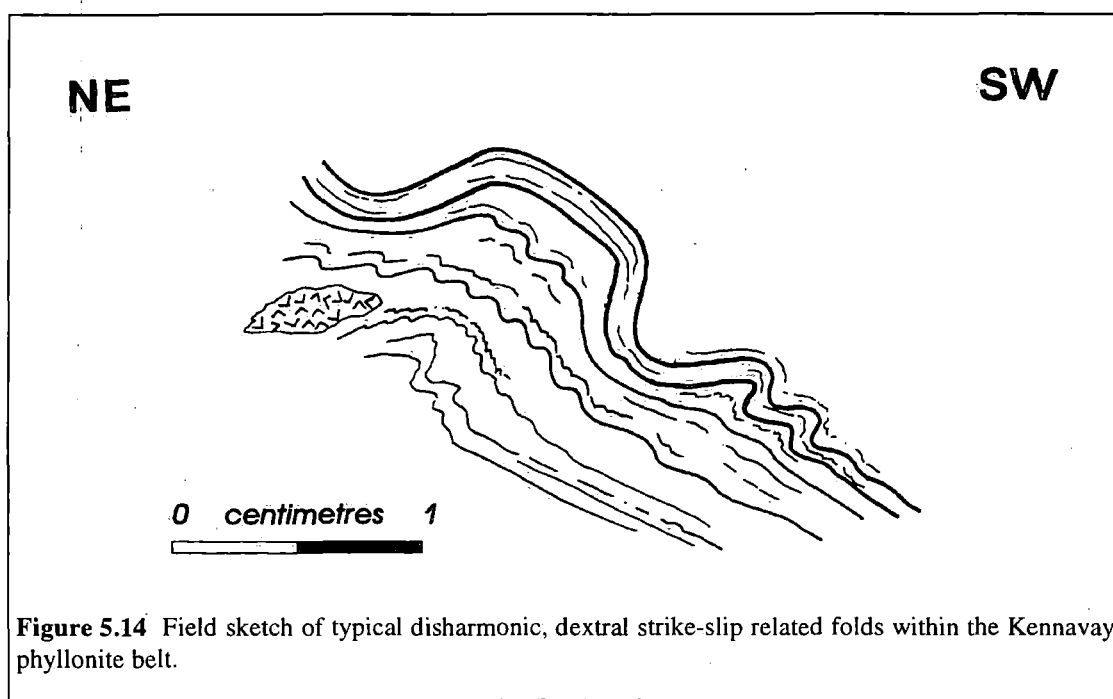
Bands of lower (and locally upper) greenschist facies phyllonite are commonly observed to have been deformed by cascades of SW- and (locally) SE-verging folds. The folds are thought to have developed during a phase of top-to-the-SW dextral strike-slip, which followed the cessation of top-to-the-NE displacements (section 3.2.3.5). A number of foliation-parallel brittle detachment faults cross-cut both the upper and lower greenschist facies phyllonitic fabrics. The aim of the following section is to describe the distribution and style of deformation associated with dextral strike-slip and subsequent brittle faulting.

### **5.5.1 REWORKED FABRICS**

#### **5.5.1.1 Field relationships**

Bands of upper greenschist facies phyllonite, which are preserved within a package of highly strained, thrust-related mylonite at Geo an Ear (NG 247 948) (Fig. 3.7), are commonly observed to have been deformed by gently ENE-plunging crenulations. Centimetre-scale SE-verging folds are locally developed and are characterised by open to close interlimb angles and angular to rounded hinges (see also Sibson 1977b).

The lower greenschist facies phyllonites preserved within the Cnoc na Croich and Kennavay belts are commonly observed to be deformed by millimetre-scale crenulations or cascades of centimetre-scale, SW-verging folds. The intensity of folding within the phyllonite belts is very heterogeneous, although folds tend to be particularly well developed within bands of dark-green (mafic) phyllonite and ultraphyllonite (e.g. NG 2316 9473). The rounded to angular, open to isoclinal folds are typically disharmonic in style, but are characterised by moderately NE-dipping axial planes and by sub-horizontal, predominantly SW-plunging curvilinear fold axes (Figs. 5.9a & b). Box folds and kink bands are locally developed (Fig. 5.14). Asymmetric shear bands fabrics, whose geometry is consistent with top-to-the-SW dextral strike-slip, are locally preserved within the Kennavay belt (NG 2309 9454).



Packages of folded and crenulated lower greenschist facies phyllonite are typically associated with discordant and foliation-parallel quartz-calcite-albite veins and / or with coarse grained polymineralic quartz-calcite-albite 'porphyroclasts' ( $\leq 25\text{cm}$  diameter). The foliation-parallel veins ( $\leq 10\text{cm}$  long;  $\leq 2\text{cm}$  thick) are locally infilled by aggregates of fibrous quartz and calcite. The orientation of the fibres is consistent with vein opening in a direction perpendicular to the phyllonitic foliation. Comparison with similar structures preserved within the better exposed North Uist phyllonite belts (section 6.4.3) suggests that the foliation-parallel veins opened *synchronous* with macroscopically ductile deformation within the Cnoc na Croich and Kennavay belts. Limited exposure precludes detailed study of the quartz-calcite-albite 'porphyroclasts', but it is possible that these polymineralic aggregates may have developed during macroscopically ductile reworking of the syn-tectonic foliation-

parallel veins. Quartz-calcite-albite veins and 'porphyroclasts' are *locally* preserved within packages of unmodified sinistral strike-slip related phyllonite. These observations suggest that whilst the majority of veins and 'porphyroclasts' developed synchronous with dextral strike-slip, some veins probably opened during the earlier phase of sinistral strike-slip related deformation.

### 5.5.1.2 Microstructure

Folded mafic phyllonites comprise alternating bands ( $\leq 0.3\text{mm}$  thick) of chlorite and fine grained albite + sericite + quartz (Plate 5.14). Folded felsic phyllonites comprise alternating bands of quartz and ultrafine grained albite  $\pm$  sericite. Individual chlorite and sericite needles display strong patchy undulose extinction, and are commonly observed to be kinked, especially in fold hinge regions. A weak axial planar fabric is locally developed and is defined by abrupt changes in grain shape preferred orientation within the chlorite-rich layers and / or by variations in the crystallographic preferred orientation of the ultrafine albite grains. Partially sericitised feldspar porphyroclasts and prismatic opaque grains ( $\leq 0.1\text{mm}$  diameter) are commonly observed within phyllosilicate-rich layers. The opaque minerals are typically fringed by aggregates of fibrous quartz and / or calcite, which are oriented parallel to the local trace of the foliation.

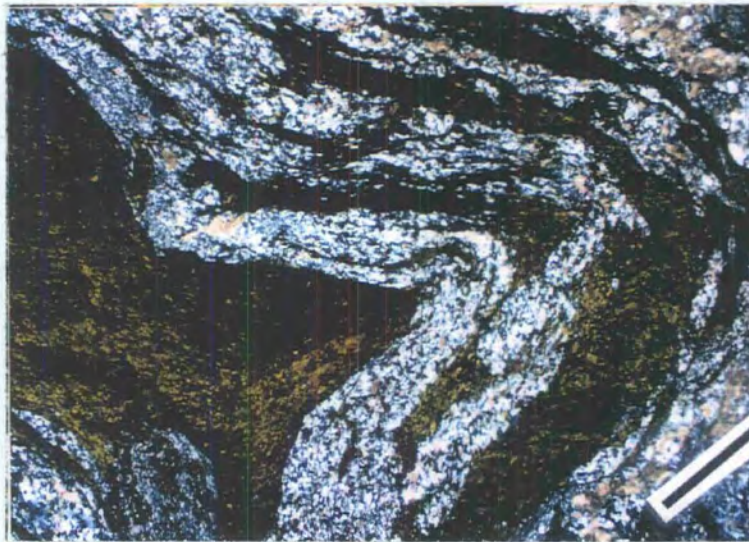


**Plate 5.14** Folded lower greenschist facies mafic phyllonite. The foliation is defined by alternating bands of chlorite and recrystallised quartz and feldspar. Bar parallel to the axial planar foliation, which is defined by changes in extinction of chlorite across the fold axial plane. SSW to right, top-to-SSW shear. Field of view  $12 \times 7.2\text{mm}$ , crossed polars.

Deformed foliation-parallel quartz-calcite-albite veins are widely preserved in packages of folded mafic and felsic phyllonite. The calcite grains ( $\leq 10\text{mm}$  long;

aspect ratios  $\leq 5:1$ ) are typically flattened parallel to either the fold axial planes or parallel to the local trace of the foliation. Flattened calcite grains display sweeping undulose extinction and are cross-cut by two sets of narrow, intersecting deformation twins ( $\leq 0.02\text{mm}$  thick; angle of intersection  $\cong 60^\circ$ ). Quartz-calcite-albite 'porphyroclasts' and / relict feldspar grains are locally preserved in the hinge-zones of millimetre-scale crenulations (see section 5.5.1.3).

### **5.5.1.3 Summary and discussion**

SW- and (locally) SE-verging folds are developed within packages of reworked lower and upper greenschist facies phyllonite. Reworking is thought to have been synchronous with an episode of top-to-the-SW dextral strike-slip. It is important to emphasise that reworked fabrics have *not* been observed anywhere in packages of quartzo-feldspathic mylonite.

#### ***Retrogression and metamorphism during dextral strike-slip***

The reworked phyllonites comprise a stable assemblage of sericite, chlorite, fine grained albite, quartz, calcite, epidote and opaque minerals. The original plagioclase, K-feldspar and hornblende grains have suffered intense (typically complete) alteration to aggregates of hydrous phyllosilicate minerals  $\pm$  albite and epidote. The retrograde minerals display a strong grain shape preferred orientation. In particular, quartz and calcite fibres are locally developed in strain shadows around the margins of opaque grains, whilst the (001) cleavage planes of chlorite and sericite grains are oriented parallel to the trace of the macroscopic foliation. These observations suggest that dextral strike-slip related deformation occurred under hydrous, lower greenschist facies conditions. Furthermore, the presence of intersecting calcite deformation twins is consistent with deformation at temperatures of between  $200^\circ\text{C}$  and  $250^\circ\text{C}$  (Burkhard 1993).

#### ***Operative deformation mechanisms during dextral strike-slip***

Deformation appears to have been accommodated by macroscopically ductile folding and shear band development, and by localised brittle deformation during vein opening. It is postulated that the foliation-parallel veins developed in response to transient, localised increases in the pore fluid pressure during macroscopically ductile deformation (Handy 1989). The orientation of the quartz-calcite vein fibres is consistent with the veins having opened in a purely extensional manner. These observations suggest (a) that the pore fluid pressure locally exceeded the tensile strength of the host rocks, and (b) that the differential stress was relatively low (see

Chapter 6 for a more detailed description and discussion of the syn-tectonic veins formed during reworking).

The precise mechanism of folding is unclear. However, deformed quartz-calcite-epidote veins ('porphyroclasts') are commonly preserved within the hinges of millimetre-scale folds and crenulations, and are widely distributed throughout packages of folded phyllonite. These observations suggest that there may be a causal link between the presence of coarse grained 'porphyroclasts' and the development of folds. It has been proposed that buckle folds are likely to nucleate at point irregularities within a deforming medium (Chapter 10 of Price & Cosgrove 1990). Furthermore, experimental simple shearing of rigid layers within a relatively weak, homogeneous matrix demonstrate that as the competent layers are boudinaged, curvilinear folds develop in the boudin neck regions (Cobbold & Quinquis 1980). It is therefore postulated that flow perturbations adjacent to deformed (possibly boudinaged) quartz-calcite-albite veins and 'porphyroclasts' could have controlled the nucleation of millimetre-scale folds and crenulations. Continued macroscopically ductile deformation may have amplified the original crenulations to produce cascades of asymmetric, centimetre-scale folds.

The different mineralogical layers within packages of felsic and mafic phyllonite appear to have accommodated macroscopic folding by a number of different deformation mechanisms. The presence of kinks and strong patchy undulose extinction suggests that chlorite- and sericite-rich layers accommodated folding by intracrystalline plastic deformation (?dislocation glide) (Bons 1988; Mares & Kronenberg 1993). The fine grain size precludes positive identification of the operative deformation mechanisms within quartz- and albite-rich bands. However, the presence of a weak, axial planar crystallographic fabric in some quartz / albite layers is consistent with the operation of intracrystalline crystal plastic deformation mechanisms. Fibrous strain shadows locally fringe opaque minerals and feldspar porphyroclasts preserved within packages of folded phyllonite. This observation suggests that sites of localised dilatation at the margins of relatively competent grains acted as fluid-assisted diffusive mass transfer sinks during folding.

### **5.5.2 DETACHMENT FAULTS**

SE-dipping, foliation-parallel brittle detachment faults have been observed within, and / or along the margins of the Cnoc na Croich, Kennavay and Aird Riabhach phyllonite belts, and along the upper margin of the Scoravick mylonite belt (Fig. 5.10). The geometries of subsidiary fracture arrays are generally consistent with top-to-the-SE, extensional displacements across the main detachment surfaces. The fault planes are

typically associated with SE- to SSE-plunging slickenlines (Fig. 5.15) and are lined by bands ( $\leq 10\text{cm}$  thick) of gouge and / or brecciated phyllonite / mylonite. The composition of the fault gouge varies from detachment to detachment. Yellow and brown clay-rich gouges, which possess a scaly fault-parallel foliation, are preserved along faults developed within the Cnoc na Croich belt. In contrast, massive carbonate-rich gouges have been observed along faults developed at the margins of the Cnoc na Croich and Aird Riabhach belts. An unusual fault rock, in which angular clasts of brecciated phyllonite 'float' in a matrix of fine grained undeformed chlorite laths, is developed in a detachment fault near the base of the Kennavay belt. The relative ages of the different gouges is unclear from the available field evidence. However, it is apparent that the latest movements along the detachment faults post-date the cessation of macroscopically ductile dextral strike-slip.

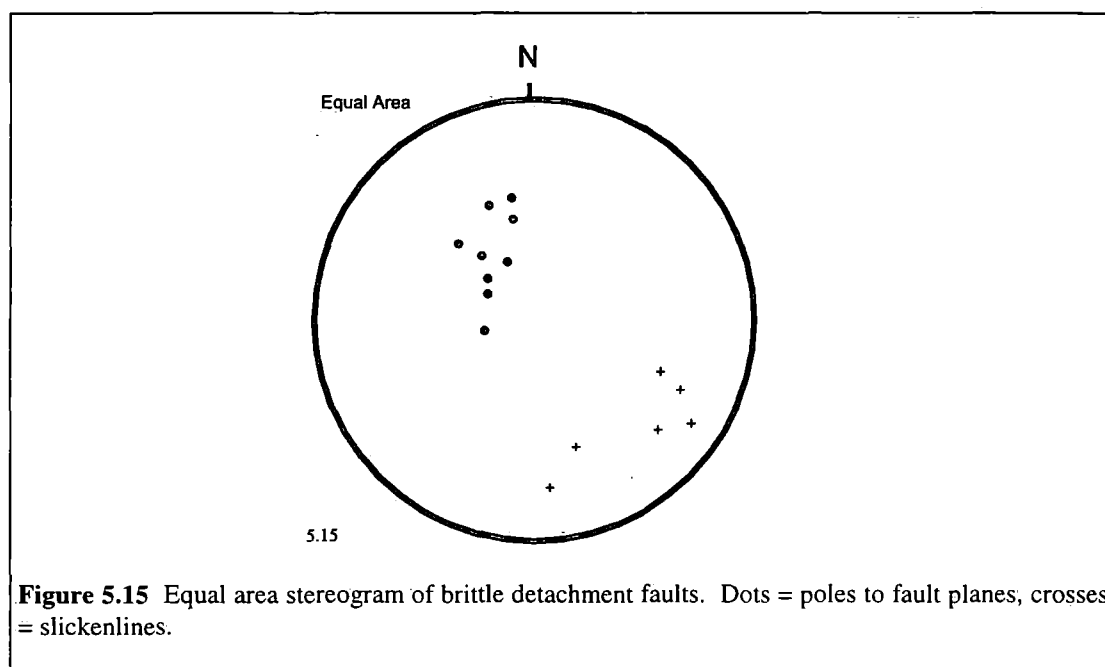


**Figure 5.15** Equal area stereogram of brittle detachment faults. Dots = poles to fault planes, crosses = slickenlines.

### 5.5.3 SYNTHESIS

#### 5.5.3.1 Summary

There is unequivocal evidence that the phyllosilicate-rich fault rocks were reworked during a phase of dextral strike-slip. In contrast, the quartzo-feldspathic mylonites were *not* reworked during dextral strike-slip. Macroscopically ductile, lower greenschist facies reworking within the Cnoc na Croich and Kennavay phyllonite belts was associated with localised, transient brittle deformation caused by high pore fluid pressures. Top-to-the-SE brittle deformation along a number of foliation-parallel detachment faults followed the cessation of macroscopically ductile dextral strike-slip.

### 5.5.3.2 Controls on the distribution of dextral strike-slip related deformation

The available field and microstructural evidence suggests that dextral strike-slip related deformation was preferentially focused into belts of lower and (locally) upper greenschist facies phyllonite. This observation suggests that *the phyllosilicate-rich faults rocks were weak relative both to the upper and lower greenschist facies mylonites and to the relatively unmodified gneisses of the 'foreland' region.*

Two principal mechanisms have been proposed which could account for the apparent weakness of the phyllonite bands on Scalpay. Firstly, high pore fluid pressure during deformation may result in a decrease in the critical shear stress needed for frictional failure and sliding to occur (Rice 1992). Secondly, it has been suggested that the development of intensely aligned aggregates of intrinsically weak phyllosilicate minerals could substantially weaken a fault zone relative to the surrounding quartzofeldspathic crust (so-called 'reaction-softening' processes) (White & Knipe 1978; Janecke & Evans 1988; Rubie 1990) (Chapter 1).

There is little evidence to suggest that reworking within the upper greenschist facies phyllonite band preserved at Geo an Ear occurred under a high pore fluid pressure regime. This observation is consistent with *the intrinsic weakness of the phyllosilicate-rich faults rocks having been the principal control on reworking at Geo an Ear.* In contrast, the abundance of deformed syn-tectonic veins within the lower greenschist facies Cnoc na Croich and Kennavay belts is consistent with a high pore fluid pressure regime during reworking. The veins are predominantly tensile, which suggests (a) that the *differential* stress during vein opening was low ( $[\sigma_1 - \sigma_3] \leq 4T$ ; where  $[\sigma_1 - \sigma_3]$  = differential stress; T = tensile strength of the host rock), and (b) that the pore fluid pressure locally exceeded the minimum principal stress ( $\sigma_3$ ). The role of hydraulic fracturing during reworking is discussed further, in relation to the better exposed and more extensively reworked North Uist phyllonite belts, in Chapters 6 and 9.

### 5.5.3.3 Age and significance of detachment faults

The observed field relationships clearly demonstrate that the latest phase of movement along the foliation-parallel brittle detachment faults must post-date the cessation of macroscopically ductile strike-slip. However, the age of detachment *initiation* is equivocal. Regional strain compatibility and kinematic considerations suggest that the detachment faults may have initiated synchronous with top-to-the-SW dextral strike-slip reworking, in order to accommodate the imposed regional top-to-the-S shear (Fig. 3.22; section 3.2.3.5). Whether detachment initiation was synchronous with, or subsequent to macroscopically ductile reworking, the distribution of detachment faults is consistent with the faults having localised along pre-existing competence

contrasts i.e. *the geometry of the brittle detachment faults was inherited from that of the pre-existing ductile fabrics.*

## 5.6 SUMMARY

- Macroscopically ductile top-to-the-NW thrusting was associated the development of upper greenschist facies mylonite and phyllonite.
- Deformation was accommodated by intracrystalline crystal plastic deformation in quartz and phyllosilicate grains. Transient increases in pore fluid pressure resulted in localised brittle deformation.
- Mylonitisation was followed by the development of predominantly SE-dipping brittle compressional faults and cataclasites.
- Bands of highly strained upper greenschist facies phyllonite were reworked during lower greenschist facies phyllonitisation and sinistral strike-slip.
- Deformation during sinistral strike-slip was ultimately controlled by fluid-assisted diffusive mass transfer processes within the lower greenschist facies phyllonite belts.
- Deformation within the lower greenschist facies phyllonite belts led to channelled fluid flow. The brittle thrust faults and cataclasite seams were *not* important fluid pathways during phyllonitisation.
- Subsequent dextral strike-slip was accommodated entirely within pre-existing upper and lower greenschist facies phyllonite belts.
- Fault zone weakening was primarily caused by reaction softening processes.

The textural evolution of the OHFZ on Scalpay is summarised in Figure 9.3a, and will be discussed further in Chapter 9.

## 6. NORTH UIST

### 6.1 INTRODUCTION

#### 6.1.1 INTRODUCTION AND AIMS

The predominantly N-S trending segment of the Outer Hebrides Fault Zone exposed on North Uist has experienced a complex, polyphase kinematic, textural and metamorphic evolution (Fig. 3.28; section 3.4; Table 3.2).

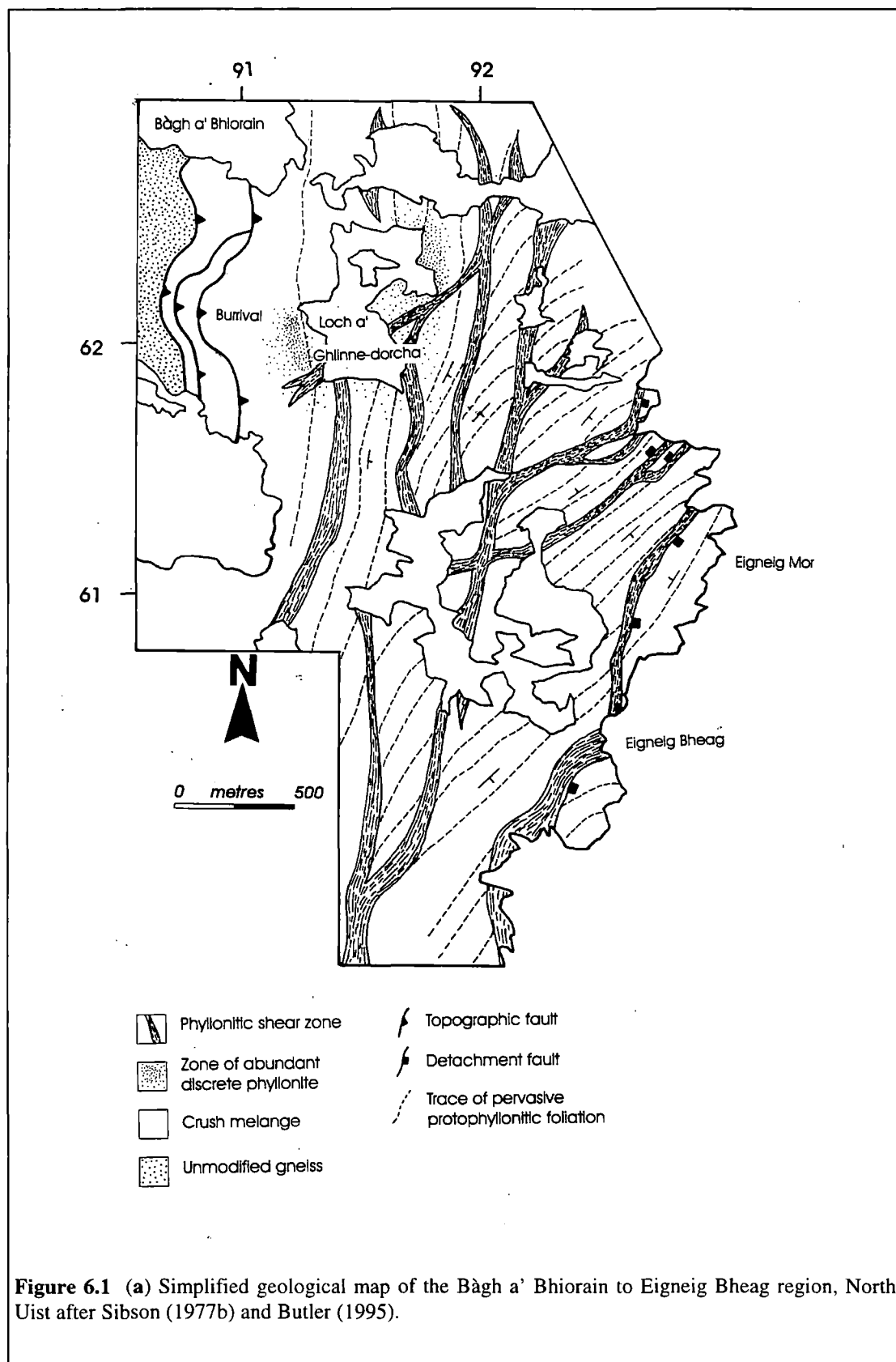
Regional top-to-the-W thrusting was associated with the development of cataclasites, pseudotachylytes and brittle faults (the 'crush melange' and 'pseudotachylyte-ultracataclaste crush zones' of Sibson 1977b; section 3.4.2). Brittle deformation was followed by an episode of lower greenschist facies retrogression, hydration and phyllonitisation during regional sinistral transpression and subsequent top-to-the-NE sinistral strike-slip (section 3.4.3). The locus of intense retrogression and / or fluid-rock interaction corresponds closely to the outcrop of the crush melange, which suggests that the primary fabric (i.e. the crush melange and associated faults) exerted a strong control on distribution of the phyllonitic fabrics (Figs. 3.44 & 3.45; sections 3.7.2 & 3.7.3).

The phyllonitic shear zones were subsequently reworked during regional top-to-the-E or -SE transtension or extension. The locus of intense retrogression and / or fluid-rock interaction appears to have been focused into actively deforming shear zones and areas of strike-slip related phyllonite (Fig. 3.44; sections 3.7.1 & 3.7.2). These observations suggest (a) that phyllonitic shear zones were weak relative to both the Lewisian gneisses and to the cataclastically-deformed host rocks (see also Butler *et al.* 1995), and (b) that phyllonitic shear zones acted as long-lived fluid pathways within the OHFZ on North Uist (section 3.7).

The aims of this chapter are twofold:

- (1) To establish the nature, distribution and principal controls on phyllonitisation along the OHFZ on North Uist, and in particular, to examine the relationships between the crush melange (i.e. the primary fabric) and the transpression / strike-slip related phyllonitic fabrics (i.e. the derived fabrics).
- (2) To determine the distribution of extensionally reworked phyllonites, and to describe the different styles of deformation associated with extensional reworking within the phyllonite belts.

The role played by fluids during deformation will be emphasised throughout this chapter.



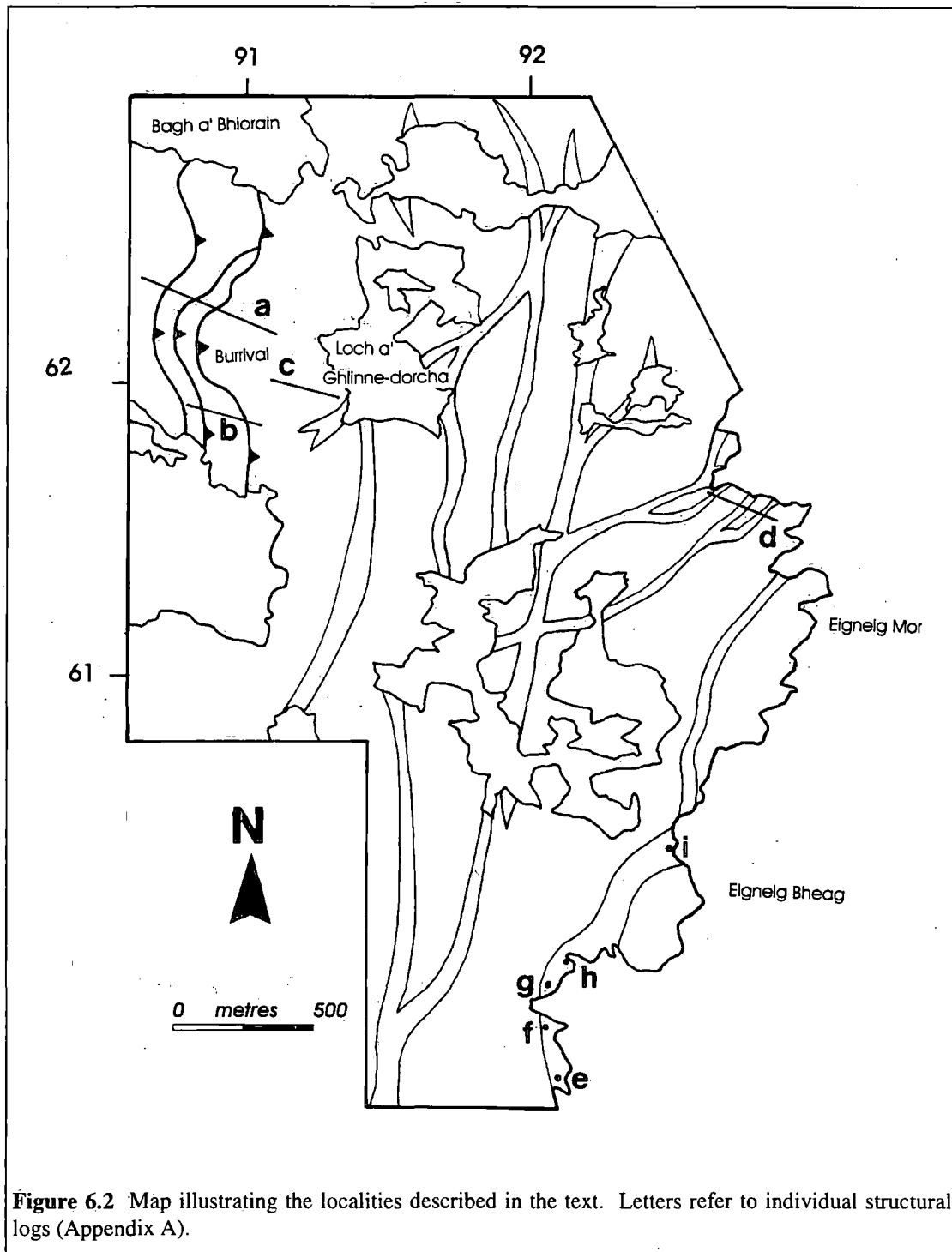


**Figure 6.2** Map illustrating the localities described in the text. Letters refer to individual structural logs (Appendix A).

### 6.1.2 STUDY AREA AND CHAPTER LAYOUT

Extensive field studies of the Outer Hebrides Fault Zone on North Uist have been conducted in the region between Burrival (NF 909 622) and Eigneig Bheag (NF 920 595) (Figs. 6.1 & 6.2). The fault rocks and structures which outcrop in the Burrival to Eigneig Bheag region are easily accessible and are representative of the fault rocks

and structures which outcrop along the OHFZ in eastern North Uist as a whole (Fig. 3.28; section 3.4) (Sibson 1977b; Butler 1995; Imber *et al.* 1997).

The western limit of the study area is dominated by Burrival hill (NF 909 622), which rises abruptly from the flat moorland to the west of the fault zone. To the east, between Burrival and Eigneig Bheag, the topography of the fault zone is more subdued and is characterised by low, undulating moorland which is dissected by numerous lochs, gullies and coastal inlets. Exposure is excellent along coastal sections, but the rocks are badly weathered and less well exposed further inland.

The base of the Outer Hebrides Fault Zone is marked by a number of eastward dipping 'topographic' faults (Sibson 1977b) which cross-cut the crush melange and outcrop along the western and southern flanks of Burrival hill. The crush melange is at least 1000m thick and outcrops between Burrival and the east coast. The crush melange is deformed and overprinted by a heterogeneously developed, macroscopically ductile phyllonitic fabric (section 3.4.3). Bands of discrete phyllonite outcrop between Burrival (NF 909 622) and Loch a' Ghlinne-dorcha (NF 913 625). In the region to the east of Loch a' Ghlinne-dorcha, the crush melange is overprinted by a pervasive protophyllonitic fabric and by a network of lower greenschist facies phyllonitic shear zones (Figs. 3.31 & 6.1).

The remainder of this chapter comprises detailed field and microstructural descriptions of the different fault rocks and structures which outcrop between Burrival and Eigneig Bheag. Each section focuses on particularly well exposed examples of each fault rock or structure, and the distribution of field localities is illustrated in Figure 6.2. A description of the crush melange (i.e. the primary fabric) (section 6.2) is followed by an account of the transpression- and strike-slip related phyllonitic fabrics (i.e. the derived fabrics) (section 6.3). The fault rocks and structures associated with extensional reactivation (i.e. the reworked fabrics) are described in section 6.4.

## **6.2 PRIMARY FABRIC: THE CRUSH MELANGE**

The crush melange developed in response to regional top-to-the-W thrusting along the OHFZ in North Uist (section 3.4.2.4). The crush melange is believed to represent the earliest phase of post-Laxfordian deformation (post D<sub>13</sub>' of Fettes *et al.* 1992), and is therefore considered to be the 'primary fabric' on North Uist. The aim of the following section is to describe the fault rocks and structures developed within the crush melange, as a context in which to understand the development of the overprinting phyllonitic fabrics.

## 6.2.1 FIELD RELATIONSHIPS

Structural logs have been constructed along well exposed sections within the crush melange, to the west and to the southeast of Burrival summit (NF 9054 6233 to NF 9091 6217 and NF 9073 6195 to NF 9100 6191 respectively) (Fig. 6.2a & b).

### 6.2.1.1 The fault zone base

In the Burrival region, the base of the Outer Hebrides Fault Zone is marked by a series of faults which dip at between 25° and 35° towards the east (Sibson 1977b; Butler 1995) (Fig. 6.1). The lowermost fault forms an abrupt boundary between the relatively unmodified banded gneisses of the 'foreland' and the highly deformed crush melange to the east (section 3.4.1). The actual fault surfaces are poorly exposed, and their outcrop is marked by distinct topographic breaks in slope. The largest of these 'topographic' faults (Butler 1995) may be traced for a few hundred metres along the southern and western flanks of Burrival hill (Fig. 6.1). The topographic faults appear to cross-cut all the other fault rocks and structures developed within crush melange (section 6.2.1.2) and may thus be relatively late features. Where topographic faults are exposed (e.g. NF 908 619), the fault planes are typically associated with down-dip plunging slickenlines and an array of subsidiary faults and fractures. The geometries of the minor faults are consistent with either localised extensional or localised compressional displacements along the main fault planes.

### 6.2.1.2 The crush melange

The crush melange comprises blocks of relatively undeformed gneiss which 'float' in a pale green matrix of crushed gneiss, cataclasite and devitrified pseudotachylyte (Plate 6.1). On textural grounds, the crush melange may be described as a 'protocataclasite' (*sensu* Sibson 1977a), although it is important to emphasise that the intensity of deformation varies significantly throughout the crush melange.

In the lowermost 100m of the crush melange (i.e. in the region to the west of Burrival summit), the gneissose banding is widely preserved, but is cross-cut by multiple generations of brittle faults, cataclasite seams and devitrified pseudotachylyte veins (Figs. 6.3a & b). However, bands ( $\leq 2\text{m}$  thick) of more intense brittle deformation, in which the gneissose fabric is completely destroyed, are locally developed in the hangingwalls of topographic faults (section 6.2.1.1; see also Sibson 1977b) (Fig. 6.2a & b). These zones of intense brittle deformation comprise angular to rounded clasts of randomly oriented, fractured gneiss ( $\leq 20\text{cm}$  diameter) which 'float' in a matrix of pale green ultracataclasite and / or devitrified pseudotachylyte.

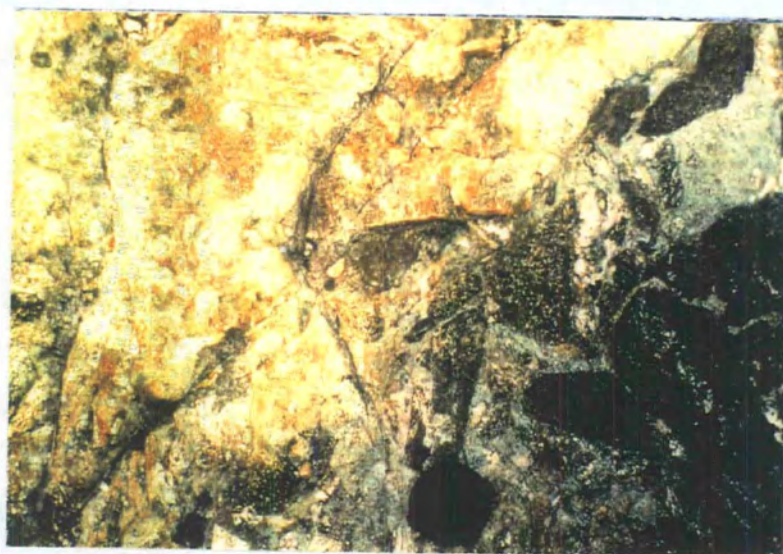
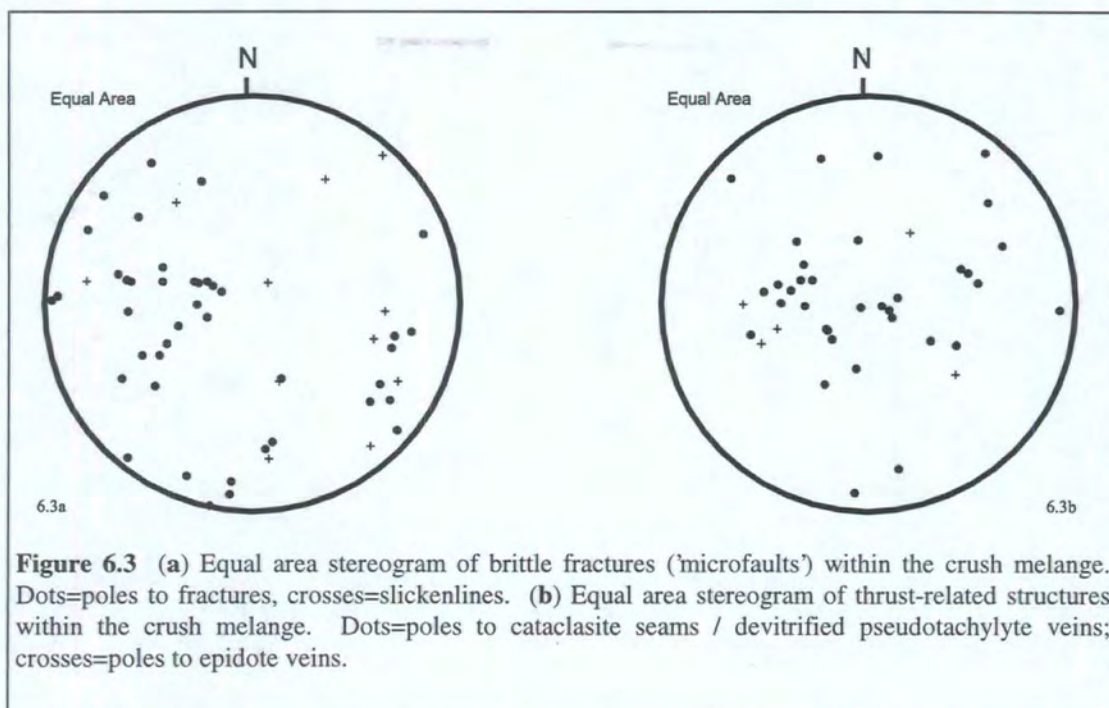


**Plate 6.1** Crush melange from Burrival region (NF 908 619). Randomly oriented blocks of felsic and mafic gneiss (black / creamy) 'float' in an ultrafine-grained matrix of cataclasite / devitrified pseudotachylyte (grey / brown). Entire assemblage is cross-cut by brittle 'microfaults' (arrowed).

In the uppermost 900m of the crush melange (i.e. in the region to the east of Burrival summit), the *overall* intensity of brittle deformation appears to be greater than that observed in the region to the west of Burrival summit. To the east of Burrival, the crush melange comprises blocks of randomly oriented, fractured gneiss which 'float' in an apparently isotropic matrix of pale green cataclasite and / or devitrified pseudotachylyte (Fig. 6.2b). The blocks of gneiss range from microscopic grain-scale

aggregates up to 100m in diameter (e.g. Eigneig Bheag; NF 920 595). The largest blocks are typically massive amphibolites and were probably derived from Older Basic pods (section 2.2.2.1).

The blocks of gneiss, the cataclasites and the devitrified pseudotachylyte veins are commonly observed to be cross-cut by networks of predominantly E- or W-dipping brittle faults and fractures (the 'microfaults' of Sibson 1977b & Butler 1995) (Plate 6.1). The 'microfaults' are associated with predominantly down-dip plunging slickenlines (Fig. 6.3a), and the geometries of subsidiary fracture arrays are consistent with either localised compressional or localised extensional displacements during faulting. Butler (1995) has stated that compressional 'microfaults' outnumber extensional 'microfaults' by a ratio of 3:2.

Both the crush melange and the microfaults are locally cross-cut by an array of sub-vertical, N-S trending quartz  $\pm$  quartz-chlorite veins. These veins are thought to have developed during a phase of regional top-to-the-E or -SE extension along the OHFZ in North Uist (section 3.4.3.5) and are discussed more fully in a later part of this chapter (section 6.4).

## 6.2.2 MICROSTRUCTURES

The microstructures observed within the crush melange are extremely heterogeneous, and reflect (a) the variety of fault rocks and structures observed at the outcrop scale and (b) the effects of lower greenschist facies retrogression (section 3.4.2.4).

### 6.2.2.1 Deformation microstructures

Three distinct microstructural domains have been recognised within the crush melange, which correspond to the lithologies observed in the field.

#### *Domains of relatively undeformed gneiss*

Domains of relatively undeformed gneiss comprise interlocking aggregates of equigranular feldspar (or hornblende) grains ( $\leq$  1mm diameter), which isolate pockets of flattened quartz ( $\leq$  6mm long), laths of biotite and / or euhedral to subhedral hornblende grains (cf. section 2.2.2.1). The feldspar grains display strong patchy undulose extinction and are partially altered to aggregates of fine-grained sericite and epidote (see section 6.2.2.2). Quartz grains also display strong patchy undulose extinction and poorly defined optical subgrains are locally developed. Intragranular fractures are commonly observed to cross-cut both quartz and feldspar grains. The fractures are *locally* infilled by aggregates of fine-grained quartz ( $\leq$  0.02mm diameter) or feldspar ( $\leq$  0.005mm diameter)  $\pm$  calcite  $\pm$  opaque minerals  $\pm$  trails of ultrafine high

relief fluid inclusions ( $\ll 0.005\text{mm}$  diameter). Significant shear displacements of the host grains have not been observed across the traces of the intragranular fractures, which is consistent with a purely tensile mode of fracture opening.

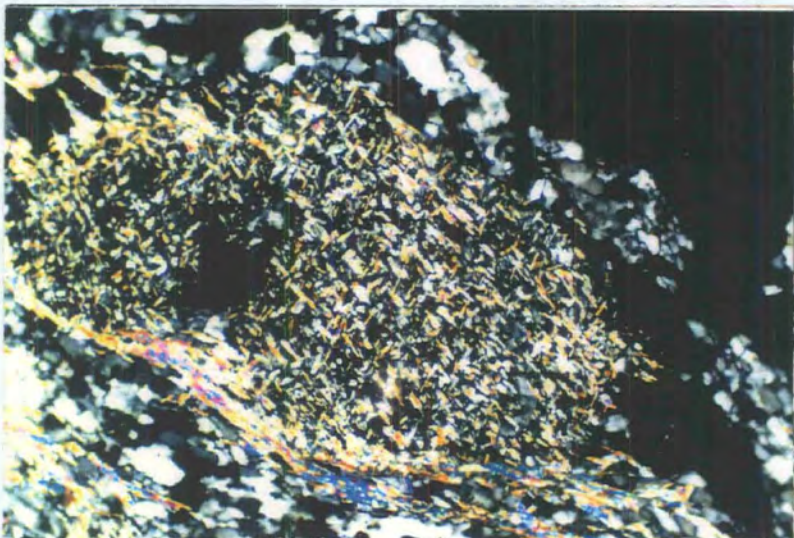


**Plate 6.2** (a) Transgranular shear fractures (dark seams oriented at  $c.45^\circ$  to long axis of photomicrograph) cross-cut relatively undeformed banded gneiss host rock. Feldspar grains partially altered to aggregates of sericite (grey / brown speckles). Field of view  $6 \times 3.7\text{mm}$ , crossed polars. (b) Detail of partially altered feldspar grain. Note that sericite needles *within* feldspar grain define an interlocking 'mesh' texture. Field of view  $0.66 \times 0.4\text{mm}$ , crossed polars.

### *Domains of intensely fractured gneiss*

Domains of intensely fractured gneiss typically form sub-planar bands, of variable width, which cross-cut domains of relatively undeformed gneiss. The domains of intensely fractured gneiss comprise a network of closely spaced, interconnected

transgranular fractures which locally dismember the original gneissose fabric (Plate 6.2). The closely-spaced fractures anastomose around slivers and wedges (aspect ratios  $\leq 6:1$ ) of relatively undeformed gneiss and clasts of quartz, hornblende and partially sericitised feldspar. The size of these clasts is very variable and is controlled by the fracture spacing. The fractures are typically infilled by aggregates of fine-grained epidote, quartz and feldspar. Structures preserved within the wall rocks cannot be correlated across these zones of intense brittle deformation, which suggests that the transgranular fractures have accommodated significant shear displacements.

#### *Domains of cataclasite / devitrified pseudotachylyte*

Glassy (vitreous) pseudotachylyte is not preserved within the crush melange. Cataclasite and devitrified pseudotachylyte both comprise randomly oriented clasts of quartz, partially sericitised feldspar  $\pm$  hornblende which 'float' in a matrix of ultrafine-grained quartz, albite, epidote, sericite and opaque minerals (individual grain  $\ll 0.005\text{mm}$  diameter) (Plate 6.3).



**Plate 6.3** 'Cataclasite' seam (dark band oriented at  $c.45^\circ$  to long axis of photomicrograph) cross-cuts banded gneiss host rocks. Dark brown matrix comprises aggregates of ultrafine-grained quartz, feldspar, hornblende and opaque minerals. Note that feldspar grains preserved in the host rock have suffered partial alteration to fine grained sericite needles. Field of view  $1.3 \times 0.77\text{mm}$ , crossed polars.

The devitrified nature of the fine-grained matrix makes distinction between pseudotachylyte and cataclasite extremely difficult, both in the field and in thin section (Walker 1990). The most reliable method for distinguishing the two types of fault rock is based on the nature of the clasts which are preserved within the fine grained matrix, and is summarised in Table 6.1. The obvious shortcoming of this

classification scheme is that it is extremely difficult to distinguish clast-poor devitrified pseudotachylyte from clast-poor ultracataclasite. As a result, it is not possible to make any meaningful estimates of the relative proportions of cataclasite and pseudotachylyte preserved within the crush melange. Where it is not possible to distinguish cataclasite from pseudotachylyte, these fault rocks will henceforth be referred to as 'cataclasites'.

<b>Clasts</b>	<b>Cataclasite</b>	<b>Devitrified pseudotachylyte</b>
<b>Size</b>	Very variable (may vary by up to 3 orders of magnitude within a single thin section).	Very variable (may vary by up to 3 orders of magnitude within a single thin section).
<b>Composition</b>	Hornblende, quartz and feldspar.	Predominantly quartz and feldspar; hornblende rare to absent.
<b>Roundness</b>	Predominantly angular.	Rounded to angular.
<b>Margins</b>	Injection veins within clast margins generally absent.	Matrix-infilled injection veins and 'plucking' along intersecting mineral cleavage planes at clast margins.

**Table 6.1** Summary of the main microstructural features used to distinguish devitrified pseudotachylyte from cataclasite. Based on Sibson (1977b), Walker (1990), Butler (1995), and on the present author's own observations.

### 6.2.2.2 Microstructures associated with low grade alteration

It has been demonstrated that the crush melange has experienced partial retrogression under fluid-rich, lower greenschist facies conditions (section 3.4.2.4) (see also Butler 1995). The following sections describe the nature and distribution of low grade alteration observed throughout the crush melange.

### ***Retrogression within domains of relatively undeformed gneiss***

Over 70% of the feldspar grains preserved within domains of relatively undeformed gneiss display evidence for partial alteration to aggregates of fine grained sericite and epidote. Sericite needles ( $\leq 0.003\text{mm}$  wide) define well developed mesh textures (Plate 6.2b), and occupy between 20% and 60% of the surface area of host feldspar grains. Laterally discontinuous sericite strands ( $\leq 0.05\text{mm}$  thick;  $\leq 0.5\text{mm}$  long) are *locally* developed, both within feldspar grains (intragranular sericite strands) and along feldspar grain boundaries (intergranular sericite strands).

Biotite grains are pseudomorphed by chlorite, but hornblende appears to have largely escaped the effects of low grade alteration.

### ***Retrogression within domains of intensely fractured gneiss, cataclasite and devitrified pseudotachylyte***

Cataclasite seams, devitrified pseudotachylyte veins, transgranular fractures and associated clasts preserved within the crush melange are typically overprinted by aggregates of fine grained ( $\ll 0.01\text{mm}$  diameter) epidote, opaque minerals  $\pm$  chlorite (Plate 6.4). At high magnifications (using backscattered SEM imaging) individual epidote grains appear to be completely undeformed (Fig. 6.4), which suggests that epidote growth must post-date pervasive fracturing, cataclasis and pseudotachylyte generation.

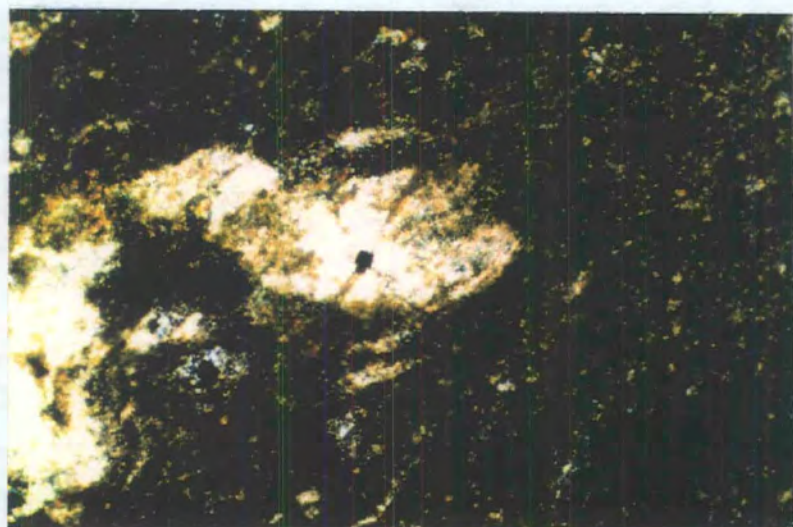


**Plate 6.4** Detail of partially sericitised feldspar clast preserved within a 'cataclasite' seam (dark brown matrix) in the crush melange. Note that the margins of the clast appear to be 'fuzzy' owing to post-tectonic epidote overgrowths. Field of view  $1.3 \times 0.77\text{mm}$ , plane polarised light.

Feldspar clasts preserved within 'cataclasite' seams are partially altered to aggregates of fine-grained sericite and epidote. Sericite accounts for between 20% and 60% of the surface area of host grains, meaning that the feldspar grains preserved within domains of cataclasite / devitrified pseudotachylyte have experienced a similar degree of alteration as the feldspar grains preserved in domains of relatively undeformed gneiss.

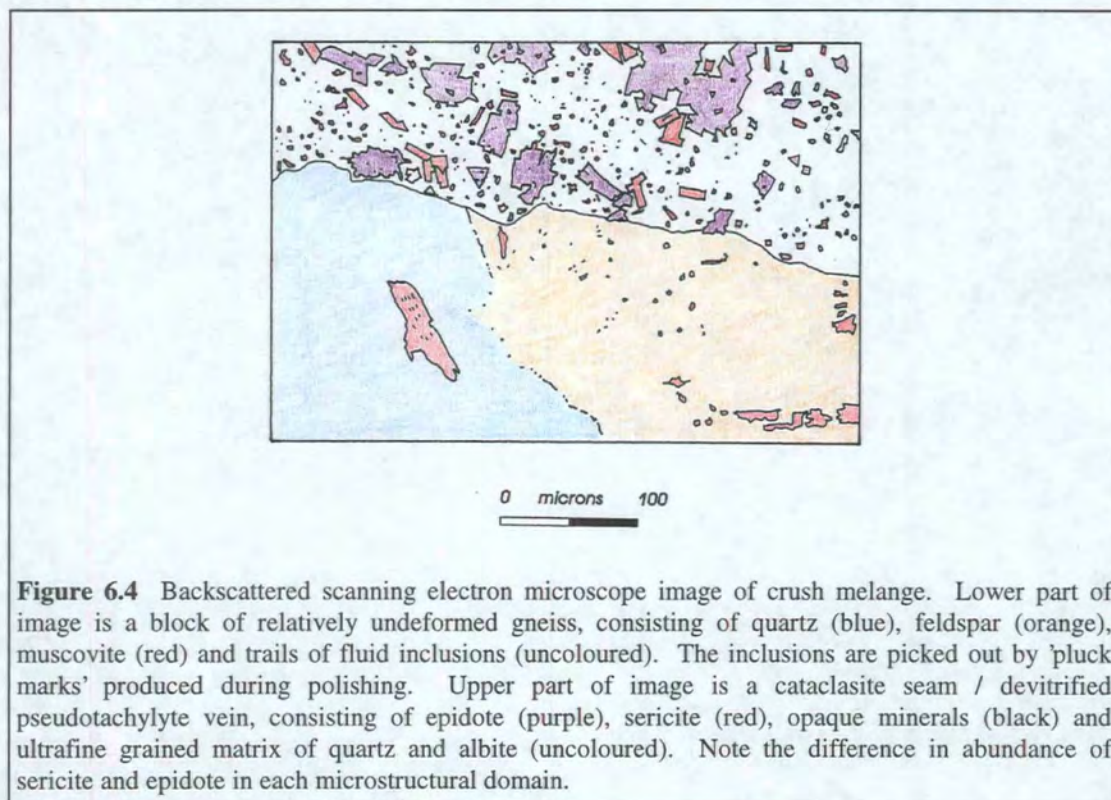


**Figure 6.4** Backscattered scanning electron microscope image of crush melange. Lower part of image is a block of relatively undeformed gneiss, consisting of quartz (blue), feldspar (orange), muscovite (red) and trails of fluid inclusions (uncoloured). The inclusions are picked out by 'pluck marks' produced during polishing. Upper part of image is a cataclasite seam / devitrified pseudotachylyte vein, consisting of epidote (purple), sericite (red), opaque minerals (black) and ultrafine grained matrix of quartz and albite (uncoloured). Note the difference in abundance of sericite and epidote in each microstructural domain.

### 6.2.3 SUMMARY AND DISCUSSION

The crush melange comprises an assemblage of fractured gneisses, cataclasite seams and devitrified pseudotachylyte veins. The intensity of brittle deformation is extremely heterogeneous at all scales of observation. In regions of relatively undeformed gneiss (e.g. to the west of Burrival summit), the banding is cross-cut by isolated brittle fractures, cataclasite seams and devitrified pseudotachylyte veins. More highly deformed regions (e.g. to the east of Burrival summit) are characterised by blocks of randomly oriented, fractured gneiss (whose dimensions may vary by up to five orders of magnitude) which 'float' in a matrix of ultrafine-grained quartz, feldspar and epidote.

### 6.2.3.1 Development of the crush melange

The onset of brittle deformation appears to be marked by the development of intragranular extension fractures and networks of through-going transgranular shear fractures. Continued shearing along the networks of transgranular fractures may have resulted in widespread cataclasis and pseudotachylyte generation (see Lloyd & Knipe 1992; Magloughlin 1992; Swanson 1992). However, intragranular tensile fractures developed within quartz and feldspar grains are locally infilled by trails of fluid inclusions and aggregates of fine-grained quartz, feldspar and / or calcite. These observations are consistent with syn-tectonic fracture healing, which was probably controlled by localised (?grain-scale) diffusive mass transfer processes (Lloyd & Knipe 1992). However, diffusive mass transfer does not appear to have been an important mechanism of strain accommodation. It is therefore postulated that the crush melange developed entirely within the 'frictional regime' described by Schmid & Handy (1991) (see also Sibson 1977a; Butler 1995).

### 6.2.3.2 The distribution of low grade alteration

Evidence for lower greenschist facies alteration is widespread, but heterogeneously distributed throughout the crush melange. Feldspar grains are partially altered to aggregates of fine-grained sericite and epidote, and the intensity of feldspar alteration appears to be similar in each microstructural domain. Aggregates of undeformed epidote and opaque minerals are commonly observed to overprint the 'cataclasite' seams and transgranular fractures, but have *not* been observed within domains of relatively undeformed gneiss (Fig. 6.4). Two important conclusions may be drawn from these observations.

Firstly, greenschist facies alteration must entirely post-date the main phase of pervasive brittle deformation within the crush melange. The timing of low grade alteration relative to 'microfaulting' (section 6.2.1.2) will be discussed further in section 6.3.

Secondly, the absence of undeformed epidote and opaque minerals in domains of relatively undeformed gneiss suggests that the transgranular fractures, cataclasite seams and pseudotachylyte veins have experienced a *greater* degree of alteration than the blocks of relatively intact gneiss. The results of whole-rock geochemical analyses of the crush melange are also consistent with enhanced alteration along transgranular fractures and 'cataclasite' seams (see Chapter 8). These observations suggest that *the distribution of low grade alteration within the crush melange was strongly influenced by the pre-existing brittle deformation microstructures*. If correct, this hypothesis has important implications for the mechanisms of phyllonitisation on North Uist, and is discussed further in the following section.

### 6.3 DERIVED FABRICS: TRANSPRESSION AND STRIKE-SLIP RELATED PHYLONITES

A macroscopically ductile phyllonitic fabric is widely developed in the region to the east of Burrival hill (Fig. 6.1). The fabric is extremely heterogeneous and preserves evidence for at least three different phases of deformation.

It has been demonstrated that the oldest phyllonitic fabrics directly overprint the crush melange, and developed synchronous with regional sinistral transpression and subsequent sinistral strike-slip along the OHFZ (section 3.4.3.5). The following section describes the relationship between the crush melange (i.e. the primary fabric) and the transpression / strike-slip related phyllonites (i.e. the derived fabrics), with the aim of understanding the processes which controlled phyllonitisation along the OHFZ on North Uist.

#### 6.3.1 DISCRETE PHYLONITES

Bands of discrete phyllonite are commonly observed in the region between Burrival and Loch a' Ghlinne-dorcha (NF 909 622 to NF 913 618), and are locally preserved in the region between Loch a' Ghlinne-dorcha and Eigneig Mor (NF 915 622 to NF 930 613) (Figs. 6.1 & 6.2c).

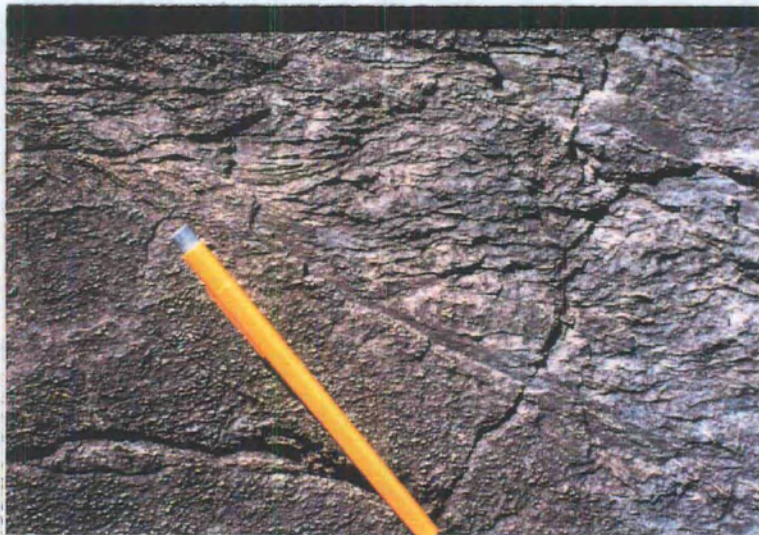


**Plate 6.5** Type 1' discrete phyllonite band developed in block of relatively undeformed gneiss preserved within the crush melange, Burrival region (NF 910 622). Note that the margins of the band are extremely abrupt and the host rocks do not appear to be foliated. Horizontal surface, NE to right.

### 6.3.1.1 Field relationships

Discrete phyllonites are laterally discontinuous (on the outcrop-scale), centimetre- to metre-scale bands of finely foliated, pale green phyllonite, protophyllonite and / or ultraphyllonite. The undulating foliation is defined by aggregates of aligned phyllosilicate minerals and flattened feldspar grains (aspect ratios typically  $\geq 10:1$ ), and is typically oriented parallel to the margins of the host phyllonite band. The phyllonitic foliation is associated either with a WNW-ESE trending *transpression*-related mineral lineation, or with a NE-SW trending *strike-slip* related mineral lineation (Fig. 3.32; section 3.4.3.1). Two types of discrete phyllonite have been recognised in North Uist. Type 1' phyllonites are isolated bands which occur within regions of unmodified crush melange (section 6.2) or in regions of pervasive protophyllonite (section 6.3.2) (Plate 6.5; Fig. 6.5). Type 2' phyllonite bands form anastomosing, metre-scale networks and are developed within regions of pervasive protophyllonite (section 6.3.2) (Fig. 6.6).

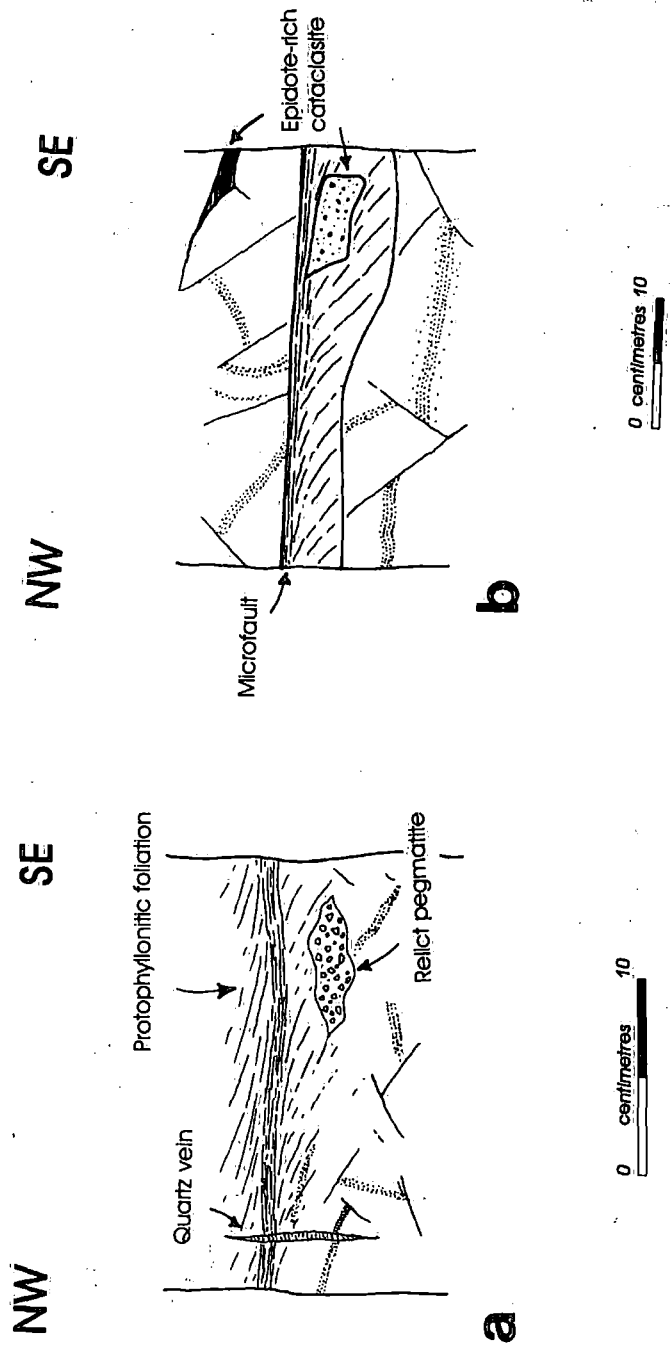


**Figure 6.5** Thrust-related Type 1 discrete phyllonite bands, Loch a' Ghlinne-dorcha region. (a) Continuous Type 1 phyllonite band developed in fractured gneiss. Note extension-related vein (section 6.4) cross-cuts crush melange and thrust-related phyllonitic fabric (vertical surface) (NF 9182 6247). (b) Discontinuous Type 1 phyllonite band developed within a relict 'cataclasite' seam in region of fractured gneiss. Note the upper margin of the phyllonite band is bounded by a brittle 'microfault' (vertical surface). (NF 9083 6209).

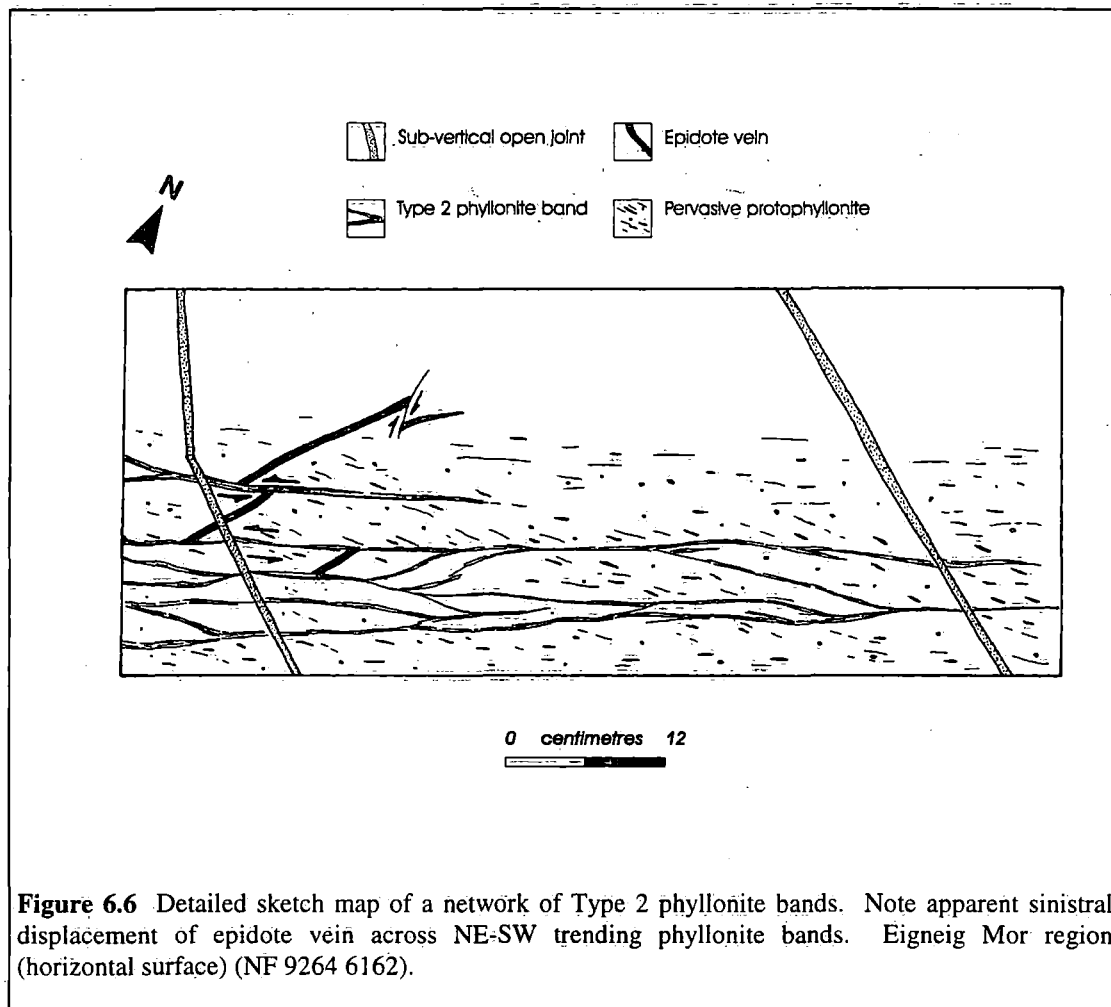


**Figure 6.6** Detailed sketch map of a network of Type 2 phyllonite bands. Note apparent sinistral displacement of epidote vein across NE-SW trending phyllonite bands. Eigneig Mor region (horizontal surface) (NF 9264 6162).

Type 1 phyllonite bands are widely developed in the region between Burrival and Loch a' Ghlinne-dorcha (NF 909 622 to NF 913 618). The bands are between 0.5cm and 2m thick, the thickest bands being preserved in the region immediately to the west of Loch a' Ghlinne-dorcha (e.g. NF 913 618) (Fig. 6.2c). Type 1 phyllonite bands are either developed within, or along the margins of 'cataclasite' seams. Both continuous and discontinuous (*sensu* Tourigny & Tremblay 1997) Type 1 phyllonite bands have been observed. The wall rocks adjacent to *continuous* Type 1 phyllonite bands are overprinted by a protophyllonitic foliation, which locally displays a well developed sigmoidal geometry (Fig. 6.5a). Viewed in surfaces parallel to the mineral lineation and perpendicular to the foliation, the geometry of the sigmoidal fabric is consistent either with regional sinistral transpression or regional sinistral strike-slip. The intensity of the protophyllonitic fabric tends to decrease away from the margins of the discrete phyllonite band. *Discontinuous* Type 1 phyllonite bands typically display massive (i.e. non-foliated) wall rocks, and are locally bounded by foliation-parallel 'microfaults' (*sensu* Sibson 1977b; Butler 1995) (Figs. 6.5b & 6.7).

Type 2 phyllonite bands ( $\leq 3$ cm thick) are particularly well exposed around Eigneig Mor (NF 9281 6156 to NF 9264 6162). Lithological markers (e.g. sets of epidote veins) are typically displaced in an apparent sinistral sense across the sub-vertical,

NE-SW to ENE-WSW trending Type 2 phyllonite bands (Fig. 6.6). The phyllonitic / ultraphyllonitic foliation is *continuous* with the pervasive protophyllonitic foliation developed in the wall rocks. Type 2 phyllonite bands are never cross-cut by 'microfaults'.

### 6.3.1.2 Microstructure

Type 1 and Type 2 discrete phyllonite bands comprise isolated quartz, feldspar or hornblende porphyroclasts ( $\leq 10\text{mm}$  diameter, but grain size may vary by up to three orders of magnitude within a single thin section) which 'float' in an ultrafine grained matrix of quartz, albite, sericite, chlorite, epidote and opaque minerals. The foliation is defined by flattened, partially sericitised feldspar porphyroclasts and aggregates of aligned sericite and chlorite needles (Plate 6.6; Fig. 6.7).

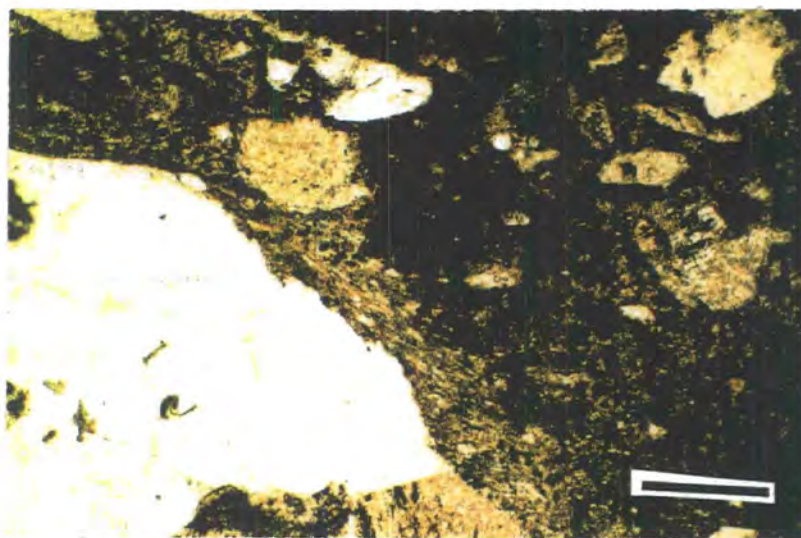


**Plate 6.6** Quartz grain (colourless) adjacent to the margin of 'Type 1' discrete phyllonite band (dark brown) is fringed by aggregates of fibrous chlorite (arrowed) which appear to be growing into the phyllonite band. See also Figure 6.7. Bar parallel mineral lineation, sense of shear not known. Field of view  $3 \times 1.9\text{mm}$ , plane polarised light.

The quartz porphyroclasts display strong patchy undulose extinction, and are cross-cut by arrays of randomly oriented intragranular tensile fractures. The fractures are healed either by polycrystalline quartz aggregates (individual grains  $\leq 0.05\text{mm}$  diameter) or by massive calcite grains ( $\leq 0.1\text{mm}$  diameter). Almost all the feldspar grains preserved within discrete phyllonite bands have experienced some degree of sericitisation. In general, sericite needles account for between 40% and 80% of the total surface area of host feldspar grains. Well-developed sericite mesh textures are commonly observed within sub-angular to sub-rounded *equant* feldspar porphyroclasts. In contrast, *flattened* feldspar porphyroclasts (aspect ratios  $\leq 5:1$ ) are

cross-cut by networks of foliation-parallel intragranular sericite strands. Hornblende porphyroclasts preserved within discrete phyllonite bands are equant, sub-angular to sub-rounded and are partially replaced by chlorite along their cleavage planes. Fibrous actinolite  $\pm$  chlorite strain shadows, which are oriented parallel to the macroscopic mineral lineation locally fringe the margins of individual hornblende porphyroclasts and / or the margins of discontinuous phyllonite bands (Fig. 6.7).

The microstructures of the rocks preserved in the hangingwalls / footwalls of *discontinuous* Type 1 phyllonite bands are indistinguishable from the microstructures observed within the crush melange (section 6.2.2). In contrast, the microstructures of the rocks preserved in the hangingwalls / footwalls of *continuous* Type 1 and Type 2 phyllonite bands are similar to the microstructures observed in regions of pervasive protophyllonites (section 6.3.2.2). The significance of the pervasive protophyllonitic fabric, and its relationship to the discrete phyllonite bands will be discussed in section 6.3.2.

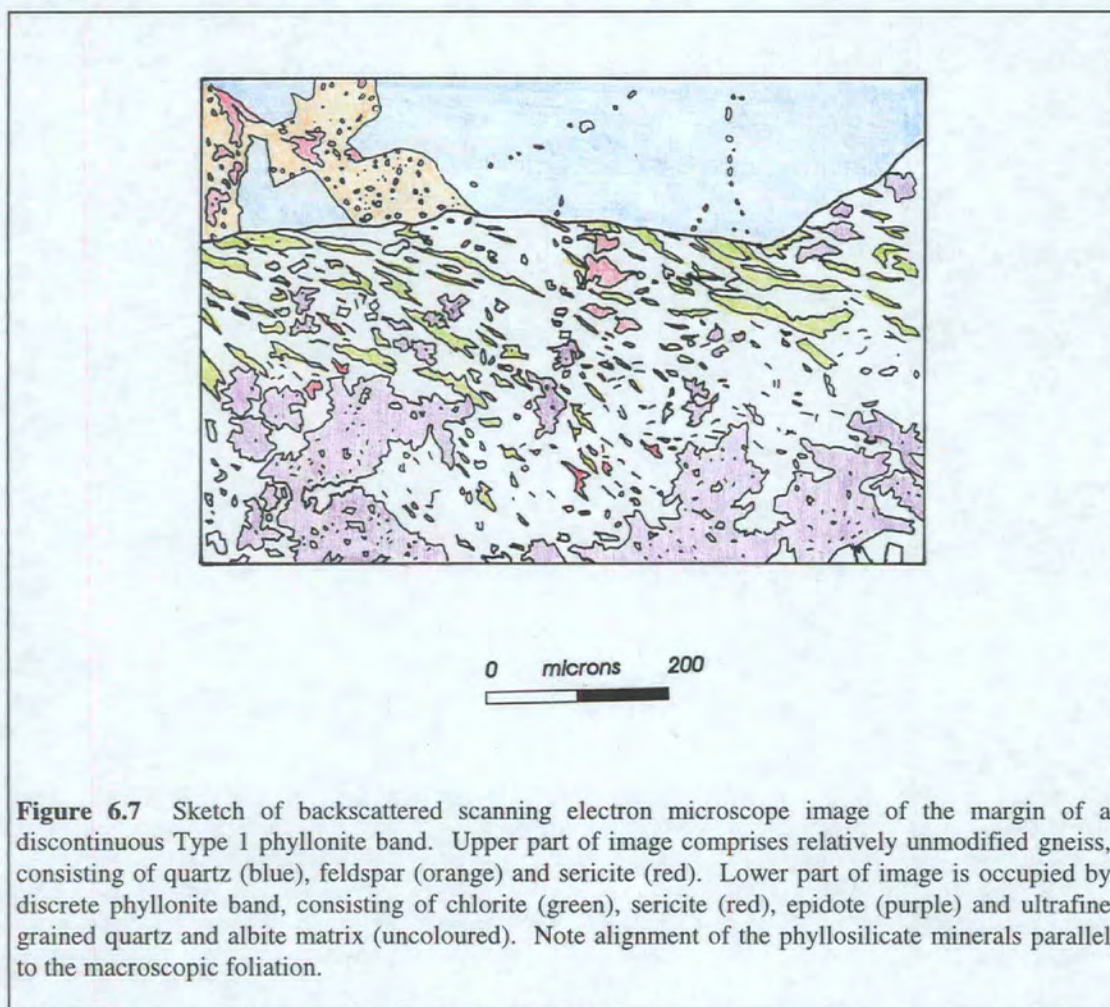


**Figure 6.7** Sketch of backscattered scanning electron microscope image of the margin of a discontinuous Type 1 phyllonite band. Upper part of image comprises relatively unmodified gneiss, consisting of quartz (blue), feldspar (orange) and sericite (red). Lower part of image is occupied by discrete phyllonite band, consisting of chlorite (green), sericite (red), epidote (purple) and ultrafine grained quartz and albite matrix (uncoloured). Note alignment of the phyllosilicate minerals parallel to the macroscopic foliation.

### 6.3.1.3 Summary and discussion

Discrete phyllonites are isolated (Type 1) or interconnected (Type 2), centimetre- to metre-scale bands of finely foliated phyllonite or ultraphyllonite. Discrete phyllonite bands are developed either in foliated protophyllonitic host rocks, or in massive non-foliated host rocks.

The discrete phyllonite bands are characterised by equant or flattened feldspar, quartz and hornblende porphyroclasts which 'float' in a matrix of ultrafine-grained quartz, albite, epidote and aligned phyllosilicate needles. Discrete phyllonites typically display a greater degree of alteration than the crush melange (section 6.2.2.2).

#### *Origin of the discrete phyllonite bands*

Discrete phyllonites are generally finer grained and more highly altered than the surrounding crush melange. This observation suggests either (a) that *grain size reduction was synchronous with phyllonitisation*, or (b) that *the discrete phyllonites developed along bands of pre-existing fine grained material* within the crush melange. There are three possible mechanisms of syn-tectonic grain size reduction. Firstly, dynamic recrystallisation processes are commonly inferred to have been operative in macroscopically ductile mylonitic fault rocks. During dynamic recrystallisation, coarse grained porphyroclasts are replaced by aggregates of relatively fine, recrystallised grains (e.g. White 1976; Drury & Urai 1990). However, microstructural observations of the quartz, feldspar and hornblende porphyroclasts preserved in both Type 1 and Type 2 phyllonites suggest that dynamic recrystallisation mechanisms were *not* widely operative during phyllonitisation (section 6.3.1.2). It is therefore unlikely that dynamic recrystallisation processes could account for the observed grain size decrease within the phyllonite bands. Secondly, pervasive grain-scale fracturing and cataclasis could produce fine grained, macroscopically ductile fault rocks (Chester *et al.* 1985; Tullis & Yund 1992). Quartz and feldspar porphyroclasts preserved within discrete phyllonite bands are commonly observed to be cross-cut by arrays of intragranular fractures. However, the intragranular fractures are typically healed and therefore did *not* result in the wholesale fragmentation of the host grains. It is therefore unlikely that the discrete phyllonite bands developed in response to during cataclastic flow. Finally, microstructural observations suggest that feldspar and hornblende porphyroclasts preserved within the discrete phyllonite bands have suffered widespread alteration to aggregates of fine grained sericite and chlorite respectively. However, the overall proportion of phyllosilicate minerals within the fine grained matrix is relatively low (the ratio of [sericite + chlorite] to [albite + epidote + quartz] is approximately 3:7). Syn-tectonic alteration alone cannot therefore account for the observed grain size distribution within the discrete phyllonite bands.

The intriguing possibility which remains is that the discrete phyllonites developed along bands of *pre-existing* fine grained material within the crush melange.

Field and microstructural relationships suggest that Type 1 phyllonite bands are developed within, or along the margins of relict 'cataclasite' seams preserved within the crush melange (Figs. 6.5b & 6.7). Furthermore, microstructural observations of the porphyroclasts preserved in both Type 1 and Type 2 phyllonites demonstrate (a) that the porphyroclasts are sub-angular to sub-rounded, (b) that the porphyroclast dimensions are extremely variable, and (c) that both quartz and feldspar porphyroclasts are more abundant than hornblende porphyroclasts. The porphyroclasts preserved in Type 1 and Type 2 phyllonite bands thus display similar morphologies and grain size distributions as the clasts preserved within the crush melange (see Table 6.1). It is therefore postulated that the Type 1 and Type 2 phyllonite bands *developed along pre-existing networks of transgranular fractures, cataclasite seams and pseudotachylyte veins preserved within the crush melange.*

#### ***Retrogression and deformation within the discrete phyllonite bands***

Type 1 and Type 2 phyllonite bands comprise an assemblage of quartz, feldspar (mostly K-feldspar and albite), hornblende, chlorite, actinolite, epidote, calcite and opaque minerals. The abundance of albite and the growth of 'new' sericite, epidote, actinolite and chlorite grains suggests that retrogression took place under fluid-rich, lower greenschist facies conditions. The retrograde minerals typically display strong grain shape preferred orientations. In particular, fibrous actinolite and chlorite aggregates develop in strain shadows around hornblende grains and are aligned parallel to the macroscopic mineral lineation. The (001) cleavage planes of sericite grains preserved within the ultrafine grained matrix are oriented parallel to the trace of the macroscopic foliation. These observations suggest (a) that deformation was accommodated by fluid assisted diffusive mass transfer processes, and (b) that deformation was broadly synchronous with retrogression.

Quartz porphyroclasts are cross-cut by arrays of intragranular fractures and thus deformed in a predominantly brittle manner. The fractures are commonly observed to be healed by aggregates of quartz and calcite. The presence of calcite suggests (a) that fracture healing was probably controlled by fluid assisted diffusive mass transfer (DMT) processes, (b) that fractures acted as DMT sinks and (c) that the diffusion path lengths were relatively long (i.e. the path lengths were greater than the dimensions of the host quartz grains) (Knipe 1989).

In contrast, feldspar porphyroclasts experienced pervasive alteration to aggregates of fine grained sericite and epidote, but are not cross-cut by significant numbers of intragranular fractures. Sericitisation reactions require a chemically active fluid phase

and are generally considered to involve the loss of silica, potassium, sodium and calcium from the host grain (e.g. Hemley & Jones 1964; Beach 1980). These observations are consistent with the feldspar grains having acted as DMT sources during deformation and retrogression (Knipe 1989). The role of fluid-assisted DMT during sericitisation will be discussed further in Chapter 9. Hornblende porphyroclasts are commonly observed to be 'fringed' by actinolite / chlorite strain shadows. The development of strain shadows suggests that sites of localised dilatation around the margins of hornblende grains acted as DMT sinks during phyllonitisation.

In conclusion, it is postulated that the discrete phyllonite bands developed in response to simultaneous deformation and retrogression along pre-existing networks of transgranular fractures, fine grained cataclasite seams and devitrified pseudotachylyte veins within the crush melange. Deformation appears to have been controlled by fluid assisted diffusive mass transfer mechanisms, which were especially important within regions of pre-existing ultrafine-grained matrix.

### **6.3.2 PERVASIVE PROTOPHYLLONITES**

It has been demonstrated that pervasive protophyllonites developed synchronous with regional top-to-the-NE sinistral strike-slip along the OHFZ in North Uist (section 3.4.3.2) (see also Butler 1995). Pervasive protophyllonites are widely observed in the region between Loch a' Ghlinne-dorcha and Eigneig Bheag (NF 915 622 to NF 925 600), and are locally preserved around Burrival (e.g. NF 909 620) (Fig. 6.1). Pervasive protophyllonites are well exposed along coastal sections, but are often badly weathered further inland.

#### **6.3.2.1 Field relationships**

Pervasive protophyllonite comprises elongate, flattened augen of felsic and mafic gneisses ( $\leq 100\text{m}$  long, but size varies by up to four orders of magnitude; aspect ratios  $\leq 10:1$ ), which 'float' within an ultrafine grained pale green phyllonitic or ultraphyllonitic matrix. Overall, the matrix accounts for between 40% and 60% of the total rock. The gneissose augen are overprinted by a crude protophyllonitic fabric, which is defined by coarse quartz ribbons ( $\leq 3\text{mm}$  thick; average aspect ratio  $\approx 3:1$ ), aggregates of aligned phyllosilicate minerals and re-oriented lithological banding. This fabric is particularly well developed in felsic host rocks, but is less well defined in mafic lithologies.

The orientation of the pervasive protophyllonitic foliation varies systematically throughout the study area. Around Eigneig Mor (NF 930 613) (Fig. 6.1), the foliation

strikes NE-SW, and dips moderately towards the northwest or towards the southeast (Fig. 6.8a). However, to the south of Eigneig Bheag (NF 925 603 to NF 920 598) (Fig. 6.1), the protophyllonitic foliation dips gently towards the east or southeast (Fig. 6.8b). The foliation is consistently associated with a sub-horizontal, NE-SW trending mineral lineation (Plate 6.7), which is defined by elongate quartz grains and aggregates of fibrous calcite, actinolite or chlorite (Figs. 6.8a & b) (section 6.3.2.2). The pervasive protophyllonites are commonly observed to be cross-cut by arrays of sub-vertical, NNW-SSE to N-S trending quartz or quartz-chlorite veins. Individual veins are locally up to 5m long, although the veins never exceed more than about 5cm in width. The orientation of the vein fibres is consistent with vein opening during regional east-west extension. The significance of these veins will be discussed in section 6.4.

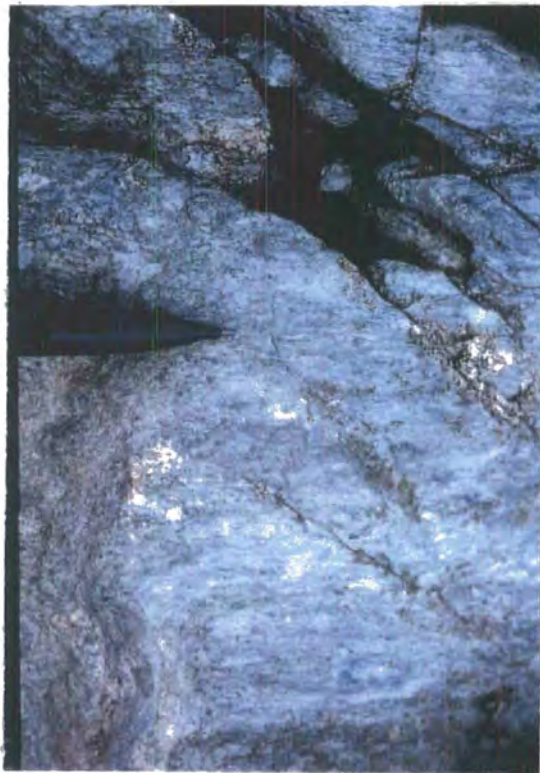


**Plate 6.7** Sub-horizontal, strike-parallel mineral lineation developed in pervasive protophyllonite, Eigneig Bheag region (NF 926 606).

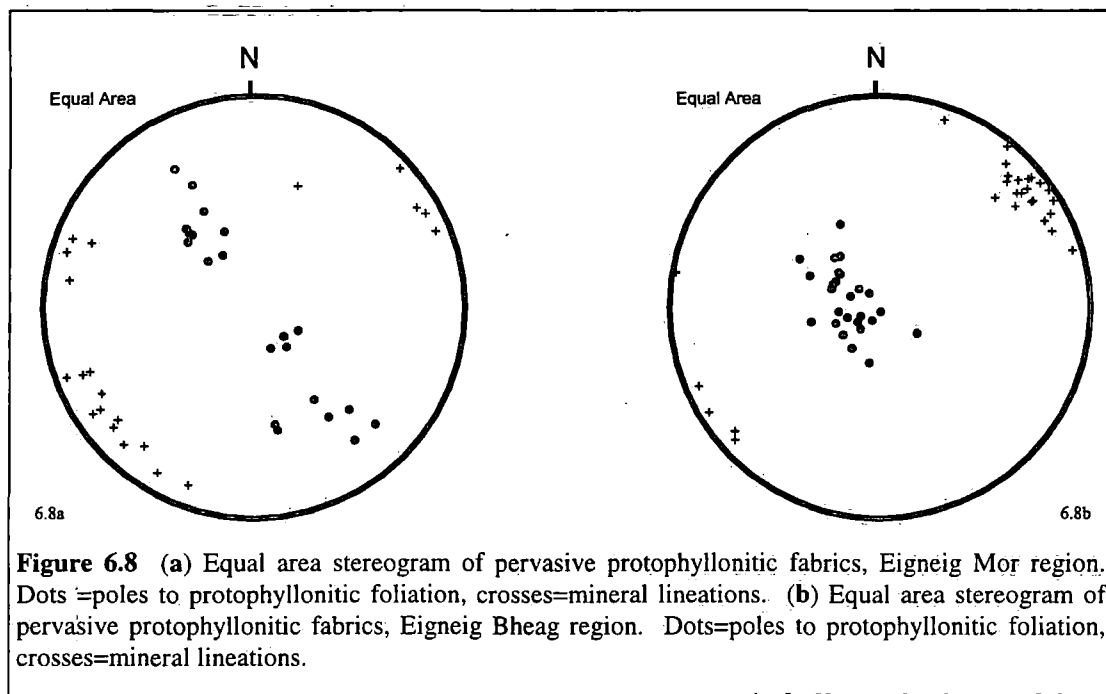


**Figure 6.8** (a) Equal area stereogram of pervasive protophyllonitic fabrics, Eigneig Mor region. Dots = poles to protophyllonitic foliation, crosses = mineral lineations. (b) Equal area stereogram of pervasive protophyllonitic fabrics, Eigneig Bheag region. Dots = poles to protophyllonitic foliation, crosses = mineral lineations.

### 6.3.2.2 Microstructure

Three distinct microstructural domains have been recognised within the pervasive protophyllonites. The microstructural domains correspond to the different lithological units observed in the field.

#### *Domains of felsic protophyllonite*

Felsic protophyllonites comprise coarse quartz ( $\leq 8\text{mm}$  long) and feldspar ( $\leq 5\text{mm}$  diameter) porphyroclasts, which are wrapped by laterally discontinuous (on the scale of a thin section) aggregates of aligned sericite needles (sericite strands) and trails of fine grained epidote (Plate 6.8a).

Quartz porphyroclasts are locally cross-cut by arrays of brittle intragranular extension fractures. The fractures are oriented at high angles to the trace of the foliation and are typically infilled by aggregates of massive or fibrous calcite and quartz. The fibres are oriented parallel to the macroscopic, NE-SW trending mineral lineation. Fibrous aggregates of polycrystalline quartz or quartz-calcite-chlorite are commonly observed in strain shadows which develop (a) around the margins of isolated quartz porphyroclasts, and (b) in the regions between pulled-apart quartz grains. Internally, quartz porphyroclasts display strong patchy undulose extinction, although optical subgrains are rarely observed.

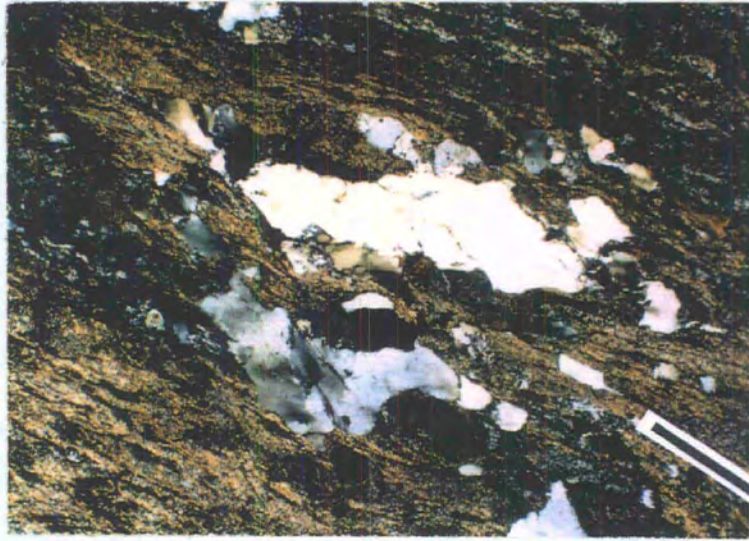


**Plate 6.8** (a) Felsic protophyllonite. Note relatively undeformed quartz porphyroclasts (white to dark grey) are locally wrapped by strands of sericite, derived from the chemical breakdown of feldspar (see text for discussion). Bar parallel mineral lineation, sense of shear not known. Field of view  $3 \times 1.9\text{mm}$ , crossed polars. (b) Partially altered feldspar grain in felsic protophyllonite. Relatively unaltered region (dark grey, locally with albite twins) is cross-cut by tensile intragranular fractures (arrowed) and thus deforms in a brittle manner. Highly sericitised margins (brown speckles) begin to deform in a macroscopically ductile manner as the sericite needles become aligned parallel to the foliation. See Chapter 9 for further discussion of mechanisms controlling sericitisation. Bar parallel trace of foliation, sense of shear not known. Field of view  $1.3 \times 0.77\text{mm}$ , crossed polars.

Approximately 25% of the feldspar grains preserved within domains of felsic protophyllonite are completely unaltered. These 'pristine' feldspar grains (moderately calcic plagioclase and K-feldspar) are characterised by patchy undulose extinction and are locally associated with irregular mantles of fine grained albite (individual albite grains  $\leq 0.02\text{mm}$  diameter). Arrays of intragranular tensile fractures, which are typically infilled by aggregates of albite, calcite or epidote are commonly observed to cross-cut relatively unaltered feldspar porphyroclasts. However, the majority ( $\cong 75\%$ ) of the feldspar grains preserved within domains of felsic protophyllonite have experienced partial or total alteration to aggregates of fine grained sericite and epidote. Sericite mesh textures are commonly observed in partially altered feldspar grains (sericite accounts for up to 70% of the surface area of host feldspar grains). These partially altered grains are flattened parallel to the trace of the foliation (aspect ratios  $\leq 6:1$ ) and are locally cross-cut or wrapped by a network of anastomosing intra- and transgranular sericite strands (Plate 6.8b).

#### ***Domains of mafic protophyllonite***

Mafic protophyllonites comprise aggregates of partially altered feldspar and hornblende grains. The partially altered feldspar grains are typically flattened parallel to the trace of the foliation and display well developed sericite mesh textures (sericite accounts for  $\leq 50\%$  of the surface area of host feldspar grains). The mesh textures are locally cross-cut by anastomosing intragranular sericite strands.

The degree of alteration observed experienced by hornblende grains preserved within domains of mafic protophyllonite is extremely variable. The least altered grains are cross-cut by arrays of intragranular extension fractures, which are typically oriented at high angles to the trace of the macroscopic foliation. The fractures are infilled by aggregates of fibrous actinolite and chlorite, and locally display good evidence for crack-seal opening (Ramsay 1980a). In contrast, the most highly altered hornblende grains are pseudomorphed by aggregates of apparently undeformed chlorite and / or acicular actinolite. Actinolite / chlorite strain shadows are commonly developed along the margins of both altered and unaltered hornblende grains (Plate 6.9).

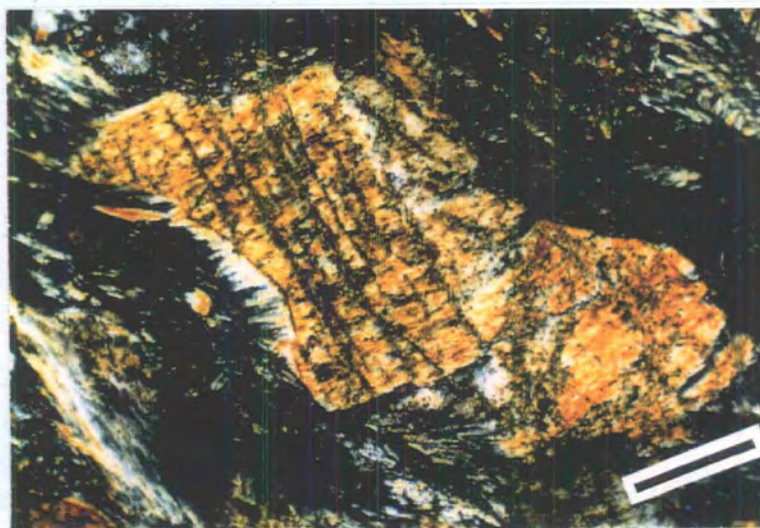


**Plate 6.9** Hornblende porphyroblast (straw yellow) preserved in mafic protophyllonite. Note fibrous actinolite overgrowths (moderate relief, pale grey to colourless) which fringe the porphyroblast margins oriented at high angles to the trace of the foliation. Bar parallel mineral lineation, sense of shear not known. Field of view 1.3×0.77mm, crossed polars.

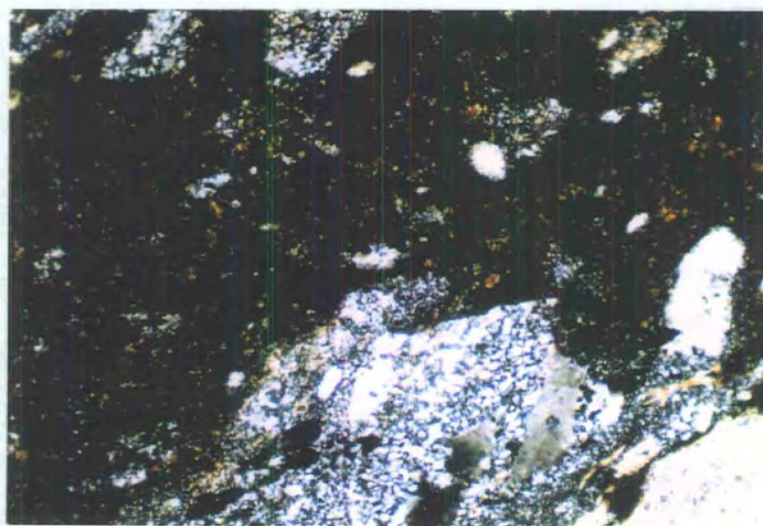


**Plate 6.10** Epidote-rich protophyllonite. Partially recrystallised quartz porphyroclasts (grey) 'float' in an ultrafine grained matrix of albite, epidote, albite, quartz and opaque minerals (dark brown). Field of view 3×1.9mm, crossed polars.

***Domains of epidote-rich phyllonite and ultraphyllonite***

The fine grained phyllonitic / ultraphyllonitic matrix, which is widely observed within regions of pervasive protophyllonite, contains a high modal abundance of epidote in comparison with felsic and mafic protophyllonite (section 6.3.2.1).

The 'epidote-rich' phyllonites and ultraphyllonites comprise fragments of felsic and mafic gneiss and isolated quartz and feldspar porphyroclasts (whose grainsize varies by up to 3 orders of magnitude within a single thin section), which 'float' within an ultrafine grained matrix of quartz, albite, epidote, sericite, chlorite and opaque minerals (Plate 6.10).

Quartz porphyroclasts are cross-cut by intragranular extension fractures, which are typically infilled by aggregates of fibrous calcite and quartz. Aggregates of fibrous, polycrystalline quartz and chlorite are commonly observed in strain shadows around the margins of quartz porphyroclasts. The porphyroclasts display strong patchy undulose extinction, although there is very little evidence to suggest that either recovery or recrystallisation processes were significant during phyllonitisation.

The feldspar grains display evidence of pervasive sericitisation (sericite accounts for up to 70% of the surface area of host grains). Well-developed sericite mesh textures are commonly observed. The most highly altered feldspar grains are typically flattened parallel to the trace of the foliation (aspect ratios  $\leq 10:1$ ) and are cross-cut by well developed intragranular sericite strands.

Foliation-parallel veins ( $\leq 0.1$ mm thick) are commonly observed to cross-cut domains of phyllonite and ultraphyllonite. The veins are either infilled by massive or bladed aggregates of epidote  $\pm$  quartz. Some of the veins appear to be undeformed, but the majority have been stretched in a direction parallel to the macroscopic mineral lineation. Boudin necks are typically infilled by fibrous chlorite strain shadows. These observations suggest that vein opening was synchronous with deformation and phyllonitisation.

### **6.3.2.3 Summary and discussion**

Pervasive protophyllonite comprises flattened, elongate lenses of felsic and mafic protophyllonite, which 'float' in an ultrafine grained, epidote-rich phyllonitic or ultraphyllonitic matrix. Feldspar and hornblende grains have experienced widespread, albeit heterogeneous alteration to aggregates of fine grained epidote, albite and phyllosilicate minerals. The overall degree of retrogression observed throughout the pervasive protophyllonite appears to be greater than that observed in regions unmodified crush melange.

#### ***Origin of the epidote-rich matrix***

The observed textures can be explained either by (a) syn-tectonic grain size reduction during phyllonitisation, or (b) by phyllonitisation within a pre-existing, matrix-supported aggregate (e.g. cataclasite and / or devitrified pseudotachylite).

There are three possible end-member mechanisms of syn-tectonic grain size reduction: (a) dynamic recrystallisation of the quartz, feldspar and / or hornblende porphyroclasts, (b) alteration of feldspar and hornblende porphyroclasts to aggregates of fine grained actinolite and / or phyllosilicate minerals, and (c) pervasive grain-scale fracturing of the porphyroclasts leading to cataclasis (see discussion in section 6.3.1.3).

Microstructural observations suggest that neither the quartz or hornblende experienced significant dynamic recrystallisation during phyllonitisation. However, unaltered feldspar grains are locally mantled by aggregates of ultrafine grained albite. These mantles appear to have developed during phyllonitisation (see section 6.3.3.4), and comprise less than 5% of the total material preserved within the fine grained matrix.

Feldspar and hornblende porphyroclasts have suffered widespread partial or total alteration to aggregates of fine grained phyllosilicates and / or actinolite. Overall, however, secondary sericite, chlorite and actinolite account for less than 20% of the total material preserved within the fine grained matrix. It is therefore unlikely that syn-tectonic alteration processes could account for the observed grain size distribution.

Quartz and hornblende grains are commonly observed to be cross-cut by arrays of intragranular fractures. However, the intragranular fractures are typically healed and therefore did *not* cause wholesale fragmentation of the host grains. It is therefore unlikely that pervasive grain-scale fracturing (i.e. cataclasis) during phyllonitisation could account for the observed grain size distribution within the pervasive protophyllonite. The intriguing possibility which remains is that the pervasive protophyllonites overprinted a pre-existing matrix-supported aggregate.

To the east of Burrival hill, unmodified crush melange comprises isolated blocks of felsic and mafic gneiss which 'float' in a fine grained matrix of quartz, feldspar and epidote (section 6.2.3.1). The blocks of gneiss vary in size from grain-scale aggregates up to 100m in diameter. The grain size distribution observed within the crush melange to the east of Burrival hill is thus similar to the grain size distribution observed in the pervasive protophyllonites. It is therefore postulated that *the epidote-rich matrix developed in regions of pre-existing, pervasive brittle deformation within crush melange.*

#### ***Retrogression and deformation within the pervasive protophyllonite***

The pervasive protophyllonites comprise an assemblage of quartz, feldspar (albite, moderately calcic plagioclase and K-feldspar), hornblende, chlorite, actinolite, epidote, calcite and opaque minerals. The abundance of albite and the growth of 'new' sericite, epidote, calcite, actinolite and chlorite grains suggests that retrogression took

place under fluid-rich, lower greenschist facies conditions. The retrograde minerals typically display strong grain shape preferred orientations. In particular, fibrous quartz, calcite, actinolite and chlorite aggregates, which are aligned parallel to the macroscopic mineral lineation, typically occur in boudin necks or strain shadows around the margins of quartz and hornblende porphyroclasts. In addition, sericite strands comprise intensely aligned aggregates of fine grained sericite needles, whose (001) cleavage planes appear to be oriented parallel to the trace of the macroscopic foliation. These observations suggest (a) that deformation was associated with the operation of fluid assisted diffusive mass transfer (DMT) mechanisms, and (b) that strike-slip deformation was synchronous with retrogression.

The local mineralogy and grain size distribution are likely to have influenced the dominant operative deformation mechanisms within each microstructural domain (Jordan 1987; Handy 1990; Wheeler 1992). Felsic protophyllonites are essentially aggregates of quartz, feldspar and sericite. Quartz porphyroclasts are commonly observed to be cross-cut by arrays of intragranular extension fractures. The fractures are typically infilled by massive or fibrous quartz and quartz-calcite aggregates. Crack-seal textures have not been identified, but it is likely that fracture healing was broadly synchronous with fracture opening (Lloyd & Knipe 1992). These observations suggest that intragranular fractures acted as diffusive mass transfer sinks during deformation and retrogression. The presence of calcite infills suggests that the diffusion pathways may have been significantly longer than the dimensions of the host grain. The feldspar grains have experienced pervasive alteration to aggregates of fine grained sericite and epidote. Sericitisation reactions generally involve the loss of silica, potassium, sodium and calcium from the host grain (e.g. Hemley & Jones 1964; Beach 1980), which is consistent with the feldspar grains having acted as DMT sources during deformation and retrogression (section 6.3.1.3 & Chapter 9). Feldspar grains outnumber quartz grains by a ratio of approximately 7:3, and the majority of feldspar grains have suffered pervasive sericitisation. These observations suggest that *domains of felsic protophyllonite may have acted as net DMT sources during deformation and retrogression*, and explain why augen of feldspar-rich felsic gneiss are commonly observed to be overprinted by a well developed protophyllonitic fabric (section 6.3.2.1).

Mafic protophyllonites comprise partially sericitised feldspar grains, which are isolated by networks of altered and partially altered hornblende grains. Relatively unaltered hornblende grains are typically cross-cut by intragranular extension fractures. The fractures are infilled by aggregates of fibrous actinolite and / or chlorite, and well developed crack-seal textures are locally preserved. These observations suggest that the intragranular extension fractures acted as DMT sinks

during deformation and alteration. Aggregates of fibrous actinolite and chlorite are commonly observed in strain shadows around the margins of both 'pristine' and highly altered hornblende grains. This observation suggests that sites of localised dilatation around the margins of some hornblende porphyroclasts acted as DMT sinks during deformation and retrogression. However, both actinolite and chlorite may be derived from the alteration of hornblende (Beach 1980), which suggests that the diffusion path lengths may have been of the same order of magnitude as the dimensions of the host hornblende grain. If this inference is correct, it is possible that individual hornblende grains may *not* have experienced significant losses or gains of chemical components during retrogression. However, it has been postulated that during sericitisation, the feldspar grains may have behaved as DMT sources. These observations suggest that *domains of mafic protophyllonite may have behaved as net DMT sources during deformation and retrogression*. However, the relatively low modal abundance of feldspar is consistent with *less* material having diffused away from domains of mafic protophyllonite than from domains of feldspar-rich felsic phyllonite. The patchily developed nature of the protophyllonitic fabric within domains of mafic protophyllonite (section 6.3.2.1) probably reflects the relatively small mass / volume losses during phyllonitisation.

The ultrafine grained nature of the polymineralic matrix makes it difficult to identify the dominant operative deformation mechanism(s) within domains of epidote-rich phyllonite and ultraphyllonite. However, foliation-parallel, syn-tectonic quartz-epidote veins are commonly observed within packages of epidote-rich phyllonite. The veins may have been important fluid pathways during phyllonitisation. Furthermore, quartz porphyroclasts preserved within domains of ultrafine grained phyllonite are typically fringed by fibrous chlorite / actinolite strain shadows. These observations are consistent with the operation of fluid-assisted diffusive mass transfer processes during deformation and retrogression within domains of epidote-rich phyllonite / ultraphyllonite (see section 6.3.3.4).

In conclusion, it has been demonstrated that the pervasive protophyllonites overprint and deform regions of intense cataclastic deformation within the crush melange. The heterogeneous nature of the primary fabric strongly influenced the style of deformation observed within each microstructural domain. However, it is likely that fluid assisted diffusive mass transfer processes were the single most important group of deformation mechanisms during the development of the pervasive protophyllonites.

### 6.3.3 PHYLLONITE BELTS

A network of anastomosing, NNE-SSW to NE-SW trending macroscopically ductile phyllonitic shear zones outcrops in the region between Loch a' Ghlinne-dorcha and Eigneig Bheag (NF 913620 to NF 925 600) (Fig. 6.1). It has been demonstrated that shear zone *initiation* was synchronous with sinistral strike-slip, but that the shear zone fabrics were *reworked* during subsequent E-directed extension. The strike-slip and extension-related fabrics are both cross-cut by networks of foliation-parallel, brittle detachment faults (section 3.4.3) (Butler *et al.* 1995). The aims of this section are (a) to describe the overall geometry of the phyllonitic shear zones (i.e. the macrostructure) and (b) to describe the lithologies and textures of the macroscopically ductile fabrics (i.e. the mesostructure). The extension-related phyllonites and the brittle detachment faults will be discussed in section 6.4.

Exposure is superb along coastal sections (NF 919 594 to NF 925 616), but the shear zones are highly weathered and often inexposed further inland. As a result, detailed studies of the phyllonitic shear zones have concentrated along the well exposed coastal sections. A major N-S to NE-SW trending phyllonite belt has been studied in the Eigneig Bheag region (NF 921 596 to NF 924 604) (Plate 6.11), whilst a number of smaller NE-SW trending phyllonite belts have been studied in the region to the north of Eigneig Mor (NF 930 613 to NF 925 616) (Figs. 6.1 & 6.2).

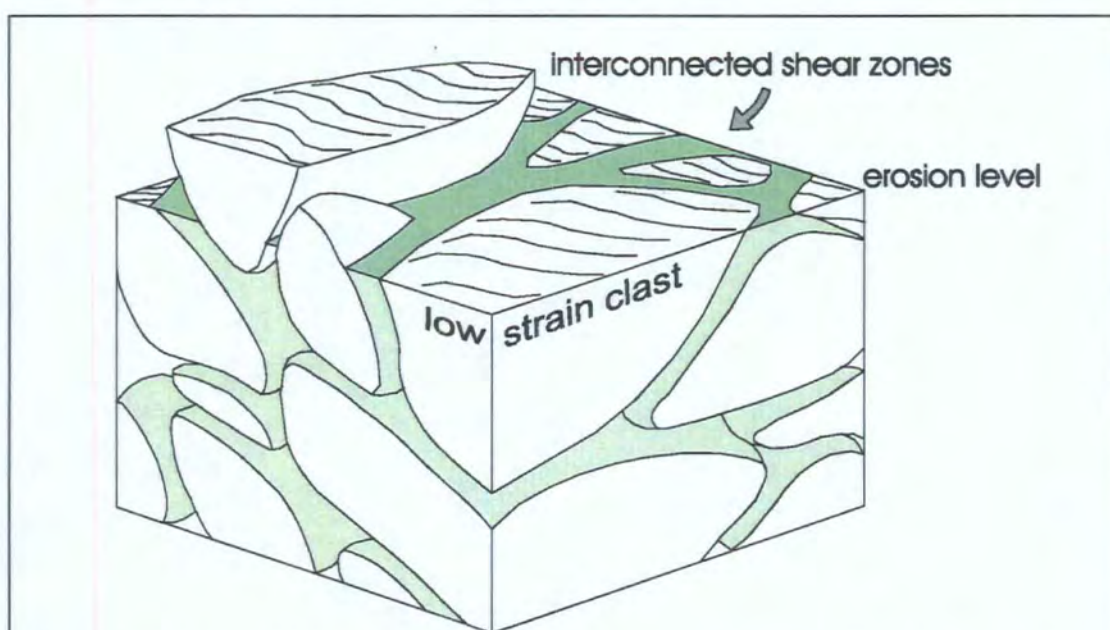


**Figure 6.9** Schematic block diagram illustrating geometry of the phyllonitic shear zone network (after Butler 1995). Similar geometries have been observed on the regional- (i.e. kilometre-) scale, and on the meso- (i.e. metres- to tens-of-metres-) scale (see Fig. 6.10).

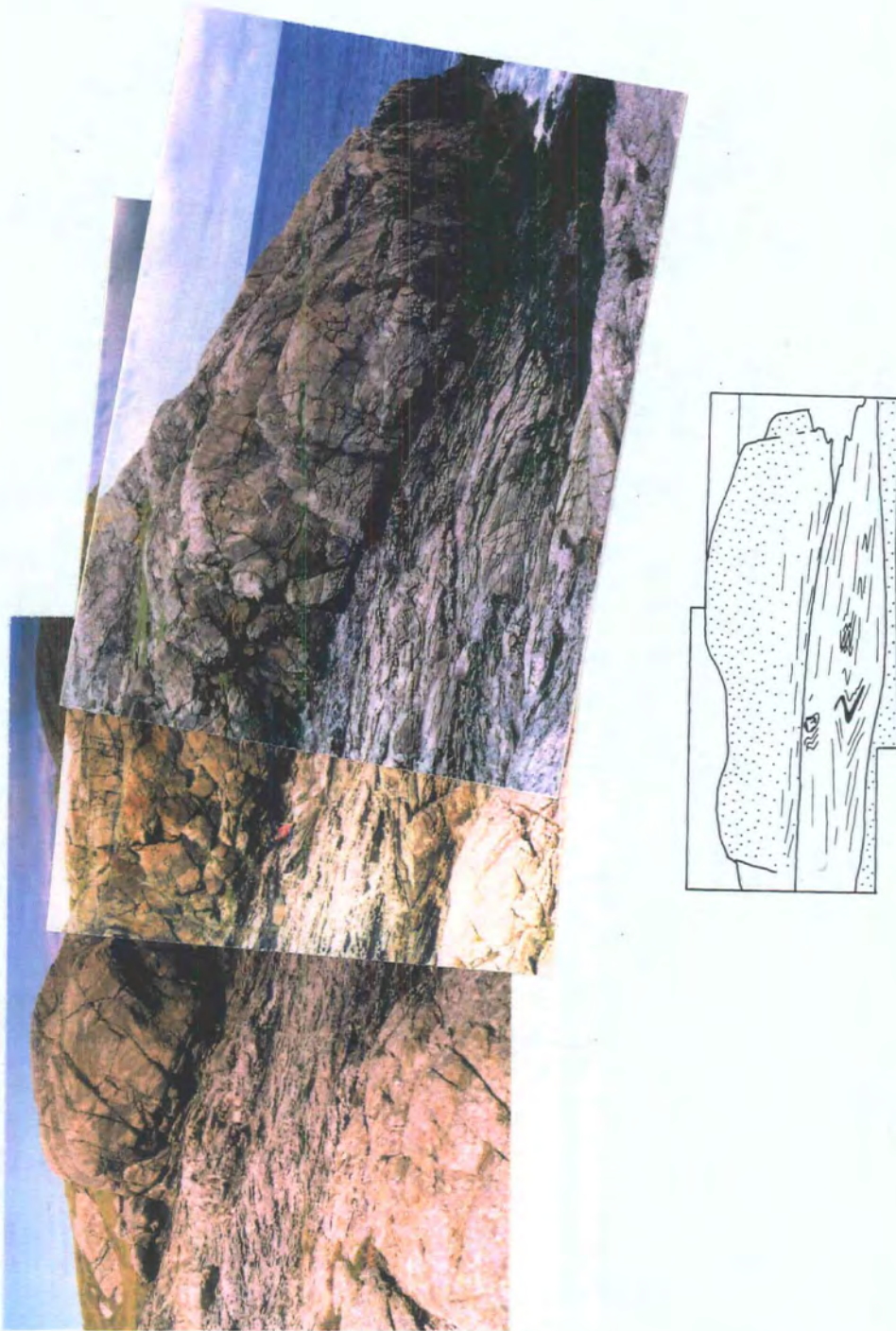


**Plate 6.11** Exceptionally well exposed gently E-dipping phyllonitic shear zone, Eigneig Bheag region (NF 921 596). Shear zone (pale grey / green) is 'capped' by a large block of pervasive protophyllonite (brown, rounded appearance; dotted ornament in drawing). Strike-slip related fabrics are preserved in the protophyllonitic block, and along the shear zone margins. Extension-related folded fabrics are preserved *within* the shear zone (highlighted in drawing). Rucksack (red) for scale, E to right.

### 6.3.3.1 Field relationships: macrostructure

It has been demonstrated that subsequent E-directed extension was focused almost entirely within the pre-existing strike-slip related shear zones (section 3.4.3, but cf. Chapter 7). This observation suggests that the regional geometry and distribution of the phyllonitic shear zones were probably established during sinistral strike-slip along the OHFZ in North Uist.

The shear zones vary from approximately 2m to 30m in thickness. N-S trending phyllonite belts tend to be thicker than NE-SW trending phyllonite belts. However, individual belts may display significant along-strike variations in thickness and / or trend. The interconnected phyllonite belts define a kilometre-scale network of braided shear zones, which isolate elongate augen of protophyllonitic crush melange (section 6.3.2) (Fig. 6.1). Viewed in horizontal surfaces (i.e. parallel to the sub-horizontal mineral lineation), the pervasive protophyllonitic foliation undergoes a marked, regional-scale sigmoidal strike-swing in the immediate hangingwall and / or footwall of each phyllonite belt (Fig. 6.1). The sigmoidal geometry is consistent with sinistral strike-slip displacements along the phyllonitic shear zone network (Butler 1995; Butler *et al.* 1995), and suggests that the pervasive protophyllonitic fabric was originally continuous with the phyllonitic shear zone fabrics.

The orientation of the phyllonite belts varies systematically between Eigneig Bheag and Eigneig Mor (NF 919 594 to NF 925 616). Around Eigneig Bheag, the N-S to NE-SW trending phyllonite belts dip towards the E or towards the SE respectively. However, in the Eigneig Mor region, the consistently NE-SW trending phyllonite belts dip either towards the NW or towards the SE (Fig. 6.1). Butler (1995) has suggested that the variably oriented phyllonitic shear zones define an interconnected, three dimensional network which wraps around augen of protophyllonitic crush melange (Fig. 6.9). The variation in the orientation of the phyllonite belts is reflected in the variable orientation of the pervasive protophyllonitic foliation (Figs. 6.8a & b; section 6.3.2.1). The relationships between the phyllonitic shear zones and the pervasive protophyllonitic fabric will be discussed in section 6.3.4.

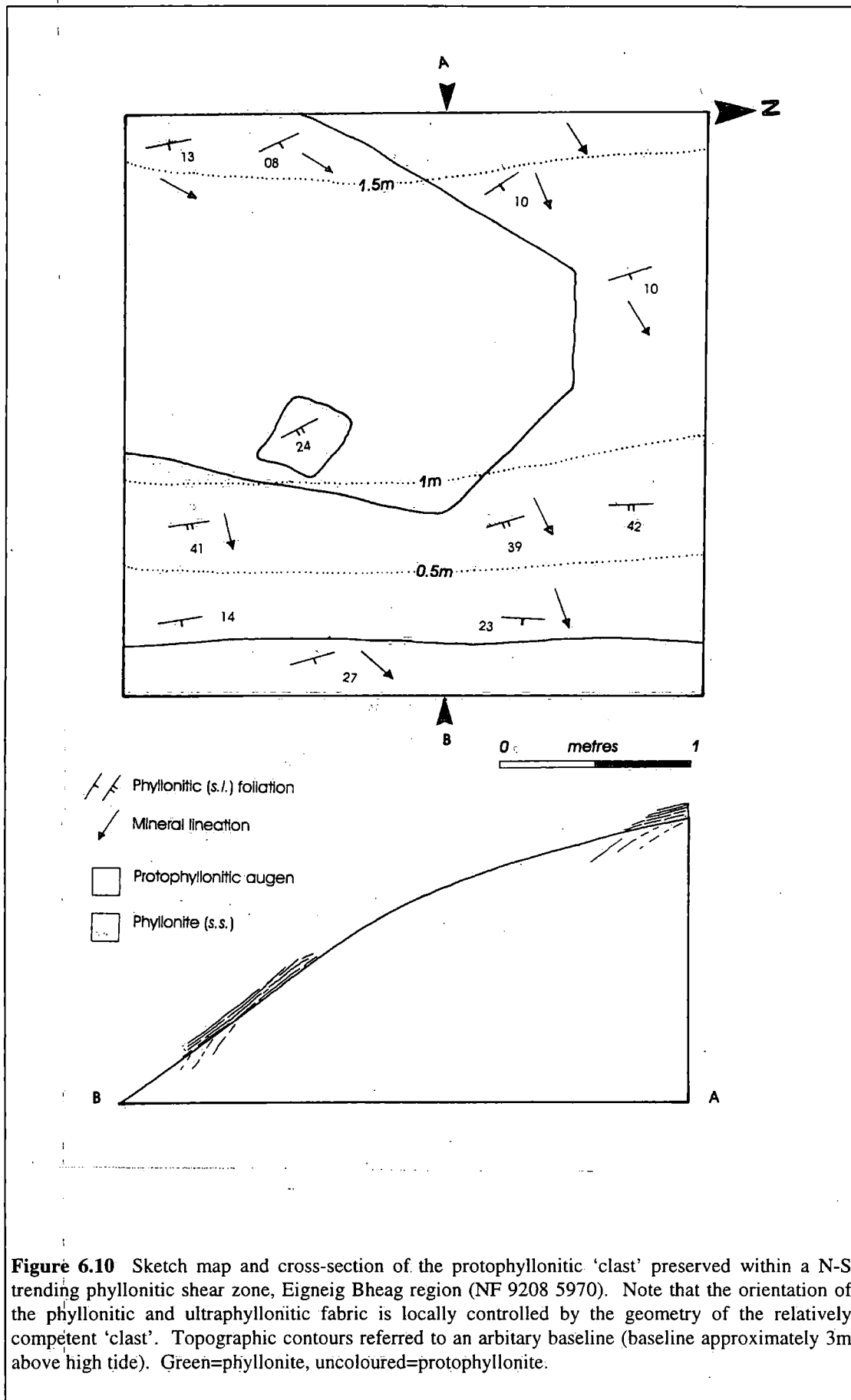
### 6.3.3.2 Field relationships: lithology and mesostructure

The phyllonite belts comprise interbanded packages (between 1cm and 5m thick) of distinctive 'dark-green' and 'grey-green' phyllonite, ultraphyllonite and protophyllonite. The ratio of dark-green phyllonite to grey-green phyllonite is typically around 7:3, although this ratio is locally very variable. In general, packages of grey-green phyllonite are laterally discontinuous ( $\leq 2\text{m}$  long) and form isolated lenses within an interconnected matrix of dark-green phyllonite.

Dark-green phyllonite comprises aggregates of intensely aligned phyllosilicate minerals and ultrafine grained epidote. Porphyroclasts are rarely observed in the field, and microstructural observations suggest that packages of dark-green phyllonite were derived either from 'cataclasite' or amphibolite protoliths (see section 6.3.3.3). Packages of grey-green phyllonite comprise finely interbanded aggregates of epidote, stretched quartz and feldspar grains (aspect ratios locally  $\geq 10:1$ ) and intensely aligned phyllosilicate minerals.  $\phi$ -type,  $\delta$ -type and  $\sigma$ -type quartz and feldspar porphyroclasts are locally preserved within units of grey-green phyllonite and ultraphyllonite, whilst highly deformed, sub-concordant 'cataclasite' seams and / or pegmatite veins are locally preserved within packages of strike-slip related grey-green protophyllonite. Microstructural observations suggest that packages of grey-green phyllonite were predominantly derived from felsic or banded gneiss protoliths (section 6.3.3.3).

Flattened, metre-scale augen of mafic and felsic protophyllonite locally outcrop *within* phyllonitic shear zones. These augen are indistinguishable from the blocks of flattened, protophyllonitic gneiss observed within regions of pervasive protophyllonite (section 6.3.2.1). Detailed mapping of a protophyllonitic 'clast' (at least 1.5m thick) which outcrops within a phyllonite belt to the south of Eigneig Bheag (NF 9208 5970) suggests that the clast is wrapped by, and thus locally controls, the orientation of the shear zone foliation (Fig. 6.10).

The phyllonitic foliation (in both dark-green and grey-green units) is typically oriented parallel to the margins of the host shear zone. The phyllonitic foliation preserved in the Eigneig Bheag region therefore dips moderately towards the E or SE (Fig. 6.11a), whilst around Eigneig Mor, the NE-SW trending foliation dips either towards the NW or towards the SE (Fig. 6.11b) (see section 6.3.2.1). The phyllonitic foliation is associated with a strike-parallel (i.e. strike-slip related) to down-dip plunging (i.e. extension-related) mineral lineation (Figs. 6.11a & b), and is commonly observed to be deformed by cascades of E-, SE- or NW-verging folds. As a result of this extensive extensional overprint, strike-slip related fabrics tend to be preserved either along the margins of phyllonite belts, or within protophyllonitic 'clasts' (Fig. 6.10). The contacts between packages of strike-slip and extension-related phyllonite are typically marked by foliation-parallel detachment faults (section 6.4.1). However, where the original shear zone geometries are preserved (e.g. NF 926 158 & NF 921 596), the contact between packages of strike-slip and extension-related phyllonite is marked by a progressive clockwise rotation of the mineral lineation, from a NE-SW to an E-W or NW-SE trend (see also Butler 1995). The relationship between shear zone kinematics, orientation, structure and lithology will be described in more detail in section 6.4.



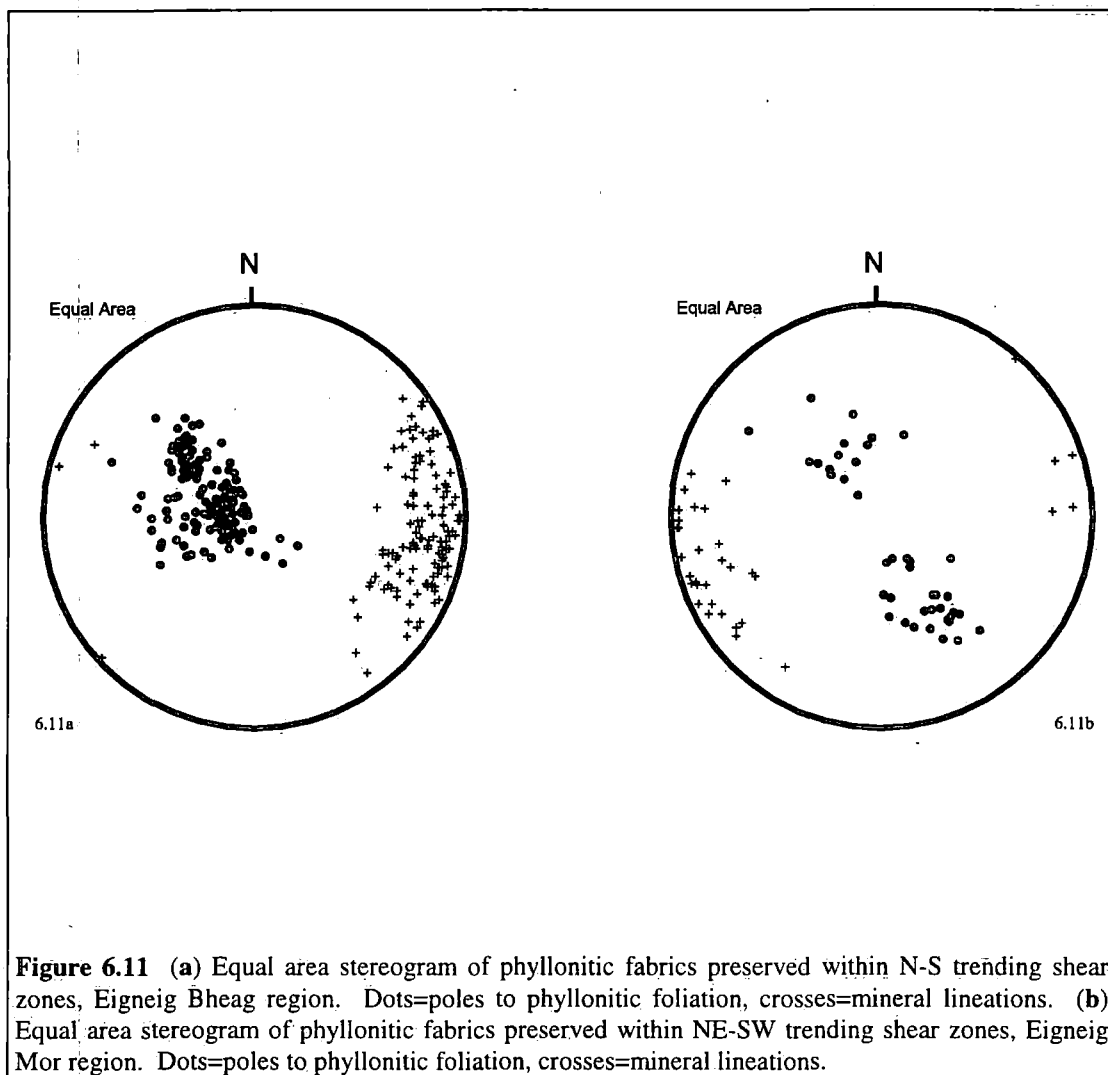


**Figure 6.11** (a) Equal area stereogram of phyllonitic fabrics preserved within N-S trending shear zones, Eigneig Bheag region. Dots=poles to phyllonitic foliation, crosses=mineral lineations. (b) Equal area stereogram of phyllonitic fabrics preserved within NE-SW trending shear zones, Eigneig Mor region. Dots=poles to phyllonitic foliation, crosses=mineral lineations.

### 6.3.3.3 Microstructure

Three distinct microstructural domains have been recognised within packages of strike-slip related phyllonite. The 'dark-green' phyllonites comprise (a) domains of epidote-rich phyllonite and ultraphyllonite and (b) domains of mafic phyllonite and protophyllonite. The overall ratio of mafic phyllonite to epidote-rich phyllonite is approximately 1:9. Packages of grey-green phyllonite comprise domains of felsic phyllonite and protophyllonite.

#### *Epidote-rich phyllonite and ultraphyllonite* ('dark-green phyllonite')

Many packages of dark-green phyllonite display a high modal abundance of epidote in comparison with packages of felsic and mafic phyllonite. Domains of 'epidote-rich' phyllonite and ultraphyllonite are characterised by quartz and highly altered feldspar porphyroclasts ( $\leq 1\text{mm}$  diameter) which 'float' within an ultrafine grained matrix of quartz, albite, epidote, sericite, chlorite and opaque minerals (Plate 6.12). Detailed study of the matrix microstructure is hampered by the fine grain size, but the (001)

cleavage traces of the phyllosilicate minerals preserved in the matrix tend to be oriented parallel to the trace of the macroscopic foliation and are rarely kinked or fractured (cf. Bell *et al.* 1986). Euhedral opaque grains (square to prismatic cross-sections;  $\leq 0.1\text{mm}$  diameter) are locally wrapped by fibrous quartz and / or quartz-chlorite strain shadows (Plate 6.13).

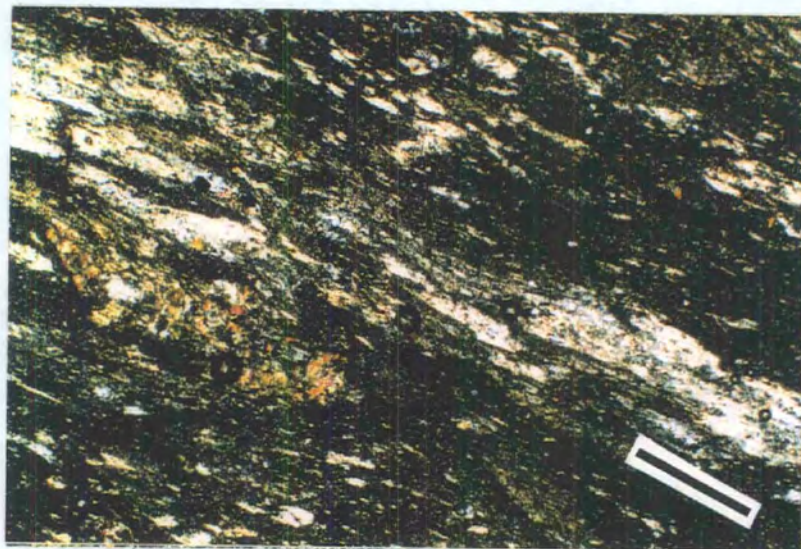


**Plate 6.12** Epidote-rich phyllonite. Polycrystalline quartz ribbons and highly sericitised, flattened feldspar grains 'float' in an ultrafine-grained matrix of epidote, albite, quartz and opaque minerals. Bar parallel mineral lineation, sense of shear not know. Field of view  $3 \times 1.9\text{mm}$ , crossed polars.



**Plate 6.13** Opaque grain preserved in epidote-rich phyllonite. Grain is fringed by quartz-chlorite strain shadows (pale green / colourless, low relief). Bar parallel mineral lineation, shear sense not known. Field of view  $1.3 \times 0.77\text{mm}$ , plane polarised light.

Quartz porphyroclasts ( $\leq 0.5\text{mm}$  diameter) display strong patchy undulose extinction, and are *locally* mantled by polycrystalline, seriate-interlobate aggregates of fine grained quartz (individual grains  $\leq 0.01\text{mm}$  diameter). Aggregates of fibrous chlorite are locally preserved in strain shadows around the margins of quartz porphyroclasts.

Many ( $\geq 70\%$ ) of the feldspar grains are cross-cut by intragranular sericite strands (sericite typically accounts for up to 80% of the surface area of host grains), and are flattened parallel to the trace of the foliation (aspect ratios  $\leq 10:1$ ). Feldspar porphyroclasts are locally surrounded by mantles of fine grained albite (individual grains  $\leq 0.025\text{mm}$  diameter). These mantles comprise equigranular- to seriate-interlobate aggregates of albitic feldspar, which appear to have escaped the effects of pervasive sericitisation. The margins of individual albite grains are decorated by arrays of ultrafine, optically high relief fluid inclusions ( $\ll 0.005\text{mm}$  diameter). However, the albite grains themselves appear to be free from inclusions (cf. Drury & Urai 1990). The mechanisms of grain size reduction in feldspar are discussed further in section 6.3.3.4.

Foliation-parallel to discordant epidote and quartz-epidote veins ( $\leq 0.1\text{mm}$  thick) are commonly observed to cross-cut domains of phyllonite and ultraphyllonite. Undeformed veins are locally preserved, but the majority have either been boudinaged parallel to the macroscopic mineral lineation, or folded and flattened into the plane of the foliation. The boudin necks are typically infilled by aggregates of fibrous chlorite. These observations suggest that vein opening and subsequent deformation were synchronous with phyllonitisation.

#### ***Felsic phyllonite and protophyllonite*** ('grey-green phyllonite')

Domains of felsic phyllonite and protophyllonite comprise quartz and feldspar porphyroclasts, which are wrapped by a network of anastomosing, interconnected transgranular sericite strands and strung-out trails of fine grained epidote (Plate 6.14).

The quartz porphyroclasts ( $\leq 1\text{mm}$  diameter) are locally cross-cut by intragranular extension fractures. The fractures are typically infilled by aggregates of fine grained quartz (individual grains  $\leq 0.1\text{mm}$  diameter), calcite and / or chlorite fibres. Chlorite fibres are also commonly observed in strain shadows around the margins of quartz grains. Quartz is characterised by strong patchy undulose extinction and arrays of poorly developed optical subgrains and / or deformation bands. The porphyroclasts are *locally* mantled by equigranular- to seriate-interlobate aggregates of fine grained quartz (individual grains  $\leq 0.05\text{mm}$  diameter).

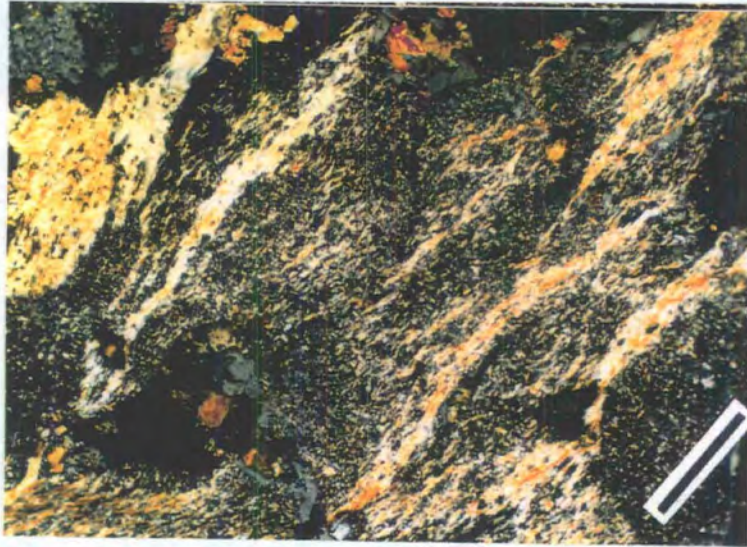


**Plate 6.14** Felsic protophyllonite. Partially altered feldspar grains (black / dark grey) (which display well developed mesh textures - Plate 6.2b) are wrapped by laterally discontinuous sericite strands (yellow, high birefringence). Bar parallel mineral lineation, shear sense not known. Field of view  $6 \times 3.7\text{mm}$ , crossed polars.

The majority ( $\geq 60\%$ ) of feldspar grains preserved within domains of felsic phyllonite have experienced intense alteration to aggregates of fine grained sericite (sericite accounts for  $\geq 80\%$  of the surface area of host grains). The sericite needles locally define well developed mesh textures, though in general, the needles display a strong grain shape preferred orientation and form a networks of intra- and transgranular sericite strands. Some ( $\cong 40\%$ ) feldspar grains have escaped the effects of pervasive sericitisation. These 'pristine' feldspars are typically cloudy in plane polarised light, and are locally surrounded by patchily developed mantles of ultrafine, equigranular- to seriate-interlobate albite grains (individual grains  $\leq 0.025\text{mm}$  diameter) (Fig. 6.12).

Concordant quartz-calcite veins are locally preserved in domains of felsic protophyllonite. The veins appear to have been stretched in a direction parallel to the macroscopic mineral lineation and comprise angular to sub-rounded, polygonal to lobate quartz grains, which 'float' in a calcite-rich matrix. This matrix is composed of inequigranular- to seriate-interlobate aggregates of coarse and fine grained calcite ( $\leq$  individual grains between  $0.5\text{mm}$  and  $0.05\text{mm}$  diameter). The coarse calcite grains are cross-cut by two sets of straight, intersecting deformation twins (twins  $\leq 0.05\text{mm}$  wide; angle of intersection  $\cong 60^\circ$ ) (cf. Type III' twins of Burkhard 1993).



0 microns 20

**Figure 6.12** Sketch of backscattered scanning electron microscope image illustrating feldspar microstructures observed in phyllonite. Left hand part of image comprises aggregates of ultrafine grained albite (uncoloured) and sericite (red). Albite grain boundaries defined by 'pluck marks' produced during polishing. Right hand part of image comprises partially sericitised albite porphyroclast, and epidote aggregates (purple). Note the relative scarcity of sericite in regions of ultrafine grained albite.

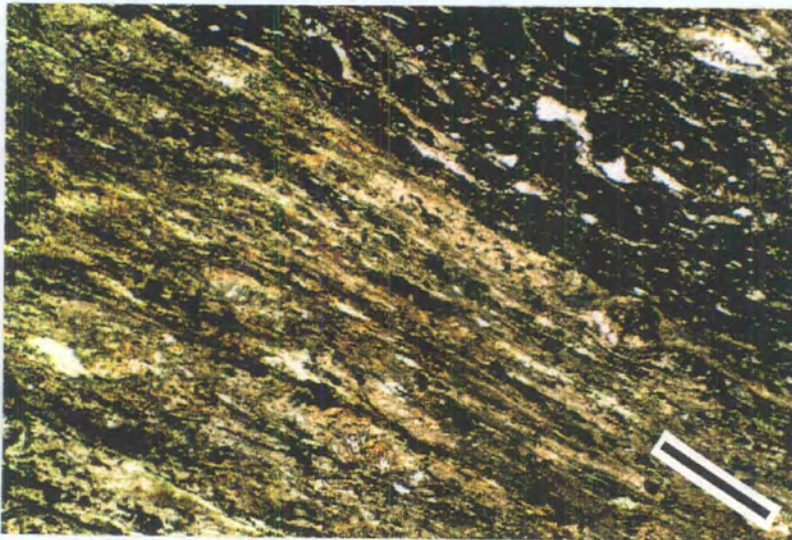


**Plate 6.15** Mafic phyllonite. Partially altered feldspar grains (brown speckles) wrapped by networks of interconnected chlorite strands (green brown). Bar parallel mineral lineation, shear sense not known. Field of view 3×1.9mm, plane polarised light.

### ***Mafic phyllonite and protophyllonite*** ('dark-green phyllonite')

Mafic phyllonite comprises partially altered feldspar and hornblende grains, which are wrapped by an interconnected network of chlorite and / or sericite strands (Plate 6.15). The hornblende grains are locally pseudomorphed by undeformed actinolite and / or chlorite fibres. Fibrous aggregates of actinolite / chlorite are commonly observed in strain shadows around the margins of partially altered hornblende porphyroclasts. The feldspar grains are flattened parallel to the trace of the macroscopic foliation (aspect ratios  $\leq 3:1$ ) and are locally cross-cut by intragranular sericite strands.

#### **6.3.3.4 Summary and discussion**

An anastomosing network of phyllonitic shear zones outcrops throughout eastern North Uist. Overall, the shear zones comprise approximately 60% epidote-rich phyllonite / ultraphyllonite, around 30% felsic phyllonite / protophyllonite and less than 10% mafic phyllonite / protophyllonite. Although these ratios are locally very variable, meso- and microstructural observations suggest that the shear zone fabrics are characterised by isolated, centimetre- to metre-scale lenses of felsic phyllonite and mafic protophyllonite, which 'float' in an interconnected matrix of epidote-rich phyllonite and ultraphyllonite. Owing to the pervasive extensional overprint, strike-slip related fabrics are typically preserved only along the shear zone margins, or adjacent to protophyllonitic low strain 'windows'. The intensity of retrogression observed throughout the phyllonite belts appears to be greater than the that observed either in the pervasive protophyllonites or the discrete phyllonite bands.

#### ***Origin of the epidote-rich phyllonite***

Field and microstructural observations suggest that the phyllonitic shear zones are predominantly composed of fine grained, dark-green epidote-rich phyllonite and ultraphyllonite. Quartz and feldspar porphyroclasts preserved within domains of epidote-rich phyllonite display widespread evidence of syn-tectonic grain size reduction (see below). However, the discrete phyllonite bands and the pervasive protophyllonitic fabrics appear to have developed within *pre-existing* regions of fine grained material (e.g. cataclasite seams or pseudotachylyte veins) within the crush melange (sections 6.3.1 & 6.3.2). The aim of the following section is to determine the relative importance of syn-tectonic grain size reduction processes during the development of the epidote-rich phyllonites.

Aggregates of seriate-interlobate quartz grains are locally preserved along the margins of quartz porphyroclasts. These polycrystalline aggregates, which are thought to have developed in response to dynamic recrystallisation of the parent grain (see below), account for around 5% of the total groundmass. Feldspar porphyroclasts preserved in

domains of epidote-rich phyllonite have experienced partial or total alteration to aggregates of fine grained sericite needles. Overall, sericite needles derived from altered porphyroclasts account for approximately 30% of the total material preserved within the fine grained groundmass. Aggregates of ultrafine grained, polycrystalline albite (see below), are widely observed within domains of epidote-rich phyllonite. Overall, fine grained albitic feldspar accounts for approximately 5% of the total material preserved within the matrix.

The products of syn-tectonic grain size reduction thus account for approximately 40% of the fine grained phyllonitic / ultraphyllonitic matrix. This observation suggests that the ultrafine grained material preserved within the phyllonitic / ultraphyllonitic matrix cannot have *wholly* have originated during syn-tectonic grain size reduction. It is therefore postulated that *the epidote-rich phyllonites must have been derived from pre-existing fine grained material, such as cataclasite seams and devitrified pseudotachylyte veins, preserved within the crush melange.*

#### ***Retrogression within the phyllonitic shear zones***

The abundance of albite and the growth of 'new' sericite, epidote, calcite and chlorite grains suggests that the phyllonite belts have experienced widespread retrogression under fluid-rich, lower greenschist facies conditions. The retrograde minerals typically display strong grain shape preferred orientations. In particular, fibrous quartz and / or chlorite aggregates are commonly observed to develop in boudin necks and in strain shadows. In addition, sericite strands comprise intensely aligned aggregates of fine grained sericite needles, whose (001) cleavage planes appear to be oriented parallel to the trace of the macroscopic foliation. These observations suggest (a) that deformation was associated with the operation of fluid assisted diffusive mass transfer (DMT) mechanisms, and (b) that deformation was synchronous with lower greenschist facies retrogression.

#### ***Deformation within the phyllonitic shear zones***

In highly strained, polymineralic fault rocks, it is widely accepted that the observed structures and microstructures will be strongly influenced by the competence contrasts between different mineral phases and / or mineral aggregates (e.g. Ramsay & Huber 1987; Handy & Zingg 1991). In particular, the most competent mineral phases / mineral aggregates tend to form isolated boudins or porphyroclasts, whilst the least competent mineral phases / mineral aggregates tend to form an interconnected matrix (Handy 1990, 1994). The phyllonitic shear zones comprise isolated quartz and feldspar porphyroclasts, and packages of boudinaged felsic phyllonite, which 'float' in an interconnected matrix of epidote-rich phyllonite and ultraphyllonite. These

observations therefore suggest that *the epidote-rich phyllonites and ultraphyllonites were the least competent lithologies during deformation within the phyllonite belts*. Experimental and microstructural studies have demonstrated that the relatively weak, interconnected matrix effectively controls the rheology of most polymineralic fault rocks (Jordan 1987; Handy 1990). It is therefore postulated that the rheology of the phyllonitic shear zones was primarily controlled by the behaviour of the ultrafine grained phyllonitic / ultraphyllonitic matrix. The aim of the following section is to determine the possible operative deformation mechanism(s) within the phyllonitic / ultraphyllonitic matrix. Unfortunately, the ultrafine grained nature of the groundmass makes it virtually impossible to directly determine the operative deformation mechanisms without the use of transmission electron microscopy (TEM). An alternative approach, which has been employed in this study, is to examine the intragranular and marginal porphyroclast microstructures in order to establish the overall deformation environment during strike-slip. This information may then be used to infer the possible operative deformation mechanisms within the ultrafine grained matrix.

Quartz porphyroclasts are commonly observed in domains of epidote-rich phyllonite and ultraphyllonite, and are typically fringed by quartz and quartz-chlorite strain shadows. These observations suggest that sites of localised dilatation around the *margins* of quartz porphyroclasts acted as diffusive mass transfer sinks during deformation and retrogression. Internally, the quartz porphyroclasts are characterised by strong patchy undulose extinction and poorly-defined optical subgrains. Core-and-mantle microstructures (White 1976) are locally developed. These observations are consistent with the limited operation of intracrystalline crystal plastic deformation mechanisms (e.g. recovery- / recrystallisation-accommodated dislocation creep) (Hirth & Tullis 1992).

The majority of the feldspar porphyroclasts preserved within domains of epidote-rich phyllonite / ultraphyllonite have experienced pervasive alteration to aggregates of fine grained sericite and epidote. Sericitisation reactions generally involve the loss of silica, potassium, sodium and calcium from the host grain (e.g. Hemley & Jones 1964; Beach 1980), which suggests that altered feldspar grains may have behaved as DMT sources during deformation and retrogression (see discussion in Chapter 9). However, relatively *unaltered* feldspar porphyroclasts are locally preserved. Unaltered feldspar porphyroclasts display patchy undulose extinction and are commonly observed to be surrounded by irregular mantles of fine grained, equigranular- to seriate-interlobate albite (Fig. 6.12). Experimental evidence suggests that neither recovery or dynamic recrystallisation are significant processes in plagioclase or K-feldspar at temperatures of less than 400°C to 500°C (i.e. at temperatures significantly higher than lower

greenschist facies conditions) (e.g. Tullis & Yund 1992). The aggregates of fine grained albitic feldspar are therefore unlikely to have formed in response to dynamic recrystallisation or recovery processes. Two mechanisms have been proposed to account for the presence of fine grained feldspar aggregates in low grade, greenschist facies tectonites. Firstly, it has been proposed that optical microstructures resembling those produced by dynamic recrystallisation may develop in response to grain-scale fracturing ('micro-cataclasis') of feldspar grains (Tullis & Yund 1992). Secondly, Fitz Gerald & Stünitz (1993) have proposed that both plagioclase and K-feldspar porphyroclasts may breakdown to aggregates of fine grained albite, white mica, clinozoisite and quartz during deformation in a *fluid-rich*, greenschist facies environment. This process, whereby the mineralogy and / or chemical composition of the 'daughter' grains differ significantly from the mineralogy and / or chemical composition of the parent porphyroclast has been termed 'neocrystallisation' (Fitz Gerald & Stünitz 1993). The aggregates of fine grained feldspar preserved within the phyllonite belts are consistently more albitic in composition than the coarse grained feldspar porphyroclasts. This observation suggests that neocrystallisation mechanisms may have been responsible for the observed grain size reduction. However, it could be argued that micro-cataclasis of the feldspar porphyroclasts would render the resulting fine grained plagioclase / K-feldspar more susceptible to albitisation (i.e. alteration) than the relatively coarse grained porphyroclasts. There are two lines of microstructural evidence which suggest that cataclasis was unlikely. Firstly, the aggregates of fine grained albite tend to be equigranular and lobate, whilst cataclasis is expected to produce angular, random-sized fragments. Secondly, the feldspar porphyroclasts are characteristically 'cloudy' in plane polarised light. In contrast, fluid inclusions are concentrated albite along grain boundaries, whilst the albite grains themselves appear to be clear in plane polarised light. These observations suggest (a) that the porphyroclasts display a 'microporous' texture (i.e. pores are distributed throughout the parent grain), and (b) that pores are restricted to the margins of the albite grains (David *et al.* 1995). Drury & Urai (1990) have demonstrated that although fluid inclusions may be homogeneously distributed within quartz *porphyroclasts*, the inclusions tend to become concentrated into grain boundary networks within aggregates of *dynamically* recrystallised quartz. It is therefore postulated that similar processes may occur in feldspars during syn-tectonic neocrystallisation of the plagioclase and K-feldspar porphyroclasts.

Microstructural observations of the quartz and feldspar porphyroclasts therefore suggest that deformation was accommodated by fluid assisted diffusive mass transfer mechanisms, and by localised intragranular fracturing, intracrystalline crystal plasticity and neocrystallisation processes. However, an apparent anomaly exists

between the relatively undeformed state of the porphyroclasts and the highly strained macro- and mesoscopic (i.e. regional-scale) fabrics observed in the field i.e. *the phyllonitic shear zone fabrics appear to exhibit strong strain intensity partitioning* (cf. the concept of 'phenomenological superplasticity' described by Gilotti & Hull 1990). This paradox can be explained if it is assumed that most of the strain has been accommodated by deformation in the relatively weak epidote-rich phyllonitic / ultraphyllonitic matrix. The ultrafine grained matrix comprises a mixture of albite, quartz, sericite, epidote, chlorite and opaque minerals. Preliminary observations suggest (a) that the quartz and albite grains are equant and display a weak crystallographic preferred orientation, and (b) that the (001) cleavage planes of the sericite and chlorite grains are aligned parallel to the macroscopic foliation. The cleavage planes of both minerals rarely display evidence of fracturing or kinking, and aggregates of recrystallised sericite / chlorite have *not* been identified. These observations suggest that there is little evidence for significant intracrystalline deformation within the ultrafine grained quartz, albite or phyllosilicate grains (cf. Bell *et al.* 1986; Hirth & Tullis 1992; Mares & Kronenberg 1993; Stünitz & Fitz Gerald 1993). The apparent lack of intracrystalline deformation, together with the observed high mesoscopic strains are consistent with deformation having been controlled by diffusion-dominated grain size sensitive mechanisms, such as grain-boundary sliding (Stünitz & Fitz Gerald 1993). In conclusion, it is postulated that grain boundary sliding was accommodated by grain scale fluid-assisted diffusive mass transfer processes within the ultrafine grained matrix, and by a combination of intracrystalline deformation, fracturing, neocrystallisation and fluid-assisted DMT within and around the margins of the relatively coarse grained quartz and feldspar porphyroclasts.

### 6.3.4 SYNTHESIS

#### 6.3.4.1 Summary

Three distinct types of phyllonite have been recognised along the OHFZ in North Uist.

- ***Discrete phyllonite bands*** are associated with thrust-, transpression- or strike-slip related fabrics and are typically preserved in western regions of the fault zone. Field and microstructural observations suggest that the discrete phyllonite bands have experienced relatively low magnitudes of macroscopically ductile, finite strain.
- ***Pervasive protophyllonite*** is associated with a NE-SW trending strike-parallel mineral lineation and is widely observed throughout the fault zone. Meso- and

microstructural observations suggest that the pervasive protophyllonites have experienced relatively low magnitudes of macroscopically ductile, finite strain.

*Phyllonitic shear zones* are associated with NE-SW trending, strike-parallel mineral lineations, which are locally rotated into NW-SE trending, down-dip plunging orientations (see section 6.4). Strike-slip related fabrics are typically preserved along shear zone margins. Macro- and mesostructural observations suggest that the strike-slip related shear zone fabrics have accommodated significant magnitudes of macroscopically ductile, finite strain.

All these fabrics appear to overprint regions of pre-existing fractured gneiss, cataclasite and / or pseudotachylyte. At relative low magnitudes of macroscopically ductile strain, deformation was accommodated by brittle intragranular fracturing, fluid assisted diffusive mass transfer and limited intracrystalline plasticity. At higher magnitudes of macroscopically ductile finite strain, deformation was accommodated predominantly by viscous grain boundary sliding, fluid-assisted DMT, neocrystallisation, recrystallisation and limited brittle intragranular fracturing.

In order to gain further insights into the mechanisms of phyllonitisation, it is important to understand the precise relationships between the primary fabric (i.e. the crush melange) and each of the different the derived fabrics (i.e. the discrete phyllonites, the pervasive protophyllonites and the phyllonitic shear zones). Section 6.3.4.2 describes the spatial and temporal relationships between the different phyllonitic fabrics, whilst section 6.3.4.3 synthesises these observations and inferences into a model of phyllonitisation on North Uist.

#### **6.3.4.2 The spatial and temporal distribution of the phyllonitic fabrics**

##### ***Discrete phyllonites and protophyllonites***

The relationships between discrete phyllonite bands and their host rocks are complex. Discontinuous, fault-bounded Type 1 phyllonite bands are developed in massive host rocks. However, Type 1 phyllonite bands are also developed in protophyllonitic host rocks, and the shear zone foliation is continuous with the regional protophyllonitic foliation (Fig. 6.5). Centimetre- to metre-scale networks of continuous Type 2 phyllonite bands are developed in regions of pervasive protophyllonite (Fig. 6.6). The sigmoidal geometry of the protophyllonitic foliation suggests that continuous Type 1 and Type 2 phyllonite bands are zones of relatively high shear strain in comparison with the protophyllonitic host rocks (Ramsay & Graham 1970) (Fig. 6.5b & 6.6). Microstructural observations are also consistent with the continuous and

discontinuous phyllonite bands being more highly strained than the protophyllonitic fabrics.

It is important to determine the *temporal* relationships between the different phyllonitic fabrics. However, in the absence of precise and accurate isotopic age dates, it is difficult to determine the relative ages of the different fabrics. The approach adopted below is to describe two possible 'end-member' models for the fabric evolution during phyllonitisation, and to compare the likely outcomes of these models to the observed field evidence.

- **Model 1** The spatial fabric sequence of protophyllonite (low strain) → discrete phyllonite (relatively high strain) tracks the fabric evolution through time (cf. Chapter 4 of Means 1976).
- **Model 2** The spatial fabric sequence of protophyllonite (low strain) → discrete phyllonite (relatively high strain) does *not* track the fabric evolution through time i.e. the pervasive protophyllonites and the discrete phyllonite bands followed different incremental strain paths.

Model 1 suggests that the relatively highly strained fabrics preserved in the discrete phyllonite bands were derived from relatively unstrained protophyllonitic fabrics. The implication of Model 1 is that all the observed fabrics have followed the same 'incremental strain path'. *Strain incompatibilities are therefore unlikely to have developed during phyllonitisation* (Means 1976).

In contrast, Model 2 suggests that the relatively highly strained fabrics preserved in the discrete phyllonite bands may *not* have been directly derived from relatively unstrained protophyllonitic fabrics. The implication of Model 2 is that the observed fabrics may have followed different incremental strain paths. If this inference is correct, it is possible that *strain incompatibilities between the phyllonite bands and the wall rocks may have developed during phyllonitisation*.

Field observations clearly demonstrate that many Type 1 phyllonite bands are bounded by brittle 'microfaults' (*sensu* Sibson 1977b; Butler 1995). Although it is not possible to unequivocally determine the age of microfaulting relative to phyllonitisation, the field relationships suggest that microfaults are only developed at the margins of those Type 1 phyllonite bands which occur in massive or weakly foliated host rocks. This observation is consistent with there being a causal link between the presence or absence of microfaults and the evolution of the phyllonitic fabrics. It is therefore postulated that the microfaults may have developed in order to accommodate strain incompatibilities between the Type 1 discrete phyllonite bands and the relatively undeformed wall rocks. If this argument is correct, it is likely that *the material within*

*the discrete phyllonite bands and the material within the wall rocks followed different incremental strain paths.* The continuous Type 1 and Type 2 phyllonite bands are *not* cross-cut by microfaults. This observation suggests that once the protophyllonitic fabrics in the wall rocks were established, the strain incompatibilities between the phyllonites bands and their host rocks diminished. The implications of this argument are discussed in section 6.3.4.3.

#### ***Phyllonitic shear zones and pervasive protophyllonites***

The spatial relationships between the phyllonitic shear zone fabrics and the pervasive protophyllonites are complex, and have been obscured (a) by the pervasive extensional overprint (section 6.4) and (b) by the presence of brittle detachment faults along the margins of many phyllonite belts. However, on a regional scale the trace of the protophyllonitic foliation clearly displays a sigmoidal geometry in the immediate hangingwall and / or footwall of each phyllonite belt (Fig. 6.1). This observation suggests that the phyllonite belts are zones of high shear strain in comparison with the protophyllonitic wall rocks (Ramsay & Graham 1970). Microstructural observations are also consistent with the shear zones having experienced a greater magnitude of finite strain than the protophyllonitic host rocks.

It is not clear from the field relationships whether the protophyllonitic wall rocks and the phyllonitic shear zones have followed the same incremental strain path. However, the overall geometry of the kilometre-scale shear zone network is exactly analogous to the geometries of the centimetre- to metre-scale networks of Type 2 phyllonite bands (compare Fig. 6.1 with Fig. 6.6). It is therefore postulated that the phyllonitic shear zones may have developed in a similar way to the discrete phyllonite bands i.e. *at the onset of phyllonitisation, the protophyllonitic host rocks may have followed a different incremental strain path to the phyllonitic and ultraphyllonitic shear zone fabrics.* The corollaries of this argument are discussed in the next section.

#### **6.3.4.3 A model of phyllonitisation on North Uist**

Field and microstructural observations suggest that at the *onset* of phyllonitisation, deformation and retrogression were initially focused into narrow, planar zones within the crush melange (i.e. into discrete phyllonite bands and phyllonitic shear zones). Relatively unstrained, discontinuous Type 1 phyllonite bands are typically developed within massive, non-foliated wall rocks. Strain incompatibilities at the margins of discontinuous phyllonite bands were accommodated by brittle, foliation-parallel 'microfaults'. In contrast, well developed, continuous pervasive protophyllonitic fabrics are typically developed in the wall rocks adjacent to more highly strained phyllonite bands and shear zones. An important corollary of these observations is that

*at the onset of phyllonitisation, both the strain rate and the rate of phyllonitisation are likely to have been significantly higher within the discrete phyllonite bands and phyllonitic shear zones than within the protophyllonitic wall rocks.*

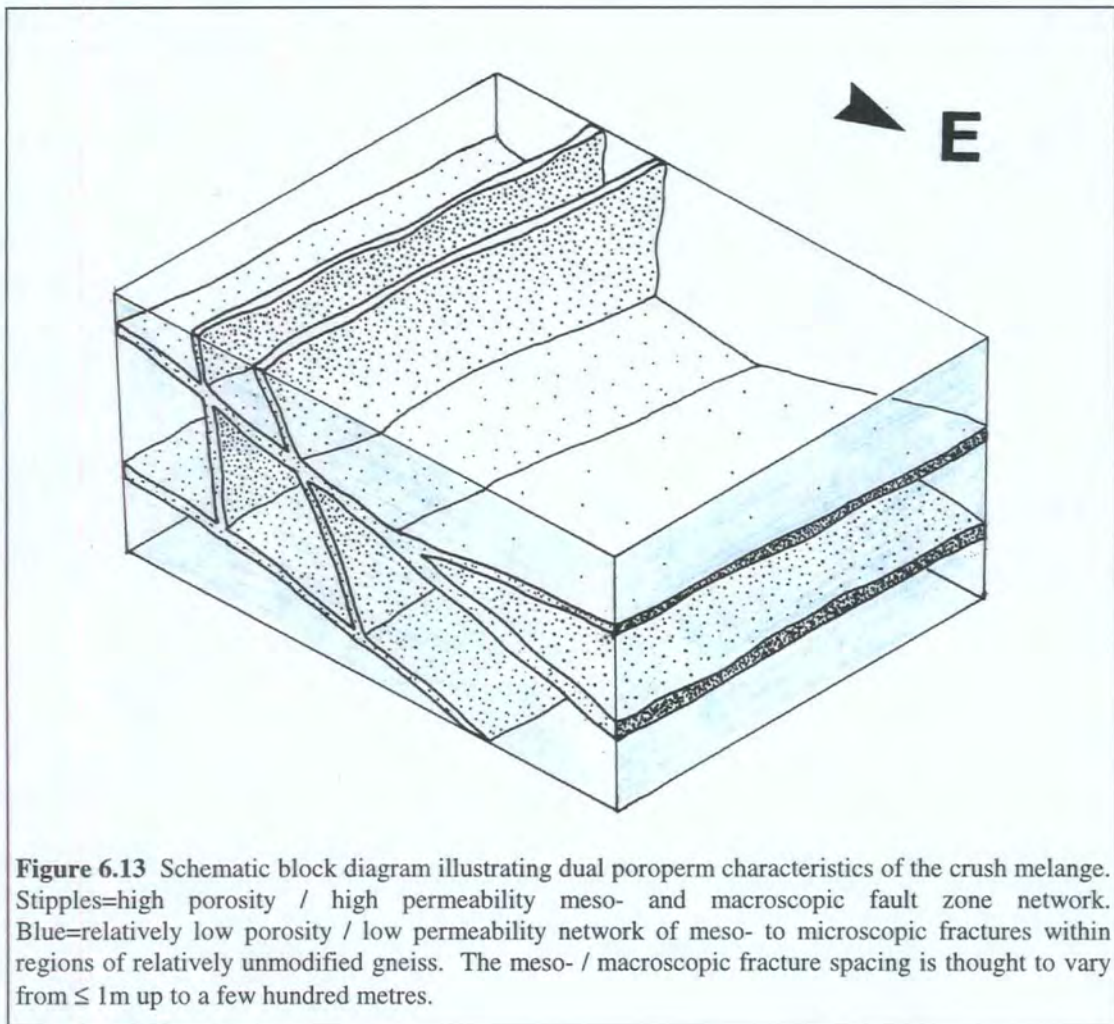
Microstructural studies suggest that deformation and syn-tectonic retrogression were strongly influenced by fluid-assisted diffusive mass transfer (DMT) mechanisms. It is widely accepted that diffusive mass transfer mechanisms are promoted by fine-grain size (e.g. Rutter 1983; Knipe 1989), which suggests that at the onset of phyllonitisation, deformation would have been focused into regions of pre-existing fine grained material within the crush melange. The availability of fluids must also have been an important control on the operation of fluid-assisted diffusive mass transfer mechanisms during phyllonitisation (Rutter 1983; Etheridge *et al.* 1984). These observations and inferences are synthesised below, to provide a model of phyllonitisation on North Uist.

### ***Role of the primary fabrics during phyllonitisation***

Microstructural observations have demonstrated that both the discrete phyllonites and the phyllonitic shear zones localised along relatively narrow bands of pre-existing fine grained material within the crush melange. However, fine grained cataclasite and devitrified pseudotachylyte are also commonly observed within regions of unmodified crush melange and within regions of relatively unstrained pervasive protophyllonite (sections 6.2.1 & 6.3.2). These observations suggest that the distribution of fine grained protoliths, although important, was unlikely to have been the *primary* control on shear zone localisation during phyllonitisation.

The availability of fluids is likely to have been a major influence on the distribution and development of the phyllonitic fabrics. The distribution of fluids at the onset of phyllonitisation is likely to have been controlled by the porosity and permeability ('poroperm') characteristics of the the crush melange. Although it has not been possible to directly measure the porosity / permeability characteristics (cf. Géraud *et al.* 1995), the distribution and intensity of hydrous, low grade alteration products give some indication of the distribution of fluids at the onset of phyllonitisation (cf. McCaig 1987; McCaig & Knipe 1990). Microstructural observations suggest that the distribution of low grade alteration within the crush melange is extremely heterogeneous (section 6.2.2.2). Feldspar grains preserved throughout the crush melange have experienced partial alteration to aggregates of fine grained sericite and epidote. However, alteration appears to have been particularly intense along networks of transgranular fractures, cataclasite seams and pseudotachylyte veins. The distribution of low grade alteration is therefore consistent with the crush melange having experienced relatively low levels of *pervasive* fluid-rock interaction, and more

intense, *localised* fluid-rock interaction (these inferences are also supported by geochemical studies, which are described in Chapter 8). These observations suggest that the crush melange was characterised by *dual-porosity / dual-permeability* ('*dual poroperm*') *fluid transport properties* (e.g. Choi *et al.* 1997). The dual poroperm system appears to have been composed of a relatively high porosity / high permeability network of interconnected, meso- and macroscopic (i.e. outcrop-scale and regional-scale) transgranular fractures, cataclasite seams and pseudotachylite veins, which was interconnected with a comparatively low porosity / low permeability network of micro-scale fractures and grain-boundaries (the poroperm characteristics of the micro-scale fracture / grain boundary network are discussed in Chapter 9) (Fig. 6.13). It is postulated that at the onset of phyllonitisation, *the discrete phyllonite bands and phyllonitic shear zone fabrics localised along the macro- and mesoscopic high porosity / high permeability network*. In particular, the centimetre- to metre-scale discrete phyllonite bands may have developed along mesoscopic fractures (section 6.2.2.1), whilst the phyllonitic shear zones probably localised along macroscopic cataclastic fault zones (?pseudotachylite-ultracataclasite crush zones) (section 3.4.2.1) developed within the crush melange.



The field relationships suggest that at the onset of phyllonitisation, both the strain rate and the rate of phyllonitisation were significantly lower within the protophyllonitic wall rocks than within the discrete phyllonite bands / phyllonitic shear zones (see above). The rate of phyllonitisation must have been influenced by the availability of fluids, which in turn was largely determined by the porosity and permeability characteristics of the host rock. It is therefore postulated that *the protophyllonitic fabrics* (section 6.3.2.1) *developed within regions of relatively low porosity and low permeability.*

### **Summary**

Field and microstructural observations suggest that the discrete phyllonite bands and the phyllonitic shear zones localised along networks of highly permeable, outcrop- and regional-scale cataclastic fault zones. In contrast, the protophyllonitic fabrics appear to have developed within regions of relatively low porosity and permeability (e.g. within augen of relatively intact gneiss and intervening regions of 'catclasite'). Relatively unstrained phyllonite bands are typically bounded by foliation-parallel 'microfaults', which are thought to have developed in order to maintain strain compatibility with the massive, non-foliated (i.e. undeformed) wall rocks. In contrast, highly strained phyllonitic shear zone fabrics appear to have been continuous with the foliated wall rocks. These observations suggest (a) that both the strain rate and rate of phyllonitisation were significantly greater within the discrete phyllonite bands and phyllonitic shear zones than within the protophyllonitic wall rocks, and (b) that the rate of phyllonitisation was a function of inherited permeability.

The heterogeneous distribution of intense low grade alteration suggests that fluid-rock interactions were focused within the high porosity / high permeability meso- to macro-scale fracture network. This observation is consistent with fluid flow having been focused along the pre-existing, highly permeable fracture / fault zone network. However, although characterised by relatively low permeability, the wall rocks do not appear to have been *totally* impermeable (see discussion in Chapter 9) (Fig. 6.13). It is therefore postulated that small volumes of fluid were able to penetrate the wall rocks adjacent to highly permeable fractures. The onset of fluid-assisted DMT within the wall rocks may have permitted continuous, macroscopically ductile deformation across margins of discrete phyllonite bands / phyllonitic shear zones, and could explain the outcrop- and regional-scale sigmoidal fabrics observed in the field (Figs. 6.1, 6.5b & 6.6). The implications of this model are (a) that the pervasive protophyllonitic fabrics *initially* developed in regions immediately adjacent to discrete phyllonite bands / phyllonitic shear zones, and (b) that the youngest, least strained pervasive protophyllonitic fabrics should be developed in regions away from discrete

phyllonite bands / phyllonitic shear zones. Further field studies in North Uist should therefore concentrate on the poroperm characteristics of the crush melange, and on the detailed relationships between the pervasive protophyllonites and the shear zone fabrics in order to prove (or disprove) this hypothesis.

## 6.4 REWORKED FABRICS & DETACHMENT FAULTS

The phyllonitic shear zone fabrics are commonly observed to have been reworked during regional transtension and subsequent extension along the OHFZ in North Uist (section 3.4.3.5). Both the reworked fabrics and unmodified strike-slip related fabrics are cross-cut by networks of foliation-parallel to discordant brittle detachment faults (section 3.4.3.3). The aims of this section are (a) to describe the overall distribution of transtension- and extension-related phyllonitic fabrics on North Uist (section 6.4.1), (b) to determine the dominant operative deformation mechanisms during reworking (sections 6.4.2 & 6.4.3), and (c) to describe the distribution and geometries of the detachment faults (section 6.4.4). The final section highlights the possible controls on extensional reworking along the OHFZ on North Uist.

### 6.4.1 THE DISTRIBUTION OF REWORKED FABRICS IN NORTH UIST

It has been demonstrated that the phyllonitic shear zone fabrics preserve evidence of a *progressive* change in the regional kinematic regime, from top-to-the-NE sinistral strike-slip, to sinistral transtension, to top-to-the-ESE extension (section 3.4.3.5) (see also Butler 1995). In order to systematically describe the reworked fabrics the following scheme has been adopted:

- **Strike-slip related phyllonites** are packages of phyllonite which are associated with a sub-horizontal, NE-SW trending mineral lineation. Kinematic indicators viewed in surfaces parallel to the mineral lineation and perpendicular to the foliation are consistent with top-to-the-NE shear.
- **Transtension-related phyllonites** are packages of phyllonite which are associated with an ENE-WSW to E-W trending mineral lineation. Kinematic indicators viewed in surfaces parallel to the mineral lineation and perpendicular to the foliation are consistent with top-to-the-ENE to -E shear.
- **Extension-related phyllonites** comprise interbanded packages of planar phyllonite and folded phyllonite. The planar phyllonites are associated with an E-W to NW-SE trending mineral lineation. Kinematic indicators viewed in surfaces parallel to the mineral lineation and perpendicular to the foliation are

consistent with top-to-the-E or -SE shear. The folds predominantly verge towards the E or SE (and locally towards the NW).

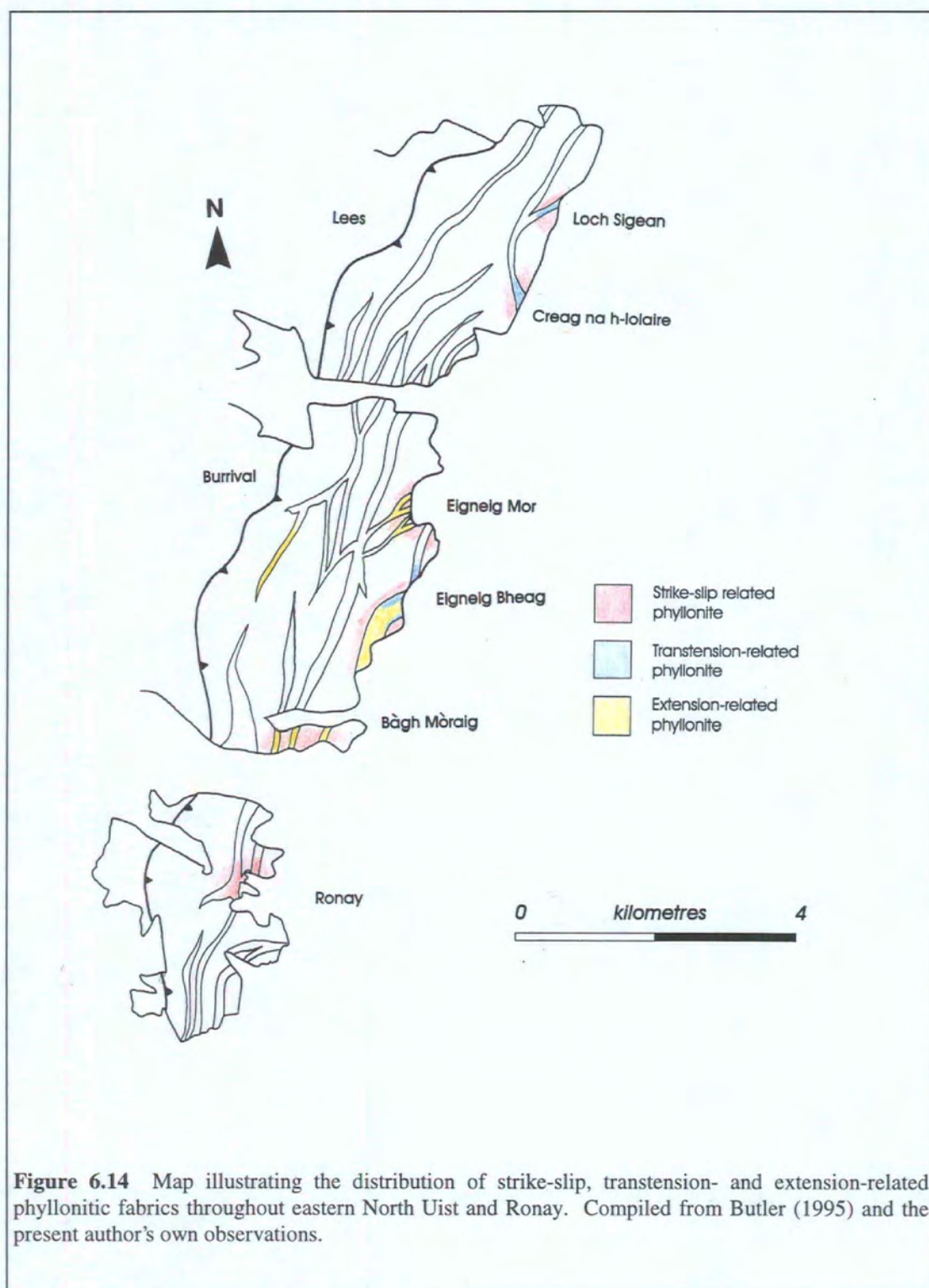


**Figure 6.14** Map illustrating the distribution of strike-slip, transtension- and extension-related phyllonitic fabrics throughout eastern North Uist and Ronay. Compiled from Butler (1995) and the present author's own observations.

The distribution of the different phyllonitic fabrics is summarised in Figure 6.14. Strike-slip related fabrics are widely observed throughout North Uist, and are typically preserved within augen of pervasive protophyllonite (section 6.3.2.1) and at the

margins of phyllonitic shear zones (section 6.3.3.2). In contrast, transtension- and extension-related fabrics tend to be preserved at the *centres* of the phyllonite belts. Transtension-related phyllonites are most commonly observed within SE- and NW-dipping, NE-SW trending shear zones (e.g. Loch Sigean, NF 947 662 and Eigneig Mor, NF 930 613 to NF 925 616), but are locally preserved in N-S and NW-SE trending shear zone segments (e.g. Eigneig Bheag, NF 925 606 and Creag na h-Iolaire, NF 945 653, respectively) (Fig. 6.14). Extension-related fabrics are widely developed within N-S trending shear zones (e.g. Eigneig Bheag, NF 9207 5957 to NF 9212 5929 and Bàgh Mòraig, NF 906 584 to NF 916 585), although thin ( $\leq 5$  m thick), detachment-bounded packages of extension-related phyllonite are locally preserved within units of predominantly transtension-related phyllonite. The N-S trending Bàgh na Caiplich phyllonite belt on Ronay (NF 901 560) is somewhat anomalous, and appears to be composed entirely of strike-slip related phyllonite (Fig. 6.14).

The crush melange, pervasive protophyllonites and strike-slip related shear zone fabrics (i.e. those rocks which were *not* reworked during regional transtension / extension) are widely observed to be cross-cut by an array of sub-vertical N-S to NNW-SSE trending quartz veins. The orientation of the fibrous quartz vein infill is generally consistent with ENE-WSW extension. It is thought that the veins developed synchronous with the onset of regional transtension along the OHFZ on North Uist (see also Butler 1995). On Ronay, the strike-slip related fabrics preserved within the Bàgh na Caiplich phyllonite belt are locally cross-cut by an array of sub-vertical NW-SE trending veins. The veins are infilled by quartz and quartz-chlorite fibres, which record two increments of vein opening. The orientation of the older quartz fibres is consistent with ENE-WSW extension, whilst the orientation of the younger quartz-chlorite fibres is consistent with ESE-WNW extension (Figs. 3.36b). It is postulated that the quartz and quartz-chlorite vein fibres preserve evidence of a progressive change from regional top-to-the-ENE transtension to regional top-to-the-ESE extension along the OHFZ on North Uist (section 3.4.3.5) (see also Butler 1995).

## 6.4.2 TRANSTENSION-RELATED FABRICS

### 6.4.2.1 Field relationships

Transtension-related shear zone fabrics comprise finely interbanded packages (typically  $\leq 2$  cm thick) of 'grey-green' and 'dark-green' phyllonite, ultraphyllonite and protophyllonite. The ratio of grey-green to dark-green phyllonite is typically around 2:1, but is locally very variable. Microstructural observations suggest that packages of grey-green phyllonite were predominantly derived from felsic protoliths, whilst packages of dark-green phyllonite and ultraphyllonite were predominantly derived

from cataclasite / pseudotachylyte protoliths (see section 6.4.2.2). Bands of relatively coarse grained protophyllonite are locally preserved in a NW-dipping shear zone to the north of Eigneig Mor (NF 9279 6156). Transtension-related protophyllonite comprises bands of coarse, angular to sub-rounded polymineralic calcite-albite-quartz-chlorite 'porphyroclasts' ( $\leq 2\text{mm}$  diameter) which are wrapped by a foliated, dark-green matrix. The origin and significance of these unusual polymineralic 'porphyroclasts' is discussed in section 6.4.3.1.

The transtension-related foliation is typically oriented sub-parallel to the margins of the host shear zone and consequently dips predominantly towards the SE, although NW- and NE-dipping fabrics are locally preserved around Eigneig Mor (NF 928 616) and Creag na h-Iolaire (NF 945 653) respectively (Figs. 3.34a, 6.1 & 6.11b). The contacts between packages of strike-slip and transtension-related phyllonite are typically defined by brittle detachment faults (section 6.4.4). However, the original shear zone fabrics are preserved at localities to the south of Eigneig Bheag (NF 9208 5970) and to the north of Eigneig Mor (NF 926 626). At NF 9208 5970, the contact between packages of strike-slip and transtension-related phyllonite is marked by a band ( $\leq 3\text{cm}$  thick) of highly weathered, moderately E-dipping en-echelon veins, which appear to be infilled by aggregates of calcite, quartz and albite. The geometry of the en-echelon vein array is consistent with the veins having opened during top-to-the-E shear (e.g. Fig. 6.16). The significance of the syn-tectonic vein arrays is discussed in section 6.4.2.3. At NF 926 626, the boundary between packages of strike-slip and transtension-related phyllonite is gradational, and is defined by a progressive clockwise rotation in the orientation of the mineral lineation.

Detailed mapping of the transtension-related phyllonites preserved within a NE-SW trending shear zone (Eigneig Bheag, NF 9248 6041) suggests that at relatively low strains, the orientation of the mineral lineation is strongly influenced by lithology (Fig. 6.15). Bands of quartz-rich, grey-green phyllonite are associated with a predominantly ENE-WSW trending mineral lineation, whilst bands of quartz-poor, dark-green phyllonite and ultraphyllonite are associated with a predominantly ESE-WNW trending mineral lineation (Figs. 6.15a & b). The implications of these observations are discussed in section 6.4.5.1.

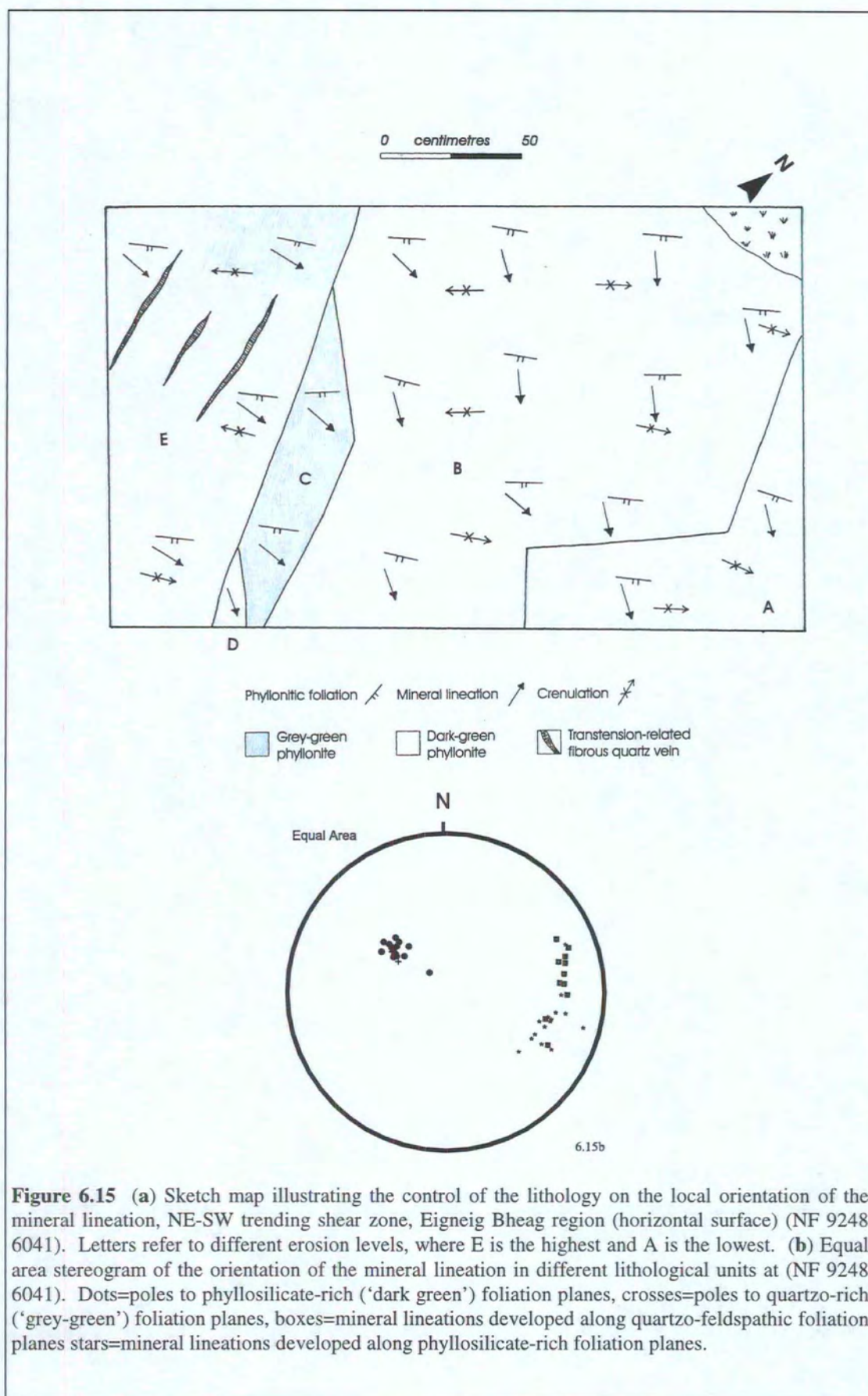


**Figure 6.15** (a) Sketch map illustrating the control of the lithology on the local orientation of the mineral lineation, NE-SW trending shear zone, Eigneig Bheag region (horizontal surface) (NF 9248 6041). Letters refer to different erosion levels, where E is the highest and A is the lowest. (b) Equal area stereogram of the orientation of the mineral lineation in different lithological units at (NF 9248 6041). Dots=poles to phyllosilicate-rich ('dark green') foliation planes, crosses=poles to quartzo-rich ('grey-green') foliation planes, boxes=mineral lineations developed along quartzo-feldspathic foliation planes stars=mineral lineations developed along phyllosilicate-rich foliation planes.

#### 6.4.2.2 Microstructure

Packages of dark-green phyllonite comprise domains of epidote-rich phyllonite and ultraphyllonite, whilst packages of grey-green phyllonite comprise domains of felsic phyllonite and protophyllonite.

##### *Epidote-rich phyllonite and ultraphyllonite* ('dark-green phyllonite')

Domains of transtension-related, epidote-rich phyllonite and ultraphyllonite comprise flattened, intensely sericitised feldspar grains (aspect ratios  $\leq 20:1$ ; sericite accounts for  $\leq 90\%$  of the surface area of host grains), chlorite aggregates and polycrystalline quartz porphyroclasts, which 'float' in an ultrafine grained matrix of sericite, albite, quartz, epidote and opaque minerals (individual grains  $\ll 0.005\text{mm}$  diameter). The foliation is defined by flattened feldspar grains, aligned sericite needles and chlorite laths and by a well developed disjunctive cleavage (*sensu* Passchier & Trouw 1996) (Plate 6.16). The disjunctive cleavage comprises finely spaced, alternating bands ( $\leq 0.01\text{mm}$  thick) of albite-quartz and sericite-epidote. Prismatic opaque minerals ( $\leq 0.1\text{mm}$  diameter), which are typically fringed by quartz or quartz-chlorite strain shadows, are commonly observed within the fine grained quartz-albite bands.

The microstructures of the quartz and feldspar porphyroclasts are similar to those observed in domains of strike-slip related epidote-rich phyllonite (see section 6.3.3.3).

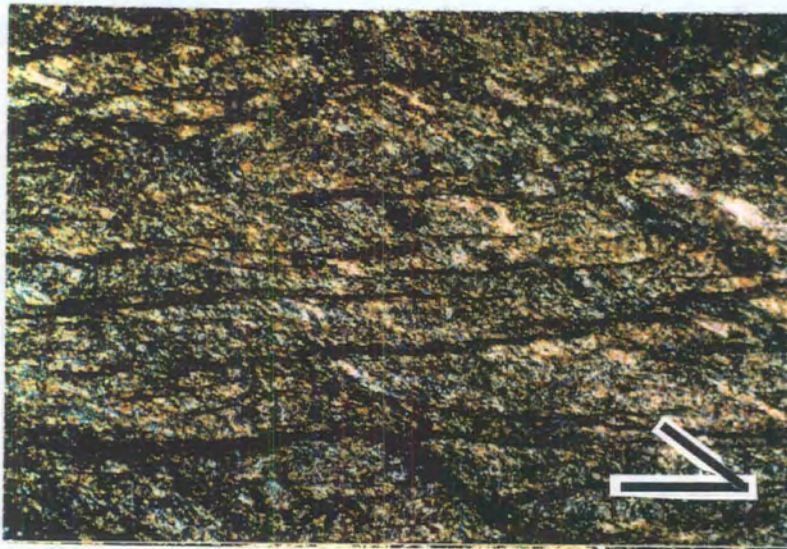


**Plate 6.16** Transtension-related reworked epidote-rich phyllonite. Disjunctive cleavage (parallel to longer bar), which is defined by concentrations of opaque grains and sericite needles, cross-cuts earlier, strike-slip related foliation (parallel to shorter bar). Field of view  $1.3 \times 0.77\text{mm}$ , crossed polars.

***Felsic phyllonite and protophyllonite*** ('grey-green phyllonite')

Domains of felsic phyllonite comprise aggregates of quartz and pristine or partially sericitised feldspar porphyroclasts ( $\leq 0.3\text{mm}$  diameter), which are wrapped by interconnected networks of sericite strands and bands of ultrafine grained albite. The sericite strands are commonly observed to be deformed by arrays of closely spaced kink bands. The kink bands ( $\cong 0.01\text{mm}$  wide) are oriented at approximately  $50^\circ$  to the trace of the foliation and are defined by an abrupt change in the grain shape preferred orientation of the sericite needles. Individual sericite needles do *not* appear to be kinked.

The partially altered feldspar grains (sericite accounts for  $\leq 80\%$  of the surface area of host grains) are typically flattened parallel to the trace of the macroscopic foliation (aspect ratios  $\leq 7:1$ ) and display well developed sericite mesh textures which are locally cross-cut by intra- and transgranular sericite strands. In contrast, pristine feldspar grains (K-feldspar and moderately Ca-rich plagioclase) are characterised by strong patchy undulose extinction and are locally surrounded by irregular mantles of ultrafine, lobate albite grains (individual grains  $\ll 0.005\text{mm}$  diameter). Sericite needles are rarely observed within albite-rich domains (Plate 6.17).

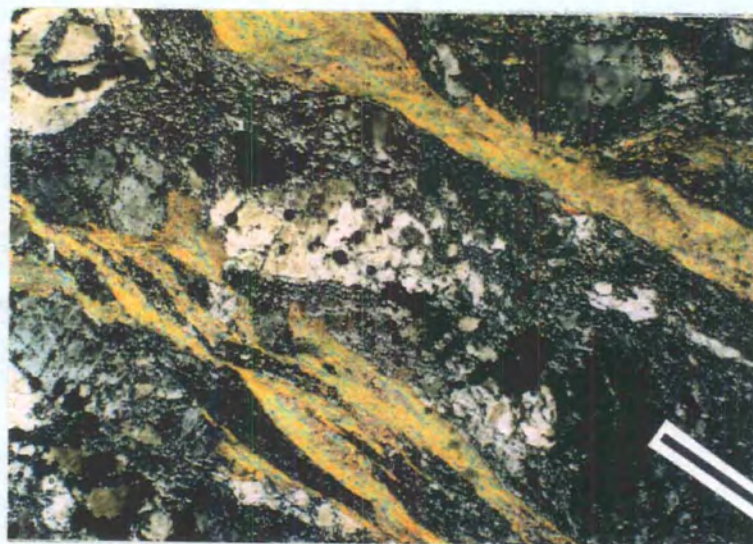


**Plate 6.17** Transtension-related reworked felsic phyllonite. Relatively unaltered feldspar porphyroclasts (pale to dark grey) 'float' in an ultrafine-grained matrix of neocrystallised albite (dark grey) and sericite strands (green). Porphyroclasts locally cross-cut by tensile intragranular fractures (arrowed). Bar parallel mineral lineation. Field of view  $6 \times 3.7\text{mm}$ , crossed polars.

Quartz porphyroclasts are characterised by strong patchy undulose extinction and locally display poorly developed 'core-and-mantle' microstructures (White 1976). The porphyroclasts are commonly observed to be cross-cut by intragranular tensile fractures (see section 6.3.3.3 for a more detailed description) and are locally fringed

by fibrous quartz-chlorite strain shadows. Where sericite strands wrap around *non*-recrystallised quartz porphyroclasts, the margins of these grains appear to be 'intruded' by a number of small embayments ( $\leq 0.02\text{mm}$  long), which are occupied by randomly oriented sericite needles.

Domains of transtension-related *protophyllonite* are characterised by abundant, coarse grained polymineralic 'porphyroclasts' ( $\leq 2\text{mm}$  diameter, typically  $\cong 0.5\text{mm}$  diameter). These 'porphyroclasts' comprise aggregates of calcite, albite, quartz, opaque minerals and chlorite, and are clearly wrapped by the phyllonitic matrix. The origin and significance of the polymineralic porphyroclasts is discussed in section 6.4.2.3.

#### **6.4.2.3 Summary and discussion**

Packages of transtension-related phyllonite are generally preserved in the centres of NE-SW trending shear zones and are characterised (a) by a well developed disjunctive cleavage and (b) by bands of calcite-rich *protophyllonite*. The transition between units of strike-slip and transtension-related phyllonite is typically very abrupt, and at lower strains, the orientation of the transtension-related mineral lineation appears to be influenced by lithology.

#### ***Origin of the transtension-related phyllonite***

In regions where the original shear zone geometries have not been modified by subsequent brittle deformation, the contacts between packages of strike-slip and transtension-related phyllonite are marked either by (a) a progressive clockwise rotation in the orientation of the mineral lineation, or (b) by arrays of en-echelon, syn-tectonic veins. These observations suggest that the original strike-slip related fabrics were deformed and overprinted during subsequent sinistral transtension. Furthermore, the microstructures observed within packages of transtension-related phyllonite are similar to the microstructures observed within packages of strike-slip related phyllonite, except that the transtension-related phyllonites appear to have experienced an additional phase of fabric development (i.e. the development of a disjunctive cleavage). These observations are consistent with *packages of strike-slip related phyllonite having been reworked during regional sinistral transtension.*

#### ***Metamorphic conditions during transtension***

Transtension-related phyllonite comprises aggregates of albite, moderately calcic plagioclase, K-feldspar, quartz, sericite, chlorite, epidote, calcite and opaque minerals. Albite, sericite and epidote appear to have been derived during neocrystallisation and alteration of the more calcic plagioclase and K-feldspar porphyroclasts, whilst chlorite was probably derived from the chemical breakdown of hornblende (see discussion in

section 6.3.3.4). The stable mineral assemblage of quartz, albite, sericite, chlorite, epidote, calcite and opaque minerals therefore suggests that retrogression occurred under fluid-rich, lower greenschist facies metamorphic conditions. In contrast to the strike-slip related phyllonites (section 6.3.3), actinolite is never observed within packages of transtension-related phyllonite. The absence of actinolite may reflect subtle changes either in the composition of the metamorphic fluid, or in the ambient pressure and temperature conditions (see discussion in Chapter 9). Fibrous quartz-chlorite aggregates are commonly observed in strain shadows around the margins of quartz and opaque grains. The quartz-chlorite fibres are oriented parallel to the macroscopic, transtension-related mineral lineation. This observation is consistent with the operation of fluid-assisted diffusive mass transfer mechanisms during transtension (see below), and suggests that lower greenschist facies retrogression was synchronous with transtension-related deformation.

#### ***Operative deformation mechanisms during transtension***

*Epidote-rich phyllonite* Domains of epidote-rich phyllonite and ultraphyllonite are characterised by intensely sericitised feldspar grains which 'float' in an ultrafine-grained matrix of quartz, albite, sericite, epidote and chlorite.

These observations suggest that the overall rheological behaviour of the epidote-rich phyllonites was controlled by the rheological behaviour of the ultrafine grained matrix (Jordan 1987; Handy 1990). The matrix is characterised by a disjunctive cleavage, which comprises alternating bands of albite-quartz and sericite-epidote. The trace of the (001) cleavage planes of the sericite needles are typically aligned parallel to the trace of the macroscopic foliation, but there is little evidence to suggest that individual sericite grains have been kinked or fractured. Opaque minerals preserved within albite-quartz bands are typically fringed by fibrous quartz or quartz-chlorite strain shadows. These observations suggest that deformation and differentiation of the albite- and sericite-rich layers may have been controlled by pressure solution and fluid-assisted diffusion processes (Wintsch 1978).

*Felsic phyllonite* Domains of felsic phyllonite comprise quartz and pristine or partially sericitised feldspar porphyroclasts ( $\leq 0.3\text{mm}$  diameter), which are wrapped by interconnected networks of kinked sericite strands and bands of ultrafine grained albite. These observations suggest that the rheological behaviour of the felsic phyllonites was controlled by the rheological behaviour of the sericite strands and aggregates of ultrafine grained albite. The intensely aligned, euhedral sericite needles typically display strong patchy undulose extinction, although individual grains are rarely observed to be kinked or fractured. Previous authors have postulated that such microstructures are consistent with the sericite grains having deformed by

intracrystalline crystal plastic mechanisms (e.g. dislocation creep) (Mares & Kronenberg 1993; Goodwin & Wenk 1995). Alternatively, strain within the sericite strands may have been accommodated by *aggregate-scale* deformation mechanisms, such as viscous grain boundary sliding (Behrmann & Mainprice 1987; Stünitz & Fitz Gerald 1993). Unfortunately, it is not possible to determine which, (if either), of these models is correct without detailed TEM studies. The fine-grained nature of the albite aggregates has hampered detailed optical study, and it has not been possible to positively identify the dominant operative deformation mechanism(s). However, Stünitz & Fitz Gerald (1993) have proposed that fine grained, greenschist facies albite-rich mylonites may accommodate deformation by viscous grain boundary sliding mechanisms.

The margins of undulose quartz porphyroclasts preserved within domains of felsic phyllonite are commonly observed to be 'intruded' by randomly oriented sericite needles. The sericite needles appear to be growing outwards from adjacent sericite strands into the margins of the quartz porphyroclasts. Similar microstructures have been described in low grade, sheared quartzites and phyllonites from Brazil, and have been attributed to localised dissolution of silica at the interfaces between quartz grains and neighbouring sericite strands (Hippertt 1994a).

*En-echelon veins* Arrays of E-dipping, en-echelon quartz-calcite-albite veins locally cross-cut the macroscopically ductile, transtension-related phyllonitic fabrics. The geometries of the vein arrays are consistent with top-to-the-E shear, which suggests that vein opening was synchronous with sinistral transtension. It is postulated that the veins developed during transient episodes of localised high pore fluid pressure within the phyllonite belts (Etheridge *et al.* 1984; Kennedy & Logan 1997). The significance of syn-tectonic veining and high pore fluid pressures during reworking will be discussed in the following section.

### **6.4.3 EXTENSION-RELATED FABRICS**

#### **6.4.3.1 Field relationships**

Extension-related shear zone fabrics comprise interbanded packages of dark-green and grey-green phyllonite, ultraphyllonite and protophyllonite. Protophyllonitic fabrics appear to be more abundant in packages of extension-related phyllonite than in packages of transtension-related phyllonite. The ratio of grey-green to dark-green phyllonite is extremely variable. The most highly strained shear zones comprise up to 70% dark-green phyllonite, whilst less highly strained shear zones comprise approximately equal proportions of grey-green and dark-green phyllonite. The style of deformation associated with extensional reworking varies systematically with the

orientation of the host shear zones. The structures developed along NE-SW and N-S trending shear zone segments will therefore be described separately.

### *NE-SW trending shear zones*

Detailed studies of the extension-related fabrics preserved in NE-SW trending shear zones have been conducted in the region to the north of Eigneig Mor (NF 930 613 to NF 925 616) (Figs. 6.1 & 6.2). The SE- and NW-dipping shear zones comprise packages of planar ( $\leq 5\text{m}$  thick) and folded ( $\leq 8\text{m}$  thick) phyllonite, ultraphyllonite and protophyllonite. Grey-green and dark-green phyllonites are preserved in approximately equal proportion. Microstructural observations (section 6.4.3.2) suggest that packages of grey-green and dark-green phyllonite were derived from felsic gneiss and cataclasite / pseudotachylite protoliths respectively.

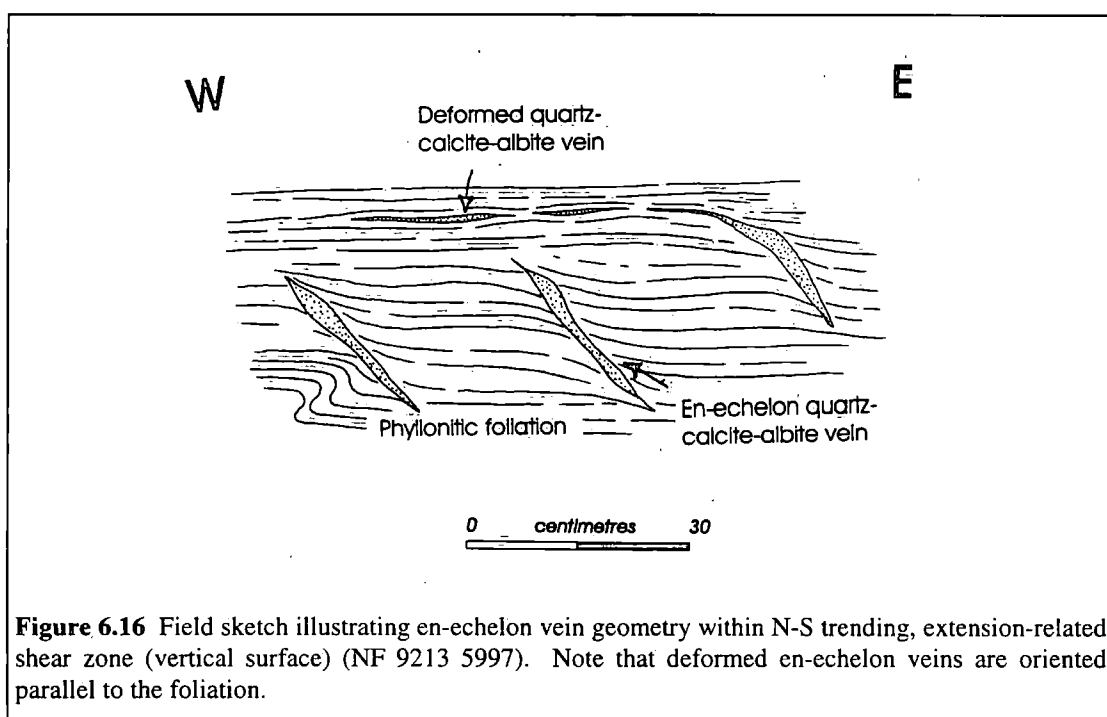


**Figure 6.16** Field sketch illustrating en-echelon vein geometry within N-S trending, extension-related shear zone (vertical surface) (NF 9213 5997). Note that deformed en-echelon veins are oriented parallel to the foliation.

Planar extension-related fabrics dip moderately towards the SE or NW, and are associated with an E-W to ESE-WNW trending mineral lineation (Fig. 6.11b). Planar phyllonites and ultraphyllonites are characterised by a strong, platy foliation, which is locally cross-cut by en-echelon arrays of E- and ESE-dipping quartz and quartz-calcite veins. The geometries of the en-echelon vein arrays are consistent with vein opening during top-to-the-E or -ESE shear (Fig. 6.16). Concordant bands and lenses of protophyllonite ( $\leq 0.5\text{m}$  thick) are commonly observed within packages of extension-related phyllonite and ultraphyllonite. These protophyllonite bands are characterised by a 'honeycomb' weathering texture and contain abundant sub-angular to rounded polymineralic quartz-calcite-albite-chlorite 'porphyroclasts' (individual

'porphyroclasts'  $\leq 3\text{cm}$  diameter). The origin of these polymineralic 'porphyroclasts' is discussed below. The contacts between packages of planar strike-slip and extension-related phyllonite are typically defined by brittle detachment faults (section 6.4.4). However, at localities where the original shear zone geometries are preserved (e.g. NF 928 617), the transition between packages of strike-slip and extension-related phyllonite is defined by a progressive change in the orientation of the mineral lineation, from a NE-SW to an ESE-WNW trend. This apparent clockwise rotation of the mineral lineation typically occurs within packages of phyllonite of less than 1m in thickness.

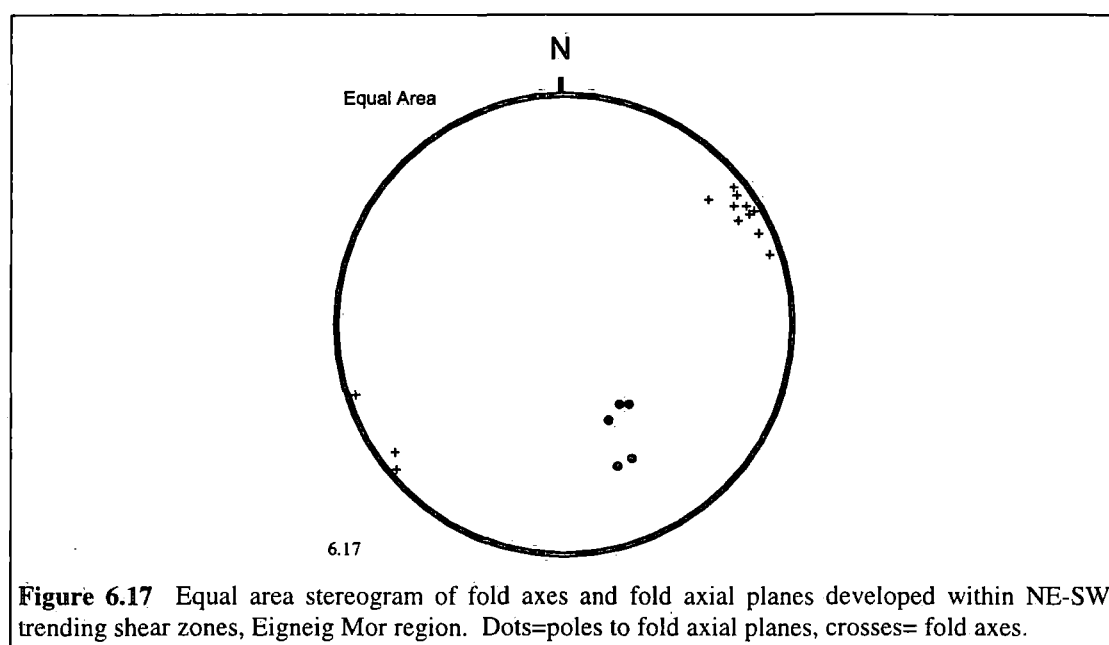


**Figure 6.17** Equal area stereogram of fold axes and fold axial planes developed within NE-SW trending shear zones, Eigneig Mor region. Dots=poles to fold axial planes, crosses= fold axes.

Packages of detachment-bounded folded phyllonite have been observed in both SE- and NW-dipping shear zones. The folds are highly asymmetric and are characterised by rounded to angular hinges, with open to tight interlimb angles. The fold axial planes dip moderately towards the NW and are associated with slightly curvilinear, sub-horizontal NE-SW trending fold axes (Fig. 6.17). Up to four orders of parasitic folds have been observed in the field, with wavelengths ranging from a few millimetres up to approximately 2m. The overall vergence direction is towards the SE, although parasitic folds preserved in the short limbs of larger folds locally verge towards the NW (cf. Fig. 3.17b) (see also Butler 1995). Packages of folded *protophyllonite* typically display a well developed 'honeycomb' weathering texture owing to the presence of numerous quartz-albite-calcite-chlorite 'porphyroclasts'. The folds are commonly observed to be cross-cut by quartz-albite-epidote veins. Undeformed veins are typically oriented parallel to the fold axial planes and cross-cut both the phyllonitic foliation and older, deformed quartz-albite-epidote veins.

Deformed veins are typically folded, and are discordant both to the foliation and to the fold axial planes (Fig. 6.18). These observations suggest that the axial planar veins may have developed synchronous with folding and macroscopically ductile extensional reworking.

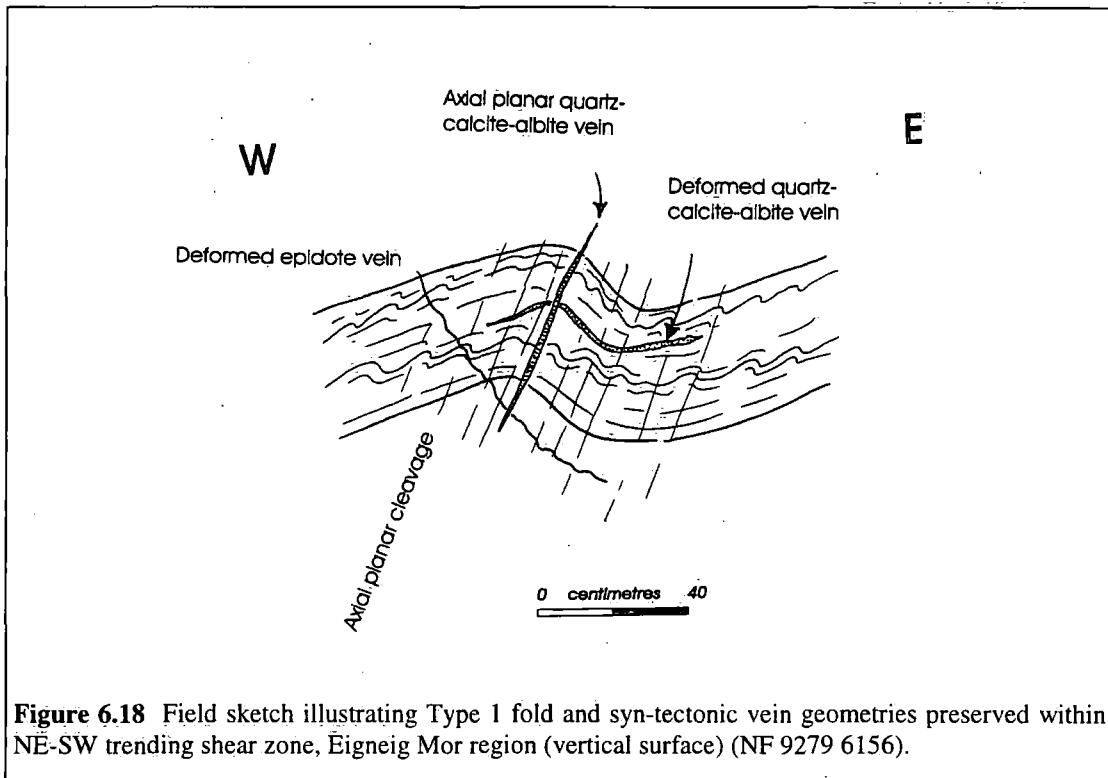


**Figure 6.18** Field sketch illustrating Type 1 fold and syn-tectonic vein geometries preserved within NE-SW trending shear zone, Eigneig Mor region (vertical surface) (NF 9279 6156).

### *N-S trending shear zones*

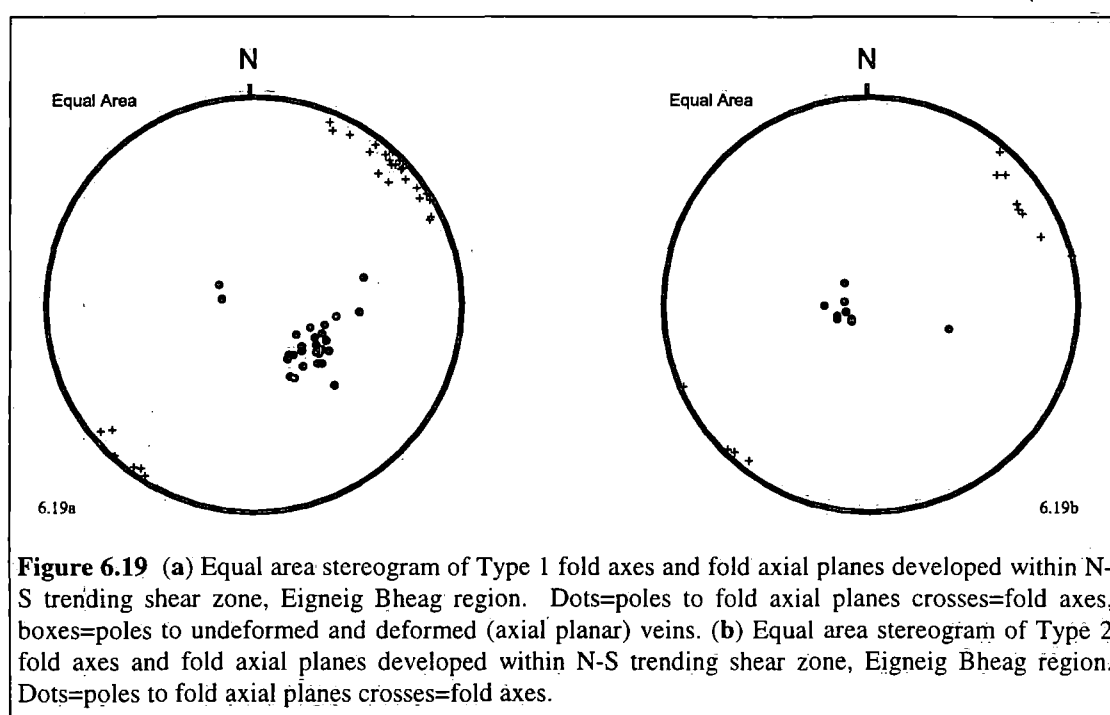
Detailed studies of the extension-related fabrics preserved in a N-S trending shear zone have been conducted in the region to the south of Eigneig Bheag (NF 9207 5957 to NF 9212 5929) (Figs. 6.1 & 6.2). The shear zone comprises packages of planar ( $\leq 3\text{m}$  thick) and folded ( $\leq 5\text{m}$  thick) phyllonite, ultraphyllonite and protophyllonite. Packages of dark-green phyllonite outnumber packages of grey-green phyllonite by a ratio of approximately 6:1. Microstructural observations (section 6.4.3.2) suggest that the dark-green phyllonites were derived predominantly from highly deformed cataclasite and / or pseudotachylite protoliths, with subordinate amounts (probably  $\leq 10\%$ ) derived from mafic protoliths. Packages of grey-green phyllonite were derived from felsic gneiss protoliths. The contacts between packages of strike-slip and packages of extension-related phyllonite are typically defined by brittle detachment faults (section 6.4.4). However, the original shear zone fabrics are preserved at a locality to the south of Eigneig Bheag (NF 9207 5957), where the transition from strike-slip and extension-related phyllonite is defined by an abrupt change in the orientation of the mineral lineation, from a NE-SW to an ESE-WNW trend.

*Planar phyllonite* Planar extension-related phyllonite dips moderately towards the southeast, and is associated with a ESE-WNW to SE-NW trending mineral lineation. Planar phyllonites and ultraphyllonites are characterised by a very well developed, platy foliation. The foliation is commonly observed to be disrupted (a) by arrays of centimetre-scale en-echelon E- to ESE-dipping quartz-calcite-albite-chlorite veins (Fig. 6.16) and (b) by metre-scale arrays of foliation-parallel calcite-albite-chlorite veins. The geometries of undeformed en-echelon veins are consistent with top-to-the-E or -ESE shear. Deformed en-echelon veins are typically oriented sub-parallel to the phyllonitic foliation, and are commonly observed to be boudinaged (Fig. 6.16). These observations suggest that there may have been several cycles of en-echelon vein emplacement during macroscopically ductile extension. Foliation-parallel vein arrays are commonly observed to line Type 1' detachment fault planes (see section 6.4.4) (e.g. south of Eigneig Bheag, NF 9212 5929 & north of Eigneig Mor NF 9279 6156). The veins form laterally continuous bands ( $\leq 15\text{m}$  long;  $\leq 10\text{cm}$  thick) which contain angular clasts of brecciated phyllonite (clasts  $\leq 0.5\text{cm}$  diameter). The foliation-parallel veins are locally overprinted by a macroscopically ductile fabric, which is defined by flattened clasts of phyllonite (aspect ratios  $\leq 4:1$ ), calcite ribbons and aggregates of aligned chlorite grains (e.g. NF 9279 6156). These observations suggest that the foliation-parallel vein arrays (and the Type 1' detachment faults) developed synchronous with macroscopically ductile extension. The relative age and significance of the Type 1 detachments is discussed further in section 6.4.4.

Laterally continuous (on the scale of metres to tens-of-metres) bands of *protophyllonite* are commonly observed within packages of extension-related phyllonite and ultraphyllonite. The *protophyllonite* bands are characterised by a 'honeycomb' weathering texture and contain abundant sub-angular to rounded polymineralic quartz-albite-calcite-chlorite 'porphyroclasts' ( $\leq 3\text{cm}$  diameter). Direct field evidence for the origin of these unusual, polymineralic 'porphyroclasts' is lacking. However, the laterally continuous nature of the *protophyllonite* bands, the mineralogy of the 'porphyroclasts' and microstructural evidence (see section 6.4.3.2) are all consistent with the *protophyllonite* bands having been derived from highly deformed and dismembered foliation-parallel vein arrays. If this inference is correct, the abundance of *protophyllonite* bands suggests that there were several episodes of foliation-parallel vein emplacement during extensional reworking.

*Folded phyllonite* Two distinct types of folded phyllonite have been recognised within N-S trending shear zones. Type 1' folds are typically preserved either at the shear zone margins or within isolated fault-bounded packages at the centre of the shear zone. In contrast, Type 2' folds are widely observed in the centre of the shear zone. Type 1 folds are identical to the folds preserved within the NE-SW trending

shear zones at Eigneig Bheag (see above), and are characterised by rounded to angular hinges, with open to tight interlimb angles (Fig. 6.18). The fold axial planes dip moderately towards the NW or SE and are associated with slightly curvilinear, sub-horizontal NE-SW trending fold axes (Fig. 6.19a). At least three orders of folds have been observed in the field (wavelengths vary from 20cm to a few millimetres), although the highest order folds are only developed in bands of dark-green phyllonite. The overall fold vergence is always towards the ESE or SE and an axial planar crenulation cleavage is locally developed within bands of dark-green phyllonite and ultraphyllonite. Packages of Type 1 folded phyllonite typically display very well developed 'honeycomb' weathering textures, owing to the presence of coarse polymineralic quartz-calcite-albite 'porphyroclasts' (individual porphyroclasts  $\leq 2$ cm diameter).



Type 2 folds are characterised by angular to sub-angular fold hinges, and tight to isoclinal interlimb angles. The axial planes dip gently towards the east and are associated with slightly curvilinear, sub-horizontal NE-SW trending fold axes (Fig. 6.19b). Viewed in the profile plane, Type 2 structures define cascades of chevron folds, which predominantly verge towards the ESE. Type 2 folds are associated with a well developed axial planar crenulation cleavage. The crenulation cleavage, which carries an ESE- to SE-plunging mineral lineation (Fig. 6.11b), is oriented parallel to the margins of the shear zone. In places, the crenulation cleavage completely transposes the folded fabric. In regions where the planar fabric is dominant, millimetre- and centimetre-scale rootless chevron folds locally deform the crenulation

cleavage. These observations suggest that the Type 2 folds presently exposed within the shear zone may have developed over one or more 'cycles' of folding, crenulation, transposition and refolding. Type 1 and Type 2 folds are commonly observed to be cross-cut by narrow, quartz-albite-epidote veins ( $\leq 3\text{mm}$  thick). Undeformed veins are typically oriented parallel to the fold axial planes and cross-cut both the phyllonitic foliation and older, deformed quartz-albite-epidote veins. Highly deformed veins are oriented parallel to the foliation and are highly attenuated, whilst less deformed veins typically cross-cut the foliation (e.g. Figs. 6.18, 6.19a & 6.20). These observations suggest that vein opening may have been broadly synchronous with extensional reworking and folding.

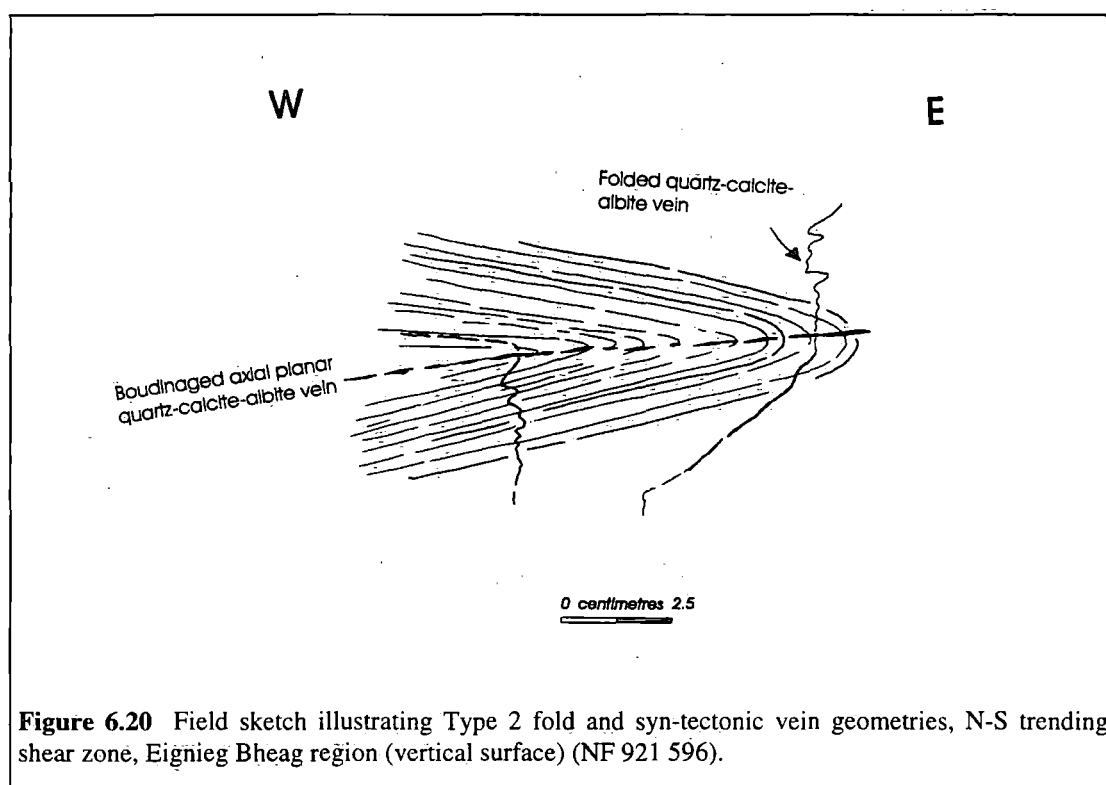


**Figure 6.20** Field sketch illustrating Type 2 fold and syn-tectonic vein geometries, N-S trending shear zone, Eignieg Bheag region (vertical surface) (NF 921 596).

#### 6.4.3.2 Microstructure

Five distinct microstructural domains have been recognised within packages of extension-related phyllonite. Domains of planar and folded felsic phyllonite correspond to the planar and folded grey-green phyllonites observed in the field. Domains of planar and folded epidote-rich phyllonite and domains of mafic phyllonite correspond to the planar and folded dark-green phyllonites observed in the field.

The following section comprises descriptions of (a) the syn-tectonic veins and 'porphyroclasts', (b) mafic phyllonite, (c) folded felsic phyllonite and (d) folded epidote-rich phyllonite. The microstructures of the planar, extension-related felsic and epidote-rich phyllonites are indistinguishable from the microstructures of the planar,

transtension-related felsic and epidote-rich phyllonites, which are described in section 6.4.2.2.

### *Syn-tectonic veins and 'porphyroclasts'*

The phyllonitic fabric is commonly observed to be cross-cut by arrays of en-echelon and foliation-parallel veins. Field evidence suggests that the veins were emplaced synchronous with macroscopically ductile deformation. The bands of coarse grained, polymineralic 'porphyroclasts' are thought to have been derived from highly dismembered, deformed veins.

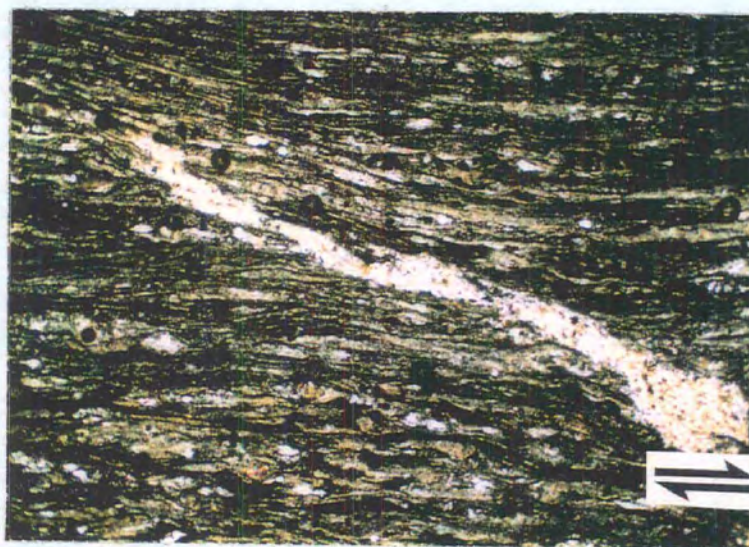


**Plate 6.18** En-echelon vein in extension-related reworked epidote-rich phyllonite. Vein infilled by aggregates of polycrystalline calcite. Split arrows parallel mineral lineation, top-to-ESE shear. Field of view 12×7.2mm, crossed polars.

En-echelon and foliation-parallel veins typically comprise aggregates of calcite, albite, quartz and chlorite (Plates 6.18 & 6.19). The modal percentages are very variable, although overall, calcite and albite appear to be the most abundant minerals. Relatively undeformed veins comprise equigranular- to seriate-interlobate aggregates of fine grained calcite (individual grains  $\leq 0.05\text{mm}$  diameter), twinned albite grains ( $\leq 2\text{cm}$  diameter) and aggregates of massive or fibrous quartz ( $\leq 2\text{cm}$  diameter). The albite grains appear to be completely unaltered. More highly deformed veins comprise calcite ribbons ( $\leq 0.05\text{mm}$  thick; aspect ratios  $\leq 10:1$ ) and equigranular- to seriate-interlobate aggregates of fine grained, untwinned albite and / or quartz (individual grains  $\leq 0.05\text{mm}$  diameter). The calcite ribbons are typically oriented parallel to the macroscopic foliation and are locally cross-cut by two sets of narrow, intersecting deformation twins (twins  $\leq 0.025\text{mm}$  wide; angle of intersection between

40° and 60°). Chlorite laths preserved in both deformed and relatively undeformed veins typically display strong patchy undulose extinction.

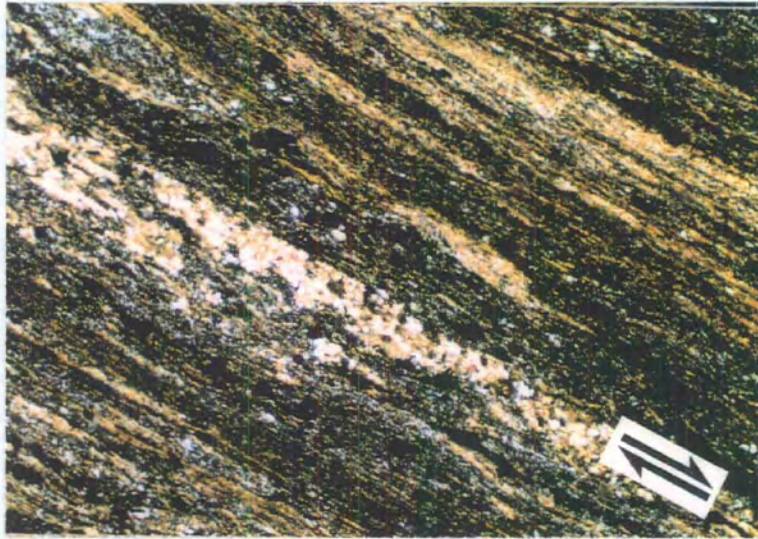


**Plate 6.19** Foliation-parallel vein in extension-related reworked epidote-rich phyllonite. Vein infilled by aggregates of polycrystalline calcite and albite. Split arrows parallel mineral lineation, top-to-ESE shear. Field of view 12×7.2mm, crossed polars.

Coarse, polymineralic 'porphyroclasts' are commonly observed within packages of extension-related protophyllonite. The 'porphyroclasts' comprise aggregates of quartz, albite, calcite and chlorite (Plates 6.20a & b). The grain size is extremely variable. Twinned albite grains ( $\leq 2\text{cm}$  diameter) (Plate 6.20b) are typically mantled by seriate-interlobate aggregates of ultrafine grained albite (individual grains  $\leq 0.005\text{mm}$  diameter). Coarse quartz grains ( $\leq 1\text{cm}$  diameter) display intense, patchy undulose extinction and are locally cross-cut by intragranular extension fractures.

It is postulated that such 'porphyroclasts' were derived from boudinated syn-tectonic veins and Type 1' detachment faults (see discussion below).

### ***Mafic phyllonite and ultraphyllonite***

Mafic phyllonite comprises an assemblage of chlorite, feldspar, sericite, quartz, opaque minerals, epidote  $\pm$  calcite. The foliation is defined by interconnected networks of chlorite strands, flattened feldspar grains and strung-out trails of fine grained epidote and opaque minerals. The flattened feldspar grains ( $\leq 0.01\text{mm}$  wide; aspect ratios  $\leq 6:1$ ) are partially sericitised (sericite accounts for  $\leq 50\%$  of the surface area of host grains) and are locally cross-cut by foliation-parallel, intragranular sericite strands.

Angular quartz porphyroclasts ( $\leq 0.2\text{mm}$  diameter; aspect ratios  $\cong 1:1$ ) are locally preserved within the chlorite strands. The quartz grains display strong patchy undulose extinction, and are typically fringed by fibrous chlorite strain shadows.

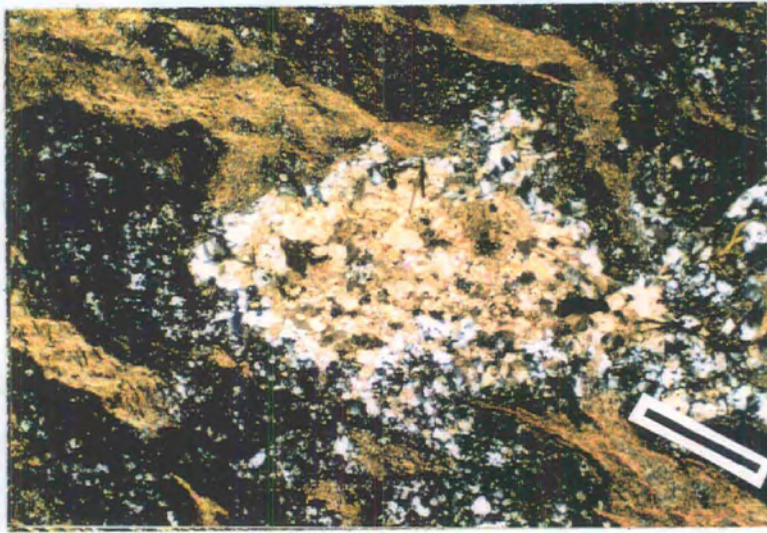


**Plate 6.20** Polymineralic / polycrystalline 'porphyroclasts' preserved in extension-related reworked epidote-rich phyllonite. (a) Calcite 'porphyroclast' wrapped by sericite strands. Bar parallel mineral lineation. Field of view  $12 \times 7.2$  mm, crossed polars. (b) Albite 'porphyroclast' wrapped by sericite strands. Bar parallel mineral lineation. Field of view  $12 \times 7.2$  mm, crossed polars. Both 'porphyroclasts' are thought to have been derived from dismembered syn-tectonic veins. See text for discussion.

### *Folded felsic phyllonite and ultraphyllonite*

Folded felsic phyllonite and ultraphyllonite comprise quartz and feldspar porphyroclasts, which are wrapped by sericite strands and bands of ultrafine grained quartz and albite. Coarse, polymineralic calcite-albite-quartz 'porphyroclasts' are locally preserved in fold hinges. Three orders of folds are visible on the thin section scale. First and second order folds (wavelength  $\leq 2\text{cm}$ ) display similar geometries to the 'Type 1' folds observed in the field (section 6.4.3.1). Third order folds are kink bands within sericite strands. The kink bands are oriented sub-parallel to the axial planes of the larger folds and are defined by abrupt changes in the grain shape preferred orientation of the sericite needles. Individual sericite needles display patchy undulose extinction, but do not appear to be kinked or fractured. In regions where sericite strands impinge upon quartz porphyroclasts, the margins of the porphyroclasts appear to be 'intruded' by numerous small embayments ( $\leq 0.02\text{mm}$  long) which contain apparently randomly oriented sericite needles (see section 6.4.2.2) (Plate 6.21).

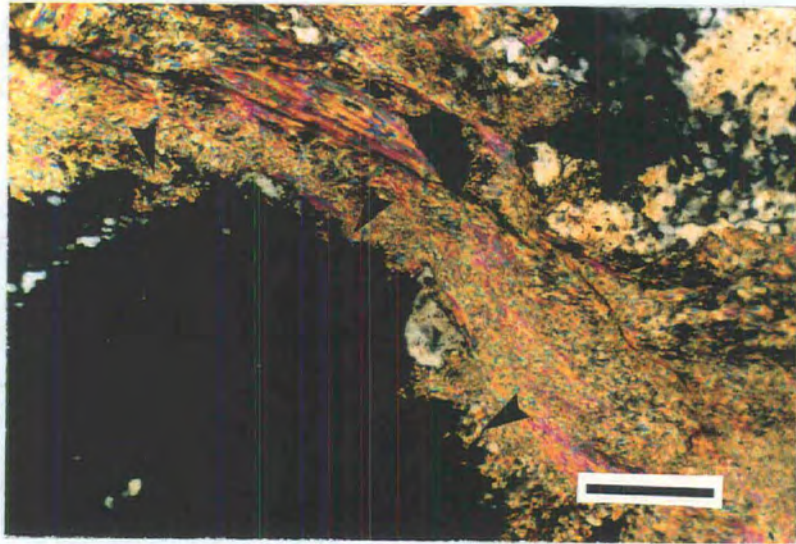


**Plate 6.21** Extension-related reworked phyllonite. Feldspar porphyroclast (black) is locally intruded by irregular embayments containing sericite needles (arrowed). Such microstructures are thought to have developed in response to pressure solution of feldspar grains along sericite strands. See text for discussion. Bar parallel mineral lineation. Field of view  $1.3 \times 0.77\text{mm}$ , crossed polars.

The Type 1 folds are commonly observed to be cross-cut by deformed and undeformed axial planar veins, which are typically infilled by fibrous quartz and / or massive quartz-albite-epidote-chlorite aggregates (Plate 6.22). In undeformed veins, the orientation of the fibres is consistent with vein opening in a direction

perpendicular to the fold axial planes (i.e. tensile opening). The relationships between folding and vein opening during reworking will be discussed in section 6.4.3.3.



**Plate 6.22** Type 1 folds in extension-related reworked felsic phyllonite. Layering defined by sericite strands and bands of fine grained recrystallised quartz. Note axial planar quartz-albite vein (arrowed). Top-to-ESE shear. Field of view 6×3.7mm, crossed polars.



**Plate 6.23** Type 2 folds (highlighted) in extension-related reworked epidote-rich phyllonite. Top-to-ESE shear. Field of view 6×3.7mm, crossed polars.

### ***Folded epidote-rich phyllonite and ultraphyllonite***

Folded epidote-rich phyllonite and ultraphyllonite comprise an ultrafine grained assemblage of albite, sericite, quartz, epidote, chlorite and opaque minerals. Cascades

of angular to subangular, tight to isoclinal Type 2 folds (wavelength  $\leq 1\text{mm}$ ) are commonly observed within thin sections (Plate 6.23). The fold limbs are defined by aggregates of epidote and aligned sericite  $\pm$  chlorite needles, whilst fold hinges comprise aggregates of ultrafine grained albite and quartz  $\pm$  epidote grains and chlorite laths. Insertion of a sensitive tint plate suggests that the crystallographic preferred orientation of the ultrafine albite and quartz grains changes abruptly across fold axial planes. An axial planar crenulation cleavage is locally well developed and is defined by alternating sericite-epidote-chlorite and albite-quartz-chlorite layers ( $\leq 0.025\text{mm}$  thick). The intensity of the crenulation cleavage is extremely variable.

#### **6.4.3.3 Summary and discussion**

Packages of extension-related phyllonite tend to be preserved in the centres of N-S trending shear zones, and comprise interbanded packages of epidote-rich phyllonite, felsic phyllonite and mafic phyllonite. Extensional reworking was associated with the development of folds and syn-tectonic veins.

#### ***Origin of the extension-related phyllonite***

The boundaries between packages of strike-slip and extension-related phyllonite are characterised by a progressive clockwise rotation of the mineral lineation, from a NE-SW to an ESE-WNW trend. Packages of planar felsic phyllonite, which are lithologically and microstructurally indistinguishable from strike-slip and transtension-related felsic phyllonites (section 6.4.2) are commonly observed to be deformed by E- to SE-verging folds. These observations suggest that *packages of strike-slip and / or transtension-related phyllonite were reworked during regional extensional displacements along the OHFZ* (cf. the Usinish Phyllonite; Chapter 7).

#### ***Retrogression and metamorphism during reworking***

The extension-related phyllonites comprise a stable mineral assemblage of albite, quartz, sericite, chlorite, epidote, calcite and opaque minerals. Syn-tectonic veins developed during extensional reworking typically contain aggregates of quartz, albite, calcite and chlorite. These observations suggest that extensional reworking took place in a fluid rich, lower greenschist facies metamorphic environment. Deformed calcite aggregates are locally cross-cut by arrays of narrow, intersecting deformation twins, which is consistent with deformation having taken place at temperature of between  $200^{\circ}\text{C}$  and  $250^{\circ}\text{C}$  (Burkhard 1993).

### ***Operative deformation mechanisms during macroscopically ductile reworking***

***Planar phyllonite*** The microstructures observed packages of planar, extension-related felsic and epidote-rich phyllonite are indistinguishable from those observed in packages of planar, *transtension*-related felsic and epidote-rich phyllonites (section 6.4.2.2), suggesting that the operative deformation mechanisms were the same in both cases i.e. dislocation creep and / or grain boundary sliding within sericite strands, and fluid-assisted diffusion-dominated viscous grain boundary sliding in ultrafine grained quartz-albite layers. Deformation within packages of planar epidote-rich phyllonite was probably accommodated by pressure solution and fluid-assisted diffusion (see section 6.4.2.3).

***Folded phyllonite*** Two distinct styles of folding have been observed within units of extension-related phyllonite. Type 1 folds are developed in packages of (predominantly) felsic phyllonite and ultraphyllonite. The available field evidence suggests that the Type 1 folds developed during a *single* phase of folding, and may thus represent regions of relatively low strain. Coarse, polymineralic calcite-albite-quartz-chlorite 'porphyroclasts' are commonly observed in the hinges of Type 1 folds. It is postulated that flow perturbations adjacent to these 'porphyroclasts' may have localised fold nucleation during macroscopically ductile reworking (Cobbold & Quinquis 1980; Chapter 10 of Price & Cosgrove 1990) (see Chapter 5 for a more detailed discussion of fold nucleation during reworking). Sericite strands which have been deformed by Type 1 folds are cross-cut by closely spaced kink bands. Individual sericite needles display strong patchy undulose extinction, but are rarely kinked or fractured. The margins of quartz porphyroclasts preserved within folded sericite strands are commonly observed to be 'intruded' by numerous fine grained sericite needles and laths. Such microstructures are thought to have developed during dissolution of silica along the margins of the quartz porphyroclasts (Hippertt 1994a) (section 6.4.2.3). These observations suggest that during folding, the sericite strands deformed by aggregate-scale (as opposed to grain-scale) kinking, which was accommodated by dislocation glide within individual sericite needles (Mares & Kronenberg 1993). Strain incompatibilities at the margins of folded sericite strands were removed by localised dissolution of silica. Quartz-albite aggregates which have been deformed by Type 1 folds typically display well developed crystallographic fabrics. This observation suggests that folding may have been accommodated by intracrystalline deformation within the quartz and albite grains. However, given their ultrafine grained nature, it is not possible to rule out the involvement of fluid-assisted, grain size sensitive deformation mechanisms during folding within the quartz-albite bands.

Type 2 folds are developed in packages of epidote-rich phyllonite and ultraphyllonite, and are particularly common in N-S trending shear zones. Type 2 folds are associated with a well developed axial planar crenulation cleavage, which locally transposes the folded fabric. The available field and microstructural evidence suggests that the folds may have developed over one or more 'cycles' of folding, crenulation, transposition and refolding. The Type 2 folds may therefore represent regions of relatively high extension-related strain. The fold limbs are comprised of aggregates of epidote and aligned sericite and chlorite needles, whilst the hinges comprise aggregates of albite, quartz and chlorite. The crenulation cleavage is characterised by alternating sericite-epidote-chlorite and albite-quartz-chlorite bands. Individual phyllosilicate grains do not appear to be kinked or fractured, and the albite-quartz aggregates typically display a strong crystallographic fabric. These observations suggest that folding and crenulation development may have been accommodated by fluid-assisted diffusion-dominated and / or intracrystalline crystal plastic mechanisms, rather than by frictional sliding or mechanical rotation of grains (Wintsch 1978).

#### ***Role of syn-tectonic veins during extensional reworking***

There is widespread field and microstructural evidence for the development of syn-tectonic vein arrays during reworking. Packages of planar phyllonite are commonly observed to be cross-cut by arrays of en-echelon and foliation-parallel calcite-albite-quartz-chlorite veins. Type 1 and Type 2 folds are typically associated with axial planar quartz-calcite-albite-epidote veins.

The geometries of undeformed en-echelon veins are consistent with emplacement during top-to-the-E or -ESE extension. There is no evidence to suggest that vein emplacement was associated with significant brittle deformation or disruption of the macroscopically ductile phyllonitic fabrics. It is therefore unlikely that vein opening contributed significantly to the finite strain experienced by the host rocks. En-echelon veins are commonly observed to be deformed and boudinaged parallel to the mineral lineation. These observations are consistent with continued macroscopically ductile deformation following vein emplacement. It is therefore postulated that the en-echelon veins developed during transient episodes of localised high pore fluid pressure within packages of viscously deforming planar phyllonite (Cox & Etheridge 1989; Kennedy & Logan 1997). The abundance of deformed veins, and their variable ages relative to the folds and phyllonitic fabrics, suggest that there may have been several episodes of high pore fluid pressure and en-echelon vein emplacement during reworking.

Arrays of foliation-parallel veins are commonly observed to line Type 1 detachment fault planes (see section 6.4.4). The phyllonitic fabrics preserved within the

detachment faults are highly disrupted and locally appear to be brecciated. In general, structures preserved in the hangingwalls and footwalls cannot be correlated across detachment faults. These observations suggest that Type 1 detachments represent localised zones brittle shearing, which probably contributed significantly to the finite strain accommodated within the phyllonite belts. The abundance of foliation-parallel veins is consistent with faulting and shearing having occurred during episodes of localised, high pore fluid pressure within the reworked phyllonite belts (Cox & Etheridge 1989). If this inference is correct, it is likely that the foliation-parallel veins originated as shear hydraulic fractures. It has been suggested that the stress conditions required for shear hydraulic fracture are that  $[\sigma_1 - \sigma_3] = 8T$ , and that the pore fluid pressure is equal to  $\sigma_3$ , (where  $[\sigma_1 - \sigma_3]$  is the differential stress;  $T$  = the tensile strength of the phyllonite;  $\sigma_3$  = the minimum principal compressive stress) (Etheridge 1983) (Table 1.1). The breccias / vein arrays are locally overprinted by a ductile fabric (section 6.4.3.1), which is consistent with continued macroscopically ductile deformation following the cessation of brittle shearing. Furthermore, it has been postulated that the bands of coarse, polymineralic 'porphyroclasts' may have been derived from highly deformed, dismembered foliation-parallel vein arrays (sections 6.4.3.1 & 6.4.3.2). It is therefore likely that there were several cycles of high pore fluid pressure, vein emplacement and localised brittle shearing during reworking (Cox & Etheridge 1989) (see Chapter 9 for further discussion).

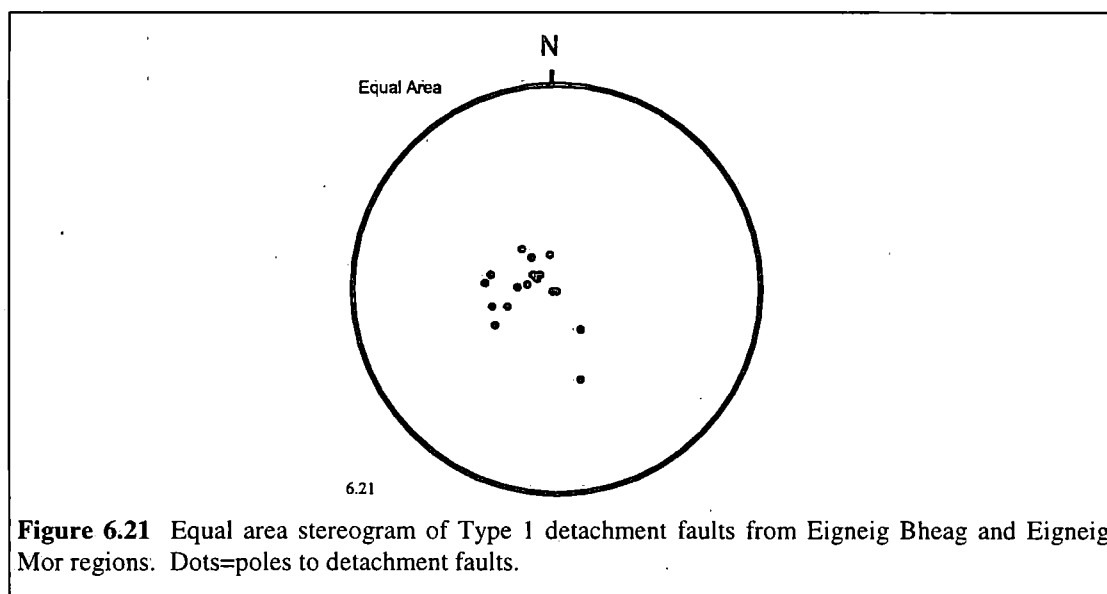
Axial planar albite-epidote-quartz veins are commonly observed in packages of Type 1 and Type 2 folded phyllonite. The orientation of the quartz fibres is consistent with vein opening in a direction perpendicular to the fold axial planes. In contrast to the foliation-parallel veins, there is no evidence to suggest that emplacement of the axial planar veins was associated with significant shear strain. It has been suggested that the stress conditions required for tensile fracture are that  $[\sigma_1 - \sigma_3] \leq 4T$ , and that the pore fluid pressure is less than  $\sigma_3$ , (where  $[\sigma_1 - \sigma_3]$  is the differential stress;  $T$  = the tensile strength of the phyllonite;  $\sigma_3$  = the minimum principal compressive stress) (Etheridge 1983) (Table 1.1).

In conclusion, extensional reworking appears to have been accommodated by (a) macroscopically ductile, grain size sensitive viscous creep processes (pressure solution and fluid assisted diffusive mass transfer)  $\pm$  intracrystalline deformation, and by (b) localised brittle faulting and veining during transient episodes of high pore fluid pressure. It is postulated that most of the observed finite strain accumulated by viscous creep processes, although localised slip along Type 1 detachments / foliation-parallel veins may have contributed significantly both to the strain and to the strain rate. The role of hydraulic fracture during reactivation is discussed further in Chapter 9.

## 6.4.4 DETACHMENT FAULTS

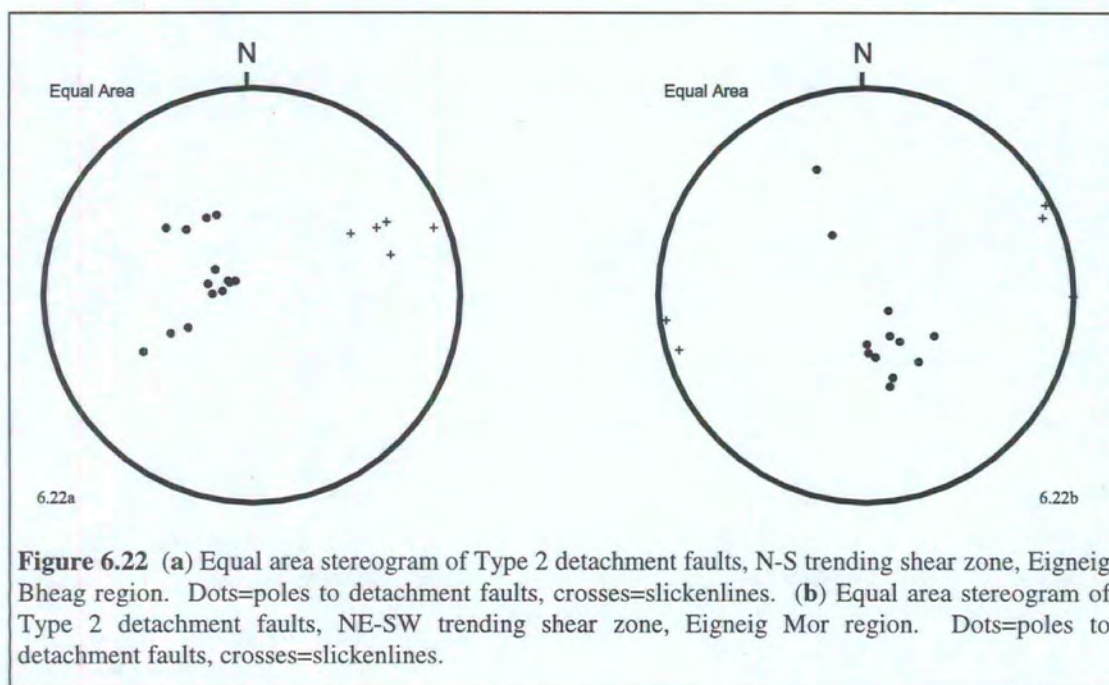
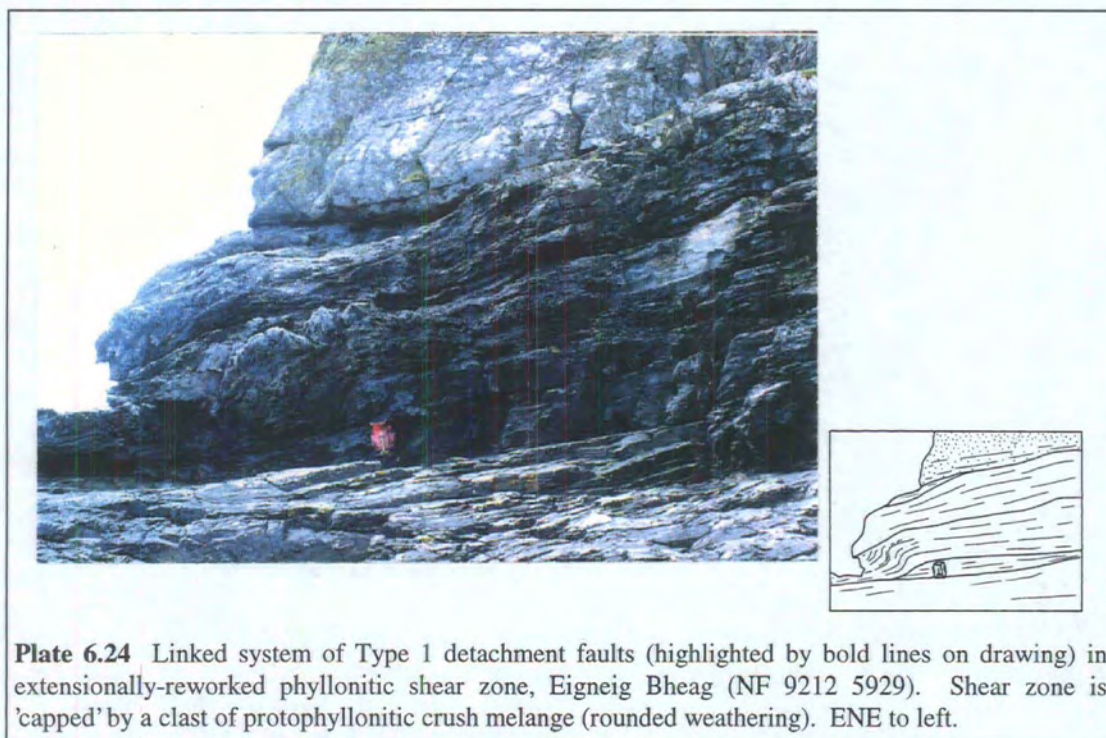
### 6.4.4.1 Field relationships

Detachment faults are commonly observed throughout eastern North Uist. The style of deformation and / or the nature of the brittle fault rocks suggest that there are two distinct types of detachment fault developed on North Uist. Extensional, 'Type 1' detachments are E- to ENE-dipping surfaces (Fig. 6.21), which are typically lined by arrays of foliation-parallel calcite-albite-chlorite veins and clasts of brecciated phyllonite (see more detailed descriptions in section 6.4.3). Type 1 detachment faults are *not* associated with arrays of subsidiary fractures (e.g. Riedel shears). In contrast, 'Type 2' detachments are planar to undulating surfaces, which are commonly observed to be associated with arrays of subsidiary fractures (e.g. Riedel shears). The detachment surfaces are oriented parallel to the phyllonitic foliation, thus Type 2 faults from around Eigneig Bheag tend to dip towards the east (Fig. 6.22a), whilst Type 2 faults from Eigneig Mor either dip towards the NW or SE (Fig. 6.22b). Type 2 detachments (and the subsidiary fractures) are typically lined by bands of clay-rich (locally chlorite-rich) gouge ( $\leq 20\text{cm}$  thick), although discrete, 'polished' fault surfaces are locally preserved. NE-SW to ENE-WSW trending slickenlines are typically developed along Type 2 detachment surfaces (Figs. 6.22a & b). The geometries of the subsidiary fracture arrays are consistent with top-to-the-NE or -ENE directed shear (i.e. sinistral strike-slip or transtension).



Type 1 detachments are either preserved within, or at the margins of reworked phyllonitic shear zones. A linked system of gently eastward-dipping 'Type 1' detachments is particularly well exposed a cliff section ( $\cong 15\text{m}$  high) through a N-S

trending segment of an extensionally reworked shear zone to the south of Eigneig Bheag (NF 9212 5929) (Plate 6.24; Figs. 6.1 & 6.2). There is little evidence to suggest that detachment fault system developed in an in-sequence manner (cf. foreland / hinterland propagating thrust systems). Type 1 detachments are also exposed within a NW-dipping extensionally-reworked shear zone to the north of Eigneig Mor (NF 9279 6156) (Figs. 6.1 & 6.2).



Type 2 detachments are preserved at the margins of the strike-slip related Bàgh na Caiplich phyllonite belt (NF 901 560), at the margins of SE- and NW-dipping transtension-related phyllonite belts to the north of Eigneig Mor (NF 9281 6156 to NF 9279 6156) and at the margins of an extension-related phyllonite belt at Eigneig Bheag (NF 9242 6042). Detachment faults are locally developed *within* shear zones, and either separate packages of planar phyllonite from packages of folded phyllonite, or units of strike-slip related phyllonite from units of transtension- or extension-related phyllonite. In the area to the east of North Lee, Type 2 detachments locally cross-cut regions of pervasive protophyllonite and unmodified gneiss (NF 9512 6690 to NF 9512 6700) (Figs. 6.1 & 6.2). A number of moderately E-dipping Tertiary dolerite sills are exposed along the coast to the east of North Lee (Walker 1990; Fettes *et al.* 1992). In places, the sills appear to have been intruded along Type 2 detachment planes (e.g. NF 9523 6725; NF 9512 6700; NF 9513 6671). However, there is no evidence to suggest that magma injection was synchronous with faulting. This observation suggests that the Type 2 detachment faults are of pre-Tertiary age.

#### **6.4.4.2 Origin and relative age of the detachment faults**

The breccias and foliation-parallel vein arrays preserved along Type 1 detachment planes are commonly observed to be overprinted by a macroscopically ductile fabric. It has therefore been postulated that the Type 1 detachment faults developed in response to transient episodes of localised high pore fluid pressure during macroscopically ductile reworking (see discussion in section 6.4.3.3).

Type 2 detachments cross-cut regions of unmodified gneiss, pervasive protophyllonite, reworked phyllonite and strike-slip related phyllonite. These faults are commonly observed to separate packages of phyllonite which have experienced differing magnitudes of finite strain. It is likely that the Type 2 detachment faults localised along pre-existing competence boundaries (see also Butler 1995). The fault planes are either polished surfaces, or are lined by bands of clay-rich fault gouge. The brittle fault rocks are *not* overprinted by a macroscopically ductile fabric. These observations suggest (a) that the Type 2 detachment faults developed following the cessation of macroscopically ductile reworking, and (b) that the faults probably developed within the uppermost 5km of the earth's surface (Sibson 1982, 1983). An important corollary of this argument is that the Type 2 detachment faults are significantly younger, and therefore unrelated to the Type 1 detachment faults. It is tentatively suggested that the Type 2 detachment faults may be the onshore expression of Mesozoic extension in the hangingwall of the OHFZ (Chapter 2). The significance of the Type 2 detachments will be discussed further in Chapter 9.

## 6.4.5 SYNTHESIS

The available field and microstructural evidence suggests that pre-Mesozoic transtensional and extensional displacements were accommodated by deformation within the pre-existing network of strike-slip related phyllonitic shear zones. More specifically, the strike-slip related fabrics were *reworked* during transtension and extension. These observations suggest that the phyllonitic shear zones were weak, relative to the unmodified Lewisian gneisses, to the cataclastically deformed rocks of the crush melange and to the protophyllonitic fabrics (see also Butler 1995; Butler *et al.* 1995).

The relatively poor inland exposure precludes a detailed analysis of the distribution of strike-slip, transtension- and extension-related fabrics. However, studies conducted along well exposed coastal sections suggest that both the regional distribution of transtension- and extension-related fabrics, and the magnitude of finite strain observed within individual reworked shear zones, are extremely heterogeneous (Fig. 6.14). The overall picture that emerges is that the most highly strained *extension*-related fabrics are preserved in N-S trending shear zones which are predominantly composed of epidote-rich ('dark-green') phyllonite and ultraphyllonite (e.g. NF 9207 5957). In NE-SW trending shear zones (e.g. NF 9242 6042), the observed magnitude of finite strain and the ratio of extension- to transtension-related phyllonite are both *lower* than within N-S trending shear zone segments, regardless of shear zone lithology (Fig. 6.14). However, both the observed magnitude of finite strain and the relative proportion of transtension- to extension-related phyllonite appear to be similar in NW- and SE-dipping shear zones (e.g. NF 9281 6156 to NF 9279 6156) (Fig. 6.14). These observations suggest that *shear zone trend* and the *shear zone lithology* were important controls on the distribution and intensity of reworking (see also Butler *et al.* 1995). However, the dip direction of the shear zones does *not* appear to have been an important factor. Both the shear zone geometries and the shear zone lithologies were established during sinistral strike-slip, which suggests that reactivation was principally controlled by *long-term* weakening mechanisms (Chapter 1).

The phyllonitic shear zones preserved on Ronay are lithologically indistinguishable from the phyllonitic shear zones preserved in the Burrival to Eigneig Bheag region of North Uist (Fig. 3.28). However, the epidote-rich phyllonites and ultraphyllonites preserved within the N-S trending Bàgh na Caiplich phyllonite belt on Ronay are anomalous in that all the fabrics preserve strike-parallel mineral lineations (Figs. 3.28 & 3.34c) i.e. *reworked fabrics have not been observed within the Bàgh na Caiplich belt*. The only evidence of regional transtension / extension preserved on Ronay are the arrays of quartz and quartz-chlorite veins which locally cross-cut the strike-slip

related shear zone fabrics. These observations suggest that other factors, such as shear zone interconnectivity (e.g. Fig. 3.28), must also have influenced shear zone reworking.

The controls on fault zone reactivation on North Uist are discussed further in Chapter 9.

## 6.5 SUMMARY

- The crush melange (i.e. the primary fabric) comprises blocks of fractured gneiss which 'float' in an interconnected matrix of cataclasite, ultracataclasite and devitrified pseudotachylyte.
- The crush melange is characterised by dual porosity / dual permeability fluid transport properties. A relatively high porosity / high permeability network of meso- to macroscopic cataclastic fault zones was superimposed upon a relatively low porosity / low permeability network of microscopic fractures and grain boundaries.
- The phyllonite belts (i.e. the derived fabrics) localised along the high porosity / high permeability network of meso- and macroscopic fault zones.
- The phyllonite belts were reworked during macroscopically ductile transtension and extension.
- During reworking, strain was accommodated by viscous grain boundary sliding, fluid-assisted DMT and frictional sliding and veining during transient episodes of high pore fluid pressure.
- The distribution of reworked fabrics is heterogeneous. In general, the most highly strained, extension-related fabrics are epidote-rich ('dark-green') phyllonites and ultraphyllonites.

The textural evolution of the OHFZ on North Uist is summarised in Figure 9.3a, and is discussed further in Chapter 9.

## 7. USINISH PHYLLONITE

### 7.1 INTRODUCTION

#### 7.1.1 INTRODUCTION AND AIMS

The predominantly N-S trending segment of the Outer Hebrides Fault Zone exposed in South Uist has experienced a complex, polyphase kinematic and textural evolution. Regional top-to-the-W thrusting was associated with intense brittle deformation and the development of thick pseudotachylyte-ultracataclasite crush zones (section 3.5.2.2). Brittle deformation was followed by an episode of lower greenschist facies retrogression, hydration and phyllonitisation during regional top-to-the-NE sinistral strike-slip. The locus of intense retrogression and deformation appears to have been restricted to the region along the east coast of South Uist, and was associated with the development of the N-S to NNE-SSW trending Usinish Phyllonite belt (section 3.5.1). During subsequent top-to-the-ENE transtension and top-to-the-E extension along the OHFZ, deformation was strongly focused into the Usinish Phyllonite belt. However, in contrast either to Scalpay or North Uist (Chapters 5 & 6), transtension- and extension-related deformation appears to have been accommodated by the generation of *new* phyllonitic fabrics as well as by the reworking of pre-existing strike-slip related fabrics (section 3.5.3.3). Following the cessation of macroscopically ductile deformation, the phyllonitic fabrics were disrupted by predominantly top-to-the-ENE displacements along networks of brittle detachment faults. The relatively poor exposure in eastern South Uist has meant that the internal structure of the Usinish Phyllonite is not well understood, particularly in comparison with better exposed Scalpay and North Uist phyllonite belts. The aims of this chapter are therefore:

- (1) To systematically describe the fault rocks and structures observed along the Usinish Phyllonite belt.
- (2) To determine the *spatial* and *temporal* distribution of the strike-slip, transtension- and extension-related fabrics.
- (3) To determine the metamorphic conditions and operative deformation mechanisms during each episode of phyllonitisation and reworking.

## **7.1.2 STUDY AREA AND CHAPTER LAYOUT**

The Usinish Phyllonite belt is exposed in a series of isolated promontories and islands along the east coast of South Uist. Detailed field studies have been conducted on the well exposed headlands of Rubha Rossel (NF 858 365) and Rubha Bolum (NF 828 284), and on the island of Stuley (NF 830 235). The results of additional reconnaissance mapping in the region between Rubha Hellisdale (NF 840 307) and Abhainn Liadale (NF 837 304) will also be presented (Fig. 3.38).

Owing to the limited exposure, the structural relationships between each of the different field areas are uncertain. Section 7.2 therefore provides descriptions of the fault rocks and structures observed at *each* locality and then synthesises these results in terms of (a) the overall structure of the Usinish Phyllonite belt, and in terms of (b) the spatial and temporal distribution of the different phyllonitic fabrics.

The fractured Corodale Gneiss and the Mashed Gneiss (i.e. the primary fabrics) (sections 3.5.1.2 & 3.5.4) are briefly described in section 7.3 in order to provide a context in which to understand the development of the derived fabrics (i.e. the strike-slip and the 'new' transtension- and extension-related phyllonites) (section 7.4). Section 7.5 describes the structures and fabrics associated with the reworked phyllonites, and discusses the possible mechanisms of fault zone reactivation in South Uist.

## **7.2 REGIONAL STRUCTURE OF THE USINISH PHYLLONITE**

The aim of this section is to systematically describe the fault rocks and structures exposed along the strike of the Usinish Phyllonite belt and in particular, to determine the spatial and temporal relationships between the different phyllonitic fabrics (section 7.2.5).

### **7.2.1 RUBHA ROSSEL**

The small headland of Rubha Rossel (NF 858 365) is situated 3.5km to the southeast of Loch Skipport pier, close to the northern extremity of the exposed Usinish Phyllonite (Fig. 3.38). This study focuses on the wave-washed exposures encountered along the north coast of the promontory (Fig. 7.1).

### 7.2.1.1 Macrostructure

The footwall of the phyllonite belt comprises Corodale Gneiss, which passes upwards into a number of detachment-bounded packages of phyllonite, protophyllonite and

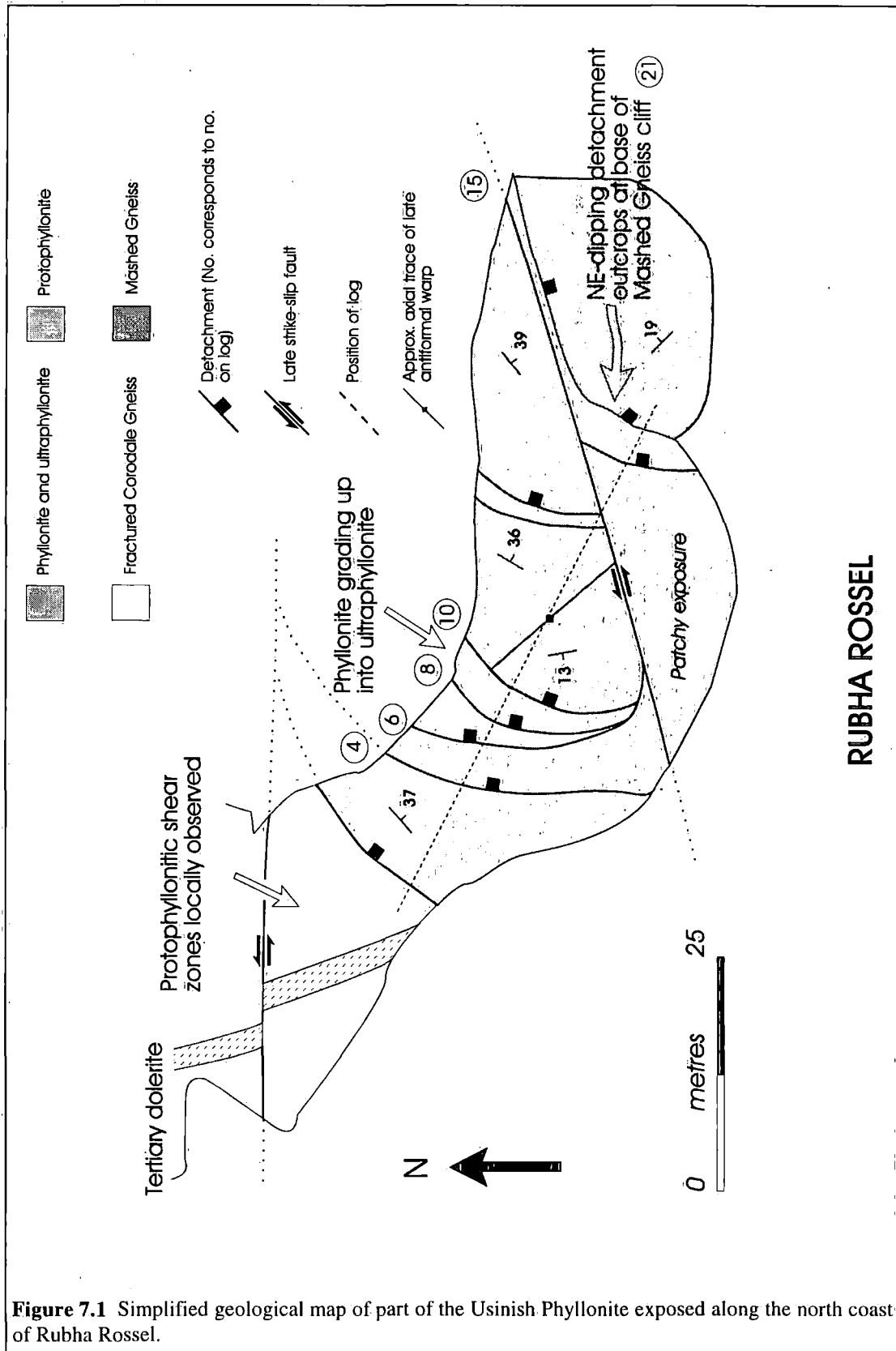


**Figure 7.1** Simplified geological map of part of the Usinish Phyllonite exposed along the north coast of Rubha Rossel.

ultraphyllonite. The phyllonitic foliation predominantly dips towards the southeast, but is deformed by a gentle, upright SSE-trending antiform. The fold axial trace is cross-cut by both detachment faults and by a sub-vertical, E-W trending strike-slip fault (Fig. 7.1). These observations suggest that folding occurred relatively early during the structural evolution of the Usinish Phyllonite. It has been postulated that the orientation of the phyllonitic foliation may reflect the presence of a relatively undeformed, metre-scale protophyllonitic 'clast' at depth (Butler 1995; cf. section 6.3.3.1 of the present work). The upper margin of the phyllonite belt is defined by a prominent, moderately ENE-dipping detachment fault (Figs. 7.1 & 7.2).

### **7.2.1.2 Mesostructure**

The following section describes the fault rocks and structures observed in the field within the phyllonite belt, and in its footwall and hangingwall.

#### ***Footwall***

The footwall of the phyllonite belt comprises quartz-poor Corodale Gneiss, discordant quartzo-feldspathic pegmatite veins and Corodale Gneiss-derived protophyllonite (section 3.5.2.1). The gneissose banding is locally cross-cut by brittle faults and / or by veins of devitrified pseudotachylyte. Previous authors have suggested that these brittle structures developed during regional top-to-the-W thrusting (Coward 1969; Sibson 1977b), although the present author could find little evidence to substantiate their claims.

Bands of discrete phyllonite ( $\leq 10\text{cm}$  thick;  $\leq 3\text{m}$  long) are commonly observed in the uppermost 5m of the footwall (Figs. 7.1 & 7.2). The predominantly ENE-WSW trending phyllonitic foliation is typically oriented parallel to the margins of the host phyllonite band, and is associated with a gently SSW-plunging mineral lineation (Fig. 7.3a). Both discontinuous and continuous phyllonite bands have been observed (*sensu* Tourigny & Tremblay 1997). The wall rocks adjacent to continuous phyllonite bands are locally overprinted by a protophyllonitic foliation. The sigmoidal trajectory of the protophyllonitic foliation is consistent with top-to-the-NNE shear across the neighbouring phyllonite band. The phyllonite bands are locally displaced in an apparent dextral sense by steeply dipping N-S trending brittle fractures (displacements  $\leq 3\text{cm}$ ).

### The phyllonite belt

The basal 5m of the Usinish Phyllonite comprises three detachment-bounded packages of protophyllonite (Figs. 7.1 & 7.2; section 7.2.1.3).  $\phi$ -type feldspar porphyroclasts are abundant, although quartz appears to be absent. These observations suggest that

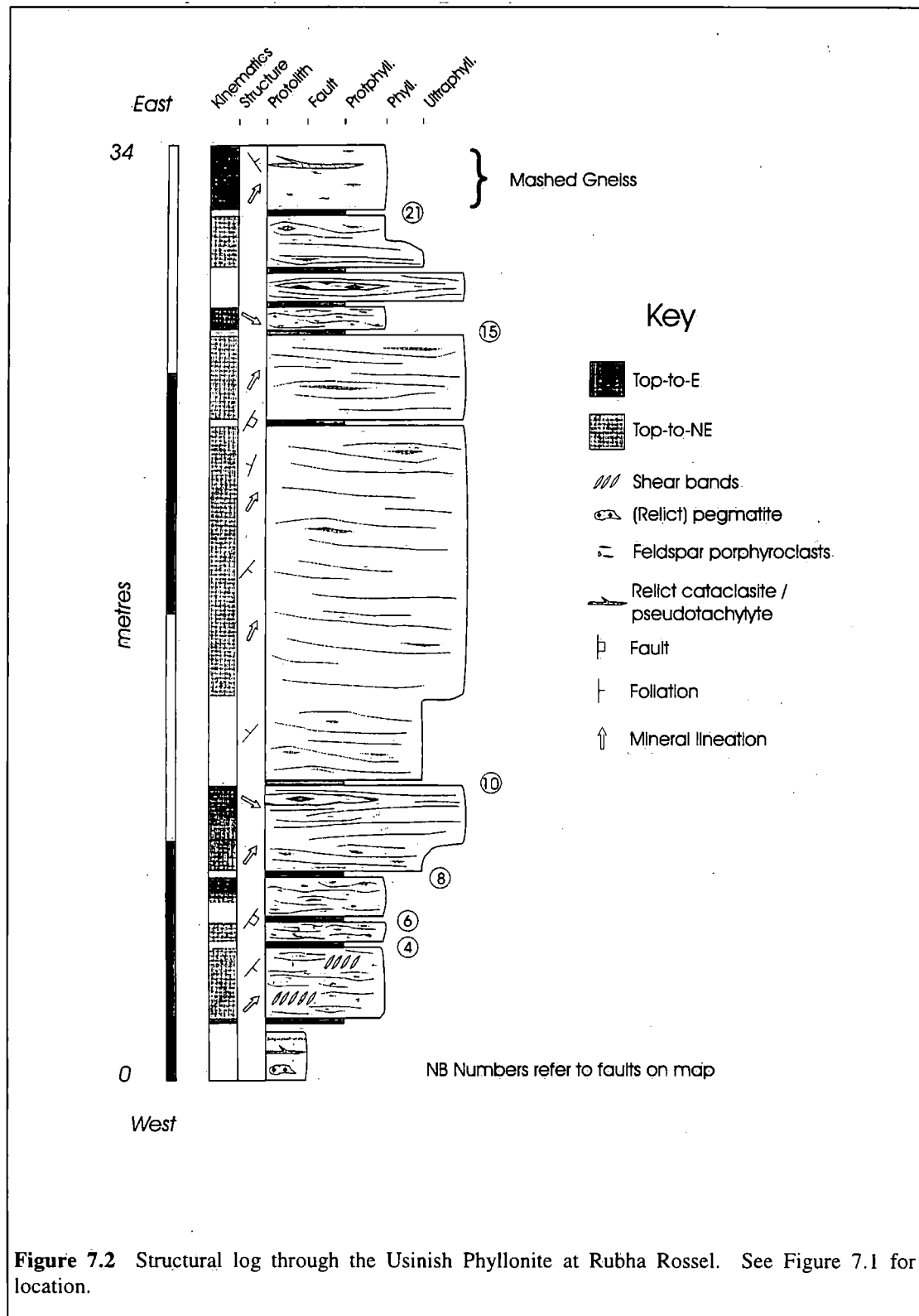
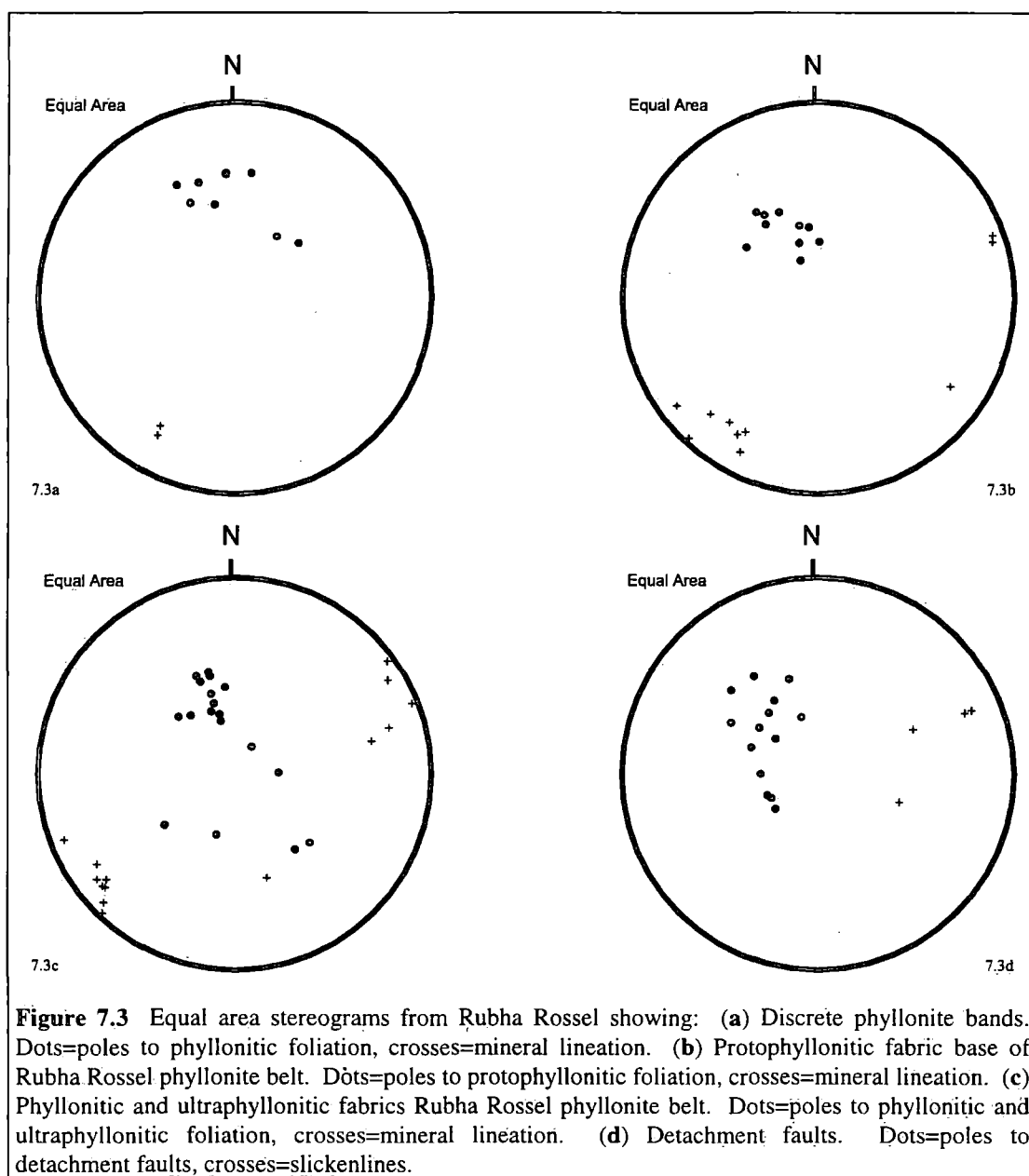


**Figure 7.2** Structural log through the Usinish Phyllonite at Rubha Rossel. See Figure 7.1 for location.

the protophyllonite was probably derived from quartz-poor Corodale Gneiss protoliths. The undulating, moderately SE- to SSE-dipping protophyllonitic foliation is associated with a SW- (locally E-) plunging mineral lineation (Fig. 7.3b). Arrays of en-echelon quartz veins (similar to those illustrated in Fig. 7.10) viewed in surfaces parallel to the mineral lineation and perpendicular to the foliation are consistent with top-to-the-NE shear (i.e. regional sinistral strike-slip). The significance of the E-plunging mineral lineation and the en-echelon veins will be discussed in sections 7.2.5 and 7.4 respectively.



The uppermost 20m of the phyllonite belt comprises a number of detachment-bounded packages of phyllonite and ultraphyllonite (Figs. 7.1 & 7.2; section 7.2.1.3).  $\phi$ - and  $\delta$ -

type feldspar porphyroclasts are widespread, although quartz is only preserved within bands of relict pegmatite ( $\leq 25\text{cm}$  thick). These observations suggest that once again, the phyllonites and ultraphyllonites were probably derived from quartz-poor Corodale Gneiss protoliths. The platy, SE- or NW-dipping foliation is associated with a sub-horizontal NE-SW to ENE-WSW trending mineral lineation (Fig. 7.3c). Asymmetric shear bands and rootless, centimetre-scale folds *locally* deform the phyllonitic foliation and are developed in the hangingwalls of detachment faults (see section 7.2.1.3). Viewed in surfaces parallel to the mineral lineation and perpendicular to the foliation, the asymmetry of these structures is consistent with top-to-the-ENE shear (Fig. 7.4). The observations are consistent with top-to-the-NE shear having been followed by localised top-to-the-ENE shear.

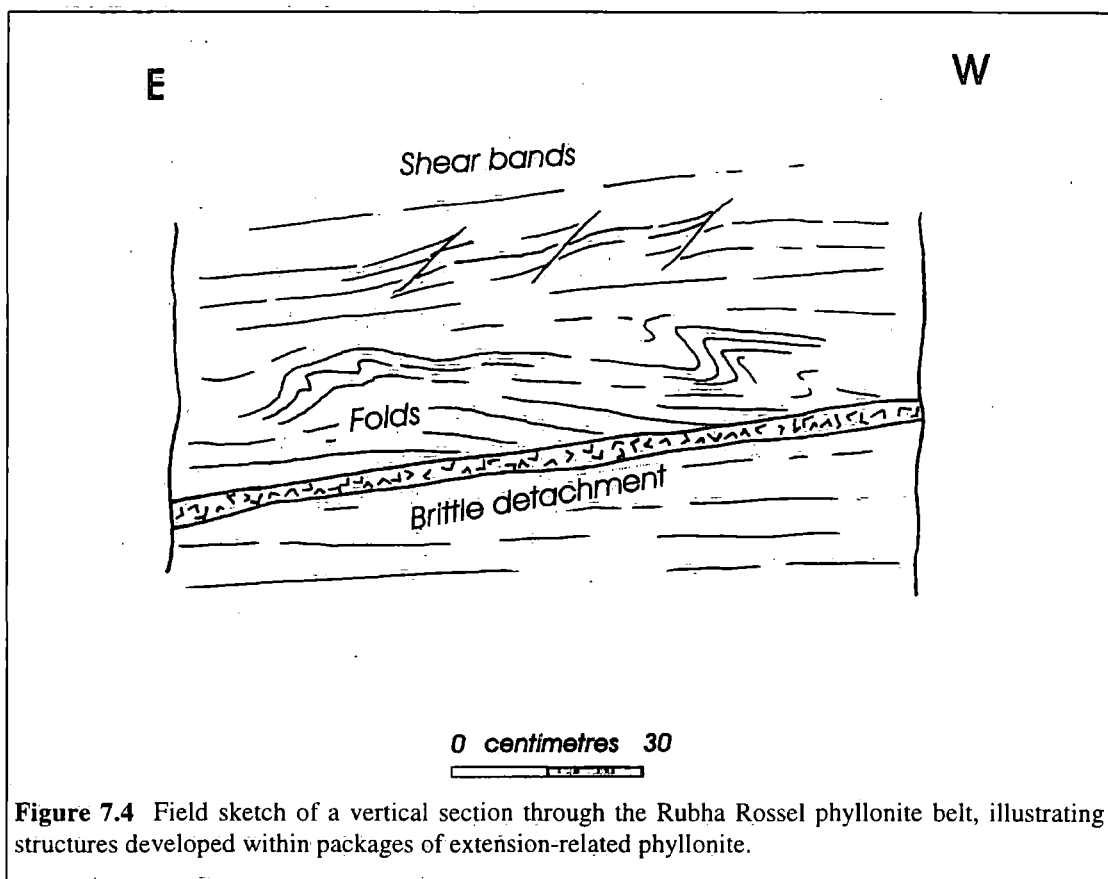


**Figure 7.4** Field sketch of a vertical section through the Rubha Rossel phyllonite belt, illustrating structures developed within packages of extension-related phyllonite.

### ***The hangingwall***

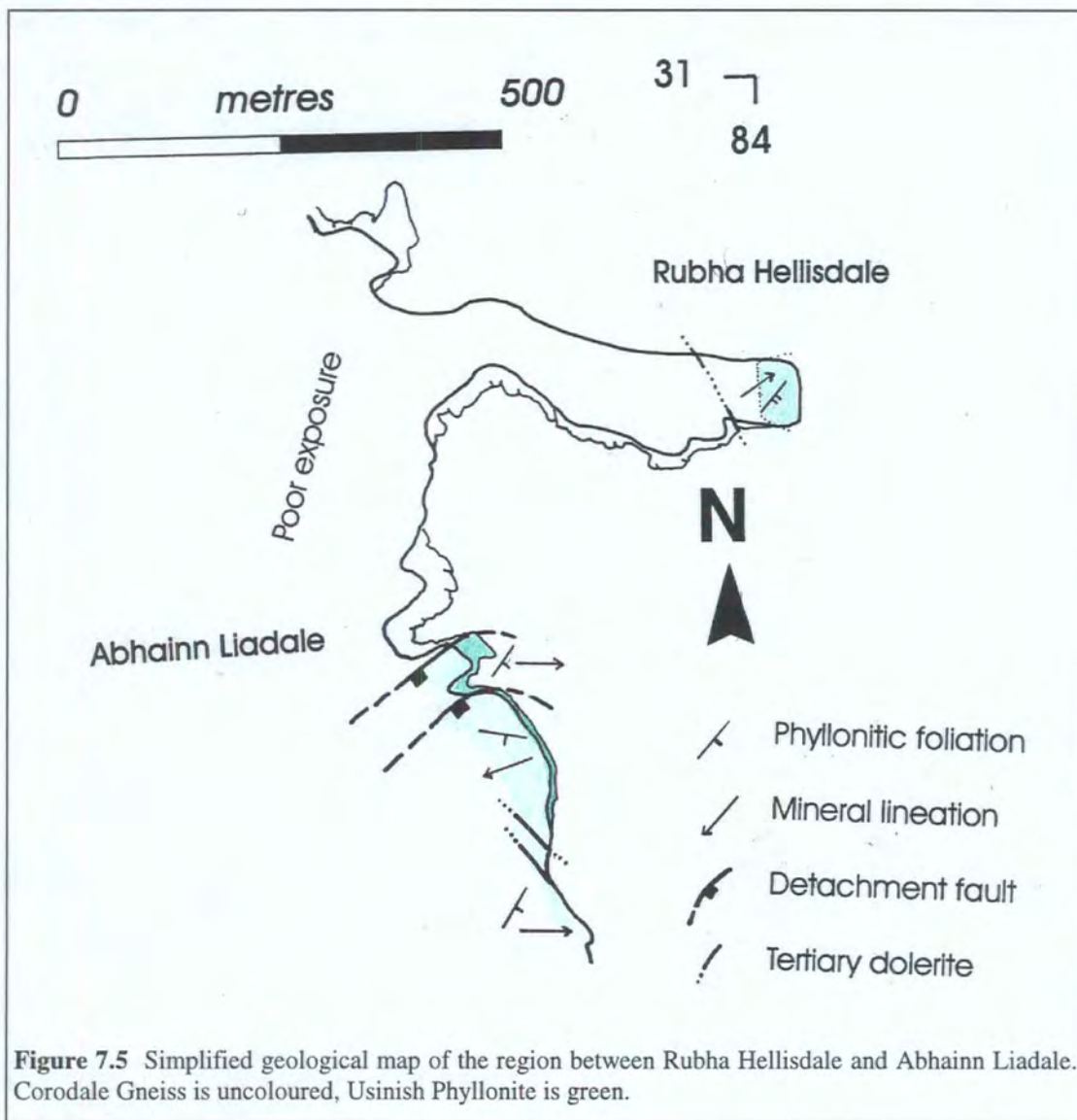
The hangingwall comprises a unit of protophyllonitic Mashed Gneiss ( $\leq 50\text{m}$  thick, although the top of this unit is not exposed onshore) (section 3.5.4). The undulating, moderately NE-dipping foliation is associated with an ENE-plunging mineral lineation (Fig. 7.2).  $\sigma$ -type quartz and feldspar porphyroclasts viewed in surfaces parallel to the mineral lineation and perpendicular to the foliation are consistent with top-to-the-ENE shear. The macroscopically ductile fabric clearly overprints and deforms relict cataclasite seams and pseudotachylite veins (cf. section 6.3.2).

### 7.2.1.3 Detachment faults

The phyllonite belt is cross-cut by arrays of interconnected, SE- to NE-dipping detachment faults (Figs. 7.1, 7.2 & 7.3d). The fault planes are typically 'polished' surfaces, but are locally lined by thin bands of gouge or breccia ( $\leq 10\text{cm}$  thick). The breccia comprises angular clasts of phyllonite which 'float' in a matrix comprising either a soft clay-rich gouge, or arrays fault-parallel quartz veins (individual veins  $\leq 1\text{cm}$  thick). Slickenlines have not been observed along breccia-lined fault planes. In contrast, 'polished' fault surfaces are typically associated with ENE-plunging slickenlines (Fig. 7.3d). The geometries of subsidiary fracture planes are consistent with top-to-the-ENE shear along the 'polished' detachment faults.

## 7.2.2 RUBHA HELLISDALE TO ABHAINN LIADALE

Reconnaissance mapping at a scale of 1:10 000 was carried out along the coast between Rubha Hellisdale (NF 840 307) and Abhainn Liadale (NF 837 304) (Figs 3.38 & 7.5). Rubha Hellisdale comprises intensely crushed and fractured Corodale Gneiss, which is overprinted by a patchily developed protophyllonitic fabric. Platy, SE-dipping phyllonite outcrops on the extreme tip of Rubha Hellisdale and is associated with a well developed ENE-plunging mineral lineation. Fractured, SW-dipping Corodale Gneiss is exposed in the region between of Rubha Hellisdale and Abhainn Liadale (NF 8370 3036). At the mouth of Abhainn Liadale several moderately SSE-dipping detachment faults juxtapose banded Corodale Gneiss, which is exposed in the footwall, against protophyllonite, which is exposed in the hangingwall (Fig. 7.5) (NF 937 304). The NNE-dipping protophyllonitic foliation is associated with a consistently E-W trending mineral lineation. Platy, SSW-dipping phyllonite is widely observed in the region immediately to the south of Abhainn Liadale (NF 839 298). The foliation is associated with an ENE-WSW trending mineral lineation, and asymmetric shear bands viewed in surfaces parallel to the lineation and perpendicular to the foliation are consistent with top-to-the-ENE shear (Fig. 7.5). The phyllonitic fabric is locally deformed by centimetre-scale, eastward verging folds. The folds are typically associated with a S-dipping axial planar crenulation cleavage, which carries a well developed E-W trending mineral lineation. The observations are consistent with top-to-the-ENE shear having been followed by *localised* top-to-the-E shear.



### 7.2.3 RUBHA BOLUM

The promontory of Rubha Bolum (NF 830 284) lies 2 km to the north of Loch Eynort (Fig. 3.38). Exposure is excellent around the coast, but is rather poor further inland.

#### 7.2.3.1 Macrostructure

The footwall of the phyllonite belt comprises relatively unmodified Corodale Gneiss, which passes upwards into several detachment-bounded packages of phyllonite, ultraphyllonite and protophyllonite. The internal structure of the Usinish Phyllonite at Rubha Bolum appears to be rather complex owing to (a) the effects of subsequent brittle deformation along the network of detachment faults (Fig. 7.7a), and to (b) the presence of a large 'clast' of relatively undeformed protophyllonitic Mashed Gneiss ( $\leq 70\text{m}$  thick), which is exposed on Bolum Island and on the extreme southeastern tip of Rubha Bolum itself (Fig. 7.6; Butler 1995). In the following description, Rubha

Bolum has been divided into four detachment-bounded 'structural domains', which have been defined on the basis of fault rock distribution and on variations in the orientation of the phyllonitic foliation and mineral lineation. Domains 1 and 4 define the structural base of the phyllonite belt, whilst Domain 2 occupies to highest structural level (Fig. 7.6).

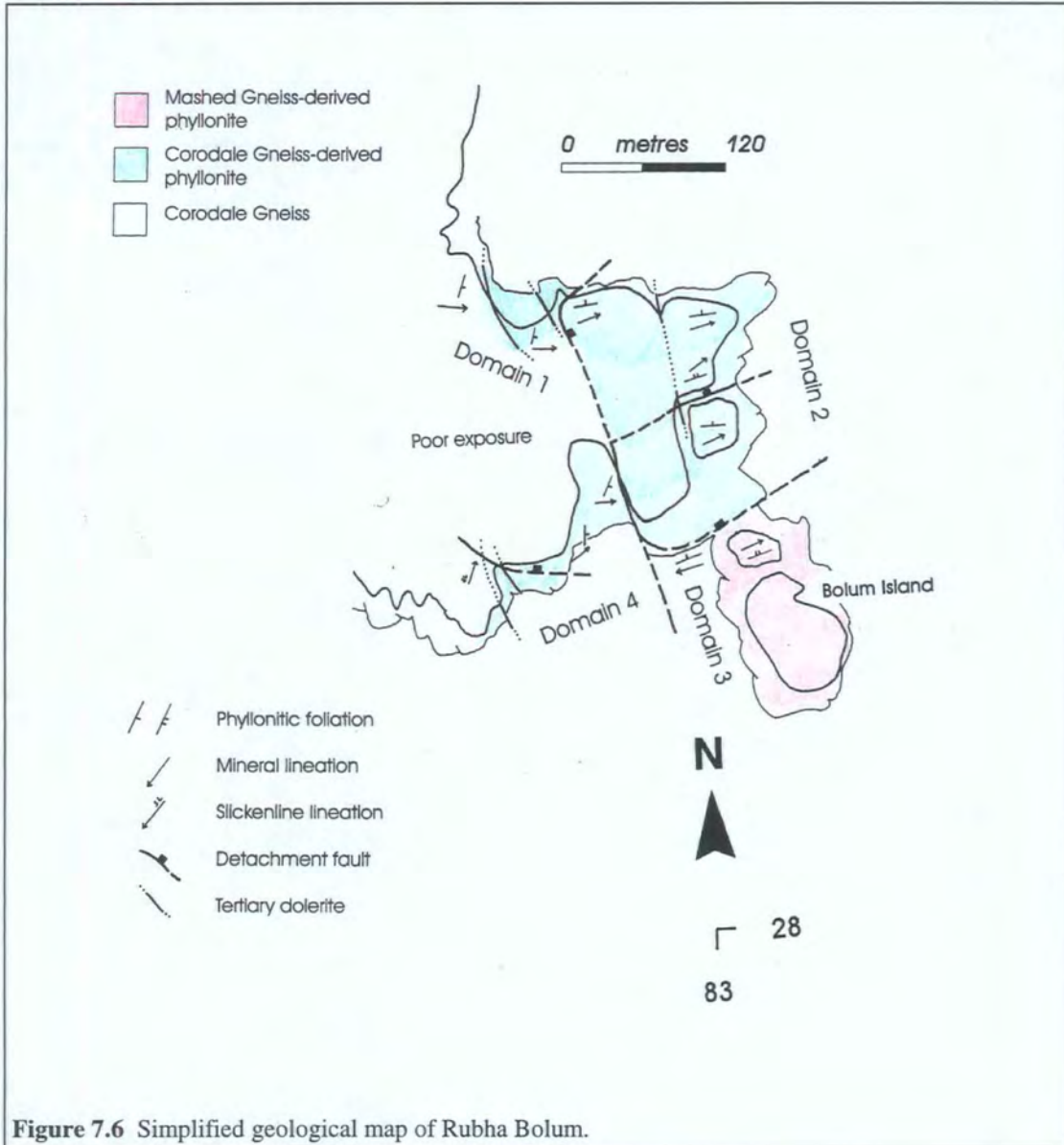


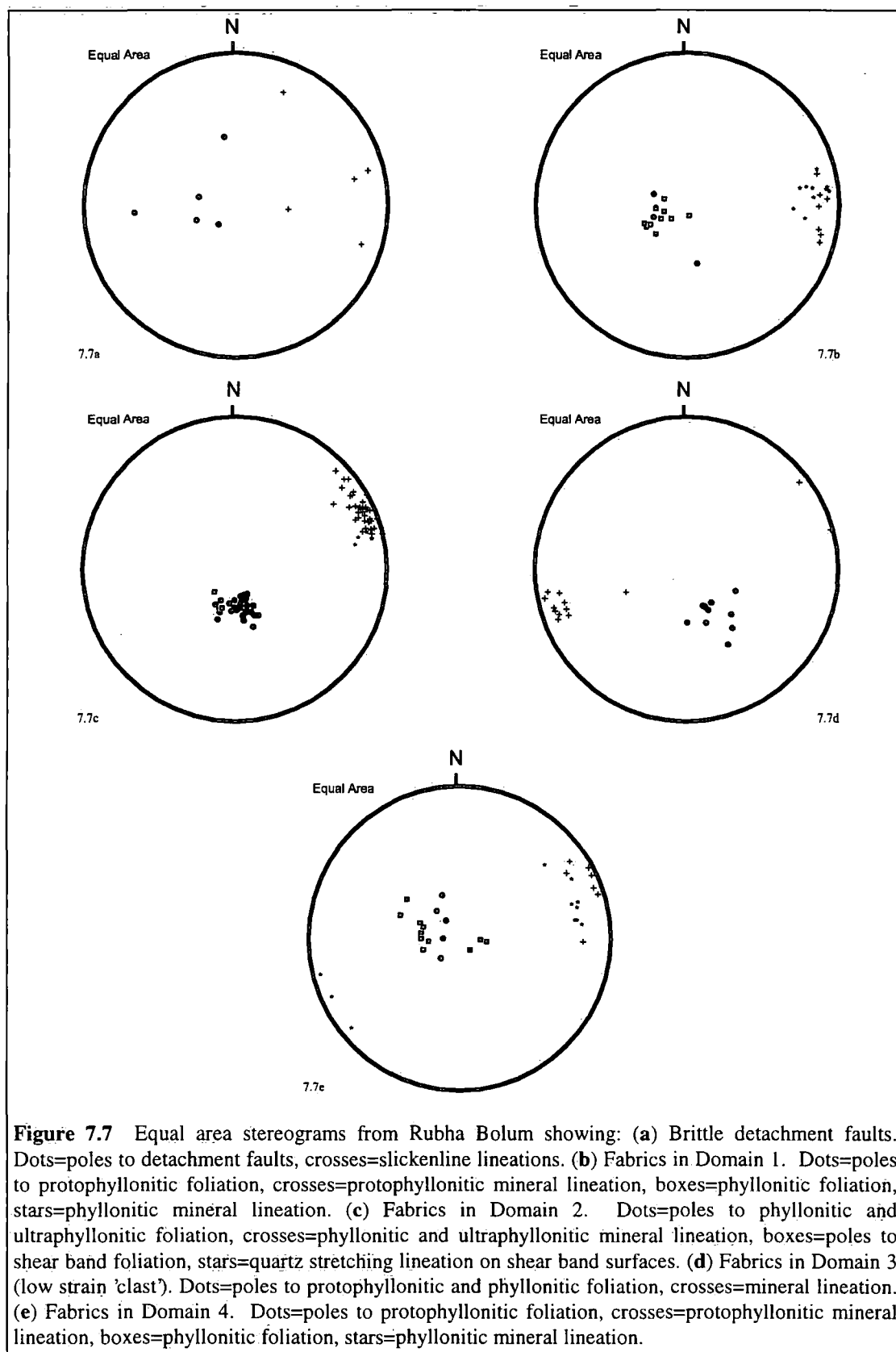
Figure 7.6 Simplified geological map of Rubha Bolum.

### 7.2.3.2 Mesostructure

#### *Domain 1*

Domain 1 occupies the northwestern corner of Rubha Bolum. The base of Domain 1 is defined by a gradational contact between fractured Corodale Gneiss and pegmatite veins to the west and protophyllonitic Corodale Gneiss and pegmatite to the east (Fig.

7.6). The patchily developed, undulating protophyllonitic foliation dips predominantly



towards the east, and is associated with an E- to ESE-plunging mineral lineation (Fig. 7.7b). The foliation locally cross-cuts highly discordant relict pegmatite veins.  $\delta$ -type quartz porphyroclasts (in protophyllonitic pegmatites) and asymmetric shear bands viewed in surfaces parallel to the mineral lineation and perpendicular to the foliation are consistent with top-to-the-E or -ESE shear. The uppermost 10m of Domain 1 are characterised by platy ENE-dipping phyllonite, which is associated with an E-plunging mineral lineation (Fig. 7.7b). The phyllonitic fabric is commonly observed to be cross-cut by sub-vertical, predominantly N-S trending quartz veins. The orientation of the quartz fibres is consistent with E-W extension. A gently ENE-dipping, gouge-lined detachment fault truncates the quartz veins and marks the boundary between Domains 1 and 2 (Fig. 7.6).

### ***Domain 2***

Domain 2 occupies the northeast quadrant of Rubha Bolum (Fig. 7.6). Domain 2 is characterised by packages of platy, gently N-dipping phyllonite and ultraphyllonite, which are associated with a sub-horizontal, NE-SW trending mineral lineation (Fig. 7.7c).  $\delta$ -type quartz (in phyllonitic pegmatite) and feldspar porphyroclasts, asymmetric shear bands and arrays of en-echelon quartz veins viewed in surfaces parallel to the mineral lineation and perpendicular to the foliation are consistent with top-to-the-NE shear. The macroscopically ductile fabric is cross-cut by sub-vertical, N-S trending quartz veins. The orientation of the vein fibres is consistent with E-W extension. The significance of the en-echelon veins and the sub-vertical veins will be discussed in sections 7.4 and 7.5.

### ***Domain 3***

Domain 3 occupies southeast quadrant of Rubha Bolum and contains a 'clast' of protophyllonitic Mashed Gneiss (Fig. 7.6). The upper margin of Domain 3 is defined by a moderately N-dipping detachment fault, which is inferred to outcrop in an eroded gully to the north of Bolum Island (Fig. 7.6). The base of Domain 3 is not exposed. The patchily developed, moderately NW-dipping protophyllonitic foliation is associated with a sub-horizontal, NE-SW trending quartz stretching lineation (Fig. 7.7d). The foliation appears to intensify towards the northwest, although exposure is poor and kinematic indicators have not been observed.

### ***Domain 4***

Domain 4 occupies the southwestern corner of Rubha Bolum (Fig. 7.6). The base of Domain 4 is defined by a gradational contact between fractured Corodale Gneiss to the west and protophyllonitic Corodale Gneiss to the east. The protophyllonitic

foliation dips towards the east or southeast, and is associated with a sub-horizontal, NE-SW trending mineral lineation (Fig. 7.7e). The uppermost 5m of Domain 4 is characterised by platy, E-dipping phyllonite and ultraphyllonite. The foliation is associated with an ENE-plunging mineral lineation, and asymmetric shear bands viewed in surfaces parallel to the lineation and perpendicular to the foliation are consistent with top-to-the-ENE shear.

### 7.2.3.3 Detachment faults

The brittle detachment faults, which form the boundaries to the different structural domains, are poorly exposed, but appear to dip predominantly towards the east (Fig. 7.7a). The detachment surfaces are typically lined by narrow bands ( $\leq 10\text{cm}$  thick) of soft, clay-rich gouge, and are locally associated with eastward plunging slickenlines. The geometries of subsidiary fracture arrays (e.g. Riedel shears) viewed in surfaces parallel to the slickenlines, are consistent with predominantly extensional (i.e. top-to-the-E or ENE) displacements along the main detachment surfaces.

## 7.2.4 STULEY

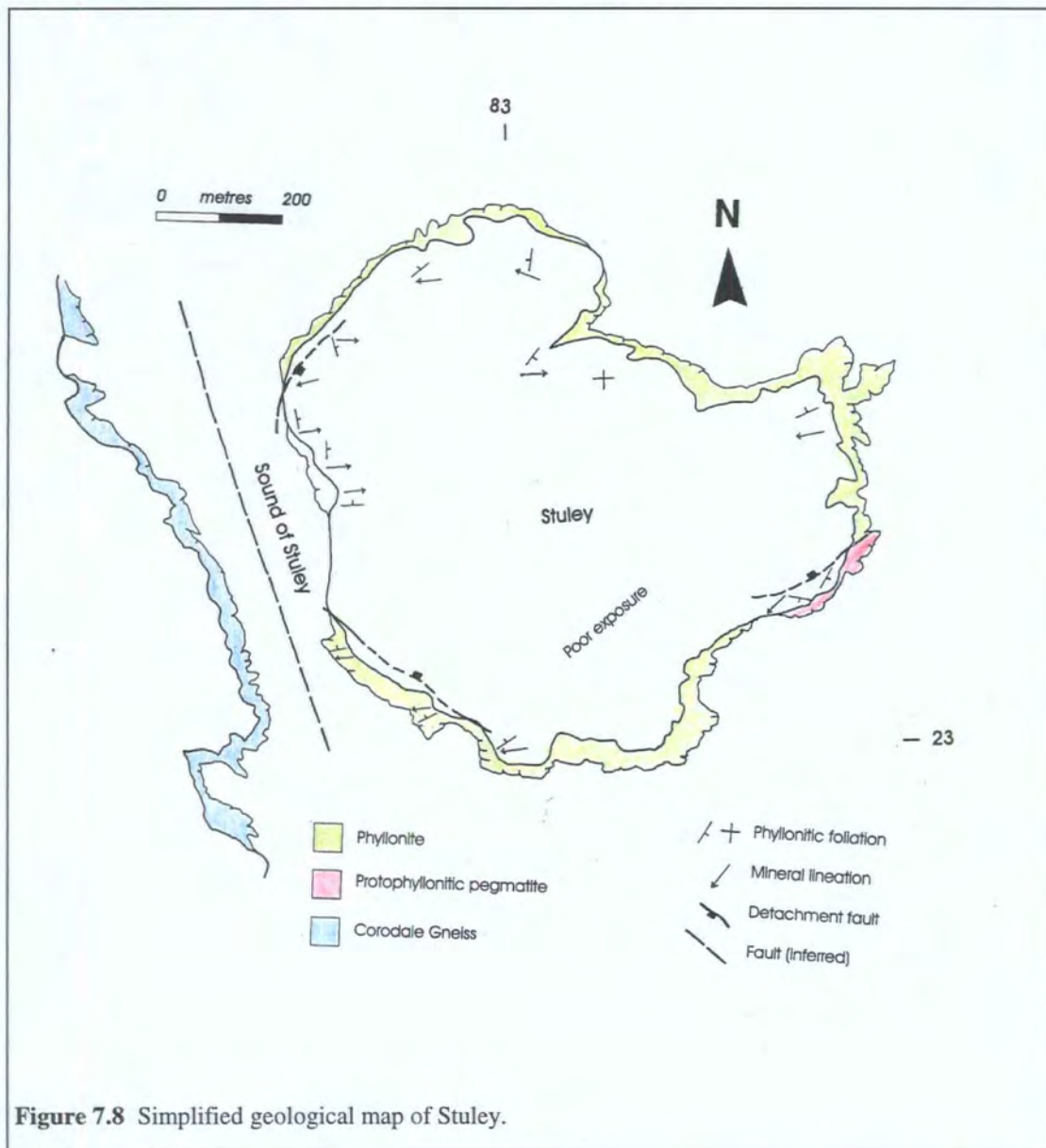
### 7.2.4.1 Macrostructure

The island of Stuley (NF 830 235) ( $\leq 40\text{m}$  high) lies approximately 200m off the east coast of South Uist, and represents the southernmost exposure of the Usinish Phyllonite. The island is composed almost entirely of flat-lying phyllonite. However, phyllonite does *not* outcrop immediately to the west, which suggests that a Stuley is separated from mainland South Uist by a moderately to steeply E-dipping fault (Fig. 7.8).

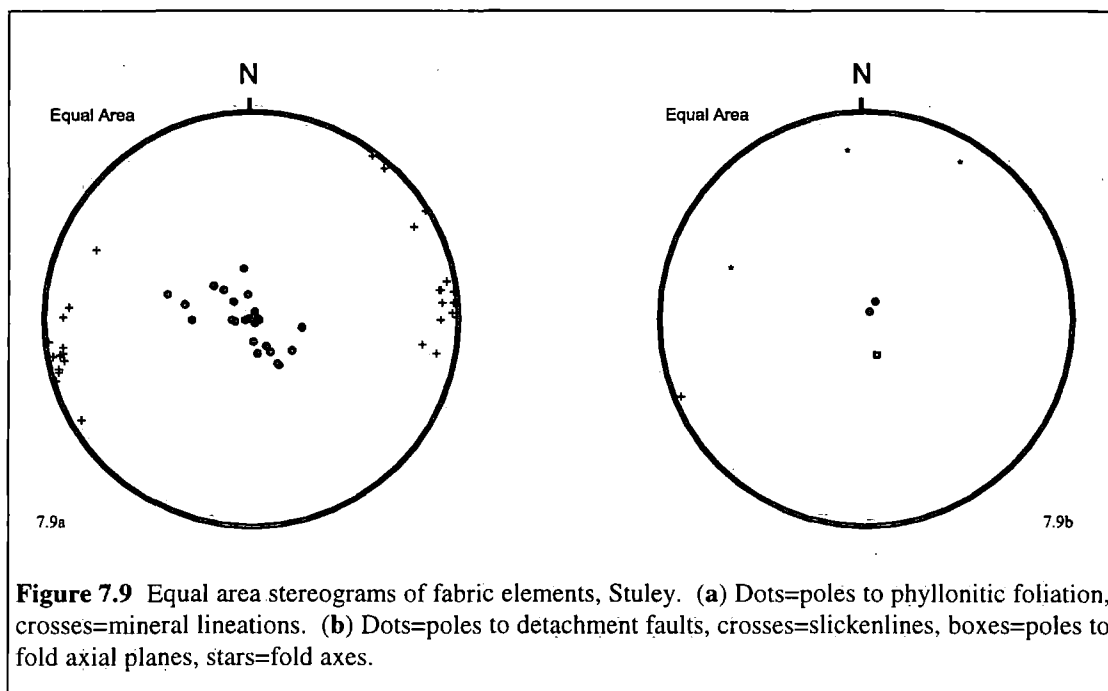
### 7.2.4.2 Mesostructure

Stuley is dominated by packages of flat-lying, platy phyllonite and ultraphyllonite. The sub-horizontal foliation is associated with a predominantly E-W trending mineral lineation (Fig. 7.9a). Asymmetric shear bands ( $\leq 30\text{cm}$  long), mica fish and  $\delta$ -type quartz and feldspar porphyroclasts ( $\leq 1\text{mm}$  diameter) viewed in surfaces parallel to the mineral lineation and perpendicular to the foliation are consistent with top-to-the-E shear. Discordant quartz and quartz-epidote veins ( $\leq 2\text{mm}$  thick) are locally deformed by cascades of recumbent, E-verging curvilinear folds (wavelength  $\leq 5\text{cm}$ ) (e.g. NF 828 231) (Fig. 7.9b). Butler (1995) has suggested that the deformed veins preserve vestiges of an early, strike-slip related phyllonitic fabric which was completely transposed during subsequent top-to-the-E extension. A metre-scale 'clast' of relatively undeformed protophyllonitic pegmatite is exposed along the east coast (NF 835 233) (Fig. 7.8). The moderately SE-dipping foliation is associated with a

poorly developed NE-SW trending quartz stretching lineation (Fig. 7.9a) (note that quartz stretching lineations have only been observed in packages of phyllonitic pegmatite). Kinematic indicators have not been observed.



Gently N- and S-dipping foliation-parallel brittle detachment faults are widely exposed. The detachment surfaces are associated with ENE-WSW trending slickenlines, and are typically lined by bands of clay-rich gouge ( $\leq 10\text{cm}$  thick). The gouges locally contain angular clasts of phyllonite and / or display a scaly fabric. Poorly developed shear band fabrics developed within gouge-rich layers are consistent with top-to-the-ENE shear.



## 7.2.5 SUMMARY AND DISCUSSION

The predominantly E-dipping Usinish Phyllonite outcrops along the east coast of South Uist. The phyllonitic fabrics developed during episodes of macroscopically ductile top-to-the-NE or top-to-the-E shear. However, the internal structure of the Usinish Phyllonite appears to be extremely complex. This complexity is in part due to displacements along a network of brittle detachment faults, which post-date the cessation of macroscopically ductile deformation. The detachment faults, which have accommodated predominantly extensional displacements, dismember the pre-existing shear zone architecture. Packages of phyllonite were probably faulted-out during brittle deformation. Consequently, it is very difficult to determine the original relationships between individual packages of detachment-bounded phyllonite.

### 7.2.5.1 Kinematic evolution and regional structure of the Usinish Phyllonite

An appreciation of how individual localities and packages of phyllonite relate to one another is central to any discussion of the spatial and temporal distribution of the different phyllonitic fabrics (section 7.1.1). However, interpretation of the regional structure is hampered (a) by the lack of exposure and (b) by the effects later brittle deformation. Two important questions to be addressed are:

- What are the relative ages of the different phyllonitic fabrics?
- Why does the outcrop width of the Usinish Phyllonite increase towards the south?

### ***Relative ages and kinematic evolution of the phyllonitic fabrics***

The phyllonitic fabrics preserved along the Usinish Phyllonite consistently display evidence for either top-to-the-NE, top-to-the-ENE or top-to-the-E shear. However, for the reasons outlined above, it is difficult either to determine the relative ages of the different phyllonitic fabrics.

The phyllonitic fabrics preserved at Rubha Rossel typically display evidence for top-to-the-NE shear (section 7.2.1.2). However, asymmetric shear bands, which extend the foliation towards the ENE, are locally observed to overprint the phyllonitic fabrics exposed in the hangingwalls of brittle detachment faults (e.g. Fig. 7.4). These observations suggest that *top-to-the-NE shear was followed by localised top-to-the-ENE deformation*. To the south of Abhainn Liadale, the phyllonitic fabric, which appears to have developed during top-to-the-ENE shear, is locally deformed by E-verging folds (section 7.2.2). These observations are consistent with *localised top-to-the-E deformation having followed a phase of top-to-the-ENE shear*. In eastern Stuley, a 'clast' of protophyllonitic pegmatite is associated with a poorly developed NE-SW trending mineral lineation. The 'clast' is wrapped by packages of highly deformed phyllonite which preserve evidence for top-to-the-E shear (section 7.2.4.2). These observations suggest that the protophyllonitic 'clast' is older than the phyllonitic foliation.

If it is assumed that the strike-slip, transtension- and extension-related fabrics can be correlated along the entire length of the Usinish Phyllonite, the field available evidence is consistent with *a progressive change in the kinematic regime, from macroscopically ductile top-to-the-NE shear, to macroscopically ductile top-to-the-ENE shear, to macroscopically ductile top-to-the-E shear* (see also Butler 1995). The timing and significance of the brittle detachment faults will be discussed in section 7.5.2.

### ***Width of the Usinish Phyllonite***

The outcrop of the Usinish Phyllonite progressively widens towards the south (Fig. 3.38). Previous authors have suggested that the increase in outcrop width is due to an increase in the *thickness* of the phyllonite belt, which in turn relates an along-strike increase in the magnitude of extensional deformation accommodated along the phyllonite belt (Butler 1995). It has been proposed that the phyllonite belt varies from c.10m thick in the region to the north of Rubha Rossel (NF 858 376) to over 200m thick around Stuley (NF 830 235) (Butler 1995). However, it is clear that the overall dip of the phyllonitic foliation also decreases towards the south, and that the foliation on Stuley is generally horizontal (compare Figs. 7.3 and 7.9). These observations

suggest that although its upper and lower margins are not exposed, the minimum thickness of the phyllonite belt on Stuley is c.40m. It is therefore postulated that whilst the *thickness* of the phyllonite belt does increase slightly towards the south, the increase in *outcrop width* is primarily a function of the diminishing dip of the phyllonitic foliation. However, the effects of detachment faulting on the thickness of the phyllonite belt are unconstrained.

#### **7.2.5.2 Distribution and origin of the phyllonitic fabrics**

The overprinting relationships described in the previous section suggest that the pre-existing strike-slip related fabrics were reworked during top-to-the-ENE transtension and top-to-the-E extension. These observations are consistent with the overprinting relationships observed on North Uist (Chapter 6). However, it has been suggested that some of the phyllonitic fabrics were *generated* during transtension and extension (section 3.5.3). The following section summarises and discusses the distribution and origin of the transtension- and extension-related phyllonites preserved along the Usinish Phyllonite.

#### ***Rubha Rossel*** (Figs. 7.1 & 7.2)

Slivers of detachment-bounded extension-related phyllonite are locally preserved at Rubha Rossel (Fig. 7.2; section 7.2.1.2). Overprinting relationships between packages of strike-slip and extension-related phyllonite are not generally preserved. However, a band of strike-slip related phyllonite, which is exposed 6m above the base of the phyllonite belt, appears to grade into a package of extension-related ultraphyllonite (Fig. 7.2). The boundary is marked by an abrupt clockwise rotation of the mineral lineation azimuth. This observation suggests that the *extension-related phyllonite preserved within the phyllonite belt at Rubha Rossel may have largely been derived from reworked strike-slip related phyllonite*. However, the protophyllonitic Mashed Gneiss preserved in the hangingwall of the phyllonite belt displays an ENE-plunging, transtension-related mineral lineation. The undulating protophyllonitic foliation cross-cuts relict cataclasite seams and pseudotachylyte veins. These observations suggest that the protophyllonitic fabric has accommodated relatively low magnitudes of finite strain, and is therefore unlikely to have been derived from a pre-existing strike-slip related fabric. Assuming that there has been no block-rotation in the hangingwall of the Rubha Rossel phyllonite belt (for which there is no evidence), it is postulated that *the protophyllonitic fabric was generated during top-to-the-ENE transtension*.

### ***Rubha Bolum and Abhainn Liadale*** (Figs. 7.5 & 7.6)

Strike-slip related fabrics are preserved adjacent to the lower margin of Domain 4 at Rubha Bolum. However, the uppermost 5m of Domain 4 comprises transtension-related phyllonite. The boundary between the strike-slip and transtension-related fabrics is marked by a gradual clockwise rotation of the mineral lineation azimuth. These observations suggest that *within Domain 4, the transtension-related fabrics may have largely been derived from reworked strike-slip related phyllonite.*

In contrast, Domain 1 is characterised by extension-related phyllonites and protophyllonites. The undulating protophyllonitic foliation is patchily developed and cross-cuts highly discordant, relict pegmatite veins. These observations suggest that the protophyllonitic fabric has accommodated very low magnitudes of finite strain. If this inference is correct, it is unlikely that these protophyllonitic fabrics rework pre-existing strike-slip related fault rocks. It is therefore postulated that *in Domain 1, top-to-the-E extension was associated with a phase of renewed phyllonitisation.* Similar extension-related protophyllonites have also been observed near the mouth of Abhainn Liadale (section 7.2.2), which suggests that phyllonitisation during extension may have been fairly widespread in eastern South Uist.

### ***Stuley*** (Fig. 7.8)

The highly strained nature of the extension-related phyllonitic fabrics preserved on Stuley has largely obscured evidence of their origins. However, the presence of a relatively undeformed protophyllonitic 'clast', which preserves a NE-SW trending mineral lineation (section 7.2.4.2), suggests that at least *some of the extension-related fabrics may have been derived from reworked strike-slip related phyllonite* (see also Butler 1995).

#### **7.2.5.3 Summary**

The present day distribution of strike-slip, transtension- and extension-related fabrics along the Usinish Phyllonite is in part the result of movements along the brittle extensional detachment faults following the cessation of macroscopically ductile deformation. However, it has been demonstrated that:

- The Usinish Phyllonite belt mostly originated during macroscopically ductile top-to-the-NE sinistral strike-slip.
- There was a progressive change in the regional kinematic regime, from top-to-the-NE strike-slip to top-to-the-ENE transtension to top-to-the-E extension.

- Transtension and extension were accommodated by the reworking of pre-existing phyllonitic fabrics *and* by the localised generation of new phyllonitic fabrics in regions of previously non-phyllonitised rock.
- The thickness of the Usinish Phyllonite belt increases towards the south, although the observed increase in outcrop width is primarily due to a decrease in average dip of the phyllonitic foliation.

The following sections provide detailed descriptions of the different fault rocks and fabrics, and discuss the possible mechanisms of phyllonitisation and reactivation along the Usinish Phyllonite.

### **7.3 PRIMARY FABRIC: FRACTURED CORODALE GNEISS AND MASHED GNEISS**

Brittle faults, cataclasite seams and devitrified pseudotachylyte veins are commonly observed to cross-cut the Corodale Gneiss and Mashed Gneiss preserved in eastern South Uist. The aim of the following sections is to describe the effects of brittle deformation (i.e. the primary fabrics) as a context in which to understand the development of the overprinting phyllonitic (i.e. derived) fabrics.

#### **7.3.1 FRACTURED CORODALE GNEISS**

Fractured Corodale Gneiss outcrops in the immediate footwall of the Usinish Phyllonite belt and is particularly well exposed in the regions to the west of Rubha Rossel (NF 857365) and Rubha Bolum (NF 827 284).

##### **7.3.1.1 Field relationships**

In the immediate footwall of the Usinish Phyllonite, the Corodale Gneiss comprises a coarse grained assemblage of feldspar, hornblende, biotite  $\pm$  quartz. The gneissose banding is commonly observed to be cross-cut by devitrified pseudotachylyte fault veins ( $\leq 2\text{m}$  long) and randomly oriented brittle fractures. The overall intensity of brittle deformation is *less* than that observed either in the pseudotachylyte-ultracataclasite crush zones preserved at the base of the Corodale Gneiss to the west (section 3.5.2.2), or in the crush melange of North Uist (section 6.2).

### 7.3.1.2 Microstructure

The microstructure of fractured Corodale Gneiss reflects (a) the effects of brittle deformation and (b) the effects of greenschist facies retrogression.

#### *Deformation microstructures*

The Corodale Gneiss comprises equigranular-polygonal aggregates of partially sericitised plagioclase grains, which isolate pockets of hornblende, biotite, opaque minerals and less commonly, rounded quartz grains. The entire assemblage is cross-cut by transgranular fractures, cataclasite seams and devitrified pseudotachylyte veins (Plate 7.1).

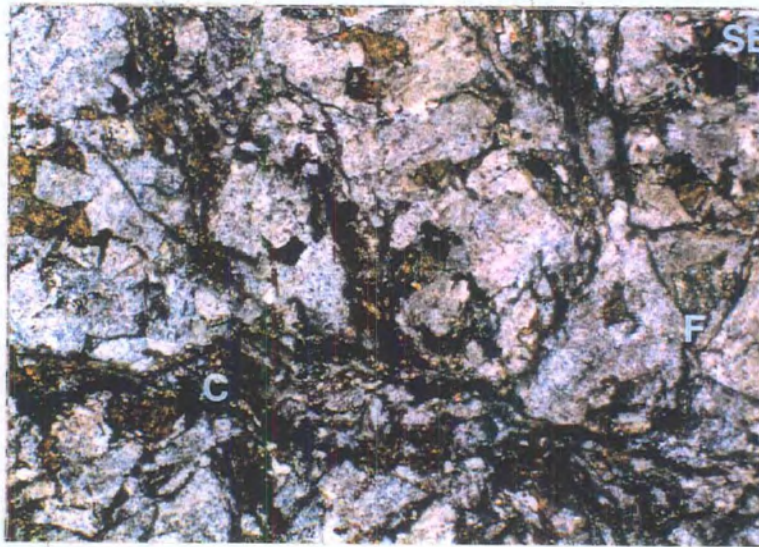


**Plate 7.1** Transgranular 'cataclasite' seam (C) and intragranular fractures (F) cross cutting interlocking network of feldspar grains in Corodale Gneiss. Field of view 6x3.7mm, crossed polars.

Relatively unaltered feldspar grains ( $\leq 1$ mm diameter) are characterised by strong patchy undulose extinction and are *locally* cross-cut by intragranular extension fractures. The fractures are infilled by seriate-polygonal or seriate-interlobate aggregates of fine grained feldspar (individual grains  $\leq 0.01$ mm diameter). The biotite laths also display strong patchy undulose extinction and the (001) cleavages planes are typically kinked. In contrast, hornblende grains appear to be undeformed, but have locally suffered partial alteration to aggregates of coarse grained epidote (epidote grains  $\leq 0.1$ mm diameter).

The cataclasite seams and devitrified pseudotachylyte veins ( $\leq 5$ mm wide) comprise angular clasts of hornblende and partially sericitised feldspar ( $\leq 1$ mm diameter), which 'float' in an ultrafine grained matrix of albite, epidote and opaque minerals (individual grains  $\leq 0.0025$ mm diameter). Randomly oriented transgranular fractures,

which are typically lined by aggregates of ultrafine grained epidote, locally cross-cut the cataclasite / pseudotachylyte veins. Structures preserved within the wall rocks cannot be correlated, which suggests that the transgranular fractures have accommodated significant shear displacements.

***Microstructures associated with low grade alteration***

The effects of low grade alteration are commonly observed throughout the Corodale Gneiss. Feldspar grains preserved within regions of intact gneiss have suffered partial alteration to aggregates of fine grained sericite needles (individual sericite grains  $\leq 0.01\text{mm}$  long). Sericite accounts for up to 20% of the surface area of the host feldspar grain and the sericite needles typically define well developed mesh textures. Feldspar clasts preserved within cataclasite seams / devitrified pseudotachylyte veins appear to have suffered a similar degree of alteration as the feldspar grains preserved in regions of intact gneiss.

The margins of the transgranular fractures, cataclasite seams, devitrified pseudotachylyte veins and associated clasts are commonly observed to be overprinted by aggregates of ultrafine grained epidote and opaque minerals (Plate 7.2). However, ultrafine grained epidote has *not* been observed in regions of intact gneiss. These observations suggest that *low grade alteration largely post-dates cataclasis, pseudotachylyte generation and brittle fracturing within the Corodale Gneiss.*

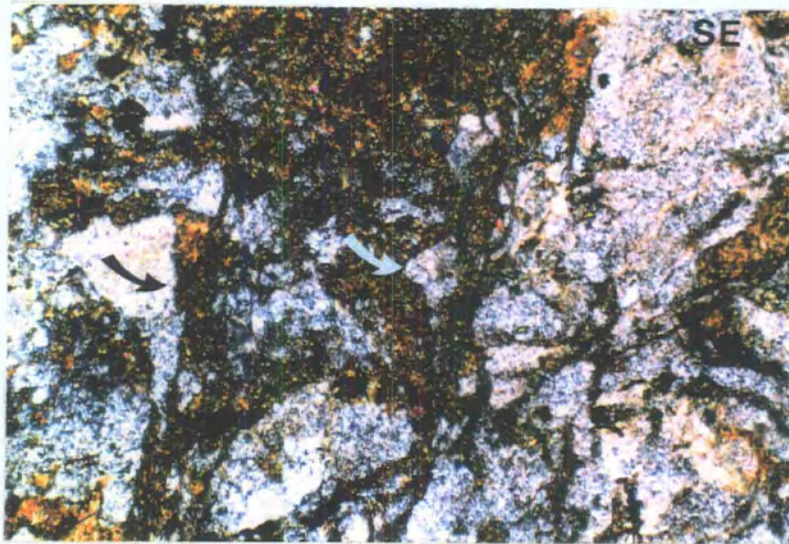


**Plate 7.2** Detail of 'cataclasite' seam within Corodale Gneiss host. 'Cataclasite' consists of fine grained epidote and chlorite matrix (brown) containing angular feldspar clasts. Note that margins of clasts preserved within the 'cataclasite' seam (arrowed) appear to be 'fuzzy' due to late overgrowths of epidote. Field of view  $3 \times 1.9\text{mm}$ , crossed polars.

### 7.3.2 MASHED GNEISS

Mashed Gneiss outcrops in the hangingwall of the Usinish Phyllonite belt and is particularly well exposed at Rubha Rossel (NF 859 365) and Rubha Hallagro (NF 870 360). A metre-scale 'clast' of Mashed Gneiss is preserved *within* the Usinish Phyllonite at Rubha Bolum (section 7.2.3.2).

#### 7.3.2.1 Field relationships

Mashed Gneiss is a predominantly quartzo-feldspathic rock. The gneissose banding appears to have been destroyed by brittle fracturing, cataclasis and localised melting along pseudotachylyte-bearing fault veins. The Mashed Gneiss closely resembles the most highly deformed regions within the crush melange of North Uist (section 6.2.1.2).

#### 7.3.2.2 Microstructure

The microstructure of fractured Mashed Gneiss reflects (a) the effects of brittle deformation and (b) the effects of greenschist facies retrogression. Apart from the relatively low abundance of calcite, the Mashed Gneiss is microstructurally indistinguishable from domains of intensely fractured crush melange observed elsewhere in the Outer Hebrides (e.g. section 6.2.2).

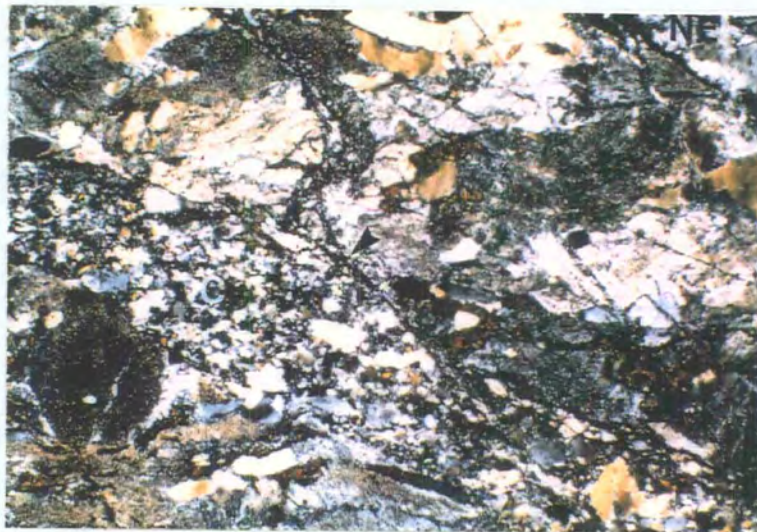


**Plate 7.3** Typical Mashed Gneiss. Granoblastic quartz and partially sericitised feldspar grains are cross cut by cataclasite seams (C) and fractures (arrow). Field of view 6x3.7mm, crossed polars.

### ***Deformation microstructures***

Mashed Gneiss comprises equigranular-polygonal aggregates of partially sericitised feldspar grains (plagioclase and K-feldspar), which isolate pockets of flattened quartz, equant hornblende grains, opaque minerals, chlorite and epidote. The entire assemblage is cross-cut by transgranular brittle fractures, cataclasite seams and devitrified pseudotachylyte veins (Plate 7.3). Multiple generations of brittle fractures can be distinguished on the scale of a single thin section.

Relatively unaltered feldspar grains ( $\leq 2\text{mm}$  diameter) display strong patchy undulose extinction and are typically cross-cut by arrays of intragranular extension fractures. The fractures are generally infilled by aggregates of fine grained feldspar (?albite). The flattened quartz grains ( $\leq 4\text{mm}$  long; aspect ratios  $\leq 5:1$ ) display strong patchy to sweeping undulose extinction, and coarse optical subgrains ( $\leq 0.03\text{mm}$  diameter) are locally developed. Intragranular extension fractures, which are infilled by seriate-interlobate aggregates of fine grained quartz, are commonly observed to cross-cut undulose quartz grains. In contrast, the hornblende grains appear to be relatively undeformed and unaltered.

The cataclasite seams and devitrified pseudotachylyte veins ( $\leq 5\text{mm}$  wide) comprise angular clasts of quartz and partially sericitised feldspar ( $\leq 1\text{mm}$  diameter), which 'float' in an ultrafine grained matrix of albite, epidote and opaque minerals (individual grains  $\leq 0.0025\text{mm}$  diameter). Randomly oriented transgranular fractures, which appear to be lined by aggregates of ultrafine grained epidote and opaque minerals are commonly observed. Structures preserved within the wall rocks cannot be correlated, which suggests that the transgranular fractures have accommodated significant shear displacements.

### ***Microstructures associated with low grade alteration***

The effects of low grade alteration are commonly observed throughout the Mashed Gneiss. Feldspar grains preserved within regions of relatively intact Mashed Gneiss and within cataclasite seams and devitrified pseudotachylyte veins have suffered partial alteration to aggregates of fine grained sericite needles (individual sericite grains  $\leq 0.01\text{mm}$  long). Sericite needles account for up to 50% (typically  $\cong 20\%$ ) of the surface area of host feldspar grains, and the needles generally define well developed mesh textures.

The margins of the transgranular fractures, cataclasite seams and pseudotachylyte veins are commonly observed to be overprinted by aggregates of ultrafine grained epidote and opaque minerals. Such epidote aggregates have only been observed within zones of intense brittle deformation. These observations suggest that *low*

*grade alteration largely post-dates cataclasis, pseudotachylyte generation and brittle fracturing within the Mashed Gneiss.*

### **7.3.3 SUMMARY AND DISCUSSION**

Packages of Corodale Gneiss and Mashed Gneiss preserved in the regions immediately adjacent to the Usinish Phyllonite are commonly observed to be cross-cut by brittle fractures, cataclasite seams and devitrified pseudotachylyte veins. The overall effect of brittle fracturing, cataclasis and pseudotachylyte generation was to cause localised, albeit extreme, grain size reduction in the gneissose protoliths. Both the Corodale Gneiss and the Mashed Gneiss appear to have suffered partial alteration following the cessation of brittle deformation.

#### **7.3.3.1 Deformation mechanisms**

The abundance of fractures, cataclasite seams and pseudotachylyte veins suggests that deformation and grain size reduction were dominated by brittle processes. However, quartz and relatively unaltered feldspar grains typically display strong patchy undulose extinction. These microstructures are consistent with the operation of intracrystalline crystal plastic deformation mechanisms, such as dislocation glide (Hirth & Tullis 1992). However, crystal plastic deformation does not appear to have been a significant mechanism for accommodating aggregate-scale strains. Furthermore, low temperature crystal plasticity is widely accepted to be a precursor to brittle fracturing (e.g. Lloyd & Knipe 1992). It is therefore postulated that *deformation occurred entirely within the frictional regime* described by Schmid & Handy (1991).

#### **7.3.3.2 Distribution of low grade alteration**

Evidence for partial alteration is widespread, although heterogeneously distributed throughout the Corodale Gneiss and the Mashed Gneiss. The growth of sericite, albite and epidote are consistent with alteration having occurred in a fluid-rich greenschist facies environment. Secondary epidote and opaque minerals are commonly observed to overprint the transgranular fractures, cataclasite seams and pseudotachylyte veins. These observations suggest that retrogression within the Corodale Gneiss and the Mashed Gneiss largely post-dates brittle deformation. However, it is clear that the pre-existing deformation microstructures influenced the distribution of retrogression. In particular, the aggregates of ultrafine grained epidote and opaque minerals are entirely restricted to transgranular fractures, cataclasite seams and pseudotachylyte seams. These observations suggest that *alteration was most intense within pre-existing zones of intense brittle deformation and extreme grain size reduction* (cf.

section 6.2.3). These inferences have important implications for the mechanisms of phyllonitisation, and are discussed further in section 7.4.

## **7.4 DERIVED FABRICS: STRIKE-SLIP AND 'NEW' TRANSTENSION- AND EXTENSION-RELATED PHYLLONITES**

Macroscopically ductile phyllonitic fabrics are commonly observed to overprint fractured Corodale Gneiss and Mashed Gneiss (i.e. the primary fabrics). The aim of this section is to determine the metamorphic conditions, the operative deformation mechanisms and the principal controls on phyllonitisation during strike-slip, transtension and extension.

### **7.4.1 CORODALE GNEISS-DERIVED PHYLLONITE**

#### **7.4.1.1 Protophyllonite**

Unequivocal Corodale Gneiss-derived strike-slip related protophyllonite has been observed at the base of the phyllonite belt exposed at Rubha Rossel (section 7.2.1.2) and in Domain 4 at Rubha Bolum (section 7.2.3.2). Corodale Gneiss-derived extension-related protophyllonite has been observed in Domain 1 at Rubha Bolum (section 7.2.3.2) and near the mouth of Abhainn Liadale (section 7.2.2).

#### *Field relationships*

The strike-slip related protophyllonites preserved in Domain 4 at Rubha Bolum are characterised by a patchily developed undulating foliation. The foliation cross-cuts and deforms highly discordant relict pegmatite veins, cataclasite seams and pseudotachylyte veins. These observations suggest that the protophyllonitic fabrics preserved in Domain 4 have accommodated relatively low magnitudes of finite strain. The strike-slip related protophyllonites preserved at the base of the Rubha Rossel phyllonite belt are characterised by a well developed, undulating foliation. Relict cataclasite seams and pseudotachylyte veins are typically oriented parallel to the foliation. These observations suggest that the protophyllonites at Rubha Rossel may have accommodated high magnitudes of finite strain in comparison with those preserved in Domain 4 at Rubha Bolum. The protophyllonitic foliation is locally cross-cut by arrays of en-echelon quartz veins (Fig. 7.2). The geometries of the vein arrays are consistent with top-to-the-NE shear, which suggests that vein opening was broadly synchronous with macroscopically ductile sinistral strike-slip. However, the veins are relatively undeformed, and there is no evidence that there was more than one

generation of syn-tectonic veins. It is therefore postulated that the veins developed *towards the end of macroscopically ductile strike-slip* at Rubha Rossel.

The Corodale Gneiss-derived extension-related protophyllonites preserved in Domain 1 at Rubha Bolum are characterised by a patchily developed, undulating foliation. Apart from the difference in inferred kinematic regime, the extension-related protophyllonitic fabrics are almost indistinguishable in the field from the strike-slip related protophyllonites observed in Domain 4.

### **Microstructure**

Packages of relatively unstrained Corodale Gneiss-derived protophyllonite comprise laterally discontinuous (on the grain scale) sericite strands, which wrap around partially altered plagioclase and hornblende grains. Randomly oriented cataclasite seams and devitrified pseudotachylyte veins are commonly observed. Cataclasite seams and pseudotachylyte veins which are oriented at high angles to the trace of the macroscopic foliation are generally folded and flattened into the plane of the foliation (i.e. the fold axial planes are oriented sub-parallel to the foliation) (fold wavelengths  $\leq 0.5\text{mm}$ ) (Plate 7.4). The feldspar grains are highly altered (sericite accounts for up to 50% of the surface area of host grains) and typically display well developed sericite mesh textures. Hornblende grains are locally pseudomorphed by aggregates of coarse grained epidote (individual grains  $\leq 0.05\text{mm}$  diameter) and / or by aggregates of fibrous actinolite. However, actinolite is more commonly observed in strike-slip related phyllonite than in extension-related phyllonite.

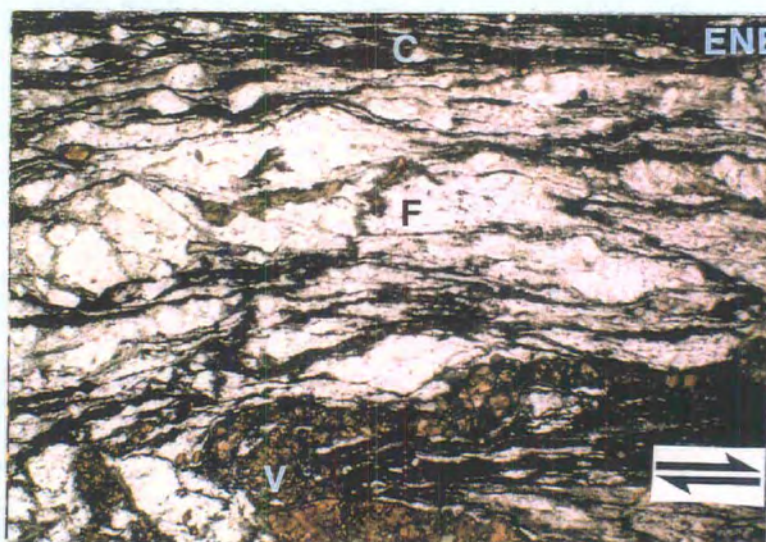


**Plate 7.4** Strike-slip related protophyllonitic Corodale Gneiss. C = sheared 'cataclasite' seam, F = feldspar-rich augen, V = sheared and folded epidote vein. Split arrows parallel mineral lineation, top-to-NE shear. Field of view 6x3.7mm, plane polarised light.

Packages of *highly strained Corodale Gneiss-derived protophyllonite* comprise interconnected networks of sericite strands, which wrap around highly altered feldspar and hornblende grains. Relict cataclasite seams and pseudotachylyte veins are typically oriented parallel to the trace of the macroscopic foliation, and comprise aggregates of ultrafine grained epidote, albite, sericite and chlorite. The (001) cleavage planes of the sericite and chlorite needles are oriented parallel to the foliation. Relict feldspar grains typically display well developed sericite mesh textures, and sericite locally accounts for up to 70% of the surface area of host grains. The hornblende grains have also experienced intense alteration, and are commonly observed to be pseudomorphed by aggregates of epidote or actinolite. Intragranular extension fractures locally cross-cut relict hornblende grains. The fractures are infilled either by aggregates of fibrous actinolite (in strike-slip related protophyllonite), or fibrous quartz-chlorite (in extension-related protophyllonite).

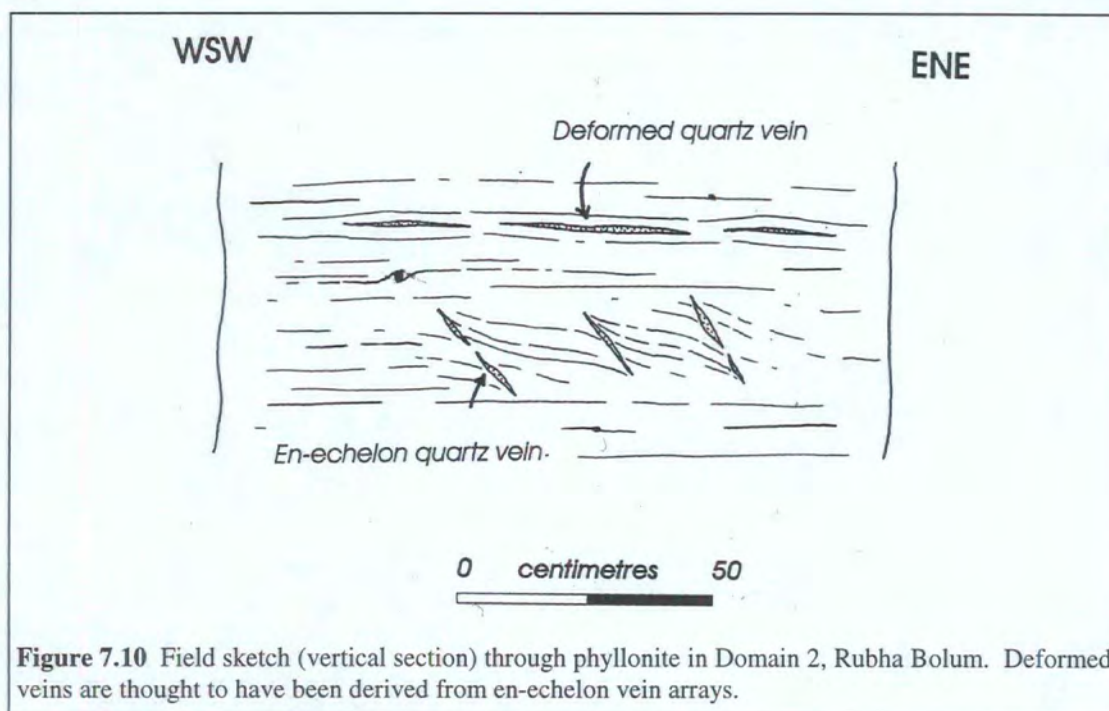
#### **7.4.1.2 Phyllonite and ultraphyllonite**

Packages of Corodale Gneiss-derived strike-slip related phyllonite and ultraphyllonite are preserved at Rubha Rossel (section 7.2.1.2) and in Domain 2 at Rubha Bolum (section 7.2.3.2). Corodale Gneiss-derived extension-related phyllonite has been observed in the uppermost 10m of Domain 1 at Rubha Bolum (section 7.2.3.2).

#### ***Field relationships***

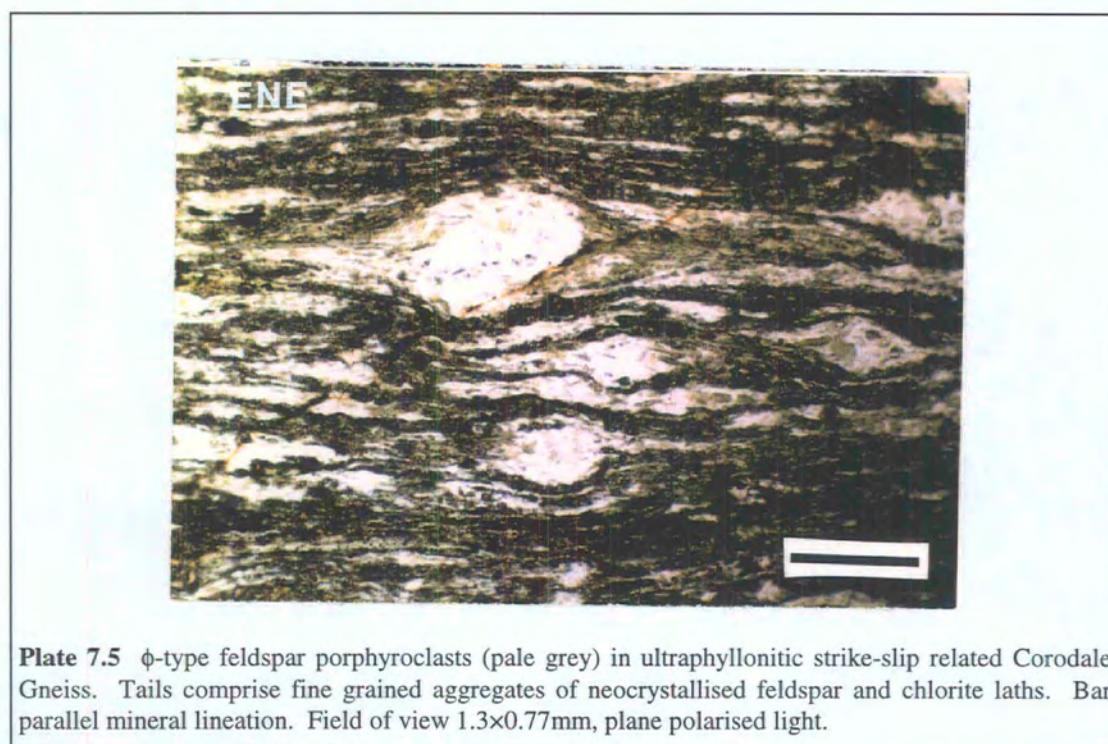
Packages of Corodale Gneiss-derived phyllonite and ultraphyllonite are characterised by a well developed planar foliation. Apart from the difference in inferred kinematic regime, packages of strike-slip related phyllonite are almost indistinguishable in the field from packages of extension-related phyllonite.

Arrays of foliation-parallel and en-echelon quartz-albite veins ( $\leq 1\text{cm}$  thick) are commonly observed within packages of strike-slip and extension-related phyllonite. The geometries of the en-echelon vein arrays are consistent with either top-to-the-NE or top-to-the-E shear. *Undeformed* en-echelon veins are oriented at up to  $30^\circ$  to the foliation. In contrast, *deformed* en-echelon veins are oriented sub-parallel to the foliation and appear to have been boudinaged (Fig. 7.10). These observations suggest (a) that vein opening was synchronous with macroscopically ductile deformation, and (b) that there is more than one generation of syn-tectonic veins. Both strike-slip and extension-related fabrics are cross-cut by sets of undeformed, predominantly N-S trending sub-vertical quartz veins. The orientation of the fibrous quartz infill is consistent with vein opening in a regime of E-W extension. The significance of the syn- and post-tectonic quartz veins is discussed in section 7.5.3.

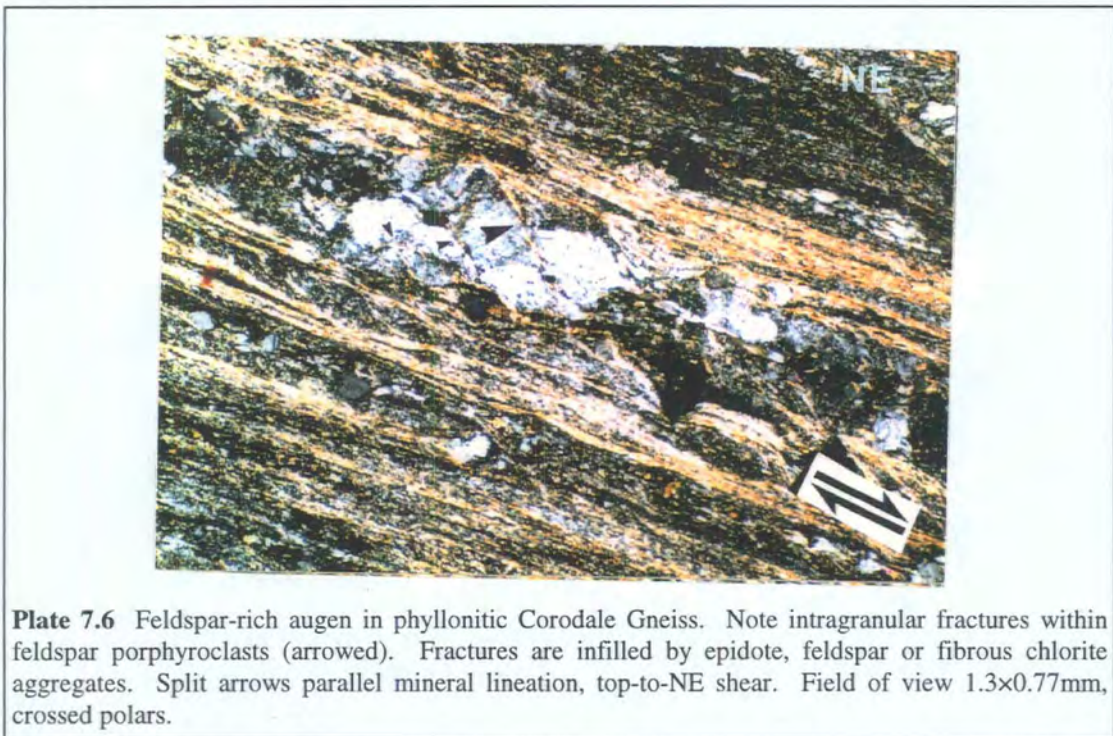


### *Microstructure*

Packages of Corodale Gneiss-derived phyllonite and ultraphyllonite comprise isolated  $\phi$ -type (locally  $\delta$ - or  $\sigma$ -type) feldspar and hornblende porphyroclasts, which are wrapped by laterally continuous sericite strands, aggregates of ultrafine grained albite and highly deformed, concordant cataclasite seams and pseudotachylyte veins (Plate 7.5).



The sericite strands (typically  $\cong 0.02\text{mm}$  wide) appear to be finely interbanded with laterally discontinuous, polycrystalline albite ribbons ( $\leq 0.01\text{mm}$  wide;  $\leq 0.1\text{mm}$  long). The ribbons comprise seriate-interlobate aggregates of ultrafine grained albite. Individual albite grains are typically less than  $0.005\text{mm}$  in diameter, and the grain boundaries are commonly observed to be decorated by low-relief fluid inclusions (inclusions  $\leq 0.0025\text{mm}$  diameter). Relict cataclasite seams and pseudotachylyte veins, which locally account for up to 50% of the total rock volume, comprise aggregates of ultrafine grained albite, epidote, sericite and chlorite. The (001) cleavage planes of the phyllosilicate minerals are typically oriented parallel to the macroscopic foliation, and chlorite is particularly common in packages of extension-related phyllonite.



Feldspar porphyroclasts ( $\leq 0.2\text{mm}$  diameter) display strong patchy undulose extinction and are commonly observed to be cross-cut by intragranular extension and shear fractures. The fractures, which are infilled by quartz-actinolite fibres, extend the deformed porphyroclasts in a direction parallel to the macroscopic mineral lineation (Plate 7.6). Feldspar porphyroclasts are either wrapped by 'tails' of ultrafine grained albite, or are fringed by fibrous actinolite or quartz-chlorite strain shadows. Unaltered hornblende grains have not been observed, and in general, hornblende is completely replaced by aggregates of actinolite, chlorite and / or coarse grained epidote (epidote grains  $\leq 0.05\text{mm}$  diameter).

### 7.4.1.3 Summary and discussion

Packages of strike-slip and extension-related Corodale Gneiss derived phyllonite are widely preserved along the length of the Usinish Phyllonite belt. Chlorite appears to be more abundant in packages of extension-related phyllonite, although overall, the deformation microstructures of the strike-slip and extension-related fabrics are very similar. Syn-tectonic quartz-albite veins are commonly observed.

#### *Retrogression and metamorphism during phyllonitisation*

Strike-slip and extension-related phyllonites comprise a stable assemblage of sericite, actinolite, chlorite, albite, epidote  $\pm$  quartz. The original plagioclase and hornblende grains have suffered intense alteration to aggregates of hydrous phyllosilicates, albite, actinolite and epidote. The retrograde minerals typically display a strong grain shape preferred orientation. In particular, fibrous actinolite is locally developed in strain shadows around the margins of feldspar porphyroclasts, whilst aggregates of sericite form interconnected strands in which the (001) cleavage planes are oriented parallel to the trace of the macroscopic foliation. These observations suggest (a) that during strike-slip and extension, *phyllonitisation occurred under lower greenschist facies conditions*, and (b) that *retrogression and hydration were synchronous with deformation*. The relatively high abundance of chlorite in packages of extension-related phyllonite may reflect subtle changes either in the ambient pressure and temperature conditions, or in the composition of the metamorphic fluid (see below). The nature of the fluid phase is discussed further in Chapter 9.

#### *Operative deformation mechanisms*

Packages of relatively unstrained protophyllonite are likely to preserve information on the deformation mechanisms which were operative at the *onset* of phyllonitisation. Corodale Gneiss-derived protophyllonite is characterised by highly altered feldspar and hornblende grains, which are wrapped by aggregates of intensely aligned sericite needles. The most important microstructural process at the onset of phyllonitisation thus appears to have been the development of sericite strands. Sericitisation reactions require a chemically active fluid phase and are generally thought to result in the loss of silica from the host feldspar grain (e.g. Hemley & Jones 1964; Beach 1980). It is therefore postulated that *the feldspar grains behaved as fluid-assisted diffusive mass transfer (DMT) sources at the onset of phyllonitisation* (see Chapter 9 for further discussion). Intragranular extension fractures are commonly observed within hornblende grains. The fractures are typically infilled by aggregates of actinolite fibres, which are oriented parallel to the macroscopic mineral lineation. This observation is consistent with the fractured hornblende grains having behaved as

fluid-assisted DMT *sinks*, and emphasises the likely importance of fluid-assisted deformation processes at the onset of phyllonitisation.

Packages of highly strained Corodale Gneiss-derived phyllonite and ultraphyllonite are characterised by a very planar foliation, which is defined by sericite strands, deformed cataclasite seams / devitrified pseudotachylyte veins and by laterally discontinuous, ultrafine grained albite ribbons. These observations suggest that the overall rheological behaviour of the highly strained phyllonitic fault rocks was probably controlled by the rheological behaviour of the sericite strands and relict cataclasite seams / pseudotachylyte veins. Individual sericite needles display a strong grain shape preferred orientation and are characterised by strong patchy undulose extinction. Kinks and fractures are rarely observed. TEM investigations of experimentally deformed muscovite grains suggest that undulose extinction develops during dislocation glide (i.e. intracrystalline crystal plastic deformation) (Bell *et al.* 1986). Previous authors have proposed that naturally deformed aggregates of intensely aligned, undulose biotite grains deformed by dislocation creep mechanisms (Goodwin & Wenk 1995). It is therefore postulated that the sericite stands may have accommodated deformation primarily by intracrystalline crystal plastic mechanisms (e.g. dislocation creep). However, detailed TEM studies are necessary to confirm this hypothesis. It is not possible to directly determine the operative deformation mechanisms within the ultrafine grained cataclasite seams / pseudotachylyte veins. However, actinolite strain shadows are commonly observed to fringe feldspar porphyroclasts preserved within the ultrafine grained matrix. This observation suggests that fluid-assisted diffusive mass transfer processes were operative within packages of highly-strained phyllonite and ultraphyllonite. Furthermore, the fine grained nature of the matrix is likely to have promoted diffusion-dominated (i.e. grain size sensitive) deformation mechanisms. It is therefore suggested that deformation within the ultrafine grained cataclasite seams / pseudotachylyte veins may have been controlled by fluid-assisted diffusion-accommodated grain size sensitive mechanisms (e.g. viscous grain boundary sliding).

The macroscopically ductile strike-slip and extension-related fabrics are locally cross-cut by arrays of syn-tectonic quartz-albite veins. It is likely that the veins developed during transient episodes of localised high fluid pressure within the Usinish Phyllonite belt (cf. Cox & Etheridge 1989; Kennedy & Logan 1997). However, there is no evidence that vein opening was associated with frictional sliding (cf. North Uist, Chapter 6). This observation suggests that veining was *not* a significant mechanism of strain accommodation during macroscopically ductile deformation.

In conclusion, the *onset* of phyllonitisation appears to have been dominated by fluid-assisted diffusive mass transfer processes, which were responsible the alteration of

feldspar porphyroclasts to aggregates fine grained sericite. However, in packages of highly strained phyllonite and ultraphyllonite, deformation appears to have been accommodated (a) by intracrystalline crystal plastic processes (within sericite grains), and (b) by continued aggregate-scale fluid-assisted DMT. Brittle deformation was not an important mechanism of aggregate-scale strain accommodation.

## **7.4.2 MASHED GNEISS-DERIVED PHYLLONITE**

### **7.4.2.1 Protophyllonite**

Mashed Gneiss-derived strike-slip related protophyllonite has been observed in Domain 3 at Rubha Bolum (section 7.2.3.2). Mashed Gneiss-derived transtension-related protophyllonite is preserved in the hangingwall of the Rubha Rossel phyllonite belt (section 7.2.1.2).

#### ***Field relationships***

Mashed Gneiss-derived protophyllonite has a very 'blocky' appearance and is characterised by a patchy to well developed undulating foliation. The protophyllonitic fabric overprints and deforms concordant and discordant cataclasite seams and pseudotachylyte veins.

#### ***Microstructure***

Unfortunately, samples of transtension-related protophyllonite have not been collected. The following descriptions are therefore pertinent only to the strike-slip related protophyllonites from the low strain 'clast' at Rubha Bolum. These rocks comprise partially altered feldspar (K-feldspar and oligoclase / andesine) and fractured quartz grains, which are wrapped by networks of deformed cataclasite seams / pseudotachylyte veins and laterally discontinuous (on the scale of a thin section) sericite strands.

The partially altered feldspar grains display well developed sericite mesh textures, and sericite typically accounts for c.40% of the surface area of host grains. However, sericite accounts for up to 70% of the surface area of feldspar grains preserved within deformed cataclasite seams / pseudotachylyte veins. This observation has important implications for the mechanisms of phyllonitisation, and is discussed further in sections 7.4.2.3 and 7.4.3. Quartz porphyroclasts typically display strong patchy undulose extinction, and are commonly observed to be fringed by fibrous quartz or actinolite strain shadows.

#### 7.4.2.2 Phyllonite and ultraphyllonite

Mashed Gneiss-derived strike-slip related phyllonite is preserved along the margins of the low strain 'clast' at Rubha Bolum (section 7.2.3.2). Mashed Gneiss-derived extension-related phyllonite has *not* been observed.

##### *Field relationships*

The Mashed Gneiss-derived phyllonite preserved at Rubha Bolum is poorly exposed and few structures can be discerned in the field.

##### *Microstructure*

Mashed Gneiss-derived strike-slip related phyllonite comprises isolated K-feldspar, plagioclase and quartz porphyroclasts which 'float' in a matrix of ultrafine grained albite (individual grains  $\leq 0.005\text{mm}$  diameter), and laterally discontinuous (on the scale of a thin section) polycrystalline quartz ribbons and sericite strands (Plate 7.7). Overall, sericite accounts for less than 10% of the total rock, and is therefore much less abundant than in Corodale Gneiss-derived phyllonite. Deformed cataclasite seams and pseudotachylite veins are also relatively uncommon and comprise less than 10% of the total rock volume.

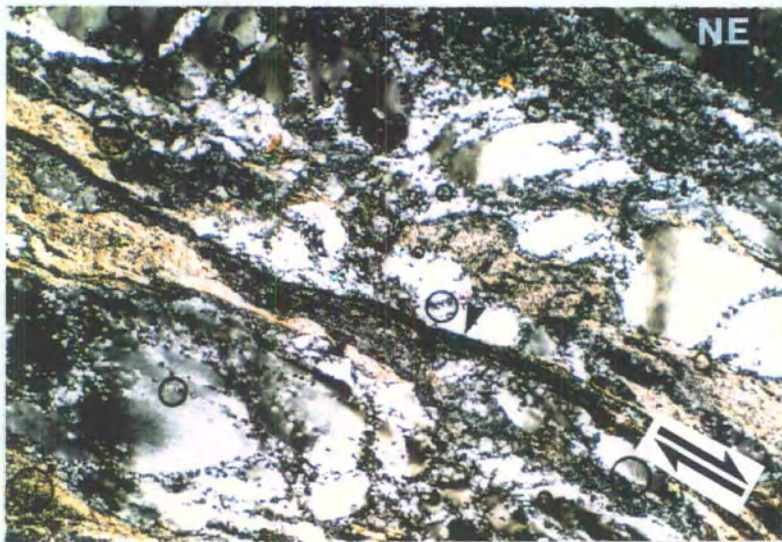


**Plate 7.7** Strike-slip related protophyllonitic Mashed Gneiss. Quartz porphyroclasts wrapped by laterally discontinuous sericite strands (speckled brown). Note late pressure solution seam which trends sub-parallel to the foliation and locally truncates quartz porphyroclasts (arrow). Split arrows parallel mineral lineation, top-to-NE shear. Field of view 1.3x0.77mm, crossed polars.

The angular to sub-rounded feldspar porphyroclasts ( $\leq 0.6\text{mm}$  diameter) display strong patchy undulose extinction and twin planes are commonly observed to be offset across hairline fractures (apparent offsets  $\leq 0.01\text{mm}$ ). Intragranular extension

fractures are locally developed, and are typically infilled by aggregates of fibrous quartz or quartz-chlorite. Both plagioclase and K-feldspar porphyroclasts are commonly observed to be surrounded by tails and mantles of ultrafine grained albite (individual grains  $\leq 0.005\text{mm}$  diameter), which appear to be in optical continuity with the albite-rich matrix. The ultrafine albite grains preserved with the matrix are characterised by lobate grain boundaries, which are commonly observed to be decorated arrays of low relief fluid inclusions (inclusions  $\leq 0.0025\text{mm}$  diameter).

Quartz porphyroclasts display strong patchy to sweeping undulose extinction, and are locally surrounded by mantles of optical subgrains and seriate-interlobate or seriate-polygonal aggregates of fine grained quartz (individual grains and subgrains  $\leq 0.01\text{mm}$  diameter). Where core-and-mantle microstructures are not developed, the quartz porphyroclasts are commonly observed to be fringed by chlorite strain shadows.

#### **7.4.2.3 Summary and discussion**

Mashed Gneiss-derived phyllonite from the low strain 'clast' at Rubha Bolum is characterised by isolated quartz and feldspar porphyroclasts which 'float' in an ultrafine grained matrix of polycrystalline albite and quartz. Sericite is relatively scarce in comparison with Corodale Gneiss-derived phyllonite.

#### ***Retrogression and metamorphism during phyllonitisation***

Mashed Gneiss-derived phyllonite is characterised by a stable assemblage of albite, quartz, sericite, chlorite and epidote. K-feldspar and plagioclase porphyroclasts are typically wrapped by tails of ultrafine grained albite and the (001) cleavage planes of the phyllosilicate minerals are oriented parallel to the trace of the macroscopic foliation. These observations suggest (a) that retrogression was synchronous with deformation, and (b) that retrogression occurred under lower greenschist facies conditions. However, the abundance of hydrous phyllosilicate minerals appears to be relatively low in comparison with the Corodale Gneiss-derived phyllonites (section 7.4.1.3). Furthermore, syn-tectonic veins have not been observed within packages of Mashed Gneiss-derived phyllonite. These observations are consistent with *the local chemical activity and / or partial pressure of the hydrous fluid phase having been relatively low during deformation within Domain 3 at Rubha Bolum*. Possible controls on the distribution of hydrous fluids during phyllonitisation are discussed in section 7.4.3.

### ***Operative deformation mechanisms***

Mashed Gneiss-derived protophyllonite comprises quartz and partially sericitised feldspar grains, which are locally wrapped by sericite strands and deformed cataclasite seams / pseudotachylyte veins. Feldspar grains preserved within relict cataclasite seams / pseudotachylyte veins appear to have experienced particularly intense sericitisation. For reasons outlined previously (section 7.4.1.3), it is conceivable that the feldspar grains behaved as fluid-assisted diffusive mass transfer sources during phyllonitisation. If this inference is correct, the most highly altered feldspar grains are likely to occur in regions of significant fluid-rock interaction. It is therefore postulated that at the onset of phyllonitisation, *fluid-rock interaction was particularly intense within deformed cataclasite seams / pseudotachylyte veins*. The corollaries of this hypothesis are discussed in section 7.4.3.

Mashed Gneiss-derived phyllonite comprises K-feldspar, plagioclase and quartz porphyroclasts which 'float' in a matrix of ultrafine grained albite and laterally discontinuous sericite strands and polycrystalline quartz ribbons. These observations suggest that the overall rheological behaviour of the Mashed Gneiss-derived phyllonite was controlled by the rheological behaviour of the interconnected albite-rich aggregates (Jordan 1987; Handy 1990). Unfortunately, the fine grained size precludes detailed optical study of the operative deformation mechanisms within the matrix. However, fibrous chlorite strain shadows are commonly observed to fringe quartz porphyroclasts preserved within the matrix. This observation is consistent with sites of localised dilatation along the margins of quartz porphyroclasts having behaved as fluid-assisted diffusive mass transfer sinks. Furthermore, the ultrafine grained nature of the matrix is likely to have promoted the operation of diffusion-dominated deformation mechanisms. It is therefore postulated that the albite-rich matrix deformed by diffusion-accommodated grain size sensitive processes (e.g. viscous grain boundary sliding) (cf. Stünitz & Fitz Gerald 1993).

## **7.4.3 SYNTHESIS**

### **7.4.3.1 Summary**

Field and microstructural observations suggest that phyllonitisation in eastern South Uist was characterised by intense, though spatially restricted, lower greenschist facies retrogression and hydration. The microstructural evolution of both strike-slip and extension-related phyllonites was primarily controlled by fluid-assisted diffusive mass transfer processes. It is therefore important to identify the mechanisms by which fluids gained access to the fault zone at the onset of retrogression and deformation.

#### 7.4.3.2 A model of phyllonitisation in South Uist

In packages of highly strained phyllonite, the pre-existing fabrics have been all but obliterated by the breakdown of the original feldspar and hornblende grains to aggregates of fine grained phyllosilicate minerals. In order to determine how fluids may have gained access to the fault zone at the *onset* of phyllonitisation, one must therefore examine (a) the primary fabrics and (b) packages of relatively unstrained protophyllonite.

The primary fabrics (i.e. fractured Corodale Gneiss and Mashed Gneiss) comprise randomly oriented brittle fractures, cataclasite seams and devitrified pseudotachylyte veins which cross-cut coarse grained, granoblastic host rocks. Both the Corodale Gneiss and Mashed Gneiss have suffered partial greenschist facies retrogression. However, it has been demonstrated that retrogression was most intense along the networks of fractures, cataclasite seams and pseudotachylyte veins (section 7.3.3). These observations suggest that *prior* to the onset of macroscopically ductile deformation, fluid-rock interactions were strongly focused into pre-existing brittle structures.

Mashed Gneiss-derived protophyllonite comprises quartz and partially sericitised feldspar grains, which are wrapped by laterally discontinuous sericite strands and deformed cataclasite seams / pseudotachylyte veins. Microstructural observations suggest that the most highly sericitised feldspar grains are preserved within relict cataclasite seams / pseudotachylyte veins (section 7.4.2.1). It has been proposed that sericitisation is primarily controlled by fluid-assisted diffusive mass transfer processes (section 7.4.2.3). The corollary of this argument is that the most highly sericitised feldspar grains must occur in regions of intense fluid-rock interaction. These observations suggest that at the *onset* of macroscopically ductile deformation, fluid-rock interactions were focused within networks of pre-existing brittle fractures, cataclasite seams and pseudotachylyte veins. The mesoscale fractures, cataclasite seams and devitrified pseudotachylyte veins thus appear to have acted as important fluid pathways within the OHFZ, and are therefore inferred to have been highly permeable in comparison with the relatively undeformed country rocks. Deformed cataclasite seams / pseudotachylyte veins are extremely abundant within packages of highly strained and retrogressed, sericite-rich phyllonite and ultraphyllonite (section 7.4.1.2). In contrast, deformed cataclasite seams / pseudotachylyte veins are relatively scarce within the sericite-poor low strain 'clast' at Rubha Bolum. It is therefore concluded that *the most highly strained and retrogressed phyllonitic rocks localised along pre-existing, highly permeable zones of intense brittle deformation*. The present-day low strain 'clasts' preserved within the Usinish Phyllonite were probably derived from blocks of relatively undeformed gneiss which largely escaped the effects

of intense brittle deformation i.e. regions of relatively *low* permeability. On a larger scale, it is suggested that the Usinish Phyllonite developed along a pre-existing brittle fault zone (?crush zone) which originally marked the contact between the Corodale Gneiss and the Mashed Gneiss (see also Walker 1990; Butler 1995).

## **7.5 REWORKED FABRICS & DETACHMENT FAULTS: TRANSTENSION- AND EXTENSION-RELATED PHYLLONITE**

The aim of this section is to determine the metamorphic conditions and operative deformation mechanisms during macroscopically ductile reworking and subsequent brittle deformation along the Usinish Phyllonite. The final part of this chapter (section 7.5.3) synthesises the previous observations and inferences to produce a model for reactivation along the OHFZ in eastern South Uist.

### **7.5.1 REWORKED FABRICS**

Packages of transtension- and extension-related reworked Corodale Gneiss-derived phyllonite have locally been observed at Rubha Bolum (section 7.2.3.2). Reworked Mashed Gneiss-derived extension related phyllonite is widely preserved on Stuley (section 7.2.4.2). Unfortunately, poor exposure and / or limited outcrop precludes detailed study of the reworked phyllonites preserved either at Rubha Bolum or at Rubha Rossel (section 7.2.3.2). The following field and microstructural descriptions therefore relate to the Mashed Gneiss-derived phyllonite from Stuley.

#### **7.5.1.1 Field relationships**

Apart from a small package of protophyllonitic pegmatite preserved along the east coast of the island, Stuley is composed entirely of highly strained, sub-horizontal Mashed Gneiss-derived phyllonite and ultraphyllonite. The macroscopically ductile fabric is characterised by a well developed, platy foliation, which is associated with a predominantly E-W trending mineral stretching lineation (section 7.2.4.2). Concordant quartz-chlorite and quartz-albite veins (between 2mm and 10cm thick) are commonly observed throughout the island. The veins locally truncate the foliation, but more typically, are stretched and boudinaged parallel to the mineral lineation. However, in contrast to the deformed veins observed in packages of reworked phyllonite in North Uist (section 6.4.3), the deformed veins observed on Stuley have *not* been completely dismembered by intense macroscopically ductile deformation. These observations suggest that whilst the quartz-rich veins preserved on Stuley were emplaced during top-to-the-E shear, the veins probably developed *towards the end* of

the macroscopically ductile deformation event. There is no evidence to suggest that vein opening was associated with frictional sliding (cf. the reworked phyllonite belts from North Uist; Chapter 6). *Discordant* quartz-epidote veins are preserved in southern Stuley (NF 828 231), and are locally deformed by centimetre-scale E-verging chevron folds (section 7.2.4.2).

### 7.5.1.2 Microstructure

Reworked Mashed Gneiss-derived extension-related phyllonite comprises isolated, polycrystalline quartz porphyroclasts ( $\leq 0.5\text{mm}$  long; aspect ratios  $\leq 3:1$ ), which 'float' in a matrix of ultrafine grained albite (individual grains  $\leq 0.005\text{mm}$  diameter) and epidote (individual grains  $\leq 0.005\text{mm}$  diameter) (Plate 7.8). Albite accounts for up to 60% of the matrix. The albite grain boundaries are lobate and are commonly observed to be decorated either by fluid inclusions ( $\ll 0.0025\text{mm}$  diameter) or by ultrafine grained sericite laths ( $\leq 0.005\text{mm}$  long).



**Plate 7.8** Extension-related reworked Mashed Gneiss-derived ultraphyllonite from Stuley. Matrix (M) comprises aggregates of fine grained recrystallised quartz and neocrystallised albite and epidote (Ep). Note angular folds (highlighted) defined by deformed quartz vein. Bar parallel mineral lineation. Field of view  $3 \times 1.9\text{mm}$ , crossed polars.

The polycrystalline quartz porphyroclasts comprise (a) relatively coarse, equigranular-polygonal aggregates, in which individual grains ( $\leq 0.05\text{mm}$  diameter) display straight to faintly undulose extinction, or (b) relatively fine, equigranular-interlobate aggregates, in which individual grains ( $\leq 0.02\text{mm}$  diameter) display aspect ratios of up to 4:1. The long axes of the elongate grains are oriented parallel to the macroscopic foliation and insertion of a sensitive tint plate suggests that the elongate grains display

a strong crystallographic preferred orientation. In contrast, the crystallographic axes of the polygonal quartz grains appear to be randomly oriented. Aggregates of fine grained chlorite are locally observed along the margins of quartz porphyroclasts which are oriented at low angles to the macroscopic foliation. Individual chlorite grains are oriented parallel to the macroscopic foliation.

### **7.5.1.3 Summary and discussion**

Packages of reworked phyllonite and ultraphyllonite are exposed at Rubha Rossel, Rubha Bolum and on Stuley. Reworked phyllonites are characterised by a platy foliation, which is locally folded. Syn-tectonic veins are locally developed, although there is little evidence to suggest that vein opening was associated with significant frictional sliding events.

#### ***Retrogression and metamorphism during extensional reworking***

Packages of extensionally reworked phyllonite comprise an assemblage of albite, epidote, chlorite and sericite. Plagioclase, K-feldspar and hornblende porphyroclasts have not been observed. These observations suggest that packages of extension-related phyllonite have suffered intense (locally complete) retrogression under lower greenschist facies conditions.

#### ***Operative deformation mechanisms***

Reworked Mashed Gneiss-derived phyllonite comprises isolated quartz porphyroclasts which 'float' in an interconnected matrix of ultrafine grained albite and epidote. This observation suggests that the overall rheological behaviour of the Mashed Gneiss-derived phyllonite was controlled by the rheological behaviour of the interconnected albite-rich aggregates (Jordan 1987; Handy 1990). Unfortunately, the fine grain size precludes detailed optical studies. However, ultrafine grained sericite laths are commonly observed to decorate the margins of individual albite grains. It has been suggested that sericitisation reactions involve the loss of silica from the host feldspar grain. Sericitisation reactions are thus ultimately controlled by fluid-assisted diffusive mass transfer processes (section 7.4.2.3). If this inference is correct, it is likely that the albite grain boundaries locally acted as diffusive mass transfer sources during deformation. Furthermore, the fine grained nature of the matrix is likely to have promoted grain size sensitive, diffusion-dominated deformation processes. It is therefore postulated that the rheology of the reworked phyllonites was controlled by grain size sensitive, fluid-assisted diffusion-dominated mechanisms.

The relatively coarse grained polymineralic quartz porphyroclasts display two distinct microstructures. Faintly undulose polygonal quartz grains, which are characterised by 120° triple junctions, are commonly observed. Stain-free polygonal grains are thought

to develop in response to grain boundary area reduction (GBAR) processes, and are consistent with a phase of static recrystallisation following the cessation of active deformation (Passchier & Trouw 1996). These observations therefore suggest (a) that many of the quartz porphyroclasts experienced an episode of static recrystallisation following the cessation of reworking, and (b) that the quartz deformation microstructures were largely destroyed by GBAR. However, aggregates of elongate, lobate quartz grains are locally observed. It is postulated that these lobate grains may have escaped the effects of static recrystallisation and therefore preserve the original quartz deformation microstructures. The lobate quartz grains are commonly observed to be flattened parallel to the macroscopic foliation and aggregates of flattened quartz grains typically display a well developed crystallographic fabric. These observations are consistent with the quartz porphyroclasts having deformed predominantly by intracrystalline crystal plastic mechanisms.

Syn-tectonic foliation-parallel quartz-albite and quartz-chlorite veins are commonly observed throughout Stuley. It is likely that the veins developed during transient episodes of localised high pore fluid pressure within the phyllonite belt (Cox & Etheridge 1989; Kennedy & Logan 1997). However, there is no evidence for frictional sliding during vein opening, which suggests that veining was *not* a significant mechanism of strain accommodation during reworking.

#### ***Timing and significance of static recrystallisation***

Evidence for static recrystallisation has only been observed in quartz porphyroclasts preserved within packages of reworked, extension-related phyllonite from Stuley. This observation suggests that static recrystallisation must post-date the cessation of macroscopically ductile extension along the Usinish Phyllonite. Static recrystallisation is thought to be controlled by grain boundary area reduction (GBAR) processes. GBAR is promoted either by elevated temperatures or by the presence of fluids along grain boundaries following the cessation of deformation (Passchier & Trouw 1996). There is no evidence to suggest that there was a major heating event following top-to-the-E extension in South Uist. However, it is clear that fluids were abundant within the Usinish Phyllonite during macroscopically ductile extension. It is therefore postulated that static recrystallisation was caused by fluids 'trapped' within the fault rocks after deformation had ceased (see also Stewart 1997 and Chapter 5 of the present work).

## 7.5.2 DETACHMENT FAULTS

### 7.5.2.1 Field relationships

E- to SE-dipping brittle detachment faults are commonly observed to cross-cut the macroscopically ductile strike-slip, transtension- and extension-related phyllonitic fabrics. In general, the detachments faults either localise along lithological boundaries (e.g. between packages of Corodale Gneiss-derived phyllonite and Mashēd Gneiss-derived protophyllonite; section 7.2.1.2), or between packages of phyllonite with different orientations (e.g. between Domains 1 and 2 at Rubha Bolum; section 7.2.3.2). However, the foliation-parallel detachment faults preserved on Stuley (section 7.2.4.2) appear to have developed within packages of lithologically and structurally homogeneous ultraphyllonite.

The fault planes are locally lined either by quartz-rich breccias (section 7.2.1.3) or by clay-rich gouges (section 7.2.4.2), and are typically associated with E- to ENE-plunging slickenlines (Fig. 3.41b). The geometries of subsidiary fracture arrays and / or shear bands in gouge-rich layers are consistent with top-to-the-E or -ENE displacements across the main fault planes (sections 7.2.1.3 & 7.2.4.2). However, the relative ages of top-to-the-E and top-to-the-ENE displacements are unclear from the available field evidence.

### 7.5.2.2 Microstructure

Brecciated phyllonite comprises angular quartz and feldspar grains (between 0.1mm and 1mm diameter), which 'float' in a matrix of randomly oriented, kinked sericite needles. The sericite needles locally define rootless, sub-angular to rounded 'brittle' folds or crenulations (wavelength  $\leq 2$ mm) (Plate 7.9). Although asymmetric, the folds do not display a consistent sense of vergence. Seams ( $\leq 0.01$ mm wide) of ultrafine opaque grains ( $\leq 0.0025$ mm diameter) and amorphous ?clay minerals locally cross-cut the sericite-rich matrix, and are occasionally observed to truncate angular feldspar clasts. Unfortunately, it was not possible to analyse any samples of fault gouge.

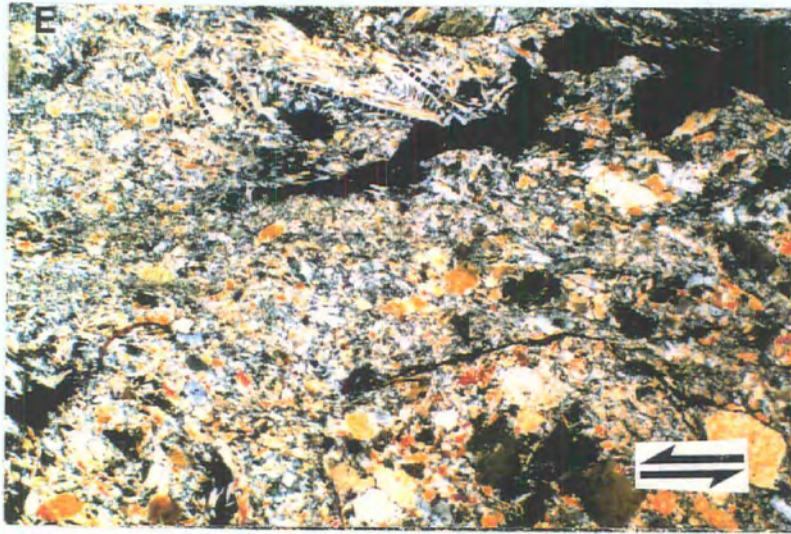


**Plate 7.9** Brecciated phyllonite from along foliation-parallel detachment fault. Note the brittle folds (highlighted) defined by aligned and kinked sericite needles. A late, anastomosing pressure solution fabric (arrow) cross cuts the chaotic fabric. Split arrows parallel transport direction, top-to-SE shear. Field of view 6×3.7mm, crossed polars.

### 7.5.2.3 Summary and discussion

The similarities in kinematics and style of deformation suggest that the detachment faults observed in eastern South Uist are of the same age as the detachment faults observed in North Uist (Chapter 6). The *latest* movements along the South Uist detachment faults clearly post-date the cessation of macroscopically ductile extension. However, the age of detachment *initiation* is unclear from the available field evidence. In general, brittle deformation appears to have been localised along pre-existing lithological or structural boundaries. However, in regions of relatively homogeneous ultraphyllonite (e.g. Stuley), the detachment faults appear to have developed along pre-existing foliation planes. It is therefore postulated that brittle deformation was focused either along pre-existing competence boundaries, or along relatively weak, micaceous foliation planes within the Usinish Phyllonite belt.

Preliminary microstructural observations are consistent with displacements along the detachment faults having been accommodated primarily by grain-scale fracturing and brecciation. However, clay-rich seams are locally observed to truncate feldspar clasts preserved along the fault planes. This observation suggests that pressure solution processes may have been important towards the end of active deformation along the detachment faults (Knipe & Lloyd 1994). The observed deformation microstructures are consistent with brittle deformation having occurred in the uppermost 5km of the crust (Sibson 1982, 1983).

### 7.5.3 SYNTHESIS

#### 7.5.3.1 Summary

The available field and microstructural evidence demonstrates that the Usinish Phyllonite belt initiated during an episode of regional sinistral strike-slip along the OHFZ in South Uist. The phyllonite belt was subsequently reactivated during episodes of regional transtension and top-to-the-E extension. Transtension- and extension-related deformation was accommodated by (a) the reworking of pre-existing lower greenschist facies phyllonitic fabrics, and (b) by the generation of *new* macroscopically ductile, lower greenschist facies phyllonitic fabrics. Deformation within packages of new and reworked phyllonite was accommodated by fluid-assisted diffusive mass transfer and / or intracrystalline crystal plastic mechanisms. Extensional displacements along networks of brittle detachment faults entirely post-date macroscopically ductile deformation.

#### 7.5.3.2 A model of reactivation in South Uist

The Usinish Phyllonite is unique along the Outer Hebrides Fault Zone in that reactivation was associated with the development of *new* extension-related phyllonitic fabrics in previously non-phyllonitised regions. There are two possible 'end-member' scenarios which could explain why phyllonite generation during occurred during regional extension. Firstly, it is possible that the pre-existing phyllonitic fabrics experienced significant *strain hardening* during reworking, and thus were unable to accommodate extension-related deformation. Strain was therefore accommodated within regions of newly formed phyllonite. Secondly, it is possible that regional extension was accompanied by significant *fluid influx* into the fault zone. Fluid influx may have resulted in a further episode of phyllonitisation.

The available mineralogical evidence is consistent with regional strike-slip, transtension and extension in South Uist all having occurred under fluid-rich, lower greenschist facies conditions. The metamorphic and microstructural evolution of the phyllonitic fabrics during strike-slip, transtension and extension were primarily controlled by fluid-assisted diffusive mass transfer processes. These observations suggest that the rheological behaviour of the phyllonitic fault rocks is likely to have been similar during strike-slip, transtension- and extension-related deformation. If this inference is correct, it is highly unlikely that the new phyllonitic fabrics developed in response to strain hardening during reworking. It is therefore postulated that the new phyllonitic fabrics developed in response to renewed fluid influx into the OHFZ during regional transtension and extension. However, it is important to explain why

evidence for a renewed phase of phyllonitisation during reactivation has only been observed in South Uist.

In North Uist and on Scalpay, the extensionally reworked lower greenschist facies phyllonite belts are developed within regions of pervasive protophyllonite and upper greenschist facies mylonite respectively (Chapters 5 & 6). There is little evidence to suggest that either the pervasive protophyllonitic fabrics or the upper greenschist facies mylonitic fabrics were reworked during transtension / extension i.e. *deformation was entirely concentrated into the lower greenschist facies phyllonite belts*. Previous authors have postulated that fluid flow during metamorphism tends to be concentrated within actively deforming shear zones (Oliver 1996; Ord & Oliver 1997). It is therefore suggested that during reactivation, the effective permeability of the actively deforming lower greenschist facies phyllonitic shear zones was significantly higher than the effective permeability of either pervasive protophyllonites or the upper greenschist facies mylonites. The corollary of this hypothesis is that the host rocks did *not* experience a further phase of phyllonitisation during transtension / extension. In South Uist, however, the Usinish Phyllonite belt is developed within fractured Corodale Gneiss and Mashed Gneiss host rocks. Pervasive protophyllonite has *not* been observed. It is postulated that fluid influx during transtension / extension was to some extent focused within actively deforming, reworked regions within the Usinish Phyllonite. However, the fractures within the surrounding Corodale Gneiss and Mashed Gneiss probably also acted as high permeability pathways, with the result that fluids were able to enter the non-deforming wall rocks. Significant fluid-rock interaction (fluid-assisted DMT) within the fractured Corodale Gneiss and Mashed Gneiss may have ultimately caused the development of new, extension-related phyllonite within previously non-phyllonitised rocks.

Arrays of foliation-parallel syn-tectonic veins are widely observed within packages of reworked phyllonite in South Uist. The syn-tectonic veins are thought to have developed towards the *end* of the macroscopically ductile deformation event, and there is no evidence to suggest that vein opening was associated with widespread frictional sliding (section 7.5.1.1). These observations suggest (a) that cyclic increases in pore fluid pressure (Cox & Etheridge 1989) were relatively infrequent, and were only significant towards the end of macroscopically ductile reworking, and (b) that increases in pore fluid pressure were not directly responsible for accommodating large magnitudes of finite strain (cf. the reworked phyllonite belts in North Uist; Chapter 6). It is postulated that the relatively permeable nature of the fractured Corodale Gneiss and Mashed Gneiss host rocks may have allowed fluids to 'bleed off' from the phyllonite belt into the wall rocks, thus preventing the

development of significant high pore fluid pressures within the Usinish Phyllonite. The role of fluids during reworking on Scalpay, North Uist and South Uist is discussed further in Chapter 9.

Packages of strike-slip related phyllonite preserved at Rubha Bolum are commonly observed to be cross-cut by arrays of sub-vertical, fibrous quartz veins. The orientation of the vein fibres is consistent with vein opening in a regime of E-W extension (section 7.2.3.2). It is postulated that the steeply dipping veins developed synchronous with regional extension in South Uist.

## 7.6 SUMMARY

- The Usinish Phyllonite initiated during regional top-to-the-NE sinistral strike-slip along the OHFZ in South Uist.
- The phyllonitic fabrics appear to have localised within a zone of intense thrust-related brittle deformation which originally marked the contact between the Corodale Gneiss and the Mashed Gneiss.
- Phyllonitisation occurred in a fluid-rich lower greenschist facies environment. The fluids probably gained access to the fault zone through pre-existing networks of brittle fractures, cataclasite seams and devitrified pseudotachylyte veins.
- Deformation during sinistral strike-slip was accommodated by fluid-assisted diffusive mass transfer mechanisms and, to a lesser extent, by intracrystalline crystal plastic mechanisms.
- There was a progressive change in the regional kinematic regime, from top-to-the-NE sinistral strike-slip, to sinistral transtension, to top-to-the-E extension.
- Transtension- and extension-related deformation was accommodated by the reworking of pre-existing strike-slip related fabrics, and by the generation of new lower greenschist facies phyllonitic fabrics in previously non-phyllonitised regions.
- The new transtension- and extension-related phyllonitic fabrics localised within intensely fractured Corodale Gneiss and Mashed Gneiss host rocks adjacent to the Usinish Phyllonite belt.
- Transtension- and extension-related deformation within packages of new and reworked phyllonite was accommodated by fluid-assisted diffusive mass transfer processes and, to a lesser extent, by intracrystalline crystal plastic mechanisms.
- Macroscopically ductile extension was post-dated by top-to-the-E or -ENE displacements along a network of brittle detachment faults. The geometry and

distribution of the brittle structures were strongly influenced by the pre-existing macroscopically ductile phyllonitic fabrics.

The textural evolution of the Usinish Phyllonite is summarised in Figure 9.5a, and will be discussed further in Chapter 9.

## 8. GEOCHEMICAL EVOLUTION OF THE LOWER GREENSCHIST FACIES PHYLLONITES, NORTH UIST

### 8.1 INTRODUCTION

#### 8.1.1 INTRODUCTION AND AIMS

Regional top-to-the-W brittle thrusting along the OHFZ occurred under dry, anhydrous conditions. However, it has been demonstrated that localised sinistral transpression and subsequent regional sinistral strike-slip were associated with widespread phyllonitisation and lower greenschist facies retrogression. Textural evidence suggests that phyllonitisation was primarily controlled by fluid-assisted diffusive mass transfer processes. The lower greenschist facies shear zones were reworked during subsequent regional eastward-directed extension. Microstructural observations are consistent with the continued operation of fluid-assisted DMT processes, and the abundance of syn-tectonic veins further emphasises the importance of fluid-rock interaction during extension. The profound mineralogical and microstructural changes caused by syn-tectonic fluid-rock interaction suggest that phyllonitisation is unlikely to have occurred under isochemical conditions (Walker 1990). The aims of this chapter are thus:

- To evaluate the geochemical effects of syn-tectonic fluid-rock interaction and retrogression, and in particular:
- To relate the *microstructural* and geochemical evolution of the phyllonitic fault rocks.
- To relate the *kinematic* and geochemical evolution of the phyllonitic fault rocks.

It should be emphasised that the aim of this study was *not* to provide a comprehensive geochemical analysis of the different fault rocks from along the entire Outer Hebrides Fault Zone, as this would have largely duplicated the work of Walker (1990). The results of the present study will be compared with Walker's (1990) results, and with geochemical analyses obtained from other highly retrogressed basement fault zones (e.g. O'Hara 1988; Condie & Sinha 1996; Hippertt 1998), in Chapter 9.

### 8.1.2 STUDY AREA AND ANALYTICAL METHODS

A representative suite of fault rocks and their protoliths were collected from several well exposed localities in the North Uist region (section 8.2 & Table 8.1). The whole-rock major element compositions were determined using X-ray fluorescence (XRF) techniques, whilst the whole-rock trace element concentrations were determined using an inductively coupled plasma mass spectrometer (ICP-MS) (Appendix B). Fault rocks from the North Uist region were selected for two important reasons. Firstly, the meso- and microstructural evolution of the Outer Hebrides Fault Zone on North Uist is very well constrained (Walker 1990; Butler 1995; Butler *et al.* 1995; Imber *et al.* 1997; Chapter 6 of the present work). Secondly, the phyllonites preserved in the North Uist region are thought to be broadly representative of the phyllonites observed along the Outer Hebrides Fault Zone as a whole (Chapters 3).

### 8.2 SAMPLES

Sixteen samples (three protoliths and thirteen fault rocks) from North Uist and the adjacent island of Ronay were selected for whole-rock geochemical analysis (Table 8.1). The sample microstructures are briefly described in the following section (see Chapter 6 for more comprehensive descriptions).

<b>Sample</b>	<b>Location</b>	<b>Rock type</b>	<b>Kinematic regime</b>
<b>LB1</b>	Foreland, North Uist.	Banded gneiss.	N/A
<b>NU7</b>	Foreland, North Uist.	Felsic gneiss.	N/A
<b>NU9</b>	Foreland, North Uist.	Younger Basic (amphibolite).	N/A
<b>BU15a</b>	Burrival region.	Fractured banded gneiss.	Top-to-W thrusting.
<b>BU15b</b>	Burrival region.	Fractured banded gneiss, locally with discrete phyllonite bands.	Top-to-W thrusting / sinistral transpression.
<b>BU20</b>	Burrival region.	Cataclasite.	Top-to-W thrusting.
<b>BU21</b>	Burrival region.	Cataclasite.	Top-to-W thrusting.
<b>RON2</b>	Isle of Ronay.	Protophyllonite.	Sinistral strike-slip.
<b>BU5</b>	Eigneig Bheag region.	Protophyllonite.	Sinistral strike-slip.
<b>BU11i</b>	Eigneig Bheag region.	Protophyllonite.	Sinistral strike-slip.
<b>SP13</b>	Eigneig Bheag shear zone (N-S trending segment).	Phyllonite.	Sinistral strike-slip.
<b>SP22</b>	Eigneig Bheag shear zone (N-S trending segment)	Ultraphyllonite.	Sinistral strike-slip.
<b>EB5</b>	Eigneig Bheag shear zone (NE-SW trending segment).	Ultraphyllonite.	Top-to-ENE extension / transtension.
<b>SP3</b>	Eigneig Bheag shear zone (N-S trending segment).	Ultraphyllonite.	Top-to-ESE extension.
<b>SP5</b>	Eigneig Bheag shear zone (N-S trending segment).	Ultraphyllonite.	Top-to-ESE extension.
<b>SP6</b>	Eigneig Bheag shear zone (N-S trending segment).	Ultraphyllonite.	Top-to-ESE extension.

**Table 8.1** Summary of the locations, rock type and kinematic regime of each of the samples.

## 8.2.1 SAMPLE DESCRIPTIONS

### 8.2.1.1 Protoliths

Field and microstructural observations suggest (a) that banded gneisses are the most abundant rock type in the 'foreland' to the west of the OHFZ, and (b) that the fault rocks preserved in North Uist are derived from either banded gneiss, felsic (quartzo-feldspathic) gneiss or amphibolite protoliths (Chapters 2 & 6). The Lewisian rocks selected for geochemical analysis thus included:

- (1) A sample of typical amphibolite facies banded gneiss (LB1).
- (2) Amphibolite facies felsic (quartzo-feldspathic) gneiss (NU7).
- (3) A sample of amphibolite (Younger Basic - see Chapter 2) (NU9).

LB1 is characterised by centimetre- to millimetre-scale mafic (hornblende  $\pm$  biotite) bands interlayered within a granular quartzo-feldspathic matrix. The felsic gneiss (NU7) comprises a coarse grained assemblage of quartz and feldspar  $\pm$  isolated hornblende grains (Chapter 6). There is little evidence for significant post-Laxfordian retrogression in either LB1 or NU7.

NU9 is comprises a coarse grained assemblage of rounded garnets which 'float' in a granular matrix hornblende and plagioclase grains (Chapter 6). NU9 appears to be fresh and unaltered.

It should be emphasised that there is no evidence to suggest that the Lewisian gneisses of North Uist were ever metamorphosed at conditions higher than the amphibolite facies (Fettes *et al.* 1992).

### 8.2.1.2 Primary fabrics

Field and microstructural observations have demonstrated that the phyllonitic fabrics preferentially localised along pre-existing zones of intense brittle deformation (i.e. cataclasite seams, devitrified pseudotachylyte veins and brittle fractures) within the crush melange. The microstructure of the crush melange is characterised by domains of relatively undeformed banded gneiss, domains of intensely fractured gneiss and seams of cataclasite / devitrified pseudotachylyte (Chapter 6). The samples selected for geochemical analysis thus included:

- (1) Relatively undeformed banded gneisses, locally cross-cut by networks of transgranular fractures. The fractures are infilled by aggregates of epidote  $\pm$  sericite and chlorite (BU15a).
- (2) Relatively undeformed banded gneiss, locally cross-cut by millimetre- to centimetre-scale discrete phyllonite bands (BU15b).

- (3) Seams of cataclasite and / or devitrified pseudotachylyte (henceforth referred to in this chapter as 'cataclasite' seams) which contain angular clasts of banded gneiss (BU20 & BU21).

Sericite mesh textures are widespread and are well developed in feldspar grains preserved within the samples of fractured banded gneiss (BU15a). BU15b is locally cross-cut by laterally discontinuous (on the scale of a thin section) discrete phyllonite bands. The phyllonite bands are thought to have developed during regional sinistral transpression along the Outer Hebrides Fault Zone in North Uist (Chapter 6; Table 6.10). The 'cataclasites' (BU20 & BU21) comprise fine grained aggregates of albite, quartz, sericite and epidote and are thought to have developed during top-to-the-W thrusting.

### **8.2.1.3 Pervasive protophyllonites**

Strike-slip related pervasive protophyllonites are microstructurally very heterogeneous and appear to be derived from both gneissose and 'cataclasite' protoliths (Chapter 6; Table 6.7). The samples selected for geochemical analysis thus included:

- (1) Protophyllonites derived from banded gneiss  $\pm$  'cataclasite' seams (RON2 & BU11i).
- (2) Protophyllonite derived from felsic (quartzo-feldspathic) gneiss (BU5).

The banded gneiss-derived pervasive protophyllonites (RON2 & BU11i) comprise aggregates of fractured, partially sericitised feldspar grains, relatively undeformed quartz grains and networks of interconnected sericite strands. BU11i also contains chlorite-rich strands and minor 'cataclasite'-derived domains. Opaque minerals (e.g. ilmenite) are particularly abundant within chlorite-rich strands.

The felsic gneiss-derived protophyllonite (BU5) is characterised by laterally discontinuous (on the scale of a thin section) sericite strands and aggregates of fine grained recrystallised quartz and albitic feldspar. Feldspar porphyroclasts preserved in BU5 are relatively unaltered, but are cross-cut by arrays of intra- and transgranular fractures. The fractures are typically infilled by seriate-interlobate aggregates of ultrafine grained albite.

### **8.2.1.4 Strike-slip related phyllonites and ultraphyllonites**

The strike-slip related phyllonites and ultraphyllonites preserved within the lower greenschist facies shear zones are typically derived from highly deformed 'cataclasite' seams  $\pm$  clasts of banded gneiss (Chapter 6; Table 6.8). The samples selected for geochemical analyses thus included:

- (1) A phyllonite comprising 'cataclasite'- and banded gneiss-derived domains (SP13).
- (2) A 'cataclasite'-derived ultraphyllonite (SP22).

The strike-slip related phyllonites and ultraphyllonites comprise aggregates of fine grained quartz, albitic feldspar, sericite, chlorite, epidote and opaque minerals (e.g. ilmenite and pyrite) (Chapter 6). Sericite and epidote appear to be less abundant in the banded gneiss-derived domains than in the 'cataclasite'-derived domains.

### 8.2.1.5 Extension-related phyllonites and ultraphyllonites

Extension-related phyllonites and ultraphyllonites rework pre-existing strike-slip related fabrics, which were typically derived from 'cataclasite' seams  $\pm$  clasts of banded gneiss (Chapter 6; Tables 6.8 & 6.9). The samples selected for geochemical analyses thus included:

- (1) A phyllonite comprising 'cataclasite'- and banded gneiss-derived domains (SP6).
- (2) 'Cataclasite'-derived folded (EB5 & SP3) and planar (SP5) ultraphyllonites.

The extensionally reworked phyllonites comprise aggregates of fine grained quartz, albitic feldspar, sericite, chlorite, epidote and opaque minerals (e.g. ilmenite and pyrite). SP6 contains numerous deformed and undeformed syn-tectonic calcite veins (Chapter 6).

SP3 (folded ultraphyllonite) is overprinted by a weakly developed axial planar crenulation fabric. In contrast, the crenulation cleavage observed in EB5 is very strong and locally obliterates the pre-existing foliation.

## 8.2.2 FAULT ROCK DERIVATION

In order to assess how much of the observed geochemical variation was caused by fluid-rock interaction during phyllonitisation, and how much was due to variations in *protolith* geochemistry, it is important to identify the exact Lewisian protolith for each of the fault rock samples. However, the fault rocks are typically very fine grained and may have suffered several phases of deformation and / or retrogression (e.g. Table 6.10). Consequently, it is difficult to determine the precise nature of the Lewisian protolith using petrographic techniques alone. An alternative approach is to compare the chondrite-normalised *immobile* trace element compositions of each fault rock with the immobile trace element compositions of the Lewisian protoliths (see explanation

in section 8.4). It is thus possible to distinguish a 'textural protolith' (determined by petrographic observations) and a 'geochemical protolith' (determined by comparison of trace element patterns) for each of the fault rock samples. The textural and geochemical protoliths to each of the different fault rock samples are listed in Table 8.2.

<b>Fault rock sample</b>	<b>Textural protolith</b>	<b>Geochemical protolith</b>
<b>Fractured gneiss; BU15a</b>	Banded gneiss-derived.	Banded gneiss.
<b>Fractured gneiss with discrete phyllonite bands; BU15b</b>	Banded gneiss-derived.	Banded gneiss.
<b>'Cataclasite'; BU20</b>	Contains banded gneiss-derived clasts.	Banded gneiss.
<b>'Cataclasite'; BU21</b>	Contains banded gneiss-derived clasts.	Banded gneiss.
<b>Protophyllonite; RON2</b>	Banded gneiss-derived.	Banded gneiss.
<b>Protophyllonite; BU5</b>	Felsic (quartzo-feldspathic) gneiss-derived.	Felsic (quartzo-feldspathic) gneiss.
<b>Protophyllonite; BU11i</b>	Banded gneiss + minor cataclasite-derived domains.	Banded gneiss.
<b>Phyllonite; SP13</b>	Banded gneiss + cataclasite-derived domains.	Banded gneiss.
<b>Phyllonite; SP22</b>	Cataclasite-derived.	Banded gneiss.
<b>Reworked phyllonite; EB5</b>	Cataclasite + banded gneiss-derived domains.	Banded gneiss.
<b>Reworked phyllonite; SP3</b>	Cataclasite + banded gneiss-derived domains	Banded gneiss.
<b>Reworked phyllonite; SP5</b>	Cataclasite + banded gneiss-derived domains	Banded gneiss.
<b>Reworked phyllonite; SP6</b>	Banded gneiss + cataclasite-derived domains.	?Banded gneiss.

**Table 8.2** Textural and geochemical protoliths of the fault rock samples. The textural protoliths were determined using optical and backscattered SE microscopy. The geochemical protoliths were determined by comparing the immobile trace element signatures of the fault rocks and the Lewisian rocks.

## 8.3 MAJOR ELEMENTS

The samples were analysed for the ten standard major elements ( $\text{SiO}_2$ ,  $\text{Al}_2\text{O}_3$ ,  $\text{Fe}_2\text{O}_3$ ,  $\text{MgO}$ ,  $\text{CaO}$ ,  $\text{Na}_2\text{O}$ ,  $\text{K}_2\text{O}$ ,  $\text{TiO}_2$ ,  $\text{MnO}$  and  $\text{P}_2\text{O}_5$ ) using XRF fusion discs. The preparation and analytical techniques used, and the major element compositions of individual samples are presented in Appendix B.

The data have been summarised by grouping individual samples into five different categories, namely: protoliths (LB1, NU7 & NU9), crush melange (BU15a, BU15b, BU20 & BU21), strike-slip related pervasive protophyllonites (BU5, BU11i & RON2), strike-slip related shear zone phyllonites (SP13 & SP22) and extensionally reworked shear zone phyllonites (EB5, SP3, SP5 & SP6). The *mean* major element composition for each group of samples was calculated (Table A2) and the results are summarised in Figure 8.1.

### 8.3.1 MAJOR ELEMENT COMPOSITION

The major element compositions of both the protoliths and the fault rocks are dominated by  $\text{SiO}_2$  and  $\text{Al}_2\text{O}_3$ , which reflects the abundance of silicates such as quartz, feldspar, sericite and epidote. The concentration of  $\text{SiO}_2$  varies considerably (from 54 wt% in strike-slip related phyllonites to 68 wt% in protophyllonites) although  $\text{Al}_2\text{O}_3$  appears to be more or less constant ( $\cong 15$  wt%) (Fig. 8.1).

All the other major elements are present in much lower concentrations (typically < 10 wt%). The concentrations of both  $\text{Fe}_2\text{O}_3$  (total iron) and  $\text{MgO}$  are variable but are most abundant in the strike-slip related phyllonites and extensionally reworked phyllonites. The ratio of wt%  $\text{Fe}_2\text{O}_3$  to wt%  $\text{MgO}$  is approximately 2 : 1 in all groups of rock. The concentration of  $\text{CaO}$  is variable (from approximately 3 wt% in the protophyllonites up to 8 wt% in the strike-slip related phyllonites). The concentration of  $\text{Na}_2\text{O}$  (typically  $\leq 5$  wt%) is generally greater than that of  $\text{K}_2\text{O}$ , although the ratio of wt%  $\text{Na}_2\text{O}$  to wt%  $\text{K}_2\text{O}$  is different in each group of rocks.

$\text{TiO}_2$ ,  $\text{MnO}$  and  $\text{P}_2\text{O}_5$  are most abundant in the strike-slip related phyllonites and the extensionally reworked phyllonites, although overall, the variation in the concentrations of these elements is small. Loss on ignition (LOI) is negligible in the amphibolite grade Lewisian protoliths, but typically accounts for between 2wt% and 3 wt% in the fault rocks.

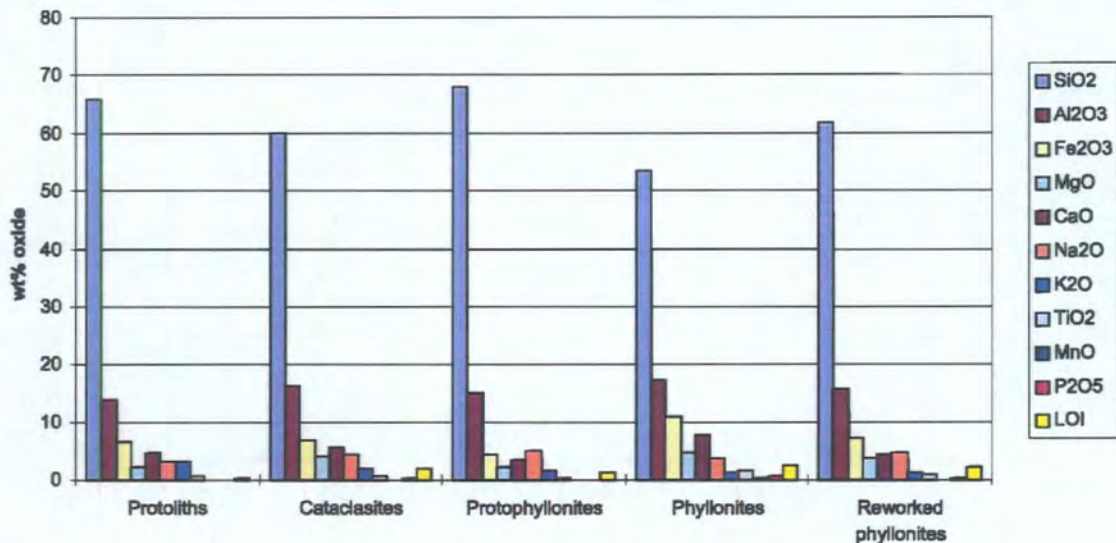


**Figure 8.1** Mean major element compositions for the protoliths, crush melange samples, protophyllonites, strike-slip related phyllonites and the extensionally reworked phyllonites.

### 8.3.2 PROTOLITH-NORMALISED MAJOR ELEMENT COMPOSITION

Variation in the concentrations of the less abundant major elements may not be apparent owing to the high concentrations of SiO<sub>2</sub> and Al<sub>2</sub>O<sub>3</sub> (the 'constant sum effect' e.g. Rollinson 1993). An alternative approach is to calculate the amount of enrichment or depletion of each major element in each fault rock relative to the protolith. The major element composition of each fault rock was thus normalised to the major element composition of its 'geochemical protolith' (Table 8.2). The data have been summarised by calculating the *mean* protolith-normalised compositions for each category of fault rock and the results are presented on a major element enrichment-depletion diagram (Fig. 8.2).

The overall pattern observed in Figure 8.2 is one of *increasing* enrichment / depletion from pervasive protophyllonite to crush melange to extensionally reworked phyllonite to strike-slip related phyllonite. The implication of this trend is that the crush melange has experienced a greater degree of alteration than the pervasive protophyllonites and that the strike-slip related phyllonites are apparently *more* altered than the extensionally reworked phyllonites. The reasons for these trends are discussed below (sections 8.4.5, 8.5.5 & 8.6.5).

SiO<sub>2</sub> follows the general trend described above and is *depleted* in all fault rocks (Fig. 8.2). The apparent loss of SiO<sub>2</sub> is consistent with the breakdown of plagioclase and K-feldspar to white mica (sericite), epidote, SiO<sub>2(aq)</sub>, Na<sup>+</sup><sub>(aq)</sub> and K<sup>+</sup><sub>(aq)</sub> (e.g. Beach 1980; Chapter 9 of the present work). It is possible that further silica loss occurred

through dissolution of quartz and feldspar porphyroclasts along sericite seams (Hippertt 1994a; Chapter 6 of the present work).

$\text{Al}_2\text{O}_3$  displays a slight, but *constant* enrichment in all groups of fault rock (Fig. 8.2). There are two explanations for this behaviour. Firstly, it is possible that  $\text{Al}_2\text{O}_3$  was actually immobile and that the observed 'enrichment' is an artefact caused by selection of incorrect normalisation factors. The second possibility is that the observed enrichment in  $\text{Al}_2\text{O}_3$  is real and may be associated with the growth of aluminosilicates such as epidote. Element mobility is discussed further in section 8.5.

$\text{Fe}_2\text{O}_3$  and MgO are enriched in all groups of fault rock. The maximum enrichment is observed in the strike-slip related phyllonites, whilst the minimum enrichment is observed in the pervasive protophyllonites (Fig. 8.2). In general, MgO is more highly enriched than  $\text{Fe}_2\text{O}_3$ , although the ratio of their enrichment factors is extremely variable (Fig. 8.2). The enrichment in MgO and  $\text{Fe}_2\text{O}_3$  is consistent with the petrographic evidence for chlorite growth during phyllonitisation (particularly within 'cataclasite'-derived domains) and the presence of opaque grains within mafic phyllonites and 'cataclasite'-derived domains (Chapter 6).

CaO is moderately enriched in the crush melange, strike-slip related phyllonites and extensionally reworked phyllonites and is slightly enriched in the protophyllonites (Fig. 8.2). Enrichment in CaO reflects the growth of epidote and the development of syn-tectonic calcite veins.

The alkali metals ( $\text{Na}_2\text{O}$  and  $\text{K}_2\text{O}$ ) display very variable patterns of enrichment / depletion and do *not* follow the overall trend described above. In general,  $\text{K}_2\text{O}$  is more strongly enriched / depleted than  $\text{Na}_2\text{O}$ , although the ratio of their enrichment factors is not constant (Fig. 8.2). These patterns are consistent with the highly mobile nature of the alkali metals in aqueous solutions (e.g. Rollinson 1993 - Table 3.4).

$\text{TiO}_2$ , MnO and  $\text{P}_2\text{O}_5$  are strongly enriched in all groups of fault rock (Fig. 8.2). The observed enrichments are consistent with the growth of apatite and opaque minerals, particularly within 'cataclasites' and 'cataclasite'-derived phyllonites (Chapter 6).

Loss on ignition (LOI) is strongly enriched in all fault rock groups (Fig. 8.2). The enrichment in LOI reflects (a) the breakdown of anhydrous mineral phases (e.g. feldspar) and their replacement by syn-tectonic OH-bearing mineral phases (e.g. sericite and epidote), and (b) the abundance of fluid inclusions around the margins of recrystallised (i.e. syn-tectonic) quartz and albite grains (see Chapter 6).

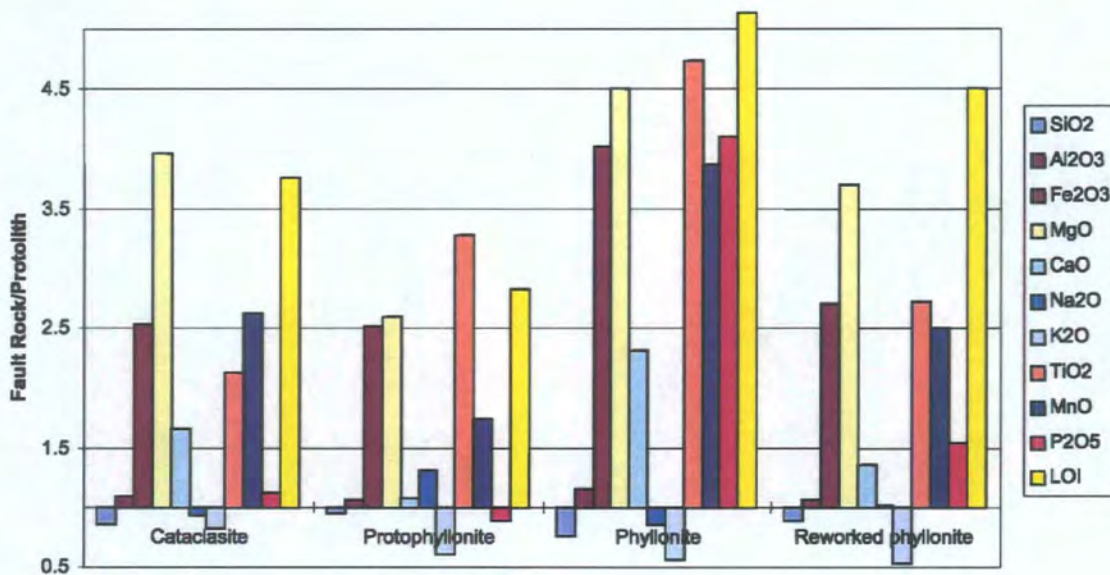


**Figure 8.2** Mean protolith-normalised major element compositions for the crush melange samples, protophyllonites, strike-slip related phyllonites and the extensionally reworked phyllonites.

#### 8.4 RARE EARTH ELEMENTS

The rare earth element (REE) (La, Ce, Pr, Nd, Sm, Eu, Gd, Tb, Dy, Ho, Er, Tm, Yb and Lu) concentrations were analysed using ICP-MS. The REEs behave as a geochemically coherent group and are widely used in petrogenetic studies (Wilson 1989). The atomic number of the REEs increases progressively from La ( $Z = 57$ ) to Lu ( $Z = 71$ ) and a distinction may be drawn between the 'light rare earth elements' (LREE) (La, Ce, Pr, Nd and Sm) and the 'heavy rare earth elements' (HREE) (Gd, Tb, Dy, Ho, Er, Tm, Yb and Lu). The HREEs are preferentially accommodated into garnet and zircon  $\pm$  hornblende. In contrast, apatite, sphene, allanite and monazite are enriched in LREEs (Le Marchand *et al.* 1987). The REEs are believed to be relatively immobile during hydrothermal alteration. However, they may become increasingly mobile at higher metamorphic grades (greenschist facies and above) and / or in the presence of halogen- or carbonate-rich fluids (Humphries 1984; Grauch 1989).

REE data is conventionally normalised to chondritic abundances (Rollinson 1993). An alternative approach is to normalise the REE concentrations in the 'daughter' rocks (in this case the fault rocks) to those in the 'parent' rocks (in this case the Lewisian 'geochemical protolith'). During the present study, the chondrite-normalised REE compositions of the Lewisian protoliths were compared with the chondrite-normalised REE compositions of the faults rocks in order to determine the 'geochemical protolith' to each of the fault rocks (Table 8.2). The protolith-normalised REE concentrations were calculated and the resulting protolith-normalised REE plots were then used to

determine the amount of REE enrichment and / or depletion experienced by each of the fault rocks.

**N.B.** Large ( $\leq$  one order of magnitude) positive and negative Gd and Tb anomalies have been obtained from quartzo-feldspathic ('felsic band', NU7 and BU5) and from hornblende-rich mafic ('mafic band' and RON2) samples respectively. A negative Tb anomaly is also obtained for the phyllonite SP6 (Tables 8.1 and 8.2). These anomalies are probably due to analytical / calibration errors and do *not* reflect the actual REE compositions of the fault rocks (D. G. Pearson and C. J. Ottley *pers. comm.* 1997). The Gd and Tb analyses are therefore ignored in the following descriptions and graphs.

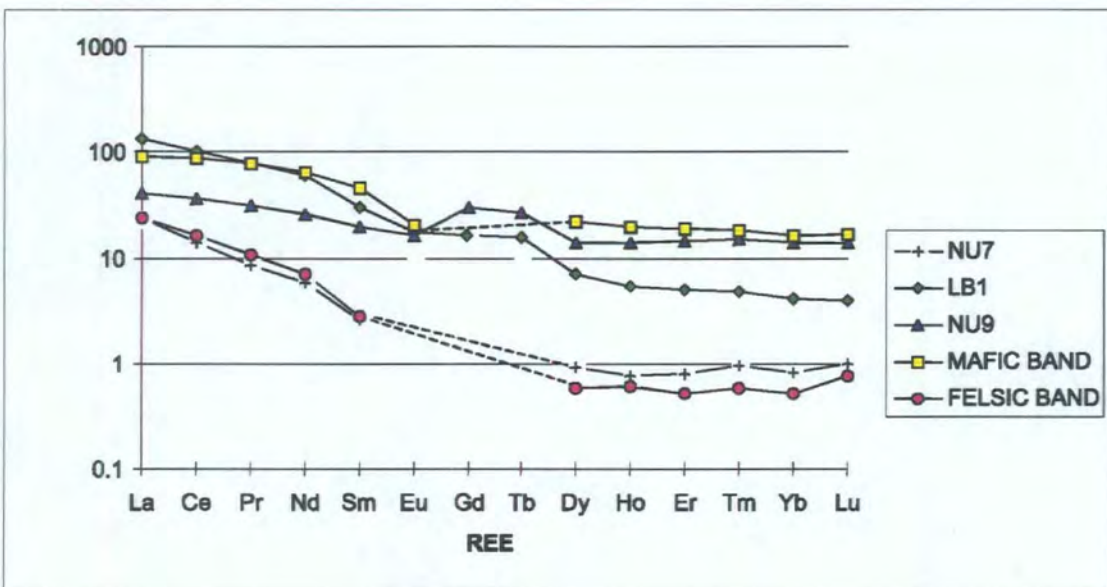


**Figure 8.3** Chondrite-normalised REE concentrations for the protoliths.

### 8.4.1 PROTOLITHS

Whole-rock analyses were conducted on the three Lewisian protoliths (LB1, NU7 & NU9). In addition, the mafic and felsic bands from a sample of banded gneiss (LB1) were separated and analysed individually. The chondrite-normalised REE concentrations are presented in Figure 8.3.

Four distinct trends (described from LREE to HREE) are apparent from Figure 8.3:

- A 'banded gneiss trend' (LB1), which is characterised by a smooth decrease in REE concentration (from LREE to HREE). La is approximately one order of magnitude more abundant than Lu.

- A 'Younger Basic trend' (NU9), which is characterised by a slight decrease in the abundance of the LREEs and by a flat HREE pattern. The concentration of La is approximately twice that of Lu.
- A 'felsic gneiss' trend (NU7 and 'felsic band'), which is characterised by a sharp decrease in the abundance of the LREEs and by a flat HREE pattern. Note that the HREE concentration in felsic gneiss is less than the chondritic abundance. La is over one order of magnitude more abundant than Lu.
- A 'mafic gneiss' trend ('mafic band'). The mafic gneiss trend is sub-parallel to the banded gneiss trend for the LREEs, but is characterised by a flat HREE curve. La is less than one order of magnitude more abundant than Lu.

#### 8.4.2 CRUSH MELANGE

The chondrite-normalised REE concentrations obtained from the 'cataclasites' (BU20 and BU21), the fractured gneiss (BU15a) and the discrete phyllonite band (BU15b) follow a 'banded gneiss-type' chondrite-normalised REE pattern (compare Fig. 8.3 with Fig. 8.4a), which is consistent with the petrographic observations presented in section 8.2.2.

The protolith-normalised REE concentrations are illustrated in Figure 8.4b. The protolith-normalised REE concentrations obtained from the fractured gneiss (BU15a) is not significantly enriched or depleted relative to banded gneiss and plots along a trend parallel to the  $x$ -axis.

In contrast, the 'cataclasites' (BU20 and BU21) and the discrete phyllonite (BU15b) display progressively increasing protolith-normalised LREE concentrations. The protolith-normalised HREE concentrations obtained from the 'cataclasites' are not significantly enriched or depleted and plot along a trend parallel to the  $x$ -axis. In contrast, the protolith-normalised HREE concentrations obtained from BU15b display a slight, albeit progressively increasing enrichment (Fig. 8.4b).

The implication of these protolith-normalised REE patterns is that the REE composition of the crush melange is heterogeneous and appears to be related to the fault rock microstructure of the fault rocks. The relationships between fault rock microstructure, REE composition and fluid-rock interaction are discussed in section 8.4.5.

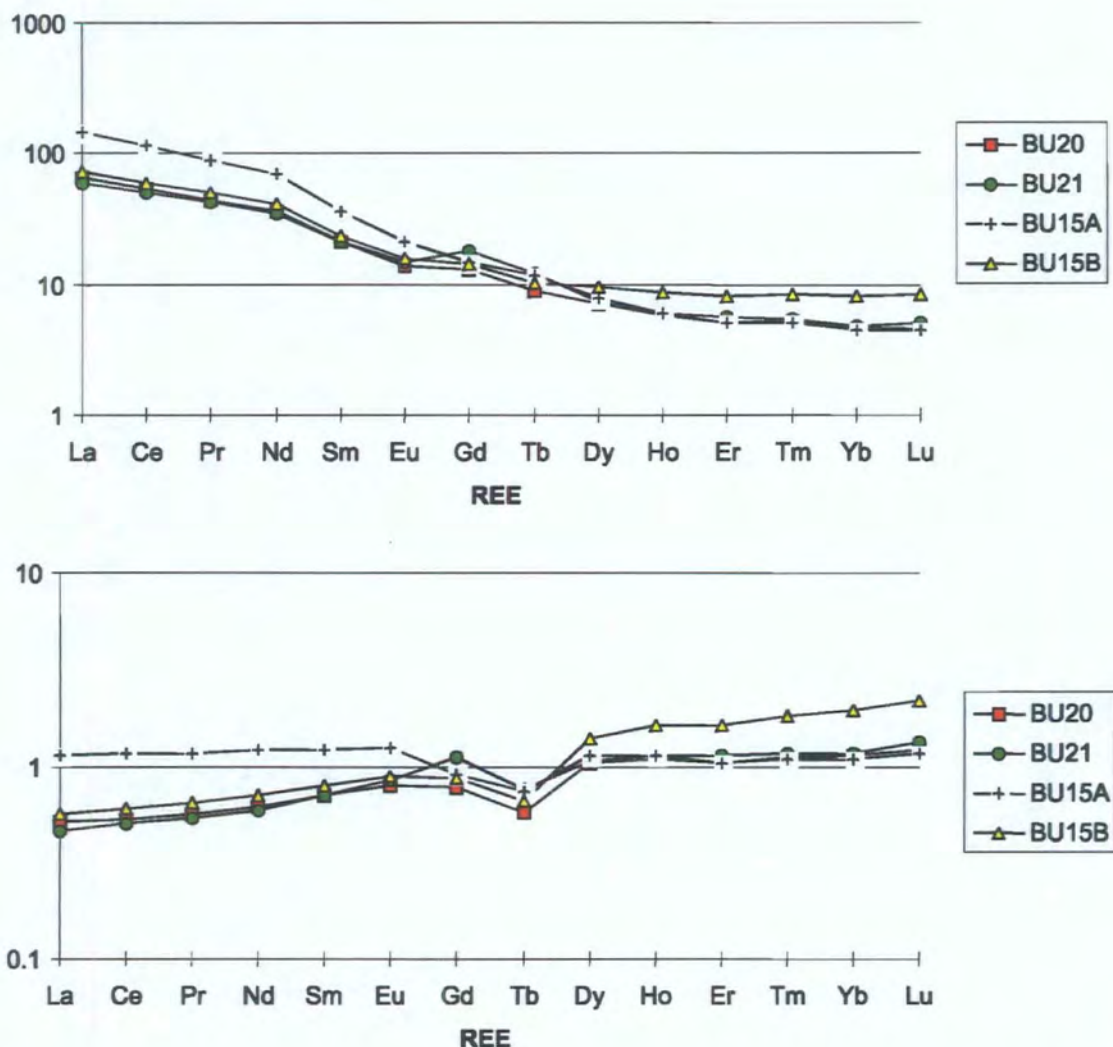


Figure 8.4 (a) Chondrite-normalised and (b) protolith-normalised REE concentrations for the crush melange samples.

### 8.4.3 PERVASIVE PROTOPHYLLONITES AND STRIKE-SLIP RELATED PHYLONITES

The chondrite-normalised REE compositions of the pervasive protophyllonites BU11i and RON2 (Fig. 8.5a) follow a 'banded gneiss-trend' (compare Fig. 8.3 with Fig. 8.5a). The REE concentrations obtained from BU11i and RON2 do not appear to be significantly enriched or depleted relative to banded gneiss (Fig. 8.5b).

The pervasive protophyllonite BU5 clearly follows a 'felsic gneiss' trend (compare Fig. 8.3 with Fig. 8.5a), which is consistent with petrographic observations (section 8.2.3). The protolith-normalised LREE concentrations obtained from BU5 are characterised by a slight, progressively *decreasing* enrichment from La to Dy (Fig. 8.5b). The HREE (Dy to Lu) composition of BU5 is not significantly enriched or depleted relative to felsic gneiss.

The chondrite-normalised REE compositions of the strike-slip related phyllonites (SP13 & SP22) (Fig. 8.5b) follow a 'banded gneiss trend' (compare Fig. 8.3 with Fig. 8.5a). The protolith-normalised LREE concentrations (from La to Eu) obtained from these phyllonites (SP13 and SP22) display a slight, albeit progressively increasing enrichment (Fig. 8.5b). The HREE concentrations obtained from the strike-slip related phyllonites follow a flat trend parallel to the  $x$ -axis of the graph (Fig. 8.5b). The implication of these protolith-normalised REE patterns is that the pervasive protophyllonites are relatively unaltered, whilst the strike-slip related phyllonites have experienced significant alteration (see section 8.4.5).

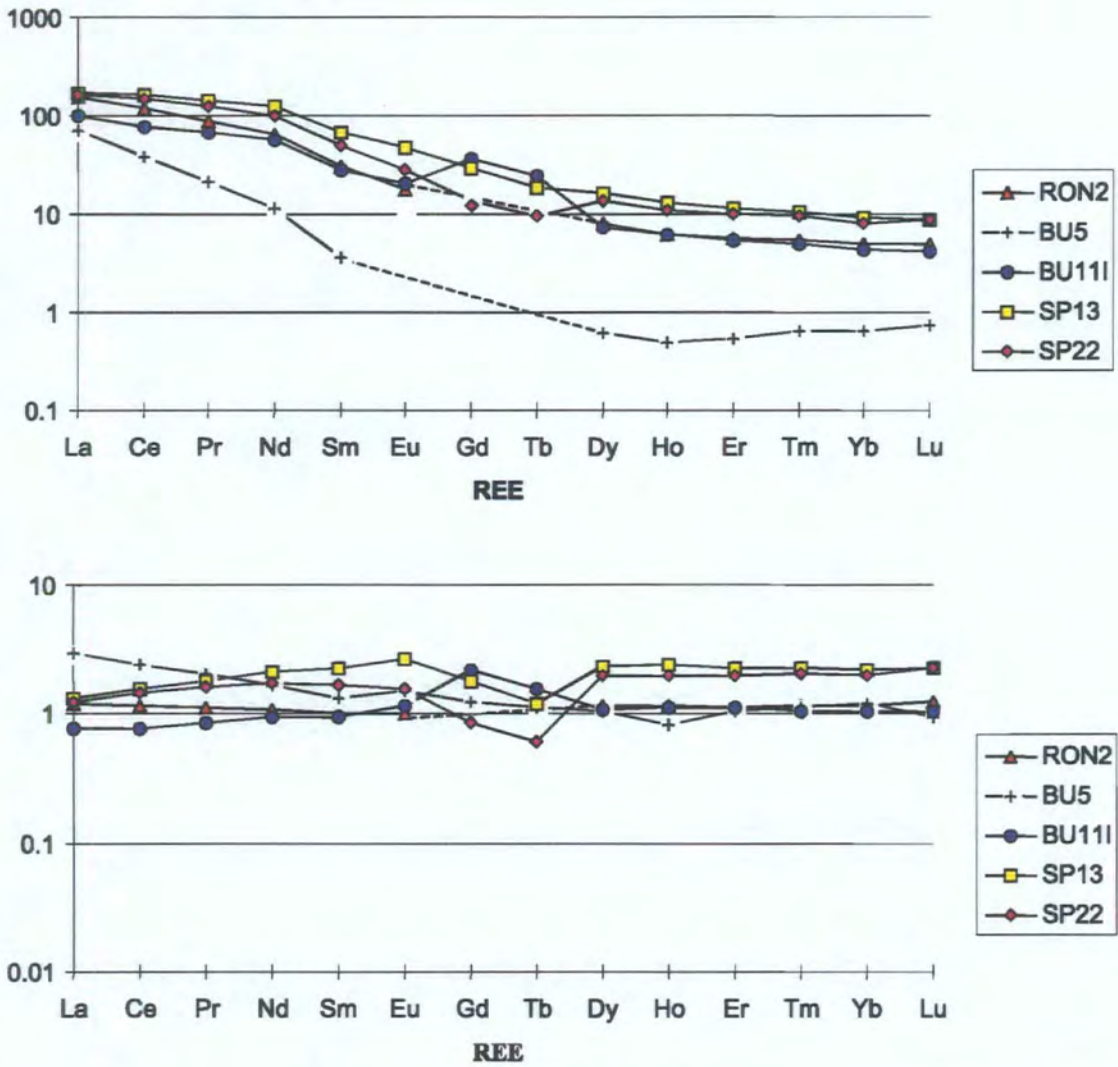


**Figure 8.5** (a) Chondrite-normalised and (b) protolith-normalised REE concentrations for the protophyllonites and the strike-slip related phyllonites.

### 8.4.4 EXTENSIONALLY REWORKED PHYLONITES

The chondrite-normalised REE concentrations obtained from the extensionally reworked phyllonites follow a 'banded gneiss-trend' (compare Fig. 8.3 with Fig. 8.6a) and the REE compositions of the different samples appears to be extremely homogeneous (Figs. 8.6a & b). The protolith-normalised LREE concentrations typically plot parallel to the  $x$ -axis and are not significantly enriched or depleted relative to banded gneiss. The protolith-normalised concentrations of the elements from Dy to Tm appear to be slightly enriched and plot along a trend parallel to the  $x$ -axis. The elements Tm to Lu display a slight, albeit progressively increasing enrichment. Overall, the HREEs are slightly more enriched than the LREEs (Fig. 8.6b).

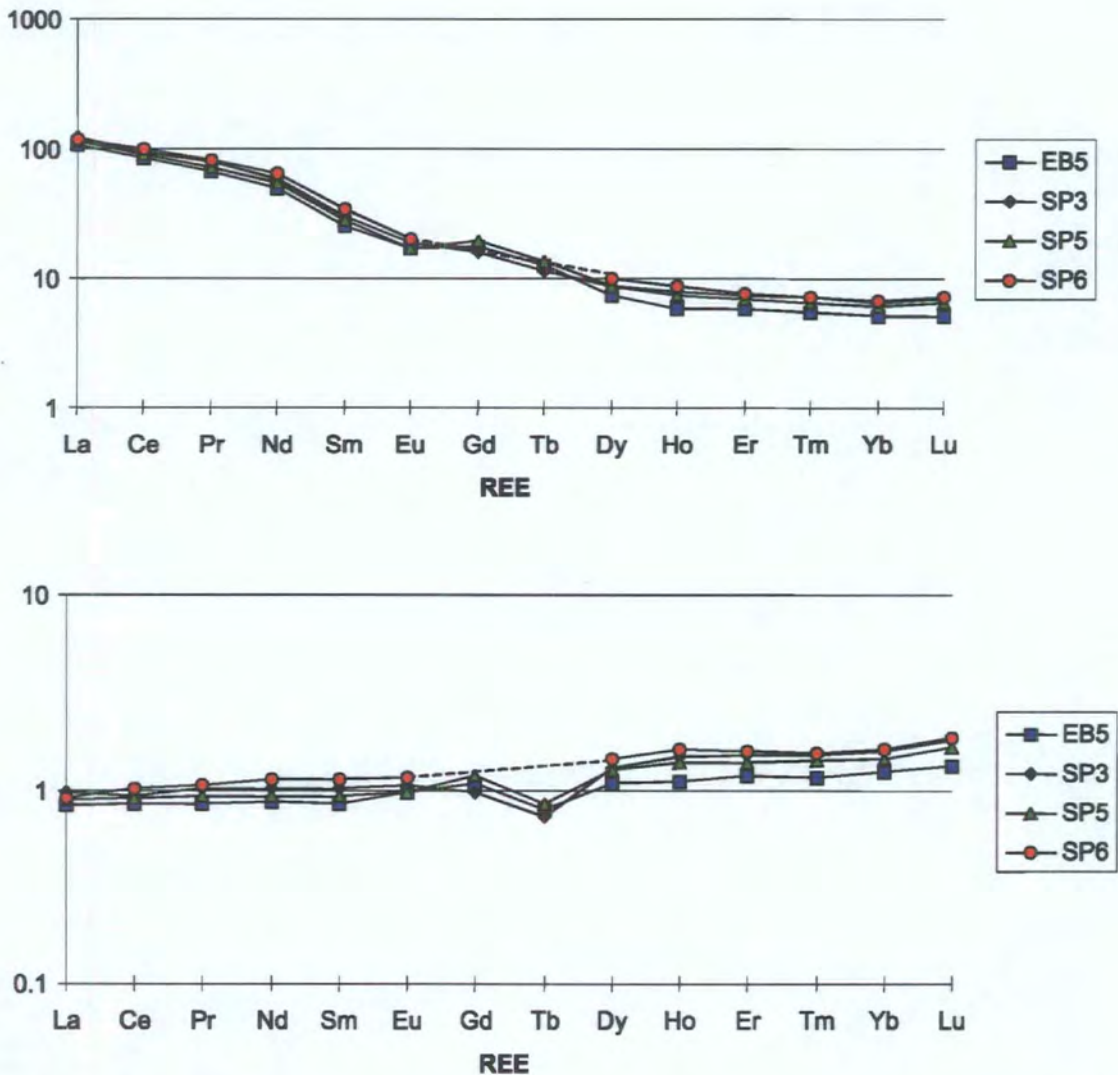


**Figure 8.6** (a) Chondrite-normalised and (b) protolith-normalised REE concentrations for the extensionally reworked phyllonites.

## 8.4.5 SUMMARY & DISCUSSION OF THE REE DATA

### 8.4.5.1 Summary

The protolith-normalised REE plots remove the effects of protolith geochemistry and can therefore be used to directly compare the amount of alteration experienced by the different fault rocks. However, insufficient analyses were carried out to be able to determine the amount of geochemical variation amongst the *protoliths*. It is therefore possible that groups of elements whose protolith-normalised REE compositions plot parallel to the *x*-axis (e.g. BU15a, Fig. 8.4b) display an 'apparent' enrichment (or depletion) caused by choosing slightly too low (or too high) normalisation factors. In order to overcome this uncertainty, the following interpretations are based on protolith-normalised REE *trends* and on the *relative* amount of REE enrichment / depletion experienced by each of the fault rocks.

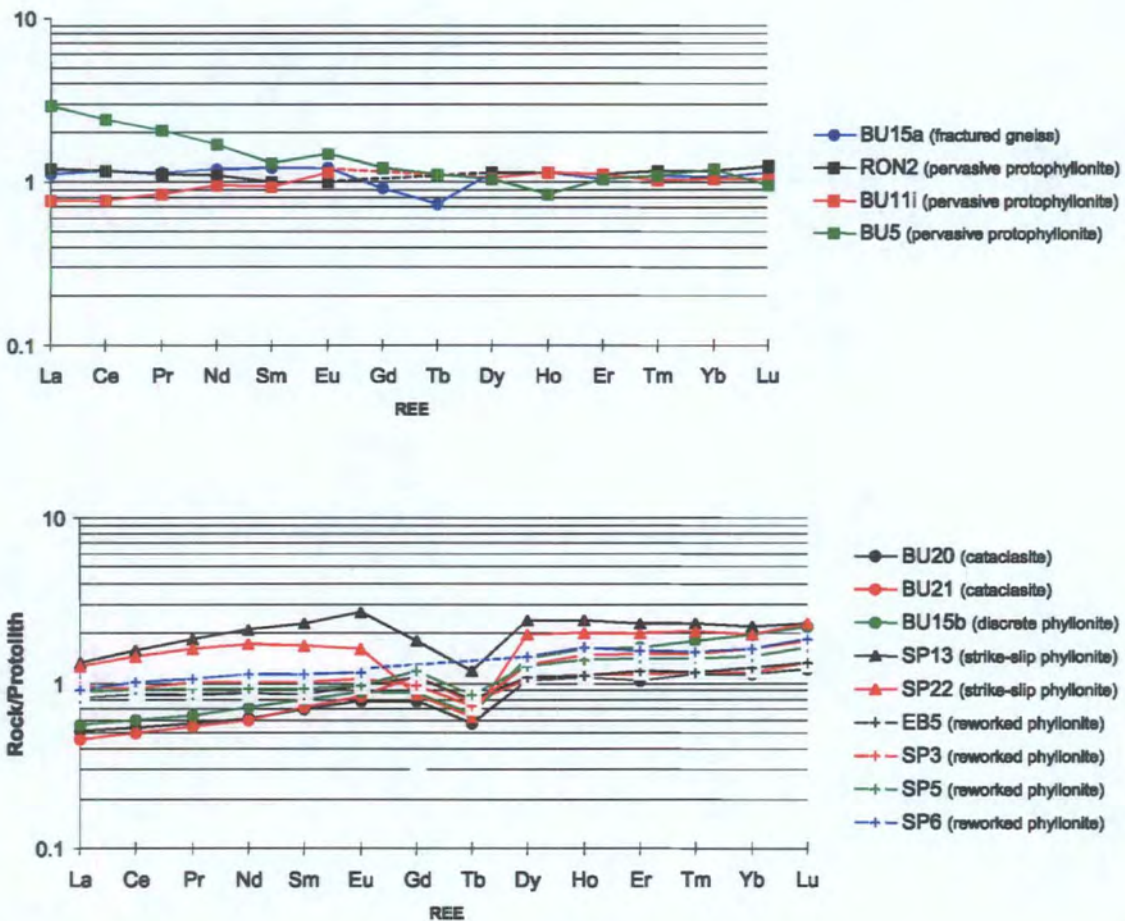


**Figure 8.7** Summary of the protolith-normalised REE concentrations for (a) Group 1 (circles and black & red squares) and (b) Groups 2 (circles), 3 (triangles) and 4 (crosses). See text for explanation.

The protolith-normalised REE compositions of the fault rocks define four distinct 'geochemical groups' (Figs. 8.7a & b). These geochemical groups are defined by different REE trends and / or by different amounts of *relative* REE enrichment or depletion. 'Group 1' (Fig. 8.7a) is characterised by protolith-normalised REE concentrations which plot parallel to the *x*-axis and do not display significant enrichment / depletion. Group 1 comprises the fractured gneiss (BU15a; section 8.4.2) and the pervasive protophyllonites RON2 and BU11i (section 8.4.3). 'Group 2' (Fig. 8.7b) is characterised by progressively increasing protolith-normalised LREE concentrations and by a relatively flat HREE pattern. Group 2 comprises the 'cataclasites' (BU20 & BU21) and the discrete phyllonite (BU15b). The protolith-normalised REE patterns obtained from the fault rocks in 'Group 3' (strike-slip related phyllonites SP13 & SP22) follow similar trends as Group 2, but are *enriched* in comparison with Group 2. 'Group 4' (Fig. 8.7b) (extensionally reworked phyllonites EB5, SP3, SP5 & SP6) is characterised by a relatively flat protolith-normalised LREE pattern and a slight enrichment in HREEs relative to banded gneiss. Group 4 appears to have experienced *less* alteration than Groups 2 and 3, but is more altered than Group 1.

#### 8.4.5.2 Fault rock microstructure and REE composition

This pattern of relative / enrichment depletion, which is also highlighted by the major element data (section 8.3), can be related to the microstructure of the fault rocks. The *most* altered fault rocks (i.e. those fault rocks belonging to 'Groups' 2, 3 & 4) are typically 'cataclasites' (BU20 & BU21) or are derived from 'cataclasite' protoliths (SP13, SP22, EB5, SP3, SP5 & SP6; Table 8.2). In contrast, the *least* altered fault rocks (i.e. those fault rocks belonging to 'Group 1') are either relatively undeformed fractured gneisses (BU15a) or are pervasive protophyllonites derived from gneisses which have *not* experienced significant cataclastic deformation (RON2 & BU11i) (Table 8.2). This correlation between the relative magnitude of REE enrichment / depletion and the presence of 'cataclasite' and 'cataclasite'-derived fault rock suggests that the fine grained 'cataclasite' seams may have been preferentially altered. Coupled with the microstructural evidence for syn-tectonic retrogression along 'cataclasite' seams (Chapter 6), the REE data suggests that *fluid-rock interaction was preferentially focused along the pre-existing, ultrafine-grained 'cataclasite' seams / cataclastic fault zones during phyllonitisation.*

However, two of the fault rocks which were analysed do not fit this pattern. The felsic gneiss-derived protophyllonite (BU5; section 8.2.1.3) and the discrete phyllonite (BU15b; section 8.2.1.2) do not contain notable amounts of 'cataclasite'-derived material. However, the REE compositions of these fault rocks differ significantly

from that of their geochemical protoliths (Figs. 8.5b, 8.7a, 8.4b & 8.7b). BU5 and BU15b are cross-cut by networks of intra-, inter- and / or transgranular fractures. The fractures are commonly observed to be infilled by epidote, albite  $\pm$  phyllosilicate aggregates. The presence of these retrograde mineral aggregates suggests that the fractures experienced a greater degree of alteration than the relatively undeformed wallrock. It is therefore likely that *fluid-rock interaction was also focused along networks of pre-existing fractures during phyllonitisation.*

The fault rocks in 'Group 1' (BU15a, RON2 & BU11i) (sections 8.2.2 & 8.2.3) also preserve microstructural evidence for enhanced alteration / retrogression along fractures, yet their REE compositions almost identical to the REE composition of the banded gneiss protolith. Humphries (1984) stated that REEs are more easily lost from basaltic glasses than from crystalline basalts. It is thus possible that during phyllonitisation, REEs were preferentially released from the ultrafine-grained to glassy pseudotachylytes and cataclasites (e.g. BU20 & BU21), but were generally *retained* by the crystalline gneisses and banded gneiss-derived pervasive protophyllonites (e.g. BU15a, RON2, & BU11i). This hypothesis is discussed further in section 8.6.5.

#### **8.4.5.3 Geochemical nature of the fluid phase**

It is, of course, not possible to directly determine the composition of the fluid(s) using whole-rock geochemical techniques. However, the REE geochemistry of the fault rocks may provide some indication of (a) whether or not we can recognise different 'phases' of fluid flow along the OHFZ in North Uist and (b) how these might relate to the changing kinematic regime.

The protolith-normalised REE compositions define four distinct groups of fault rock, which are distinguished on the basis of different amount of relative REE enrichment / depletion or by different REE trends (see above). Three different REE *trends* can be recognised (Figs. 8.7a & b). Group 1 (BU15a, RON2 & BU11i) follows a banded gneiss trend (Fig. 8.7a). Groups 2 (BU15b, BU20 & BU21) and 3 (SP13 & SP22) follow very similar trends, which are characterised by progressively increasing protolith-normalised LREE concentrations and by a relatively flat HREE pattern (Fig. 8.7b). Group 4 (EB5, SP3, SP5 & SP6) is characterised by a relatively flat protolith-normalised LREE pattern and a slight, albeit progressively increasing enrichment in HREEs (Fig. 8.7b).

As discussed above, the relative *magnitude* of REE enrichment / depletion can be related to the magnitude of alteration experienced by each fault rock. In contrast, the protolith-normalised REE *trends* reflect the metamorphic behaviour of the different

mineral species which make up each of the fault rocks. The exact shape of each REE trend must therefore be influenced by a number of different factors, including:

- The whole-rock geochemistry of the host rock.
- The prevailing pressure and temperature conditions (i.e. crustal depth / geothermal gradient).
- The composition of the fluid phase.
- The partial pressure / chemical activity of the fluid phase.

(Grauch 1989; Miyashiro 1994)

The majority of the fault rocks analysed during the present study are derived from banded gneiss protoliths, therefore the REE trends observed in Figures 8.7a and 8.7b are real and are not simply a function of different host rock geochemistries.

Although Groups 2 and 3 follow almost identical trends, Group 3 (strike-slip related phyllonites) is significantly enriched relative to Group 2 ('cataclasites' and transpression-related discrete phyllonites). The relative magnitude of REE enrichment suggests that the strike-slip related phyllonites have experienced a greater degree of alteration than either the 'cataclasites' or the discrete phyllonite. This observation is consistent with the microstructural evidence presented in Chapter 6 and in section 8.2. However, the similarity of the REE trends suggests that the prevailing P-T-fluid composition-fluid pressure conditions during alteration of the 'cataclasites', during transpression-related phyllonitisation *and* during strike-slip related phyllonitisation were almost identical. In contrast, the fault rocks in Group 4 (extensionally reworked phyllonites) produce a very different protolith-normalised REE trend. These REE trends have two important implications. Firstly, the prevailing P-T-fluid composition-fluid pressure conditions were almost identical during transpression and strike-slip related phyllonitisation ('Event 1'), but were significantly different during extensional reworking ('Event 2'). Secondly, partial alteration of the crush melange probably occurred either during during sinistral transpression or during sinistral strike-slip, but *not* during extension.

Unfortunately, the protolith-normalised REE trends obtained from RON2 and BU11i (Group 1; Fig. 8.7a) do not yield any information on the prevailing P-T-fluid composition-fluid pressure conditions during the development of the pervasive protophyllonites.

## 8.5 MULTI-ELEMENT SPIDERDIAGRAMS

Trace element abundances are commonly presented on multi-element 'spiderdiagrams' (e.g. Thompson *et al.* 1984). Spiderdiagrams are designed so that trace elements with similar geochemical properties are grouped together. The trends produced by plotting the trace element concentrations thus approximate to smooth curves, which may be associated with marked positive or negative anomalies at particular elements. The trend of the curves and the position of the anomalies may provide information on the petrogenesis of the rock (Wilson 1989).

The spiderdiagrams devised for the present study are based upon those of Pearce (1983). The elements are arranged according to their mobility in an aqueous environment. The elements on the left hand side (Cs, Pb, Ba, Rb, Sr and U) are generally considered to be mobile in aqueous environments. The elements on the right hand side (Nb, Th, La, Ce, Nd, Sm, Zr, Hf, Ti, Tb, Y and Tm) are considered to be relatively immobile in aqueous environments (Pearce 1983; Rollinson 1993). For the present study, both chondrite-normalised and protolith-normalised spiderdiagrams have been constructed in order to provide a direct comparison with the REE data (section 8.4). The chondrite-normalised spiderdiagrams have been used to confirm the choice of 'geochemical protoliths' which were selected using the chondrite-normalised REE data (section 8.4; Table 8.2). The protolith-normalised spiderdiagrams have been used to examine the geochemical effects of fluid-rock interaction on each of the fault rocks analysed.

### 8.5.1 PROTOLITHS

The chondrite-normalised trace element concentrations obtained from the Lewisian protoliths are presented in Figure 8.8.

The mobile trace element concentrations define 'sawtooth' curves on the spiderdiagram. Although the concentrations of the mobile trace elements are very variable (up to two orders of magnitude difference in the concentrations of the most abundant and the least abundant mobile elements in any given sample), Cs and Pb are comparatively depleted ( $<$  ten times chondritic abundance), whilst Ba, Rb, Sr and U are comparatively enriched ( $\leq$  five hundred times chondritic abundance) in each of the samples analysed.

In contrast, the 'immobile' trace element concentrations define relatively smooth curves on the spiderdiagram (Fig. 8.8). The gradients of the immobile element curves are characteristic for each of the different gneisses:

- The 'banded gneiss curve' (LB1) is characterised by a marked decrease in the concentrations of the elements Th to Sm and Hf to Tm. The concentrations of the elements Sm, Zr and Hf plot sub-parallel to the x-axis.
- The 'Younger Basic curve' (NU9) is characterised by a progressive decrease in the concentrations of the elements Th to Tm.
- The 'felsic gneiss curve' (NU7 and 'felsic band') is characterised by a rapid decrease in the concentrations of the elements Th to Sm, a 'plateau' from Zr to Hf and a marked 'trough' from Tb to Tm.
- The 'mafic gneiss curve' ('mafic band') is characterised by a progressive decrease in the concentrations of the elements Th to Sm, a marked 'trough' from Zr to Hf and a progressive decrease in the concentrations of the elements Tb to Tm.

All the samples are characterised by a trough at Nb and a major increase in trace element concentration from Tm to Yb.

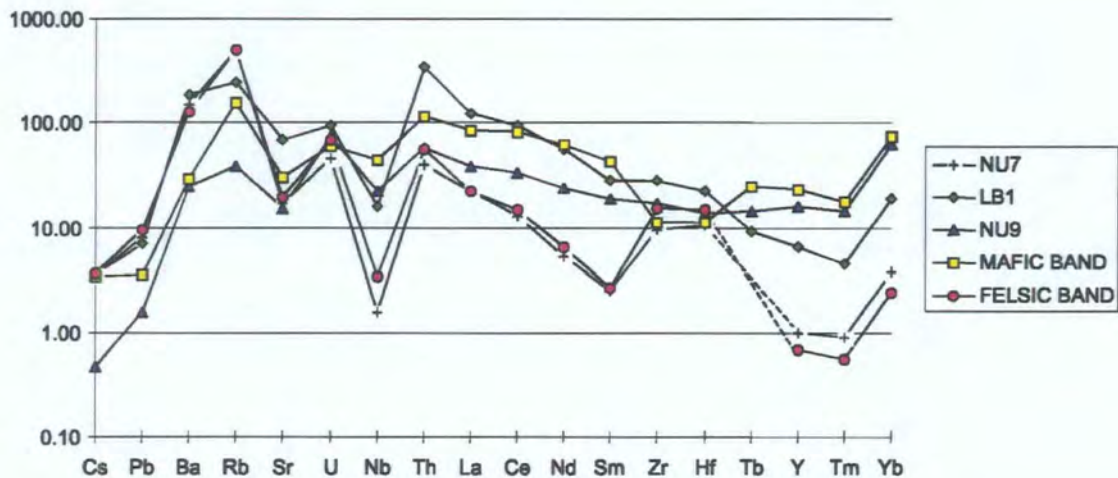


Figure 8.8 Chondrite-normalised multi-element spiderdiagram for the protoliths.

### 8.5.2 CRUSH MELANGE

The chondrite-normalised immobile trace element concentrations obtained from the 'cataclasites' (BU20 & BU21), the fractured gneiss (BU15a) and the discrete phyllonite (BU15b) follow a 'banded gneiss curve' (Fig. 8.9a). Note that chondrite-normalised immobile element abundances obtained from the *least* deformed sample (fractured gneiss BU15a) are generally greater than those obtained from the more highly deformed rocks (BU20, BU21 and BU15b).

The protolith-normalised trace element concentrations are presented in Figure 8.9b.

The protolith-normalised mobile trace element concentrations obtained from each of the samples produce 'sawtooth' curves on the spiderdiagram (Fig. 8.9b). BU15a is

depleted in Pb, Ba, Rb and U relative to banded gneiss, although the concentrations of Cs and Sr obtained from BU15a are comparable to those obtained from the protolith. The 'cataclasites' (BU20 & BU21) are depleted in Pb, Ba, Sr and U, although Cs and Rb are not significantly enriched / depleted with respect to banded gneiss. The greatest variability in protolith-normalised mobile trace element concentrations is observed in the discrete phyllonite (BU15b). BU15b is depleted in Ba, Rb and Sr, is enriched in Pb and is not significantly enriched / depleted in Cs or U with respect to banded gneiss.

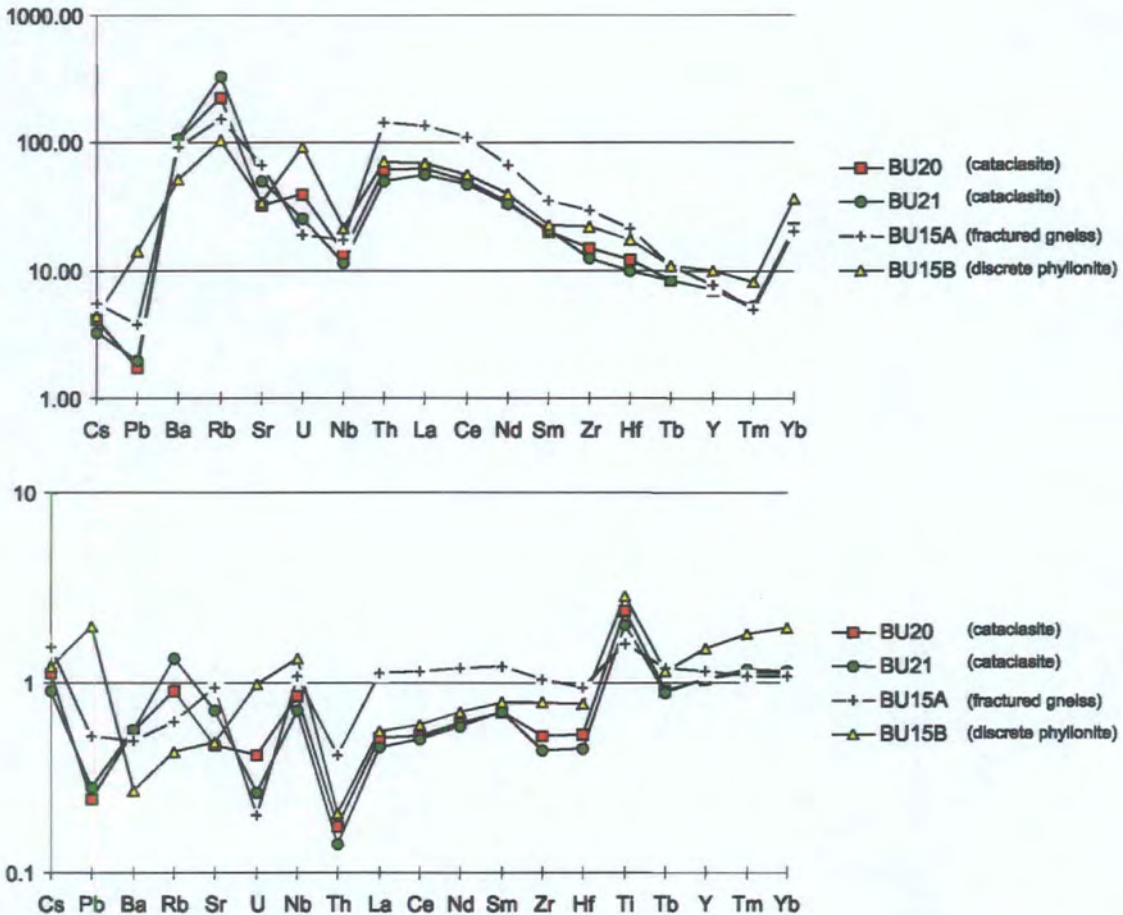


**Figure 8.9** (a) Chondrite-normalised and (b) protolith-normalised multi-element spiderdiagrams for the crush melange samples.

The protolith-normalised immobile trace element concentrations obtained from each of the samples define similar curves, which are characterised by large negative Th anomalies and large positive Ti anomalies (Fig. 8.9b). In the relatively undeformed gneiss (BU15a), the concentrations of the elements La to Hf and Tb to Yb plot sub-parallel to the *x*-axis and are not significantly enriched or depleted with respect to banded gneiss. In contrast, the protolith-normalised concentrations of the elements La

to Sm obtained from the 'cataclasites' (BU20 & BU21) and the discrete phyllonite (BU15b) display progressively *decreasing* depletion, whilst the elements Tb to Yb display progressively *increasing* enrichment.

### 8.5.3 PERVASIVE PROTOPHYLLONITES AND STRIKE-SLIP RELATED PHYLLONITES

The chondrite-normalised trace element concentrations obtained from the protophyllonites and strike-slip related phyllonites either follow a 'banded gneiss trend' (BU11i, RON2, SP13 and SP22) or a 'felsic gneiss trend' (BU5) (Fig. 8.10a). The chondrite-normalised concentrations obtained from the *protophyllonites* (BU5, BU11i and RON2) display considerable scatter, which in part reflects the variable protolith geochemistry. In contrast, the chondrite-normalised trace element concentrations obtained from each of the strike-slip related phyllonites (SP13 and SP22) are very similar (Fig. 8.10a).

The protolith-normalised trace element concentrations are presented in Figure 8.10b.

The protolith-normalised mobile trace element concentrations obtained from the protophyllonites produce 'sawtooth' curves on the spiderdiagram (Fig. 8.10b). The banded gneiss-derived protophyllonite RON2 is depleted in Cs, Pb, Rb and U, whilst Ba and Sr are not significantly depleted with respect to the protolith. The protolith-normalised mobile trace element concentrations obtained from BU11i and BU5 follow similar trends, although BU11i is slightly enriched in Pb, whilst BU5 is slightly enriched in Ba. The mobile trace element concentrations obtained from the strike-slip related phyllonites (SP13 & SP22) produce 'sawtooth' curves on the spiderdiagram. SP13 and SP22 are depleted in Cs, Ba, Rb and U, whilst Pb and Sr are not significantly enriched / depleted relative to the banded gneiss protolith (Fig. 8.10b).

The protolith-normalised immobile trace element concentrations obtained from each of the protophyllonites (RON2, BU11i & BU5) and phyllonites (SP13 & SP22) are characterised by marked negative Th and positive Ti anomalies. Nb is not significantly enriched or depleted with respect to the protoliths. The protolith-normalised concentrations of the elements La to Hf and Tb to Yb obtained from the banded gneiss-derived protophyllonites (RON2 & BU11i) plot parallel to the *x*-axis and are not significantly enriched or depleted. In contrast, the concentrations of the elements La to Hf obtained from the felsic gneiss-derived protophyllonite (BU5) are characterised by progressively decreasing enrichment relative to the protolith. The immobile trace-element concentrations obtained from the strike-slip related phyllonites (SP13 & SP22) are typically enriched with respect to the protolith. The elements La to Sm display progressively increasing enrichment, whilst the elements Tb to Yb plot parallel to the *x*-axis (Fig. 8.10b).

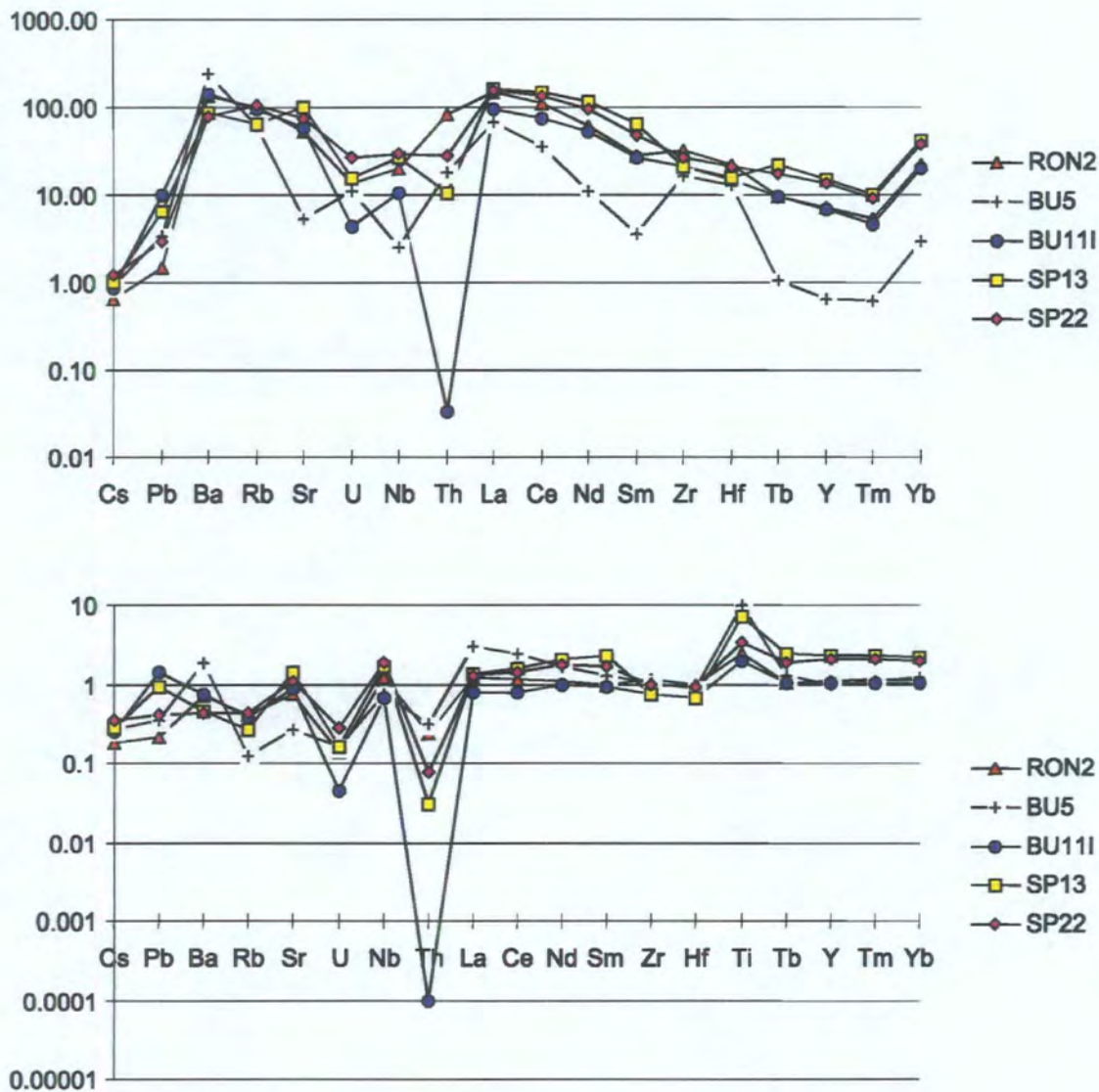


Figure 8.10 (a) Chondrite-normalised and (b) protolith-normalised multi-element spiderdiagrams for the protophyllonites and the strike-slip related phyllonites.

#### 8.5.4 EXTENSIONALLY REWORKED PHYLLOMITES

The chondrite-normalised trace element compositions obtained from the extensionally reworked phyllonites follow a 'banded gneiss trend'. The chondrite-normalised mobile element compositions are slightly more scattered than the immobile elements compositions (Fig. 8.11a), but are much less variable than the mobile element concentrations obtained from the protophyllonites and strike-slip related phyllonite (section 8.5.3; Fig. 8.10a).

The protolith-normalised mobile trace element concentrations obtained from the extensionally-reworked phyllonites are generally depleted, although the amount of depletion varies between samples (Fig. 8.11b). Sr does not appear to be significantly

enriched or depleted relative to the banded gneiss protolith. The elements Nb and La to Hf are not significantly enriched or depleted relative to the protolith. The extensionally reworked phyllonites show marked negative Th and positive Ti anomalies. The elements Tb to Yb display a slight, but progressively increasing enrichment with respect to the protoliths.

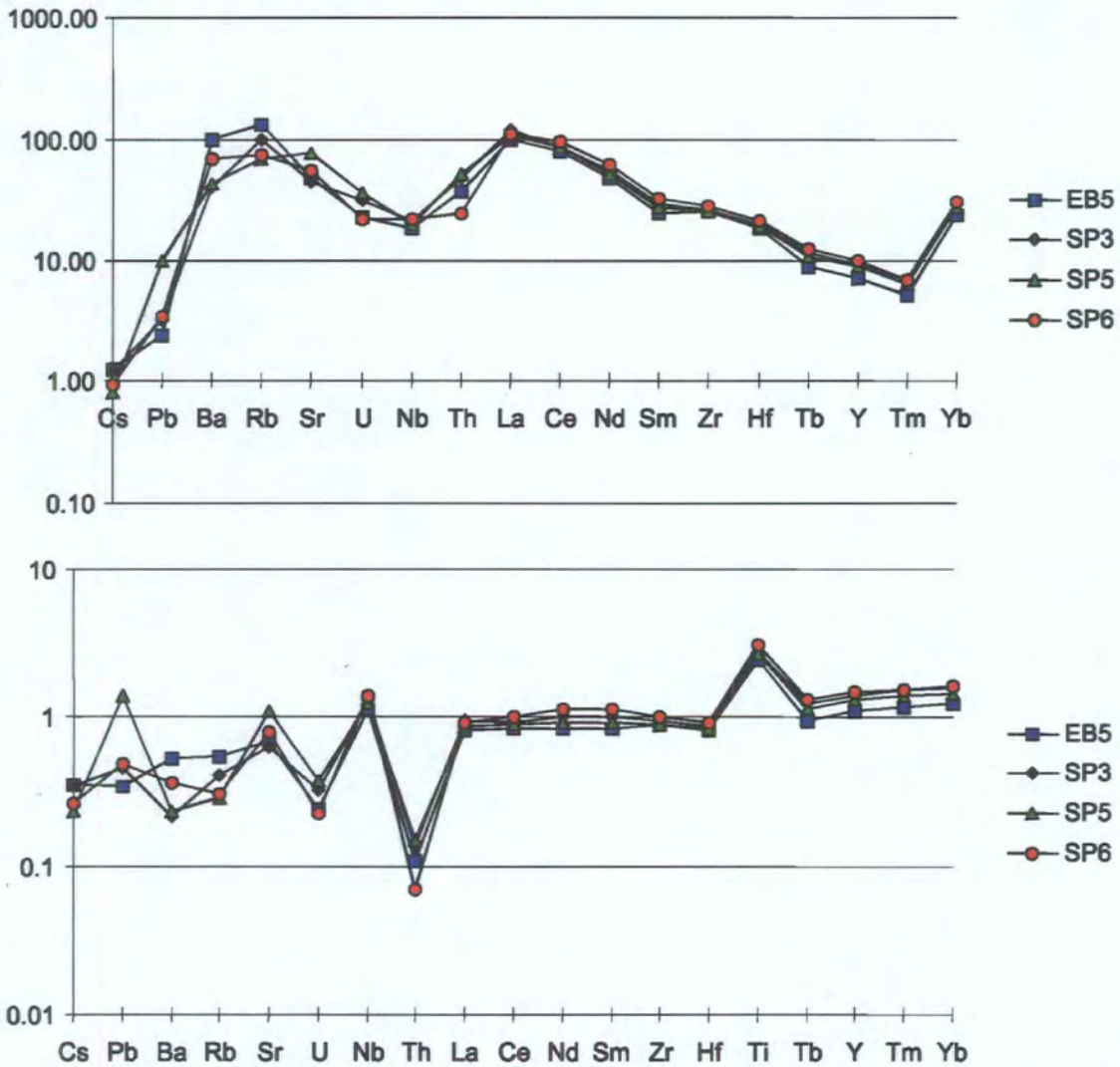


**Figure 8.11** (a) Chondrite-normalised and (b) protolith-normalised multi-element spiderdiagrams for the extensionally reworked phyllonites.

### 8.5.5 SUMMARY & DISCUSSION

The *absolute* values of protolith-normalised trace element concentration must be treated with caution, owing to the unknown geochemical variability of the Lewisian protoliths. The following interpretations are therefore based on enrichment / depletion *trends* and on the *relative* amount of enrichment / depletion experienced by each fault rock (see section 8.4.5 for further explanation).

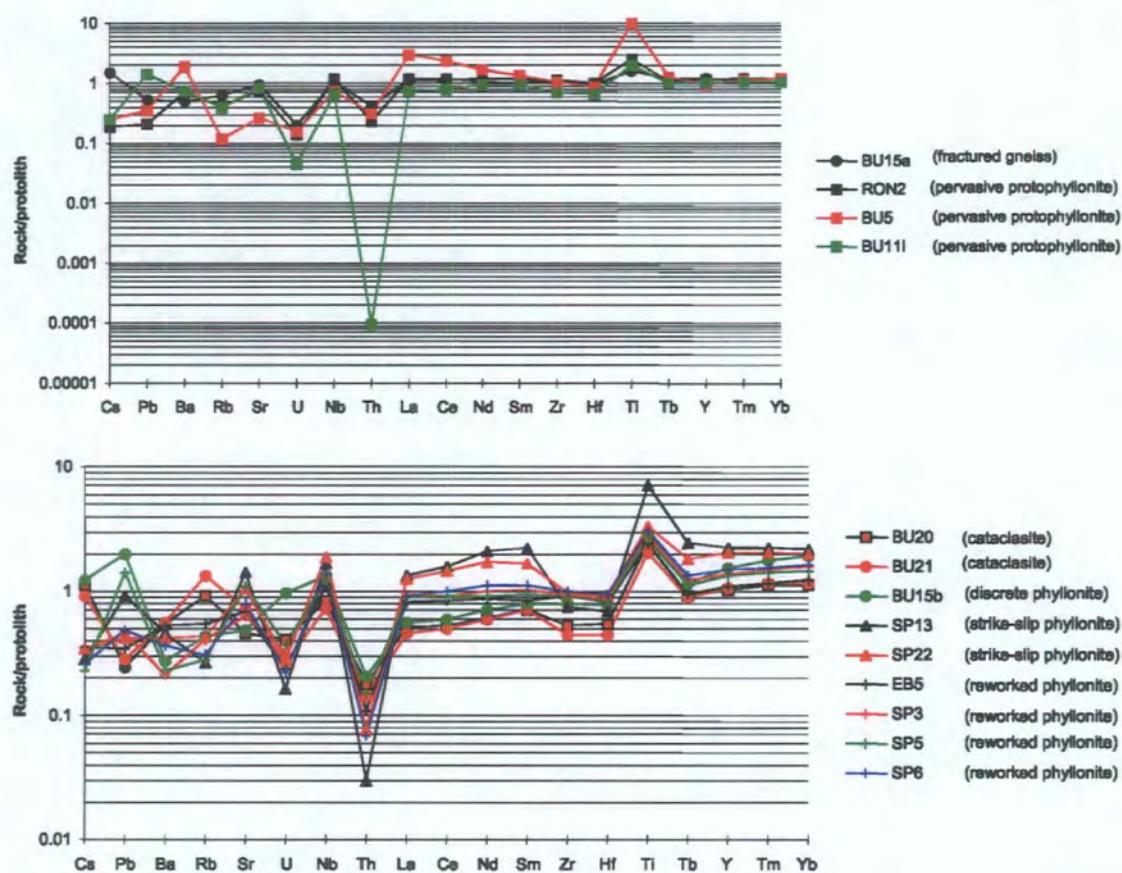


**Figure 8.12** Summary spiderdiagrams showing the protolith-normalised trace element concentrations for (a) Group 1 (circles and black & red squares) and (b) Groups 2 (circles), 3 (triangles) and 4 (crosses). See text for explanation.

### 8.5.5.1 Immobile trace element data

The protolith-normalised trace element data are summarised in Figure 8.12. The 'immobile' trace elements (i.e. the REEs + Nb, Th, Zr, Hf, Ti and Y) define four distinct geochemical groups (Figs. 8.11a & b), which are exactly analogous to the four geochemical groups defined by the protolith-normalised REE data (section 8.4.5; 'Group 1' = BU15a, RON2, BU11i & BU5; 'Group 2' = BU20, BU21 & BU15b; 'Group 3' = SP13 & SP22; 'Group 4' = EB5, SP3, SP5 & SP6). The behaviour of the REEs is discussed in section 8.4.5. Of the other 'immobile' elements, Nb, Zr and Hf are *not* significantly enriched or depleted relative to the Lewisian protoliths in any group of fault rocks. This observation suggests that Nb, Zr and Hf were relatively immobile during alteration. In contrast, Th is strongly depleted and Ti is markedly enriched in each group of fault rocks, relative to both the Lewisian protoliths *and* to the immobile elements Nb, Zr and Hf. The greatest Ti (and Th) anomalies are observed in Groups 2, 3 and 4 (i.e. in 'cataclasites' and 'cataclasite'-derived fault rocks) (Fig. 8.12b), whilst the smallest Ti (and Th) anomalies are observed Group 1 (i.e. the relatively undeformed fractured gneisses and the pervasive protophyllonites) (Fig.

8.12a). The relative magnitudes of the Ti anomaly are consistent with the petrographic observation that opaque minerals, such as ilmenite, are concentrated along 'cataclasite' seams and within 'cataclasite'-derived phyllonites (Chapter 6). Furthermore, the enrichment in Ti relative to Nb, Zr and Hf suggests that *additional* Ti was added to the 'cataclasite' seams and to the 'cataclasite'-derived phyllonites during alteration i.e. *the 'cataclasite'-derived fault rocks behaved as a 'geochemically open' system during alteration / phyllonitisation*. This observation is discussed in relation to the mobile trace element data in section 8.6.5.

#### 8.5.5.2 Mobile trace element data

In contrast to the relatively 'ordered' spiderdiagrams defined by the protolith-normalised 'immobile' trace element data, the protolith-normalised *mobile* trace element data produce noisy, sawtooth spiderdiagrams, and the distinction between the different geochemical groups (section 8.4.5) appears to break down (Figs. 8.12a & b; but see section 8.6.5). The most obvious feature of the mobile element spiderdiagrams is that the mobile elements are typically depleted, relative to both the Lewisian protoliths and to the immobile elements Nb, Zr and Hf. *All* the different fault rocks, (including those belonging to 'Group 1'), have experienced loss (or more rarely, gain) of mobile elements. The most mobile elements appear to have been Cs, Rb, Ba, Pb and U. The mobility of U probably reflects the relative ease of apatite dissolution, whilst the behaviour of Rb and Ba may have been controlled by the breakdown of K-feldspar  $\pm$  plagioclase. Rb and Cs are also influenced by the growth of sericite and may substitute for potassium in the mica lattice (Smith 1975, 1983; Deer *et al.* 1992) (Chapters 6 & 9).

Sr is unusual in that it is *not* significantly enriched or depleted in the highly altered phyllonites SP22 and SP5, whilst it *does* appear to be strongly depleted in the 'cataclasites' (BU20 & BU21) and in the discrete phyllonite (BU15b) (Fig. 8.12b). The Sr depletion observed in the crush melange samples can be attributed to the breakdown of Ca-rich plagioclase to aggregates of albite and sericite during strike-slip related phyllonitisation and extensional reworking (Chapters 6 & 9). However, petrographic observations suggest that epidote is exceptionally abundant in all the phyllonitic and ultraphyllonitic rocks, whilst carbonate veins are commonly observed only in extensionally reworked phyllonites (section 8.2). It is therefore possible that Sr substitutes for Ca into the epidote / carbonate lattice and thus 'masks' the effects of plagioclase breakdown.

The extensionally reworked phyllonites, which have experienced intense deformation and fluid-rock interaction, are characterised by relatively homogeneous mobile (and immobile) trace element concentrations. Microstructural observations suggest that

strain was accommodated by fluid-assisted diffusion-dominated mechanisms during reworking. It is postulated that the relatively homogeneous trace element concentrations resulted from diffusion  $\pm$  mechanical mixing during reworking. This hypothesis is consistent with the inference that the actively deforming phyllonitic shear zones were 'geochemically open' systems (section 8.4.5).

## 8.6 ELEMENT RATIO DIAGRAMS

The protolith-normalised multi-element spiderdiagrams demonstrate that in each group of fault rocks, the mobile elements have been either depleted or enriched relative to Nb, Zr and Hf (Figs. 8.11a & b; section 8.5.5). This observation suggests (a) that *all* the fault rocks behaved in a 'geochemically open' manner during alteration and / or phyllonitisation (section 8.5.5) and (b) that the pervasive protophyllonites and the fractured gneisses (i.e. 'Group 1'; section 8.4.5) have in fact experienced a greater degree of alteration than is implied by the REE data alone (section 8.4.5). In order to test these conclusions, 'mobile element ratio diagrams' (e.g. Rollinson 1993) have been constructed in order to examine the behaviour of four different mobile elements (Figs. 8.13, 8.14, 8.15 & 8.16).

The element ratio diagrams are scatter plots of (chondrite-normalised concentration of mobile element A in sample S / chondrite-normalised concentration of immobile element C in sample S) *versus* (chondrite-normalised concentration of mobile element B in sample S / chondrite-normalised concentration of immobile element C in sample S), where, in this case A = U, B = Rb, Sr, Cs or Ba and C = Nb. Nb was selected as the normalisation factor owing to its extremely immobile behaviour (section 8.5.5; Fig. 8.12). U was selected to plot along the ordinate owing to its extremely mobile behaviour (section 8.5.5; Fig. 8.12), which ensures that the data is not 'bunched up' on the element ratio diagrams.

### 8.6.1 U/Nb versus Rb/Nb DIAGRAM

The Lewisian gneisses occupy a broad compositional field, although the principal 'geochemical protoliths' (i.e. LB1, NU7 and 'felsic band') plot along a straight line (highlighted in Fig. 8.13). The different 'geochemical groups' (section 8.4.5) occupy distinct compositional fields on the element ratio diagram. Group 2 (i.e. BU15b, BU20 & BU21) plots closest to the 'geochemical protolith line' whilst Group 3 (i.e. SP13 & SP22) plots furthest from the 'geochemical protolith line'. The Rb/Nb ratio of Group 2 partly overlaps with the Rb/Nb ratio of the 'geochemical protoliths'. Groups 1 and 4 (i.e. RON2 & BU11i and EB5, SP3, SP5 & SP6 respectively) occupy

intermediate positions in between 2 and 3. The Rb/Nb ratio of Group 1 is greater than the Rb/Nb ratio of Group 4.

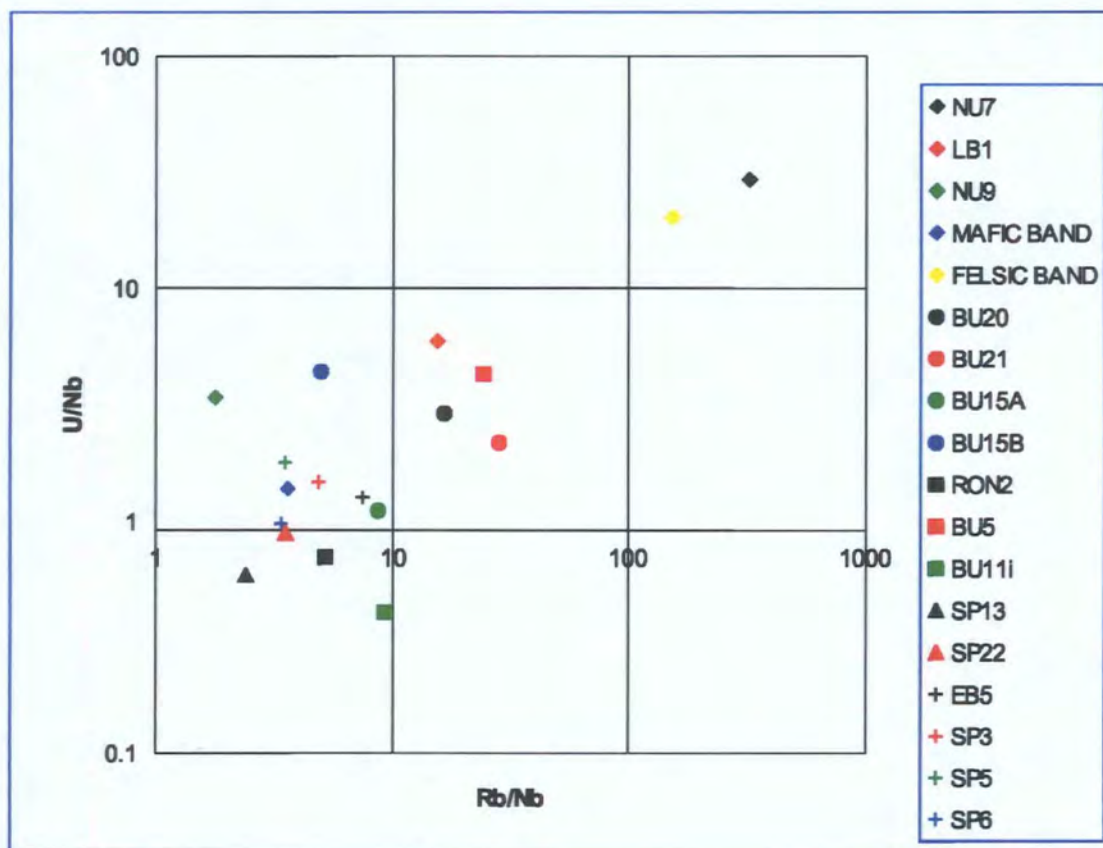


**Figure 8.13** U/Nb versus Rb/Nb element ratio diagram. Group 1 (circles and black & red squares), Group 2 (circles), Group 3 (triangles) and Group 4 (crosses). Heavy line represents region occupied by geochemical protoliths.

### 8.6.2 U/Nb versus Sr/Nb DIAGRAM

The Lewisian gneisses occupy a broad compositional field, although the principal 'geochemical protoliths' (i.e. LB1, NU7 and 'felsic band') define more tightly constrained region on the element ratio diagram (highlighted in Fig. 8.14). The compositions of the fault rocks do not overlap with the 'geochemical protolith field'. The different 'geochemical groups' generally occupy distinct compositional fields, although the fields occupied by Groups 1 and 3 partly overlap one another. Group 2 (i.e. BU15b, BU20 & BU21) occupies the region closest to the 'geochemical protolith field', whilst Groups 1 and 3 (i.e. RON2 & BU11i and SP13 & SP22 respectively) lie furthest from the 'geochemical protolith field'. Group 4 (i.e. EB5, SP3, SP5 & SP6) occupies an intermediate position in between Group 2 and Groups 1 & 3 (Fig. 8.14). Note that the Sr/Nb ratio of each group of fault rocks is approximately constant.

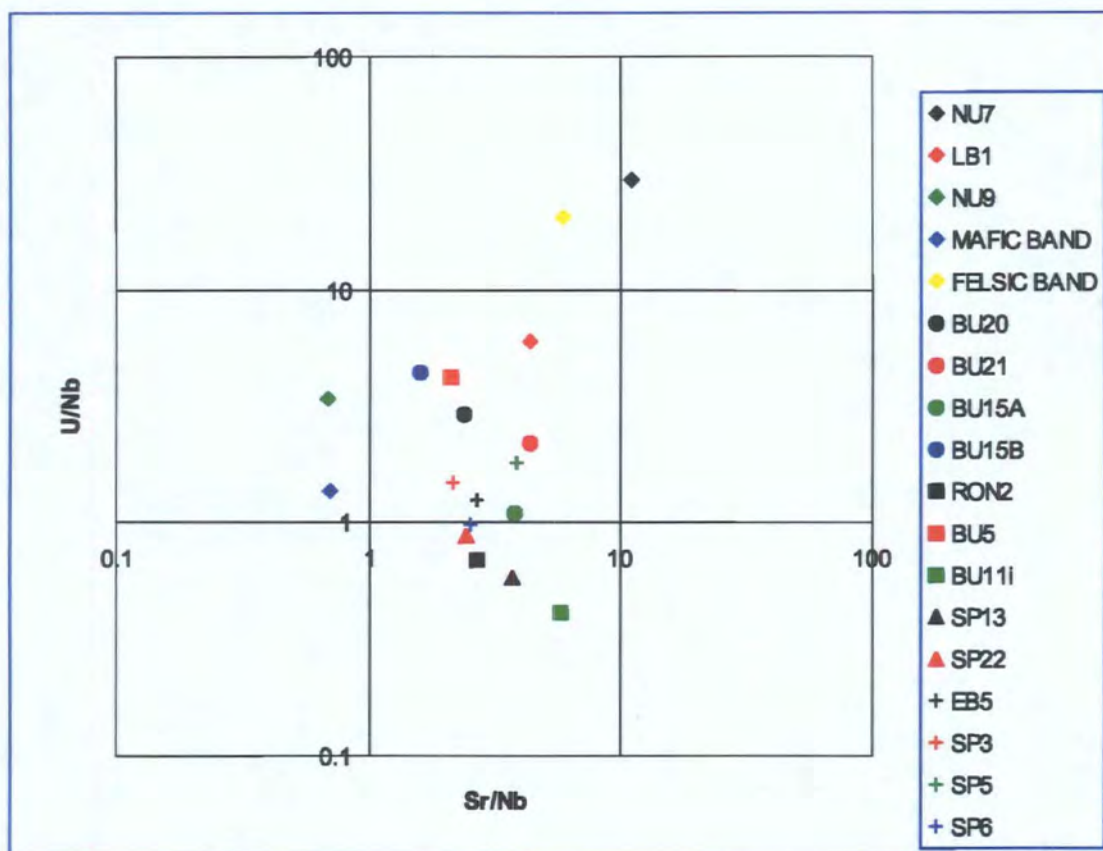


**Figure 8.14** U/Nb versus Sr/Nb element ratio diagram. Group 1 (circles and black & red squares), Group 2 (circles), Group 3 (triangles) and Group 4 (crosses). Hatched box represents region occupied by geochemical protoliths.

### 8.6.3 U/Nb versus Ba/Nb DIAGRAM

The principal 'geochemical protoliths' (i.e. LB1, NU7 and 'felsic band') occupy a distinct geochemical field on the element ratio diagram (highlighted in Fig. 8.15). The different 'geochemical groups' have lower Ba/Nb ratios than the 'geochemical protoliths' and each group of fault rocks occupies a distinct compositional field. Group 2 (i.e. BU15b, BU20 & BU21) occupies the region closest to the 'geochemical protolith field', whilst Group 3 (i.e. SP13 & SP22) plots furthest from the 'geochemical protolith field'. Groups 1 and 4 (i.e. RON2 & BU11i and EB5, SP3, SP5 & SP6 respectively) occupy intermediate positions in between 2 and 3. The Ba/Nb ratio of Group 1 is greater than the Ba/Nb ratio of Group 4.

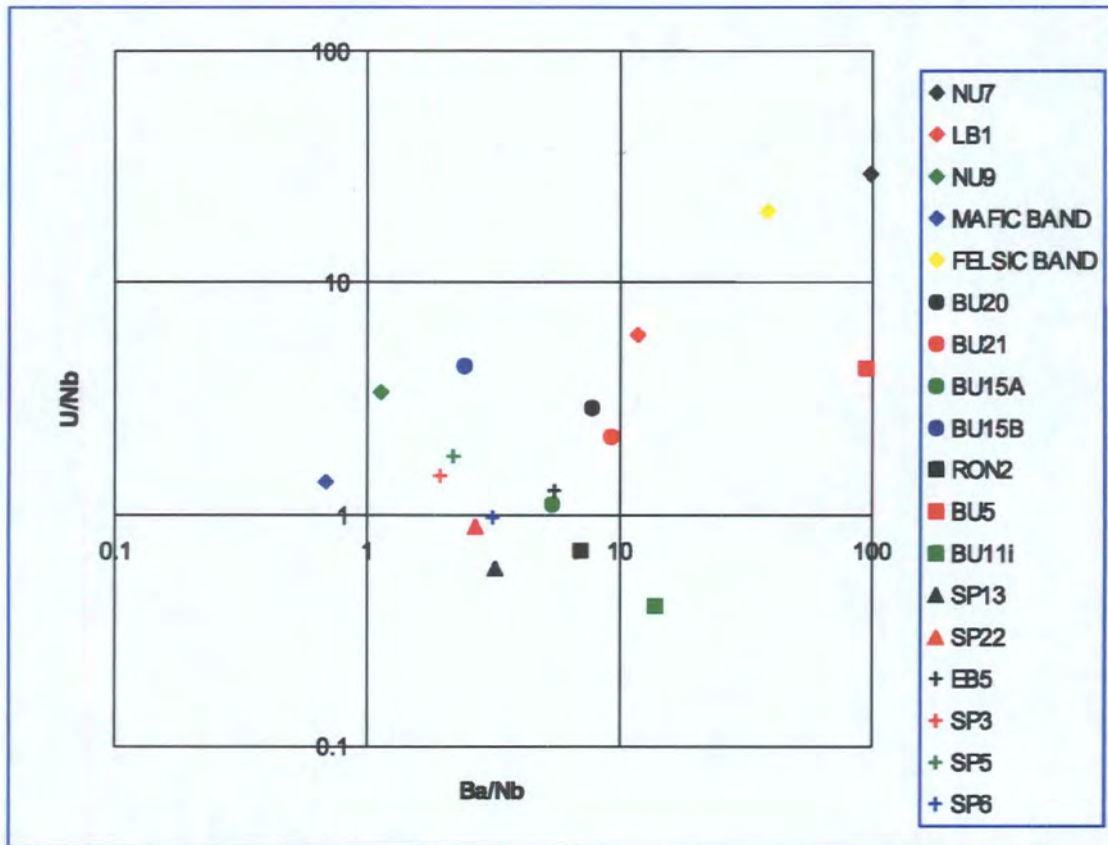


**Figure 8.15** U/Nb versus Ba/Nb element ratio diagram. Group 1 (circles and black & red squares), Group 2 (circles), Group 3 (triangles) and Group 4 (crosses). Hatched box represents region occupied by geochemical protoliths.

### 8.6.4 U/Nb versus Cs/Nb DIAGRAM

The Lewisian protoliths occupy a broad compositional field although the principal 'geochemical protoliths' (i.e. LB1, NU7 and 'felsic band') plot along a straight line (highlighted in Fig. 8.16). The different 'geochemical groups' generally occupy distinct compositional fields. Group 2 (i.e. BU15b, BU20 & BU21) occupies the region closest to the 'geochemical protolith field', whilst Groups 1 and 3 (i.e. RON2 & BU11i and SP13 & SP22 respectively) plot furthest from the 'geochemical protolith field'. Note that the Cs/Nb ratio of Group 2 is comparable to the Cs/Nb ratio of LB1 (banded gneiss), whilst Groups 1 and 3 partly overlap. Group 4 (i.e. EB5, SP3, SP5 & SP6) occupies an intermediate position in between Groups 2 and 3.

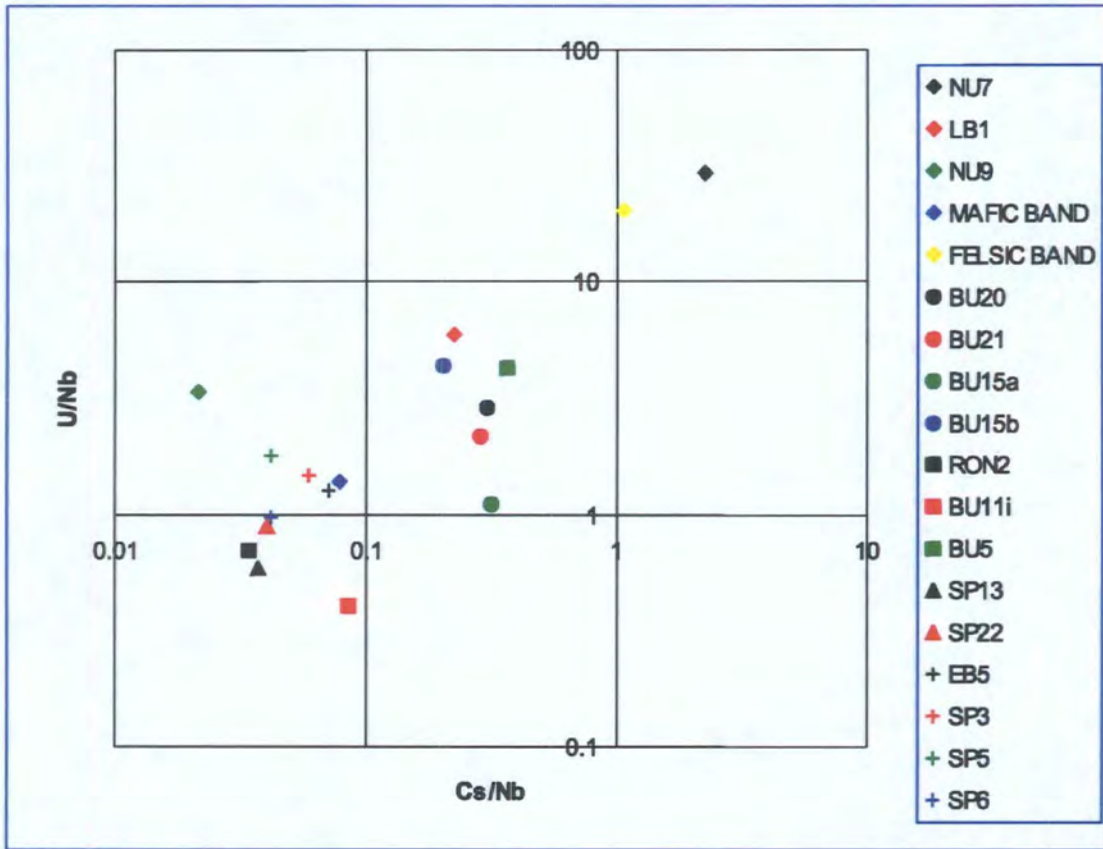


**Figure 8.16** U/Nb versus Cs/Nb element ratio diagram. Group 1 (circles and black & red squares), Group 2 (circles), Group 3 (triangles) and Group 4 (crosses). Hatched box represents region occupied by geochemical protoliths.

### 8.6.5 SUMMARY AND DISCUSSION

The 'geochemical groups' defined by the protolith-normalised REE data (section 8.4.5) occupy distinct compositional fields in all the element ratio diagrams (sections 8.6.1, 8.6.2, 8.6.3 & 8.6.4). There are two important observations which can be made from analysis of the element ratio diagrams:

- (1) The compositional fields occupied by the different groups of fault rocks are distinct from the compositional field occupied by the geochemical protoliths.
- (2) The relative positions of each group of fault rocks are similar in each diagram.

The absence of any overlap between the compositional fields occupied by the fault rocks and the compositional fields occupied the 'geochemical protoliths' suggests that the observed fault rock compositions *cannot* have been produced by either physical or chemical mixing of the different Lewisian protoliths. The implication is that mobile

components must have been either removed from, or gained by the fault rocks i.e. *the fault rocks* (including Group 1) *must have behaved as a 'geochemically open' system during alteration and phyllonitisation.*

#### **8.6.5.1 Intensity of alteration**

The relative displacement of each 'fault rock field' away from the position of the 'geochemical protolith field' reflects the relative degree of alteration experienced by each group of fault rocks. The relative positions occupied by each group of fault rocks on the element ratio diagrams consistently suggest that (a) Group 2 ('cataclasites' and discrete phyllonite) has experienced the least alteration, (b) that Group 3 (strike-slip related phyllonites) has experienced the greatest degree of alteration and (c) that Groups 1 (fractured gneiss and pervasive protophyllonites) and 4 (extensionally reworked phyllonites) have experienced intermediate amounts of alteration. The relative degree of alteration experienced by Groups 3 and 4 inferred from the element ratio diagrams is consistent with the relative degree of alteration experienced by Groups 3 and 4 inferred from the protolith-normalised REE data. However, the relative degree of alteration experienced by Groups 1 and 2 inferred from the element ratio diagrams is the exact *opposite* to the relative degree of alteration experienced by Groups 1 and 2 inferred from the protolith-normalised REE data (section 8.4.5). This observation suggests that the fractured gneisses were open to the mobile trace elements but were closed to the REEs, whilst the glassy / fine grained 'cataclasites' were relatively closed to the mobile trace elements but were open to the REEs (section 8.4.5).

Both the REE data (section 8.4.5) and the element ratio diagrams imply that the extensionally reworked phyllonites (Group 4) are apparently *less* altered than the strike-slip related phyllonites (Group 3). The field relationships clearly demonstrate that the strike-slip related phyllonites were reworked during extension i.e. the *Group 4 phyllonites are clearly derived from the Group 3 phyllonites* (Chapter 6). It is therefore extremely unlikely that the extensionally reworked phyllonites can be less altered than the strike-slip related phyllonites. The relative positions of the compositional fields defined by Groups 3 and 4 can be explained by the *addition* of mobile components to the phyllonites during extensional reworking. Field and petrographic observations suggest that quartz-carbonate-albite-chlorite veins were widely developed during extensional reactivation of the pre-existing phyllonitic shear zones Chapter 6). It is therefore likely that the variation in the mobile element and REE concentrations between Groups 3 and 4 was caused by the precipitation of veins during extensional reworking.

### 8.6.5.2 Volume changes

In order to determine whether or not phyllonitisation was associated with significant volume changes, it is necessary to ascertain (a) the chemical compositions of the fault rocks and their protoliths, and (b) the *densities* of the fault rocks and their protoliths (Gresens 1967). Unfortunately, the fault rock densities were not determined during the present study. However, Walker (1990) has carried out detailed geochemical mass balance calculations for the different fault rocks and their protoliths. The *overall* loss in mobile elements observed in Groups 1, 2, 3 and 4 is consistent with *overall* volume loss during alteration and phyllonitisation reported by Walker (1990). However, the slight *gain* in mobile elements and REEs observed in extension-related phyllonites suggests that reworking was associated with a slight volume *increase*. This inferred volume increase is consistent with field and microstructural observations of abundant syn-tectonic veins in packages of extensionally-reworked phyllonite. The mechanical and hydrogeological implications of volume change during phyllonitisation are discussed in Chapter 9.

## 8.7 SUMMARY

Whole-rock major and trace element analysis of a suite of fault rocks and their protoliths from the Outer Hebrides Fault Zone in North Uist suggests that:

- The majority of the fault rocks were derived from banded gneiss protoliths.
- The major, trace and rare earth element compositions of the phyllonitised and / or altered fault rocks differ significantly from the composition of the protolith.
- Alteration was not isochemical and the fault rocks behaved in a 'geochemically open' manner.
- The microstructure of the fault rocks strongly influenced the intensity of geochemical alteration. 'Cataclasite' seams, fractures and 'cataclasite'-derived phyllonites experienced the greatest degree of alteration and probably acted as fluid pathways.
- At least two distinct episodes of fluid-rock interaction have been recognised in North Uist. 'Event 1' was related to phyllonitisation during transpression and strike-slip, whilst 'Event 2' was related to extensional reworking of the phyllonitic shear zones.

- Phyllonitisation and / or alteration was associated with an overall volume loss, although extensional reworking was associated with a (relatively) small volume increase.

To conclude, this study has demonstrated that whole-rock geochemical techniques can be applied to reactivated, retrogressed basement fault zones *provided that the geochemical data is interpreted in the context of the kinematic, mesostructural and microstructural evolution of the fault zone*. It is important that individual datasets (e.g. REE data) are not treated in isolation but are analysed in conjunction with the other structural and geochemical datasets. In particular, it is important to relate the geochemistry to the microstructure of the fault rocks.

## 9. SUMMARY, DISCUSSION AND CONCLUSIONS

### 9.1 INTRODUCTION

Detailed field and microstructural studies (Chapters 3 to 7) have clearly demonstrated that the Outer Hebrides Fault Zone is a long-lived structure, which has experienced a complex history of repeated reactivation. The aims of this chapter are:

- To summarise and discuss the structural, textural and metamorphic evolution of fault rocks preserved along the length of the OHFZ.
- To discuss the controls on fault zone weakening and reactivation along the OHFZ.
- To discuss the reasons why some segments of the OHFZ have *not* been extensively reactivated.
- To present a generalised model to explain reactivation of retrogressed basement fault zones.

### 9.2 TECTONIC AND METAMORPHIC EVOLUTION OF THE OHFZ

A complex array of different fault rocks and structures is presently exposed along the length of the OHFZ. The aims of the following section are:

- To summarise and discuss the available age constraints and kinematic and metamorphic data for each *individual* group of fault rocks and their protoliths (sections 9.2.1 to 9.2.5),
- To synthesise this information into a series of models explaining the tectonic and metamorphic evolution of the OHFZ (section 9.2.6).

#### 9.2.1 LEWISIAN PROTOLITHS

The fault rocks preserved along the OHFZ were, without exception, ultimately derived from gneissose Lewisian protoliths. The principal protoliths lithologies appear to have been quartzo-feldspathic banded gneiss and, to a lesser extent, amphibolite (Chapter 8). The granoblastic, banded gneisses comprise networks of interlocking plagioclase and K-feldspar grains, which isolate pockets of quartz, biotite and garnet (section 2.2.2.1). The amphibolites comprise interlocking networks of equigranular

hornblende and plagioclase grains, which isolate pockets of quartz, garnet and, less commonly, pyroxene (sections 2.2.2.1 & 2.2.2.4).

Experimental evidence suggests that feldspar is unable to accommodate significant crystal plastic deformation at temperatures below c.450°C (Tullis & Yund 1992). Experimental data for hornblende is lacking, but observations of naturally deformed rocks suggest that amphiboles do not readily deform by dislocation creep, except at very high temperatures (e.g. during mantle deformation) (Passchier & Trouw 1996). In contrast, quartz is able to accommodate significant strains by dislocation creep at temperatures above c.300°C (Hirth & Tullis 1992; Passchier & Trouw 1996). Thus, at any given temperature, feldspar and hornblende are likely to be significantly stronger than quartz. This observation suggests that both banded gneiss and amphibolite are characterised by *load-bearing framework* (LBF) microstructures (Handy 1990) (section 1.5.2.2). If this inference is correct, it is likely the rheologies of the unmodified felsic and mafic protoliths were controlled by the rheological behaviour of feldspar and hornblende respectively.

## 9.2.2 PERVASIVE MYLONITE

A NE-SW to N-S trending, eastward dipping belt of upper greenschist to lower amphibolite facies mylonite (the 'pervasive mylonite belt') outcrops extensively throughout southeast Lewis and Scalpay (i.e. within the Northern Zone of the OHFZ) (Figs. 3.3 & 3.13). Pervasive mylonites are not exposed in the Southern Zone of the OHFZ (Fig. 2.5).

### 9.2.2.1 Timing of mylonitisation

The mylonitic fabrics are commonly observed to deform both Younger Basic (Scourie) dykes and Laxfordian pegmatite sheets (section 2.2.2) (Figs. 5.4 & 5.12). Mylonitisation must therefore post-date the intrusion of the amphibolite dykes and pegmatite sheets. Whole-rock Rb-Sr ages obtained from Laxfordian granites in southwest Harris (Fig. 2.3) suggest that the pegmatite sheets were intruded c.1750Ma (Van Breemen *et al.* 1971). Mylonitisation must therefore have occurred sometime after 1750Ma.

Butler (1995) has argued that the present-day outcrop pattern, in which the pervasive mylonite belt is only exposed in the Northern Zone of the OHFZ, can be explained by oblique dextral movements across the NW-SE trending South Harris Shear Zones, following the cessation of mylonitisation (see section 2.3.3.3). Rb-Sr ages obtained from biotite grains preserved in unmodified Lewisian gneisses from regions within, and to the north, of the South Harris Shear Zones are consistent with the exhumation of Lewis and north Harris relative to south Harris and the Uists around c.1100Ma

(Cliff & Rex 1989). Butler (1995) has suggested that exhumation of the northern Outer Hebrides is compatible with oblique dextral movements across the South Harris Shear Zones, and has therefore argued that mylonitisation along the OHFZ must have ceased prior to 1100Ma. Observations made during the present study are entirely consistent with Butler's (1995) hypothesis. In the absence other evidence, it is therefore concluded that mylonitisation must have occurred some time between the late Laxfordian (c.1700Ma) and Grenvillian (c.1100Ma) 'events' in the Outer Hebrides.

#### **9.2.2.2 Kinematic evolution of the pervasive mylonite belt**

The mylonitic foliation is associated with a well developed, SE-plunging mineral lineation (Figs. 3.5, 3.8 & 3.10). Shear sense criteria viewed in surfaces parallel to the mineral lineation and perpendicular to the foliation are everywhere consistent with top-to-the-NW thrusting (Chapters 4 & 5).

#### **9.2.2.3 Textural evolution of the pervasive mylonite belt**

##### ***Lower amphibolite facies mylonite***

A N-S trending belt of lower amphibolite facies mylonite is exposed in the region between Loch Erisort and Loch Sgibacleit (Figs. 3.3 & 3.4; section 3.2.2.1). The lower amphibolite facies mylonites were derived directly from Lewisian protoliths, and comprise interbanded packages of quartzo-feldspathic mylonite, protomylonite, ultramylonite and mafic protomylonite (Chapter 4). During macroscopically ductile deformation of the gneissose protoliths, the quartz grains were progressively flattened parallel to the regional foliation. The quartz ribbons, which typically display extremely high aspect ratios ( $\leq 100:1$ ) (section 4.2.2.1), appear to have deformed predominantly by dislocation glide and subgrain rotation recrystallisation at low strains, and by grain boundary migration recrystallisation at higher strains (section 4.2.3.2). In contrast, the feldspar and hornblende grains deformed predominantly by intragranular fracture  $\pm$  limited dynamic recrystallisation along grain margins (sections 4.2.3.2). Consequently, packages of highly strained, lower amphibolite facies mylonite and ultramylonite are characterised by isolated, sub-equant feldspar and / or hornblende porphyroclasts, which 'float' in a fine grained, contiguous matrix of dynamically recrystallised quartz ( $\pm$  dynamically recrystallised feldspar, hornblende and biotite). These observations suggest that the load-bearing framework microstructure of the protolith gneisses was replaced by an *interconnected weak layer* (IWL) microstructure (Handy 1990) (section 1.5.2.2). If this inference is correct, the rheological behaviour of highly strained lower amphibolite facies mylonite is likely to have been controlled by the rheological behaviour of the quartz ribbons and

dynamically recrystallised feldspar. The breakdown of the feldspar- / hornblende-dominated load-bearing framework was clearly brought about by progressive crystal plastic deformation (i.e. ribboning) of quartz and by intragranular fracturing / dynamic recrystallisation of the feldspar and hornblende porphyroclasts i.e. *the transition from a LBF microstructure to an IWL microstructure was strain-induced*. Breakdown of the load-bearing framework was *locally* enhanced by melt generation and subsequent grain-size sensitive, viscous deformation of the glassy / cryptocrystalline pseudotachylyte veins (sections 4.2.3.3 & 4.2.3.4).

### ***Upper greenschist facies mylonite***

NE-SW trending belts of upper greenschist facies mylonite are exposed on Scalpay and around Loch Bhrollum, whilst N-S trending mylonite belts are exposed at Kebock Head and Aird Raerinish (Figs. 3.3, 3.7, 3.9 & 3.19) (sections 3.2.2.2, 3.2.2.3 & 3.2.2.4). The upper greenschist facies mylonites were derived directly from Lewisian protoliths, and comprise interbanded packages of quartzo-feldspathic mylonite and protomylonite, mafic protomylonite and banded gneiss-derived phyllonite (Chapter 5). Packages of quartzo-feldspathic mylonite are characterised by plastically deformed, dynamically recrystallised quartz ribbons, which wrap around isolated aggregates and porphyroclasts of relatively unaltered, fractured feldspar. The quartzo-feldspathic mylonites are therefore characterised by an interconnected weak layer microstructure, similar to that observed in the lower amphibolite facies mylonites. If this inference is correct, it is likely that (a) the rheological behaviour of the quartzo-feldspathic mylonites was controlled by the rheological behaviour of the interconnected quartz ribbons, and that (b) the breakdown of the feldspar-dominated, load-bearing framework of the banded gneiss protoliths was controlled by progressive crystal plastic deformation of quartz and fracturing of feldspar grains i.e. *the transition from a LBF microstructure to an IWL microstructure was strain-induced*.

In contrast, packages of upper greenschist facies phyllonite comprise isolated, partially altered, fractured feldspar porphyroclasts and aggregates, which are wrapped networks of interconnected sericite strands and quartz ribbons (section 5.2.2.2). Experimental evidence suggests that under given temperature and strain rate conditions, both quartz *and* sericite are significantly weaker than feldspar (e.g. Tullis & Yund 1992; Mares & Kronenberg 1993; Shea & Kronenberg 1993) (section 1.5.2.1). Thus, packages of upper greenschist facies phyllonite are characterised by an IWL microstructure. This observation is consistent with the rheological behaviour of the phyllonite bands having been controlled by the rheological behaviour of the contiguous quartz ribbons and sericite strands. Detailed microstructural studies have demonstrated that the sericite strands developed in response to syn-tectonic retrogression and hydration of

existing feldspar grains (section 5.2.3.1). It is therefore postulated that the breakdown of the feldspar-dominated, load-bearing framework of the banded gneiss protoliths was controlled (a) by progressive crystal plastic deformation of quartz, and fracturing of feldspar, and (b) by syn-tectonic breakdown of feldspar to aggregates of fine-grained sericite, in response to the influx of chemically active hydrous fluids during thrusting. *Thus, the transition from a load-bearing framework microstructure to an interconnected weak layer microstructure was partly strain-induced and partly reaction-modified.*

Packages of upper greenschist facies mafic protomylonite comprise interlocking aggregates of granoblastic hornblende grains, which surround pockets of partially altered, flattened feldspar grains  $\pm$  quartz. The hornblende grains are commonly observed to be cross-cut by intra- and transgranular tensile veins. However, the LBF microstructure of the amphibolite protoliths appears, in essence, to be intact. Thus, deformation was strongly partitioned into packages of upper greenschist facies quartzo-feldspathic mylonite and phyllonite.

The effects of upper greenschist facies retrogression on the rheology of the fault zone will be discussed further in sections 9.5 and 9.6.

#### **9.2.2.4 Metamorphic conditions and crustal depths**

The lower amphibolite facies mylonites appear to have developed in 'dry', fluid-absent crust (Chapter 4). In contrast, the upper greenschist facies mylonites appear to have developed in 'wet', fluid-rich crust (Chapter 5). On the basis of the observed field relationships, and qualitative considerations of metamorphic reaction kinetics, it has been argued that the lower amphibolite and upper greenschist facies fabrics developed synchronously, during regional top-to-the-NW thrusting (section 3.2.2.5). The temperature at which deformation occurred can be estimated either by locating the syn-tectonic mineral assemblage on a petrogenetic grid (e.g. O'Hara 1988) (Fig. 1.8) (Table 9.2), or by comparing the observed deformation microstructures with the microstructures of experimentally deformed rocks (e.g. O'Hara 1988; Stewart 1997) (Tables 1.1 & 9.2).

*Temperature estimates from syn-tectonic mineral assemblages*

<b>Fault rock</b>	<b>Syn-tectonic mineral assemblage</b>	<b>Temperature estimate</b>
<b>Lower amphibolite facies mylonite</b>	Ca-plagioclase, K-feldspar, quartz, hornblende, garnet, biotite.	450 to 500°C
<b>Upper greenschist facies mylonite</b>	Ca-plagioclase, K-feldspar, albite, quartz, hornblende, actinolite, biotite, epidote.	400 to 450°C

**Table 9.1** Temperature estimates for deformation within the pervasive mylonite belt, based on syn-tectonic mineral assemblages (see Fig. 1.8).

*Temperature estimates from deformation microstructures*

<b>Fault rock</b>	<b>Deformation microstructures</b>	<b>Temperature estimate</b>
<b>Lower amphibolite facies mylonite</b>	Dynamically recrystallised quartz ribbons with oblique foliations; intragranular fracturing and limited dynamic recrystallisation of feldspar and hornblende.	450 to 500°C. Oblique foliation in quartz suggests higher end of this range may be more appropriate.
<b>Upper greenschist facies mylonite</b>	Dynamically recrystallised quartz ribbons, local core-and-mantle structures; fracturing and local neocrystallisation of feldspar; undulose hornblende.	400 to 450°C. Presence of hydrous fluids suggests that lower end of this range may be more appropriate.

**Table 9.2** Temperature estimates for deformation within the pervasive mylonite belt, based on the observed deformation microstructures (see Table 1.1).

Assuming an average geothermal gradient of  $c.30^{\circ}\text{C km}^{-1}$ , it is postulated that lower amphibolite facies deformation occurred at depths of between 15km and 17km. However, it is unclear if the observed difference in metamorphic grade within the pervasive mylonite belt reflects deformation at different crustal levels, or whether it

can be attributed to the influx of relatively cool, hydrous fluids during upper greenschist facies deformation. If it is assumed that the geothermal gradient was *not* significantly perturbed by fluid influx (i.e. the geotherm remained at c.30°C km<sup>-1</sup>), deformation during upper greenschist facies mylonitisation probably occurred at between 13km and 15km depth. Given the uncertainties inherent in the temperature estimates (Chapter 1), it is postulated (a) that mylonitisation during upper greenschist and lower amphibolite facies deformation occurred at similar crustal depths, and (b) that the apparent difference in metamorphic grade was caused by localised influx of hydrous fluids. The geochemical and thermodynamic characteristics of the fluids are discussed in sections 9.3 & 9.4.

### 9.2.3 CATACLASITE AND PSEUDOTACHYLYTE

Four distinct groups of cataclasite- and / or pseudotachylyte-bearing structures have been recognised along the OHFZ.

- *'Early' pseudotachylyte veins*, which developed synchronously with viscous, lower amphibolite facies mylonitisation at Loch Sgibacleit. The 'early' pseudotachylyte veins have been discussed extensively in Chapter 4, and are not considered further in this section.
- *Foliation-parallel, pseudotachylyte-bearing fault zones* and associated *pseudotachylyte-ultramylonite crush zones*, which are commonly observed within, and were derived from, packages of lower amphibolite facies mylonite (section 4.3).
- *Pseudotachylyte-ultracataclasite crush zones*, which are commonly observed throughout the Uists, Eriskay and the Barra Isles (Chapters 3, 6 & 7).
- *Crush melange*, which is preserved on North Uist and Eriskay (Chapters 3 & 6). The pseudotachylyte-ultracataclasite crush zones and crush melange were derived directly from gneissose protoliths.

#### 9.2.3.1 Timing of brittle deformation

##### *Foliation-parallel fault zones and pseudotachylyte-ultramylonite crush zones*

The foliation-parallel fault zones and pseudotachylyte-ultramylonite crush zones are thought to have developed around the level of the primary frictional to viscous creep transition, immediately after the cessation of macroscopically ductile, lower amphibolite facies mylonitisation (section 4.3.3.2). If the upper greenschist and lower amphibolite facies mylonites are late Laxfordian or Grenvillian (c.1700Ma to

c.1100Ma) (sections 2.3.3.3 & 3.7.1), it is likely that these pseudotachylytes are the same age.

#### ***Crush melange and pseudotachylyte-ultracataclasite crush zones***

Laser-probe  $^{40}\text{Ar} / ^{39}\text{Ar}$  dating of a pseudotachylyte vein from the 'foreland' region (Grimsay; Fig. 3.28) immediately to the west of the OHFZ on North Uist has yielded a Caledonian age of  $430 \pm 6\text{Ma}$  (Kelley *et al.* 1994) (section 2.2.3.2). The age of the pseudotachylyte veins preserved in the 'foreland' relative to the crush melange / pseudotachylyte-ultracataclasite crush zones is unclear from the available field evidence. However, previous authors have argued that localised deformation and pseudotachylyte generation in the 'foreland' was synchronous with pseudotachylyte generation within the crush melange and crush zones (Sibson 1977b; Butler 1995) (sections 3.4.2.4 & 3.5.2.4). If this inference is correct, it is likely that *the crush melange and the pseudotachylyte-ultracataclasite crush zones are significantly younger than the foliation-parallel, pseudotachylyte-bearing fault zones preserved on Lewis.*

#### **9.2.3.2 Fault zone kinematics during pseudotachylyte generation**

##### ***Foliation-parallel fault zones and pseudotachylyte-ultramylonite crush zones***

Pseudotachylyte veins preserved within the foliation-parallel fault zones and pseudotachylyte-ultramylonite crush zones at Loch Sgibacleit appear to have developed either during localised *compression* or localised *extension* (section 4.3.1). Thus, it has not been possible to directly determine the overall sense of shear during late Laxfordian / Grenvillian brittle deformation. However, it has been argued that both the lower amphibolite facies mylonites and the foliation-parallel fault zones developed during a single, progressive deformation event. If this inference is correct, it is likely that the foliation-parallel fault zones developed during regional top-to-the-NW thrusting (see discussion in section 4.3.3.2).

##### ***Crush melange and pseudotachylyte-ultracataclasite crush zones***

The fine grained, jointed nature of the crush melange and pseudotachylyte-ultracataclasite crush zones precludes detailed kinematic analysis (sections 3.4.2 & 3.5.2). It has not, therefore, been possible to directly determine the overall sense-of-shear during cataclasis and pseudotachylyte generation. Previous authors have suggested that localised deformation in the 'foreland' was synchronous with cataclasis and pseudotachylyte-generation within the crush melange and pseudotachylyte-ultracataclasite crush zones. It has therefore been suggested that the preponderance of

E- and (locally) W-dipping *compressional* structures in the 'foreland' is consistent with brittle deformation having occurred during regional, top-to-the-W thrusting along the OHFZ (Sibson 1977b; Butler 1990) (sections 3.4.2.4 & 3.5.2.4). However, the pseudotachylyte-bearing faults exposed in the 'foreland' region on the Barra Isles are predominantly *extensional* in nature (section 3.6). Owing to limited exposure in the Sound of Barra region, the relationship between these structures and the compressional structures exposed in the Uists is unclear (Figs. 3.3, 3.42 & 3.43) (see discussions in section 3.6.2). In the absence of more compelling evidence to the contrary, the present author therefore concurs with Sibson (1977b) and Butler (1995) and concludes that cataclasis and pseudotachylyte generation in the Uists were synchronous with regional, top-to-the-W Caledonian thrusting.

### 9.2.3.3 Textural evolution during brittle deformation

#### *Foliation-parallel fault zones and pseudotachylyte-ultramylonite crush zones*

The foliation-parallel fault zones and crush zones were derived directly from lower amphibolite facies mylonite. Foliation-parallel fault zones are relatively narrow, tabular bands ( $\leq 2\text{m}$  thick) of intense brittle deformation which are enclosed, or bounded on one side, by pseudotachylyte-bearing, foliation-parallel faults. The intensely deformed bands comprise randomly oriented blocks of fractured mylonite, which are locally intruded by pseudotachylyte injection veins (section 4.3.1.2). The overall effect of brittle deformation has been to *locally disrupt* the continuity of the pre-existing mylonitic fabric (Fig. 4.5).

The pseudotachylyte-ultramylonite crush zones ( $\leq 5\text{m}$  thick) comprise aggregates of ultrafine-grained, intensely fractured pseudotachylyte and ultramylonite. Detailed microstructural observations suggest that the crush zones are the result of many episodes of melting and pseudotachylyte generation (section 4.3.2.2). The overall effect of repeated melt generation has been to cause extreme, *localised grain-size reduction, and to locally destroy the pre-existing mylonitic fabric*. The rheological evolution and fluid transport properties of the OHFZ during late Laxfordian / Grenvillian brittle thrusting will be discussed in sections 9.4, 9.5 and 9.6.

#### *Crush melange and pseudotachylyte-ultracataclasite crush zones*

The crush melange ( $\geq 1000\text{m}$  thick on North Uist) was derived directly from Lewisian protoliths, and comprises fractured, angular blocks of gneiss ( $\leq 100\text{m}$  diameter, but whose dimensions vary by up to four orders of magnitude), which 'float' in a fine-grained matrix of cataclasite and devitrified pseudotachylyte (section 6.2). The crush melange appears to have developed in response to distributed, grain-scale brittle

fracturing and frictional melting. The overall effect of brittle deformation has been (a) *to cause extreme grain size reduction*, and (b) *to disrupt the pre-existing gneissose fabrics, over an extremely wide region* (e.g. Fig. 3.28).

The pseudotachylyte-ultracataclasite crush zones are bands of intense brittle deformation, which are developed either within crush melange (e.g. Fig. 3.28), or along major lithological contacts (e.g. Fig. 3.38). The crush zones comprise randomly oriented clasts of gneiss ( $\leq 1\text{m}$  diameter, but whose dimensions vary by up to four orders of magnitude), which float within an ultrafine-grained matrix of devitrified pseudotachylyte and / or ultracataclasite. Microstructural observations suggest that the crush zones developed in response to many episodes of melting and pseudotachylyte generation. The overall effect of brittle deformation has been (a) *to cause extreme grain size reduction*, and (b) *to locally destroy the pre-existing Laxfordian fabrics*. The rheological evolution and fluid transport properties of the OHFZ during Caledonian brittle thrusting will be discussed in sections 9.4, 9.5 and 9.6.

#### 9.2.3.4 Metamorphic conditions and crustal depths

Late Laxfordian / Grenvillian and Caledonian brittle deformation are both inferred to have taken place in dry, fluid-absent crust (sections 3.4.2.4 & 4.3.3.1). Retrogression, therefore, is likely to have been inhibited by the lack of hydrous fluids. Thus, deformation microstructures have therefore been used to estimate the temperatures at which brittle thrusting and pseudotachylyte generation took place.

<b>Fault rocks / structures</b>	<b>Deformation microstructures</b>	<b>Temperature estimate</b>
<b>Foliation-parallel fault zones / pseudotachylyte-ultramylonite crush zones (late Laxfordian / Grenvillian)</b>	Non-vesicular pseudotachylyte; evidence for adhesive wear (see Swanson 1992).	Direct temperature estimate not possible, but probably developed near base of 'seismogenic' crust.
<b>Crush melange / pseudotachylyte-ultracataclasite crush zones (Caledonian)</b>	Fractured quartz and feldspar; undulose quartz grains, but no evidence for recovery (low temperature plasticity).	250 to 300°C. The absence of recovery microstructures in quartz suggests that the lower end of this range may be more appropriate.

**Table 9.3** Temperature estimates of late Laxfordian / Grenvillian and Caledonian brittle thrusting along the OHFZ (see Table 1.1).

Although it is not possible to obtain *direct* estimates for the temperature of late Laxfordian / Grenvillian deformation, the deformation microstructures are consistent with brittle thrusting having occurred near the base of the crustal seismogenic zone (Swanson 1992) (see discussion in section 4.3.3.1). The distribution of earthquake hypocentres obtained from currently active fault zones, suggests that the seismogenic zone extends to between 10km and 15km depth within the continental crust (e.g. Figure 5.7 of Hill *et al.* 1990). It is therefore postulated that late Laxfordian / Grenvillian thrusting took place in dry crust, at depths of between 10km and 15km. Assuming an average geothermal gradient of  $30^{\circ}\text{C km}^{-1}$ , it is likely that Caledonian thrusting took place at 8km to 9km depth within the crust. Thus, *late Laxfordian / Grenvillian brittle thrusting probably occurred at significantly greater depths than Caledonian brittle thrusting.*

#### **9.2.4 LOWER GREENSCHIST FACIES FABRICS**

Four different types of lower greenschist facies tectonite have been recognised along the OHFZ:

- *Phyllonitic shear zone fabrics, which localised along pre-existing bands of upper greenschist facies phyllonite.* Such fabrics are commonly observed on Scalpay, in southeast Lewis and at Kebock Head (Chapter 5; sections 3.2.3.2 & 3.2.3.3).
- *Phyllonitic shear zone fabrics (including the discrete phyllonite bands), which localised along pre-existing brittle fault zones.* Such fabrics are commonly observed throughout the Uists, at Eishken and on Eriskay (Chapters 6 & 7; sections 3.2.3.1 & 3.6.1).
- *Pervasive protophyllonitic fabrics, which localised within regions of relatively undeformed, fractured gneiss.* Such fabrics are commonly observed on North Uist and Eriskay (Chapter 6; section 3.6.1)
- *Lower greenschist facies, quartzo-feldspathic mylonites, which localised along pre-existing bands of upper greenschist facies quartzo-feldspathic mylonite.* Such fabrics are locally preserved on Scalpay (Chapter 5).

##### **9.2.4.1 Timing of lower greenschist facies deformation**

The lower greenschist facies phyllonites and quartzo-feldspathic mylonites preserved in the Northern Zone of the OHFZ locally deform and overprint the late Laxfordian / Grenvillian mylonites. The lower greenschist facies phyllonites preserved in the Southern Zone of the OHFZ locally deform and overprint thrust-related, Caledonian

cataclasites and pseudotachylytes (section 9.2.4.1). It is therefore likely that phyllonitisation post-dates brittle Caledonian thrusting. Whole-rock K-Ar ages obtained from samples of lower greenschist facies phyllonite from Scalpay, North Uist, Ronay and South Uist typically fall between 471Ma and 394Ma (Sibson 1977b). These dates are consistent with a late Caledonian age for lower greenschist facies deformation.

The lower greenschist facies phyllonites are commonly observed to have been reworked during top-to-the-S or -E extension (see next section). Packages of intensely deformed, reworked phyllonite are exposed on Stuley (Chapter 7), and are locally cross-cut by undeformed, WNW-ESE trending camptonite dykes. Rb-Sr ages obtained from similar camptonite dykes which outcrop on Orkney and the Scottish mainland are consistent with intrusion having occurred around c.300Ma (i.e. during the Permo-Carboniferous) (Fettes *et al.* 1992). Macroscopically ductile, lower greenschist facies reworking within the phyllonite belts must therefore have ceased prior to the Permo-Carboniferous. Most previous authors have postulated that a late Caledonian age is most likely for extensional reworking (Sibson 1977b; Butler 1995, but cf. Walker 1990).

#### 9.2.4.2 Kinematic evolution of the lower greenschist facies fabrics

The kinematic evolution of the lower greenschist facies fault rocks has been discussed extensively in previous sections (see Chapter 3 for an overview), and is summarised in Table 9.4. The salient points to note are (a) that the lower greenschist facies fabrics developed during regional sinistral (top-to-the-NE or -E) strike-slip and (b) that the *phyllonitic* fabrics were reactivated and reworked during subsequent regional transtension / extension.

Locality	Kinematics
Southeast Lewis	1. Top-to-E sinistral strike-slip; 2. Top-to-S extension.
Scalpay	1. Top-to-NE sinistral strike-slip; 2. Top-to-SW dextral strike-slip.
North Uist	1. Top-to-WNW transpression; 2. Top-to-NE sinistral strike-slip; 3. Sinistral transtension; 4. Top-to-E extension.
South Uist	1. Top-to-NE sinistral strike-slip; 2. Sinistral transpression; 3. Top-to-E extension.

**Table 9.4** Table summarising the kinematic evolution of the lower greenschist facies phyllonite belts preserved along the OHFZ.

### 9.2.4.3 Textural evolution of the lower greenschist facies fabrics

#### ***Phyllonitic shear zone fabrics which localised along bands of upper greenschist facies phyllonite***

Phyllonitic shear zone fabrics which localised along pre-existing bands of upper greenschist facies phyllonite comprise isolated quartz and partially altered feldspar porphyroclasts, which 'float' in a matrix of interconnected sericite strands and polycrystalline quartz ribbons. These lower greenschist facies fabrics are therefore characterised by an interconnected weak layer microstructure. It is therefore likely that the rheology of such phyllonites was controlled by the rheological behaviour of the contiguous sericite strands and quartz ribbons. Detailed microstructural observations suggest that the sericite strands developed in response to syn-tectonic alteration and hydration of the existing feldspar grains. However, it is important to emphasise that the primary fabrics (i.e. the upper greenschist facies phyllonites) are also characterised by an interconnected weak layer microstructure. The breakdown of the protolith gneissés was therefore a two-stage process, which involved (a) *strain-induced (i.e. dynamic recrystallisation / neocrystallisation) and reaction-modified (i.e. sericitisation of feldspar) grain size reduction during upper greenschist facies thrusting*, followed by (b) *continued reaction-modified (i.e. sericitisation of feldspar) grain size reduction during lower greenschist facies strike-slip*, in response to the influx of chemically active hydrous fluids into the fault zone. The large-scale geometry and distribution of the lower greenschist facies fabrics appears to have been controlled by the distribution of the pre-existing upper greenschist facies fabrics (see discussion in section 5.4.4.3).

The phyllonitic fabrics are commonly observed to have been folded and / or disrupted by the emplacement of quartz-carbonate-albite-chlorite veins during subsequent extension / dextral strike-slip related reworking. Folding is locally associated with the development of a weak, axial planar crenulation cleavage. The rheological evolution of the fault zone during phyllonitisation and subsequent reworking is discussed further in sections 9.5 & 9.6.

#### ***Phyllonitic shear zone fabrics which localised along pre-existing brittle fault zones***

Phyllonites which developed along pre-existing brittle fault zones comprise isolated quartz and partially altered feldspar porphyroclasts, which 'float' in an ultrafine-grained, polymineralic matrix of albite, epidote, quartz, chlorite and sericite strands. Strain appears to have been strongly partitioned into the ultrafine grained matrix. These lower greenschist facies fabrics are therefore characterised by an interconnected weak layer microstructure. Thus, it is likely that the rheology of phyllonitic shear

zones was controlled by the rheological behaviour of the contiguous, ultrafine-grained matrix. Detailed microstructural observations suggest that the matrix was partly derived from the syn-tectonic alteration of feldspar and hornblende grains, and partly derived from pre-existing, thrust-related cataclasite and pseudotachylyte (see discussion in section 6.3.3.4). It is therefore postulated that the breakdown of the load-bearing framework of the protolith gneisses was essentially a two-stage process, which involved (a) *localised, strain-induced grain size reduction during cataclasis / pseudotachylyte generation* (section 9.2.4.2), followed by (b) *reaction-modified grain size reduction during phyllonitisation*, in response to the influx of chemically active hydrous fluids into the fault zone at the onset of sinistral transpression / strike-slip. The large-scale geometry of the phyllonitic shear zones appears to have been controlled by the architecture of pre-existing brittle fault systems (see discussion in section 6.3.4).

The phyllonitic fabrics are commonly observed to have been folded and / or disrupted by the emplacement of shear and tensile quartz-albite-chlorite-carbonate veins during subsequent transtension / extension-related reworking. Folding was associated with the development of an axial planar crenulation cleavage. The crenulation cleavage is locally dominant, and obliterates all earlier fabrics.

#### ***Pervasive protophyllonite***

Pervasive protophyllonitic fabrics are commonly observed to overprint regions of relatively undeformed, fractured gneiss within the crush melange. Pervasive protophyllonite comprises fractured quartz, feldspar and hornblende grains, which are *locally* wrapped by laterally discontinuous sericite strands. These observations suggest that the feldspar- (or hornblende-) dominated load-bearing framework was locally broken down to form a sericite-dominated interconnected weak layer microstructure. It has been demonstrated that the quartz, feldspar and hornblende grains deformed predominantly by intragranular fracturing, whilst the sericite strands developed in response to syn-tectonic retrogression and hydration of feldspar. Thus, it is postulated that the transition from a load-bearing framework to an interconnected weak layer microstructure was *partly strain- (i.e. fracture-) induced and partly reaction-modified*.

#### ***Lower greenschist facies quartzo-feldspathic mylonites***

Packages of lower greenschist facies, sinistral strike-slip related quartzo-feldspathic mylonite, which are only exposed on Scalpay, developed within pre-existing bands of upper greenschist facies, thrust-related quartzo-feldspathic mylonite. The lower greenschist facies fault rocks comprise isolated, fractured K-feldspar porphyroclasts,

which 'float' in an ultrafine grained matrix of polycrystalline quartz, albite and sericite strands. The lower greenschist facies mylonites are therefore characterised by an interconnected weak layer microstructure, whose rheology was probably controlled by the mechanical behaviour of the ultrafine grained, polymineralic matrix. Microstructural observations suggest the polycrystalline quartz aggregates developed in response to dynamic recrystallisation, and that albite and sericite were derived from neocrystallisation and / or alteration of the K-feldspar and plagioclase grains (see discussion in section 5.4.3.2). It is postulated that the breakdown of the load-bearing framework observed in the protolith gneisses was a two-stage process, which involved (a) *strain-induced grain size reduction by dynamic recrystallisation during upper greenschist facies mylonitisation*, and (b) *strain-induced and reaction-modified grain size reduction during lower greenschist facies mylonitisation*. There is no evidence to suggest that the lower greenschist facies, quartzo-feldspathic mylonites were reworked during subsequent dextral strike-slip.

#### 9.2.4.4 Metamorphic conditions and crustal depths

##### *Temperature estimates from syn-tectonic mineral assemblages*

<b>Fault rock</b>	<b>Syn-tectonic mineral assemblage</b>	<b>Temperature estimate</b>
<b>Sinistral strike-slip related phyllonite / mylonite</b>	Albite, sericite, quartz, epidote, chlorite, actinolite.	200 to 350°C
<b>Dextral strike-slip / extension-related reworked phyllonite</b>	Albite, sericite, quartz, chlorite, epidote ± calcite.	200 to 350°C

**Table 9.5** Temperature estimates for deformation during lower greenschist facies deformation, based on syn-tectonic mineral assemblages (see Fig. 1.8).

*Temperature estimates from deformation microstructures*

<b>Fault rock</b>	<b>Deformation microstructures</b>	<b>Temperature estimate</b>
<b>Sinistral strike-slip related phyllonite / mylonite</b>	Undulose quartz grains, locally recrystallised; neocrystallised albite; flame perthite locally.	250 to 400°C. Hydrolytic weakening of quartz suggests lower end of temperature range more likely.
<b>Dextral strike-slip / extension-related reworked phyllonite</b>	Undulose quartz grains, locally recrystallised; neocrystallised albite; Type III calcite deformation twins.	200 to 250°C, constrained from calcite deformation twins.

**Table 9.6** Temperature estimates for lower greenschist facies deformation, based on the observed deformation microstructures (see Table 1.1)

Packages of sinistral strike-slip related phyllonite are composed of albite, quartz, sericite, epidote, actinolite and chlorite. Packages of reworked phyllonite display similar mineralogies, but are characterised (a) by the absence of actinolite, and (b) by a relatively high modal abundance of calcite. For reasons discussed in section 9.3, it is postulated that the different mineral assemblages may reflect subtle changes in *fluid composition* in addition to possible changes in the ambient temperature and pressure conditions. Assuming an average geothermal gradient of  $30^{\circ}\text{C km}^{-1}$ , it is postulated that sinistral strike-slip occurred in wet crust at depths of between 8km and 12km. However, Caledonian thrusting, which occurred immediately prior to phyllonitisation, is inferred to have taken place at between 8km and 9km depth (section 9.2.4.3). It is therefore likely that sinistral strike-slip occurred towards the lower end of the possible depth range (i.e. at between 8km and 9km). The temperature of extension- / dextral strike-slip related reworking can be constrained fairly precisely by the presence of Type III calcite deformation twins (Burkhard 1993). Assuming a geothermal gradient of  $30^{\circ}\text{C km}^{-1}$ , it is postulated that reworking occurred in wet crust at depths of between 7km and 8km.

## **9.2.5 LATE BRITTLE DEFORMATION: LATE DETACHMENT FAULTS AND STEEPLY DIPPING NORMAL FAULTS**

Brittle detachment faults are commonly observed to localise within, or along the margins of, pseudotachylyte-ultracataclasite crush zones and macroscopically ductile phyllonitic shear zones. In contrast, steeply dipping normal faults are typically, though not exclusively, developed in regions of relatively unmodified gneiss.

Two distinct types of detachment fault have been recognised along the OHFZ. Type 1' detachments are foliation-parallel, shear hydraulic fractures which developed during macroscopically ductile, extension-related reworking within certain phyllonite belts on North Uist (sections 6.4.3.3 & 6.4.4). In contrast, Type 2' detachments are brittle, typically gouge-filled faults, the latest movements along which entirely post-date reworking within the phyllonite belts (e.g. Chapter 3; section 6.4.4). The following sections relate only to Type 2' structures, which are henceforth referred to as 'late' detachments. The significance of Type 1' detachments will be discussed in sections 9.4 and 9.5.

### **9.2.5.1 Regional distribution and kinematics**

The kinematics and regional distribution of late detachment faults / steeply dipping normal faults along the OHFZ are complex, and is summarised in Tables 9.7 & 9.8. In general, late detachment faults appear to be more abundant in the Southern Zone, whilst steeply dipping normal faults are more commonly observed in the Northern Zone (Chapter 2 & 3).

<b>Locality</b>	<b>Host rock lithology</b>	<b>Detachment orientation</b>	<b>Slickenline orientation / kinematics</b>
<b>Loch Sgibacleit</b>	Poorly exposed 'topographic faults' in lower amphibolite facies mylonite.	Moderately eastward dipping.	Unknown.
<b>Scalpay</b>	Upper and lower greenschist facies phyllonite.	SE-dipping.	SE-plunging (down dip). Extensional (top-to-SE).
<b>Lees, North Uist</b>	Lower greenschist facies phyllonite; pervasive; protophyllonite; unmodified gneiss.	E- to SE-dipping.	ENE-WSW trending (sub-horizontal). Sinistral strike-slip (top-to-ENE).
<b>Burrival to Eigneig Bheag, (North Uist) and Ronay</b>	Lower greenschist facies phyllonite, pervasive protophyllonite and 'topographic faults' in crush melange.	SE- or NW-dipping.	ENE-WSW trending (sub-horizontal). Sinistral strike-slip (top-to-ENE).
<b>South Uist</b>	Pseudotachylyte-ultracataclasite crush zones and Usinish Phyllonite belt.	NE- to SE-dipping.	NE-SW to NW-SE trending. Tend to be ENE-WSW to ESE-WNW trending in phyllonite belt (sub-horizontal to down-dip).
<b>Vatersay</b>	Pseudotachylyte-ultracataclasite crush zones and unmodified gneiss.	E-dipping.	SE-plunging (down-dip). Oblique extensional (top-to-SE)

**Table 9.7** Table summarising the regional distribution and structural geometries of the brittle detachment faults.

<b>Locality</b>	<b>Host rock lithology</b>	<b>Fault plane orientation</b>	<b>Slickenline orientation / kinematics</b>
<b>Northeast Lewis</b>	Unmodified gneiss, Stornoway Formation sediments.	Predominantly SE-dipping, also NE- and SW-dipping.	Predominantly SE-plunging (down-dip). Predominantly extensional (top-to-SE).
<b>Loch Sgibacleit</b>	Lower amphibolite facies mylonite, pseudotachylite-ultramylonite crush zones.	ESE-dipping.	SE-plunging (down-dip), locally NNE-SSW trending (sub-horizontal). Predominantly extensional (top-to-SE).
<b>Vatersay</b>	Unmodified gneiss.	E-dipping.	Apparent extensional displacements.

**Table 9.8** Table summarising the regional distribution and structural geometry of the steeply dipping normal faults.

### 9.2.5.2 Fault kinematics

#### *Detachment faults*

*Scalpay* Late detachment faults are commonly observed along the margins of the lower greenschist facies phyllonite and mylonite belts exposed in southeast Scalpay. The detachment faults are typically associated with down-dip, SE-plunging slickenlines (Fig. 3.21c). Shear sense criteria, such as the geometries of subsidiary fracture sets, are consistent with top-to-the-SE, extensional displacements along the detachment faults.

*North Uist* Late detachment faults exposed on North Uist are typically associated with sub-horizontal, ENE-WSW trending slickenlines (Figs. 3.36 a & b). The geometries of subsidiary fracture sets are consistent with sinistral strike-slip / transtensional (i.e. top-to-the-ENE) displacements along the detachment faults.

*South Uist* The distribution of late detachments on South Uist is complex. NE- to ESE-dipping detachments, associated with NE-SW to NW-SE trending slickenlines, are commonly observed within the pseudotachylite-ultracataclasite crush zones developed along the base of the OHFZ (Figs. 3.38 & 3.40) (section 3.5.2). The

geometries of subsidiary fracture arrays are consistent with either top-to-the-SE or top-to-the-NE displacements along the detachment faults. The relative timing of top-to-the-SE and top-to-the-NE movements are generally unclear, although Butler (1995) has described an ESE-dipping detachment fault which displays both ENE- and SE-plunging slickenlines (NF 813 202) (Fig. 3.38). The ENE-plunging slickenlines appear to overprint the SE-plunging slickenlines. These observations suggest that the detachment fault may have *initiated* during top-to-the-SE shear, and was subsequently *reactivated* during top-to-the-ENE shear (Butler 1995).

Detachment faults which are developed within, or along the margins of, the Usinish Phyllonite belt dip towards the SE or NE, and are associated with NE-SW to ESE-WNW trending slickenlines (Fig. 3.41b). The geometries of subsidiary fracture arrays are consistent with either top-to-the-NE or top-to-the-ESE shear along the detachment faults.

*Vatersay* Moderately E-dipping detachment faults are locally developed either along the margins of pseudotachylite-ultracataclásite crush zones, or within regions of relatively unmodified gneiss, in eastern Vatersay. The fault planes are typically associated with SE-plunging slickenlines. The geometries of subsidiary fracture arrays are consistent with extensional (i.e. top-to-the-SE) displacements along the detachment surfaces.

### ***Steeply dipping normal faults***

*Northeast Lewis and Loch Sgibacleit* Steeply dipping normal faults are commonly observed in northeast Lewis and at Loch Sgibacleit. In northeast Lewis, the SE-, NE- and SW-dipping fault planes are associated with predominantly SE-plunging slickenlines (Fig. 3.26). The geometries of subsidiary fracture arrays and metre-scale duplexes are consistent with top-to-the-SE displacements (i.e. regional extension) along the principal fault planes (e.g. Fig. 3.23). Around Loch Sgibacleit, the ESE-dipping faults are associated with SE- (locally NNE) plunging slickenlines. Centimetre-scale offsets of the mylonitic foliation are consistent with the faults having accommodated top-to-the-SE (i.e. extensional) displacements.

*Vatersay* An array of steeply E-dipping faults is developed in the hangingwall of an E-dipping detachment fault in eastern Vatersay (section 3.6.2.1). Slickenlines have not been observed, but the geometries of subsidiary fracture arrays are consistent with apparent extensional (i.e. top-to-the-E) displacements along the steeply dipping fault surfaces. The intersection between the steeply dipping structures and the shallowly dipping detachment fault is partly obscured by boulders. However, neither the detachment fault, or the steeply dipping normal faults appear to have been

significantly displaced. It is therefore postulated that both sets of structures developed during the same deformation event.

### 9.2.5.3 Timing and kinematic model for late brittle deformation

#### *Caledonian top-to-the-SE extension*

Detachment faults are commonly observed to cross-cut and disrupt the macroscopically ductile, lower greenschist facies phyllonitic fabrics. This observation demonstrates that the *latest* movements along the detachment fault must post-date macroscopically ductile reworking within the phyllonite belts. However, it has been postulated that detachment faults on Scalpay may have *initiated* synchronously with macroscopically ductile reworking within the phyllonite belts (section 3.2.3.5). Late Caledonian reworking in the Northern Zone of the OHFZ appears to have been associated with a S-directed regional displacement vector. The NE-SW trending phyllonite belts which outcrop on Scalpay were therefore oriented oblique to the regional displacement direction. The geometries of reworked fabrics preserved within these phyllonite belts are consistent with top-to-the-SW, dextral strike-slip. Thus, it has been argued that regional top-to-the-S displacements must have locally been *partitioned* into components of dextral strike-slip, within the NE-SW trending phyllonite belts, and top-to-the-SE extension, accommodated along SE-dipping detachment faults (Fig. 3.22 and see discussion in section 3.2.3.5).

#### *Mesozoic top-to-the-E and -SE extension*

Late detachment faults exposed in the Uists locally preserve evidence of top-to-the-E or -SE movements, whilst steeply dipping normal faults preserved on Vatersay and northeast Lewis typically display evidence of top-to-the-E extension (Table 9.8). In general, it is not possible to determine the relative ages of the detachment faults and steeply dipping normal faults. However, if the field relationships observed on Vatersay (section 3.6.2.1) are applicable to the OHFZ as a whole, it is likely that the detachment faults and the steeply dipping normal faults were active at broadly the same time. The faults exposed on Vatersay all appear to have developed during top-to-the-E or -SE extension. It is therefore postulated that regional, eastward directed extension along the OHFZ was accommodated by movements along moderate to shallowly dipping detachment faults *and* steeply dipping normal faults. Possible controls on fault geometry during extension are discussed in section 9.5.

Field and offshore seismic studies suggest that the steeply dipping normal faults controlled the development of the Mesozoic North Minch and Sea of the Hebrides basins, which occur in the hangingwall of the more shallowly-dipping OHFZ (Steel &

Wilson 1975; Sibson 1977b; Butler 1995; Stein 1988) (Figs. 2.7, 2.8 & 2.10) (Chapter 2). It is therefore postulated that top-to-the-E and -SE onshore displacements along the detachment faults and steeply dipping normal faults are likely to have been of Mesozoic age.

### *Oligocene sinistral strike-slip*

Butler (1995) has suggested that the detachment faults exposed in South Uist were locally reactivated during top-to-the-ENE shear (i.e. regional transtension). Although direct overprinting relationships are generally lacking, the preponderance of ENE-WSW trending slickenlines throughout the Uists is consistent with top-to-the-ENE transtension having been the *final* phase of deformation to have been accommodated along the detachment faults. If this inference is correct, it is possible that transtension in the Uists post-dates the main phase of offshore basin formation i.e. *top-to-the-ENE shear is likely to be post-Mesozoic in age*. There is insufficient onshore exposure to constrain the timing of transtension more precisely. However, Evans *et al.* (1991) have described a small, fault-bounded basin, which lies offshore immediately to the east of south Harris. The structure of the basin is poorly constrained, although it has been suggested that the deposition of Oligocene sediments was controlled by movements along the nearby Minch Fault (Fig. 9.1) (Evans *et al.* 1991). It is possible that regional top-to-the-ENE displacements along the onshore detachment faults may have been associated with Oligocene movements and basin formation along the offshore Minch Fault. Further detailed offshore studies are required to confirm this hypothesis.

The observations and inferences presented in this section are summarised in Table 9.9.

<b>Timing</b>	<b>Regional kinematic regime</b>	<b>Structures</b>
<b>Late Caledonian / pre-Mesozoic reworking within phyllonite belts</b>	Top-to-the-S extension in the Northern Zone of the OHFZ.	Dextral strike-slip related phyllonitic fabrics and SE-dipping detachment faults (on Scalpay only).
<b>Mesozoic</b>	Top-to-the-E or -SE extension.	Late detachment faults and steeply dipping normal faults.
<b>?Oligocene</b>	Top-to-the-ENE transtension (only observed in the Uists).	Reactivation of late detachment faults in the Uists.

**Table 9.9** Table summarising possible sequence of events during 'late' brittle deformation along the OHFZ.

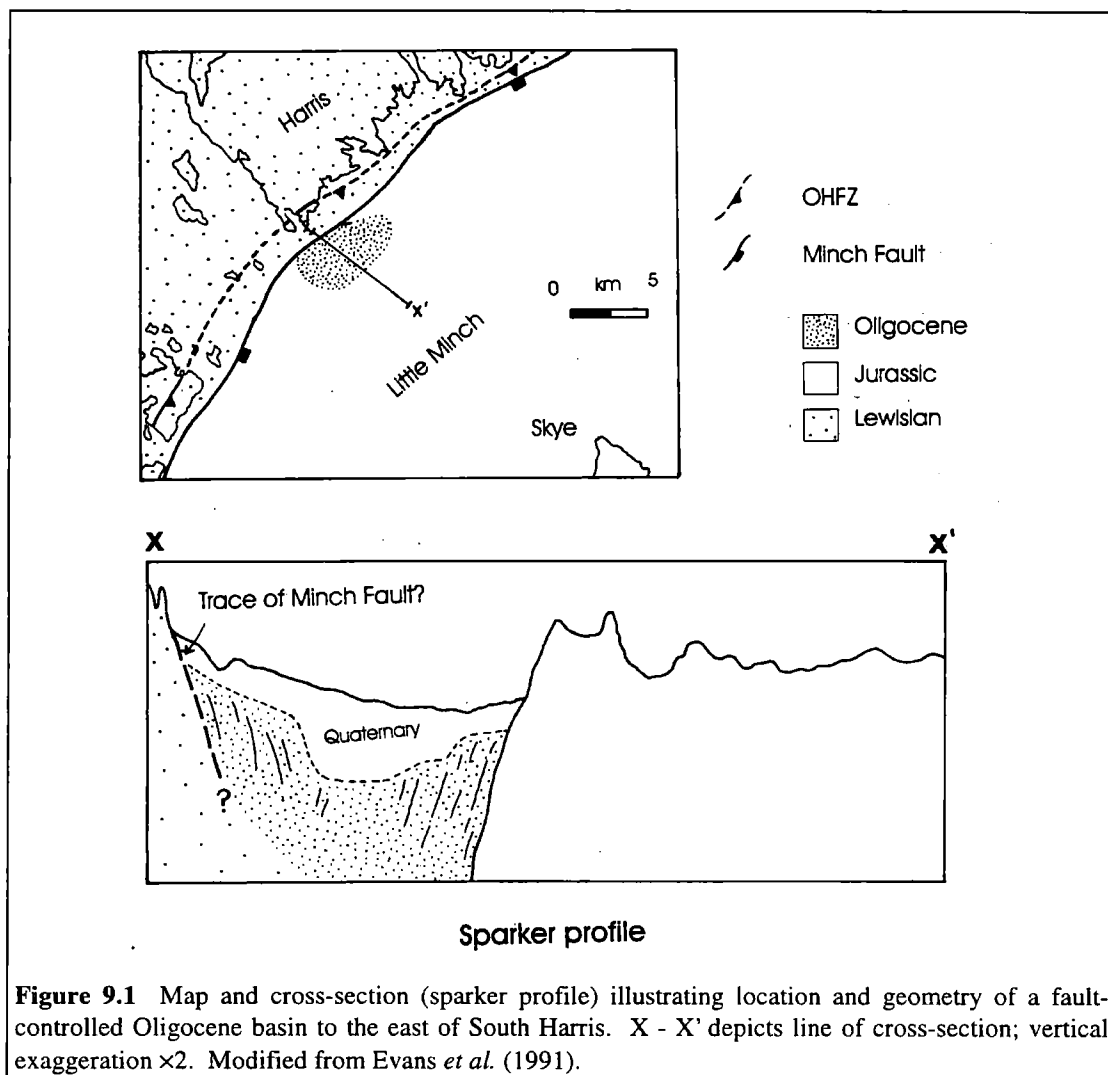


**Figure 9.1** Map and cross-section (sparker profile) illustrating location and geometry of a fault-controlled Oligocene basin to the east of South Harris. X - X' depicts line of cross-section; vertical exaggeration  $\times 2$ . Modified from Evans *et al.* (1991).

#### 9.2.5.4 Metamorphic conditions and crustal depths

The detachment faults and steeply dipping normal faults display an extremely brittle style of deformation. The fault planes are either discrete, 'polished' surfaces, or are infilled by incohesive gouges and / or breccias. Millimetre- to centimetre-scale, fault-parallel calcite and / or quartz veins are locally preserved, either within the fault gouge, or in the wall rock immediately adjacent to the fault planes (e.g. section 3.2.4). However, there is no textural evidence to suggest that deformation was controlled by hydraulic fracturing.

Detailed sedimentological studies of the Stornoway Formation sandstones and conglomerates (section 2.4) led Steel & Wilson (1975) to conclude that deposition was controlled by movements along syn-sedimentary normal faults. It is therefore postulated that the detachment faults and steeply dipping normal faults developed in the uppermost 5km of the crust, probably close to the earth's surface. Detailed studies

of the fluid inclusions preserved in syn-tectonic calcite and quartz veins are required to determine the precise pressure and temperature conditions during deformation.

### **9.2.6 TECTONIC AND METAMORPHIC MODELS OF THE OHFZ: FABRIC EVOLUTION PATHWAYS**

Observations presented in the previous sections suggest that the wide range of deformation products observed along the OHFZ can be attributed to (a) the changing *kinematic* regime and *metamorphic* conditions (i.e. pressure, temperature, fluid activity etc.) during each successive deformation event, and (b) to the effects of *geological inheritance*. Four distinct 'fabric evolution pathways', which reflect the changing tectonic and metamorphic environments during each successive deformation event, have been recognised along the OHFZ.

- *Loch Sgibacleit pathway* (Fig. 9.2): Fault rocks which developed along the 'Loch Sgibacleit pathway' are exposed in the region between Loch Erisort and Loch Sgibacleit, Lewis.
- *Scalpay pathway* (Fig. 9.3): Fault rocks which developed along the 'Scalpay pathway' are exposed on Scalpay, in southeast Lewis (between Loch Seaforth and Loch Bhrollum), at Kebock Head and possibly at Aird Raerinish and Eishken.
- *North Uist pathway* (Fig. 9.4): Fault rocks which developed along the 'North Uist pathway' are exposed in eastern North Uist, on Ronay and possibly on Eriskay.
- *South Uist pathway* (Fig. 9.5): Fault rocks which developed along the 'South Uist pathway' are only exposed in eastern South Uist.

The aim of this section is to describe the salient features of each fabric evolution pathway, as context in which to discuss the mechanisms of fault zone reactivation.

#### **9.2.6.1 Loch Sgibacleit pathway**

Rocks which have been deformed along the 'Loch Sgibacleit pathway' are characterised by a simple kinematic and structural history.

##### ***Macroscopically ductile thrusting (Late Laxfordian / Grenvillian)***

The earliest phase of late Laxfordian / Grenvillian deformation was associated with the development of macroscopically ductile, lower amphibolite facies mylonites during regional top-to-the-NW thrusting. Deformation probably took place at between 15km and 17km depth, in dry, fluid-absent crust. The main textural change

during mylonitisation was the *strain-induced* breakdown of the feldspar-dominated LBF of the protolith gneisses to produce an IWL aggregate (Fig. 9.2a). At relatively low magnitudes of macroscopically ductile finite strain, deformation was controlled by intracrystalline, crystal plastic deformation in quartz and localised, intragranular fracturing in feldspar porphyroclasts. At higher magnitudes of strain, deformation appears to have been controlled by dislocation creep within interconnected aggregates of recrystallised quartz and feldspar. Localised melting and pseudotachylyte generation during viscous deformation does not appear to have contributed significantly to the bulk strain. These observations demonstrate (a) that deformation was predominantly within the 'viscous creep regime' (Schmid & Handy 1991) (Fig. 9.2b), and (b) that viscous deformation was promoted by *thermally-activated* crystal plastic deformation in quartz and feldspar.

#### ***Reactivation of mylonitic fabrics during brittle thrusting (Late Laxfordian / Grenvillian)***

The viscously deformed mylonitic fabrics are overprinted by a series of late Laxfordian / Grenvillian thrust-related, foliation-parallel pseudotachylyte-bearing fault zones and crush zones (Fig. 9.2a). These brittle structures appear to have localised within regions of pre-existing, highly strained mylonite and ultramylonite. Thus, the strongly anisotropic primary fabrics exerted a strong control on the distribution of subsequent brittle deformation. Pseudotachylyte generation appears to have been controlled by frictional, adhesive wear mechanisms in dry crust at between 10km and 15km depth. There is little evidence to suggest that either crystal plasticity or diffusive mass transfer were important mechanisms of strain accommodation. These observations are consistent with deformation having occurred entirely within the 'frictional regime' (Schmid & Handy 1991) (Fig. 9.2b). The implications of pseudotachylyte generation in the frictional regime for fault zone rheology are discussed in sections 9.5 & 9.6.

#### ***Brittle extension (Mesozoic)***

The mylonitic fabric, foliation-parallel fault zones and pseudotachylyte-ultramylonite crush zones are locally disrupted by steeply E-dipping, Mesozoic normal faults and poorly exposed, moderately E-dipping 'topographic faults' (Fig. 9.2a). Faulting probably took place at high crustal levels ( $\leq 5$ km depth), within the frictional regime (Fig. 9.2b). The geometries of the steeply dipping normal faults were clearly *not* influenced (at least at the currently exposed levels), by the pre-existing late Laxfordian / Grenvillian fabrics.

### ***Discussion***

Each successive generation of fault rocks appears to have developed at progressively shallower levels within the crust. This observation is consistent with the Loch Sgibacleit pathway recording progressive exhumation of the OHFZ, from the late Laxfordian to the present day (Fig. 9.2b). The transition from predominantly viscous to predominantly frictional deformation occurred relatively *early* during the structural history of the OHFZ in the Loch Sgibacleit region. Microstructural observations suggest that the change from distributed, macroscopically ductile deformation to localised, brittle deformation was related to the cessation of significant crystal plasticity in quartz. Crystal plasticity is a *thermally activated* deformation mechanism (e.g. Hirth & Tullis 1992) (Chapter 1). It is therefore postulated that (a) the transition from viscous to frictional deformation was controlled by a fall in the ambient temperature during thrusting, and (b) that the decrease in temperature was related to the progressive exhumation of the fault zone (Fig. 9.2b).

### ***Summary***

The Loch Sgibacleit pathway is characterised by (a) thrust-related lower amphibolite facies quartzo-feldspathic mylonites (primary fabrics), (b) thrust-related, pseudotachylyte-bearing foliation-parallel fault zones and pseudotachylyte-ultracataclasite crush zones (derived fabrics) and (c) steeply dipping normal faults (cross-cutting fabrics) (Fig. 9.2a). The main points to note are that:

- Thrusting and subsequent normal faulting occurred in dry, fluid-absent crust.
- The thrust-related foliation-parallel fault zones and pseudotachylyte-ultramylonite crush zones localised within pre-existing bands of fine grained mylonite and ultramylonite.
- There is little evidence for repeated reactivation of the mylonitic fabrics over long periods of geological time.

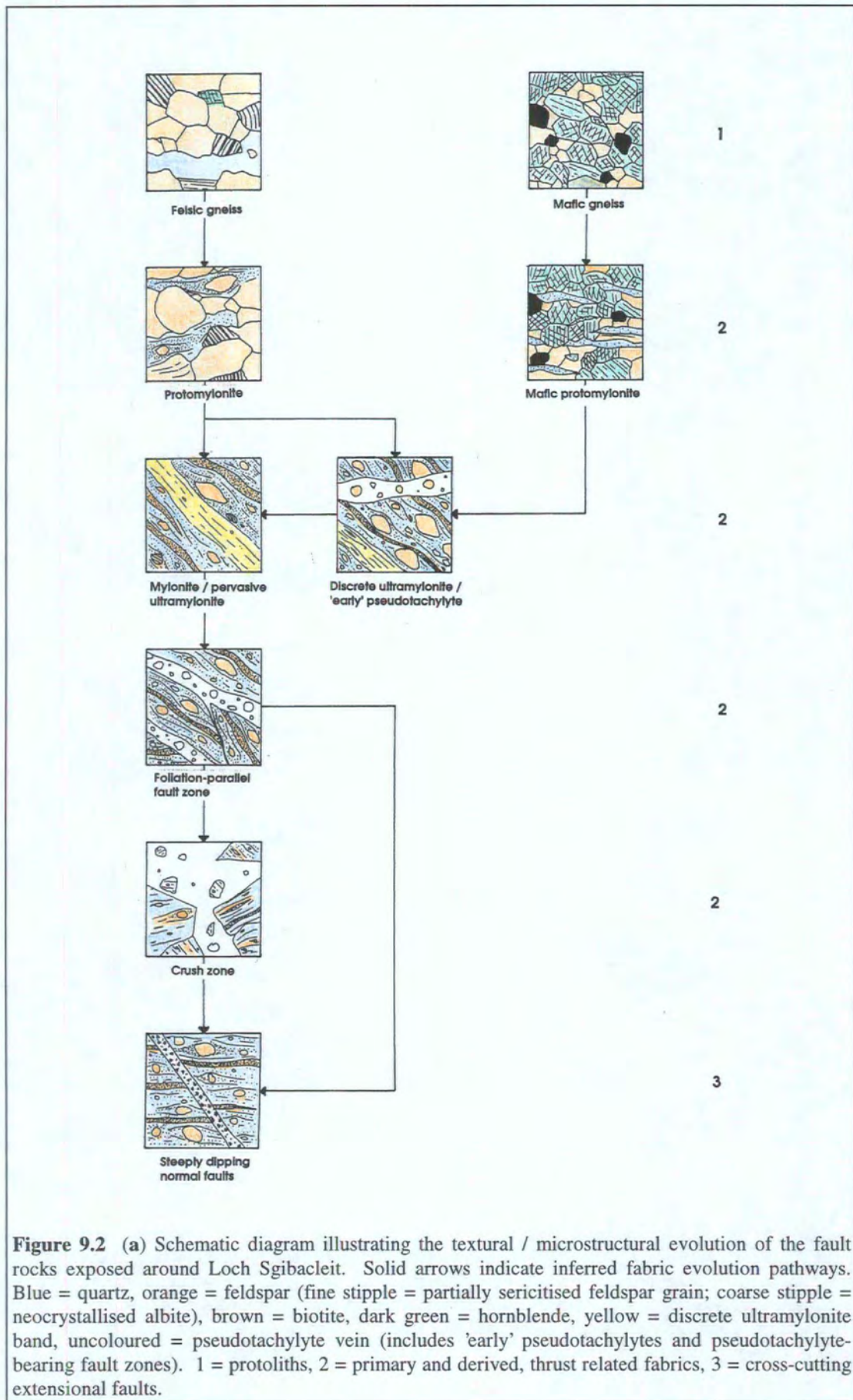
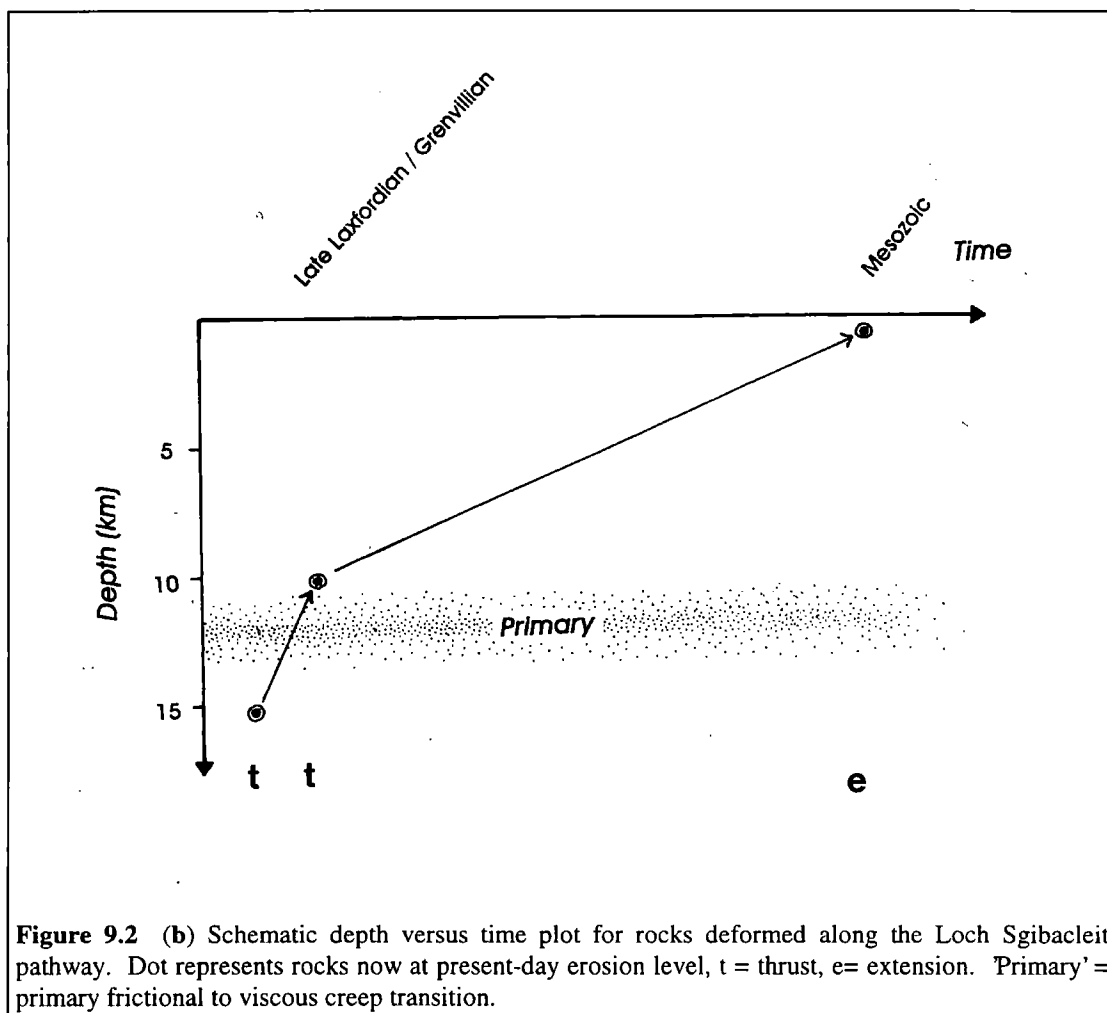


**Figure 9.2 (a)** Schematic diagram illustrating the textural / microstructural evolution of the fault rocks exposed around Loch Sgibacleit. Solid arrows indicate inferred fabric evolution pathways. Blue = quartz, orange = feldspar (fine stipple = partially sericitised feldspar grain; coarse stipple = neocrystallised albite), brown = biotite, dark green = hornblende, yellow = discrete ultramylonite band, uncoloured = pseudotachylyte vein (includes 'early' pseudotachylytes and pseudotachylyte-bearing fault zones). 1 = protoliths, 2 = primary and derived, thrust related fabrics, 3 = cross-cutting extensional faults.



### 9.2.6.2 Scalpay pathway

Rocks which have been deformed along the 'Scalpay pathway' are characterised by a complex structural, textural and metamorphic history (Fig. 9.3a).

#### *Macroscopically ductile thrusting (Late Laxfordian / Grenvillian)*

The earliest phase of deformation appears to have been late Laxfordian / Grenvillian top-to-the-NW thrusting, which was associated with the development of upper greenschist facies mylonites and phyllonites. Deformation probably occurred at between 15km and 17km depth, and was associated with significant fluid influx into the fault zone. The fluids appear to have been focused into relatively narrow, highly strained bands of phyllonite within the predominantly quartzo-feldspathic mylonite belt. The principal textural changes during mylonitisation were *strain-induced* and *reaction-modified* breakdown of the feldspar-dominated LBF of the protolith gneisses to produce IWL quartzo-feldspathic mylonites and phyllonites (Fig. 9.3a). Deformation within packages of quartzo-feldspathic mylonite appears to have been controlled by dislocation glide and dynamic recrystallisation within the interconnected

quartz ribbons, and by localised neocrystallisation and intragranular fracturing within feldspar porphyroclasts. Deformation within packages of upper greenschist facies phyllonite appears to have been controlled (a) by intracrystalline, crystal plastic deformation within the interconnected quartz ribbons and sericite strands, and (b) by neocrystallisation, intragranular fracturing and fluid-assisted diffusive mass transfer in feldspar and hornblende-rich bands. These observations are consistent with thrusting having occurred predominantly within the viscous creep regime (Fig. 9.3b).

#### ***Brittle thrusting (Caledonian)***

The upper greenschist facies mylonites are *locally* cross-cut by thrust-related cataclasite seams (Fig. 9.3a), which are thought to have developed at depths of between 8km and 9km in the crust. The precise age of brittle deformation is unclear, although a Caledonian age seems most likely (see discussion in Butler 1995). The geometries of the cataclasite seams and pseudotachylyte veins have clearly *not* been influenced by the pre-existing mylonitic fabrics, and microstructural observations suggest that cataclasis and pseudotachylyte generation occurred predominantly within the frictional regime (Fig. 9.3b).

#### ***Macroscopically ductile reactivation of upper greenschist facies thrust-related phyllonites during transpression and sinistral strike-slip (Caledonian)***

Bands of *upper* greenschist facies phyllonite are commonly observed to be overprinted macroscopically ductile, transpression and sinistral strike-slip related *lower* greenschist facies phyllonite (Fig. 9.3a). The lower greenschist facies fabrics are thought to be of Caledonian age, and probably developed at depths of between 8km and 9km. Lower greenschist facies phyllonitisation was associated with significant fluid influx into the fault zone, focused along pre-existing bands of upper greenschist facies phyllonite. The principal textural change associated with lower greenschist facies phyllonitisation was continued breakdown of feldspar (and hornblende) porphyroclasts to produce sericite- (and chlorite) dominated IWL aggregates (Fig. 9.3a). Deformation within packages of lower greenschist facies phyllonite was primarily controlled by fluid-assisted diffusive mass transfer processes, with significant contributions from intracrystalline deformation in sericite strands and by localised intragranular fracturing and neocrystallisation of the remaining feldspar porphyroclasts. These observations are consistent with deformation having occurred predominantly within the viscous creep regime (Fig. 9.3b).

***Macroscopically ductile reactivation of lower greenschist facies sinistral strike-slip related phyllonites during dextral strike-slip / extension (late Caledonian)***

The lower (and locally upper) greenschist facies fabrics are commonly observed to have been reworked during late Caledonian top-to-the-S extension / top-to-the-SW dextral strike-slip (Fig. 9.3a). Reworking is thought to have occurred at depths of between 7km and 8km. Strain was accommodated by macroscopically ductile deformation and localised, cyclic hydraulic fracturing within the phyllonite belts. The hydraulic fractures are predominantly tensile in nature, and do *not* appear to have accommodated high magnitudes of bulk strain. Microstructural observations suggest that background macroscopically ductile deformation was controlled by fluid-assisted diffusive mass transfer processes and intracrystalline crystal plasticity within sericite and chlorite strands. It is therefore postulated that deformation occurred *around the level of the frictional to viscous creep transition* (Fig. 9.3b).

***Brittle reactivation of phyllonitic fabrics during extension (Mesozoic)***

The lower greenschist facies fabrics are *locally* disrupted by Mesozoic, foliation parallel detachment faults. The detachments, which are thought to have accommodated regional E-W extension, probably developed within the uppermost 5km of the crust. These observations are consistent with deformation having occurred *within the frictional regime* (Fig. 9.3b).

***Discussion***

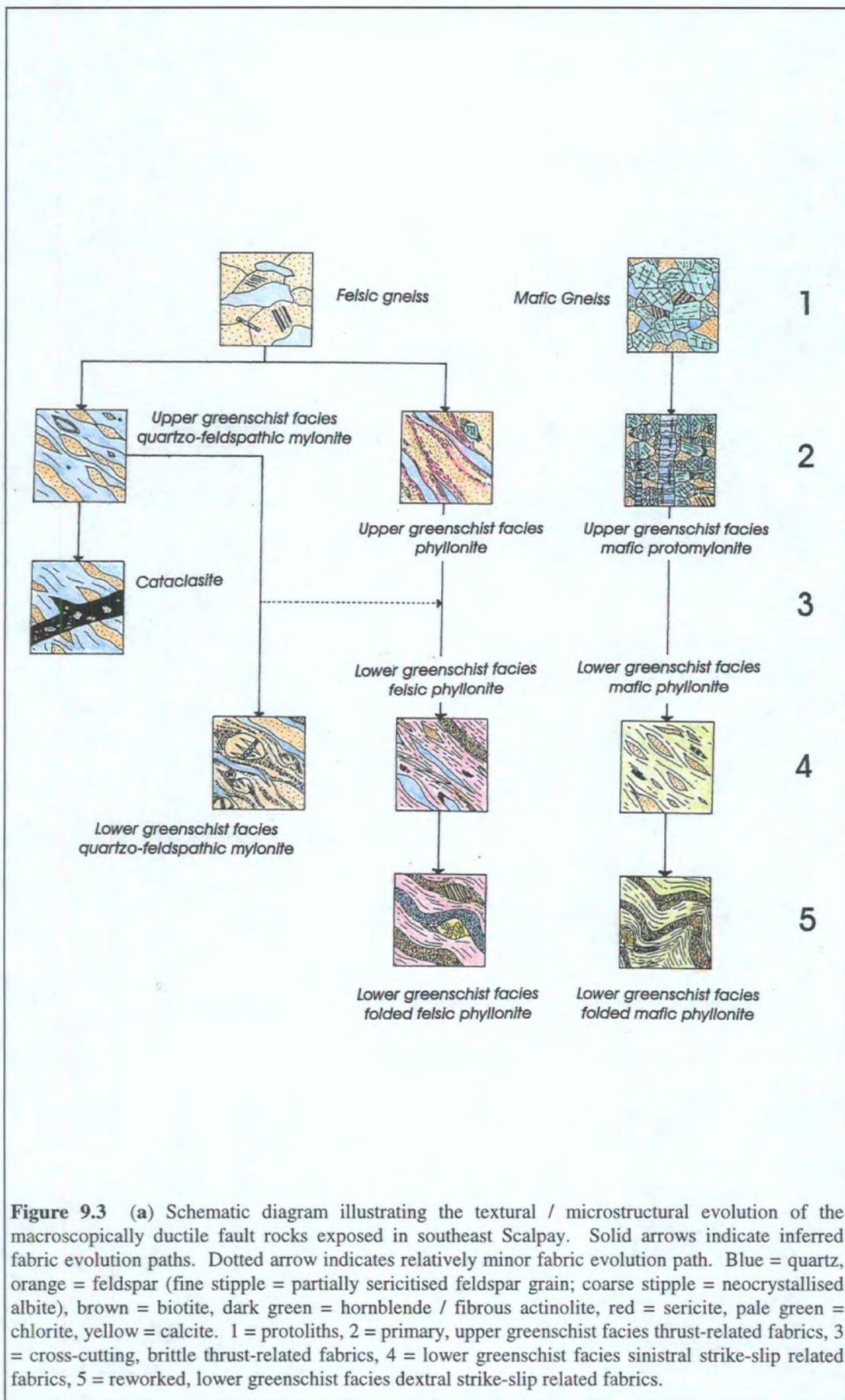
Rocks which have been deformed along the Scalpay pathway have clearly experienced a complex history of deformation, apparently at a number of different levels relative to the frictional to viscous creep transition. Following the cessation of macroscopically ductile, late Laxfordian / Grenvillian thrusting, in which deformation was dominated by both *thermally activated* and *fluid assisted* viscous creep mechanisms, the fault zone appears to have been exhumated from c.14km to c.8km depth by the Caledonian. Brittle thrusting at the onset of Caledonian deformation took place within the frictional regime. However, microstructural observations suggest that subsequent Caledonian sinistral strike-slip was controlled by predominantly *viscous* deformation mechanisms, including fluid-assisted DMT and intracrystalline deformation within sericite strands. Sinistral strike-slip was associated with localised fluid influx into the fault zone. Thus, viscous deformation during the Caledonian appears to have been promoted by the influx of fluids into the fault zone, and *not* by further burial / increase in the geothermal gradient. This important observation is discussed in detail in sections 9.5 & 9.6. During dextral strike-slip / extension-related reworking within the pre-existing phyllonite belts, strain appears to have been

accommodated both by viscous, fluid-assisted deformation mechanisms, and by periods of localised hydraulic fracturing. Reworking was probably associated with minor (c. 1km) exhumation of the fault zone. However, embrittlement of the fault zone appears to have been governed by cyclic changes in the pore fluid pressure, and *not* by a decrease in the ambient pressure and temperature conditions. Following the cessation of macroscopically ductile reworking within the phyllonite belts, the fault zone experienced significant exhumation. It is postulated that a significant drop in the ambient pressure and temperature conditions during exhumation was sufficient to promote a return to predominantly frictional deformation (Fig. 9.3b).

### **Summary**

The Scalpay pathway is characterised by (a) thrust-related upper greenschist facies mylonites and phyllonites (primary fabrics), (b) thrust-related cataclasite seams and pseudotachylyte veins (cross-cutting fabrics), (c) Transpression- and sinistral strike-slip related lower greenschist facies phyllonites and quartzo-feldspathic mylonites (reworked fabrics), (d) dextral strike-slip / top-to-the-S extension-related lower greenschist facies fabrics (reworked fabrics) and (e) extension-related, brittle detachment faults (derived fabrics) (Fig. 9.3a). The main points to note are that:

- Phyllonitisation during thrusting and subsequent strike-slip was associated with the influx of hydrous fluids into the fault zone.
- The transpression- and sinistral strike-slip related lower greenschist facies fabrics localised within, and reworked, pre-existing bands of thrust-related upper greenschist facies phyllonite.
- The sinistral strike-slip related phyllonites, and locally, the thrust-related upper greenschist facies phyllonites are commonly observed to have been reactivated and reworked during subsequent dextral strike-slip / top-to-the-S extension.
- The extension-related detachment faults are typically developed along the margins of pre-existing phyllonitic shear zones.



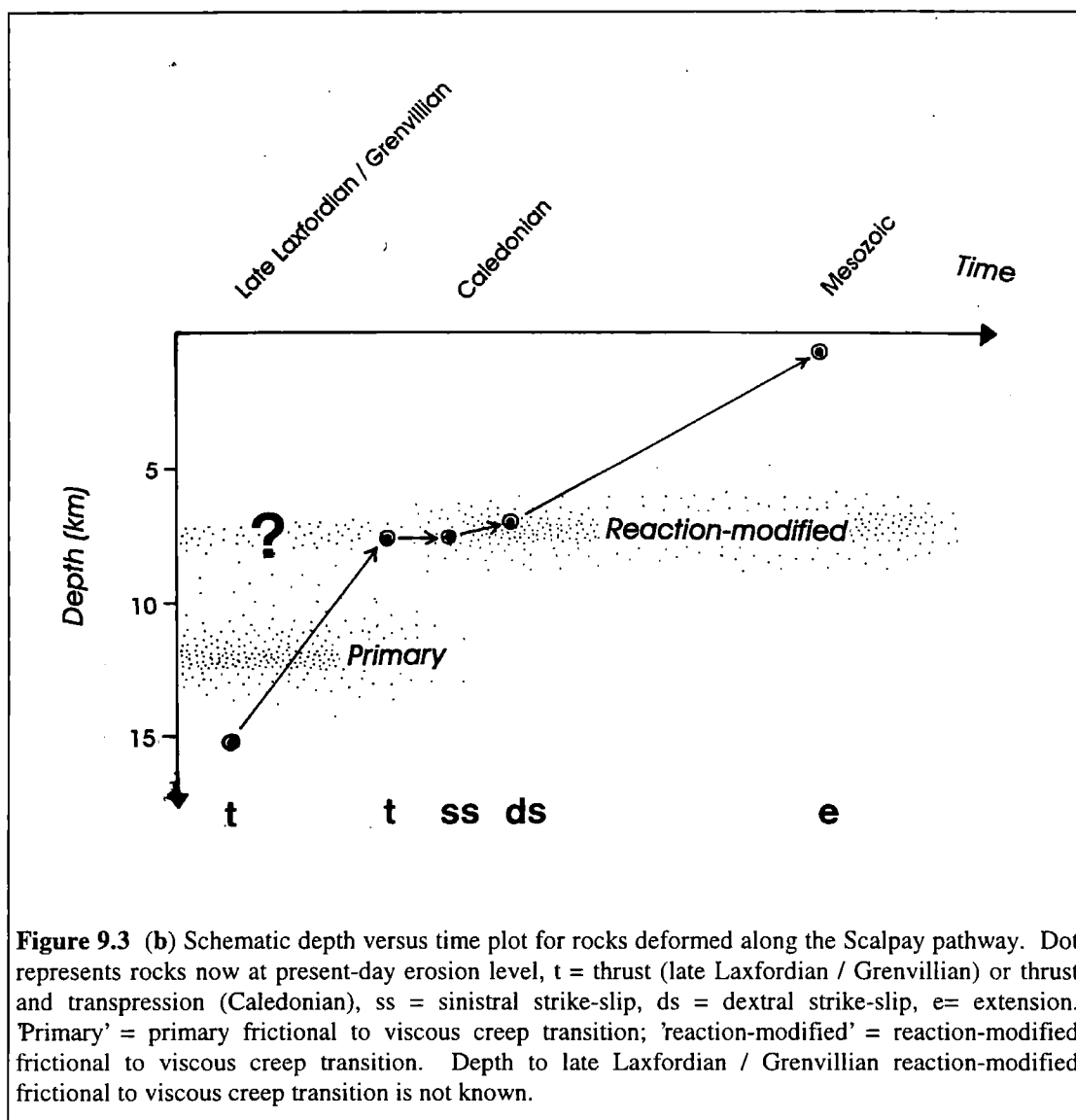


**Figure 9.3 (b)** Schematic depth versus time plot for rocks deformed along the Scalpay pathway. Dot represents rocks now at present-day erosion level, t = thrust (late Laxfordian / Grenvillian) or thrust and transpression (Caledonian), ss = sinistral strike-slip, ds = dextral strike-slip, e= extension. 'Primary' = primary frictional to viscous creep transition; 'reaction-modified' = reaction-modified frictional to viscous creep transition. Depth to late Laxfordian / Grenvillian reaction-modified frictional to viscous creep transition is not known.

### 9.2.6.3 North Uist pathway

Rocks deformed along the North Uist pathway have experienced a complex kinematic, textural and metamorphic evolution.

#### *Brittle thrusting (Caledonian)*

The earliest phase of deformation appears to have been top-to-the-W Caledonian thrusting, which occurred at depths of between 8km and 9km, in dry, fluid-absent crust. The principal textural change associated with brittle deformation was the development of the crush melange and associated pseudotachylyte-ultracataclite crush zones (Fig. 9.4a). Strain was accommodated by localised melting and pseudotachylyte generation, cataclasis and brittle intra- and transgranular fracturing. It is therefore likely that deformation occurred entirely within the frictional regime (Fig. 9.4b).

***Macroscopically ductile reactivation of brittle, thrust-related fault zones during transpression and sinistral strike-slip (Caledonian)***

The crush melange and crush zones are commonly observed to be overprinted by macroscopically ductile, transpression and strike-slip related, lower greenschist facies phyllonitic fabrics (Fig. 9.4a). The transpression and strike-slip related fabrics are thought to be of Caledonian age, and probably developed at depths of between 8km and 9km. The principal textural change accompanying phyllonitisation appears to have been the chemical breakdown of feldspar (and hornblende) grains to produce fine grained, sericite- (and chlorite) dominated IWL aggregates. Lower greenschist facies phyllonitisation was associated with widespread fluid influx into the fault zone. The distribution of fluids appears to have been extremely heterogeneous and was controlled by the dual porosity / dual permeability characteristics of the pre-existing crush melange and pseudotachylite-ultracataclasite crush zones. A network of phyllonitic shear zones appears to have localised along networks of highly permeable crush zones, whilst a pervasive protophyllonitic fabric overprints less permeable crush melange. Strain was focused into the interconnected phyllonitic shear zone network and was largely accommodated by fluid-assisted diffusive mass transfer processes. This observation suggests that deformation occurred predominantly within the viscous creep regime (Fig. 9.4b).

***Macroscopically ductile reactivation of sinistral strike-slip related phyllonites during transtension and extension (Late Caledonian)***

The phyllonitic shear zone fabrics are commonly observed to have been reworked during Caledonian transtension and subsequent top-to-the-E extension (Fig. 9.4a). However, it is important to emphasise that transpression, strike-slip, transtension and extension on North Uist are likely to have been part of a *single, progressive* deformation event (Butler 1995) (see also discussion in Chapter 3). This observation has important implications for the rheological evolution of the OHFZ, and is discussed further in section 9.5.2.3. Transtension- and extension-related deformation probably occurred at between 7km and 8km depth, and was accommodated (a) by macroscopically ductile reworking of the phyllonitic fabrics, and (b) localised, cyclic hydraulic fracturing within the otherwise ductile shear zones. In contrast to Scalpay, *shear* hydraulic fractures ('Type 1' detachments), which appear to have accommodated high magnitudes of strain, are commonly observed. These observations suggest that deformation took place in a fluid-rich environment, around the level of the frictional to viscous creep transition (Fig. 9.4b).

### ***Brittle reactivation of phyllonitic fabrics during extension (Mesozoic)***

The phyllonitic and protophyllonitic fabrics are locally disrupted by arrays of foliation-parallel detachment faults ('Type 2' detachments). It has been inferred that the detachment faults initiated during regional, top-to-the-E or -SE extension, at depths of less than 5km in the crust. It is likely that the detachment faults developed in a predominantly 'dry' environment, entirely within the frictional regime (Fig. 9.4b).

### ***Brittle reactivation of detachment fault during transtension / sinistral strike-slip (?Oligocene)***

The brittle detachment faults appear to have been reactivated during ?Oligocene transtension. Deformation was locally associated with the development of incohesive gouges and breccias. This observation is consistent with reactivation having occurred within the uppermost 5km of the crust, entirely within the frictional regime (Fig. 9.4b).

### ***Discussion***

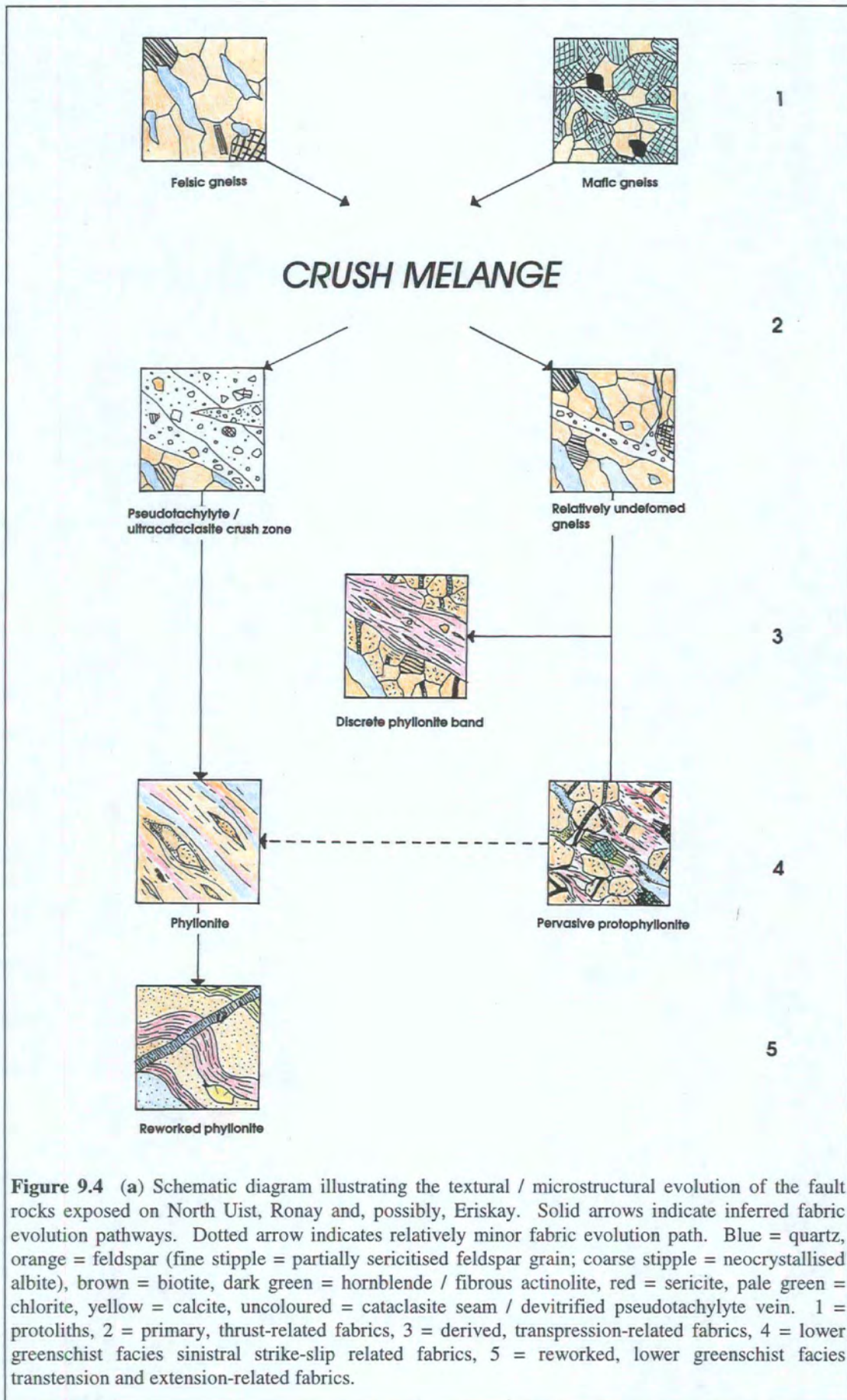
Rocks which have been deformed along the North Uist pathway have experienced a complex history of deformation, apparently at a variety of different levels relative to the frictional to viscous transition. Metamorphic and microstructural evidence suggest that viscous deformation and phyllonitisation during transpression and sinistral strike-slip occurred at similar crustal levels as frictional, top-to-the-W thrusting. This observation suggests that the onset of viscous deformation is unlikely to have been controlled by an increase in the ambient pressure and temperature conditions. Phyllonitisation was associated with widespread fluid influx into the fault zone, and deformation appears to have been controlled by fluid-assisted diffusive mass transfer processes. It is therefore postulated that the transition from frictional to viscous creep behaviour during transpression and subsequent strike-slip was principally governed by the influx of fluids into the fault zone, and *not* by burial or an increase in the geothermal gradient. Caledonian transtension- and extension-related reworking was associated with minor (c.1km) exhumation of the fault zone, and was accommodated by viscous creep and localised, transient brittle deformation within the phyllonite belts. Macroscopically ductile deformation within the phyllonite belts was accommodated by fluid-assisted diffusive mass transfer mechanisms, whilst localised embrittlement was probably controlled by cyclic changes in pore fluid pressure. Variations in pore fluid pressure are therefore thought to have been the principal cause of embrittlement, rather than a decrease in the ambient pressure and temperature conditions. Following the cessation of macroscopically ductile reworking, the fault zone appears to have been exhumed from c.8km to less than 5km depth during the

Mesozoic. There is little evidence to suggest that the Mesozoic detachment faults developed by hydraulic fracture mechanisms, which implies that the decrease in the ambient pressure and temperature conditions during exhumation was sufficient to promote a return to frictional deformation (Fig. 9.4b).

### **Summary**

The North Uist pathway is characterised by (a) thrust-related crush melange and pseudotachylyte-ultracataclasite crush zones (primary fabrics), (b) thrust, transpression and sinistral strike-slip related lower greenschist facies phyllonites and protophyllonites (derived fabrics), (c) transtension- and extension-related lower greenschist facies phyllonites (reworked fabrics) and (d) foliation-parallel detachment faults (derived fabrics) (Fig. 9.4a). The main points to note are that:

- Phyllonitisation was associated with the influx of hydrous fluids into the previously dry fault zone.
- The thrust-, transpression- and sinistral strike-slip related phyllonitic shear zones localised within pre-existing zones of intense brittle deformation (e.g. pseudotachylyte-ultracataclasite crush zones).
- Pervasive protophyllonitic fabrics overprint regions of *less* intense brittle deformation.
- The sinistral strike-slip related fabrics are commonly observed to have been reactivated and reworked during subsequent transtension and extension.
- The foliation-parallel detachment faults are typically developed within, or along the margins of pre-existing phyllonitic shear zones.



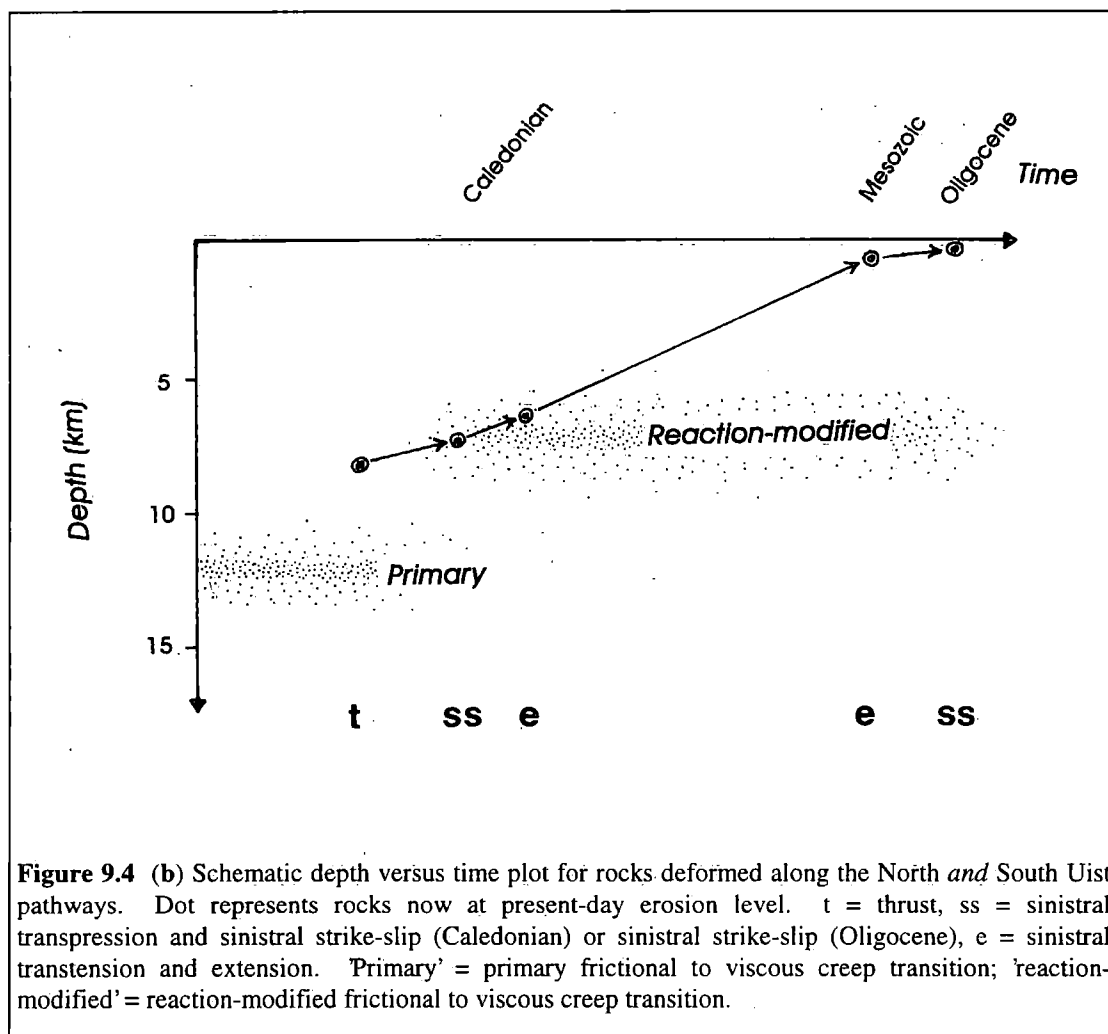


**Figure 9.4 (b)** Schematic depth versus time plot for rocks deformed along the North and South Uist pathways. Dot represents rocks now at present-day erosion level. t = thrust, ss = sinistral transpression and sinistral strike-slip (Caledonian) or sinistral strike-slip (Oligocene), e = sinistral transtension and extension. 'Primary' = primary frictional to viscous creep transition; 'reaction-modified' = reaction-modified frictional to viscous creep transition.

#### 9.2.6.4 South Uist pathway

Rocks which have been deformed along the South Uist pathway share a similar structural history as those deformed along the North Uist pathway. However, there are several important differences in fault rock distribution and fabric evolution (compare Fig. 9.4a with 9.5a).

##### *Brittle thrusting (Caledonian)*

The earliest phase of deformation in South Uist appears to have been top-to-the-W Caledonian thrusting, which is thought to have occurred at between 8km and 9km depth. Deformation appears to have been strongly focused along the contacts between the Corodale Gneiss and the surrounding banded gneisses / Mashed Gneiss and, in contrast to North Uist, crush melange is not developed (or is not exposed onshore). Thrusting was accommodated by cataclasis, pseudotachylyte generation and brittle fracturing (Fig. 9.5a). It is therefore postulated that deformation occurred in a dry environment, entirely within the frictional regime (Fig. 9.4b).

***Macroscopically ductile reactivation of brittle, thrust-related fault zones during sinistral strike-slip (Caledonian)***

The intensely fractured gneisses along the eastern margin of the Corodale Gneiss are commonly observed to be overprinted by macroscopically ductile, lower greenschist facies phyllonitic fabrics (Fig. 9.5a). The phyllonites are thought to have developed during Caledonian sinistral strike-slip, at depths of between 8km and 9km. The principal textural change accompanying phyllonitisation was breakdown of feldspar (and hornblende) to produce interconnected aggregates of intensely aligned sericite and chlorite grains. Phyllonitisation was associated with fluid influx, focused along the pre-existing fault zone at the contact between the Corodale Gneiss and the Mashed Gneiss. Pervasive protophyllonite is *not* developed on South Uist owing to the absence of crush melangé. Deformation was localised within the phyllonitic shear zone, and was largely accommodated by fluid-assisted diffusive mass transfer processes. This observation suggests that deformation occurred *below* the level of the frictional to viscous creep transition (Fig. 9.4b).

***Macroscopically ductile reactivation of pre-existing, and generation of new phyllonitic fabrics during transtension and extension (Caledonian)***

The phyllonitic fabrics are commonly observed to have been reactivated and reworked during Caledonian transtension and extension although, there is also evidence that 'new' phyllonitic fabrics developed in previously non-phyllonitised regions (Fig. 9.5a). However, it is important to emphasise that strike-slip, transtension and extension on South Uist are likely to have been part of a *single, progressive* deformation event (Butler 1995) (see also discussion in Chapter 3). This observation has important implications for the rheological evolution of the OHFZ, and is discussed further in section 9.5.2.3. Transtension- and extension-related reworking and phyllonitisation are thought to have occurred at depths of between 7km and 8km, and the development of 'new' phyllonitic fabrics is clear evidence for continued fluid influx into the fault zone during transtension / extension. Strain within packages of new and pre-existing phyllonite was accommodated by fluid-assisted diffusive mass transfer mechanisms and localised, cyclic hydraulic fracturing. It is therefore postulated that deformation occurred around the level of the frictional to viscous creep transition. However, in contrast to rocks deformed along the North Uist pathway, there is little evidence to suggest that hydraulic fracturing was associated with significant frictional sliding (i.e. Type 1' detachments have not been observed on South Uist) (Fig. 9.4b).

### ***Brittle reactivation of phyllonitic fabrics and crush zones during extension***

#### ***(Mesozoic)***

The phyllonitic fabrics and the pseudotachylyte-ultracataclasite crush zones are commonly observed to be dismembered by arrays of foliation-parallel detachment faults. It has been inferred that the detachment faults initiated during regional, top-to-the-E or -SE extension, at depths of less than 5km in the crust. It is likely that the detachment faults developed in a 'dry' environment, entirely within the frictional regime (Fig. 9.4b).

### ***Brittle reactivation of detachment faults during sinistral transtension / strike-slip***

#### ***(?Oligocene)***

The brittle detachment faults appear to have been reactivated during ?Oligocene transtension. Deformation was locally associated with the development of incohesive gouges and breccias. This observation is consistent with reactivation having occurred within the uppermost 5km of the crust, entirely within the frictional regime (Fig. 9.4b).

### ***Discussion***

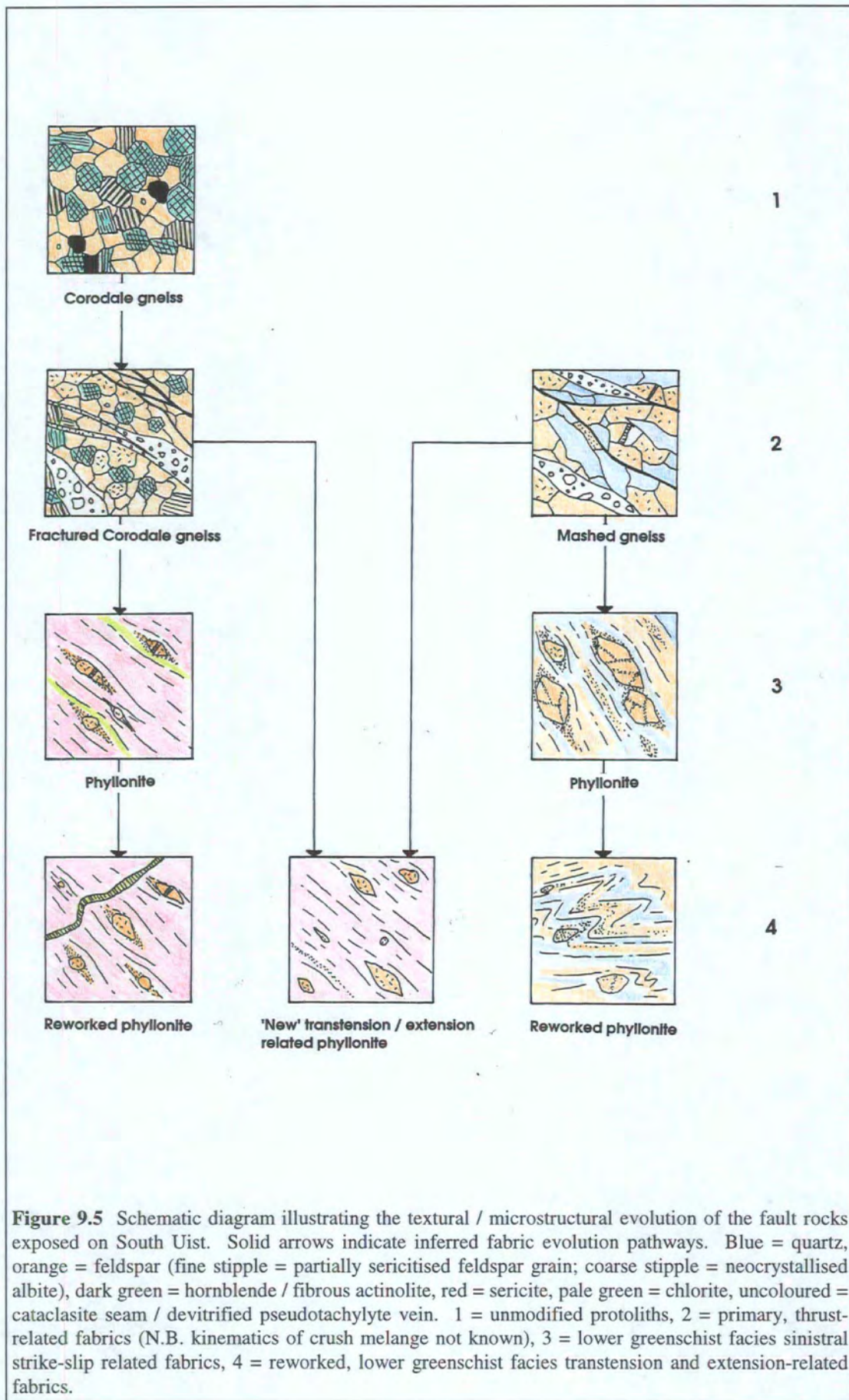
As with the North Uist pathway, viscous deformation and phyllonitisation during and sinistral strike-slip probably occurred at similar crustal levels as cataclasis and pseudotachylyte generation during earlier top-to-the-W thrusting. This observation suggests that the onset of viscous deformation is unlikely to have been controlled by an increase in the ambient pressure and temperature conditions. Phyllonitisation was associated with localised fluid influx into the fault zone, and deformation within the phyllonite belt appears to have been controlled by fluid-assisted diffusive mass transfer processes. Thus, it is postulated that the transition from frictional to viscous creep behaviour during transpression and subsequent strike-slip was principally governed by the influx of fluids into the fault zone, and *not* by burial or an increase in the geothermal gradient. Transtension- and extension-related reworking were associated with minor (c.1km) exhumation of the fault zone, and were accommodated (a) by viscous creep and localised, transient brittle deformation within the pre-existing phyllonite belt and (b) by the generation of 'new' phyllonitic fabrics. Deformation within packages of 'new' and reworked phyllonite was largely accommodated by viscous, fluid-assisted diffusive mass transfer mechanisms. Localised embrittlement of the fault zone appears to have been controlled by cyclic changes in pore fluid pressure, *not* by a decrease in the ambient pressure and temperature conditions. Following the cessation of macroscopically ductile reworking, the fault zone appears to have been exhumed from c.8km to less than 5km depth during the Mesozoic.

There is little evidence to suggest that the detachment faults developed by hydraulic fracture mechanisms, which suggests that the decrease in the ambient pressure and temperature conditions during exhumation was sufficient to promote a return to frictional deformation (Fig. 9.4b).

### **Summary**

The South Uist pathway is characterised by (a) thrust-related fractured Corodale Gneiss, Mashed Gneiss and pseudotachylyte-ultracataclasite crush zones (primary fabrics), (b) sinistral strike-slip related lower greenschist facies phyllonites (derived fabric), (c) transtension- and extension-related lower greenschist facies phyllonites (derived and reworked fabrics) and (d) foliation-parallel detachment faults (derived fabrics) (Fig. 9.5a). The main points to note are that:

- Phyllonitisation was associated with the influx of hydrous fluids into the previously dry fault zone.
- The sinistral strike-slip related phyllonitic fabrics localised within pre-existing zones of intense brittle deformation (e.g. pseudotachylyte-ultracataclasite crush zones).
- Pervasive protophyllonite does *not* appear to be developed in South Uist.
- The sinistral strike-slip related fabrics were locally reactivated and reworked during transtension and extension.
- Transtension and extension were associated with an episode of lower greenschist facies phyllonitisation.
- The foliation-parallel detachment faults are typically developed within, or along the margins of, the pre-existing phyllonitic shear zones / pseudotachylyte-ultracataclasite crush zones.



### 9.2.6.5 Summary and discussion

The fabric evolution pathways presented above clearly demonstrate that many of the fault rocks exposed along the OHFZ have experienced a complex history of alternating *frictional* and *viscous* deformation. This observation is consistent with such fault rocks having been deformed at depths both above and below the level of the frictional to viscous creep transition i.e. *deformation occurred across the frictional to viscous creep transition*. However, the inferred depth at which the transition from frictional to viscous creep behaviour (or vice-versa) took place appears to have varied both spatially (i.e. along the length of the fault zone), and temporally (i.e. between successive deformation events). It is therefore postulated that many of the fault rocks have been deformed across one or more *different* frictional to viscous creep transition zones within the crust. The transition zones recognised along the OHFZ are:

- A *primary* frictional to viscous creep transition, which occurs in quartzo-feldspathic fault rocks at depths of between 10km and 15km (e.g. Fig. 9.2b).
- A *reaction-modified* frictional to viscous creep transition, which occurs in phyllosilicate-rich fault rocks at depths of between 5km and 8km (e.g. Figs. 9.4b & 9.4b).

The main differences between fabric evolution pathways can be attributed to whether the fault rocks were deformed across the primary transition (e.g. the Loch Sgibacleit pathway), the reaction-modified transition (e.g. the North and South Uist pathways) or across both transition zones (e.g. the Scalpay pathway). The depth at which deformation occurred with respect to each transition zone appears to have been fundamental in determining whether a fault zone segment was prone to reactivation. In particular, fault rocks which were deformed *only* across the primary frictional to viscous creep transition do *not* appear to have experienced significant reactivation. In contrast, fault rocks which were deformed either across the reaction-modified transition or across *both* transition zones have experienced long histories of reactivation and reworking. Rocks which have been deformed across the reaction-modified frictional to viscous creep transition zone are characterised by intense, localised retrograde metamorphism and phyllonitisation (Figs. 9.3a, 9.4a & 9.5a). Thus, *segments of the OHFZ which have suffered extensive phyllonitisation were particularly susceptible to repeated episodes of reactivation*. In contrast, *those segments of the fault zone which have not experienced intense phyllonitisation were characterised by relatively short-lived deformation histories, and were therefore 'immune' to reactivation*.

Phyllonitisation clearly depends on a number of factors, including:

- Protolith mineralogy.
- The availability of chemically active fluids during deformation.
- The composition, temperature and pressure of the fluid phase.
- The microstructure and fluid transport properties of the pre-existing fault rocks (i.e. the primary fabrics).
- Changes in fault rock microstructure and fluid transport properties during deformation across the reaction-modified frictional to viscous creep transition.

The following sections therefore consider the controls exercised (a) by the chemical and thermodynamic characteristics of the fluid phase (section 9.3), and (b) by the fluid transport properties of the OHFZ, on the development of phyllonitic fault rocks (section 9.4). The chapter concludes with a discussion on the rheological implications of phyllonitisation (sections 9.5 & 9.6) and finally, synthesises the data presented in this thesis into a simple model to explain reactivation in continental basement fault zones (section 9.7).

### **9.3 MINERAL REACTIONS, FAULT ROCK GEOCHEMISTRY AND NATURE OF THE FLUID PHASE**

Segments of the OHFZ which are inferred to have been deformed across the reaction-modified frictional to viscous creep transition are characterised by intense, localised retrograde metamorphism and hydration within networks of greenschist facies phyllonitic shear zones. The nature of the fluid phase can be *directly* evaluated (a) by analysis of syn-tectonic fluid inclusions trapped within the fault rocks, or (b) by comparing the oxygen isotope signatures obtained from the fault rocks with those obtained from the protoliths (McCaig 1997; Streit & Cox 1998). An alternative method is to use mineralogical and geochemical data obtained from the fault rocks to assess the likely controls on syn-tectonic metamorphism. Thus, it may be possible to make inferences about the composition and geochemical nature of the fluid phase. The latter method has been employed during the present study. The following sections discuss the mineralogical (section 9.3.1) and geochemical (section 9.3.2) constraints on the nature of the fluid phase.

### 9.3.1 FAULT ROCK MINERALOGY AND METAMORPHIC REACTIONS

A range of possible retrograde metamorphic reactions has been determined for each fabric evolution pathway. Protolith (or primary fabric) mineral assemblages were compared with fault rock mineral assemblages. It was assumed that significant differences in the mineralogy of successive generations of fault rocks was likely to have been caused either by syn- or post-tectonic metamorphism (e.g. Beach 1980). The timing of metamorphism relative to deformation was constrained by relating 'new' mineral phases to the fault rock microstructure (McCaig & Knipe 1990) (see Chapter 1 for discussion of the microstructural criteria used).

#### 9.3.1.1 Syn-tectonic mineral assemblages

The characteristic protolith mineral assemblages are summarised in Table 9.10, whilst the characteristic mineral assemblages observed in fault rocks which have been deformed across the reaction-modified frictional to viscous creep transition are summarised in Table 9.11.

<b>Protolith</b>	<b>Mineral assemblage</b>
<b>Banded gneiss</b>	Plagioclase + quartz + K-feldspar ± biotite ± hornblende ± pyroxene.
<b>Amphibolite</b>	Plagioclase + hornblende + quartz + garnet ± sphene.
<b>Corodale gneiss</b>	Pyroxene + garnet + plagioclase + hornblende.

**Table 9.10** Table summarising the characteristic mineral assemblages preserved in unmodified Lewisian protoliths. Minerals listed in approximate order of decreasing modal abundance.

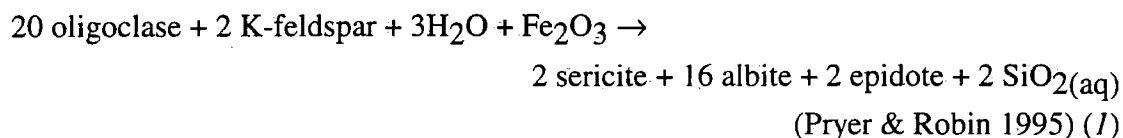
<b>Fault rocks</b>	<b>Syn-tectonic mineral assemblage</b>
<b>Upper greenschist facies mylonite and phyllonite (Northern Zone only)</b>	Albite + quartz + sericite + hornblende + biotite + epidote + actinolite.
<b>Lower greenschist facies sinistral strike-slip related phyllonite (Northern and Southern Zones)</b>	Albite + sericite + quartz + actinolite + epidote + chlorite ± sphene ± ilmenite ± calcite.
<b>Lower greenschist facies transtension-, extension- and dextral strike-slip related phyllonite (Northern Zone, North Uist and Ronay)</b>	Albite + sericite + quartz + chlorite + ilmenite + epidote.
<b>Lower greenschist facies transtension- and extension-related phyllonite (South Uist only)</b>	Albite + quartz + sericite + epidote + chlorite ± pyrite.

**Table 9.11** Table summarising the characteristic syn-tectonic mineral assemblages preserved in rocks deformed across the reaction-modified frictional to viscous creep transition. 'Syn-tectonic assemblage' includes both 'new' minerals and minerals which are found in the protoliths, but were apparently stable during deformation.

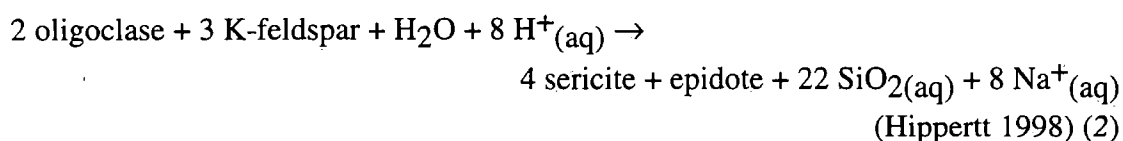
Four distinct mineral assemblages, all of which are characteristic of greenschist facies metamorphism, have been recognised in fault rocks deformed across the reaction-modified frictional to viscous creep transition along the OHFZ. Upper greenschist facies assemblages are characteristic of some late Laxfordian / Grenvillian thrust-related mylonites and phyllonites preserved in the Northern Zone of the OHFZ. Lower greenschist facies assemblages are characteristic of Caledonian sinistral strike-slip, transtension- and extension-related phyllonites preserved in both Northern *and* Southern Zones of the OHFZ. The lower greenschist facies fault rocks display subtle spatial and temporal variations in mineralogy. In particular, packages of sinistral strike-slip related phyllonite are characterised by the presence of actinolite and sphene, but very little chlorite and calcite. In contrast, packages of reworked, transtension- and extension-related phyllonite from the Northern Zone, North Uist and Ronay contain abundant calcite and chlorite, but no actinolite or sphene. Packages of reworked and 'new' transtension- and extension-related phyllonite from South Uist contain abundant chlorite and epidote, but no actinolite or calcite. These observations suggest that during phyllonitisation, the metamorphic reactions may have varied both in space (i.e. at different points along the fault zone) and in time (i.e. between successive deformation events). The following section describes a number of possible reactions which could account for the observed fault rock mineral assemblages.

### 9.3.1.2 Metamorphic reactions

One of the most important processes controlling the microstructural evolution of both upper *and* lower greenschist facies phyllonites appears to have been the syn-tectonic breakdown of plagioclase and K-feldspar to aggregates of fine grained sericite, albite and epidote. Such reactions are commonly observed in greenschist facies fault rocks (Beach 1980), and take the form:

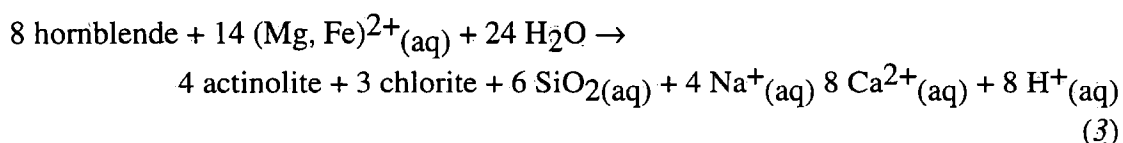


or:



The exact form of these equations will vary depending on (a) the feldspar composition, and (b) on the relative amounts of albite and sericite produced. However, it is clear that feldspar sericitisation reactions require the addition of hydrous fluids, and the involvement of  $\text{Fe}^{3+}$  suggests that such reactions may take place in oxidising environments.

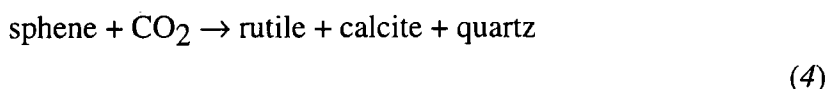
In packages of upper greenschist facies, thrust-related phyllonite and in packages of lower greenschist facies, sinistral strike-slip related phyllonite, hornblende grains are commonly observed to be fringed by actinolite + quartz  $\pm$  chlorite strain shadows. The most highly altered hornblende grains are locally pseudomorphed by actinolite fibres. These observations suggest that during phyllonitisation, the 'protolith' hornblende grains were breaking down to aggregates actinolite, quartz and chlorite. Such reactions are envisaged to be of the form:



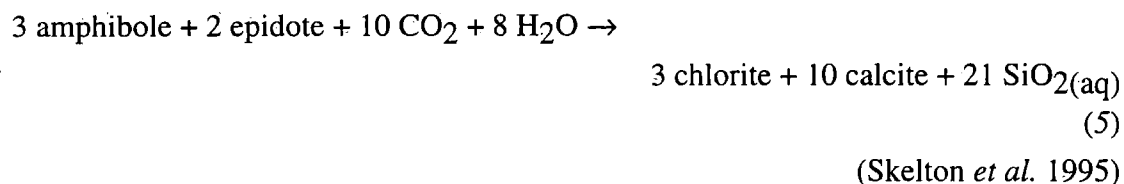
The breakdown of hornblende thus requires the addition of hydrous fluids, magnesium and ferrous iron. It is also possible that *ferric* iron ( $\text{Fe}^{3+}$ ) may also have been involved in such reactions.

Packages of reworked lower greenschist facies phyllonite preserved on Lewis, Scalpay, south Harris, North Uist and Ronay are characterised by an assemblage of

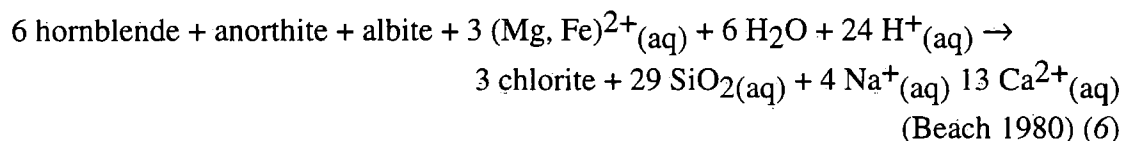
sericite, albite, chlorite, calcite. Calcic plagioclase and K-feldspar are rarely observed, and hornblende, actinolite and sphene are absent. These observations are consistent with (a) reactions (1) and (2) having virtually gone to completion, and (b) with amphibole (and sphene) having been replaced by calcite and chlorite. Such greenschist facies carbonation reactions are envisaged to be of the form:



and:



Carbonation reactions are thus promoted by the influx of CO<sub>2</sub>-bearing hydrous fluids. During transtension- and extension-related deformation on South Uist, hornblende appears to have been converted to chlorite *without* the precipitation of calcite. Chloritisation of hornblende can be described by reactions such as:



Such reactions require a source of magnesium, iron and water, and appear to be promoted by acidic conditions.

### 9.3.1.3 Summary and discussion

The metamorphic reactions described in the previous section provide some insights into the nature of the fluid phase during phyllonitisation along the OHFZ. Almost all the proposed reactions involve the addition of water, which is consistent with the fluids having been predominantly hydrous in nature. The breakdown of feldspar to sericite, albite and epidote also requires a source of ferric iron (e.g. reaction 1), which suggests that the fluids responsible for late Laxfordian / Grenvillian and Caledonian phyllonitisation had relatively high oxidation potentials.

Alteration of hornblende, either to actinolite + chlorite + quartz or to chlorite + quartz requires the addition of hydrous fluids, ferrous iron and magnesium (e.g. reactions 3 & 6). The source of iron and magnesium is unclear, but petrographic observations

suggest that hornblende is the dominant mafic mineral in the amphibolite facies gneisses of the Outer Hebrides (e.g. Table 9.10). It is therefore unlikely that iron and magnesium were derived locally from within the gneisses by the breakdown of other mafic phases. If this inference is correct, it is possible that iron and magnesium were derived from an *external* source, and transported to the reaction sites in aqueous solution. Thus, it is postulated that the fluids responsible for late Laxfordian / Grenvillian and Caledonian phyllonitisation were iron- and magnesium-bearing.

Packages of *reworked*, transtension- and extension-related lower greenschist facies phyllonite preserved on Lewis, Scalpay, south Harris, North Uist and Ronay are characterised by an abundance of chlorite and calcite. However, hornblende, actinolite and sphene are absent. These observations are consistent with hornblende, actinolite and sphene having been consumed by carbonation reactions, to produce chlorite and calcite (e.g. reactions 4 & 5). Such reactions can only proceed if the chemical potential of CO<sub>2</sub> is sufficiently high (see Graham *et al.* 1983) (Chapter 1). It is therefore postulated that during late Caledonian reworking within the phyllonite belts in the Northern Zone, North Uist and Ronay, the concentration of CO<sub>2</sub> in the fluids may have increased sufficiently to promote such carbonation reactions.

Petrographic observations suggest that although chlorite and epidote are abundant, the breakdown of hornblende during late Caledonian reworking and phyllonitisation on South Uist did *not* produce significant amounts of calcite. The chemical potential of CO<sub>2</sub> within the Usinish Phyllonite may therefore remained sufficiently low to prevent carbonation reactions from taking place (e.g. reaction 5). Possible controls on the activity of CO<sub>2</sub> during phyllonitisation are discussed in section 9.4. If this inference is correct, it is likely that hornblende breakdown during late Caledonian deformation on South Uist was controlled by hydration reactions, in the presence of iron- and magnesium-bearing fluids (e.g. reaction 6).

The pH of the fluids may, to some extent, have been buffered by the metamorphic reactions. For example, the breakdown of hornblende to aggregates of actinolite + chlorite + quartz (e.g. reaction 3) appears to *liberate* H<sup>+</sup>, whilst feldspar sericitisation reactions (e.g. reaction 2) and the breakdown of hornblende to chlorite + quartz (e.g. reaction 6) require the *addition* of H<sup>+</sup>. However, it is unclear whether such reactions would tend to buffer the pH to high or low values, and the precise value of pH is likely to have also been dependant on factors such as protolith composition and intensity of metamorphism.

In conclusion, the mineral reactions inferred to have controlled upper greenschist facies metamorphism are consistent with the influx of hydrous, iron- and magnesium-bearing fluids during late Laxfordian / Grenvillian phyllonitisation. The oxidation potential of the fluids was relatively high, and the chemical activity of CO<sub>2</sub> was

sufficiently low to suppress carbonation reactions. Reactions taking place during lower greenschist facies metamorphism are consistent with the influx of hydrous iron- and magnesium-bearing fluids during Caledonian phyllonitisation and subsequent reworking in the Northern Zone of the OHFZ, and on North Uist and Ronay. The oxidation potential of the fluids was sufficiently high for iron to exist in both ferrous and ferric states. During sinistral transpression and strike-slip, the chemical activity of CO<sub>2</sub> was low enough to suppress hornblende carbonation reactions. However, with the onset of transtension and extension (i.e. reworking within the phyllonite belts), there appears to have been a general increase in chemical activity of CO<sub>2</sub>, although on South Uist, the chemical activity of CO<sub>2</sub> appears to have been remained relatively low *throughout* Caledonian deformation. The possible controls on CO<sub>2</sub> on South Uist are discussed in section 9.4.3.4.

### 9.3.2 FAULT ROCK GEOCHEMISTRY

The geochemical behaviour of certain major and trace elements can be used to further constrain the composition and chemical characteristics of the fluid phase. The following section discusses major and trace element data, obtained from selected lower greenschist facies phyllonites and their protoliths, from North Uist and Ronay (Chapter 8).

#### 9.3.2.1 Major elements

The lower greenschist facies phyllonites are strongly enriched in loss on ignition (LOI), magnesium, iron and titanium, relative to the protolith gneisses (Fig. 8.2). Loss on ignition is a measure of the amount of fluid which is either bound into the lattices of hydrous minerals, or trapped as inclusions within the rock. An increase in LOI therefore suggests that there has been an increase in the concentration of fluid inclusions and / or an increase in the abundance of hydrous minerals, both of which are consistent with fluid-rock interaction and hydration during retrograde metamorphism.

The enrichment of iron, magnesium and titanium is consistent with these elements being *added* to the fault rocks during phyllonitisation (section 9.3.1.3).

#### 9.3.2.2 Trace elements

##### *Trace element mobility*

The mobility of particular trace elements during phyllonitisation can be used to make inferences regarding the geochemical nature of the fluid phase. Rare earth elements (REE) tend to be relatively immobile during low-grade metamorphism. However,

REEs are able to form aqueous carbonate- and halide complexes. The REEs are thus thought to be relatively mobile in carbonate- and / or halogen-bearing fluids (Grauch 1989). The protolith-normalised REE concentrations obtained from samples of lower greenschist facies phyllonite suggest that the REEs behaved in a relatively mobile manner during phyllonitisation (see discussion in section 8.4.5). It is therefore postulated that the fluids responsible for Caledonian phyllonitisation on North Uist and Ronay contained significant concentrations of carbonate- and / or halide ions.

Experimental studies conducted at room temperatures and pressures suggest that uranium will only form aqueous complexes under oxidising conditions (e.g. see Gill 1989) (Fig. 9.6). Uranium is likely to display broadly similar behaviour at higher temperatures and pressures. Protolith-normalised uranium concentrations obtained from samples of lower greenschist facies phyllonite are extremely variable, but are typically depleted with respect to the Lewisian protoliths (Fig. 8.12). These observations suggest that uranium behaved in an mobile manner during phyllonitisation. It is therefore concluded that the fluids responsible for Caledonian phyllonitisation were characterised by a relatively high oxidation potential.

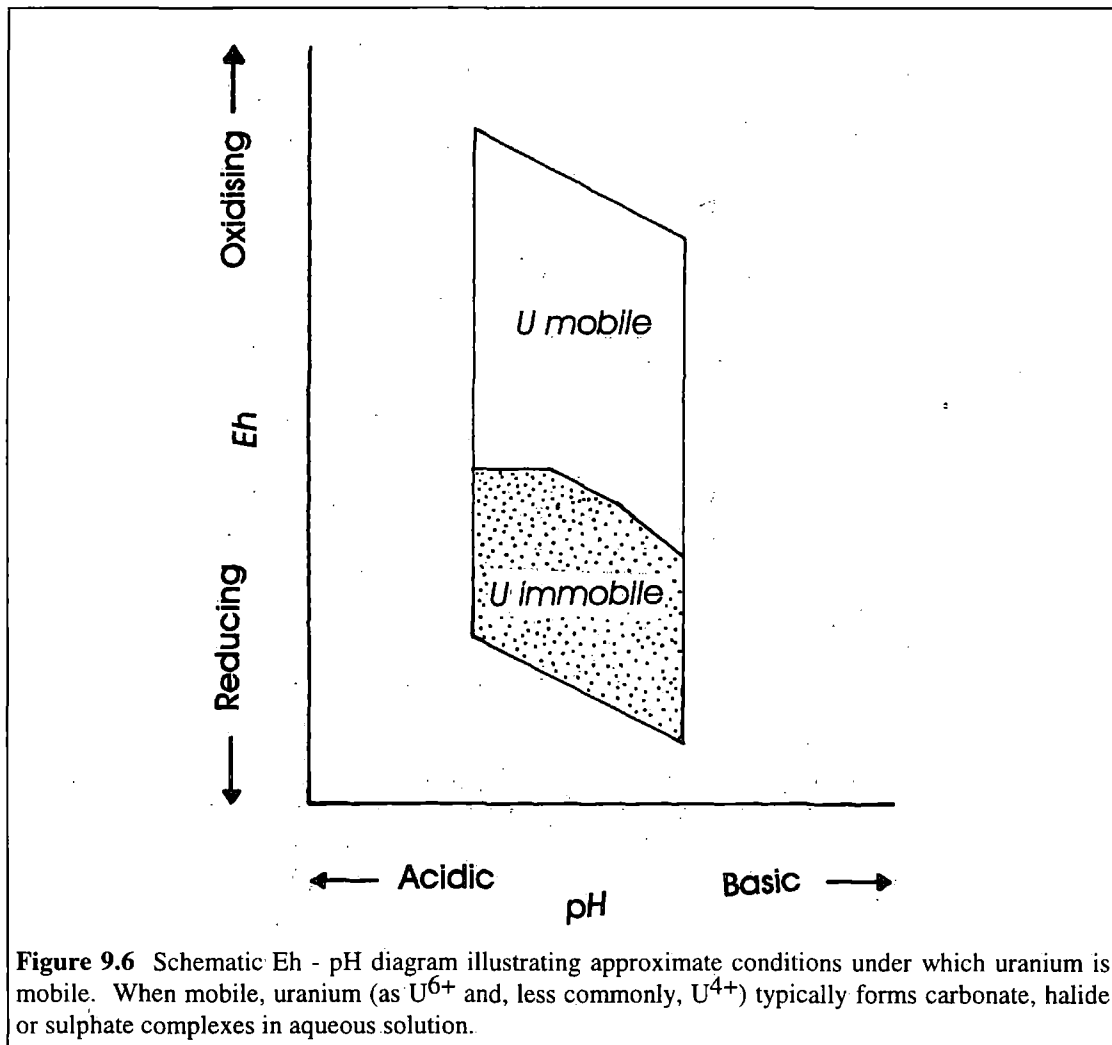


**Figure 9.6** Schematic Eh - pH diagram illustrating approximate conditions under which uranium is mobile. When mobile, uranium (as  $U^{6+}$  and, less commonly,  $U^{4+}$ ) typically forms carbonate, halide or sulphate complexes in aqueous solution.

### ***Trace element concentrations***

The protolith-normalised REE and 'immobile' trace element concentrations obtained from samples of lower greenschist facies phyllonite from North Uist and Ronay display characteristic trends, which reflect changes in the composition, fluid pressure and chemical activity of the fluid phase (see discussion in section 8.4.5.3). The REE and 'immobile' trace element patterns obtained from samples of transpression- and strike-slip related phyllonite are distinct from those obtained from samples of reworked, transtension- / extension-related phyllonite (Figs. 8.7 & 8.12). It has therefore been postulated that there was a marked change in the geochemical nature of the fluid phase at the onset of transtension / extension (see discussion in section 8.4.5.3). This observation is consistent with the inference that there was an increase in the chemical activity of CO<sub>2</sub> at the onset of transtension / extension (section 9.3.1.3).

Chondrite-normalised REE concentrations obtained from the samples of phyllonite are typically smooth and, in particular, do *not* display strong europium (Eu) anomalies (Figs. 8.4, 8.5 & 8.6). Europium exists either in a divalent (Eu<sup>2+</sup>) or trivalent (Eu<sup>3+</sup>) state, depending on the oxidation conditions. Eu<sup>2+</sup> is preferentially incorporated into plagioclase (e.g. see Hall 1987). In environments with low oxidation potential, plagioclase-rich rocks are thus expected to display strong, positive europium anomalies. The lower greenschist facies phyllonites contain abundant albite ± relict plagioclase and K-feldspar grains. The absence of a positive europium anomaly therefore suggests that phyllonitisation and retrogression occurred in a relatively oxidising environment. This is consistent with the conclusions drawn from the presence of ferric iron-bearing minerals, and from the high mobility of uranium during phyllonitisation (see above and section 9.3.1.3).

### **9.3.2.3 Summary**

In conclusion, the hydrous fluids responsible for lower greenschist facies phyllonitisation on North Uist and Ronay appear to have contained abundant dissolved iron, magnesium, titanium, uranium and rare earth elements (the latter probably as carbonate or halide complexes). It is likely that the fluids were relatively oxidising in nature, and that there was a change in the geochemical characteristics of the fluids at the onset of transtension- / extension-related deformation. The change in fluid chemistry is likely to have been related to the inferred increase in the activity of CO<sub>2</sub> at the onset of transtension / extension, although it is not possible to rule out other causes (see discussion in section 9.4).

### 9.3.3 FLUID SOURCES

Walker (1990) suggested that the fluids responsible for phyllonitisation along the OHFZ were derived from basic magmas associated with Tertiary volcanism in the North Atlantic region. However, the latest phase of phyllonitisation recognised along the OHFZ is of probable Caledonian age, and thus pre-dates Tertiary igneous activity by several hundred million years. The metamorphic fluids therefore *cannot* have been derived from Tertiary magmas. In the absence of oxygen isotope date, however, it is impossible to determine the sources of either the late Laxfordian / Grenvillian or Caledonian fluids. Consequently, no attempt has been made to speculate on the likely origins of these fluids.

## 9.4 MECHANISMS OF FLUID FLOW

Deformation across the reaction-modified frictional to viscous creep transition is likely to have been influenced by the fluid transport properties of the OHFZ. In particular, *permeable* fault rocks will be more susceptible to retrograde metamorphism than relatively impermeable fault rocks. It is important to emphasise that at the *onset* of phyllonitisation, fluid flow is likely to have been controlled by the porosity and permeability ('poroperm') characteristics of the pre-existing fault rocks (i.e. the primary fabrics). However, the fluid transport properties of the fault zone are likely to have evolved rapidly with increasing strain and retrogression. The following section therefore considers the poroperm characteristics of the primary fabrics *and* of the phyllonitic fault rocks themselves.

The likely syn-tectonic fluid pathways have been inferred from the microstructural distribution of retrograde metamorphic minerals (Chapter 1). However, it should be stressed that the absence of syn-tectonic retrogression may suggest either (a) that fluids were not present during deformation, or (b) that the fluids were in local *equilibrium* with the wall rocks (McCaig & Knipe 1990). Thus, in the absence of detailed oxygen isotope studies, the following sections can only provide crude 'first order' indications of the likely fluid transport properties of the fault zone.

## 9.4.1 UPPER GREENSCHIST FACIES MYLONITES AND PHYLLONITES

It is important to discuss the fluid transport properties of the upper greenschist facies fabrics for two reasons. Firstly, upper greenschist facies deformation was associated with an important episode of late Laxfordian / Grevillian phyllonitisation and fluid influx in the Northern Zone of the OHFZ. Secondly, phyllonitisation and fluid influx during subsequent *lower* greenschist facies Caledonian deformation appear to have been localised along pre-existing bands of upper greenschist facies mylonite (Fig. 9.3a).

### 9.4.1.1 Microstructure: evidence for fluid-rock interaction

The upper greenschist facies mylonites preserved in the Northern Zone of the OHFZ display evidence for widespread syn-tectonic retrogression and hydration (see Chapter 5 for detailed description). Packages of upper greenschist facies quartzo-feldspathic mylonite and phyllonite comprise networks of polycrystalline quartz ribbons and / or sericite strands, which wrap around the margins of highly altered hornblende and sericitised feldspar grains. Sericite needles account for up to 80% of the surface area of host feldspar grains viewed in thin section, and the effects of sericitisation are particularly intense along feldspar grain boundaries which are oriented sub-parallel to the regional foliation. The macroscopically ductile fabrics are locally cross-cut by tensile, *transgranular* hydrofractures, which are either oriented sub-parallel, or perpendicular to the foliation. Hornblende porphyroclasts preserved within packages of quartzo-feldspathic mylonite and phyllonite are typically fringed by fibrous actinolite strain shadows, and are locally cross-cut by tensile, *intragranular* fractures. The fibrous actinolite-quartz fracture infills are commonly observed to display well developed crack-seal textures (Ramsay 1980a).

Packages of protomylonitic amphibolite comprise aggregates of interlocking hornblende grains, which isolate pockets of quartz and / or partially sericitised feldspar grains. The protomylonitic fabric is locally cross-cut by tensile, *transgranular* crack-seal veins. Individual hornblende grains are commonly observed to be deformed by arrays of tensile, *intragranular* fractures, and are locally fringed by fibrous actinolite strain shadows.

### 9.4.1.2 Fluid transport properties

#### *Porosity and permeability characteristics*

The abundance of syn-tectonic, tensile hydrofractures is consistent with mylonitisation having occurred in a non-hydrostatically stressed regime, in which the pore fluid pressure locally exceeded the minimum principal stress ( $\sigma_3$ ) (Etheridge 1983).

Microstructural observations suggest that syn-tectonic fluid-rock interaction resulted in:

- Fracture opening during periods of particularly high pore fluid pressure.
- Fracture sealing, which appears to have been broadly synchronous with fracture opening.
- Pervasive alteration of feldspar to aggregates of sericite needles.
- Growth of fibrous actinolite strain shadows around hornblende porphyroclasts.

The abundance of crack-seal textures is consistent with fracture *sealing* having been broadly synchronous with fracture *opening*. This observation suggests that fracture permeability was *transient*, and decreased rapidly during sealing (Cox & Etheridge 1989). Furthermore, individual hydrofractures do not appear to display a high degree of interconnectivity. It is therefore unlikely that networks of hydrofractures ever formed permanent, 'through-going' high permeability pathways within the mylonite belt (cf. Sibson 1996). Feldspar grains preserved within the upper greenschist facies mylonite belt typically display evidence of *pervasive*, syn-tectonic sericitisation. Sericitisation reactions require a chemically active, syn-tectonic fluid phase (section 9.3.1). This observation suggests that fluid flow was *pervasive*, both on the scale of *individual feldspar grains* and on the scale of *the entire mylonite belt* i.e. fluids were not confined to the hydrofracture networks described above. Sericite needles are particularly abundant along feldspar grain boundaries, and the grain boundaries of neocrystallised albite aggregates are commonly observed to be decorated by arrays of ultrafine grained fluid inclusions (Chapter 5). It is therefore postulated that a significant proportion of the syn-tectonic porosity may have been associated with (a) networks of interconnected grain boundary voids and / or *intergranular* microfractures (Graham *et al.* 1997), and (b) with aggregates of porous (and permeable) feldspar grains (cf. David *et al.* 1995) (see section 9.4.2 for further discussion of the porosity and permeability characteristics of feldspar).

The intensity of upper greenschist facies retrogression is also heterogeneous on *outcrop-* and *regional* scales. Detailed field observations suggest that alteration was particularly intense within bands of upper greenschist facies phyllonite (Chapter 5). The controls on heterogeneous meso- and macro-scale fluid flow are a matter of speculation. However, there is a positive correlation between the magnitude of finite strain and the degree of syn-tectonic retrogression during upper greenschist facies thrusting. Thus, it is possible that fluid flow and syn-tectonic alteration were focused into high strain zones within the mylonite belt (Oliver 1996) (see discussion in Chapter 5).

### ***Fluid flow mechanisms***

The available microstructural evidence is consistent with syn-tectonic fluids having been contained within two separate, but possibly interconnected, porosity networks (see above), which comprised:

- Transient, intra- and transgranular hydrofractures (i.e. *fracture porosity*).
- Porous feldspar grains, feldspar grain boundary voids and / or intergranular microfractures (i.e. *grain porosity*).

Oliver (1996) has suggested that the overpressures required to induce hydraulic fracturing in mid crustal rocks may result from changes in porosity caused by (viscous) deformation. Fracturing increases dilatancy and causes significant localised reductions in pore fluid pressure (e.g. Sibson 1990). Consequently, hydraulic gradients within the upper greenschist facies mylonite belt are likely to have been disturbed by repeated hydrofracturing. Such perturbations in hydraulic head may have driven fluids towards dilatant regions during each hydrofracture event. If these inferences are correct, it is possible that *grain-scale dilatancy pumping* mechanisms may have controlled syn-tectonic fluid flow (Oliver 1996). In order for dilatancy pumping to have been an effective mechanism for driving syn-tectonic fluid flow, the feldspar- / feldspar grain boundary-dominated porosity network must have been sufficiently interconnected and permeable to respond to transient changes in hydraulic gradient (cf. Cox & Etheridge 1989). Further studies are required to establish the permeability characteristics of, and the degree of interconnection between, the two porosity networks within the upper greenschist facies mylonite belt (cf. Géraud *et al.* 1995).

## **9.4.2 CRUSH MELANGE AND PSEUDOTACHYLYTE-ULTRACATACLASITE CRUSH ZONES**

Phyllonitic fabrics exposed in the Southern Zone of the OHFZ appear to have localised within pre-existing regions of intense brittle deformation. It is therefore of utmost importance to discuss the fluid transport properties of the crush melange and pseudotachylyte-ultracataclasite crush zones.

### **9.4.2.1 Microstructure: evidence for fluid-rock interaction**

The crush melange comprises randomly oriented blocks of fractured gneiss, which 'float' in a matrix of ultrafine grained cataclasite seams and devitrified pseudotachylyte veins (matrix  $\leq 50\%$  by volume). The pseudotachylyte-ultracataclasite crush zones

are characterised by a higher proportion of cataclasite / pseudotachylyte (matrix c.70% by volume) than the crush melange, and are typically cross-cut by several sets of closely-spaced joints and fractures.

Retrogression within the crush melange and pseudotachylyte-ultracataclasite crush zones clearly post-dates the cessation of intense, thrust-related brittle deformation. Almost all the feldspar grains preserved within the crush melange and pseudotachylyte-ultracataclasite crush zones display evidence of pervasive sericitisation. Sericite accounts for up to 70% of the surface area of host feldspar grains, and the sericite needles typically display well developed 'mesh' textures (see below). However, brittle fractures, cataclasite seams and devitrified pseudotachylyte veins are commonly observed to be overprinted by aggregates of epidote, opaque minerals and / or chlorite. This observation is consistent with zones of intense brittle deformation having experienced particularly intense retrogression and alteration following the cessation of brittle, thrust-related deformation (see Chapters 6 & 8).

#### **9.4.2.2 Fluid transport properties**

##### ***Porosity and permeability characteristics***

It has been postulated that the heterogeneous distribution of low grade alteration products is consistent with the crush melange and pseudotachylyte-ultracataclasite crush zones having been characterised by dual porosity / dual permeability fluid transport properties (Chapter 6). In particular, it has been suggested that blocks of relatively undeformed gneiss possessed relatively low porosities and permeabilities, whilst networks of interconnected meso- and macro-scale fractures, cataclasite seams and devitrified pseudotachylyte seams ('cataclastic fault zones') possessed relatively high porosities and permeabilities (see discussion in section 6.3.4). Thus, fluid flow within intensely deformed pseudotachylyte-ultracataclasite crush zones is likely to have been dominated by the high porosity / high permeability system, whilst fluid flow through the less deformed crush melange is likely to have been dominated by the low porosity / low permeability system.

Blocks of relatively undeformed gneiss (i.e. regions characterised by especially low porosities / low permeabilities) preserved within the crush melange are primarily composed of aggregates of partially sericitised feldspar grains. The sericite needles are evenly distributed throughout host feldspar grains, and do not appear to be concentrated along grain boundaries. These observations suggest that fluids were (a) *evenly distributed throughout the low porosity / low permeability crush melange*, and (b) *that fluid infiltration was pervasive on the scale of individual feldspar grains* (see also section 9.4.1). Sericite needles preserved in partially altered feldspar grains

typically display well developed 'mesh' textures. Mesh textures are defined by up to three sets of sericite needles, which intersect at angles of between 30° and 110°. The regular arrangement of the sericite needles is consistent with alteration having been controlled by the crystallographic structure of the host feldspar grains. Feldspar grains typically display three sets of cleavages, which are developed parallel to the {001}, {010} and {110} faces (Deer *et al.* 1992). It is therefore postulated (a) that the mesh texture geometries may reflect the orientations of the feldspar cleavage planes, and (b) that fluid infiltration may have occurred along feldspar cleavage planes. In the absence of detailed TEM data, the precise nature of these intracrystalline permeability pathways is unclear. However, pervasive cleavage microfracture arrays have been observed in feldspar aggregates deformed experimentally under dry conditions at c.300°C (Tullis & Yund 1992). It is therefore not inconceivable that intracrystalline cleavage microcrack arrays may have developed in feldspar grains during dry, thrust-related deformation along the OHFZ. Furthermore, Kronenberg *et al.* (1990) have suggested that pervasive fluid infiltration occurs along dilatant microfractures and / or dislocation cores in feldspar grains. It is therefore postulated that *the fluid transport properties of the low porosity / low permeability system were dominated by interconnected, intracrystalline cleavage fracture arrays within feldspar grains.*

### ***Fluid flow mechanisms***

Butler (1995) and Butler *et al.* (1995) have postulated that fluid influx into the crush melange was controlled by a change in the regional kinematic regime, from thrusting to sinistral strike-slip. Reverse (thrust) faults display load-strengthening behaviour, whilst strike-slip faults may display load-weakening behaviour (Sibson 1993). Load-strengthening faults are generally associated with high mean stresses, which tends to reduce fault zone dilatancy and permeability. In contrast, load-weakening faults are generally associated with lower mean stresses, which tends to increase fault zone dilatancy and permeability (see Chapter 1). It was therefore been argued that the change in fault zone kinematics caused a switch from load-strengthening to load-weakening behaviour, which in turn promoted an increase in fault zone permeability allowing widespread fluid influx and retrogression within the crush melange (Butler 1995; Butler *et al.* 1995).

Field observations made during the present study suggest that the onset of regional sinistral transpression was associated with limited, localised retrogression, whilst the onset of regional sinistral strike-slip was associated with widespread, intense retrogression within the crush melange. The field relationships are therefore consistent with the notion that fluid influx was facilitated by a kinematically-controlled increase in fault zone permeability. Following the cessation of brittle

thrusting, the poroperm network within the crush melange is inferred to have been dominated by arrays of intracrystalline cleavage microfractures in feldspar grains (see above). It is therefore postulated that during transpression (i.e. load-strengthening behaviour), the high mean stresses may have effectively held the intracrystalline microfractures 'shut', resulting in very low permeabilities. The onset of sinistral strike-slip (i.e. load weakening behaviour) was probably associated with a decrease in the mean stress. A reduction in mean stress may have allowed the microfractures to dilate, hence increasing the overall permeability of the fault zone.

### **9.4.3 LOWER GREENSCHIST FACIES PHYLLONITE**

There is abundant textural evidence to suggest that during late Caledonian transtension and extension, fluid flow was predominantly (though not entirely) focused within packages of actively deforming phyllonite. It is therefore of utmost importance to discuss the fluid transport properties of the lower greenschist facies phyllonite belts.

Packages of lower greenschist facies phyllonite comprise several different microstructural domains, including:

- Domains of relatively undeformed, protophyllonitic gneiss.
- Domains of felsic phyllonite and ultraphyllonite.
- Domains of mafic phyllonite and ultraphyllonite.
- Domains of epidote-rich phyllonite.

The heterogeneous nature of the phyllonites reflects a number of different factors including protolith lithology, the structure and lithology of the primary fabrics and the effects of strain and retrogression (see discussion in Chapter 6). Thus, the fluid transport properties of a particular phyllonite belt are likely to have been characterised by considerable *spatial* and *temporal* variations. Owing to the limited data available, the conclusions presented below are therefore likely to be gross over-simplifications.

#### **9.4.3.1 Microstructure: evidence for fluid-rock interaction**

##### ***Protophyllonite***

Domains of relatively undeformed protophyllonitic gneiss appear to have developed within regions of intrinsically low *inherited* permeability (e.g. within low porosity / low permeability regions of the crush melange) (see discussions in Chapters 6 & 7). Protophyllonite is characterised by fractured quartz and / or partially sericitised feldspar grains, which are locally wrapped by networks of sericite strands. The quartz

porphyroclasts are commonly observed to be cross-cut by tensile, intragranular fractures, which are either infilled by aggregates of fibrous quartz and / or quartz-calcite. Fibrous quartz or quartz-calcite overgrowths locally fringe the margins of quartz porphyroclasts. Feldspar grains display well developed sericite mesh textures, and sericite strands are commonly observed along feldspar grain boundaries which are oriented sub-parallel to the macroscopic foliation. Relatively unaltered feldspar grains are cross-cut by arrays of tensile, *intragranular* fractures. The fractures are typically infilled by aggregates of fine-grained albite and trails of fluid inclusions. Foliation-parallel, syn-tectonic transgranular quartz-epidote veins are locally preserved.

### ***Phyllonite and ultraphyllonite***

Domains of phyllonite and ultraphyllonite appear to have developed within regions of intrinsically high *inherited* permeability (e.g. within high porosity / high permeability meso- and macro-scale fault zones within the crush melange) (see discussions in Chapters 6 & 7). Phyllonites and ultraphyllonites are characterised by isolated quartz and feldspar porphyroclasts, which are either wrapped by laterally continuous sericite and chlorite strands, or 'float' in a matrix of ultrafine-grained quartz, albite, epidote and chlorite. The porphyroclasts are typically fringed by fibrous quartz-chlorite strain shadows, and are locally cross-cut by arrays of tensile, intragranular hydrofractures. However, intragranular hydrofractures are less commonly observed in packages of phyllonite and ultraphyllonite than in packages of protophyllonite. Feldspar grains typically display evidence for intense (locally complete) sericitisation. Relatively unaltered sericite porphyroclasts are locally preserved, and are typically surrounded by mantles of ultrafine grained albite. The albite grain boundaries are commonly observed to be decorated by arrays of ultrafine fluid inclusions.

Multiple generations of syn-tectonic albite-calcite-quartz-calcite vein arrays are commonly observed in packages of *reworked* phyllonite from the Northern Zone, North Uist and Ronay. The veins comprise:

- . Centimetre-scale, foliation-parallel tensile vein arrays, within packages of planar phyllonite (particularly common on Scalpay) (see description in Chapter 5).
- . Millimetre- to centimetre-scale, en-echelon vein arrays, within packages of planar phyllonite (*locally* developed within the Usinish Phyllonite, South Uist) (see descriptions in Chapters 5, 6 & 7).
- . Metre- to tens-of-metres-scale, foliation-parallel shear hydraulic fractures ('Type 1' detachments), within packages of planar phyllonite (particularly common on North Uist) (see description in Chapter 6).

- Millimetre- to metre-scale, axial planar vein arrays, within packages of folded phyllonite (see description in Chapter 6).

#### 9.4.3.2 Fluid transport properties of protophyllonitic gneiss

##### *Porosity and permeability characteristics*

The microstructures observed in packages of lower greenschist facies protophyllonite are, in some respects, similar to those observed in packages of upper greenschist facies quartzo-feldspathic mylonite (section 9.4.1). In particular, the abundance of tensile hydrofractures is consistent with deformation having occurred in a non-hydrostatically stressed environment, in which the fluid pressure locally exceeded the minimum principal stress (Etheridge 1983) (see Chapter 1). Microstructural observations suggest that syn-tectonic fluid-rock interaction caused:

- Fracture opening during periods of particularly high pore fluid pressure.
- Fracture sealing and mineralisation.
- Pervasive alteration of feldspar to aggregates of sericite needles.
- Growth of fibrous quartz and quartz-chlorite strain shadows around hornblende porphyroclasts.

The tensile, intragranular hydrofractures display a low degree of interconnectivity. Furthermore, although crack-seal textures are not widely preserved, the abundance of fibrous fracture infills is consistent with fracture sealing having been broadly synchronous with fracture opening. These observations suggest that (a) fracture permeability was transient, and (b) that a relatively small volume of the total syn-tectonic porosity was associated with hydrofractures (see discussion in section 9.4.1.2). Feldspar grains preserved within domains of protophyllonitic gneiss typically display well developed sericite mesh textures and are locally wrapped by sericite strands. These observations suggest that fluid infiltration was pervasive on the scale of individual feldspar grains, and that a significant proportion of the syn-tectonic porosity may have been associated with networks of intracrystalline cleavage microfractures within feldspar grains, and grain boundary networks / *intergranular* microfractures around the margins of feldspar grains (see discussions in sections 9.4.1.2 & 9.4.2.2). It is likely that some of this porosity may have been *inherited* from the primary fabrics (e.g. the crush melange).

### ***Fluid flow mechanisms***

The available microstructural evidence is consistent with syn-tectonic fluids having been contained within two separate, but probably interconnected, porosity networks (see above), which comprised:

- Transient, predominantly grain-scale intra- and transgranular hydrofractures (fracture porosity).
- Porous feldspar grains, feldspar grain boundary networks and / or *intergranular* microfractures (grain porosity).

Hydrofracturing is likely to have been an important mechanism for (a) increasing dilatancy, and (b) causing perturbations in the hydraulic gradients within packages of protophyllonite. Provided that the permeability of the porous feldspar grains and feldspar grain boundary networks was sufficient for the fluids to respond to rapid changes in the local fluid pressure gradient, it is possible that fluid flow may have been controlled by grain-scale *hydrofracture-driven dilatancy pumping* mechanisms (see discussion in section 9.4.1.2). If this inference is correct, it is likely that fluid flow through packages of protophyllonite was significantly enhanced during periods of active deformation. This observation has important implications for the hydrogeological behaviour of the OHFZ during transtension- and extension-related reworking (see section 9.4.3.4).

### **9.4.3.3 Fluid transport properties of phyllonite and ultraphyllonite**

#### ***Porosity and permeability characteristics***

The microstructures observed in packages of fine grained, highly retrogressed lower greenschist facies phyllonite and ultraphyllonite differ significantly from those observed in packages of protophyllonite. In particular, the fine grain size and low abundance of porphyroclasts appears to have inhibited the development of *intragranular* hydrofractures. However, the presence of syn-tectonic transgranular shear and tensile hydraulic fractures, particularly within packages of reworked phyllonite, is consistent with deformation having occurred in a non-hydrostatically stressed environment, in which the pore fluid pressure locally exceeded the minimum principal compressive stress.

Hydrofractures are commonly observed to be infilled by aggregates of fibrous quartz, chlorite, calcite, albite or epidote. Although crack-seal textures are not commonly preserved, it is possible that fracture sealing may have been broadly synchronous with fracture opening. thus, it is postulated that fracture porosity and permeability were

*transient*, and decreased rapidly due to mineral precipitation (see discussion in section 9.4.1.2). Foliation-parallel tensile veins and en-echelon vein arrays are characterised by very low degrees of interconnectivity. However, the foliation-parallel shear hydraulic fractures and tensile axial planar vein arrays preserved in packages of reworked phyllonite typically extend over several tens-of-metres. This observation is consistent with *the shear hydraulic fractures and tensile axial planar vein arrays having been important fluid transport pathways during reworking* (cf. Skelton *et al.* 1995; Graham *et al.* 1997).

Feldspar grains preserved within packages of phyllonite and ultraphyllonite typically display evidence of intense, pervasive sericitisation. For the reasons outlined in section 9.4.2.2, it is postulated that a significant proportion of the syn-tectonic porosity was associated with intracrystalline microfractures within feldspar grains. In addition, fluid inclusions are commonly observed along grain boundaries in neocrystallised albite aggregates. Previous workers have suggested that grain boundary voids and intergranular microcracks account for a significant proportion of the total porosity in fine grained phyllonites. Thus, although the ultrafine grain size precludes detailed optical analysis, it is not inconceivable that quartz and phyllosilicate grains preserved within the phyllonitic matrix were also associated with porous grain boundary voids and / or *intergranular* microcracks.

In conclusion, it is likely that the total syn-tectonic porosity was composed of (a) transient hydrofracture porosity, (b) intracrystalline cleavage microfractures (i.e. inherited porosity) and (c) grain boundary voids and intergranular microfractures.

#### ***Fluid flow mechanisms during sinistral strike-slip***

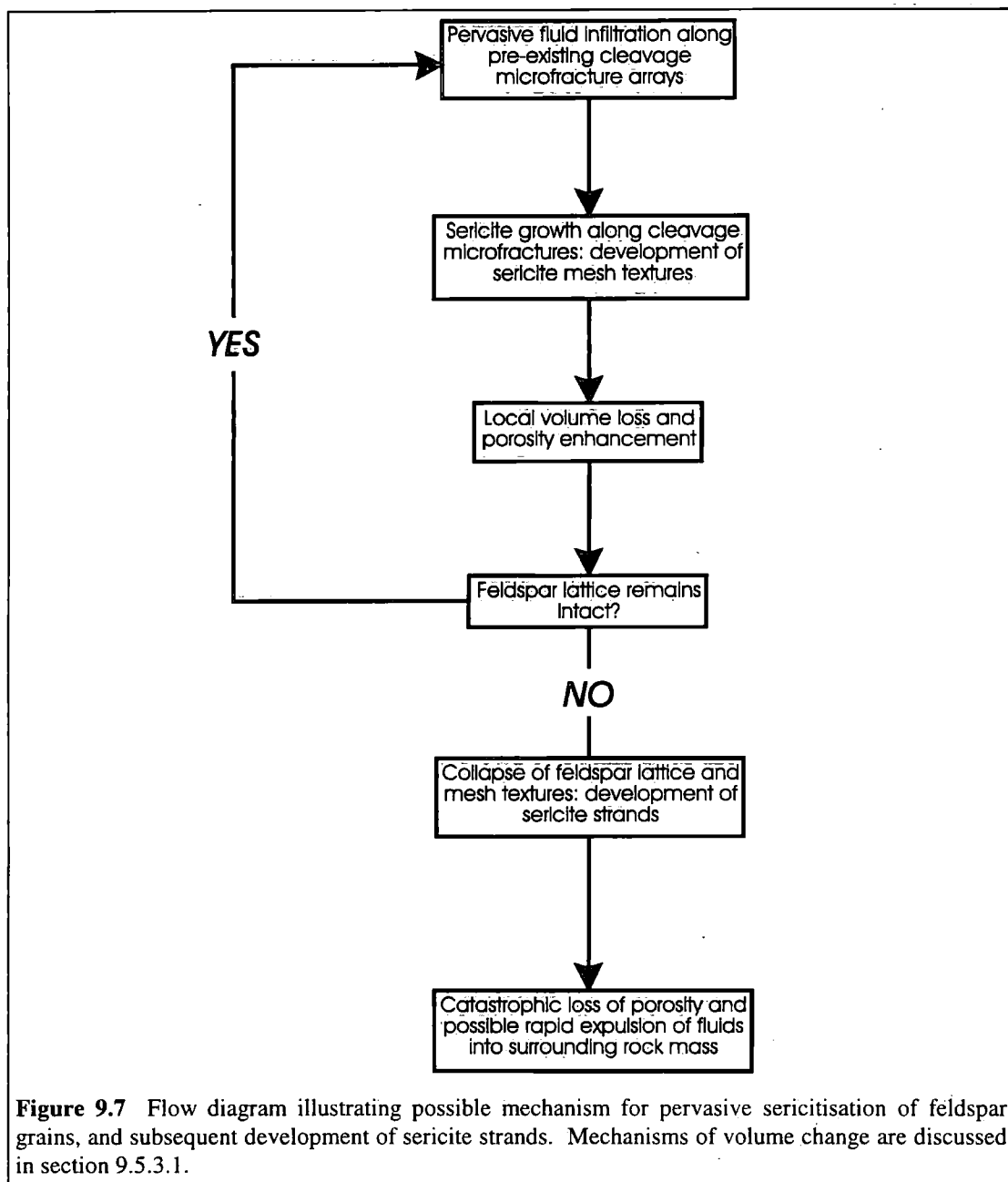
*Sinistral strike-slip* related deformation within the phyllonite belts was characterised by intense retrogression, in particular the alteration of feldspar to aggregates of fine-grained sericite. However, *reworking* within the phyllonite belts appears to have been dominated by hydrofracture and folding. It is therefore postulated that the mechanisms driving fluid flow through the phyllonitic shear zones may have changed through time. The following sections therefore discuss the possible fluid flow mechanisms (a) at the onset of phyllonitisation, and (b) during reworking.

The available textural evidence is consistent with fluids having been contained within two separate, but probably interconnected porosity networks, comprising:

- Transient, millimetre- to tens-of-metres-scale trans- and intragranular syn-tectonic hydrofractures (fracture porosity).
- Porous feldspar grains, and networks of grain boundary voids and / or intergranular microcracks (grain porosity).

However, *transgranular* hydrofractures are rarely observed in packages of non-reworked, sinistral strike-slip related phyllonite. Furthermore, *intragranular* hydrofractures have only been observed in packages of sinistral strike-slip related phyllonite which contain abundant porphyroclasts. Consequently, grain-scale hydrofracture-driven dilatancy pumping is *not* thought to have been the dominant fluid flow mechanism at the during phyllonitisation. The following section discusses other possible operative fluid flow mechanisms during sinistral strike-slip.

It has been suggested that significant volumes of fluid may have been contained in porous, intracrystalline cleavage microfracture arrays within feldspar grains. However, pervasive fluid infiltration promoted the growth of sericite needles within host feldspar grains, producing distinctive 'mesh' textures. Textural evidence suggests that provided the sericite needles were sufficiently interconnected, feldspar grains eventually 'collapse', (i.e. became flattened parallel to the regional foliation), forming strands of highly aligned sericite needles (see discussion in section 9.7). Collapse of the feldspar grains is likely to have had important consequences for fluid flow. In particular, 'compaction' of sericite mesh textures into sericite strands may have significantly reduced the porosity and permeability of the phyllonite belts. Furthermore, the permeability is likely to have become increasingly *directional*, with fluid flow focused parallel to the developing sericite strands (Graham *et al.* 1997). An interesting corollary of these arguments is that, in the absence of significant intragranular hydrofracturing, pervasive alteration and collapse of feldspar may have provided an alternative mechanism for driving fluids through the phyllonite belts. It is postulated that during collapse of the intracrystalline cleavage microfracture network, any fluids remaining within the feldspar lattice may have been rapidly expelled into the surrounding matrix (Fig. 9.7). Further detailed studies are required to investigate the viability of such 'retrogression-driven' dilatancy pumping mechanisms (see discussion in section 9.7).



### ***Fluid flow mechanisms during reworking***

Packages of reworked phyllonite are characterised by intense (locally complete) retrogression of the protolith mineral assemblages to aggregates of ultrafine-grained epidote, albite and highly aligned phyllosilicates. These observations suggest that grain-scale hydrofracture- and / or retrogression-driven dilatancy pumping mechanisms are *unlikely* to have been important in controlling fluid flow.

Most belts of reworked phyllonite are cross-cut by abundant syn-tectonic shear and tensile hydraulic fracture arrays. Field relationships suggest (a) that the largest veins originated as shear hydraulic fractures, and (b) that several episodes of vein emplacement occurred throughout macroscopically ductile reworking within the

phyllonite belts. These observations are consistent with Sibson's (1990) criteria for recognising *fault-valve* behaviour.

Fault-valve behaviour requires (a) continual fluid input into a fault zone and (b) the presence of a regional permeability barrier, in order that fluid pressures are able to build up sufficiently to cause hydrofracturing (see Chapter 1). Reworking on South Uist was accompanied by the generation of new phyllonitic fabrics in previously non-phyllonitised rocks (see Chapter 7). It has been demonstrated by previous authors that significant quantities of fluid are required to allow phyllonitisation (e.g. O'Hara 1988; Walker 1990). Furthermore, geochemical studies of samples of reworked phyllonite from North Uist suggest that the composition of syn-tectonic fluids present during reworking may have differed significantly from that of syn-tectonic fluids present during sinistral strike-slip (see discussions in Chapter 8). These observations are consistent with *significant fluid influx into the fault zone during reworking*.

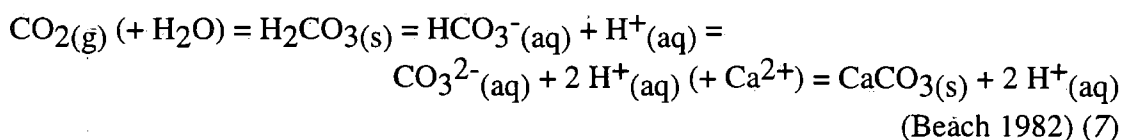
Kennedy & Logan (1997) have suggested that during mylonitisation along the McConnell thrust in Alberta, the development of fine-grained, clay-rich seams reduced the permeability of the thrust zone sufficiently to promote high fluid pressures and localised hydrofracturing. It is therefore possible that the sericite and chlorite strands preserved within the phyllonite belts may have behaved as permeability barriers during reworking. However, syn-tectonic hydrofractures are rarely observed within the phyllosilicate-rich Usinish Phyllonite belt on South Uist (see Chapter 7). This observation suggests that sericite and chlorite strands are unlikely to have behaved as *regionally significant* permeability barriers during reworking. The phyllonite belts preserved in the Northern Zone of the OHFZ, and on North Uist and Ronay are surrounded either by upper greenschist facies mylonite or by lower greenschist facies pervasive protophyllonite. Syn-tectonic fluid flow through the upper greenschist facies mylonite belt and through regions of lower greenschist facies pervasive protophyllonite appears to have been controlled by grain-scale, hydrofracture-driven dilatancy pumping (see discussions in sections 9.4.1.2 & 9.4.3.3). Thus, the *syn-tectonic* permeability of these fault rocks is likely to have been significantly higher than their *static* (i.e. intrinsic) permeability. There is no evidence to suggest that either the upper greenschist facies mylonites or the pervasive protophyllonites were reactivated during extension-related reworking within the phyllonite belts. It is therefore postulated that during reworking in the Northern Zone and on North Uist and Ronay, the fluids were effectively 'sealed' into the phyllonite belts by their relatively impermeable host rocks, thus allowing high internal fluid pressures to develop (see discussion in Chapter 7).

If these inferences are correct, it is likely that *syn-tectonic fluid flow was controlled by cyclic variations in pore fluid pressure (i.e. fault-valve behaviour) during reworking along much of the OHFZ.*

#### 9.4.3.4 Metamorphic effects of high pore fluid pressure during reworking

Reworked phyllonites preserved in the Northern Zone of the OHFZ, and on North Uist and Ronay are characterised by a high modal abundance of calcite. In contrast, calcite is rarely observed, either in packages of reworked or 'new' extension-related phyllonite preserved on South Uist. It has been postulated that fluid flow during reworking on Lewis, Harris, North Uist and Ronay was driven by cyclic variations in pore fluid pressure, and that the fluids were highly overpressured. Reworking and phyllonitisation on South Uist was also associated with syn-tectonic fluid influx along the fault zone. However, there is no evidence to suggest that reworking was accompanied by significant hydrofracturing within the Usinish Phyllonite. This observation suggests that the fluid pressures remained relatively low. It is likely that excess fluids were able to 'bleed off' into the highly permeable, fractured Corodale Gneiss / Mashed Gneiss wall rocks, thus preventing high fluid pressures from developing within the Usinish Phyllonite during reworking (see discussion in Chapter 7). These observations are therefore consistent with *calcite having been precipitated only along highly overpressured segments of the fault zone.*

In metamorphic fluids, CO<sub>2</sub> is unlikely to exist as a separate gaseous phase, but may break down to form aqueous hydrogen carbonate (HCO<sub>3</sub><sup>-</sup>) and / or carbonate complexes (CO<sub>3</sub><sup>2-</sup>) (Beach 1982). Thus, calcite (CaCO<sub>3</sub>) precipitation is controlled by the equilibrium:



Previous authors have suggested that calcite precipitation during metamorphism is promoted by fluids which are characterised by a relatively *high* mole fraction of CO<sub>2</sub>, and a relatively *low* mole fraction of H<sub>2</sub>O (i.e. the chemical potential of CO<sub>2</sub> must have been high) (Graham *et al.* 1983). Clearly, calcite precipitation from an aqueous solution will be favoured by a high concentration of carbonate (CO<sub>3</sub><sup>2-</sup>) ions (reaction 7). According to the equilibrium described by reaction 7, the concentration of carbonate anions depends on the amount of dissolved CO<sub>2</sub> in the metamorphic fluid. Since CO<sub>2</sub> is a gas, carbon dioxide will dissolve more readily, and thus the concentration of CO<sub>3</sub><sup>2-</sup> will increase, in high pressure environments. It is therefore

proposed that during reworking on South Uist, the relatively low pressure fluids contained low concentrations of dissolved CO<sub>2</sub>, thus calcite was unable to precipitate. In contrast, the highly overpressured fluids associated with reworking in the Northern Zone of the OHFZ, and on North Uist and Ronay may have contained sufficiently high mole fractions of dissolved CO<sub>2</sub> to allow calcite precipitation to occur. If these inferences are correct, it is likely that fluid *pressure* played an equally important role as fluid composition and fluid temperature in controlling syn-tectonic retrogression during phyllonitisation along the OHFZ.

#### 9.4.4 SUMMARY

The observations presented in the previous sections demonstrate that the fluid transport properties of the OHFZ evolved dramatically with increasing strain and retrogression.

At the *onset* of phyllonitisation, the fluid transport properties of the OHFZ were controlled by the primary fabrics, and appear to have been dominated by:

- Grain networks and transient, *syn-tectonic* hydrofracture networks in packages of upper greenschist facies mylonite (Northern Zone), or by:
- Networks of *pre-existing* meso- and grain-scale faults and fractures in regions of crush melange and pseudotachylite-ultracataclasite crush zones (Southern Zone).

However, with increasing strain and retrogression, grain porosity networks (i.e. grain boundary voids and intergranular microfractures) and transient, *syn-tectonic* hydrofracture- / retrogression-driven porosity networks appear to have become increasingly important in phyllonite belts preserved in both Northern *and* Southern Zones.

In the most highly strained and retrogressed *reworked* phyllonite belts, the fluid transport properties of the wall rocks played an important role in determining the mechanisms of fluid flow within the phyllonitic shear zones. Shear zones enclosed by relatively impermeable wall rocks display evidence of fault valve behaviour, whilst shear zones developed in highly permeable, fractured host rocks do not. These observations have important implications for fault zone weakening, and are discussed further in section 9.5.2.

## 9.5 REACTIVATION, LOCALISATION AND WEAKENING ALONG THE OHFZ

Reactivation, by definition, must involve strain localisation along pre-existing fabrics or structures (e.g. Holdsworth *et al.* 1997) (see Chapter 1). So far, it has tacitly been assumed that reactivation and localisation provide evidence for *fault zone weakening* (see also Watterson 1975; White *et al.* 1986). Detailed field and microstructural studies have demonstrated that during Caledonian reactivation along the OHFZ, strain was preferentially focused into *pre-existing* bands of upper and / or lower greenschist facies phyllonite (i.e. the phyllonite belts were *reworked*) (Figs. 9.3a, 9.4a & 9.5a). There is very little evidence for reactivation in the relatively un-phyllonitised host rocks. These observations are consistent with the phyllonitic shear zones having been *weak in comparison with the surrounding unmodified gneisses, upper greenschist facies mylonites, pervasive protophyllonites, crush melange and / or pseudotachylite-ultracataclasite crush zones* (Chapters 5, 6 & 7) (Butler 1995; Butler *et al.* 1995). The weakening mechanisms associated with phyllonitisation and deformation across the reaction-modified frictional to viscous creep transition are discussed further in section 9.5.2.

In contrast, late Laxfordian / Grenvillian reactivation at Loch Sgibacleit was characterised by *localised, brittle* deformation in rocks which were previously deforming in a viscous, macroscopically ductile manner. Thus, reactivation of the mylonitic fabrics was associated with the development of *new* (i.e. derived) structures within the mylonite belt. However, there is no evidence that either the macroscopically ductile mylonitic fabrics or the brittle faults were reactivated during subsequent regional Caledonian deformation (Fig. 9.2a). These observations suggest that late Laxfordian / Grenvillian brittle reactivation at Loch Sgibacleit did *not* significantly modify the long-term rheological behaviour of the fault zone. The aims of the following section, therefore, are to discuss the mechanical behaviour of the OHFZ at Loch Sgibacleit, and to determine why the late Laxfordian / Grenvillian fault rocks and structures were not susceptible to Caledonian reactivation (section 9.5.1).

### 9.5.1 REACTIVATION AND LOCALISATION: LOCH SGIBACLEIT

#### 9.5.1.1 Localisation vs. weakening: clarification

Hobbs *et al.* (1990) have pointed out that strain-softening (i.e. weakening) is not *necessarily* an essential requirement for localisation. Indeed, experimental evidence suggests that strain localisation in previously homogeneously deforming materials is possible in the *strain-hardening* regime (e.g. Griggs & Handin 1960). The aim of the following section is to clarify the differences between localisation and weakening, and

to discuss the implications for reactivation and the mechanical behaviour of the OHFZ at Loch Sgibacleit.

### ***Material behaviour***

The stress-strain response of a rock undergoing strain localisation can be evaluated in two different ways. The first approach is to consider the *constitutive behaviour* of the material undergoing deformation. The constitutive behaviour determines whether a rock is intrinsically strain-hardening, strain-softening or able to deform in a steady-state manner. The constitutive behaviour of any material depends strongly on the ambient pressure and / or temperature conditions, and on the availability of fluids. For example, at relatively low temperatures and pressures, quartz-rich rocks deform predominantly by dislocation glide (low temperature plasticity). During low temperature plastic deformation, dislocations are likely to become tangled, and strain-hardening ensues (see discussion in Lloyd & Knipe 1992). Thus, at low temperatures and pressures, the constitutive behaviour of quartz is likely to be intrinsically *strain-hardening*. In quartz-rich rocks deformed experimentally at higher temperatures and pressures, recovery and recrystallisation processes become important. Such processes remove dislocation tangles and hence counteract strain-hardening. Thus, at high temperatures and pressures, quartz is likely to display either *strain-softening* or *steady-state creep* behaviour (e.g. Hirth & Tullis 1992).

### ***System behaviour***

Material constitutive behaviour takes no account of constraints imposed by the boundary conditions during deformation. An alternative approach, therefore, is to consider to the stress-strain response of the entire *system* (i.e. stress-strain behaviour due to constitutive behaviour of the rocks + additional stresses due to constraints imposed by boundary conditions). The difference between *material* (constitutive) and *system* behaviour has been highlighted by Edmond & Paterson (1972). These authors have pointed out that even though *dilatational* materials deformed at non-zero confining pressures may display strain-softening *constitutive* behaviour (i.e. decreasing *applied* stress with strain), they are likely to display strain-hardening *system* behaviour. System hardening arises because changes in volume are constrained by the confining pressure. Hence, additional stresses are required to counteract the effects of dilatancy, and the *total* stress acting on the rock may therefore increase (Edmond & Paterson 1972). *Kinematic* constraints can also affect the stress-strain response of dilatational materials (Hobbs *et al.* 1990). For example, a rock characterised by dilatational constitutive behaviour, and subjected to plane strain deformation, is kinematically constrained to deform at a constant volume. Thus, the *system* is likely to display strain-hardening behaviour.

### ***Material and system behaviour during localisation***

In general terms, pressure-sensitive, dilational materials (e.g. rocks which deform predominantly by frictional deformation mechanisms) are strongly dependant on constraints imposed by the boundary conditions. During *unconstrained* deformation, pressure sensitive strain-softening / strain-hardening materials typically display strain-softening *system* behaviour during localisation (as one would intuitively expect). However, if boundary constraints are imposed, localisation may also be associated with *strain-hardening* system behaviour. In contrast, pressure *insensitive*, non-dilational materials (e.g. rocks which deform predominantly by crystal plastic mechanisms) are less susceptible to constraints imposed by the boundary conditions. Thus, localisation of deformation in pressure-insensitive materials is typically associated with strain-softening behaviour (see Hobbs *et al.* 1990 for a more complete discussion).

#### **9.5.1.2 Stress-strain behaviour during reactivation at Loch Sgibacleit**

Late Laxfordian / Grenvillian mylonitisation and subsequent brittle reactivation at Loch Sgibacleit occurred during top-to-the-NW thrusting, under conditions of progressively decreasing pressure and temperature (Chapter 4). Macroscopically ductile deformation was primarily accommodated by dislocation creep and dynamic recrystallisation of quartz and feldspar. However, dislocation creep is a strongly temperature sensitive deformation mechanism (e.g. Hirth & Tullis 1992). These observations suggest that the flow stresses required to maintain a constant strain rate are likely to have *increased* with progressively decreasing temperature. Palaeopiezometric estimates, obtained from measurements of recrystallised quartz and feldspar grain size and / or dislocation density, are consistent with mylonitisation having occurred under a high differential stress regime (White 1996). It is therefore proposed that top-to-the-NW thrusting in the Loch Sgibacleit region was associated with *temperature-induced strain-hardening* of the quartzo-feldspathic mylonites.

In general, the effects of brittle reactivation are confined to parallel sided, foliation-parallel fault zones. This observation is consistent with frictional sliding and pseudotachylyte generation having approximated to simple shear (plane strain). However, frictional sliding and melting are strongly pressure sensitive, dilatant processes. Thus, the mechanical behaviour of the fault zone (i.e. the 'system') during reactivation is likely to have been influenced by the boundary conditions. If this inference is correct, it is possible that the kinematic constraints of simple shear may have induced *system hardening* behaviour during brittle deformation.

### 9.5.1.3 Controls on fault zone reactivation at Loch Sgibacleit

The stress-strain behaviour of *actively* deforming systems (i.e. fault zones) is influenced both by the constitutive behaviour of the fault rocks and by the boundary constraints imposed by the prevailing kinematic regime (Hobbs *et al.* 1990). However, if a fault zone is *inactive* for significant periods of geological time, and is then subjected to renewed tectonic stresses, the *material constitutive behaviour* (i.e. the intrinsic mechanical strength of the fault rocks) is likely to be the main factor in determining whether the fault zone reactivates.

It has been demonstrated that the lower amphibolite facies mylonites exposed at Loch Sgibacleit entered the material strain-hardening regime during late Laxfordian / Grenvillian deformation across the primary frictional to viscous creep transition, at depths of between 10km and 15km (sections 9.2.7.1 & 9.5.1.2). Caledonian deformation elsewhere along the OHFZ is inferred to have taken place at depths of between 5km and 9km (section 9.2.7), which suggests that the quartzo-feldspathic mylonites at Loch Sgibacleit remained within the material hardening regime throughout the Caledonian. Furthermore, there is no evidence to suggest that the pseudotachylyte-bearing fault zones were long-lived structures. Thus, the absence of intense Caledonian deformation at Loch Sgibacleit is likely to reflect the high *absolute* material strengths of the quartzo-feldspathic mylonites and pseudotachylyte-bearing fault zones. However, given the abundance of phyllonite preserved elsewhere along the OHFZ, the lack of reactivation at Loch Sgibacleit must also reflect the high strength of the quartzo-feldspathic mylonites and pseudotachylyte-bearing fault zones *relative* to that of the phyllonite belts. The relative weakness of the phyllonite belts is discussed further in the following sections.

### 9.5.2 REACTIVATION AND WEAKENING: PHYLLONITE BELTS

The upper and lower greenschist facies phyllonite belts appear to have been weak in comparison with the surrounding, relatively un-phyllonitised fault rocks and protoliths. A number of different *syn-tectonic* and *long-term* mechanisms have been proposed which could account for the apparent mechanical weakness of many continental fault zones (Holdsworth *et al.* 1997) (see review in Chapter 1). The aims of the following section are:

- To briefly discuss the likely syn-tectonic and long-term weakening mechanisms operative during phyllonitisation and reworking across the reaction-modified frictional to viscous creep transition along the OHFZ.

- To determine the relative importance of syn-tectonic and long-term weakening mechanisms in controlling reworking within the phyllonite belts preserved along the OHFZ.
- To discuss the relationships between syn-tectonic fluid flow, retrogressive metamorphism and long-term weakening along the OHFZ.

### 9.5.2.1 Syn-tectonic weakening mechanisms

#### *Fluid-assisted diffusive mass transfer*

There is widespread microstructural evidence for the operation of fluid-assisted diffusive mass transfer deformation mechanisms within packages of upper and lower greenschist facies phyllonite. In general, rocks deforming by diffusion-dominated, grain size sensitive mechanisms sustain much lower shear stresses than rocks deforming by dislocation-dominated mechanisms, under similar pressure, temperature and strain rate conditions (e.g. Handy 1989) (section 1.5.1.1). These observations are consistent with the phyllonitic shear zones having behaved in a weak manner. The possible effect of fluid-assisted DMT on shear zone strength is discussed further in section 9.5.2.3.

#### *High pore fluid pressure and embrittlement*

*Role of grain-scale hydraulic fractures* Tensile, intragranular hydraulic fractures are commonly observed to deform porphyroclasts preserved in packages of upper and lower greenschist facies phyllonite. These observations are consistent with deformation within the phyllonite belts having been characterised by high syn-tectonic pore fluid pressures. Although the presence of intragranular hydrofractures is not in itself evidence for syn-tectonic weakening, previous authors have argued that high pressure metamorphic fluids are important means of material transport during fluid-assisted diffusive mass transfer processes (Cox & Etheridge 1989). Thus, it is postulated that grain-scale hydraulic fracturing *indirectly* contributed to syn-tectonic weakening by facilitating the operation of fluid-assisted DMT.

*Embrittlement and fault valve behaviour* Packages of reworked phyllonite preserved in the Northern Zone of the OHFZ, and on North Uist and Ronay are commonly observed to be disrupted by arrays of syn-tectonic *tensile* and *shear* hydraulic fractures. These observations suggest that high pore fluid pressures within the phyllonite belts promoted transient, localised phases of embrittlement during macroscopically ductile, viscous reworking, and appear to be consistent with brittle deformation having been controlled by fault-valve behaviour (see discussion in section 9.4.3.3). Previous authors have postulated that high pore fluid pressures can

cause weakening by reducing the critical shear stress required for frictional sliding (Rice 1992) (section 1.5.1.1). Thus, the presence of shear hydraulic fractures (Type 1' detachments) is consistent with embrittlement having resulted in fault zone weakening. It has been demonstrated that fault-valve behaviour during late Caledonian reworking within the phyllonite belts was promoted by the presence of relatively impermeable host rocks (section 9.4.3.3). Thus, *the syn-tectonic weakening effects of embrittlement appear to have been directly controlled by the fluid transport properties of the fault zone.*

***Volume change: transformational plasticity and porosity enhancement***

Syn-tectonic retrogression appears to have been controlled by three principal metamorphic reactions, involving (a) the breakdown of plagioclase and K-feldspar to sericite, albite and muscovite (upper and lower greenschist facies phyllonites) (reaction 1), (b) the breakdown of hornblende to actinolite and chlorite (upper greenschist facies phyllonites) (reaction 3), and (c) the breakdown of hornblende to chlorite (lower greenschist facies phyllonites) (reaction 6) (see section 9.3.1.2). The volume changes associated with each of these reactions have been calculated following the methods of Beach (1979) and Wintsch *et al.* (1995), and the results are presented in Table 9.12.

Reactants	Molar volume (cm <sup>3</sup> mol <sup>-1</sup> )	Actual volume (cm <sup>3</sup> )	Products	Molar volume (cm <sup>3</sup> mol <sup>-1</sup> )	Actual volume (cm <sup>3</sup> )
20 Oligoclase	101	2016	2 sericite	141	282
2 K-feldspar	109	217	16 albite	100	1601
1 Haematite	30	30	2 epidote	124	248
			(2 silica)	(23)	(46)
		<b>Total: 2264</b>			<b>Total: 2130</b> (2176)
					<b>ΔV = -6% (-4%)</b>

**Table 9.12a** Table summarising volume changes associated with reaction 1 (feldspar sericitisation).  $\Delta V = ([\text{volume products} - \text{volume reactants}] / \text{volume reactants}) \times 100$ . Totals *not* in brackets assume all silica is removed in aqueous solution, totals in brackets assume all silica remains as solid phase at the site of reaction. Molar volumes from Holland (1989), except epidote and silica, which are from Beach (1979).

Reactants	Molar volume (cm <sup>3</sup> mol <sup>-1</sup> )	Actual volume (cm <sup>3</sup> )	Products	Molar volume (cm <sup>3</sup> mol <sup>-1</sup> )	Actual volume (cm <sup>3</sup> )
8 hornblende (modelled as pargasite)	279	2235	4 actinolite	283	1131
			3 chlorite	398	1194
			(6 silica)	(23)	(138)
		<b>Total: 2235</b>			<b>Total: 2325 (2463)</b>
					<b>ΔV = +4% (+10%)</b>

**Table 9.12b** Table summarising volume changes associated with reaction 3 (hornblende breakdown under upper greenschist facies conditions).  $\Delta V = ([\text{volume products} - \text{volume reactants}] / \text{volume reactants}) \times 100$ . Total volumes *not* in brackets assume all silica is removed in aqueous solution, total volumes in brackets assume all silica remains as solid phase at the site of reaction. Molar volumes from Holland (1989), except chlorite and silica, which are from Beach (1979).

Reactants	Molar volume (cm <sup>3</sup> mol <sup>-1</sup> )	Actual volume (cm <sup>3</sup> )	Products	Molar volume (cm <sup>3</sup> mol <sup>-1</sup> )	Actual volume (cm <sup>3</sup> )
6 hornblende (modelled as pargasite)	279	1676	3 chlorite	398	1194
1 anorthite	101	101	(29 silica)	(23)	(667)
1 albite	100	100			
		<b>Total: 1877</b>			<b>Total: 1194 (1861)</b>
					<b>ΔV = -36% (-1%)</b>

**Table 9.12c** Table summarising volume changes associated with reaction 6 (hornblende breakdown under lower greenschist facies conditions).  $\Delta V = ([\text{volume products} - \text{volume reactants}] / \text{volume reactants}) \times 100$ . Total volumes *not* in brackets assume all silica is removed in aqueous solution, total volumes in brackets assume all silica remains as solid phase at the site of reaction. Molar volumes from Holland (1989), except chlorite and silica, which are from Beach (1979).

The three principal metamorphic reactions all produce significant volume changes. The precise magnitude of volume change depends on whether silica liberated during retrogression remains as a solid phase at the site of reaction, or whether it is removed in aqueous solution. Petrographic observations suggest that silica was precipitated in strain shadows, intragranular fractures and / or veins away from the immediate vicinity of the reactants (see also Walker 1990). Thus, it is postulated that much of the silica went into aqueous solution and was removed from the site of reaction.

Previous authors have proposed that stresses induced by volume change may be sufficient to overcome the plastic yield strength of the host minerals, and hence trigger the onset of intracrystalline deformation (see review in Rubie 1990) (section 1.5.1.5). However, microstructural observations of upper and lower greenschist facies phyllonites suggest that neither feldspar or hornblende experienced significant plastic deformation. It is therefore unlikely that transformational plasticity was a significant syn-tectonic weakening mechanism.

A more important effect of volume change is likely to have been syn-tectonic *porosity enhancement*. Pervasive sericitisation appears to have been promoted by the presence of porous and permeable intracrystalline cleavage microfracture arrays within host feldspar grains (see discussion in section 9.4.2.2). However, it has been demonstrated that sericitisation results in a 4% to 6% volume loss. This observation suggests, therefore, that sericite growth *created* additional porosity within the lattice of the host feldspar grain. Increased porosity may have facilitated further fluid infiltration, promoting further sericite growth. Thus, it is proposed that sericitisation was an important mechanism of progressive, syn-tectonic porosity enhancement. However, once the sericite needles become sufficiently interconnected, host feldspar grains are likely to 'collapse', causing a catastrophic decrease in porosity (see discussion in section 9.4.3.3) (Fig. 9.7). Similarly, it is likely that lower greenschist facies alteration of hornblende was an important mechanism of syn-tectonic porosity enhancement.

Porosity enhancement is not in itself a weakening mechanism. However, sericitisation and chloritisation reactions are important reaction softening and foliation weakening processes (see discussions in section 9.5.2.2). Furthermore, increased porosity may have promoted fluid-assisted diffusive mass transfer, by allowing additional fluids access to the fault zone. Thus, it is proposed that volume change and porosity enhancement may have been important *indirect* fault zone weakening mechanisms. The relationships between sericitisation, fluid-assisted DMT and fault zone weakening are discussed further in section 9.7.

### ***Hydrolytic weakening and neocrystallisation***

The abundance of fluids during greenschist facies deformation suggests that hydrolytic weakening, which promotes the crystal plastic deformation mechanisms, is likely to have been an important mechanism of syn-tectonic weakening (section 1.5.1.3).

Furthermore, both upper and lower greenschist facies phyllonites are characterised by aggregates of ultrafine grained albite. It has been postulated that the development of such albite aggregates was controlled by *feldspar neocrystallisation* mechanisms (e.g. section 5.2.3.2). Recent work by Stünitz & Fitz Gerald (1993) suggests that the development of ultrafine grained, neocrystallised albite aggregates in fluid-rich environments may promote the operation of diffusion-dominated viscous grain boundary sliding deformation mechanisms. Rocks which deform by such mechanisms are weak relative to rocks which deform by dislocation creep (e.g. Handy 1989). Thus, it is possible that feldspar neocrystallisation may have been an important syn-tectonic weakening mechanism.

Unfortunately, it is extremely difficult to assess the importance of either hydrolytic weakening or neocrystallisation compared to other mechanisms such as embrittlement and fluid-assisted DMT.

### ***Generation of transient, fine grained reaction products***

Experimental evidence suggests that when the generation of fine grained reaction products is associated with shear zone localisation, a marked weakening effect is observed (see Rubie 1990 and references therein) (section 1.5.1.4). The onset of retrogression during phyllonitisation is likely to have been associated with the generation of transient, fine grained reaction products. However, microstructural observations suggest that the most important reaction products (i.e. sericite and chlorite) tend to nucleate *within the lattices* of host feldspar and hornblende grains, and, at least initially, are not associated with shear zone localisation. Thus, generation of transient, fine grained reaction products is unlikely to have been an important mechanism of syn-tectonic weakening.

## **9.5.2.2 Long-term weakening mechanisms**

### ***Development of crystallographic fabrics***

White *et al.* (1986) have suggested that, provided the movement vectors during each successive deformation event are broadly coaxial, pre-existing crystallographic fabrics may permit 'easy' intracrystalline slip during reactivation. However, if the movement directions do *not* coincide, the presence of a strong crystallographic fabric may result in fault zone *hardening* (White *et al.* 1986) (section 1.5.2.2). Qualitative observations

using a sensitive tint plate suggest that quartz grains preserved in packages of highly strained mylonite and phyllonite preserved along the OHFZ display strong crystallographic fabrics. However, it has been demonstrated that the phyllonitic shear zones experienced *geometric* reactivation (*sensu* Holdsworth *et al.* 1997) during Caledonian deformation (see section 1.6.2) i.e. the movement vectors associated with phyllonitisation and subsequent reworking were *not* coaxial. These observations are consistent with the crystallographic fabrics *not* having significantly affected the long-term strength of the OHFZ.

### ***Foliation weakening***

The Lewisian protoliths in the Outer Hebrides are characterised by feldspar-dominated load-bearing framework (LBF) microstructures. During phyllonitisation, the LBF microstructures were replaced by interconnected weak layer (IWL) aggregates, comprising highly aligned sericite needles, chlorite laths, polycrystalline quartz ribbons and neocrystallised albite aggregates (sections 9.2.3.3 & 9.2.5.3).

Foliation-weakening appears to have been either a one- or two-stage process, depending on the nature of the primary fabric. In phyllonites derived directly from *gneissose* protoliths (e.g. upper greenschist facies phyllonites and packages of 'grey-green' lower greenschist facies phyllonite), foliation development was primarily controlled by the syn-tectonic breakdown of feldspar and hornblende to aggregates of sericite and chlorite. However, in phyllonites derived from *cataclastic* protoliths (e.g. packages of 'dark-green' lower greenschist facies phyllonite), foliation development appears to have been a two-stage process, involving (a) strain-induced breakdown of the LBF microstructure during brittle deformation, and (b) the development of an IWL microstructure during subsequent viscous deformation and syn-tectonic retrogression. Thus, foliation weakening during deformation across the reaction-modified frictional to viscous creep transition is likely to have been an important long-term weakening mechanism along the OHFZ. However, it should be emphasised that foliation weakening *alone* cannot account for the observed weakness of the OHFZ. In particular, the lower amphibolite facies mylonites preserved at Loch Sgibacleit display well developed quartz-dominated IWL microstructures (section 9.2.3.3), yet it has been demonstrated that the Loch Sgibacleit mylonite belt has experienced significant strain-hardening. These observations suggest that the differences in mechanical behaviour between the lower amphibolite facies mylonites and the greenschist facies phyllonites result from reaction softening due to the growth of phyllosilicate minerals during phyllonitisation (see below).

### ***Reaction softening***

Experimentally deformed phyllosilicate-rich rocks display low shear strengths, both in absolute terms, and in comparison with quartz-rich rocks deformed under similar pressure, temperature and strain rate conditions (Shea & Kronenberg 1992). Although the available data is limited, phyllosilicate-rich rocks appear to exhibit several important microstructural and rheological characteristics. During progressive deformation, strain typically becomes localised into networks of through-going phyllosilicate-rich strands. Strain localisation is associated with rapid *stress drops* (i.e. brittle failure), *strain-softening* or *steady-state creep* behaviour. In samples of biotite schist deformed at relatively low confining pressures ( $P_c \leq 100\text{MPa}$ ) (equivalent to depths of  $\leq c.5\text{km}$ ), deformation within biotite-rich strands is accommodated by frictional sliding and microcracking. At higher confining pressures ( $200 \leq P_c \leq 500\text{MPa}$ ) (equivalent to depths of between approximately 5 and 15km), deformation is accommodated by dislocation glide and intragranular kinking. Within the dislocation glide-dominated regime, the bulk strength of such rocks does *not* increase greatly with increasing confining pressure (Shea & Kronenberg 1992). However, bulk strength appears to decrease significantly (a) with increasing phyllosilicate *content* and with (b) increasing *contiguity* of phyllosilicate strands (Shea & Kronenberg 1993). Deformation experiments involving single mica crystals have highlighted important differences in behaviour between different phyllosilicate minerals. For example, Mares & Kronenberg (1993) have demonstrated that muscovite grains compressed at  $45^\circ$  to the (001) cleavage plane are up to two times weaker than biotite grains deformed under similar conditions. If these results can be extrapolated to natural strain rates and metamorphic conditions, foliated muscovite-rich rocks are expected to be extremely weak, over a wide range of crustal conditions (Janecke & Evans 1988; Wintsch *et al.* 1995).

The phyllonitic fault rocks preserved along the OHFZ are characterised by abundant, highly contiguous sericite (i.e. muscovite) and chlorite strands, which appear to have developed in response to syn-tectonic retrogression and chemical breakdown of feldspar and hornblende (e.g. section 9.3.1). In the absence of detailed TEM analyses, the operative deformation mechanisms within the sericite and chlorite strands are unclear. However, the results of preliminary optical studies suggest that deformation may have been accommodated by intracrystalline slip (?dislocation glide) within phyllosilicate grains (e.g. Chapter 5). The high modal abundance, and interconnected nature of the phyllosilicate strands are therefore consistent with the bulk strength of the phyllonite belts having been extremely low. Furthermore, the operation of intracrystalline slip processes suggests that the bulk strength of the phyllonites may have been largely independent of confining pressure (i.e. depth). If correct, these

inferences suggest that *reaction softening processes* (section 1.5.2.1) were important long-term weakening mechanisms along the OHFZ.

### **9.5.2.3 Controls on fault zone reactivation along the OHFZ**

The aim of the following section is to determine which weakening mechanism(s) ultimately controlled reactivation along the OHFZ and, in particular, to distinguish between the effects of long-term and syn-tectonic weakening.

#### ***Caledonian transpression- and sinistral strike-slip related reactivation of late Laxfordian / Grenvillian thrust-related phyllonites***

Packages of late Laxfordian / Grenvillian (c.1700 to 1100Ma), thrust-related upper greenschist facies phyllonite preserved in the Northern Zone of the OHFZ were reactivated and reworked during subsequent Caledonian transpression and sinistral strike-slip (c.430Ma). These observations suggest that *phyllonitisation during late Precambrian upper greenschist facies deformation resulted in long-term weakening of the OHFZ*.

There is no evidence preserved onshore in the Outer Hebrides to suggest that there was any activity along the fault zone during the period between 1100Ma and 430Ma. It is therefore extremely unlikely that syn-tectonic weakening mechanisms (e.g. high pore fluid pressure / fluid-assisted DMT) could account for the observed weakness of the upper greenschist facies phyllonites. Furthermore, although high pore fluid pressures are commonly cited as important fault zone weakening mechanisms (e.g. Rice 1992), other authors have argued that high pore fluid pressures cannot be sustained over long periods of geological time (Wintsch *et al.* 1995). Thus, it is proposed that fault zone weakening during the early history of the Northern Zone can ultimately be attributed to *reaction softening* and *foliation weakening* processes during thrust-related, late Laxfordian / Grenvillian phyllonitisation.

#### ***Caledonian transpression- and sinistral strike-slip related reactivation of earlier Caledonian thrust-related cataclastic fault rocks***

Crush melange, brittle faults and pseudotachylyte-ultracataclasite crush zones preserved throughout the Uists are commonly observed to have been overprinted and reactivated by macroscopically ductile, lower greenschist facies transpression- and sinistral strike-slip related phyllonitic fabrics (i.e. derived fabrics) (e.g. Figs. 9.4a & 9.5a). However, there is no evidence to suggest that cataclasites and pseudotachylytes are inherently weak fault rocks (see discussion in section 9.5.1). Thus, transpression- / strike-slip related reactivation in the Uists is *unlikely* to have been caused by any

long-term mechanical weakening of the OHFZ arising during earlier Caledonian thrusting.

Phyllonitisation and retrogression clearly required the influx of a chemically active fluid phase into the fault zone (e.g. sections 9.3 & 9.4). Thus, it is postulated that Caledonian transpression- and sinistral strike-slip reactivation in the Uists was ultimately controlled by the influx of hydrous fluids along pre-existing networks of macro- to micro-scale fractures within the brittle fault rocks i.e. the *inherited porosity and permeability* structure, (*not* mechanical weakness), was the principal control on fault zone reactivation in the Uists.

### ***Late Caledonian transtension- and extension-related reactivation of earlier Caledonian strike-slip related phyllonites***

Packages of lower greenschist facies, Caledonian sinistral strike-slip related phyllonite preserved along the entire length of the OHFZ are commonly observed to have been reactivated and reworked during late Caledonian sinistral transtension and subsequent extension. It has been demonstrated that sinistral strike-slip, transtension and extension are likely to have occurred during a single, progressive deformation event along the OHFZ (Butler 1995) (see also discussion in Chapter 3). Thus, it is impossible to distinguish unequivocally between the effects of syn-tectonic weakening and long-term weakening. However, detailed field studies suggest that late Caledonian reactivation in the Northern Zone of the OHFZ, and on North Uist and Ronay, was characterised by high syn-tectonic pore fluid pressures and localised embrittlement within the phyllonitic shear zones (Chapters 5 & 6). In contrast, there is little evidence for embrittlement within packages of reworked phyllonite preserved on South Uist (Chapter 7). Thus, although high syn-tectonic pore fluid pressures may have *contributed* to fault zone weakening, such mechanisms cannot explain the observed weakness of the lower greenschist facies phyllonites for the OHFZ as a whole. It is therefore postulated that *reaction softening* and *foliation weakening* during strike-slip related phyllonitisation must have been the principal controls on the rheological evolution of the OHFZ during late Caledonian deformation.

Detailed field studies conducted at well exposed localities on North Uist suggest that phyllonite belts comprising a high proportion of 'dark-green', epidote-rich cataclasite-derived phyllonite have been more extensively reworked than phyllonite belts comprising a high proportion of 'grey-green' banded gneiss-derived phyllonite. These observations suggest that packages of dark-green phyllonite may have been significantly weaker than packages of grey-green phyllonite (see discussion in Chapter 6). Dark-green, epidote-rich phyllonites comprise isolated quartz and partially sericitised feldspar porphyroclasts, which 'float' in an ultrafine-grained matrix of

albite, quartz, epidote, sericite and chlorite. Microstructural observations suggest that strain was primarily accommodated by fluid-assisted diffusion-dominated grain size sensitive processes, such as viscous grain boundary sliding within the ultrafine-grained matrix. Grey-green phyllonites comprise isolated quartz and feldspar porphyroclasts, which are wrapped by interconnected sericite strands and bands of ultrafine-grained recrystallised quartz and neocrystallised albite. Deformation within the sericite strands appears to have been dominated by dislocation glide and pressure solution, whilst deformation within the quartz and albite bands may have been accommodated by viscous grain boundary sliding processes (Chapter 6). Thus, the main microstructural differences between dark-green and grey-green phyllonite are that dark-green phyllonite is characterised by a *polymineralic* matrix, whilst grey-green phyllonite is characterised by what are effectively *monomineralic* bands of sericite, albite and quartz. Theoretical models of solid-state diffusive mass transfer suggest that the rheology of monomineralic fault rocks is controlled by the diffusion rates of the *slowest* elements. In contrast, the rheology of polymineralic fault rocks is likely to be controlled by the diffusion rates of the *fastest* elements. Thus, at constant pressures, temperatures and strain rates, polymineralic fault rocks are able to deform under significantly lower stresses than monomineralic fault rocks of the same grain size (Wheeler 1992). Assuming that rock types deforming by *fluid-assisted* diffusive mass transfer behave in a similar manner, it is possible that the relative weakness of dark-green phyllonite compared to grey-green phyllonite can be attributed to high rates of diffusion within the ultrafine-grained, polymineralic matrix.

These observations suggest that reactivation was ultimately controlled by long-term weakening mechanisms such as reaction softening and foliation weakening. However, the local strain distribution may have been influenced by transient, syn-tectonic weakening mechanisms.

### 9.5.3 SUMMARY

- Brittle, late Laxfordian / Grenvillian reactivation of the mylonitic fabrics at Loch Sgibacleit occurred as the fault rocks entered the material hardening regime during late Precambrian uplift of the fault zone. Thus, brittle reactivation and the development of 'derived' fabrics at Loch Sgibacleit represents strengthening, *not* weakening of the fault zone.
- Macroscopically ductile, Caledonian reactivation of the earlier, Caledonian thrust-related brittle fault rocks in the Southern Zone of the OHFZ occurred due to the influx of chemically active hydrous fluids into the fault zone. Reactivation was therefore controlled by the fluid transport properties of the pre-existing

brittle fault rocks, and does *not* appear to represent mechanical weakening of the fault zone.

- Bands of upper and lower greenschist facies phyllonite represent regions of long-term weakness within the fault zone. Long-term weakening appears to have been controlled by *reaction softening* and *foliation weakening* processes during retrograde metamorphism.
- Syn-tectonic weakening mechanisms may have been important in controlling the *local* strain distribution during late Caledonian reworking within the phyllonite belts.

## **9.6 WEAKENING AND RHEOLOGICAL EVOLUTION OF THE OHFZ**

It is apparent that phyllonitisation resulted in long-term weakening of the OHFZ. The aims of the following section are (a) to provide an order of magnitude estimate of the likely reduction in crustal strength during phyllonitisation, and (b) to briefly summarise the rheological evolution of the fault rocks deformed along the Loch Sgibacleit, Scalpay, North Uist and South Uist fabric evolution pathways.

### **9.6.1 EFFECT OF PHYLLOMITISATION ON CRUSTAL STRENGTH**

The effects of phyllonitisation (i.e. reaction softening and foliation weakening) on crustal strength can be modelled in a semi-quantitative manner, using schematic strength versus depth profiles through the continental crust (e.g. Janecke & Evans 1988; Wintsch *et al.* 1995). Previous authors have constructed crustal strength profiles for biotite-bearing fault rocks (Janecke & Evans; Shea & Kronenberg 1992), but to date, no attempts have been made to construct such diagrams for muscovite-(=sericite) bearing phyllonites. However, data presented by Mares & Kronenberg (1993) suggests that muscovite may be up to two times weaker than biotite under certain experimental conditions. Thus, the aim of the following section is to model the effects of sericitisation on the rheological evolution of the Outer Hebrides Fault Zone.

#### **9.6.1.1 Methods and assumptions**

Strength versus depth profiles are constructed by extrapolating experimentally determined flow laws to natural strain rates, overburden pressures, fluid pressures and temperatures. The general problems associated with extrapolating laboratory flow laws to natural conditions have been discussed in detail by Handy (1989) and Molnar (1992).

The effects of *long-term* weakening along the OHFZ are most apparent in the Northern Zone (in particular on Scalpay), where packages of late Laxfordian / Grenvillian, thrust-related upper greenschist facies phyllonite appear to have been reactivated and reworked during lower greenschist facies Caledonian sinistral strike-slip (see discussion in section 9.5). The following section therefore attempts to model the rheological behaviour of the upper greenschist facies phyllonite belts at the onset of Caledonian strike-slip. However, the results are broadly applicable to phyllonites preserved along the entire length of the OHFZ (section 9.6.2).

### ***Lower strength limit***

The lower strength limit of the OHFZ at the onset of Caledonian sinistral strike-slip has been modelled using the laboratory-derived muscovite flow laws determined by Mares & Kronenberg (1993). These flow laws are based on stress-strain data obtained from deforming *single* muscovite crystals. Previous authors have argued that, provided the phyllosilicate minerals form contiguous, through-going networks (i.e. an IWL microstructure), the *bulk* rheology of mica-bearing fault rocks will approximate to that of single phyllosilicate crystals (Shea & Kronenberg 1992; Wintsch *et al.* 1995). Sericite strands observed in upper (and lower) greenschist facies phyllonites from the Outer Hebrides typically define well developed IWL microstructures (Chapter 5). Thus, single crystal flow laws are probably valid for modelling the lower strength limit of the OHFZ at the onset of Caledonian sinistral strike-slip.

***Frictional regime*** The frictional strength of the phyllonite belts has been estimated using the failure criterion for strike-slip faults (Sibson 1974):

$$(\sigma_1 - \sigma_2) \gg \frac{2(R' - 1)}{(R' + 1)} \rho g z (1 - \lambda)$$

where  $(\sigma_1 - \sigma_3)$  = differential stress (Pa);  $R' = (\sqrt{1 + \mu^2} - \mu)^{-2}$ ;  $\rho$  = overburden density =  $2700 \text{kgm}^{-3}$  (Shea & Kronenberg 1992);  $g = 9.8 \text{ms}^{-2}$ ;  $z$  = depth of overburden (m);  $\lambda$  = (pore pressure/overburden pressure);  $\mu$  = coefficient of friction.

In order to determine the frictional failure envelope, assumptions have to be made regarding the values of  $\mu$  and  $\lambda$ . Experimental evidence suggests that at low confining pressures ( $\leq 25 \text{MPa}$ ) (equivalent to c.1km depth), muscovite crystals compressed at  $45^\circ$  to the (001) plane are characterised by a low coefficient of friction ( $\mu = 0.4$ ) (Mares & Kronenberg). Similar values for  $\mu$  have been obtained from biotite schists deformed experimentally at low confining pressures ( $\leq 100 \text{MPa}$ ) (Shea & Kronenberg 1992). Thus, a coefficient of friction of  $\mu = 0.4$  has been used to model phyllonite rheology in the frictional regime.

Field and microstructural observations suggest that reworking within the phyllonite belts was characterised by high pore fluid pressures. Furthermore, the abundance of tensile fractures is consistent with the pore fluid pressure locally having exceeded the minimum principal stress ( $\sigma_3$ ). Although these observations cannot be directly applied to the (now eroded) upper crustal fault rocks, it is postulated that frictional deformation may also have been characterised by high pore fluid pressures. Consequently, a value of  $\lambda = 0.8$  has been selected.

*Viscous creep regime* The strength of the phyllonite belts in the viscous creep regime has been estimated using the single muscovite crystal exponential flow law determined by Mares & Kronenberg (1993):

$$\dot{\epsilon} = A \exp(\alpha\sigma) \exp\left(\frac{-Q}{RT}\right)$$

where  $\dot{\epsilon}$  = strain rate ( $s^{-1}$ );  $\sigma$  = differential stress (MPa);  $T$  = temperature (K);  $A$ ,  $\alpha$ ,  $Q$  and  $R$  are constants ( $A = 4 \times 10^{-9} s^{-1}$ ,  $\alpha = 0.5 MPa^{-1}$ ;  $Q$  = activation energy =  $47 kJ mol^{-1}$ ;  $R$  = universal gas constant =  $8.31 kJ mol^{-1} K^{-1}$ ). For consistency with the depth calculations presented in section 9.2, a geothermal gradient of  $30^\circ C km^{-1}$  has been selected. Sibson (1977b) has suggested that strain rates within the phyllonitic shear zones may have been between  $10^{-10} s^{-1}$  and  $10^{-11} s^{-1}$ . Consequently, stresses within the phyllonite belts having been calculated assuming a strain rate of  $10^{-11} s^{-1}$ .

### ***Upper strength limit***

*Frictional regime* The frictional failure envelope for the quartzo-feldspathic fault rocks has been determined using the frictional failure criterion for strike-slip faults (Sibson 1974) (see above). The coefficient of friction for muscovite-poor rocks is likely to be significantly higher than that for muscovite-rich rocks. Hence, a coefficient of friction of  $\mu = 0.75$  was selected (Sibson 1977b). It has also been assumed that pore fluid pressures within the upper crust were similar throughout entire the fault zone. Consequently, a ratio of pore fluid pressure to overburden pressure of  $\lambda = 0.8$  has been selected (see above).

*Viscous creep regime* Packages of upper greenschist facies phyllonite are integral components of the predominantly quartzo-feldspathic, upper greenschist to lower amphibolite facies pervasive mylonite belt (Chapter 3). It is therefore postulated that the upper strength limit of the OHFZ at the onset of Caledonian deformation may have been defined by the strength of the mylonitic host rocks. Microstructural observations suggest (a) that the rheological behaviour of the upper greenschist facies mylonite belt

is likely to have been dominated by dislocation creep within quartz ribbons, and (b) that fluids were present during upper greenschist facies mylonitisation. Thus, assuming that fluids were also present within the mylonite belt at the onset of Caledonian deformation, it is possible to model the upper strength limit of the OHFZ using a 'wet' quartzite flow law (Koch *et al.* 1989):

$$\dot{\epsilon} = A \sigma^n \exp\left(\frac{-H}{RT}\right)$$

where  $\dot{\epsilon}$  = strain rate ( $s^{-1}$ );  $\sigma$  = differential stress (MPa);  $T$  = temperature (K);  $n$ ,  $H$  and  $R$  are constants ( $n$  = stress exponent = 2.61;  $H$  = activation energy =  $145 kJmol^{-1}$ ;  $R$  = universal gas constant =  $8.31 kJmol^{-1}K^{-1}$ ). For consistency, a geothermal gradient of  $30^{\circ}Ckm^{-1}$ , and a strain rate of  $10^{-11} s^{-1}$  were assumed (see above).

#### 9.6.1.2 Results and limitations

The estimated upper and lower strength limits provide useful insights into the behaviour of the OHFZ at the onset of Caledonian deformation, and are presented on a schematic crustal strength versus depth profile (Fig. 9.8). However, it is important to consider the following limitations:

- Large errors are likely owing to uncertainties in estimating (a) the pore fluid pressure / overburden ratios ( $\lambda$ ) in the frictional regime, (b) the strain rates in the viscous regime and (c) the geothermal gradient.
- The strength envelopes are 'static', and do not take into account factors such as cyclic variations in pore fluid pressure, or the effects of strain and syn-tectonic retrogression on fault rock rheology (see Handy 1989).
- Microstructural observations have demonstrated that fluid-assisted diffusive mass transfer deformation mechanisms were extremely important in accommodating strain during reactivation. However, both the muscovite and 'wet' quartzite flow laws ignore the effects of fluid-assisted DMT.

If it is assumed that Figure 9.8 represents the strength of the OHFZ at the very *onset* of Caledonian reactivation (i.e. at very low strains), it is possible to ignore the effects of strain and syn-tectonic weakening. The upper envelope (quartzo-feldspathic mylonite) is characterised by a major peak in strength (at depths of around 14km) at the level inferred for the *primary* frictional to viscous creep transition. In contrast, the lower envelope (muscovite-rich phyllonite) is characterised by a relatively small peak in strength (at depths of around c.4km) around the level inferred for the *reaction-modified* frictional to viscous creep transition (see section 9.2.7.5). Total crustal

strength can be estimated from the area beneath each curve. Thus, for the uppermost 16km of the crust (i.e. the depth range for which deformation along the OHFZ is exposed), the phyllonite belts are inferred to have been up to *six times* weaker than the surrounding 'wet' quartzo-feldspathic mylonites (Fig. 9.8). The crustal strength estimates are therefore consistent with the growth of phyllosilicates (such as muscovite) having been an important mechanism of long-term weakening along the OHFZ. The following section considers the effects of (or absence of) sericite growth on the long-term rheological behaviour of rocks deformed along the Loch Sgibacleit, Scalpay and North and South Uist pathways.

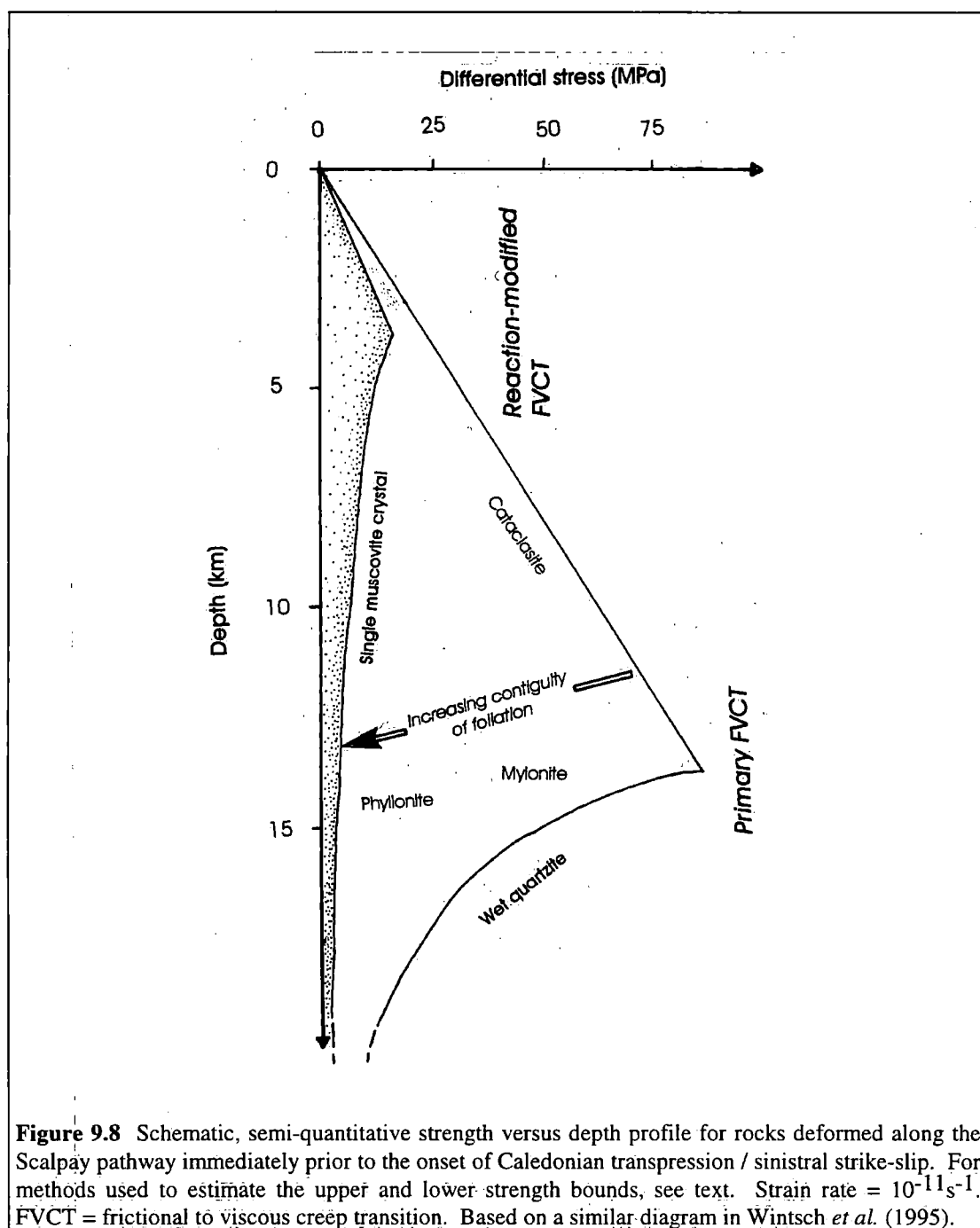


**Figure 9.8** Schematic, semi-quantitative strength versus depth profile for rocks deformed along the Scalpay pathway immediately prior to the onset of Caledonian transpression / sinistral strike-slip. For methods used to estimate the upper and lower strength bounds, see text. Strain rate =  $10^{-11} \text{ s}^{-1}$ . FVCT = frictional to viscous creep transition. Based on a similar diagram in Wintsch *et al.* (1995).

## 9.6.2 RHEOLOGICAL EVOLUTION OF THE OHFZ

The aim of the following section is to briefly consider the rheological evolution of each fabric evolution pathway, based on (a) the field and microstructural observations presented in Chapters 4, 5, 6 and 7, and on (b) the strength estimates determined in the previous section. It should be emphasised that discussions of fault zone strength / weakening are purely *qualitative* in nature. Furthermore, it has been assumed that there has been a *single* major episode of fluid influx and softening along each fabric evolution pathway. In reality, there are likely to have been several episodes of fluid influx and reaction softening (e.g. during late Caledonian transtension / extension on South Uist).

### 9.6.2.1 Loch Sgibacleit pathway

There is no evidence to suggest that the quartzo-feldspathic rocks deformed along the Loch Sgibacleit pathway have suffered significant phyllonitisation or long-term weakening (see discussion in section 9.5.1). Fault zone rheology at Loch Sgibacleit can therefore be modelled using (a) a frictional failure criterion for dry crust (i.e.  $\lambda = 0$ ), and (b) a viscous creep flow law for 'dry' quartzite (cf. White 1996). Data presented by Koch *et al.* (1989) suggest that 'dry' quartzites are up to 2.5 times stronger than 'wet' quartzites deformed under certain experimental conditions. Thus, the dry, lower amphibolite facies mylonites at Loch Sgibacleit are likely to have been significantly stronger than the 'wet' upper greenschist facies mylonites preserved elsewhere in the Northern Zone (Fig. 9.9a).

At the onset of late Laxfordian / Grenvillian top-to-the-NW thrusting, the present-day erosion level is inferred to have been below the level of the primary frictional to viscous creep transition (Fig. 9.9a). However, exhumation of the fault zone towards the end of late Precambrian thrusting brought the present-day erosion level into the high strength frictional regime (Fig. 9.9b) (see also White 1996). Exhumation following the cessation of brittle thrusting brought the present-day erosion level into the near-surface, low strength frictional environment during the Mesozoic. Brittle, Mesozoic extensional faults are locally observed to cross-cut the mylonitic fabrics. The rheological implications of brittle faulting are discussed in section 9.6.2.4.

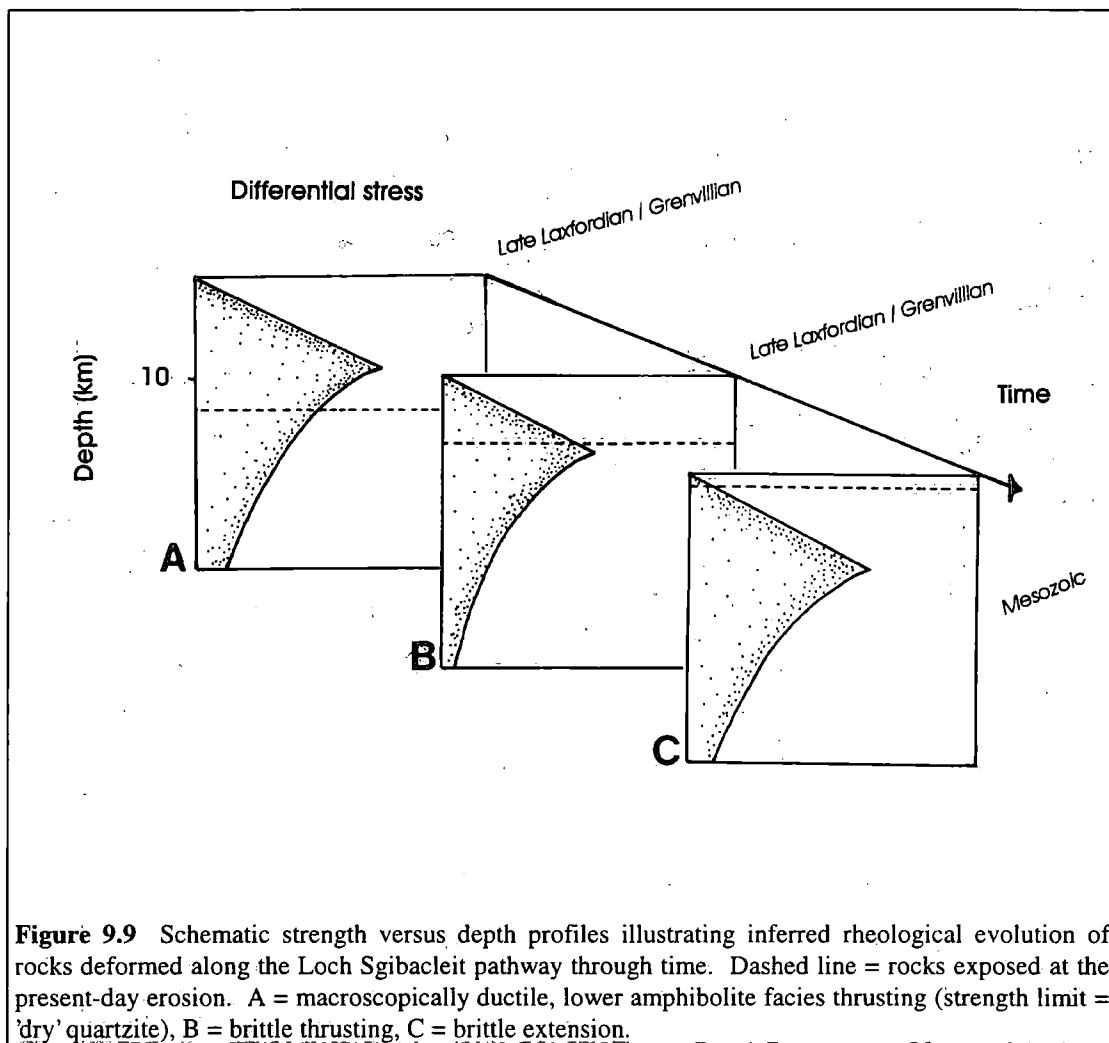
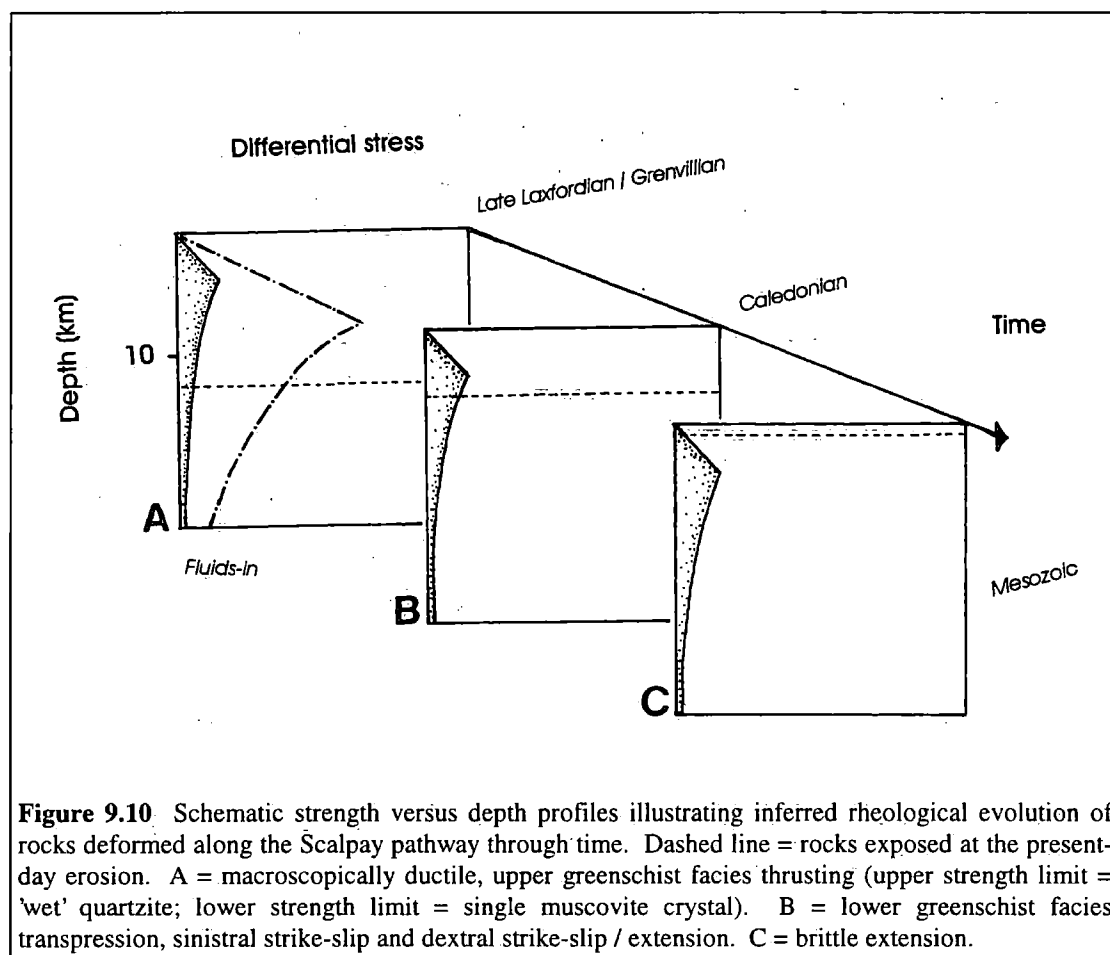


**Figure 9.9** Schematic strength versus depth profiles illustrating inferred rheological evolution of rocks deformed along the Loch Sgibacleit pathway through time. Dashed line = rocks exposed at the present-day erosion. A = macroscopically ductile, lower amphibolite facies thrusting (strength limit = 'dry' quartzite), B = brittle thrusting, C = brittle extension.

### 9.6.2.2 Scalpay pathway

Rocks deformed along the Scalpay pathway appear to have experienced a complex rheological evolution. During late Laxfordian / Grenvillian thrusting (i.e. before the development of the upper greenschist facies phyllonite belts), the rheology of the quartzo-feldspathic mylonite belt is likely to have been controlled by a 'wet' quartzite flow law (see discussion in section 9.6.1). In contrast, the rheology of the upper greenschist facies phyllonite belts is more likely to have been controlled by a muscovite flow law (e.g. Mares & Kronenberg 1993). Thus, the *overall* strength of the pervasive mylonite belt is likely to have been somewhere between these two 'end-member' flow laws (Fig. 9.10a). Exhumation of the fault zone following the cessation of late Precambrian thrusting is likely to have brought the present-day erosion level to within 8km or 9km of the surface at the onset of Caledonian transpression / sinistral strike-slip (section 9.2.7). However, shallowing of the frictional to viscous creep transition during late Laxfordian / Grenvillian thrust-related phyllonitisation ensured that the present-day erosion level remained within the viscous creep regime throughout the Caledonian (Fig. 9.10b). Exhumation of the fault zone following the

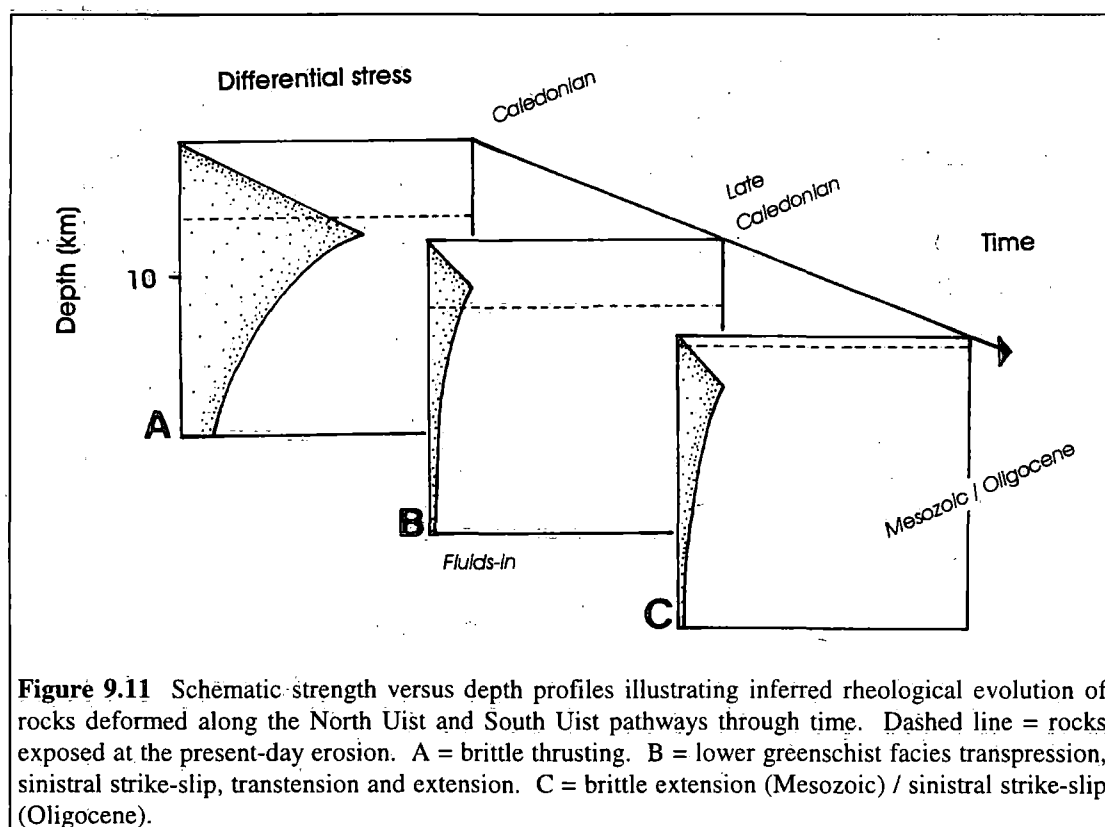
cessation of Caledonian extension / dextral strike-slip brought the present-day erosion level into the near surface, low strength frictional regime by the Mesozoic. Mesozoic, foliation-parallel extensional detachments are locally observed to disrupt the phyllonitic fabrics, and are thought to have developed along pre-existing competence boundaries. The rheological implications of brittle faulting are discussed in section 9.6.2.4.



### 9.6.2.3 North and South Uist pathways

Rocks deformed along the North and South Uist pathways are, to a first order approximation, likely to have displayed similar rheological characteristics. It has been demonstrated that the earliest phase of OHFZ-related deformation in the Southern Zone was associated with Caledonian top-to-the-W thrusting. There is no evidence to suggest that thrusting was associated with significant fluid rock interaction. Thus, at the onset of Caledonian deformation in the Uists, the rheological behaviour of the OHFZ can be modelled using the criterion for dry, frictional failure in the frictional regime (Sibson 1974), and a 'dry' quartzite flow law for deformation in the viscous creep regime (Koch *et al.* 1989). During thrusting, the rocks exposed at the present-day erosion level were clearly within the high strength frictional regime (Fig. 9.11a).

However, following the cessation of brittle thrusting, the influx of chemically active fluids into the fault zone resulted in widespread phyllonitisation throughout the Uists. As a result of reaction-modified weakening and associated shallowing of the frictional to viscous creep transition, the rocks exposed at the present-day erosion surface appear to have entered the viscous creep regime at the onset of Caledonian sinistral transpression (Fig. 9.11b). It is important to emphasise that there is *no* metamorphic or textural evidence for burial of the fault zone prior to the onset of transpression. Following, or during, top-to-the-E Caledonian extension, the fault zone was exhumationed, bringing the rocks exposed at the present-day erosion level to within a few kilometres of the Mesozoic land surface. The phyllonitic fabrics are commonly observed to be disrupted by Mesozoic extension-related detachment faults, which are thought to have developed along pre-existing competence boundaries. The rheological implications of brittle faulting are discussed in the following section.



#### 9.6.2.4 Fault zone rheology during the Mesozoic and Cenozoic

It is not possible to *directly* determine the controls on the Mesozoic - Cenozoic rheological behaviour of the OHFZ, because the principal load-bearing region of the crust during that period (i.e. the frictional to viscous creep transition zone) is still below the level of the present-day erosion surface. If it is assumed that weak phyllonite occurs at *depth* along the present-day OHFZ (i.e. the Mesozoic - Cenozoic rheology was governed by a reaction-modified frictional to viscous creep transition), it

is possible that Mesozoic (and Oligocene) faulting in the upper crustal, low strength frictional regime may have been driven by continued viscous deformation at greater depths (Figs. 9.19c & 1.10c). If correct, this scenario implies that the OHFZ is weak at the present-day, and is likely to undergo further reactivation in the future.

Shallow seismic reflection profiles of the Minch Basin, and deep seismic reflection profiles of the crust beneath northwest Scotland, suggest that the Mesozoic basin-bounding faults in the region to the east of the Outer Hebrides 'root down' into, and therefore reactivate, the OHFZ at depths of 2 to 6s two-way travel time ( $\cong$  3 to 9km depth, assuming seismic velocities of  $3\text{kms}^{-1}$ ) (Stein 1988; Smythe 1987) (Chapter 2). These observations are consistent with brittle, upper crustal faulting having been associated with viscous deformation and reactivation at depth along the OHFZ. It is therefore tentatively suggested that the Mesozoic - Cenozoic rheology of the OHFZ was governed by weak phyllonitic rocks, which occur around the level of the *present-day* frictional to viscous creep transition zone.

### 9.6.3 SUMMARY

Simple, semi-quantitative rheological models, constructed from experimentally determined flow laws, appear to be in broad agreement with inferences on fault zone rheology made from detailed field and microstructural observations (section 9.5). In particular, schematic crustal strength-depth-time diagrams emphasise that:

- Intense, pervasive phyllonitisation significantly reduces the overall strength of the continental crust.
- Phyllonitisation is associated with a marked shallowing of the frictional to viscous creep transition zone. The lower, high strength transition corresponds to the primary frictional to viscous creep transition zone. The upper, low strength transition zone corresponds to the reaction-modified frictional to viscous creep transition zone, as inferred from detailed field and microstructural observations (section 9.2).
- Rocks which have been deformed across the reaction-modified frictional to viscous creep transition are weak relative to the surrounding quartzo-feldspathic crust, and are therefore particularly susceptible to reactivation.
- In contrast, rocks which have been deformed solely across the primary frictional to viscous creep transition are characterised by high overall strength. As a result, such rocks are *not* susceptible to reactivation.

## 9.7 SYNTHESIS

This section aims to highlight the principal mechanical, metamorphic and hydrogeological controls on basement fault reactivation. The implications of basement fault reactivation are also discussed, and suggestions for further research are also made.

### 9.7.1 MECHANICAL SIGNIFICANCE OF BASEMENT FAULT REACTIVATION

This study has demonstrated that basement fault reactivation is ultimately controlled by the *long-term mechanical weakness* of continental faults and shear zones, and thus confirms predictions made by previous authors (Watterson 1975; White *et al.* 1986). However, it is clear that basement faults experience different *types* of reactivation at different stages in their evolution. Three fundamentally different types of 'reactivated' structure have been observed along segments of the OHFZ:

- *Cross-cutting structures*, which localise within pre-existing regions of fault-related deformation, but which cross-cut earlier fabrics / structures.
- *Derived fabrics and structures*, which localise along, but do not *directly* rework, pre-existing fault-related fabrics or structures i.e. *different* deformation mechanisms were operative during the development of the derived and primary fabrics / structures.
- *Reworked fabrics and structures*, which localised along, and directly deform pre-existing fault-related fabrics and structures i.e. the *same* deformation mechanisms were operative during the development of the reworked and primary fabrics / structures.

Field observations made along the OHFZ suggest that cross-cutting structures are typically brittle faults, which develop within the low strength, upper crustal frictional regime ( $\leq$  c.5km depth) (e.g. Mesozoic extensional faults). The presence of cross-cutting structures does not *necessarily* imply that the fault zone experienced significant mechanical weakening (e.g. compare Fig. 9.9c with Fig. 9.10c).

Derived structures are either brittle faults which localise along pre-existing macroscopically ductile fabrics, or are macroscopically ductile fault rocks which localise along pre-existing brittle structures. Brittle derived structures which develop within the low strength, upper crustal frictional regime (e.g. the Mesozoic detachment

faults) tend to localise along pre-existing competence boundaries (Butler 1995). The presence of such structures cannot be taken as *conclusive* evidence that a fault zone is mechanically weak, although weakness is one possible explanation (section 9.6.2.4) (e.g. Figs. 9.10c & 9.11c). Brittle derived structures which develop within the high strength, mid crustal frictional regime (e.g. foliation-parallel fault zones at Loch Sgibacleit), tend to localise along pre-existing mylonitic foliation planes (see also Beacom *et al.* 1997). Such structures develop in response to the onset of material hardening within the host rock. Thus, the presence of derived structures in mid crustal settings is consistent with a fault zone being characterised by *high mechanical strength* (Fig. 9.9b). Macroscopically ductile derived fabrics which localise along pre-existing brittle structures (e.g. the lower greenschist facies phyllonites in the Southern Zone of the OHFZ) develop in response to fluid influx into the fault zone. Thus, the presence of macroscopically ductile derived structures may reflect the *high permeability*, rather than the mechanical weakness, of the pre-existing brittle fault rocks.

Reworked fabrics preserved along the OHFZ tend to be macroscopically ductile, *viscously* deformed fault rocks which localise within, and deform, pre-existing bands of viscously deformed fault rocks (e.g. phyllonite belts). The presence of reworked fabrics is always consistent with the pre-existing fault rocks having been characterised by *low mechanical strength* (e.g. Fig. 9.11b).

These observations demonstrate that evidence for reactivation is not *necessarily* evidence for mechanical weakening of the pre-existing fault rocks, and that care must be taken in describing the relationships between different generations of fabrics and structures preserved along reactivated basement faults zones.

## 9.7.2 CONTROLS ON PHYLLONITISATION ALONG BASEMENT FAULTS

Detailed field and microstructural observations of the OHFZ demonstrate that evidence for reactivation and reworking is confined to those segments of the fault zone which have experienced *intense, pervasive phyllonitisation around the level of the frictional to viscous creep transition*. Thus, the development of mica- and chlorite-bearing phyllonites at mid crustal depths is thought to cause profound, long-term rheological weakening. This weakness stems primarily from the fact that phyllosilicate minerals display intrinsically low strengths over a wide range of crustal conditions.

Phyllonitisation in crystalline basement terranes is controlled by syn-tectonic, chemical breakdown of feldspar and hornblende to produce interconnected aggregates of fine grained, intensely aligned phyllosilicate minerals, such as sericite and chlorite.

Thus, *syn-tectonic retrograde metamorphism appears to be the ultimate control on the long-term weakness of typical quartzo-feldspathic continental basement faults and shear zones*. Syn-tectonic retrogression requires:

- Pervasive and effective permeability pathways which allow the fluids access to the fault zone.
- The presence of a fluid phase with the correct geochemical and thermodynamic characteristics to drive the retrograde metamorphic reactions.

The following sections therefore consider (a) the nature of the permeability pathways, and (b) the relationships between syn-tectonic retrogression, fluid-assisted DMT and rheology.

#### **9.7.2.1 Permeability pathways**

In order for syn-tectonic retrogression to occur, fluids must be able to gain access to a fault zone. The presence of highly retrogressed phyllonites is therefore consistent with the permeability of the fault zone having been significantly higher than that of the wall rocks. Two 'end-member' types of permeability pathway have been recognised along the OHFZ:

- Permeability pathways through intensely fractured fault rocks.
- Permeability pathways through bands of viscously deforming, macroscopically ductile fault rocks.

##### ***Permeability pathways in intensely fractured fault rocks***

Permeability pathways through intensely fractured rocks arise due to the dilatant nature of many brittle deformation mechanisms (e.g. Odling 1997). However, the permeability of brittle fault zones is unlikely to be homogeneous. Along the OHFZ, for example, zones of intense brittle deformation (e.g. pseudotachylite-ultracataclite crush zones) are characterised by relatively *high* permeabilities, whilst less deformed regions (e.g. crush melange) are characterised by relatively *low* permeabilities. Pre-existing variations in permeability may lead to complex patterns of strain and alteration during phyllonitisation (Chapter 6). Further work is required to understand how *inherited permeability* affects the distribution of retrogression and phyllonitisation along basement fault zones. In particular, it may be instructive to apply oil industry-derived porosity / permeability models (see discussion in section 6.3.4) to predict the likely pattern of syn-tectonic metamorphic fluid flow at the onset of retrogression and phyllonitisation.

### ***Permeability pathways in viscously deforming, macroscopically ductile fault rocks***

Bands of reworked phyllonite are commonly inferred to have been important permeability pathways along the OHFZ. For example, the phyllonite belts exposed on Scalpay appear to have acted as fluid conduits during late Laxfordian / Grenvillian thrusting, Caledonian sinistral strike-slip *and* late Caledonian dextral strike-slip. Thus, reworked shear zones may provide important *long-lived* permeability pathways through the crust. The reasons for such long-lived permeability enhancement are unclear, although it has been postulated that some form of 'positive feedback' mechanism may operate between active deformation, focused fluid-flow and reactivation (e.g. Fig. 5.13) (see discussion in section 5.4.4.3). Regardless of the precise mechanism of permeability enhancement, the development of long-lived permeability pathways has important implications for the siting of fault-hosted mineral deposits (cf. Sibson 1990; Cox 1995). Further research is therefore required to determine the relationships between focused fluid flow and basement fault reactivation.

In conclusion, it is suggested that permeability pathways in viscously deforming, macroscopically ductile fault rocks will be particularly important during phyllonitisation at relatively deep crustal levels (between 10 and 17km depth), whilst permeability pathways through cataclastically deformed fault rocks will be important during phyllonitisation at relatively shallow crustal levels (between 5 and 10km depth). Some 'overlap' between the two mechanisms of permeability enhancement is expected at depths of c. 10km.

#### **9.7.2.2 Role of retrograde metamorphic reactions during phyllonitisation**

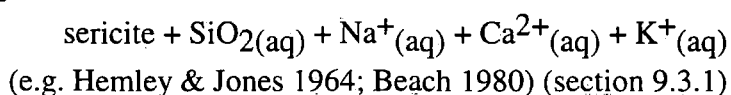
Phyllonitisation along basement faults and shear zones is ultimately controlled by retrograde metamorphic reactions, which occur once chemically active fluids have gained access to the fault zone (see previous section). Such processes include the chemical breakdown of hornblende to actinolite and chlorite, greenschist facies carbonation reactions and the breakdown of feldspar to sericite, epidote and albite (sections 9.3 & 9.4). It has been demonstrated that feldspar breakdown, and concomitant growth of intrinsically weak sericite grains, were amongst the most important weakening mechanisms during phyllonitisation along the OHFZ. More generally, feldspar is known to form a significant proportion of the continental crust, and in crystalline rocks, feldspar grains typically form strong, load-bearing framework microstructures (section 9.2.1). Metamorphic processes, such as sericitisation reactions, which ultimately destroy the load-bearing framework, are thus predicted to

be important weakening mechanisms along other reactivated basement faults. The following section discusses the relationships between phyllonitisation, deformation and rheology, with the aim of producing a general model explaining the significance of retrograde metamorphism along basement faults and shear zones. Given the obvious importance of sericite growth during phyllonitisation along the OHFZ, the following discussion focuses on feldspar sericitisation reactions. However, the results likely to be broadly applicable to a range of other reaction softening processes.

### ***Sericitisation as a metamorphic process***

Phyllonitisation reactions, such as feldspar sericitisation, are metamorphic processes, which can be modelled by chemical reactions of the general form:

Plagioclase + K-feldspar + H<sub>2</sub>O →



The silica released by such feldspar breakdown reactions is typically transported away from the site of reaction in aqueous solution, and may be re-precipitated elsewhere (Beach 1982). Furthermore, it has been demonstrated that sericitisation is associated with local volume loss (Wintsch *et al.* 1995) (see discussion in section 9.5). These observations have important implications for the operative deformation mechanisms during phyllonitisation, and are discussed in the following sections.

### ***Sericitisation as a deformation mechanism***

There is abundant microstructural evidence for the operation of fluid-assisted diffusive mass transfer (DMT) mechanisms during phyllonitisation along the OHFZ. Porphyroclasts are commonly observed (a) to be cross-cut by arrays of syn-tectonic intragranular hydrofractures, and (b) to be fringed by fibrous strain shadows. In addition, transgranular shear and tensile hydraulic fractures are widely developed, particularly within packages of reworked phyllonite. The hydrofractures and strain shadows (i.e. the DMT sinks) are typically infilled by aggregates of quartz, chlorite, calcite, albite and / or actinolite. Geochemical studies suggest that during phyllonitisation, SiO<sub>2</sub> was removed from the fault zone resulting in *overall* volume losses of up to c.40% (Walker 1990 and see also O'Hara 1988) (Chapter 8). Thus, quartz preserved within strain shadows and hydrofractures is unlikely to have been derived from an external source. It is therefore postulated that much of the quartz observed in DMT sinks may have derived from feldspar sericitisation reactions. If

correct, these inferences suggest that *feldspar grains acted as important DMT sources during sericitisation and phyllonitisation.*

In packages of highly deformed phyllonite and ultraphyllonite, the original feldspar grains are largely replaced by interconnected strands of highly aligned sericite needles. It is postulated that such sericite strands represent zones of extreme silica depletion, and may therefore be analogous to structures such as pressure solution seams in low-grade regional metamorphic rocks and / or stylolites in diagenetic limestones (see also O'Hara 1988). The development of sericite (and other phyllosilicate minerals, such as chlorite) has important implications for the mechanical behaviour of basement fault zones, which are discussed in the following section.

### ***Sericitisation as a microstructural and rheological process***

It has been demonstrated that sericitisation and feldspar breakdown had profound consequences for the microstructural and rheological evolution of the OHFZ. The onset of sericitisation is marked by the growth of sericite needles *within* host feldspar grains, forming distinctive 'mesh' textures (see discussion in section 9.4.2.2). Further pervasive sericitisation eventually weakened host grains to such an extent that the feldspar lattices and mesh textures 'collapsed', producing through-going sericite strands. Deformation within the sericite strands is likely to have been accommodated by dislocation glide-dominated mechanisms. Stress-strain data obtained from experimentally deformed mica-bearing rocks suggest that the development of interconnected phyllosilicate-rich strands is associated either with strain-softening, or the onset of steady-state creep (Shea & Kronenberg 1992, 1993). It is therefore postulated that widespread collapse of host feldspar grains, and the onset of dislocation glide within networks of interconnected sericite strands may have been associated with sudden and dramatic weakening of the OHFZ.

### ***Discussion and model of sericitisation along the OHFZ***

These observations emphasise the importance of syn-tectonic retrogression in controlling (a) the operative deformation mechanisms, (b) the microstructural development, and (c) the rheological evolution of basement faults and shear zones. So far throughout this thesis, each of these processes has been considered in isolation. However, it is apparent from the previous discussion that *interactions* between different processes have profound implications for understanding the mechanisms of fault zone weakening. The aim of the following section is to present a simple metamorphic, structural and rheological model of feldspar sericitisation, based on detailed mineralogical and microstructural observations made during this study.

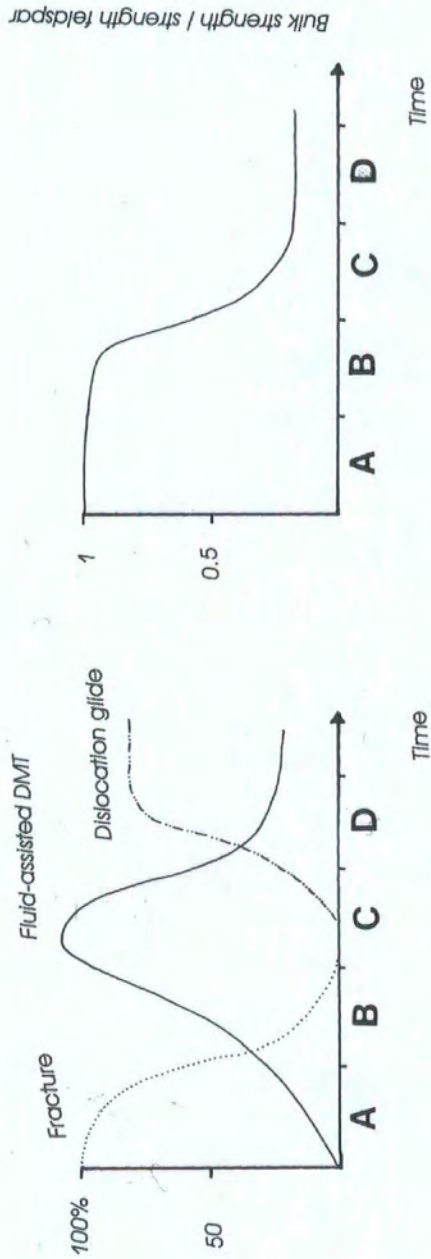
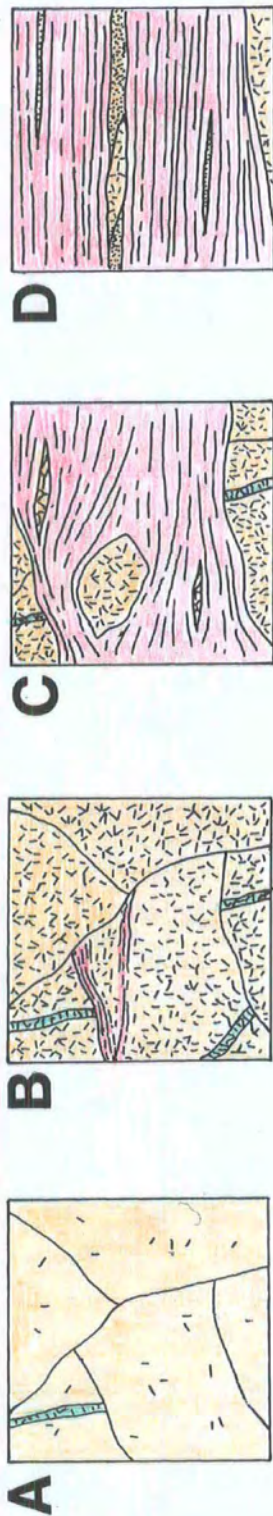


**Figure 9.12** Diagram illustrating 'ideal' microstructural sequence during feldspar sericitisation. A, B, C and D correspond to Stages 1, 2, 3 and 4 described in the text. Orange = feldspar, red = sericite, green = (hydro) fractures, fine stipple = neocrystallised albite. Graph on the lower left illustrates inferred changes in operative deformation mechanisms during sericitisation (note that DMT includes pressure solution *and* viscous grain boundary sliding). Graph on lower right illustrates how bulk rock strength is thought to change with progressive sericitisation. See text for explanation.

*Stage 1 - permeability enhancement and onset of retrogression:* The onset of retrogression depends on the ability of chemically active, hydrous fluids to gain access to the fault zone. Fault zone permeability at the onset of retrogression is likely to be controlled either by networks pre-existing of brittle fractures (i.e. *inherited* permeability) in cataclastically-deformed primary fabrics (cf. North and South Uist pathways), or by networks of transient hydrofractures / grain boundary voids and microfractures (i.e. *syn-tectonic* permeability) in bands of viscously deforming phyllonite / mylonite (cf. Scalpay pathway). Pervasive fluid infiltration through intracrystalline cleavage microfracture arrays within feldspar grains (section 9.4.2.2) triggers the onset of sericitisation and retrogression. Sericite growth along cleavage microfractures is associated with *localised* volume loss, creating additional intracrystalline porosity (section 9.5.2.1). Silica liberated during sericite growth is likely to be re-precipitated at sites of localised dilatancy elsewhere within the rock mass, and deformation is dominated by fluid-assisted DMT. Intragranular hydrofractures locally develop in feldspar grains (Figs. 9.12a & 9.13).

*Stage 2 - progressive sericitisation:* Retrogression-induced porosity enhancement promotes further fluid infiltration and sericitisation within feldspar grains (see discussion in section 9.5.2.1). Sericite needles form *mesh textures* along intersecting cleavage microfractures. If sericite needles are heterogeneously distributed, localised collapse of the feldspar lattice in highly sericitised regions may ensue, forming isolated, *intragranular sericite strands*. The development of isolated intragranular sericite strands is *not* thought to affect the bulk rheology of the host rock, and deformation continues to be dominated by fluid-assisted DMT (Fig. 9.12b & 9.13).

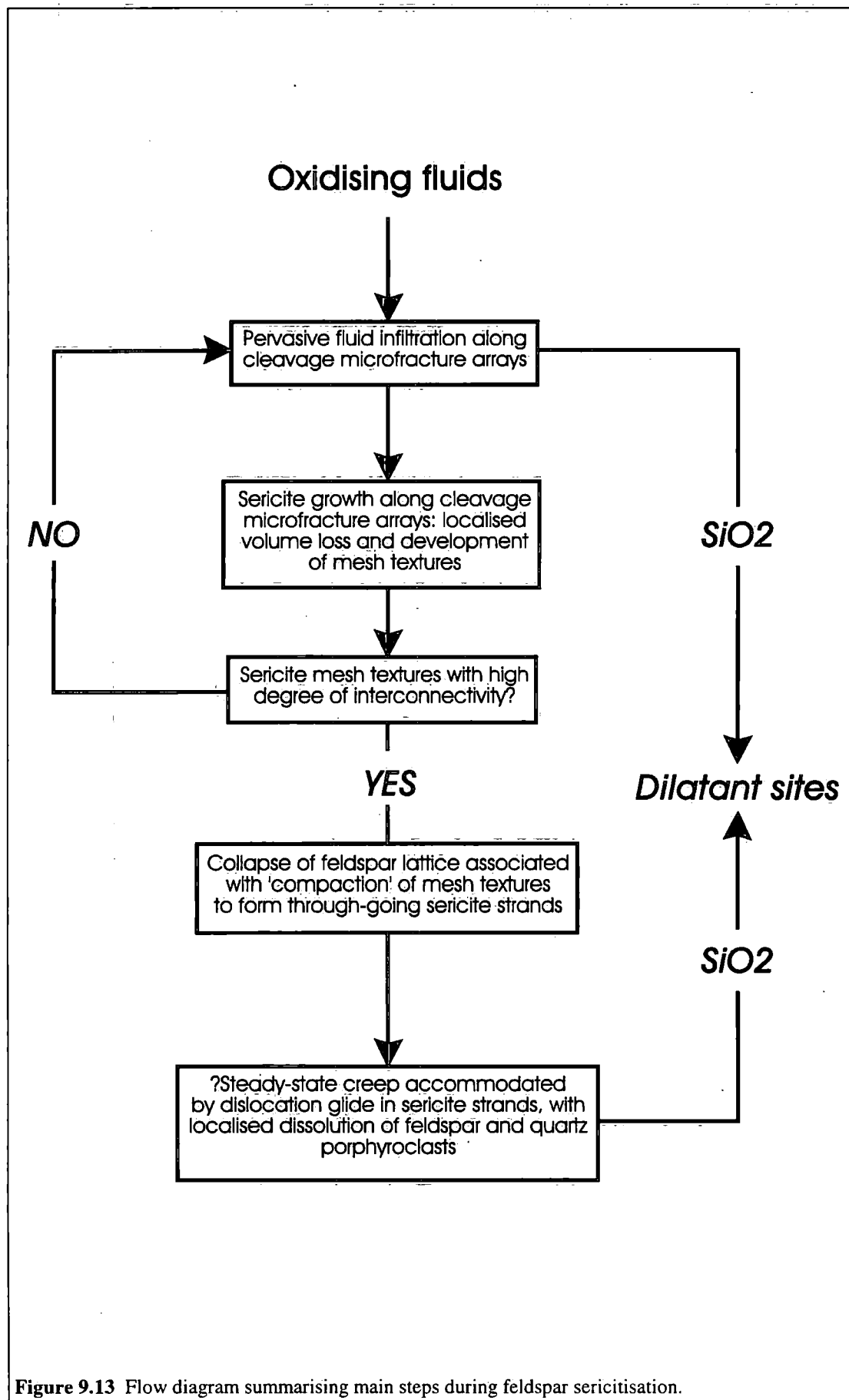
*Stage 3 - collapse of host grain:* Further pervasive sericitisation and growth of mesh textures leads to catastrophic weakening of the feldspar lattice. The host grain eventually collapses, forming interconnected, transgranular sericite strands as the mesh textures are 'compacted' parallel to the macroscopic foliation. Collapse of feldspar lattice is associated with a dramatic loss of porosity and permeability, and remaining intragranular fluids are likely to be expelled into the surrounding rock (see discussion in section 9.4.3.3). Collapse of the feldspar-dominated load-bearing framework, and concomitant development of interconnected sericite strands is likely to be associated (a) with a switch from diffusion-dominated deformation to dislocation glide-dominated deformation, and (b) with a dramatic decrease in bulk strength of the fault zone (Fig. 9.12c & 9.13). It is important to emphasise that collapse of the feldspar lattice and compaction the mesh textures does *not* cause either kinking or fracturing of

individual sericite needles. Thus, mechanical rotation of grains is unlikely to be the dominant 'compaction' mechanism. It is postulated that *viscous* grain boundary sliding mechanisms (Ashby & Verrall 1973) may control mesh texture collapse.

*Stage 4 - creep and dissolution:* Intracrystalline slip within sericite grains is accompanied by dissolution of remaining quartz and feldspar porphyroclasts which impinge upon the sericite strands (Chapter 6). Such processes are likely to increase the contiguity of the sericite grains, intensifying the effects of foliation weakening. Steady-state deformation within the sericite strands may be achieved (Fig. 9.12d & 9.13).

This model fails to take account of important factors such as lithological variation (e.g. felsic and mafic phyllonite), and the operation of other deformation mechanisms (e.g. feldspar neocrystallisation, viscous grain boundary sliding). It is, therefore, a grossly over-simplified description of the processes controlling phyllonitisation along the OHFZ. However, the model provides a basis for detailed microstructural, geochemical and thermodynamic studies aimed at understanding the interactions between metamorphic and structural processes during phyllonitisation and weakening along reactivated basement faults and shear zones. In particular, additional research is urgently required (a) to clarify the role of syn-tectonic metamorphism (in particular feldspar sericitisation) as a mechanism of diffusive mass transfer (cf. Beach 1979, 1982), (b) to investigate the precise mechanism(s) by which feldspar grains eventually 'collapse' to form interconnected sericite strands, and (c) to determine the fluid transport properties of feldspar grains preserved in deformed host rocks.

In conclusion, it is proposed that interactions between fluids and metamorphic and structural processes during phyllonitisation hold the key to understanding the long-term weakness of reactivated basement faults and shear zones.



## 9.8 CONCLUSIONS

- Two end-member frictional to viscous creep transition zones have been recognised in continental basement fault zones: (1) a high strength, *primary* transition zone at depths of between 10 and 15km; (2) a low strength, *reaction-modified* transition zone at depths of between 5 and 8km.
- Long-lived, reactivated fault zones developed in crystalline basement rocks are likely to show evidence of deformation across the reaction-modified frictional to viscous creep transition zone, and are characterised by intense, localised retrograde metamorphism and phyllonitisation.
- Weakening and phyllonitisation are ultimately controlled by retrogressive metamorphic reactions. Feldspar sericitisation reactions are likely to be particularly important mechanisms of reaction softening in quartzo-feldspathic continental crust.
- The distribution and intensity of phyllonitisation will be strongly influenced by: (1) the geochemical and thermodynamic characteristics of the metamorphic fluid phase; (2) by the pre-existing permeability structure of the fault zone.
- Fault zones which have *not* been extensively reactivated display evidence of deformation across the high strength, primary frictional to viscous creep transition zone, and are characterised by an *absence* of intense retrogression and phyllonitisation.
- Reactivation is not *necessarily* evidence of fault zone weakening. Care must be taken when describing the spatial and temporal relationships between different fabrics and structures developed along reactivated basement fault zones. It is not sufficient to simply describe a fault as being 'reactivated' - the relationships between successive generations of fault rocks and structures must be described in more rigorous terminology, such as that used throughout this thesis.
- Finally, future research should be directed at understanding the structural, microstructural, geochemical and thermodynamic relationships between metamorphism, deformation and rheology along reactivated basement faults and shear zones.

## REFERENCES CITED IN THE TEXT

- Ashby, M. F. & Verrall, R. A.** 1973. Diffusion-accommodated flow and superplasticity. *Acta Metallurgica* **21**, 149-163.
- Beach, A.** 1979. Pressure solution as a metamorphic process in deformed terrigenous sedimentary rocks. *Lithos* **12**, 51-58.
- Beach, A.** 1980. Retrogressive metamorphic processes in shear zones with special reference to the Lewisian complex. *Journal of Structural Geology* **2**, 257-263.
- Beach, A.** 1982. Deformation mechanisms in some cover sheets from the external French Alps. *Journal of Structural Geology* **4**, 137-149.
- Beacom, L., Holdsworth, B., Henderson, J., Imber, J. & Anderson, B.** 1997. *Reactivation and brittle fracture patterns in basement terrains: the Lewisian Complex, NW Scotland*. Unpublished abstract, 28th Annual General Meeting of the Tectonic Studies Group, University of Durham.
- Behrmann, J. H.** 1975. Crystal plasticity and superplasticity in quartzite: a natural example. *Tectonophysics* **115**, 101-129.
- Behrmann, J. H. & Mainprice, D.** 1987. Deformation mechanisms in a high temperature quartz-feldspar mylonite: evidence for super plastic flow in the lower continental crust. *Tectonics* **140**, 297-305.
- Bell, I. A., Wilson, C. J. L., McLaren, A. C. & Etheridge, M. A.** 1986. Kinks in mica: role of dislocations and (001) cleavage. *Tectonophysics* **127**, 49-65.
- Bickle, M. J. & Chapman, H. J.** 1990. Strontium and oxygen isotope decoupling in the Hercynian Trois Seigneurs Massif, Pyrenees: evidence for fluid circulation in a brittle regime. *Contributions to Mineralogy and Petrology* **104**, 332-347.
- Bons, A.-J.** 1988. Deformation of chlorite in naturally deformed low-grade rocks. *Tectonophysics* **154**, 149-165.

**Brodie, K. H. & Rutter, E. H.** 1985. On the relationship between deformation and metamorphism with special reference to the behaviour of basic rocks *in* **Thompson, A. B. & Rubie, D. C.** (eds) *Kinetics, Textures and Deformation*. Advanced Physical Geochemistry 4, Springer, New York. 138-179.

**Brodie, K. H. & Rutter, E. H.** 1987. The role of transiently fine grained reaction products in syntectonic metamorphism: natural and experimental examples. *Canadian Journal of Earth Science* **24**, 556-564.

**Brown, G. C., Hawkesworth, C. J. & Wilson, R. C. L.** (eds) 1992. *Understanding the Earth*. Cambridge University Press, Cambridge. 551pp.

**Burkhard, M.** 1993. Calcite twins, their geometry, appearance and significance as stress-strain markers and indicators of tectonic regime: a review. *Journal of Structural Geology* **15**, 351-368.

**Butler, C. A.** 1995. *Basement fault reactivation: the kinematic evolution of the Outer Hebrides Fault Zone, Scotland*. Unpublished PhD thesis, University of Durham.

**Butler, C. A., Holdsworth, R. E. & Strachan, R. A.** 1995. Evidence for Caledonian sinistral strike-slip motion and associated fault zone weakening, Outer Hebrides Fault Zone, NW Scotland. *Journal of the Geological Society of London* **152**, 743-746.

**Byerlee, J.** 1978. Friction of rocks. *Pure and Applied Geophysics* **116**, 615-626.

**Byerlee, J.** 1990. Friction, overpressure and fault-normal compression. *Geophysical Research Letters* **17**, 2109-2112.

**Chapman, H. J.** 1979. 2,390 M.y. Rb-Sr whole-rock age for the Scourie Dykes of north-west Scotland. *Nature* **277**, 642-623.

**Chen, W.-P. & Molnar, P.** 1983. Focal depths of intracontinental and intraplate earthquakes and their implications for the thermal and mechanical properties of the lithosphere. *Journal of Geophysical Research* **88**, 4183-4214.

**Chester, F. M., Friedman, M. & Logan, J. M.** 1985. Foliated Cataclasites. *Tectonophysics* **111**, 139-146.

**Choi, E. S., Cheema, T. & Islam, M. R.** 1997. A new dual-porosity / dual-permeability model with non-Darcian flow through fractures. *Journal of Petroleum Science and Engineering* **17**, 331-344.

**Cliff, R. A. & Rex, D. C.** 1989. Evidence for a 'Grenville' event in the Lewisian of the northern Outer Hebrides. *Journal of the Geological Society of London* **146**, 921-924.

**Cliff, R. A., Gray, C. M. & Huhma, H.** 1983. A Sm-Nd isotope study of the South Harris Igneous Complex, the Outer Hebrides. *Contributions to Mineralogy and Petrology* **82**, 91-98.

**Cobbold, P. R. & Quinquis, H.** 1980. Development of sheath folds in shear regimes. *Journal of Structural Geology* **2**, 119-126.

**Condie, K. C. & Sinha, A. K.** 1996. Rare earth and other trace element mobility during mylonitisation: a comparison of the Brevard and Hope Valley shear zones in the Appalachian Mountains, USA. *Journal of Metamorphic Geology* **14**, 213-226.

**Coward, M. P.** 1969. *The structural and metamorphic geology of South Uist, Outer Hebrides*. Unpublished PhD thesis, University of London.

**Coward, M. P.** 1972. The Eastern Gneisses of South Uist. *Scottish Journal of Geology* **8**, 1-12.

**Coward, M. P. & Park, R. G.** 1987. The role of mid-crustal shear zones in the Early Proterozoic evolution of the Lewisian in **Park, R. G. & Tarney, J.** (eds) *Evolution of the Lewisian and Comparable Precambrian High Grade Terrains*. Geological Society Special Publication **27**, 127-138.

**Coward, M. P., Francis, P. W., Graham, R. H., Myers, J. S. & Watson, J. V.** 1969. Remnants of an early metasedimentary assemblage in the Lewisian Complex of the Outer Hebrides. *Proceedings of the Geologist's Association* **80**, 387-408.

**Cox, S. F.** 1995. Faulting processes at high fluid pressures: An example of fault valve behaviour from the Wattle Gully Fault, Victoria, Australia. *Journal of Geophysical Research* **100**, 12841-12859.

**Cox, S. F. & Etheridge, M. A.** 1989. Coupled grain-scale dilatancy and mass transfer during deformation at high fluid pressures: examples from Mount Lyell, Tasmania. *Journal of Structural Geology* **11**, 147-162.

**David, F., Walker, L., Lee, M. R. & Parsons, I.** 1995. Micropores and micropermeable texture in alkali feldspars: geochemical and geophysical implications. *Mineralogical Magazine* **59**, 505-534.

**Dearnley, R.** 1962. An outline of the Lewisian complex of the Outer Hebrides in relation to that of the Scottish mainland. *Quarterly Journal of the Geological Society of London* **118**, 143-176.

**Deer, W. A., Howie, R. A. & Zussman, J.** 1992. *An introduction to the rock forming minerals*, 2nd. Edition, Longman, Harlow. 696pp.

**Dewey, J. F.** 1988. Extensional collapse of orogens. *Tectonics* **7**, 1123-1139.

**Dewey, J. F., Hempton, M. R., Kidd, W. S. F., Saroglu, F. & Sengör, A. M. C.** 1986. Shortening of continental lithosphere: the neotectonics of Eastern Anatolia - a young collision zone in **Coward, M. P. & Ries, A. C.** *Collision Tectonics*. Geological Society Special Publication **19**, 3-36.

**Drüry, M. R. & Urai, J. L.** 1990. Deformation-related recrystallisation processes. *Tectonophysics* **172**, 235-253.

**Edmond, J. M. & Paterson, M. S.** 1972. Volume changes during the deformation of rocks at high pressures. *International Journal of Rock Mechanics and Mining Sciences* **9**, 161-182.

**Etheridge, M. A.** 1983. Differential stress magnitudes during regional deformation: Upper bound imposed by tensile fracturing. *Geology* **11**, 231-234.

**Etheridge, M. A., Wall, V. J. & Vernon, R. H.** 1983. The role of the fluid phase during regional metamorphism and deformation. *Journal of Metamorphic Geology* **1**, 205-226.

**Etheridge, M. A., Wall, V. J., Cox, S. F. & Vernon, R. H.** 1984. High fluid pressures during regional metamorphism and deformation: implications for mass

transport and deformation mechanisms. *Journal of Geophysical Research* **89**, 4344-4358.

**Evans, D., Hallsworth, C., Jolley, D. W. & Morton, A. C.** 1991. Late Oligocene terrestrial sediments from a small basin in the Little Minch. *Scottish Journal of Geology* **27**, 33-40.

**Fettes, D. J. & Mendum, J. R.** 1987. The evolution of the Lewisian complex in the Outer Hebrides in **Park, R. G. & Tarney, J.** (eds) *Evolution of the Lewisian and Comparable Precambrian High Grade Terrains*. Geological Society Special Publication **27**, 27-44.

**Fettes, D. J., Mendum, J. R., Smith, D. I. & Watson, J. V.** 1992. Geology of the Outer Hebrides. *Memoir of the British Geological Survey, Sheets (solid edition) Lewis and Harris, Uist and Barra (Scotland)*. HMSO, London. 198pp.

**Fitz Gerald, J. D. & Stünitz H.** 1993. Deformation of granitoids at low metamorphic grade. I: Reactions and grain size reduction. *Tectonophysics* **221**, 269-297.

**Fleck, R. J. & Criss, R. E.** 1985. Strontium and oxygen isotopic variation in Mesozoic and Tertiary plutons of central Idaho. *Contributions to Mineralogy and Petrology* **90**, 291-308.

**Fliervoet, T. F., White, S. H. & Drury, M. R.** 1997. Evidence for dominant grain-boundary sliding deformation in greenschist- and amphibolite-grade polymineralic ultramylonites from the Redbank Deformed Zone, Central Australia. *Journal of Structural Geology* **19**, 1495-1520.

**Francis, P. W.** 1973. Scourian-Laxfordian relationships in the Barra Isles. *Journal of the Geological Society of London* **129**, 161-189.

**Fyfe, W. S., Price, N. J. & Thompson, A. B.** 1978. *Fluids in the earth's crust*. Elsevier, Amsterdam. 383pp.

**Géraud, Y., Caron, J.-M. & Faure, P.** 1995. Porosity network of a ductile shear zone. *Journal of Structural Geology* **17**, 1757-1769.

**Gill, R.** 1989. *Chemical Fundamentals of Geology*. Unwin Hyman, London. 292pp.

**Gilotti, J. A. & Hull, J. M.** 1990. Phenomenological superplasticity in rocks in **Knipe, R. J. & Rutter, E. H.** (eds) *Deformation mechanisms, Rheology and Tectonics*. Geological Society Special Publication **54**, 229-240.

**Goetze, C. & Evans, B.** 1979. Stress and temperature in the bending lithosphere as constrained by experimental rock mechanics. *Geophysical Journal of the Royal Astronomical Society* **59**, 463-478.

**Goodwin, L. B. & Wenk, H.-R.** 1995. Development of phyllonite from granodiorite: Mechanisms of grain-size reduction in the Santa Rosa mylonite zone, California. *Journal of Structural Geology* **17**, 689-707.

**Graham, C. M., Greig, K. M., Sheppard, S. M. F. & Turi, B.** 1983. Genesis and mobility of the H<sub>2</sub>O-CO<sub>2</sub> fluid phase during regional greenschist and epidote amphibolite facies metamorphism: a petrological and stable isotope study in the Scottish Dalradian. *Journal of the Geological Society of London* **140**, 577-599.

**Graham, C. M., Skelton, A. D. L., Bickle, M. & Cole, C.** 1997. Lithological, structural and deformation controls on fluid flow during regional metamorphism in **Holness, M. B.** (ed). *Deformation-enhanced Fluid Transport in the Earth's Crust and Mantle*. The Mineralogical Society Series **8**, Chapman & Hall, London. 196-226.

**Grauch, R. I.** 1989. Rare Earth Elements in Metamorphic Rocks in **Lipin, B. R. & McKay, G. A.** (eds). *Geochemistry and Mineralogy of Rare Earth Elements*. *Reviews in Mineralogy* **21**, 147-167.

**Gresens, R. L.** 1967. Composition-volume relationships of metasomatism. *Chemical Geology* **2**, 47-65.

**Griggs, D. T. & Handin, J.** 1960. Observations on fracture and a hypothesis on earthquakes in **Griggs, D. & Handin, J.** (eds) *Rock Deformation*. Memoir of the Geological Society of America **79**, 347-364.

**Grocott, J.** 1977. The relationship between Precambrian shear belts and modern fault systems. *Journal of the Geological Society of London* **133**, 257-261.

**Grocott, J.** 1981. Fracture geometry of pseudotachylyte generation zones: a study of shear fractures formed during seismic events. *Journal of Structural Geology* **3**, 169-178.

**Hall, A.** 1987. *Igneous Petrology*. Longman Scientific & Technical, Harlow. 573pp.

**Handy, M. R.** 1989. Deformation regimes and the rheological evolution of fault zones in the lithosphere: the effects pressure, temperature, grainsize and time. *Tectonophysics* **163**, 119-152.

**Handy, M. R.** 1990. The Solid-State Flow of Polymineralic Rocks. *Journal of Geophysical Research* **95**, 8647-8661.

**Handy, M. R.** 1992. Correction and Addition to "The Solid-State Flow of Polymineralic Rocks". *Journal of Geophysical Research* **97**, 1897-1899.

**Handy, M. R.** 1994. Flow laws for rocks containing two non-linear viscous phases: a phenomenological approach. *Journal of Structural Geology* **16**, 287-301.

**Handy, M. R. and Zingg, A.** 1991. The tectonic and rheological evolution of an attenuated cross section of the continental crust: Ivrea crustal section, southern Alps, northwestern Italy and southern Switzerland. *Geological Society of America Bulletin* **103**, 236-253.

**Hemley, J. J. & Jones, W. R.** 1964. Chemical aspects of hydrothermal alteration with emphasis on hydrogen metasomatism. *Economic Geology* **59**, 538-569.

**Hill, D. P., Eaton, J. P. & Jones, L. M.** 1990. Seismicity, 1980-86 in **Wallace, R. E.** (ed). *The San Andreas Fault System, California*. U.S. Geological Survey Professional Paper **1515**, 115-188.

**Hills, E. S.** 1946. Some aspects of the tectonics of Australia. *Proceedings of the Royal Society of New South Wales* **79**, 67-91.

**Hippertt, J. F.** 1994a. Microstructures and *c*-axis fabrics indicative of quartz dissolution in sheared quartzites and phyllonites. *Tectonophysics* **229**, 141-163.

**Hippertt, J. F.** 1994b. Direct observation of porosity in quartzite and phyllonite. *Neues Jahrbuch für Mineralogie-Abhandlungen* **166**, 239-259.

**Hippertt, J. F.** 1998. Breakdown of feldspar, volume gain and lateral mass transfer during mylonitization of granitoid in a low metamorphic grade shear zone. *Journal of Structural Geology* **20**, 175-193.

**Hirth, G. & Tullis, J.** 1992. Dislocation creep regimes in quartz aggregates. *Journal of Structural Geology* **14**, 145-159.

**Hobbs, B. E., Means, W. D. & Williams, P. F.** 1976. *An Outline of Structural Geology*. Wiley, New York. 571pp.

**Hobbs, B. E., Ord, A. & Teyssier, C.** 1986. Earthquakes in the ductile regime? *Pure and Applied Geophysics* **124**, 309-336.

**Hobbs, B. E., Mühlhaus, H.-B. & Ord, A.** 1990. Instability, softening and localization of deformation in **Knipe, R. J. & Rutter, E. H.** (eds) *Deformation mechanisms, Rheology and Tectonics*. Geological Society Special Publication **54**, 143-165.

**Holdsworth, R. E.** 1989. Late brittle deformation in a Caledonian ductile thrust wedge: new evidence for gravitational collapse in the Moine Thrust sheet, Sutherland, Scotland. *Tectonophysics* **170**, 17-28.

**Holdsworth, R. E.** 1994. Structural evolution of the Gander-Avalon terrane boundary - a reactivated transpression zone in the NE Newfoundland Appalachians. *Journal of the Geological Society of London* **151**, 629-646.

**Holdsworth, R. E. & Strachan, R. A.** 1991. Interlinked system of ductile strike slip and thrusting formed by Caledonian sinistral transpression in northeastern Greenland. *Geology* **19**, 510-513.

**Holdsworth, R. E., Butler, C. A. & Roberts, A. M.** 1997. The recognition of reactivation during continental deformation. *Journal of the Geological Society of London* **154**, 73-78.



**Holland, T. J. B.** 1989. Dependence of entropy on volume for silicate and oxide minerals: A review and a predictive model. *American Mineralogist* **74**, 5-13.

**Holness, M. B.** 1993. Temperature and pressure dependence of quartz-aqueous fluid dihedral angles: the control of adsorbed H<sub>2</sub>O on the permeability of quartzites. *Earth and Planetary Science Letters* **144**, 171-184.

**Holness, M. B.** 1997. The permeability of non-deforming rock in **Holness, M. B.** (ed). *Deformation-enhanced Fluid Transport in the Earth's Crust and Mantle*. The Mineralogical Society Series **8**, Chapman & Hall, London. 9-39.

**Holness, M. B. & Graham, C. M.** 1991. Equilibrium dihedral angles in the system H<sub>2</sub>O-CO<sub>2</sub>-NaCl-calcite, and implications for fluid flow during metamorphism. *Contributions to Mineralogy and Petrology* **108**, 368-383.

**Houseknecht, D. W.** 1988. Intergranular pressure solution in four quartzose sandstones. *Journal of Sedimentary Petrology* **58**, 228-246.

**Humphries, S. E.** 1984. The mobility of the rare earth elements in the crust in **Henderson, P.** (ed) *Rare earth element geochemistry*. Elsevier, Amsterdam. 315-341.

**Imber, J., Holdsworth, R. E., Butler, C. A. & Lloyd, G. E.** 1997. Fault-zone weakening processes along the reactivated Outer Hebrides Fault Zone, Scotland. *Journal of the Geological Society of London* **154**, 105-109.

**Janecke, S. U. & Evans, J. P.** 1988. Feldspar-influenced rock rheologies. *Geology* **16**, 1064-1067.

**Jehu, T. J. & Craig, R. M.** 1927. Geology of the Outer Hebrides. Part IV - South Harris. *Transactions of the Royal Society of Edinburgh* **55**, 457-488.

**Jordan, P. G.** 1987. The deformational behaviour of bimineralic limestone-halite aggregates. *Tectonophysics* **135**, 185-197.

**Kelley, S. P.** 1988. The relationship between K-Ar mineral ages, mica grain sizes and movement on the Moine Thrust Zone, NW Highlands, Scotland. *Journal of the Geological Society of London* **145**, 1-10.

**Kelley, S. P., Reddy, S. M. & Maddock, R. H.** 1994. Laser-probe  $^{40}\text{Ar} / ^{39}\text{Ar}$  investigation of a pseudotachylyte and its host rock from the Outer Isles thrust, Scotland. *Geology* **22**, 443-446.

**Kennedy, L. A. & Logan, J. M.** 1997. The role of veining and dissolution in the evolution of fine grained mylonites: the McConnell thrust, Alberta. *Journal of Structural Geology* **19**, 785-797.

**Knipe, R. J.** 1989. Deformation mechanisms-recognition from natural tectonites. *Journal of Structural Geology* **11**, 127 - 146.

**Knipe, R. J. & Lloyd, G. E.** 1994. Microstructural Analysis of Faulting in Quartzite, Assynt, NW Scotland: Implications for Fault Zone Evolution. *Pure and Applied Geophysics* **143**, 229-254.

**Koch, P. S., Christie, J. M., Ord, A. & George, R. P. Jr.** 1989. Effects of Water on the Rheology of Experimentally Deformed Quartzite. *Journal of Geophysical Research* **94**, 13975-13966.

**Korzhinsky, D. S.** 1959. *Physicochemical basis of the analysis of the paragenesis of minerals*. Consultants Bureau, New York.

**Kronenberg, A. K. & Tullis, J.** 1984. Flow strengths of quartz aggregates: grain size and pressure effects due to hydrolytic weakening. *Journal of Geophysical Research* **89**, 4281-4297.

**Kronenberg, A. K., Segall, P. & Wolf, G. H.** 1990. Hydrolytic weakening and penetrative deformation within a natural shear zone in **Duba, A. G., Durham, W.B., Handin, J. W. & Wang, H. F.** (eds) 1992. The Brittle-Ductile Transition in Rocks: the Heard volume. *Geophysical Monograph* **56**, 21-36.

**Lachenbruch, A. H. & Sass, J. H.** 1980. Heat flow and energetics of the San Andreas fault zone. *Journal of Geophysical Research* **85**, 6185-6222.

**Lailey, M., Stein, A. M. & Reston, T. J.** 1989. The Outer Hebrides fault: a major Proterozoic structure in NW Britain. *Journal of the Geological Society of London* **146**, 253-259.

- Lambert, R. St. J., Myers, J. S. & Watson, J. V.** 1970. An apparent age for a member of the Scourie dyke suite in Lewis, Outer Hebrides. *Scottish Journal of Geology* **6**, 214-220.
- Law, R. D.** 1990. Crystallographic fabrics: a selective review of their applications to research in structural geology in **Knipe, R. J. & Rutter, E. H.** (eds) *Deformation mechanisms, Rheology and Tectonics*. Geological Society Special Publication **54**, 335-352.
- Le Marchand, F., Villemant, B. & Calas, G.** 1987. Trace element distribution coefficients in alkaline series. *Geochimica and Cosmochimica Acta* **51**, 1071-1081.
- Le Pichon, X., Sibuet, J. C. & Franchéteau, J.** 1977. The fit of the continents around the North Atlantic Ocean. *Tectonophysics* **38**, 169-209.
- Lister, G. S. & Snoke, A. W.** 1984. S-C mylonites. *Journal of Structural Geology* **6**, 617-638.
- Lloyd, G. E. & Knipe, R. J.** 1992. Deformation mechanisms accommodating faulting of quartzite under upper crustal conditions. *Journal of Structural Geology* **14**, 127-143.
- MacInnes, E. A. & Alsop, G. I.** 1997. *Kinematic evolution of the Outer Hebrides Fault Zone exposed in the small isles north of Barra, NW Scotland*. Unpublished abstract, 28th Annual General Meeting of the Tectonic Studies Group, University of Durham.
- Maddock, R. H.** 1986. Partial melting of lithic porphyroclasts in fault-generated pseudotachylytes. *Neues Jahrbuch für Mineralogie-Abhandlungen* **129**, 292-311.
- Magloughlin, J. F.** 1992. Microstructural and chemical changes associated with cataclasis and frictional melting at shallow crustal levels: the cataclasite-pseudotachylyte connection. *Tectonophysics* **204**, 243-260.
- Maltman, A.** 1994. Prelithification Deformation in **Hancock, P. L.** (ed) *Continental Deformation*. Pergamon Press, Oxford. 143-158.

**Mares, V. M. & Kronenberg, A. K.** 1993. Experimental deformation of muscovite. *Journal of Structural Geology* **15**, 1061-1075.

**Means, W. D.** 1976. *Stress and Strain. Basic concepts of Continuum Mechanics for Geologists*. Springer-Verlag, New York.

**McCaig, A. M.** 1987. Deformation and fluid-rock interaction in metasomatic dilatant shear bands. *Tectonophysics* **135**, 121-132.

**McCaig, A. M.** 1997. The geochemistry of volatile fluid flow in shear zones in **Holness, M. B.** (ed). *Deformation-enhanced Fluid Transport in the Earth's Crust and Mantle*. The Mineralogical Society Series **8**, Chapman & Hall, London. 227-266.

**McCaig, A. M. & Knipe, R. J.** 1990. Mass-transport mechanisms in deforming rocks: Recognition using microstructural and microchemical criteria. *Geology* **18**, 824-827.

**Means, W. D.** 1981. The concept of steady-state foliation. *Tectonophysics* **78**, 179-199.

**Michibayashi, K.** 1996. The role of intragranular fracturing on grain size reduction in feldspar during mylonitisation. *Journal of Structural Geology* **18**, 17-25.

**Miller, E. L., Gans, P. G. & Garing, J.** 1983. The Snake Range decollement; an exhumed mid-Tertiary brittle-ductile transition. *Tectonics* **2**, 239-264.

**Miyashiro, A.** 1994. *Metamorphic Petrology*. UCL Press Ltd., London.

**Molnar, P.** 1988. Continental tectonics in the aftermath of plate tectonics. *Nature* **335**, 131-137.

**Molnar, P.** 1992. Brace-Goetze Strength Profiles, The Partitioning of Strike-slip and Thrust Faulting at Zones of Oblique Convergence, and the Stress-Heat Flow Paradox of the San Andreas Fault in **Evans, B. & Wong, T.-F.** (eds) *Fault mechanics and Transport Properties of Rocks*. Academic Press Ltd., London. 435-459.

**Murphy, F. C.** 1984. Fluidized breccias: a record of brittle transitions during ductile deformation. *Tectonophysics* **104**, 325-349.

**Myers, J. S.** 1971. The late Laxfordian granite-migmatite complex of Western Harris, Outer Hebrides. *Scottish Journal of Geology* **7**, 254-284.

**Myers, J. S.** 1987. The East Greenland Nagssugtoqidian mobile belt compared with the Lewisian complex in **Park, R. G. & Tarney, J.** (eds) *Evolution of the Lewisian and Comparable Precambrian High Grade Terrains*. Geological Society Special Publication **27**, 235-246.

**O'Brien, D. K., Wenk, H.-R., Ratschbacher, L & You, Z.** Preferred orientation of phyllosilicates in phyllonites and ultramylonites. *Journal of Structural Geology* **9**, 719-730.

**O'Hanley, D. S. & Offler, R.** 1992. Characterization of multiple serpentinisation, Woodsreef, New South Wales. *Canadian Mineralogist* **30**, 1113-1126.

**O'Hara, K.** 1988. Fluid flow and volume loss during mylonitization: an origin for phyllonite in an overthrust setting, North Carolina, USA. *Tectonophysics* **156**, 21-36.

**O'Hara, K.** 1990. State of strain in mylonites from the western Blue Ridge province, southern Appalachians: the role of volume loss. *Journal of Structural Geology* **12**, 419-430.

**Odling, N. E.** 1997. Fluid flow in fractured rocks at shallow levels in the Earth's crust: an overview in **Holness, M. B.** (ed). *Deformation-enhanced Fluid Transport in the Earth's Crust and Mantle*. The Mineralogical Society Series **8**, Chapman & Hall, London. 289-320.

**Oldow, J. S., Bally, A. W. & Avé Lallement, H. G.** 1990. Transpression, orogenic float, and lithospheric balance. *Geology* **18**, 991-994.

**Oliver, N. H. S.** 1996. Review and classification of structural controls on fluid flow during regional metamorphism. *Journal of Metamorphic Geology* **14**, 477-492.

**Ord, A. & Oliver, N. H. S.** 1997. Mechanical controls on fluid flow during regional metamorphism: some numerical models. *Journal of Metamorphic Geology* **15**, 345-359.

**Oxburgh, E. R.** 1972. Flake Tectonics and Continental Collision. *Nature* **239**, 202-204.

**Park, R. G.** 1973. The Laxfordian belts of the Scottish mainland in **Park, R. G. & Tarney, J.** (eds) *The Early Precambrian of Scotland and related rocks of Greenland*. Univeristy of Keele. 65-76.

**Passchier, C. W.** 1982. Pseudotachylyte and the development of ultramylonite bands in the Saint-Barthélemy Massif, French Pyrenees. *Journal of Structural Geology* **4**, 69-79.

**Passchier, C. W.** 1984. The generation of ductile and brittle shear bands in a low-angle mylonite zone. *Journal of Structural Geology* **6**, 273-281.

**Passchier, C. W. & Trouw, R. A. J.** 1996. *Microtectonics*. Springer-Verlag, Berlin.

**Pearce, J. A.** 1983. Role of the sub-continental lithosphere in magma genesis at active continental margins in **Hawkesworth, C. J. & Norry, M. J.** (eds) *Continental basalts and mantle xenoliths*. Shiva, Nantwich. 230-249.

**Peddy, C. P.** 1984. Displacement of the Moho by the Outer Isles Thrust shown by seismic modelling. *Nature* **312**, 628-630.

**Phillips, W. J.** 1972. Hydraulic fracturing and mineralization. *Journal of the Geological Society of London* **128**, 337-359.

**Price, N. J. & Cosgrove, J. W.** 1990. *Analysis of Geological Structures*. Cambridge University Press, Cambridge.

**Pryer, L. L. & Robin, P.-Y. F.** 1995. Retrograde metamorphic reactions in deforming granites and the origin of flame perthites. *Journal of Metamorphic Geology* **13**, 645-658.

**Ramsay, J. G.** 1980a. The crack-seal mechanism of rock deformation. *Nature* **284**, 135-139.

**Ramsay, J. G.** 1980b. Shear zone geometry: a review. *Journal of Structural Geology* **2**, 83-99.

**Ramsay, J. G. & Graham, R. H.** 1970. Strain variation in shear belts. *Canadian Journal of Earth Sciences* **7**, 787-813.

**Ramsay, J. G. & Huber, M. I.** 1987. *Techniques of Modern Structural Geology Volume 2: Folds and Fractures*. Academic Press Ltd., London.

**Rice, J. R.** 1992. Fault stress states, Pore Pressure Distributions, and the weakness of the San Andreas Fault in **Evans, B. & Wong, T.-F.** (eds) *Fault mechanics and Transport Properties of Rocks*. Academic Press Ltd., London. 476-503.

**Rollinson, H.** 1993. *Using geochemical data: evaluation, presentation, interpretation*. Longman Scientific & Technical, Harlow. 352pp.

**Rubie, D. C.** 1990. Mechanisms of reaction-enhanced deformability in minerals and rocks in **Barber, D. J. & Meredith, P. G.** (eds) *Deformation processes in minerals and rocks*. Cambridge University Press, Cambridge. 262-294.

**Rütter, E. H.** 1983. Pressure solution in nature, theory and experiment. *Journal of the Geological Society of London* **140**, 725-740.

**Rutter, E. H.** 1986. On the nomenclature of mode of failure transitions in rocks. *Tectonophysics* **122**, 381-387.

**Schmid, S. M.** 1982. Microfabric studies as indicators of deformation mechanisms and flow laws operative in mountain building in **Hsü, K. J.** (ed) *Mountain Building Processes*. Academic Press, London. 95-110.

**Schmid, S. M. & Handy, M. R.** 1991. Towards a Genetic Classification of Fault Rocks: Geological Usage and Tectonophysical Implications in **Müller, D. W., McKenzie, J. A. & Weissert, H.** (eds) 1991. *Controversies in Modern Geology: Evolution of Geological Theories in Sedimentology, Earth History and Tectonics*. Academic Press Ltd., London. 339-361.

**Scholz, C. H.** 1990. *The mechanics of earthquakes and faulting*. Cambridge University Press, Cambridge.

- Shea, W. T. & Kronenberg, A. K.** 1992. Rheology and Deformation Mechanisms of Isotropic Mica Schist. *Journal of Geophysical Research* **97**, 15201-15237.
- Shea, W. T. Jr., & Kronenberg, A. K.** 1993. Strength and anisotropy of foliated rocks with varied mica contents. *Journal of Structural Geology* **15**, 1097-1121.
- Shihe, L. & Park, R. G.** 1993. Reversals of movement sense in Lewisian brittle-ductile shear zones at Gairloch, NW Scotland, in the context of Laxfordian kinematic history. *Scottish Journal of Geology* **29**, 9-19.
- Sibson, R. H.** 1974. Frictional constraints on thrust, wrench and normal faults. *Nature* **249**, 542-543.
- Sibson, R. H.** 1975. Generation of Pseudotachylyte by Ancient Seismic Faulting. *Geophysical Journal of the Royal Astronomical Society* **43**, 775-794.
- Sibson, R. H.** 1977a. Fault rocks and fault mechanisms. *Journal of the Geological Society of London* **133**, 191-213.
- Sibson, R. H.** 1977b. *The Outer Hebrides Thrust: Its Structure, Mechanism and Deformation Environment*. Unpublished PhD thesis, University of London.
- Sibson, R. H.** 1980. Transient discontinuities in ductile shear zones. *Journal of Structural Geology* **2**, 165-171.
- Sibson, R. H.** 1982. Fault zone models, heat flow, and the depth distribution of earthquakes in the continental crust of the United States. *Bulletin of the Seismological Society of America* **72**, 151-163.
- Sibson, R. H.** 1983. Continental fault structure and shallow earthquake source. *Journal of the Geological Society* **140**, 741-767.
- Sibson, R. H.** 1985. A note on fault reactivation. *Journal of Structural Geology* **7**, 751-754.
- Sibson, R. H.** 1990. Conditions for fault-valve behaviour in **Knipe, R. J. & Rutter, E. H.** (eds) *Deformation mechanisms, Rheology and Tectonics*. Geological Society Special Publication **54**, 15-28.

**Sibson, R. H.** 1993. Load-strengthening versus load-weakening faults. *Journal of Structural Geology* **15**, 123-128.

**Sibson, R. H.** 1996. Structural permeability of fluid-driven fault-fracture meshes. *Journal of Structural Geology* **18**, 1031-1042.

**Sibson, R. H., Moore, J. M. & Rankin, A. H.** 1975. Seismic pumping - a hydrothermal fluid transport mechanism. *Journal of the Geological Society of London* **131**, 653-659.

**Skelton, A. D. L., Graham, C. M. & Bickle, M. J.** 1995. Lithological and Structural Controls on Regional 3-D Fluid Flow Patterns during Greenschist Facies Metamorphism of the Dalradian of the SW Scottish Highlands. *Journal of Petrology* **36**, 563-586.

**Smith, J. V.** 1975. Some Chemical Properties of Feldspars in **Ribbe, P. H.** (ed) *Feldspar Mineralogy*. Short Course Notes Volume 2, Mineralogical Society of America, Sm18-Sm29.

**Smith, J. V.** 1983. Some Chemical Properties of Feldspars in **Ribbe, P. H.** (ed) *Feldspar Mineralogy*, 2nd. Ed. Reviews in Mineralogy Volume 2, Mineralogical Society of America, 281-296.

**Smythe, D. K.** 1987. Deep seismic reflection profiling of the Lewisian foreland in **Park, R. G. & Tarney, J.** (eds) *Evolution of the Lewisian and Comparable Precambrian High Grade Terrains*. Geological Society Special Publication **27**, 193-203.

**Smythe, D. K., Dobinson, A., McQuillin, R., Brewer, J. A., Matthews, D. H., Blundell, D. J. & Kelk, B.** 1982. Deep structure of the Scottish Caledonides revealed by the MOIST reflection profile. *Nature* **299**, 338-340.

**Steel, R. J. & Wilson, A. C.** 1975. Sedimentation and tectonism (?Permo-Triassic) on the margin of the North Minch Basin, Lewis. *Journal of the Geological Society of London* **131**, 183-202.

**Stein, A. M.** 1988. Basement controls upon basin development in the Caledonian foreland. *Basin Research* **1**, 107-119.

**Stewart, M.** 1997. *Kinematic evolution of the Great Glen Fault Zone, Scotland*. Unpublished PhD thesis, Oxford Brookes University.

**Stewart, M., Holdsworth, R. E. & Strachan, R. A.** 1998. Sense of shear and strain localisation processes in the region of the frictional-viscous creep transition, Great Glen Fault Zone, Scotland. *In press*.

**Streit, J. E. & Cox, S. F.** 1998. Fluid infiltration and volume change during mid-crustal mylonitization of Proterozoic granite, King Island, Tasmania. *Journal of Metamorphic Geology* **16**, 197-212.

**Stünitz, H. & Fitz Gerald, J. D.** 1993. Deformation of granitoids at low metamorphic grade. II: Granular flow in albite-rich mylonites. *Tectonophysics* **221**, 299-324.

**Sutton, J. & Watson, J. V.** 1951. The pre-Torridonian metamorphic history of the Loch Torridon and Scourie areas in the North-West Highlands, and its bearing on the chronological history of the Lewisian. *Quarterly Journal of the Geological Society of London* **106**, 241-308.

**Swanson, M. T.** 1992. Fault structure, wear mechanisms and rupture processes in pseudotachylite generation. *Tectonophysics* **204**, 223-242.

**Taylor, H. P.** 1971. Oxygen isotope evidence for large-scale interaction between meteoric groundwaters and Tertiary granodiorite intrusions, western Cascade Range, Oregon. *Journal of Geophysical Research* **79**, 7855-7874.

**Terzaghi, K.** 1936. Simple tests determine hydrostatic uplift. *Engineering News and Research* **95**, 987-996.

**Teyssier, C., Tikoff, B. & Markley, M.** 1995. Oblique plate motion and continental tectonics. *Geology* **23**, 447-450.

**Thompson, R. N., Morrison, M. A., Hendry, G. L. & Parry, S. J.** 1984. An assessment of the relative roles of crust and mantle in magma genesis: an elemental approach. *Philosophical Transactions of the Royal Society* **A310**, 549-550.

**Tourigny, G. & Tremblay, A.** 1997. Origin and incremental evolution of brittle/ductile shear zones in granitic rocks: natural examples from the southern Abitibi Belt, Canada. *Journal of Structural Geology* **19**, 15-27.

**Tullis, J. & Yund, R. A.** 1980. Hydrolytic weakening of experimentally deformed Westerly granite and Hale albite rock. *Journal of Structural Geology* **2**, 439-451.

**Tullis, J. & Yund, R. A.** 1985. Dynamic recrystallization of feldspar: A mechanism for ductile shear zone formation. *Geology* **13**, 238-241.

**Tullis, J. & Yund, R.** 1992. The Brittle-ductile Transition in Feldspar Aggregates: An Experimental Study in **Evans, B. and Wong, T.-F.** (eds) 1992. *Fault Mechanics and Transport Properties of Rocks*. Academic Press Ltd., London. 89-117.

**Van Breemen, O., Aftalion, M. & Pidgeon, R. T.** 1971. The age of the granitic injection complex of Harris, Outer Hebrides. *Scottish Journal of Geology* **7**, 139-152.

**Walker, J.** 1990. *A study of the deformation environment of the Outer Hebrides Fault Zone*. Unpublished PhD thesis, University of London.

**Walther, J. V.** 1990. Fluid Dynamics During Progressive Regional Metamorphism in *The Role of Fluids in Crustal Processes*. National Academy Press, Washington, 64-71.

**Wang, C.-Y.** 1990. On the constitution of the San Andreas fault zone in central California. *Journal of Geophysical Research* **89**, 5858-5866.

**Watterson, J.** 1975. Mechanism for the persistence of tectonic lineaments. *Nature* **253**, 520-522.

**Wheeler, J.** 1987. The significance of grain-scale stresses in the kinetics of metamorphism. *Contributions to Mineralogy and Petrology* **17**, 397-404.

**Wheeler, J.** 1992. Importance of Pressure Solution and Coble Creep in the Deformation of Polymineralic Rocks. *Journal of Geophysical Research* **97**, 4579-4586.

**Wheeler, J., Windley, B. F. & Davies, F. B.** 1987. Internal evolution of the major Precambrian shear belt at Torridon, NW Scotland in **Park, R. G. & Tarney, J.** (eds) *Evolution of the Lewisian and Comparable Precambrian High Grade Terrains*. Geological Society Special Publication **27**, 153-163.

**White, J. C.** 1996. Transient discontinuities revisited: pseudotachylyte, plastic instability and the influence of low pore fluid pressure on deformation processes in the mid-crust. *Journal of Structural Geology* **18**, 1471-1486.

**White, S. H.** 1975. Tectonic deformation and recrystallization of oligoclase. *Contributions to Mineralogy and Petrology* **50**, 287-304.

**White, S.** 1976. The effects of strain on the microstructures, fabrics, and deformation mechanisms in quartzites. *Philosophical Transactions of the Royal Society, London* **A283**, 69-86.

**White, S. H.** 1982. Fault rocks of the Moine Thrust Zone: a Guide to Their Nomenclature. *Textures and Microstructures* **4**, 211-221.

**White, S. H. & Knipe, R. J.** 1978. Transformation and reaction enhanced ductility in rocks. *Journal of the Geological Society of London* **135**, 513-516.

**White, J. C. & White, S. H.** 1983. Semi-brittle deformation within the Alpine fault zone, New Zealand. *Journal of Structural Geology* **5**, 579-589.

**White, S. H. & Glasser, J.** 1987. The Outer Hebrides Fault Zone: evidence for normal movements in **Park, R. G. & Tarney, J.** (eds) *Evolution of the Lewisian and Comparable Precambrian High Grade Terrains*. Geological Society Special Publication **27**, 175-183.

**White, S. H. & Muir, M. D.** 1989. Multiple reactivation of coupled orthogonal fault systems: An example from the Kimberley region in north Western Australia. *Geology* **17**, 618-621.

- White, S. H., Bretan, P. G. & Rutter, E. H.** 1986. Fault-zone reactivation: kinematics and mechanisms. *Philosophical Transactions of the Royal Society, London* **A317**, 81-97.
- White, S. H., Burrows, S. E., Carreras, J., Shaw, N. D. & Humphreys, F. J.** 1980. On mylonites in ductile shear zones. *Journal of Structural Geology* **2**, 175-187.
- Whitehouse, M. J.** 1993. Age of the Corodale Gneisses, South Uist. *Scottish Journal of Geology* **29**, 49-58.
- Williams, H. R.** 1987. Stick-slip model for kink band formation in shear zones and faults. *Tectonophysics* **140**, 327-331.
- Williams, P. F., Goodwin, L. B. & Ralser, S.** 1994. Ductile deformation processes in **Hancock, P. L.** (ed) *Continental Deformation*. Pergamon Press, Oxford. 1-27.
- Wilson, M.** 1989. *Igneous Petrogenesis*. Chapman & Hall, London. 466pp.
- Wintsch, R. P.** 1978. A chemical approach to the preferred orientation of mica. *Geological Society of America Bulletin* **89**, 1715-1718.
- Wintsch, R. P.** 1985. The possible effects of deformation on chemical processes in metamorphic fault rocks in **Thompson, A. & Rubie, D. C.** (eds) *Kinetics, Textures and Deformation*. Advances in Physical Geochemistry **4**, Springer, New York. 251-268.
- Wintsch, R. P., Christofferson, R. and Kronenberg, A. K.** 1995. Fluid-rock reaction weakening of fault zones. *Journal of Geophysical Research* **100**, 13021-13032.
- Woodcock, N. H.** 1988. Strike-slip faulting along the Church Stretton Lineament, Old Radnor Inlier, Wales. *Journal of the Geological Society of London* **145**, 925-933.
- Woodcock, N. H.** 1992. Dolyhir Quarries, Old Radnor in **Treagus, J. E.** (ed). *Caledonian Structures in Britain South of the Midland Valley*. Chapman & Hall, London. 154-158.

**Yardley, B. W. D.** 1989. *An introduction to metamorphic petrology*. Longman Scientific & Technical, Harlow. 248pp.

**Zoback, M. D., Zoback, M. L., Mount, V. S., Suppe, J., Eaton, J. P., Healy, J. H., Oppenheimer, D., Reasenber, P., Jones, L., Raleigh, C. B., Wong, I. G., Scotti, O. & Wentworth, C.** 1987. New evidence on the state of stress on the San Andreas fault system. *Science* **238**, 1105-1111.

## APPENDIX A: STRUCTURAL LOGS

Appendix A provides brief descriptions of the main features associated with each structural log.

### LOCH SGIBACLEIT

#### NORTH OF LOCH SGIBACLEIT (NB 299 165)

W → E traverse through base of the lower amphibolite facies pervasive mylonite belt, north of Loch Sgibacleit. Section comprises mainly quartzo-feldspathic mylonite, locally with amphibolite (?Older Basic) pods. Mylonitic fabric is widely observed to be disrupted by foliation-parallel and cross-cutting brittle faults, and locally by pseudotachylyte-ultramylonite crush zones.

#### MALASGAIR (NB 167 296)

W → E traverse through base of the lower amphibolite facies pervasive mylonite belt, west face of Malasgair hill. Quartzo-feldspathic mylonites are widely disrupted by thick pseudotachylyte-ultramylonite crush zones and foliation-parallel, pseudotachylyte-bearing fault zones.

#### SOUTH OF LOCH SGIBACLEIT (NB 307 158)

E → W traverse through internal region of lower amphibolite facies pervasive mylonite belt, south of Loch Sgibacleit. Foliation-parallel, pseudotachylyte-bearing faults zones are abundant.

### SCALPAY

#### FORELAND - PERVASIVE MYLONITE TRANSITION, CNOC NA CROICH (NG 222 956)

The section is characterised by an extremely heterogeneous distribution of strain. Mylonitic fabrics are developed in pegmatites and quartzo-feldspathic gneisses along the margins of amphibolite sheets. The amphibolite sheets themselves deformed predominantly in a brittle manner, with the formation of transcrySTALLINE fibrous quartz veins.

Note that the orientation of the mylonitic foliation is extremely variable and is strongly controlled by the orientation of pre-existing lithological boundaries.

#### FORELAND - PERVASIVE MYLONITE TRANSITION, AIRD RIABHACH (NG 236 966)

The section is characterised by a heterogeneous distribution of strain. Mylonitic fabrics are localised in pegmatites and quartzo-feldspathic banded gneisses at the margins of amphibolite sheets. Note that phyllonitic fabrics are locally developed,

particularly within phyllosilicate-rich pegmatite sheets (Type 2' phyllonites). The amphibolite sheets deformed in a predominantly brittle manner (see Appendix 1 'Foreland - pervasive mylonite transition, Cnoc na Croich'), although a weak foliation may be developed in the margins of the amphibolite sheets. In the most highly strained mylonites near the top of the section, the amphibolite sheets experienced boudinage within a matrix of quartzo-feldspathic protomylonite.

#### **LOW STRAIN MYLONITES, LAG NA LAIRE (NG 233 942)**

Section through a typical package of mylonites which outcrop within the macroscopic low strain zone at Lag na Laire. A mylonitic fabric is well developed within banded gneiss-derived quartzo-feldspathic units. Within pegmatite sheets, the distribution of strain is more heterogeneous. Coarse grained, undeformed pegmatite (cross-hatched) is cross-cut by a network of Type 2' phyllonite strands which consistently display a top-to-the-NW sense of shear.

Amphibolite sheets may be either boudinaged or else appear to be completely undeformed.

#### **MODERATELY STRAINED MYLONITES, E. LAG NA LAIRE (NG 234 942)**

A fairly homogeneous mylonitic fabric is developed in most quartzo-feldspathic units. Coarse grained protomylonites derived from pegmatitic protoliths display well developed shear band fabrics which are consistent with a top-to-the-NW sense of displacement. Relict pegmatite pods appear to be flattened within the plane of the foliation and are stretched parallel to the mineral lineation.

Amphibolite bodies appear to be undeformed apart from a weak foliation developed along their margins.

Note the consistently SE-dipping orientation of the mylonitic foliation.

#### **HIGHLY STRAINED MYLONITES, GEO AN EAR (NG 247 949)**

The Geo an Ear section is characterised by a strong mylonitic fabric which locally grades rapidly into narrow phyllonitic bands. Both mylonitic and phyllonitic fabrics appear to have formed during top-to-the-NW displacements. Phyllonitic fabrics are developed in both banded gneiss- and pegmatite-derived units.

Amphibolite sheets may be either weakly foliated and appear to have deformed homogeneously, or else deformed by boudinage within a phyllonitic / quartzo-feldspathic protomylonitic matrix.

Amphibolite-derived phyllonite has not been observed at Geo an Ear.

#### **HIGHLY STRAINED MYLONITE, AIRD RIABHACH (NG 239 265)**

Note that the rocks in the footwall of the fault are shown at the *top* of the section, and the rocks in hangingwall of the fault are displayed at the *bottom* of the section, i.e. the hangingwall rocks apparently occur below the fault.

Phyllonitic fabrics are well developed in the hangingwall of the fault. Kinematic indicators suggest that the phyllonites formed during top-to-the-NW shearing. The SE-dipping fault plane is lined by a blocky carbonate breccia. Analysis of the

fractures associated with the main fault plane suggests that fault took place during top-to-the-SE (i.e. extensional) shearing.

Strongly developed thrust-related protomylonites are observed in the footwall of the fault.

#### **PHYLLONITE, CNOG NA CROICH (NG 224 957)**

The Cnog na Croich section is characterised by well developed phyllonitic fabrics. The mineral lineation generally trends parallel to the strike of the foliation and is associated with top-to-the-NE kinematic indicators.

S- to SW-verging folds are locally observed in regions where the phyllonitic fabric was reworked during dextral transtension along the OHFZ in Scalpay. The trend of the fold axes is highly variable and reflects the curvilinear nature of the folds.

Note the development of carbonate-quartz porphyroblasts in strike-slip related phyllonites.

#### **PHYLLONITE, KENNAVAY (NG 230 945)**

The base of the section is characterised by thrust-related protophyllonitic fabrics, which suggest that the Kennavay phyllonite localised along site of a pre-existing high strain mylonite zone.

A package of strike-slip related phyllonites is separated from the underlying thrust-related rocks by a SE-dipping normal fault.

## EISHKEN (NB 317 116)

The log represents a NNW → NNE traverse across the western margin of the Eishken phyllonite belt. The lower half of the log comprises discrete phyllonites, protomylonites, pseudotachylytes and cataclasites exposed in the region to the west of the Eishken phyllonite belt. The upper half of the the log comprises part of the Eishken phyllonite belt. Note that the western margin of the phyllonite belt is not exposed.

The protomylonites to the west of the phyllonite belt are highly disrupted by pseudotachylyte veins, cataclasite seams and brittle faults. Relict pegmatites and amphibolite sheets are locally preserved. Discrete phyllonite bands are typically developed along the margins of, or within pegmatite and / or amphibolite sheets. All fabrics and structures are cross-cut by an array of N-S trending sub-vertical quartz veins. The orientation of the vein fibres is consistent with E-W extension.

The phyllonite belt itself comprises predominantly fine grained, homogeneous ultraphyllonite. Quartzo-feldspathic augen are locally preserved (relict pegmatites?) and deformed cataclasite / pseudotachylyte seams have been observed in less strained protophyllonitic regions.

Towards the centre of the phyllonite belt, the phyllonitic fabrics are deformed by predominantly S-verging folds. The folds deform a set of 'early' quartz veins, but are themselves cross-cut by an array of axial planar quartz veins.

## RONAY (NF 901 560)

The log represents a W → E traverse through the Bàgh na Caiplich phyllonite belt on the Isle of Ronay.

The rocks to the west and east of the phyllonite belt comprise crush melange, in which blocks of intensely fractured gneiss 'float' in a matrix of cataclasite and / or devitrified pseudotachylyte.

The phyllonite belt itself comprises fine grained phyllonite and ultraphyllonite, which locally contains relict amphibolite and pegmatite boudins and deformed cataclasite / pseudotachylyte veins. The geometries of the phyllonitic fabrics are consistent with top-to-the-NE sinistral strike-slip. The phyllonitic fabrics are cross-cut by an array of sub-vertical N-S trending quartz and quartz-chlorite veins. The orientation of the veins fibres is consistent with E-W extension. However, there is no evidence to suggest that the Bàgh na Caiplich phyllonite belt has suffered significant reworking during top-to-the-E or -SE extension.

## RUBHA VALLERIP (NF 901 560)

The log represents a W → E traverse through the Rubha Vallerip phyllonite belt. The region to the west of the phyllonite belt is dominated by intensely deformed meta-anorthosite. Blocks of fractured meta-anorthosite 'float' in a matrix of cataclasite and devitrified pseudotachylyte veins.

The phyllonite belt comprises fine grained protophyllonite and ultraphyllonite. The protophyllonitic unit is associated with a NW-SE trending mineral lineation, whilst the ultraphyllonitic unit is associated with an E-W trending mineral lineation. The relative ages of the two units are not known.

The phyllonite belt contains numerous detachment-bounded m-scale blocks of crushed meta-anorthosite, which grade laterally and vertically into phyllonite.

## **SOUTH UIST CRUSH ZONES**

The pseudotachylyte-ultracataclasite crush zones which outcrop along the base of the OHFZ in South Uist have been logged in the Ben na Hoe (NF 8114 2849) and Bealach an Easain (NF 8155 2079) regions. Both logs represent W → E traverses through the crush zones.

The region to the west of the crush zones is dominated by quartzo-feldspathic banded gneisses, which are cross-cut by numerous pseudotachylyte veins and / or cataclasite seams. The pseudotachylyte-bearing fault veins appear to have developed in either localised compressional or localised extensional environments.

The base of the crush zones are not well exposed, but are marked by abrupt topographic breaks of slope (i.e. 'topographic faults'). The crush zones themselves comprise fine grained, apparently homogeneous masses of pseudotachylyte and / or ultracataclasite. Individual pseudotachylyte / cataclasite seams are locally preserved and the cross-cutting relationships suggest that there have been several episodes of pseudotachylyte / cataclasite generation.

The crush zones are cross-cut by a number of 'stacked' NE- to SE-dipping brittle faults. The faults are predominantly normal and displace the hangingwalls down-to-the-NE, -SE or -E.

**CRUSH MELANGE, WEST FACE OF BURRIVAL (NF 9054 6233)**

W → E traverse through the crush melange which outcrops along the west face of Burrival hill. Blocks of randomly oriented, fractured gneiss 'float' in a matrix of cataclasite and devitrified pseudotachylyte. The overall assemblage could be described as 'protocataclasite'. Crush melange is cross-cut by predominantly E- and W-dipping 'microfaults'. See Chapter 6 for more detailed description.

**CRUSH MELANGE, SOUTH FACE OF BURRIVAL (NF 9073 6195)**

W → E traverse through the crush melange which outcrops along the southern flank of Burrival hill. Protocataclastic textures, similar to those observed along the west face of Burrival. See Chapter 6 for more detailed description.

**DISCRETE PHYLLONITE BANDS, BURRIVAL - LOCH A' GHLINNE-DORCHA (NF 9133 6189)**

W → E traverse through a zone of abundant discrete phyllonite bands (green) which outcrop within the crush melange in the region between Burrival and Loch a' Ghlinne-dorcha (see Chapter 6). The phyllonite bands tend to localise along lithological contacts, such as the margins of pegmatite bodies and 'cataclasite' seams. Seams are locally fault bounded on one or both sides.

**NE-SW TRENDING PHYLLONITE BELTS, EIGNEIG MOR (NF 9260 6158)**

NW → SE traverse through zone of NE-SW trending phyllonite belts. Section is characterised by alternating packages of strike-slip and extension-related phyllonite. Contacts are generally gradational, although they are locally marked by moderately NW- or SE-dipping brittle detachment faults. In general, strike-slip related rocks display protophyllonitic / phyllonitic textures, whilst extension-related rocks are typically display phyllonitic / ultraphyllonitic fabrics. The extension-related phyllonites are locally deformed by 'Type 1' folds (see Chapter 6).

**N-S TRENDING PHYLLONITE BELT, EIGNEIG BHEAG (1) (NF 921 599)**

Vertical section through phyllonitic shear zone illustrated in Plate 6.24 (see Chapter 6). Shear zone is 'capped' by a clast of strike-slip related protophyllonite. Shear zone itself comprises packages of planar and folded extension-related phyllonite and ultraphyllonite, which are separated by networks of 'Type 1' detachment faults. Note the abundance of coarse-grained calcite-albite-chlorite 'porphyroclasts' within packages of extension-related phyllonite, particularly immediately adjacent to detachment faults.

## **N-S TRENDING PHYLLONITE BELT, EIGNEIG BHEAG (2) (NF 921 596)**

Vertical section through phyllonitic shear zone illustrated in Plate 6.11. Lowermost two thirds of shear zone comprise packages of extension-related phyllonite. 'Type 2' chevron folds are locally developed, and are commonly associated with polymineralic calcite-albite-chlorite 'porphyroclasts'. Upper part of shear zone comprises extension-related phyllonite, which is 'capped' by a clast of strike-slip related protophyllonite.

# STRUCTURAL LOGS: LEGEND

## KINEMATIC LOG

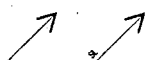
- Thrust (generally top-to-NW)
- Strike-slip (generally top-to-NE)
- Extension (generally top-to-E or -SE; *but* top-to-S or SW in Scalpay phyllonites)
- No exposure

## STRUCTURE LOG

*N.B. fabric elements represented by standard mapping symbols. North to top of page, unless otherwise shown.*

 Banding / foliation (one tick = 0 - 29; two ticks = 30 - 59; three ticks = 60 - 89 degrees dip)

 Fault (one tick = 0 - 29; two ticks = 30 - 59; three ticks = 60 - 89 degrees dip)

 Mineral lineation; slickenline lineation

 Fold axis

## LITHOLOGICAL LOG

*Protolith*

- Banded gneiss
- Amphibolite / Younger Basic dyke
- Pegmatite

*Faults*

Discrete fault plane

Breccia

Cataclasite

*Fault rocks*

Pseudotachylyte

Protomylonite / mylonite / ultramylonite

Protophyllonite / phyllonite / ultraphyllonite

*Miscellaneous*

Shear bands

Quartz ribbon / porphyroclast

Feldspar porphyroclast

Quartz - calcite - chlorite porphyroblast

Veins

Type 1' and Type 2' phyllonite (Scalpay logs)

***N.B. Scale bars refer to the vertical (distance) axis of the logs.***

## APPENDIX B: GEOCHEMICAL DATA

### X-RAY FLUORESCENCE

The major element concentrations were determined using the XRF at the Department of Geological Sciences, University of Durham. Samples were crushed, powdered and dried, then fused to form glass disks, using standard techniques. The fusion disks were analysed using a Philips PW1400 XRF machine using peak and background intensity measurements. This was conducted using the Philips X41 software package and international standards.

### ICP-MS

Trace element concentrations were determined using the ICP-MS at the Department of Geological Sciences, University of Durham. Samples were crushed, powdered and dried, then fused to form glass disks. This procedure was designed to eliminate the possibility of accessory phases not dissolving during ICP-MS preparation. The disks were then powdered. After powdering and drying, 0.1g +/- 0.001g of sample were transferred into a clean teflon vial. 2ml of Aristar HNO<sub>3</sub> were added and allowed to react with the sample. Subsequently, 4ml in mLs of Aristar HF were added to each sample. The vials were then left on a hotplate at 130 – 150°C for twenty-four hours. After being allowed to cool, the vials were replaced on the hot plate, without their lids, allowing the solution to evaporate. This process was halted prior to the sample oxidising and the samples were left to cool. Another 1ml of Aristar HNO<sub>3</sub> was added to the vials, and the samples evaporated again as before. The process was repeated with a further 1ml of HNO<sub>3</sub>. After cooling, 2.5ml of Aristar HNO<sub>3</sub> was added to each vial, and topped up with 10 – 15ml of de-ionised water. The vials were returned to the hot plate at 130 – 150°C for thirty minutes and allowed to cool. 1.25ml of internal standard was added to each sample which was then transferred to a 50ml polypropylene volumetric flask. After all the sample had been transferred, the flask was made up to 50ml with de-ionised water. After these procedures the solution comprised the sample diluted to 50ml in 3.5% HNO<sub>3</sub> with internal standards at 50ppb. The solutions were diluted with 3.5% Aristar HNO<sub>3</sub> to a ratio of 1:10 immediately prior to being run on the ICP-MS. This procedure gives a 5000-fold dilution of the original rock sample.

The major and trace element data thus obtained are presented below.

Major Element Concentrations

	SiO2	Al2O3	Fe2O3	MgO	CaO	Na2O	K2O	TiO2	MnO	P2O5	Ba ppm	Sr ppm	Total	LOI
<b>NU7</b>	75.35	13.18	0.46	0.16	1.43	2.93	5.67	0.03	0.01	0.00	923.40	173.70	99.34	0.35
<b>LB1</b>	69.45	14.92	2.68	1.00	3.27	4.50	2.38	0.30	0.04	0.14	1145.60	805.30	98.87	0.51
<b>NU9</b>	52.78	13.21	15.98	5.21	9.47	2.16	0.82	1.25	0.23	0.13	150.40	160.50	101.27	0.23
<b>BU20</b>	57.62	16.26	7.09	5.16	5.85	4.25	2.15	0.66	0.12	0.14	638.00	343.30	99.39	1.95
<b>BU21</b>	54.19	17.22	8.39	5.74	7.65	2.76	3.20	0.56	0.13	0.12	646.30	493.60	100.07	2.24
<b>RON2</b>	62.66	16.11	5.88	3.18	5.88	4.27	1.66	0.67	0.08	0.20	782.00	506.70	100.72	1.44
<b>BU15a</b>	65.03	16.42	4.01	1.43	4.02	5.50	1.58	0.44	0.06	0.22	559.10	701.30	98.82	1.33
<b>BU15b</b>	63.32	15.06	7.59	3.51	4.16	4.29	1.00	0.85	0.11	0.15	277.70	475.50	100.11	2.14
<b>BU11i</b>	64.29	16.29	6.04	2.84	4.24	4.10	2.18	0.56	0.08	0.17	860.30	622.50	100.94	1.94
<b>BU5</b>	76.46	12.95	1.42	0.28	0.19	6.02	1.23	0.15	0.02	0.01	1465.50	62.60	99.02	0.64
<b>EB5</b>	62.98	15.74	6.55	3.24	4.46	4.20	1.81	0.73	0.09	0.21	585.20	619.70	100.14	2.21
<b>SP13</b>	49.59	17.48	13.02	4.71	8.21	3.35	1.30	1.90	0.19	0.80	494.20	1069.90	100.71	2.99
<b>SP22</b>	57.49	16.83	8.52	4.29	6.94	4.33	1.37	0.90	0.12	0.35	476.00	701.30	101.27	2.24
<b>SP3</b>	63.65	15.78	7.52	3.62	3.71	4.14	1.00	0.80	0.11	0.20	222.60	597.10	100.60	2.51
<b>SP5</b>	61.13	15.65	7.21	3.79	5.41	4.76	1.03	0.80	0.09	0.20	246.90	951.50	100.19	1.92
<b>SP5</b>	61.13	15.63	7.23	3.76	5.35	4.86	1.03	0.78	0.10	0.18	259.00	890.30	100.16	1.92
<b>SP6</b>	59.30	16.45	7.71	4.16	4.04	5.10	1.27	0.89	0.11	0.25	412.80	695.30	99.39	2.55
<b>Average protolith (NU7, LB1, NU9)</b>	65.86	13.77	6.37	2.12	4.72	3.20	2.96	0.52	0.10	0.09	739.80	379.83	99.83	0.36
<b>Average cataclasite (BU20, BU21, BU15a, BU15b)</b>	60.04	16.24	6.77	3.96	5.42	4.20	1.98	0.63	0.11	0.16	530.28	503.43	99.60	1.91
<b>Average pervasive prophyllonite (RON2, BU11i, BU5)</b>	67.80	15.12	4.45	2.10	3.44	4.80	1.69	0.46	0.06	0.13	1035.93	397.27	100.23	1.34
<b>Average strike-slip phyllonite (SP13, SP22)</b>	53.54	17.16	10.77	4.50	7.58	3.84	1.34	1.40	0.16	0.58	485.10	885.60	100.99	2.62
<b>Average reworked phyllonite (EB5, SP3, SP5, SP6)</b>	61.77	15.91	7.25	3.70	4.41	4.55	1.28	0.80	0.10	0.22	366.88	715.90	100.08	2.30

Protolith-normalised Major Element Concentrations

(All normalised to LB1, except BU5)	SiO2	Al2O3	Fe2O3	MgO	CaO	Na2O	K2O	TiO2	MnO	P2O5	Ba ppm	Sr ppm	Total	LOI
BU20	0.83	1.09	2.65	5.16	1.79	0.94	0.90	2.23	3.00	1.00	0.56	0.43	1.01	3.83
BU21	0.78	1.15	3.13	5.74	2.34	0.61	1.35	1.90	3.23	0.86	0.56	0.61	1.01	4.40
BU15a	0.94	1.10	1.50	1.43	1.23	1.22	0.66	1.49	1.43	1.57	0.49	0.87	1.00	2.61
BU15b	0.91	1.01	2.83	3.51	1.27	0.95	0.42	2.86	2.85	1.07	0.24	0.59	1.01	4.19
BV3	0.75	0.65	4.78	15.18	2.17	0.33	0.44	1.90	5.93	1.14	2.66	0.34	1.02	6.66
RON2	0.90	1.08	2.19	3.18	1.80	0.95	0.70	2.26	2.08	1.43	0.68	0.63	1.02	2.83
BU11i	0.93	1.09	2.25	2.84	1.30	0.91	0.92	1.89	2.00	1.21	0.75	0.77	1.02	3.82
BU5 (Normalised to NU9)	1.01	0.98	3.09	1.75	0.13	2.05	0.22	5.70	1.14	0.00	1.59	0.36	1.00	1.83
EB5	0.91	1.05	2.44	3.24	1.36	0.93	0.76	2.46	2.23	1.50	0.51	0.77	1.01	4.34
SP13	0.71	1.17	4.86	4.71	2.51	0.74	0.55	6.42	4.70	5.71	0.43	1.33	1.02	5.87
SP22	0.83	1.13	3.18	4.29	2.12	0.96	0.58	3.04	3.05	2.50	0.42	0.87	1.02	4.40
SP3	0.92	1.06	2.81	3.62	1.13	0.92	0.42	2.70	2.68	1.43	0.19	0.74	1.02	4.93
SP5	0.88	1.05	2.69	3.79	1.65	1.06	0.43	2.70	2.35	1.43	0.22	1.18	1.01	3.77
SP5	0.88	1.05	2.70	3.76	1.64	1.08	0.43	2.65	2.38	1.29	0.23	1.11	1.01	3.77
SP6	0.85	1.10	2.88	4.16	1.24	1.13	0.53	3.01	2.75	1.79	0.36	0.86	1.01	5.00
SCM2	1.04	1.01	0.88	0.94	0.62	0.95	1.14	1.08	0.78	0.71	0.72	0.57	1.01	2.62
Average protolith-normalised cataclasite (BU20, BU21, BU15a, BU15b)	0.86	1.09	2.53	3.96	1.66	0.93	0.83	2.12	2.63	1.13	0.46	0.63	1.01	3.76
Average protolith-normalised pervasive prophyllonite (RON2, BU11i, BU5)	0.95	1.05	2.51	2.59	1.08	1.30	0.61	3.29	1.74	0.88	1.01	0.59	1.01	2.83
Average protolith-normalised strike-slip phyllonite (SP13, SP22)	0.77	1.15	4.02	4.50	2.32	0.85	0.56	4.73	3.88	4.11	0.42	1.10	1.02	5.14
Average protolith-normalised reworked phyllonite (EB5, SP3, SP5, SP6)	0.89	1.07	2.70	3.70	1.35	1.01	0.54	2.72	2.50	1.54	0.32	0.89	1.01	4.51

	Atomic Mass	nu7	lb1	nu9	mafic band : felsic band	bu20	bu21	bu15a	bu15b	bv3	ren2	bu5	bu111	sp13	sp22	eb5	sp3	sp5	sp6	acm2	
La	139	7.40	40.18	12.51	27.64	7.34	20.56	18.32	44.99	22.49	37.69	47.90	21.72	30.99	53.36	50.52	32.91	38.42	35.34	36.60	28.89
Ce	140	11.14	81.53	28.78	70.25	12.85	43.04	40.89	94.09	48.70	78.23	95.58	30.91	63.10	129.00	117.94	68.99	74.74	73.94	81.94	50.52
Pr	141	1.03	9.54	3.70	9.51	1.28	5.40	5.17	10.92	6.09	9.02	10.72	2.64	8.08	17.37	15.40	8.07	9.74	8.81	10.15	4.68
Nd	143	3.39	34.92	15.07	38.96	4.10	21.35	20.80	41.81	24.60	31.68	37.73	6.92	33.08	73.28	60.33	29.95	35.08	32.42	39.40	14.66
Sm	147	0.56	5.63	3.72	8.58	0.57	4.04	3.99	6.96	4.65	5.12	5.57	0.75	5.43	12.86	9.40	4.75	5.71	5.63	6.66	1.76
Sr	149	0.46	6.01	3.85	9.07	0.52	4.12	4.27	7.25	4.50	5.43	6.04	0.68	5.46	13.52	10.05	5.03	6.17	5.24	6.64	1.75
Eu	151	0.56	1.21	1.17	1.49	0.44	0.95	1.04	1.56	1.12	1.17	1.22	0.62	1.39	3.38	2.04	1.19	1.38	1.23	1.46	0.65
Er	153	0.79	1.37	1.18	1.48	0.58	1.08	1.11	1.61	1.19	1.78	1.36	0.92	1.56	3.48	2.08	1.32	1.28	1.28	1.55	0.86
Gd	157	0.43	3.86	4.24	7.64	0.39	3.13	3.30	4.66	3.84	3.66	4.22	0.56	3.81	9.42	7.57	3.59	4.58	4.12	5.04	1.24
Tb	159	0.05	0.48	0.75	1.27	0.04	0.44	0.43	0.57	0.55	0.49	0.50	0.05	0.49	1.16	0.88	0.46	0.59	0.54	0.63	0.13
Dy	161	0.33	2.19	4.62	7.05	0.18	2.25	2.33	2.47	3.15	2.68	2.44	0.20	2.42	5.17	4.33	2.46	2.70	2.83	3.21	0.67
Y	163	0.26	2.25	4.29	7.04	0.19	2.32	2.41	2.58	3.05	2.53	2.62	0.19	2.37	5.37	4.44	2.34	3.00	2.79	3.21	0.54
Ho	165	0.05	0.39	1.01	1.41	0.04	0.42	0.43	0.44	0.62	0.47	0.44	0.04	0.44	0.93	0.78	0.42	0.57	0.53	0.63	0.10
Er	166	0.15	1.05	3.01	3.94	0.10	1.04	1.19	1.06	1.57	1.34	1.22	0.10	1.14	2.35	2.09	1.21	1.48	1.47	1.69	0.25
Tm	167	0.19	1.02	3.01	3.86	0.12	1.10	1.15	1.10	1.80	1.34	1.09	0.12	1.16	2.43	2.03	1.26	1.43	1.43	1.65	0.29
Yb	169	0.03	0.15	0.48	0.59	0.02	0.17	0.18	0.17	0.27	0.19	0.18	0.02	0.16	0.34	0.31	0.18	0.23	0.21	0.23	0.04
Lu	172	0.16	0.83	2.84	3.40	0.09	0.99	0.94	0.90	1.62	1.22	1.03	0.12	0.92	1.94	1.76	1.11	1.45	1.25	1.35	0.23
Lu	174	0.19	0.90	2.85	3.38	0.13	0.95	1.04	0.95	1.74	1.18	0.99	0.14	0.90	1.86	1.65	1.01	1.29	1.25	1.44	0.24
Lu	175	0.03	0.12	0.44	0.54	0.02	0.15	0.16	0.14	0.27	0.19	0.16	0.02	0.13	0.29	0.28	0.16	0.22	0.21	0.23	0.04
La	7.40	40.18	12.51	27.64	7.34	20.56	18.32	44.99	22.49	37.69	47.90	21.72	30.99	53.36	50.52	32.91	38.42	35.34	36.60	28.89	Boydton: chondrite
Ce	11.14	81.53	28.78	70.25	12.85	43.04	40.89	94.09	48.70	78.23	95.58	30.91	63.10	129.00	117.94	68.99	74.74	73.94	81.94	50.52	0.31
Pr	1.03	9.54	3.70	9.51	1.28	5.40	5.17	10.92	6.09	9.02	10.72	2.64	8.08	17.37	15.40	8.07	9.74	8.81	10.15	4.68	0.81
Nd	3.39	34.92	15.07	38.96	4.10	21.35	20.80	41.81	24.60	31.68	37.73	6.92	33.08	73.28	60.33	29.95	35.08	32.42	39.40	14.66	0.12
Sm	0.51	5.62	3.78	8.83	0.55	4.08	4.13	7.10	4.58	5.27	5.80	0.71	5.44	13.19	9.73	4.89	5.94	5.44	6.60	1.78	0.60
Eu	0.66	1.29	1.17	1.49	0.51	1.01	1.08	1.59	1.15	1.48	1.29	0.77	1.47	3.43	2.06	1.26	1.38	1.26	1.50	0.76	0.20
Gd	3.86	4.24	7.64	0.39	3.13	3.30	4.66	3.84	3.66	4.22	0.56	3.81	9.42	7.57	3.59	4.58	4.12	5.04	1.24	1.24	0.07
Tb	0.48	0.75	1.27	0.04	0.44	0.43	0.57	0.55	0.49	0.50	0.05	0.49	1.16	0.88	0.46	0.59	0.54	0.63	0.13	0.13	0.26
Dy	0.30	2.22	4.46	7.04	0.19	2.29	2.37	2.53	3.10	2.60	2.53	0.19	2.40	5.27	4.39	2.40	2.85	2.81	3.21	0.60	0.05
Ho	0.06	0.39	1.01	1.41	0.04	0.42	0.43	0.44	0.62	0.47	0.44	0.04	0.44	0.93	0.78	0.42	0.57	0.53	0.63	0.10	0.02
Er	0.17	1.03	3.01	3.90	0.11	1.07	1.17	1.08	1.88	1.34	1.18	0.11	1.15	2.39	2.06	1.23	1.55	1.44	1.63	0.27	0.07
Tm	0.03	0.15	0.48	0.59	0.02	0.17	0.18	0.17	0.27	0.19	0.18	0.02	0.16	0.34	0.31	0.18	0.23	0.21	0.23	0.04	0.03
Yb	0.17	0.86	2.85	3.43	0.11	0.97	0.99	0.93	1.58	1.20	1.01	0.13	0.91	1.90	1.70	1.06	1.37	1.25	1.40	0.23	0.21
Lu	0.03	0.12	0.44	0.54	0.02	0.15	0.16	0.14	0.27	0.19	0.16	0.02	0.13	0.29	0.28	0.16	0.22	0.21	0.23	0.04	0.03
La	23.86	129.55	40.37	89.16	23.69	66.31	59.10	145.14	72.55	121.60	154.53	70.07	93.96	172.12	162.98	106.15	123.93	114.01	118.28	93.21	62.53
Ce	13.79	100.90	35.61	86.94	15.90	53.27	50.61	116.45	60.28	96.83	118.29	38.25	78.09	159.66	145.96	85.38	92.49	91.52	101.41	62.53	38.35
Pr	8.48	76.20	30.36	77.94	10.49	44.30	42.39	89.51	43.92	73.96	87.89	21.65	66.21	142.34	126.22	66.15	79.84	72.21	83.19	38.35	24.43
Nd	5.64	58.20	25.12	64.94	6.84	35.59	34.66	69.69	40.99	52.79	62.89	11.53	55.13	122.13	100.55	49.91	58.47	54.03	65.67	24.43	9.01
Sm	2.61	29.83	19.29	45.26	2.80	20.94	21.19	36.43	23.47	27.05	29.77	3.66	27.92	67.63	49.87	25.07	30.47	27.87	33.85	9.01	10.28
Eu	8.96	17.60	15.96	20.22	7.00	13.80	14.72	21.58	15.69	20.10	17.52	10.47	20.05	46.66	27.88	17.09	18.78	17.12	20.48	10.28	4.78
Gd	14.90	16.37	29.50	1.52	12.07	12.72	18.00	14.84	14.12	16.28	2.16	14.72	36.38	29.21	13.85	17.70	15.89	19.48	4.78	4.78	2.68
Tb	10.18	15.77	26.83	0.89	9.23	9.07	12.03	11.70	10.31	10.50	1.18	10.41	24.53	18.67	9.74	12.54	11.42	13.38	2.68	2.68	1.87
Dy	0.92	8.90	13.85	21.87	0.56	7.10	7.36	7.86	9.63	8.09	7.86	0.60	7.44	16.37	13.62	7.45	8.86	8.72	9.87	1.87	1.42
Ho	0.77	5.39	14.05	18.62	0.50	5.83	6.05	6.09	8.67	6.52	6.14	0.50	6.09	12.92	10.82	5.91	7.87	7.44	8.77	1.42	1.26
Er	0.80	4.92	14.33	18.58	0.52	5.11	5.55	5.12	8.02	6.39	5.51	0.54	5.48	11.37	9.83	5.87	7.40	6.86	7.74	1.26	1.18
Tm	0.95	4.70	14.82	18.26	0.58	5.25	5.44	5.11	8.47	6.02	5.45	0.64	4.84	10.83	9.67	5.47	7.10	6.57	7.20	1.18	1.12
Yb	0.83	4.13	13.62	16.41	0.53	4.64	4.74	4.43	8.02	5.75	4.83	0.63	4.34	9.09	8.16	5.07	6.55	5.99	6.68	1.12	1.31
Lu	0.99	3.88	13.69	16.62	0.75	4.67	5.11	4.43	8.43	5.88	4.82	0.72	4.05	8.85	6.76	5.09	6.94	6.39	7.15	1.31	

	Atomic Mass	nu7	lb1	nu9	mafic band	felsic band	bu20	bu21	bu15a	bu16b	bu3	ron2-	bu5	bu11	sp13	sp22	eb5	sp3	sp5	sp6	scm2	
Tl	49	0.00	0.30	1.49	0.84	0.02	0.74	0.62	0.49	0.88	0.62	0.76	0.15	0.59	2.15	1.03	0.73	0.85	0.81	0.93	0.24	
Rb	85	177.50	85.30	13.69	55.63	178.14	77.19	113.60	53.07	36.93	35.37	35.03	21.64	33.87	22.68	37.11	47.09	34.92	24.18	25.91	104.04	
Sr	88	203.21	821.80	179.48	363.53	233.97	382.66	592.41	779.12	402.39	292.68	618.58	63.24	703.15	1172.60	869.68	564.20	523.00	895.24	652.48	371.03	
Y	89	1.95	13.20	31.91	45.83	1.35	13.73	13.79	15.26	20.07	15.15	14.49	1.29	13.34	29.81	26.86	14.34	18.19	17.35	19.57	3.35	
Zr	90	65.49	191.85	115.37	76.02	104.58	101.06	85.02	198.36	150.73	59.78	216.38	110.18	139.63	145.23	186.41	173.81	180.79	174.31	192.34	158.99	
Nb	93	0.55	5.56	7.70	15.26	1.17	4.73	4.01	6.06	7.40	2.68	6.79	0.89	3.64	9.36	10.50	6.26	7.24	6.89	7.68	2.75	
Cs	133	0.67	0.67	0.09	0.64	0.68	0.76	0.61	1.04	0.81	0.61	0.12	0.17	0.17	0.19	0.23	0.24	0.23	0.15	0.18	0.24	
Ba	137	1061.77	1296.38	170.32	206.27	882.57	717.36	736.11	645.10	352.61	3643.63	927.93	1650.41	985.68	592.61	547.10	678.76	276.77	299.06	471.79	968.95	
La	139	7.40	40.16	12.51	27.64	7.34	20.56	18.32	44.99	22.49	37.69	47.90	21.72	30.99	53.36	50.52	32.91	38.42	35.34	36.66	28.89	
Ce	140	11.14	81.53	28.78	70.25	12.85	43.04	40.89	94.09	48.70	78.23	95.58	30.91	63.10	129.00	117.94	68.99	74.74	73.94	81.94	50.52	
Nd	143	3.39	34.92	15.07	38.96	4.10	21.35	20.80	41.81	24.60	31.68	37.73	6.92	33.08	73.28	60.33	29.95	35.08	32.42	39.40	14.66	
Sm	147	0.56	5.63	3.72	8.58	0.57	4.04	3.99	6.96	4.65	5.12	5.57	0.75	5.43	12.86	9.40	4.75	5.71	5.63	6.56	1.76	
Sm	149	0.46	6.01	3.85	9.07	0.52	4.12	4.27	7.25	4.50	5.43	6.04	0.68	5.46	13.52	10.05	5.03	6.17	5.24	6.64	1.75	
Tb	159	0.05	0.48	0.75	1.27	0.04	0.44	0.43	0.57	0.55	0.49	0.50	0.05	0.49	1.16	0.88	0.46	0.59	0.54	0.63	0.13	
Hf	177	2.16	4.59	2.72	2.34	2.96	2.47	2.02	4.43	3.55	1.47	4.46	2.73	3.10	3.26	4.19	3.72	3.92	3.89	4.30	3.43	
Hf	178	2.12	4.39	2.75	2.22	2.91	2.38	1.98	4.01	3.41	1.46	4.44	2.41	2.87	2.87	3.99	3.67	3.89	3.62	4.09	3.28	
Ta	181	0.00	0.01	0.20	0.75	0.00	0.00	0.00	0.00	0.29	0.00	0.00	0.00	0.00	0.12	0.15	0.00	0.03	0.08	0.00	0.00	
Pb	206	17.69	15.00	3.78	8.20	22.39	3.94	4.28	8.27	31.56	1.68	3.25	7.87	22.53	14.66	6.71	5.50	7.18	23.44	7.75	8.28	
Pb	207	21.62	17.80	3.71	8.62	24.96	4.38	5.09	9.46	36.06	1.85	3.91	8.52	25.75	17.26	7.61	6.08	8.43	24.50	8.91	9.36	
Pb	208	19.84	17.68	3.81	8.73	23.61	4.32	4.99	9.23	34.51	1.90	3.78	8.31	24.52	16.05	7.28	6.02	7.99	24.21	8.37	9.24	
Pb	208	20.15	18.89	3.87	9.02	23.65	4.47	5.29	9.60	35.28	2.02	3.97	8.44	24.97	16.22	7.41	6.23	8.20	24.46	8.44	9.65	
Th	232	1.67	14.68	2.45	4.81	2.37	2.57	2.10	6.10	3.02	2.06	3.50	0.75	0.00	0.44	1.15	1.59	2.03	2.21	1.02	3.86	
U	238	0.37	0.76	0.60	0.48	0.54	0.31	0.20	0.15	0.74	0.10	0.11	0.09	0.03	0.13	0.21	0.18	0.25	0.28	0.17	0.21	
																						Thompson Sun & McDonough
Cs		0.67	0.67	0.09	0.64	0.68	0.76	0.61	1.04	0.81	0.61	0.12	0.17	0.17	0.19	0.23	0.24	0.23	0.15	0.18	0.24	0.19
Pb		19.82	17.34	3.79	8.64	23.65	4.28	4.91	9.14	34.35	1.86	3.73	8.29	24.44	16.05	7.25	5.96	7.95	24.15	8.37	9.13	2.47
Ba		1061.77	1296.38	170.32	206.27	882.57	717.36	736.11	645.10	352.61	3643.63	927.93	1650.41	985.68	592.61	547.10	678.76	276.77	299.06	471.79	968.95	6.90
Rb		177.50	85.30	13.69	55.63	178.14	77.19	113.60	53.07	36.93	35.37	35.03	21.64	33.87	22.68	37.11	47.09	34.92	24.18	25.91	104.04	0.35
Th		1.67	14.68	2.45	4.81	2.37	2.57	2.10	6.10	3.02	2.06	3.50	0.75	0.00	0.44	1.15	1.59	2.03	2.21	1.02	3.86	0.04
U		0.37	0.76	0.60	0.48	0.54	0.31	0.20	0.15	0.74	0.10	0.11	0.09	0.03	0.13	0.21	0.18	0.25	0.28	0.17	0.21	0.01
Nb		0.55	5.56	7.70	15.26	1.17	4.73	4.01	6.06	7.40	2.68	6.79	0.89	3.64	9.36	10.50	6.26	7.24	6.89	7.68	2.75	0.35
Ta		0.00	0.01	0.20	0.75	0.00	0.00	0.00	0.00	0.29	0.00	0.00	0.00	0.00	0.12	0.15	0.00	0.03	0.08	0.00	0.00	0.02
La		7.40	40.16	12.51	27.64	7.34	20.56	18.32	44.99	22.49	37.69	47.90	21.72	30.99	53.36	50.52	32.91	38.42	35.34	36.66	28.89	0.33
Co		11.14	81.53	28.78	70.25	12.85	43.04	40.89	94.09	48.70	78.23	95.58	30.91	63.10	129.00	117.94	68.99	74.74	73.94	81.94	50.52	0.87
Sr		203.21	821.80	179.48	363.53	233.97	382.66	592.41	779.12	402.39	292.68	618.58	63.24	703.15	1172.60	869.68	564.20	523.00	895.24	652.48	371.03	11.80
Nd		3.39	34.92	15.07	38.96	4.10	21.35	20.80	41.81	24.60	31.68	37.73	6.92	33.08	73.28	60.33	29.95	35.08	32.42	39.40	14.66	0.63
Sm		0.51	5.82	3.78	8.83	0.55	4.08	4.13	7.10	4.58	5.27	5.80	0.71	5.44	13.19	9.73	4.89	5.94	5.44	6.60	1.76	0.20
Zr		65.49	191.85	115.37	76.02	104.58	101.06	85.02	198.36	150.73	59.78	216.38	110.18	139.63	145.23	186.41	173.81	180.79	174.31	192.34	158.99	6.84
Hf		2.14	4.49	2.74	2.28	2.94	2.42	2.00	4.22	3.48	1.47	4.45	2.57	2.98	3.06	4.09	3.69	3.91	3.76	4.19	3.36	0.20
Tl		0.00	0.30	1.49	0.84	0.02	0.74	0.62	0.49	0.88	0.62	0.76	0.15	0.59	2.15	1.03	0.73	0.85	0.81	0.93	0.24	620.00
Tb		0.05	0.48	0.75	1.27	0.04	0.44	0.43	0.57	0.55	0.49	0.50	0.05	0.49	1.16	0.88	0.46	0.59	0.54	0.63	0.13	0.05
Y		1.95	13.20	31.91	45.83	1.35	13.73	13.79	15.26	20.07	15.15	14.49	1.29	13.34	29.81	26.86	14.34	18.19	17.35	19.57	3.35	2.00
Tm		0.03	0.15	0.48	0.59	0.02	0.17	0.18	0.17	0.27	0.19	0.18	0.02	0.16	0.34	0.31	0.18	0.23	0.21	0.23	0.04	0.03
Yb		0.83	4.13	13.62	16.41	0.53	4.64	4.74	4.43	8.02	5.75	4.83	0.63	4.34	9.09	8.16	5.07	6.55	5.99	6.68	1.12	0.22
Cs		3.54	3.58	0.47	3.40	3.59	4.06	3.26	5.51	4.33	3.22	0.66	0.93	0.88	1.00	1.22	1.27	1.23	0.82	0.93	1.25	
Pb		8.03	7.02	1.53	3.50	9.58	1.73	1.99	3.70	13.91	0.75	1.51	3.35	9.90	6.50	2.94	2.41	3.22	9.78	3.39	3.70	
Ba		153.88	187.88	24.68	29.89	127.91	103.96	106.68	93.49	51.10	528.06	134.48	239.19	142.85	85.89	79.29	98.37	40.11	43.34	68.38	140.43	
Rb		507.15	243.72	39.12	158.93	508.96	220.56	324.57	151.63	105.51	101.07	100.10	61.82	96.78	64.80	106.02	134.53	99.77	69.08	74.02	297.27	
Sr		17.22	69.64	15.21	30.81	19.83	32.43	50.20	66.03	34.10	24.80	52.42	5.36	59.59	99.37	73.70	47.81	44.32	75.87	55.30	31.44	
U		46.26	95.14	75.00	59.49	68.04	39.23	25.09	19.09	92.94	12.01	13.53	10.86	4.25	15.65	26.45	22.65	30.68	35.41	21.51	26.53	
Nb		1.57	15.89	22.00	43.60	3.35	13.50	11.45	17.31	21.15	7.67	19.39	2.55	10.41	26.74	30.00	17.90	20.68	19.69	21.95	7.86	
Th		39.81	349.45	58.45	114.41	56.33	61.26	50.02	145.30	71.84	48.96	83.33	17.96	0.03	10.49	27.30	37.86	48.25	52.58	24.29	91.92	
La		22.48	122.07	38.04	84.01	22.32	62.48	55.68	136.76	68.36	114.57	145.61	66.02	94.18	162.18	153.56	100.02	116.77	107.43	111.43	87.82	
Ce		12.88	94.25	33.27	81.21	14.86	49.76	47.27	108.77	56.31	90.44	110.50	35.73	72.94	149.14	136.34	79.76	86.40	85.49	94.73	58.41	
Nd		5.37	55.43	23.93	61.85	6.51	33.89	33.01	66.37	39.04	50.28	59.89	10.99	52.50	116.31	95.76	47.54	55.68	51.45	62.55	23.27	
Sm		2.51	28.66	18.62	43.48	2.69	20.11	20.36	35.00	22.54	25.98	28.60	3.52	26.82	64.97	47.91	24.08	29.27	26.77	32.52	8.65	
Zr		9.57	28.05	16.87	11.11	15.29	14.77	12.43	29.00	22.04	8.											

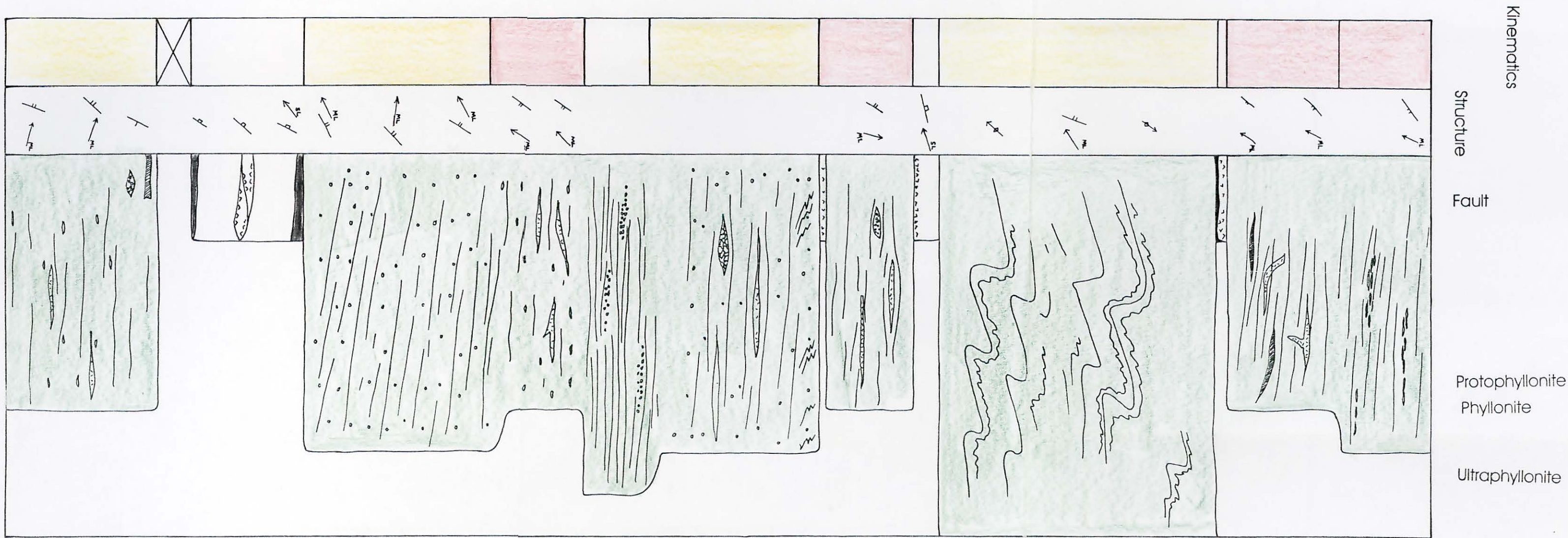
ppm	nu7	lb1	nu9	mafic band	felsic band	bu20	bu21	bu15a	bu15b	bv3	ron2	bu5	bu11i	sp13	sp22	eb5	sp3	sp5	sp6	scm2
Normalisation factor						LB1	LB1	LB1	LB1	LB1	LB1	Felsic band	LB1	LB1	LB1	LB1	LB1	LB1	LB1	LB1
<b>Cs</b>	0.67	0.67	0.09	0.64	0.68	1.13	0.91	1.54	1.21	0.90	0.18	0.26	0.25	0.28	0.34	0.35	0.34	0.23	0.26	0.35
<b>Pb</b>	19.82	17.34	3.79	8.64	23.65	0.25	0.28	0.53	1.98	0.11	0.21	0.35	1.41	0.93	0.42	0.34	0.46	1.39	0.48	0.53
<b>Ba</b>	1061.77	1296.38	170.32	206.27	882.57	0.55	0.57	0.50	0.27	2.81	0.72	1.87	0.76	0.46	0.42	0.52	0.21	0.23	0.36	0.75
<b>Rb</b>	177.50	85.30	13.69	55.63	178.14	0.90	1.33	0.62	0.43	0.41	0.41	0.12	0.40	0.27	0.44	0.55	0.41	0.28	0.30	1.22
<b>Sr</b>	1.67	14.68	2.45	4.81	2.37	0.47	0.72	0.95	0.49	0.36	0.75	0.27	0.86	1.43	1.06	0.69	0.64	1.09	0.79	0.45
<b>U</b>	0.37	0.76	0.60	0.48	0.54	0.41	0.26	0.20	0.98	0.13	0.14	0.16	0.04	0.16	0.28	0.24	0.32	0.37	0.23	0.28
<b>Nb</b>	0.55	5.56	7.70	15.26	1.17	0.85	0.72	1.09	1.33	0.48	1.22	0.76	0.65	1.68	1.89	1.13	1.30	1.24	1.38	0.49
<b>Th</b>	7.40	40.16	12.51	27.64	7.34	0.18	0.14	0.42	0.21	0.14	0.24	0.32	0.00	0.03	0.08	0.11	0.14	0.15	0.07	0.26
<b>La</b>	11.14	81.53	28.78	70.25	12.85	0.51	0.46	1.12	0.56	0.94	1.19	2.96	0.77	1.33	1.26	0.82	0.96	0.88	0.91	0.72
<b>Ce</b>	203.21	821.80	179.48	363.53	233.97	0.53	0.50	1.15	0.60	0.96	1.17	2.41	0.77	1.58	1.45	0.85	0.92	0.91	1.01	0.62
<b>Nd</b>	3.39	34.92	15.07	38.96	4.10	0.61	0.60	1.20	0.70	0.91	1.08	1.69	0.95	2.10	1.73	0.86	1.00	0.93	1.13	0.42
<b>Sm</b>	0.51	5.82	3.78	8.83	0.55	0.70	0.71	1.22	0.79	0.91	1.00	1.31	0.94	2.27	1.67	0.84	1.02	0.93	1.13	0.30
<b>Zr</b>	65.49	191.85	115.37	76.02	104.58	0.53	0.44	1.03	0.79	0.31	1.13	1.05	0.73	0.76	0.97	0.91	0.94	0.91	1.00	0.83
<b>Hf</b>	2.14	4.49	2.74	2.28	2.94	0.54	0.45	0.94	0.77	0.33	0.99	0.88	0.66	0.68	0.91	0.82	0.87	0.84	0.93	0.75
<b>Ti</b>	0.00	0.30	1.49	0.84	0.02	2.42	2.04	1.61	2.89	2.03	2.50	9.74	1.95	7.06	3.37	2.41	2.78	2.65	3.04	0.80
<b>Tb</b>	0.05	0.48	0.75	1.27	0.04	0.91	0.89	1.18	1.15	1.01	1.03	1.30	1.02	2.41	1.83	0.96	1.23	1.12	1.31	0.26
<b>Y</b>	1.95	13.20	31.91	45.83	1.35	1.04	1.05	1.16	1.52	1.15	1.10	0.95	1.01	2.26	2.03	1.09	1.38	1.31	1.48	0.25
<b>Tm</b>	0.03	0.15	0.48	0.59	0.02	1.12	1.16	1.09	1.80	1.28	1.16	1.10	1.03	2.26	2.06	1.16	1.51	1.40	1.53	0.25
<b>Yb</b>	0.83	4.13	13.62	16.41	0.53	1.12	1.15	1.07	1.94	1.39	1.17	1.20	1.05	2.20	1.98	1.23	1.59	1.45	1.62	0.27

Normalisation factor	nu7	lb1	nu9	mafic band	felsic band	bu20	bu21	bu15a	bu15b	bv3	ron2	bu5	bu11i	sp13	sp22	eb5	sp3	sp5	sp6	scm2
						LB1	LB1	LB1	LB1	LB1	LB1	Felsic band	LB1	LB1	LB1	LB1	LB1	LB1	LB1	LB1
<b>La</b>	7.40	40.16	12.51	27.64	7.34	0.51	0.46	1.12	0.56	0.94	1.19	2.96	0.77	1.33	1.26	0.82	0.96	0.88	0.91	0.72
<b>Ce</b>	11.14	81.53	28.78	70.25	12.85	0.53	0.50	1.15	0.60	0.96	1.17	2.41	0.77	1.58	1.45	0.85	0.92	0.91	1.01	0.62
<b>Pr</b>	1.03	9.54	3.70	9.51	1.28	0.57	0.54	1.14	0.64	0.95	1.12	2.06	0.85	1.82	1.61	0.85	1.02	0.92	1.06	0.49
<b>Nd</b>	3.39	34.92	15.07	38.96	4.10	0.61	0.60	1.20	0.70	0.91	1.08	1.69	0.95	2.10	1.73	0.86	1.00	0.93	1.13	0.42
<b>Sm</b>	0.51	5.82	3.78	8.83	0.55	0.70	0.71	1.22	0.79	0.91	1.00	1.31	0.94	2.27	1.67	0.84	1.02	0.93	1.13	0.30
<b>Eu</b>	0.66	1.29	1.17	1.49	0.51	0.78	0.84	1.23	0.89	1.14	1.00	1.50	1.14	2.65	1.59	0.97	1.07	0.97	1.16	0.58
<b>Gd</b>	3.86	4.24	7.64	0.39	3.13	0.78	1.10	0.91	0.86	0.99	0.13	1.22	2.22	1.78	0.85	1.08	0.97	1.19	0.29	0.29
<b>Tb</b>	0.48	0.75	1.27	0.04	0.44	0.58	0.76	0.74	0.65	0.67	0.07	1.13	1.56	1.18	0.62	0.80	0.72	0.85	0.17	0.17
<b>Dy</b>	0.30	2.22	4.46	7.04	0.19	1.03	1.07	1.14	1.40	1.17	1.14	1.04	1.08	2.37	1.97	1.08	1.28	1.26	1.45	0.27
<b>Ho</b>	0.06	0.39	1.01	1.41	0.04	1.08	1.12	1.13	1.61	1.21	1.14	0.84	1.13	2.40	2.01	1.10	1.46	1.38	1.63	0.26
<b>Er</b>	0.17	1.03	3.01	3.90	0.11	1.04	1.13	1.04	1.63	1.30	1.12	1.04	1.11	2.31	2.00	1.19	1.50	1.39	1.57	0.26
<b>Tm</b>	0.03	0.15	0.48	0.59	0.02	1.12	1.16	1.09	1.80	1.28	1.16	1.10	1.03	2.26	2.06	1.16	1.51	1.40	1.53	0.25
<b>Yb</b>	0.17	0.86	2.85	3.43	0.11	1.12	1.15	1.07	1.94	1.39	1.17	1.20	1.05	2.20	1.98	1.23	1.59	1.45	1.62	0.27
<b>Lu</b>	0.03	0.12	0.44	0.54	0.02	1.21	1.32	1.15	2.18	1.52	1.25	0.95	1.05	2.29	2.27	1.32	1.80	1.66	1.85	0.34



# Eigneig Mor

0 metres 4

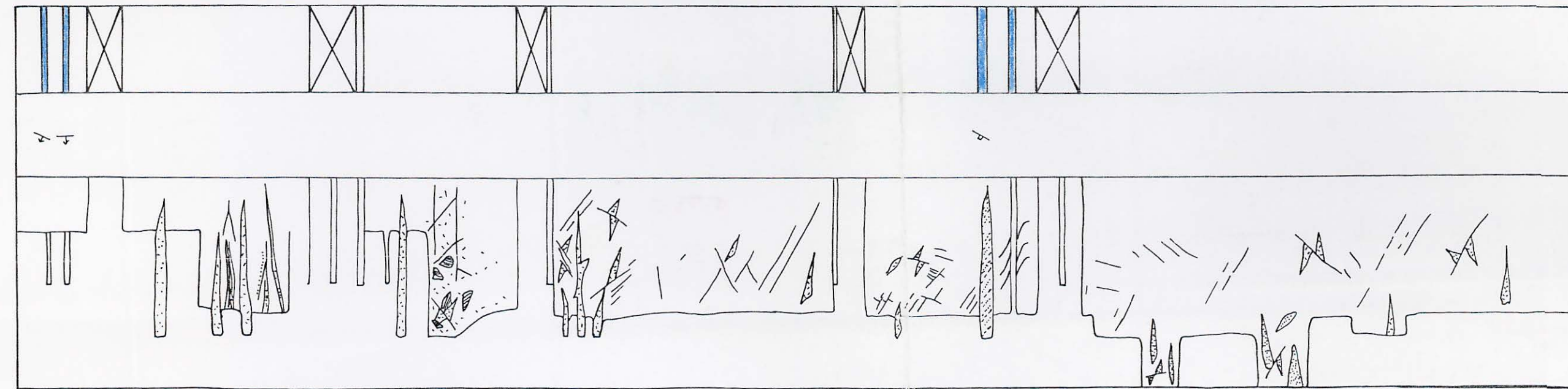


Base of log NF 9260 6158

# Base of crush melange - Burrival summit

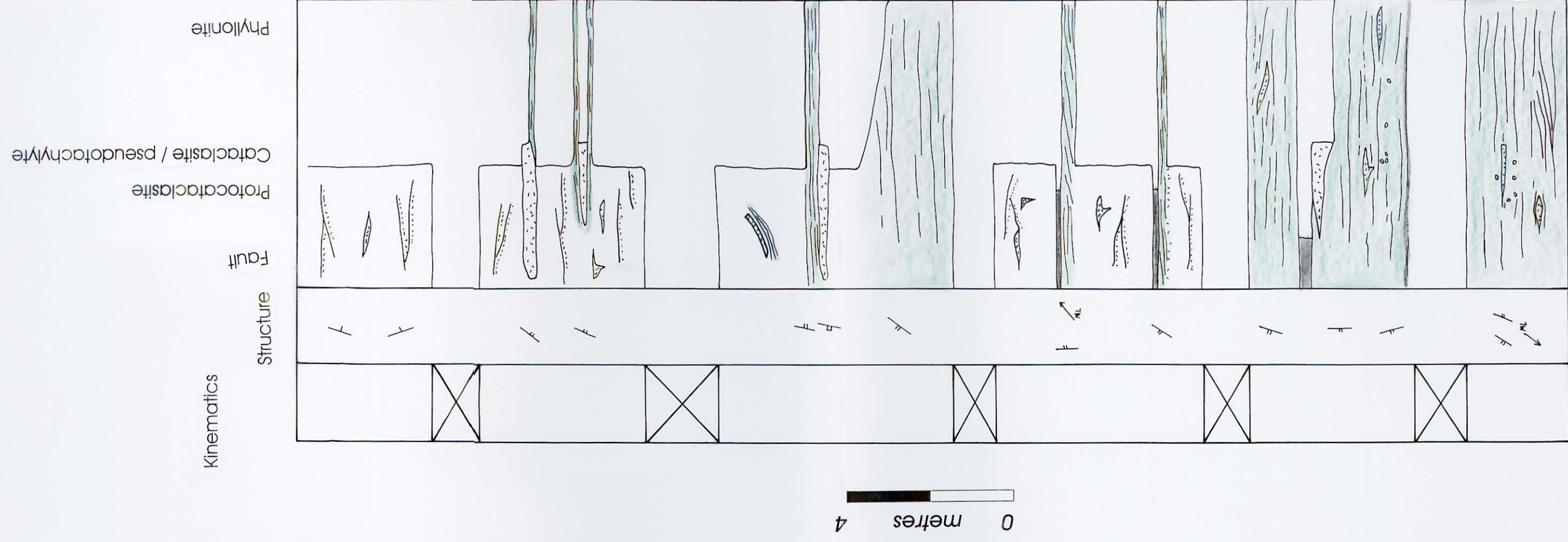
0 metres 4

Base of log NF 905 622



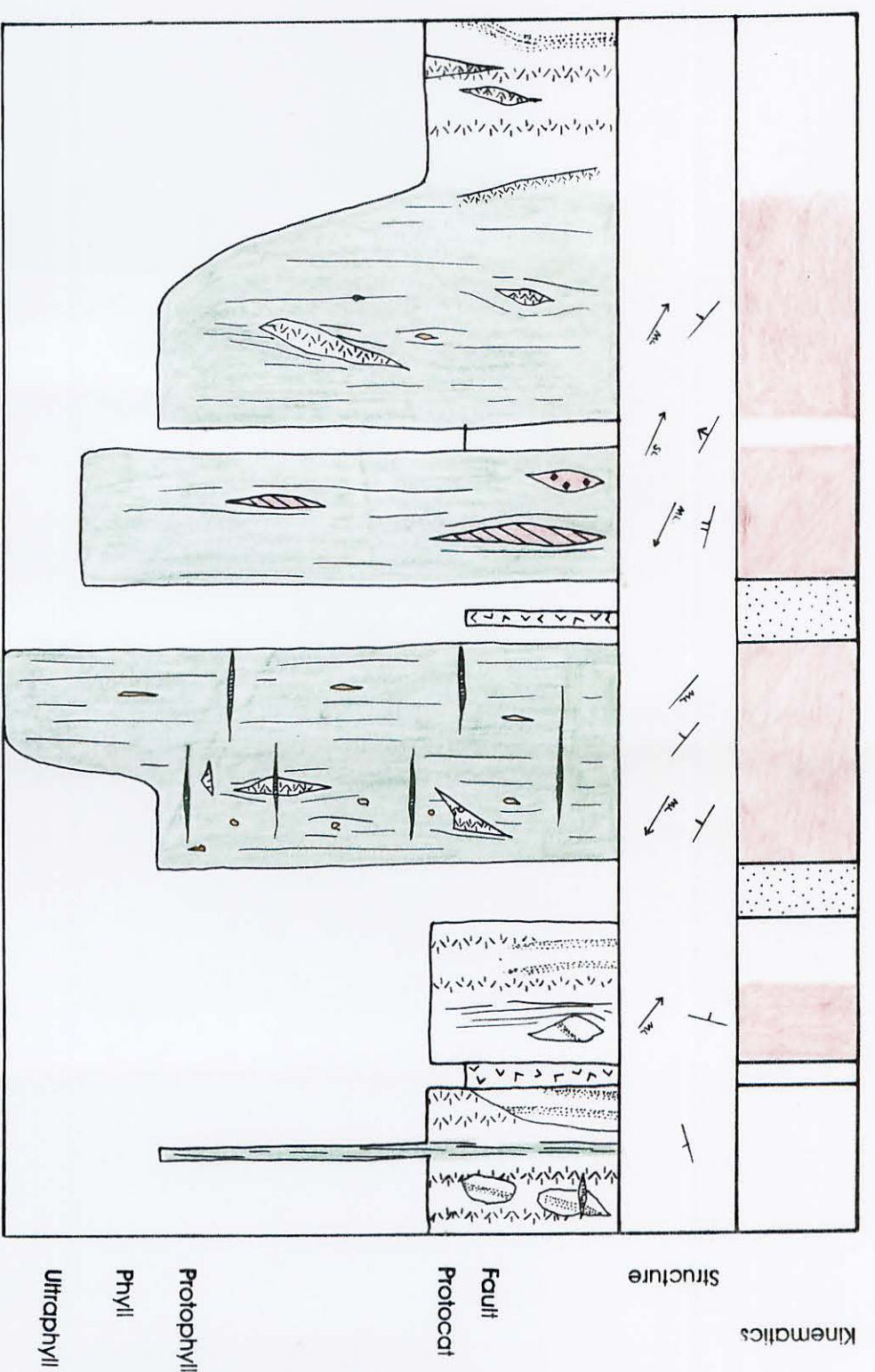
Kinematics  
Structure  
Protolith  
Fault  
Protocataclasite  
Cataclasite / pseudotachylite

# Burrival - Loch a' Ghlinne-dorcha



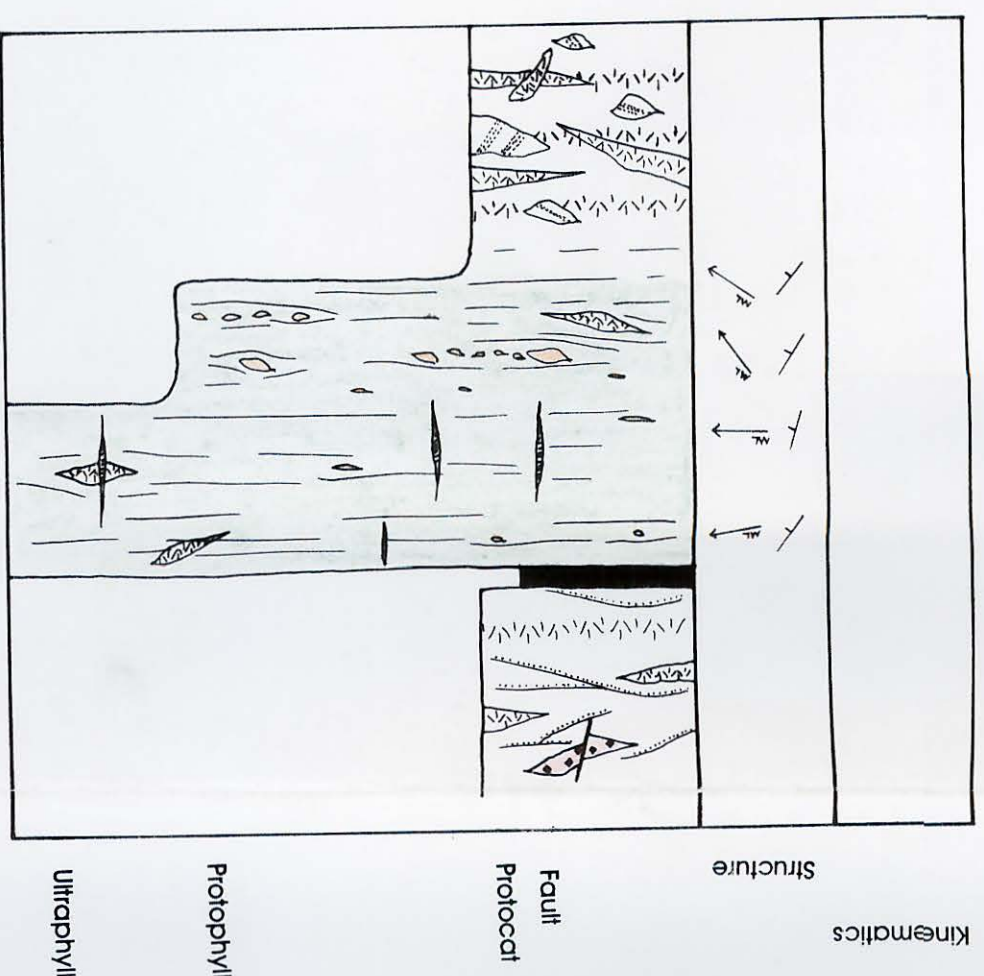
Base of log NF 9133 6189

# Bagh na Caiplich, Ronay



Base of log NF 901 560

# Rubha Vallerip



Base of log NF 059 829

0 10 metres

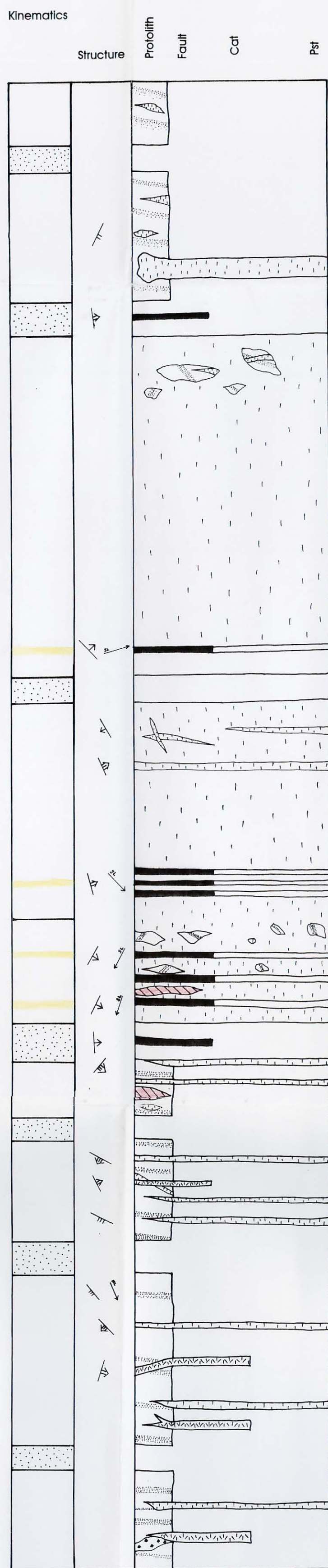
0 5 metres

# South Uist Crush Zones

0 metres 10



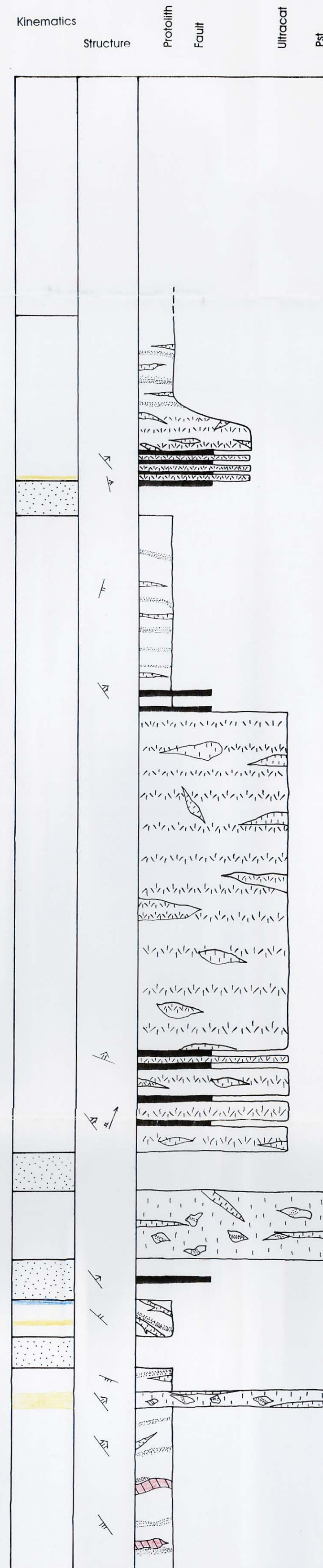
## Ben na Hoe



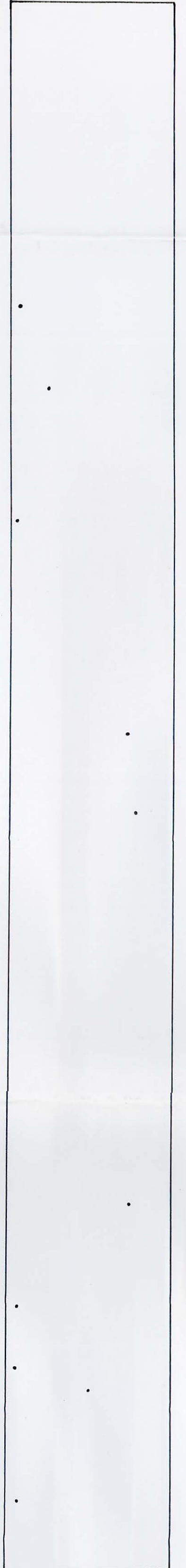
0% pst and / or ultracat 100



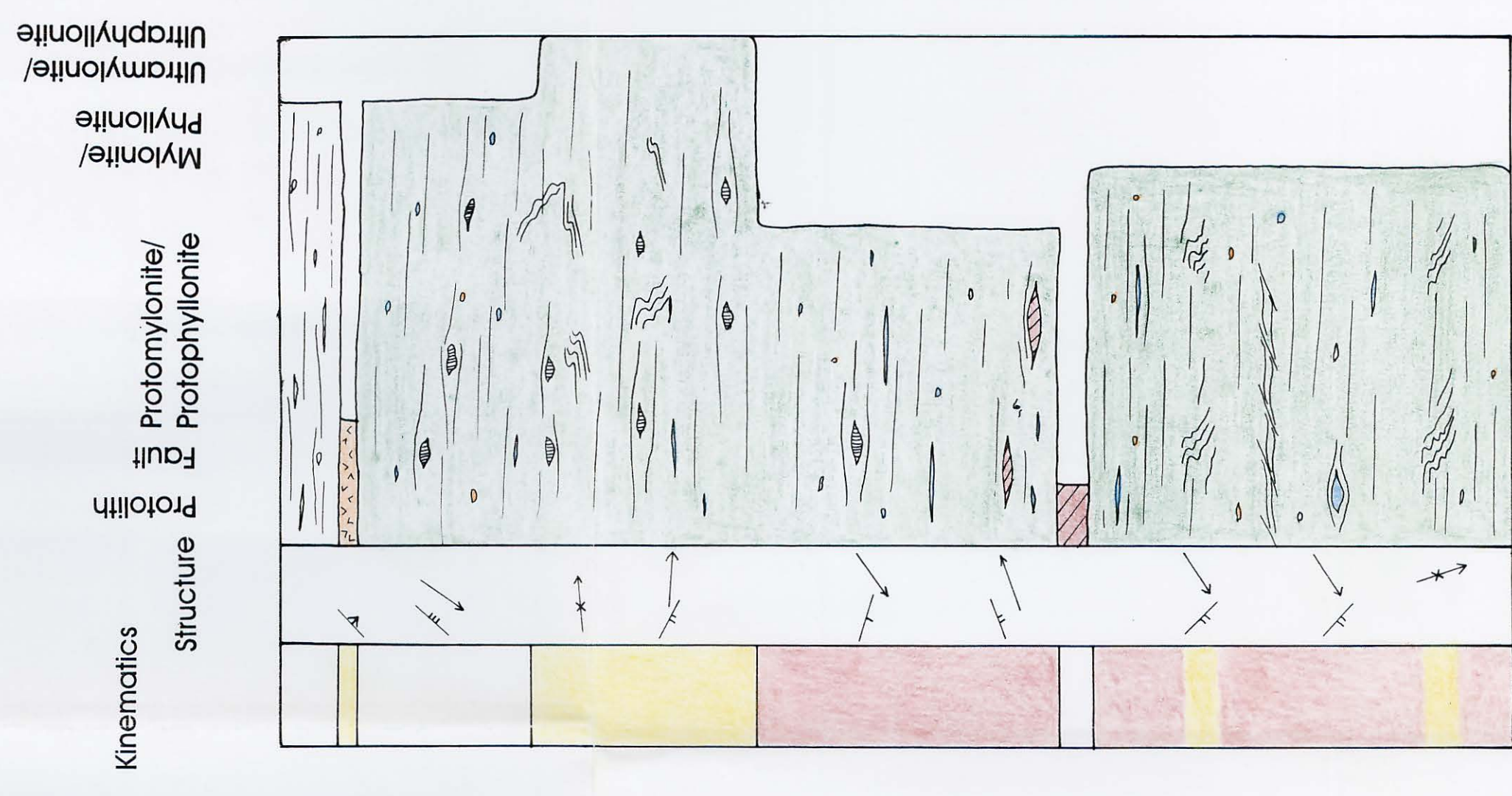
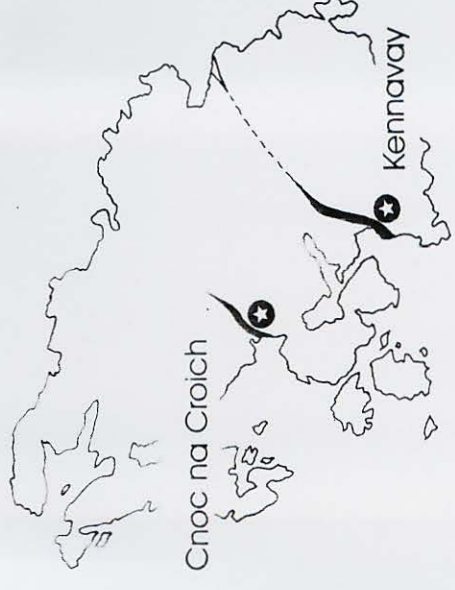
## Bealach an Easain



0% pst and / or ultracat 100



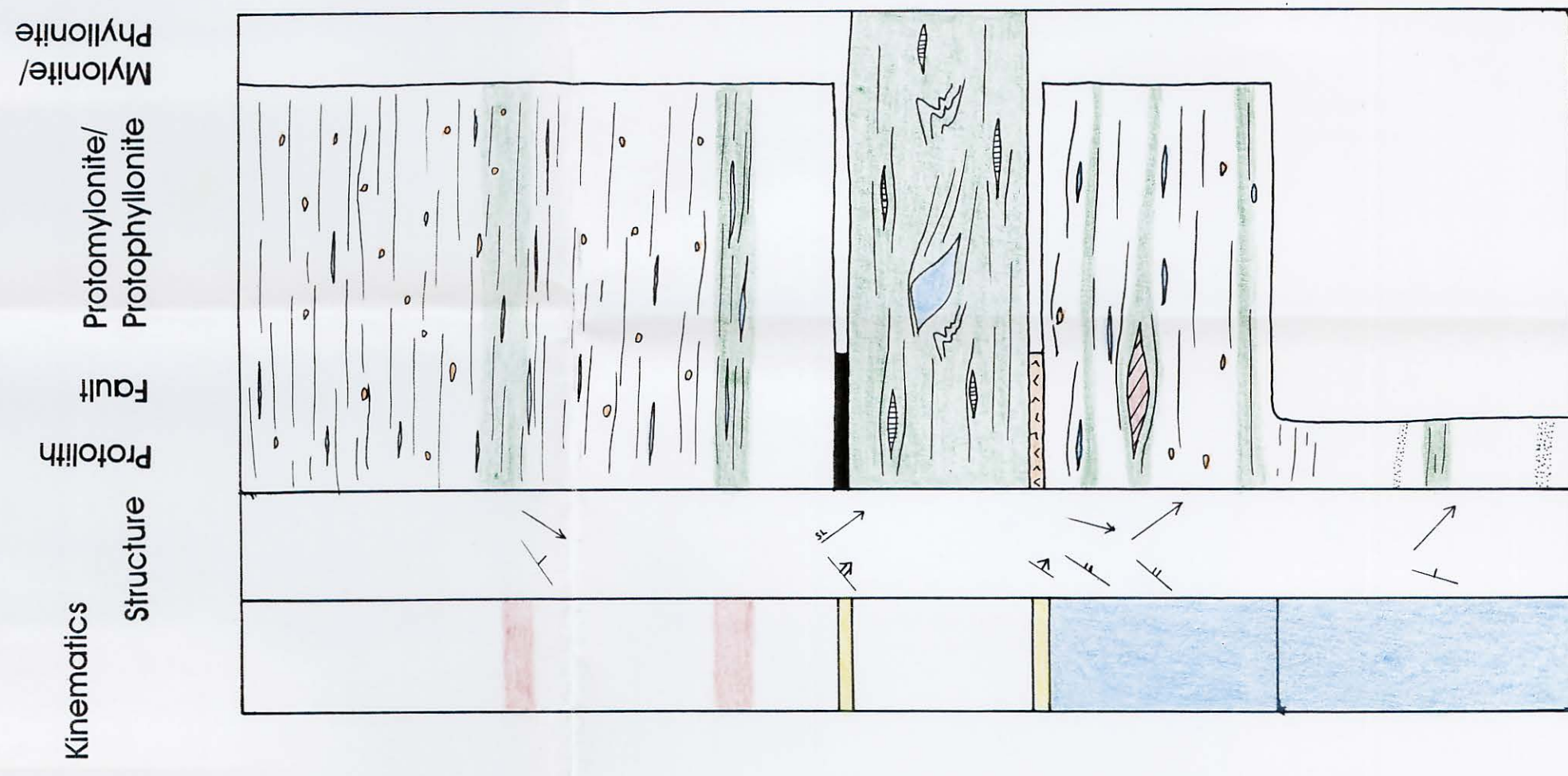
# SCALPAY (3)



0 metres  
1

Phyllonite, Cnoc na Craich

Base of log NG 224 957

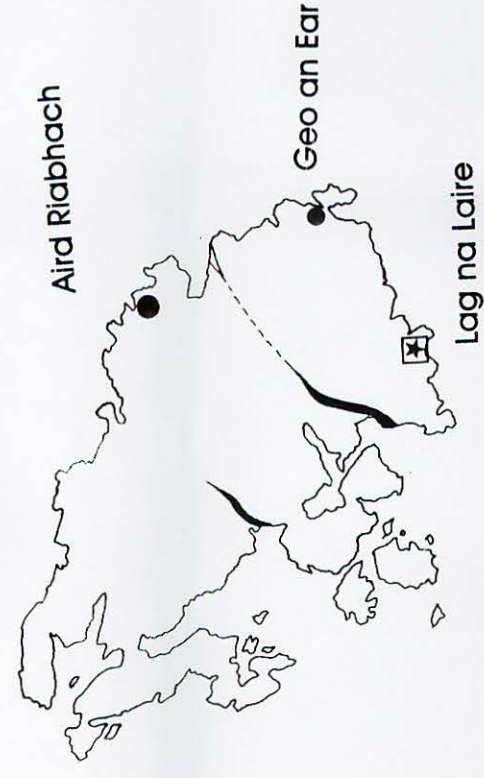


0 metres  
1

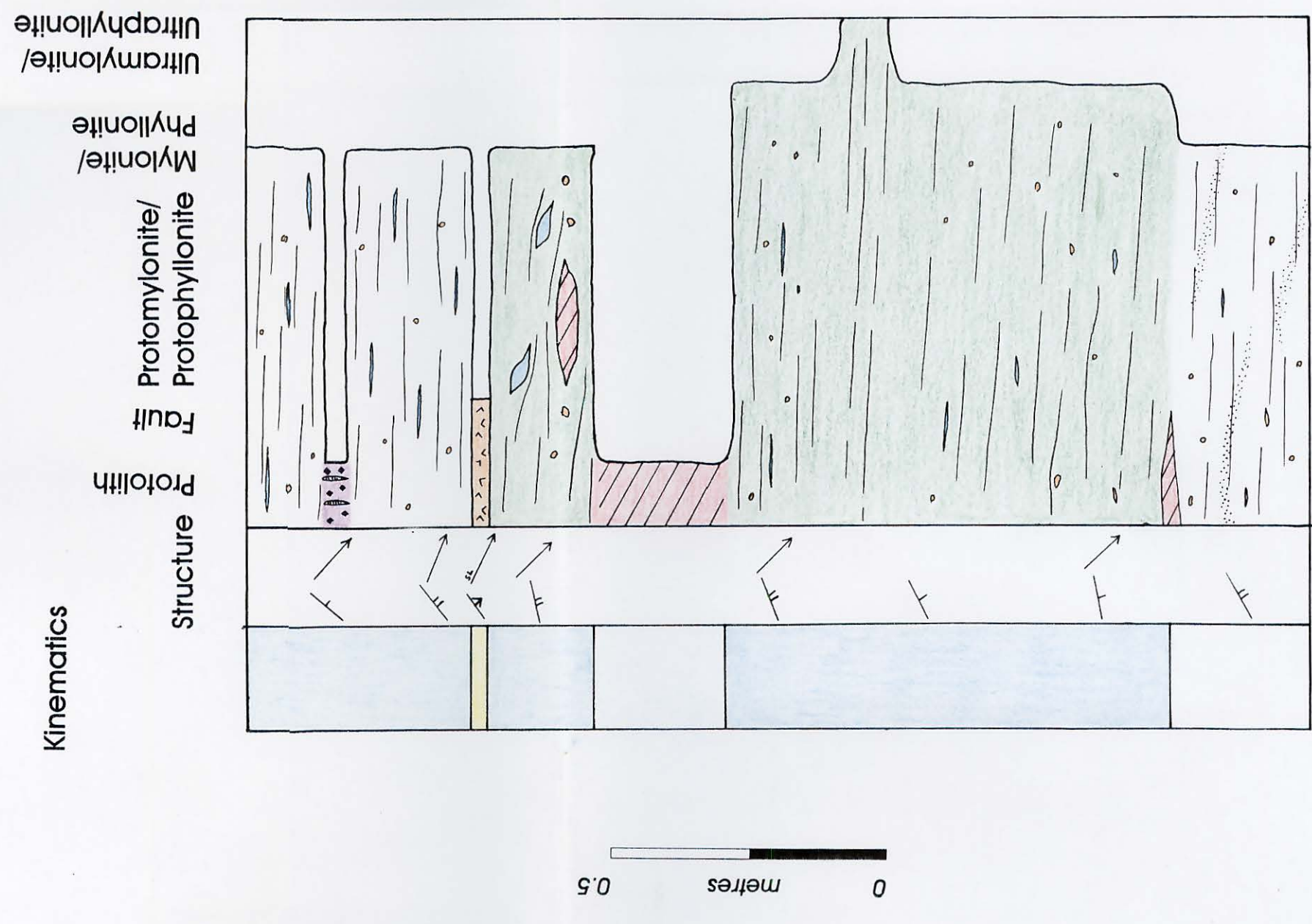
Phyllonite, Kennavay

Base of log NG 230 945

# SCALPAY (2)

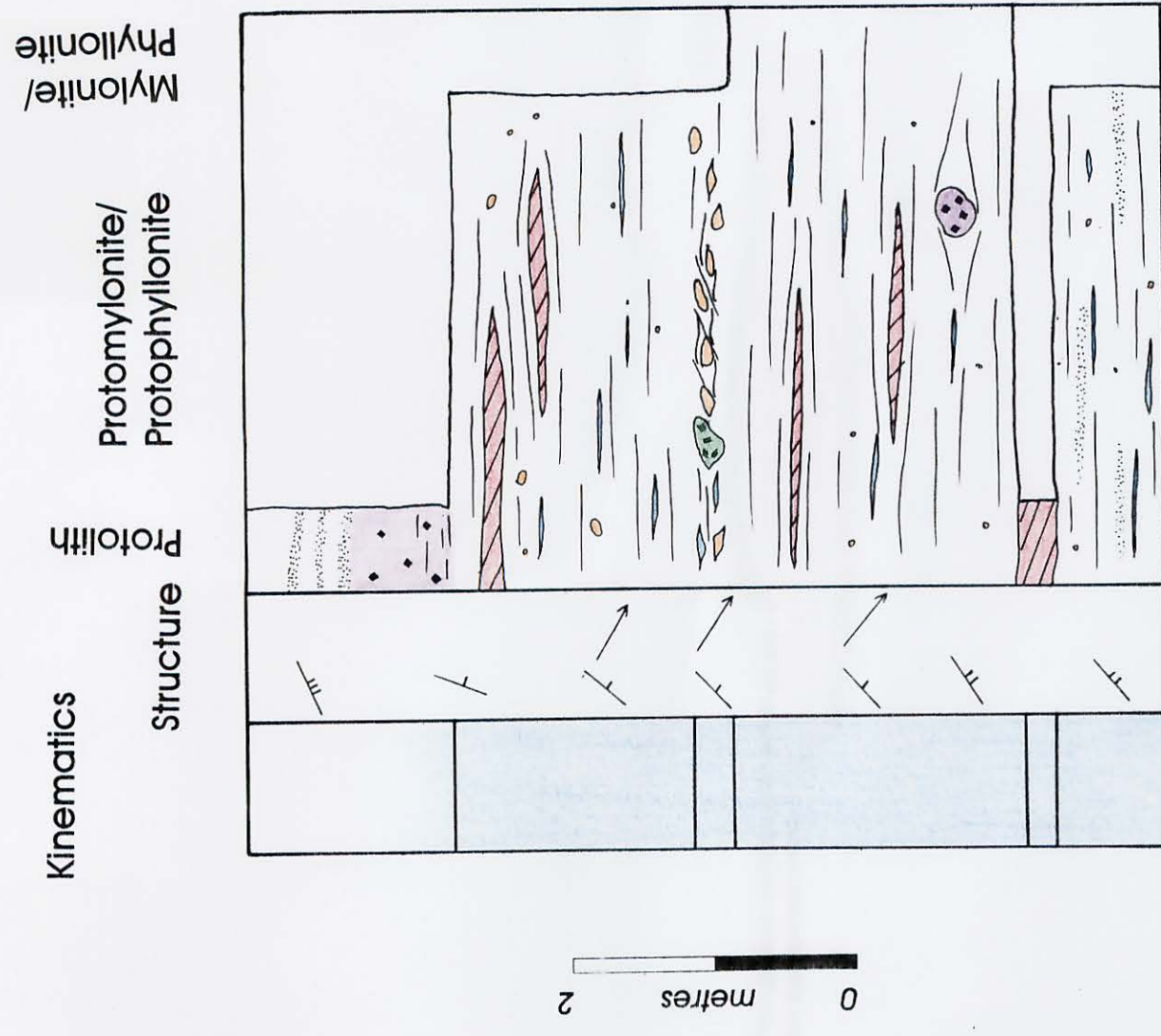


Highly strained mylonites, S. Aird Riabhach



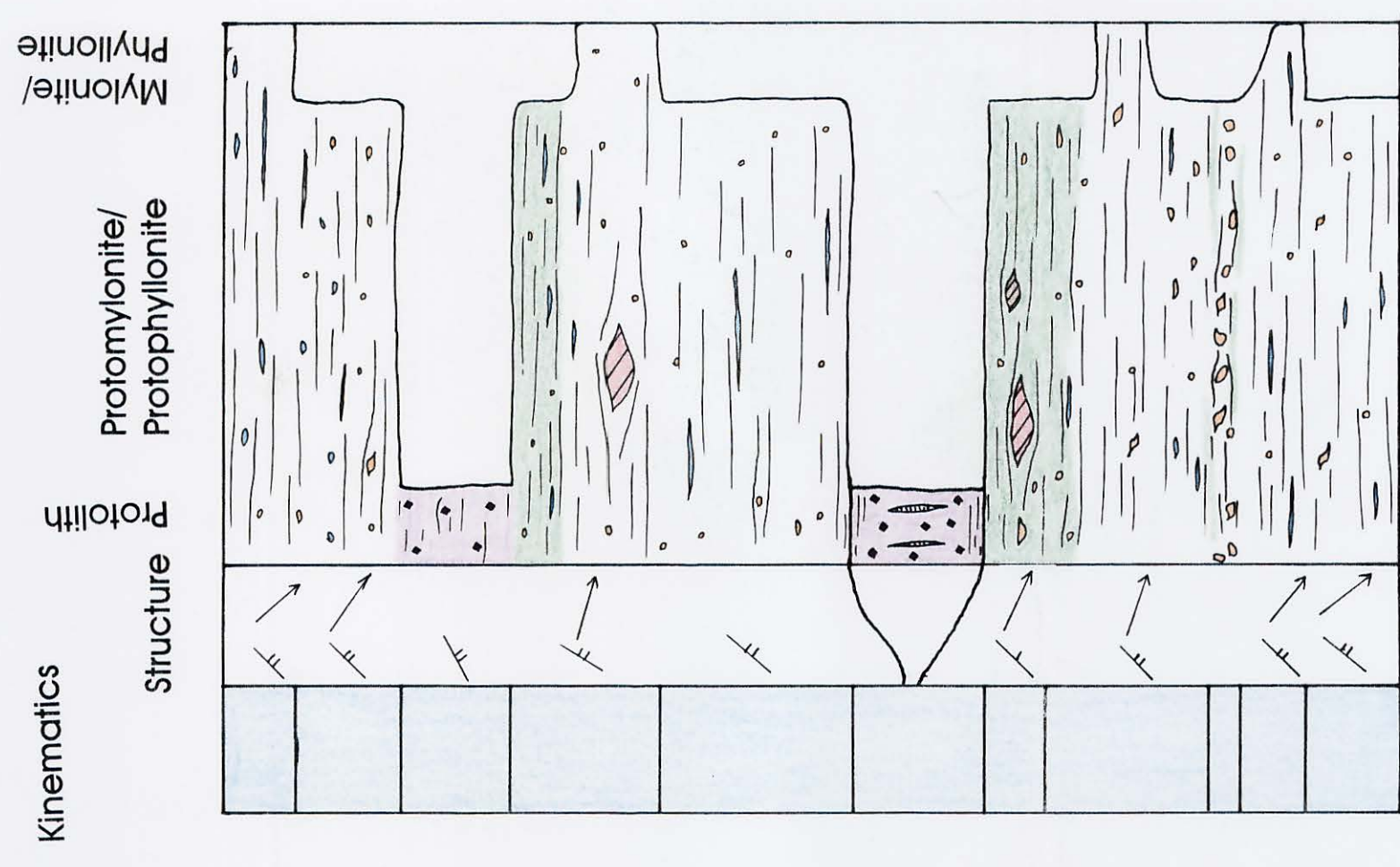
Base of log NG 239 265

Moderately strained mylonites, E. Lag na Laire



Base of log NG 234 942

Highly strained mylonites, Geo an Ear

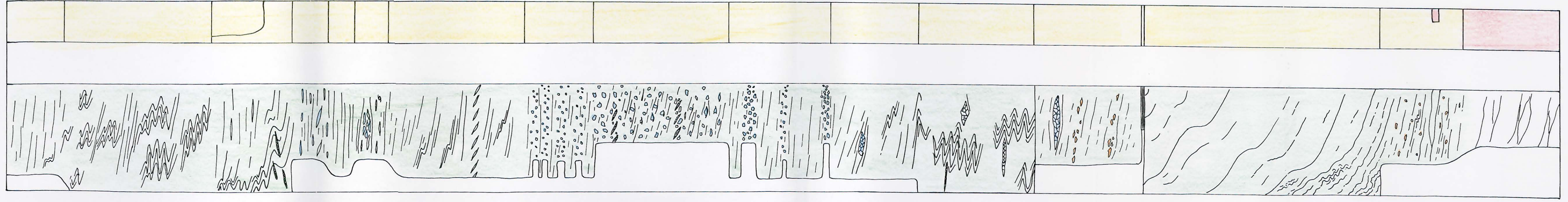


Base of log NG 247 949

# Eignieg Bheag (2)

0 metres 0.5

Base of log NF 921 596

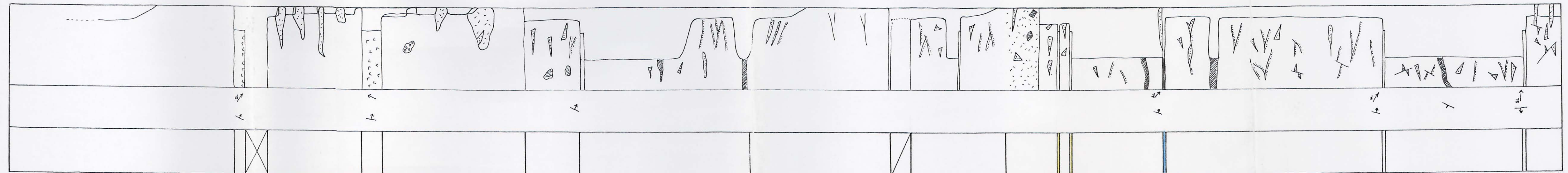


Kinematics  
Structure  
Fault  
Protophyllonite  
Phyllonite  
Ultraphyllonite

# South Burrival

0 metres 4

Kinematics  
Structure  
Protolith  
Fault  
Protoclastite  
Catclastite / pseudochylyte

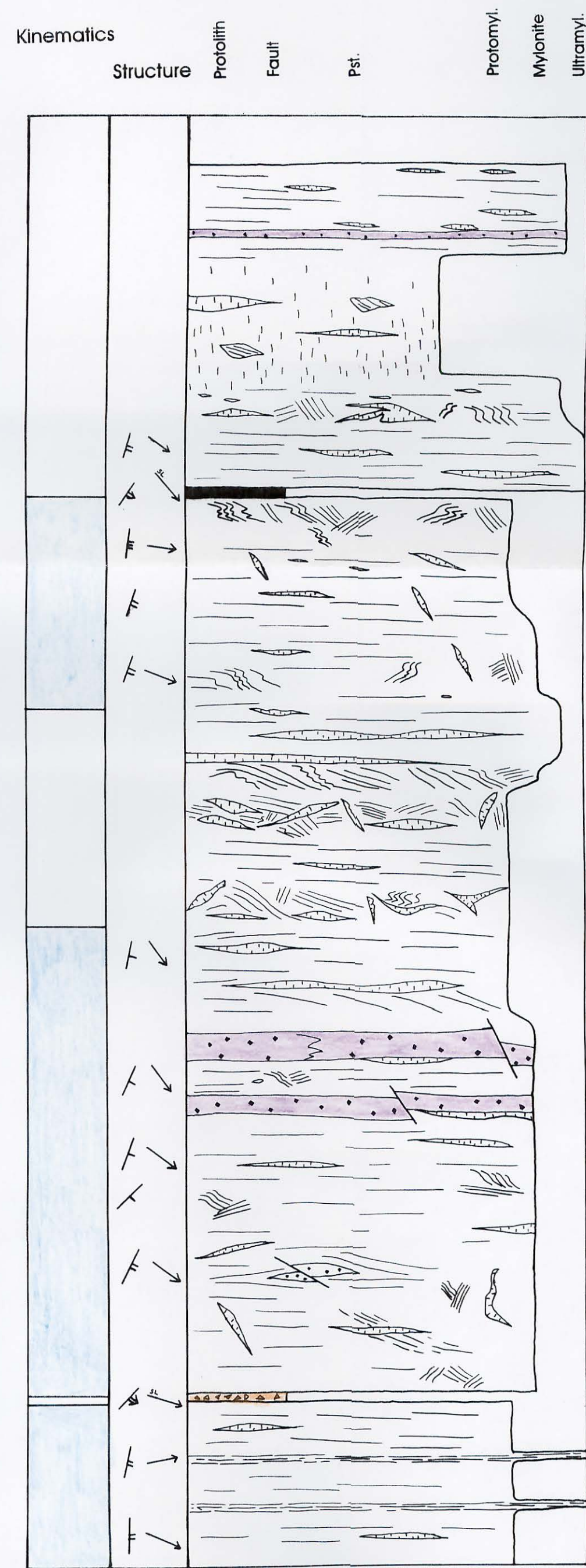


Base of log NF 9073 6195

# SEAFORTH HEAD (2)

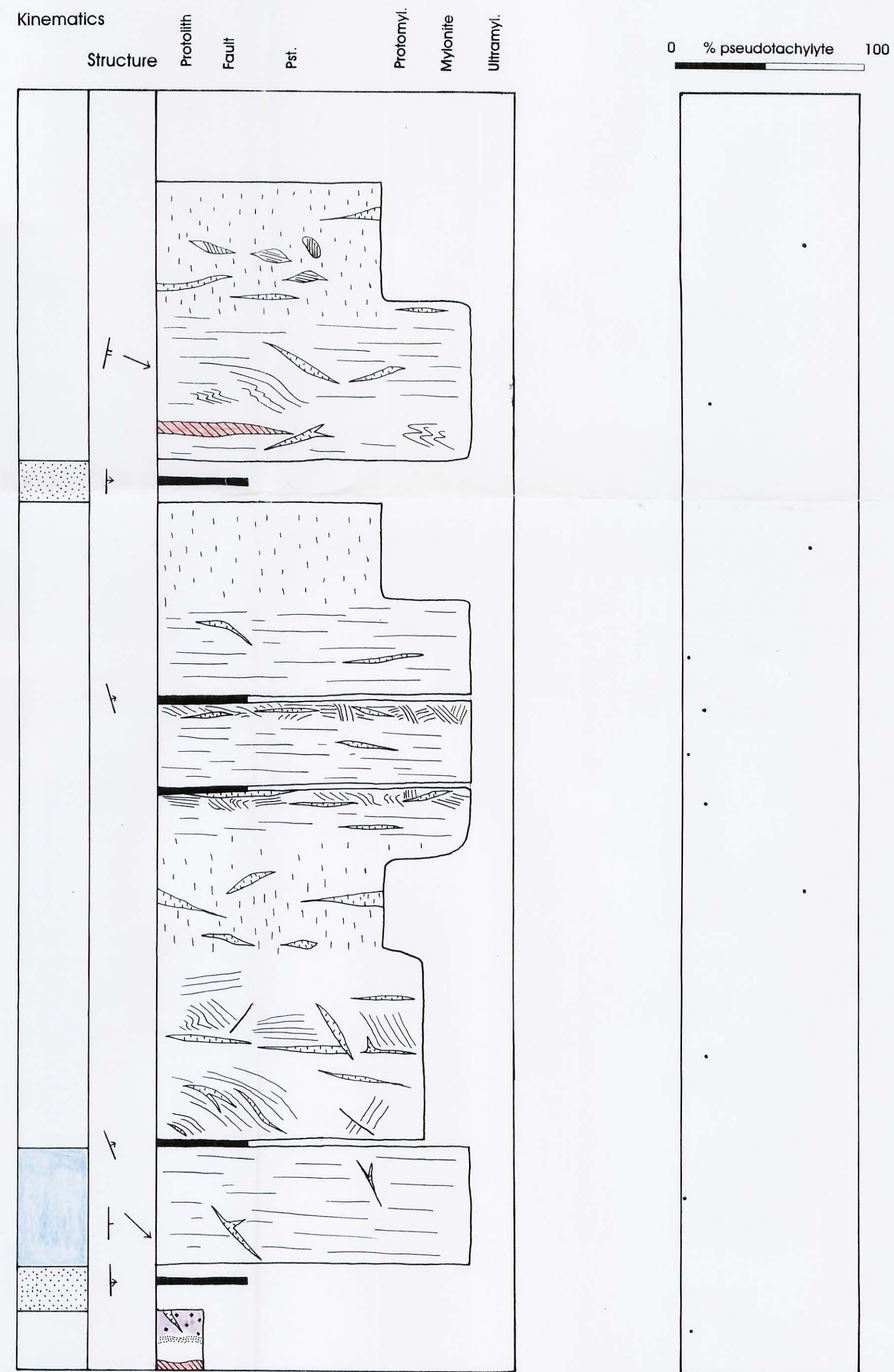


S. of Loch Sgibacleit



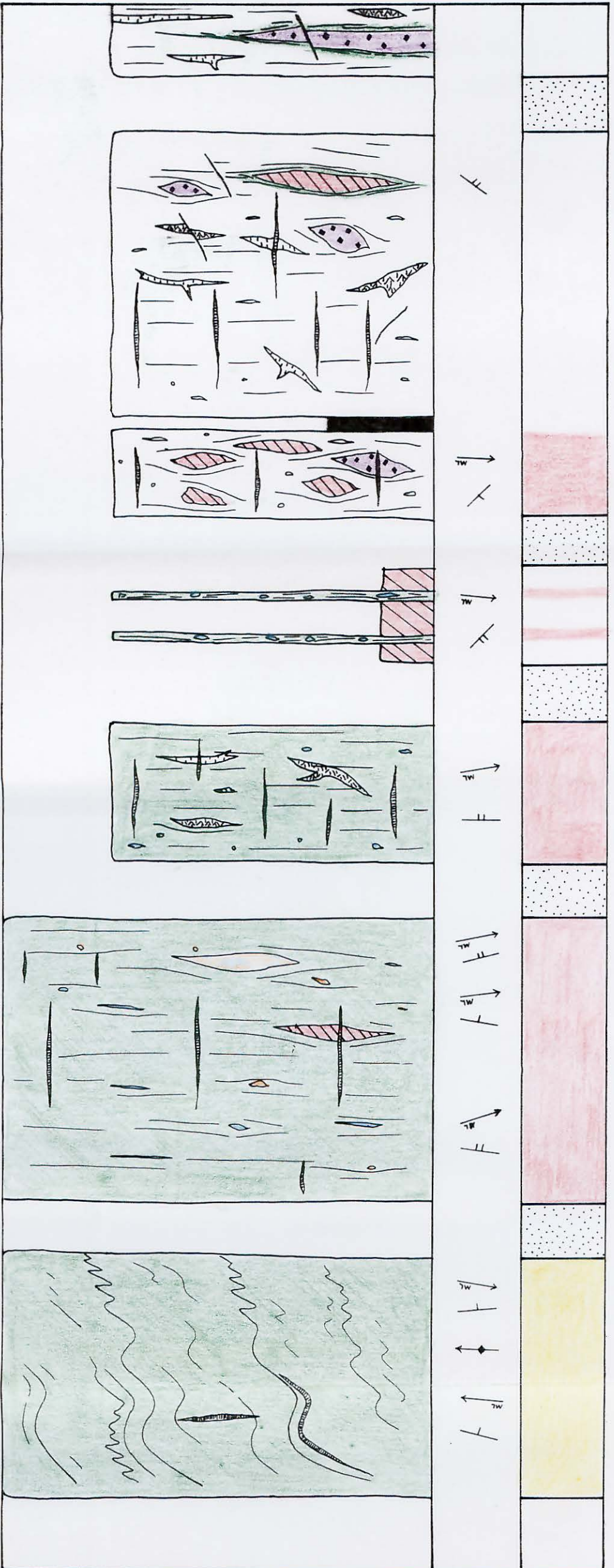
Base of log NB 307 158

Malasgair



Base of log NB 167 296

Base of log NB 317 116



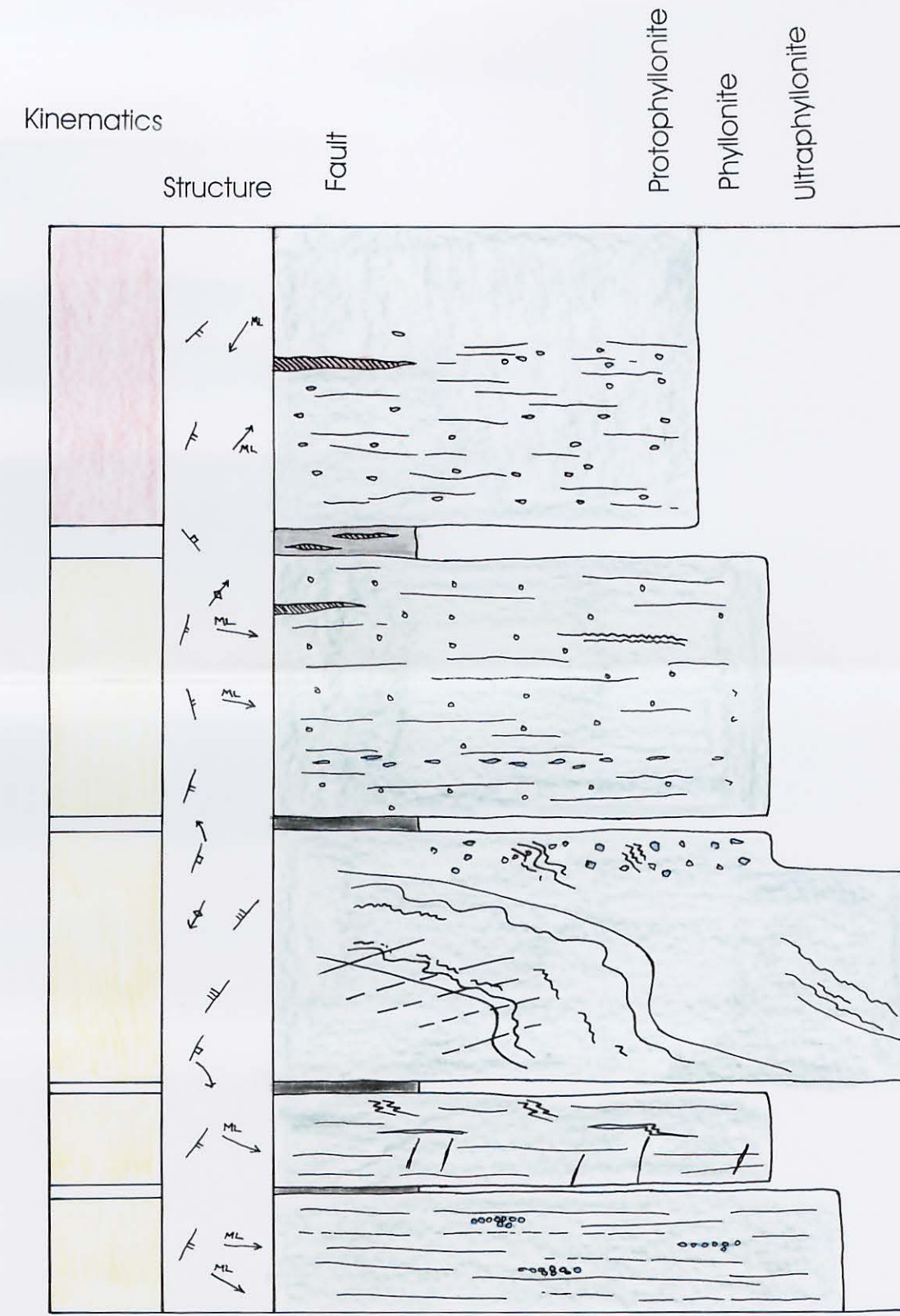
Kinematics  
Structure  
Protolith  
Fault  
Ultraphyll  
Protomyl / protophyll

0 metres 10

Eishken

# Eigneig Bheag (1)

0 metres 2



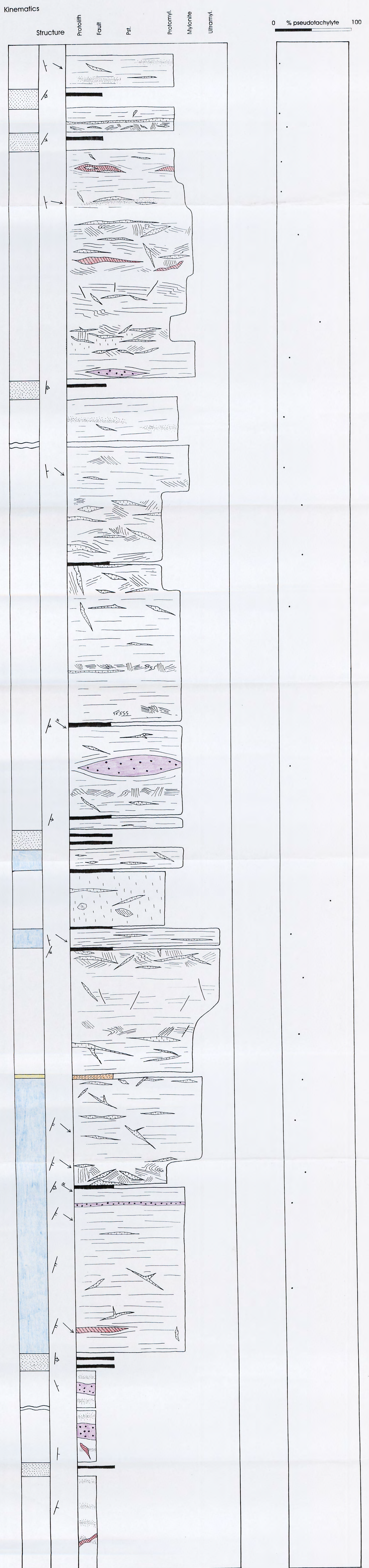
Base of log NF 921 599

# SEAFORTH HEAD (1)

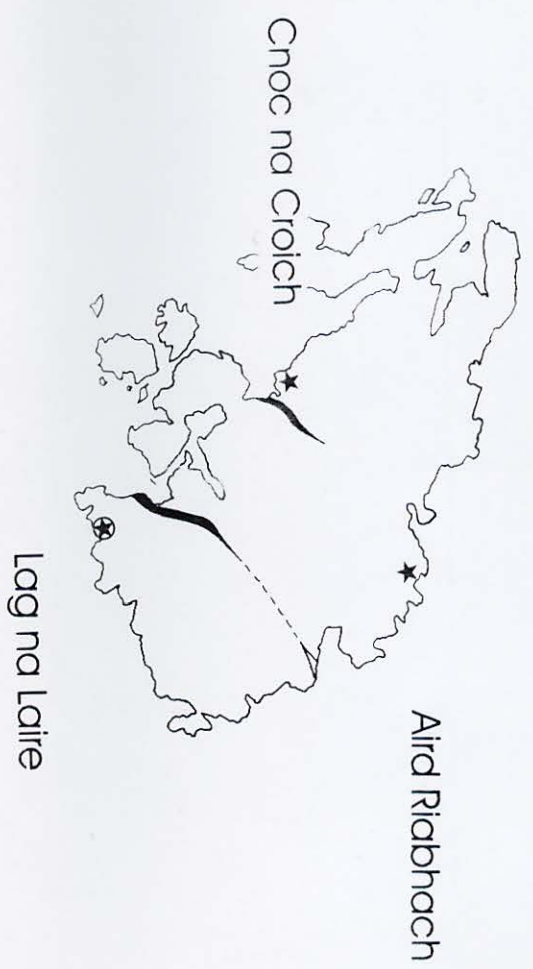
0 metres 10



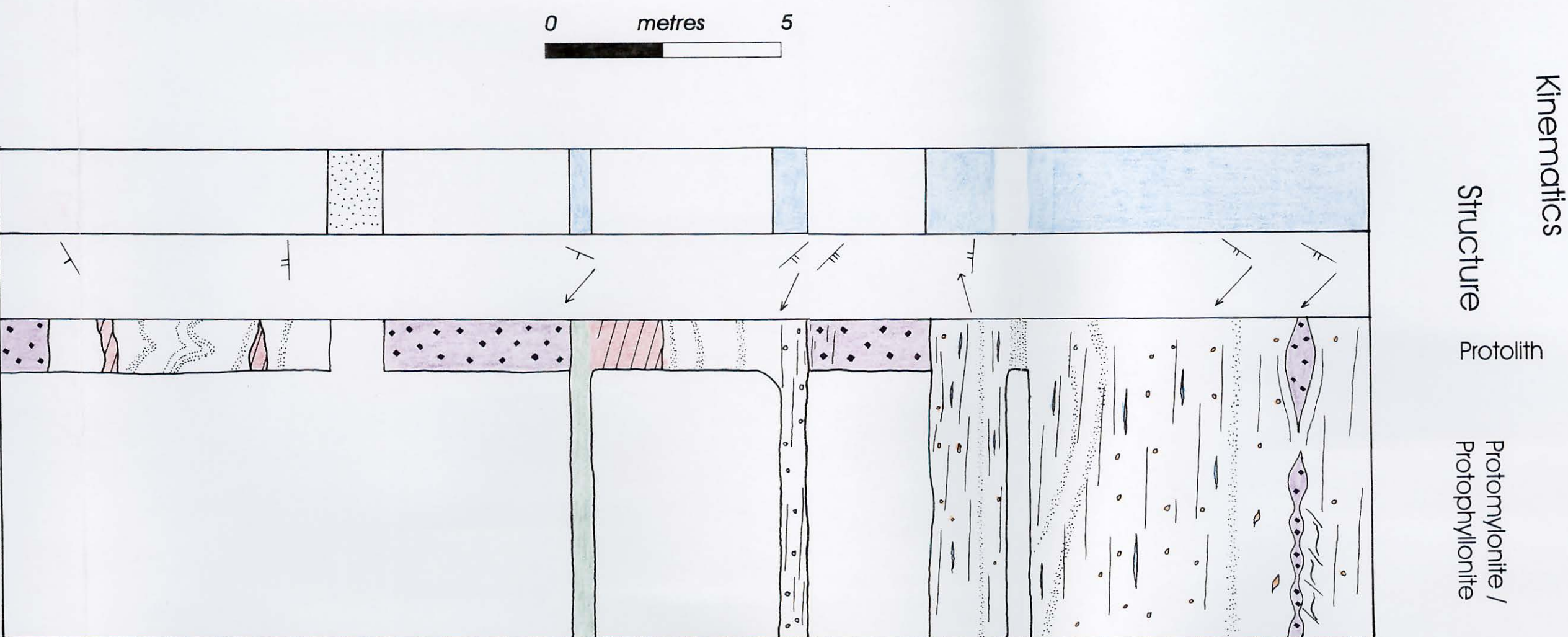
N. of Loch Sgibacleit



# SCALPAY (1)

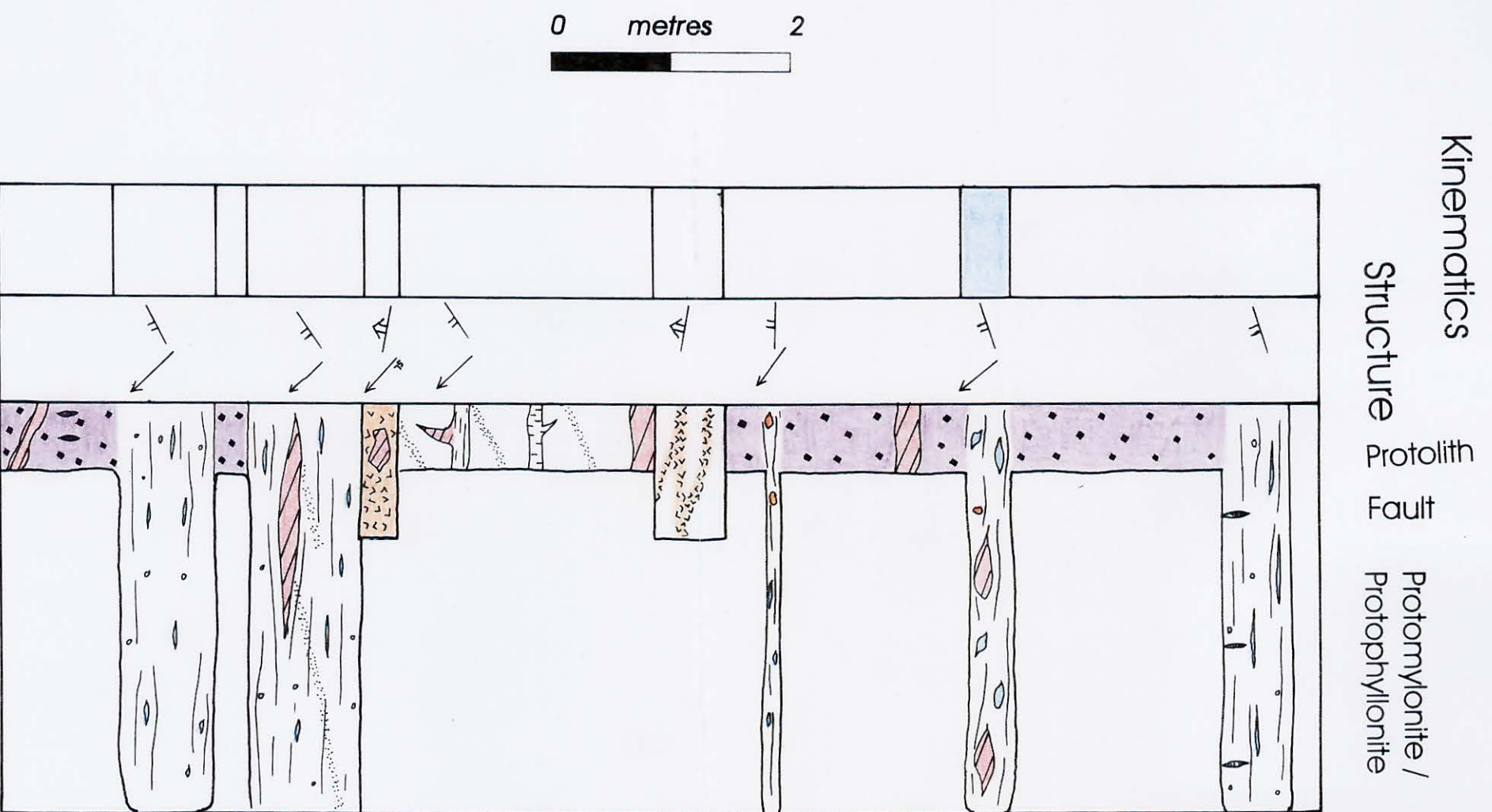


Foreland - pervasive mylonite transition; Aird Riabhach



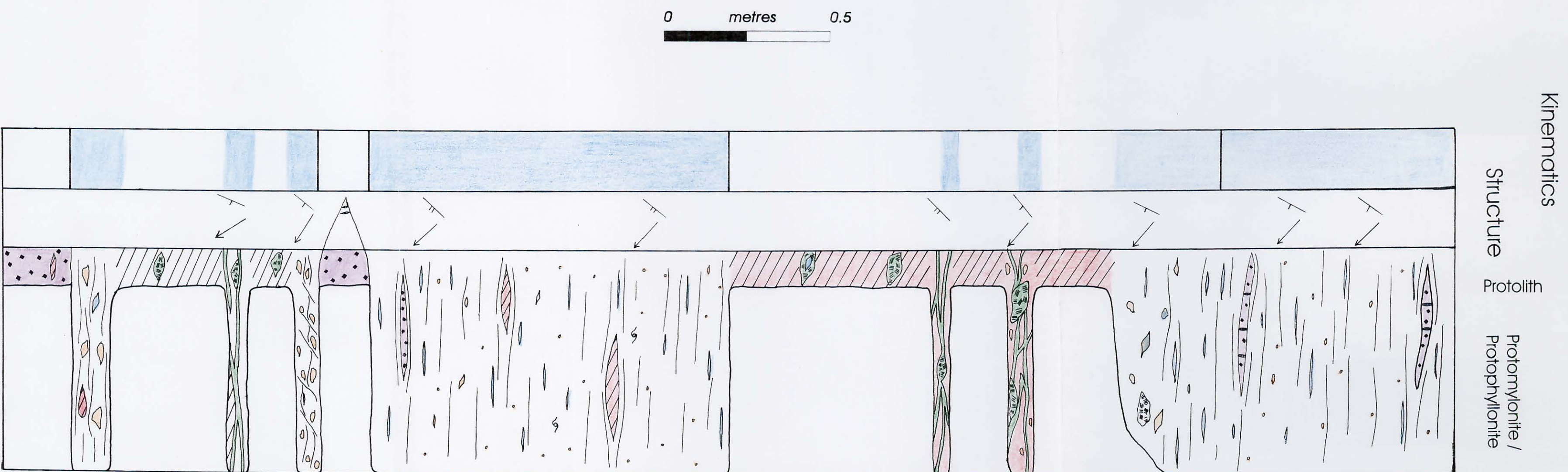
Base of log NG 236 966

Foreland - pervasive mylonite transition; Cnoc na Croich



Base of log NG 222 956

Low strain mylonites; Lag na Laire



Base of log NG 233 942